Vol. 134, January 1, 1982
Complete in one issue

ISSN 0003-2670

ANALYTICA CHIMICA ACTA

International journal devoted to all branches of analytical chemistry

ELSEVIER SCIENTIFIC PUBLISHING COMPANY

ANALYTICA CHIMICA ACTA

International journal devoted to all branches of analytical chemistry
Revue internationale consacrée à tous les domaines de la chimie analytique
Internationale Zeitschrift für alle Gebiete der analytischen Chemie

PUBLICATION SCHEDULE FOR 1982

	J	F	M	A	M	J	J	A	S	O	N	D
Analytica Chimica Acta	134	135/1	135/2	136	137	138	139	140	141	142	143	

Scope. *Analytica Chimica Acta* publishes original papers, short communications, and reviews dealing with aspect of modern chemical analysis, both fundamental and applied.

Submission of Papers. Manuscripts (three copies) should be submitted as designated below for rapid and eff handling:

Papers from the Americas to: Professor Harry L. Pardue, Department of Chemistry, Purdue University, West Lafa IN 47907, U.S.A.

Papers from all other countries to: Dr. A. M. G. Macdonald, Department of Chemistry, The University, P.O. Box Birmingham B15 2TT, England. Papers dealing particularly with computer techniques to: Professor J. T. Universität Bern, Pharmazeutisches Institut, Sahlistrasse 10, CH-3012 Bern, Switzerland.

Submission of an article is understood to imply that the article is original and unpublished and is not being consi for publication elsewhere. Upon acceptance of an article by the journal, authors resident in the U.S.A. will be ask transfer the copyright of the article to the publisher. This transfer will ensure the widest dissemination of inform under the U.S. Copyright Law.

Information for Authors. Papers in English, French and German are published. There are no page cha Manuscripts should conform in layout and style to the papers published in this Volume. Authors should co Vol. 132, p. 239 for detailed information. Reprints of this information are available from the Editors or from: El Editorial Services Ltd., Mayfield House, 256 Banbury Road, Oxford OX2 7DH (Great Britain).

Reprints. Fifty reprints will be supplied free of charge. Additional reprints (minimum 100) can be ordered. An form containing price quotations will be sent to the authors together with the proofs of their article.

Advertisements. Advertisement rates are available from the publisher.

Subscriptions. Subscriptions should be sent to: Elsevier Scientific Publishing Company, P.O. Box 211, 100 Amsterdam, The Netherlands.

Publication. *Analytica Chimica Acta* appears in 11 volumes in 1982. The subscription for 1982 (Vols. 134–14 Dfl. 1815.00 plus Dfl. 220.000 (postage) (total approx. U.S. $814.00). Journals are sent automatically by airm the U.S.A. and Canada at no extra cost and to Japan, Australia and New Zealand for a small additional postal ch All earlier volumes (Vols. 1–133) except Vols. 23 and 28 are available at Dfl. 164.00 (U.S. $66.00), plus Dfl. (U.S. $5.20) postage and handling, per volume.

Claims for issues not received should be made within three months of publication of the issue, otherwise they ca be honoured free of charge.

Customers in the U.S.A. and Canada who wish to obtain additional bibliographic information on this and Elsevier journals should contact Elsevier/North Holland Inc., Journal Information Center, 52 Vanderbilt Avenue, York, NY 10017. Tel: (212) 867-9040.

ANALYTICA CHIMICA ACTA
VOL. 134 (1982)

ANALYTICA CHIMICA ACTA

International journal devoted to all branches of analytical chemistry

ELSEVIER SCIENTIFIC PUBLISHING COMPANY

Anal. Chim. Acta, Vol. 134 (1982)

Analytica Chimica Acta, 134 (1982) 1
Elsevier Scientific Publishing Company, Amsterdam — Printed in The Netherlands

EDITORIAL

Beginning with this issue, those papers that would previously have been published in the COMPUTER TECHNIQUES AND OPTIMIZATION (CTO) section are incorporated into the regular issues of the Journal. When the CTO section was conceived some five years ago, many authors writing about computer techniques and optimizations were uncertain where their manuscripts would be welcomed. As an alternative to a separate journal, it was decided to organize the CTO section of ANALYTICA CHIMICA ACTA, to emphasize the suitability of such papers for a journal devoted to all aspects of analytical chemistry whilst retaining some separate identity of this then rather specialized subject.

The viability of ANALYTICA CHIMICA ACTA as a medium for publishing papers in this area has become well established and it now seems that any advantages associated with a separate section on the subject are outweighed by the best interests of the discipline in which computer techniques are inseparable from analytical chemistry and chemical analysis. This decision to amalgamate the specialized section with the general issues of the journal is consistent with the current trend toward the incorporation of computers as essential parts of much chemical instrumentation and the use of computers in all aspects of research, development, education and applications in analytical chemistry. An integrated format permits the most effective presentation of all chemical and instrumental aspects of the discipline.

The editors continue to welcome papers dealing with all aspects of computer applications in analytical chemistry and chemical analysis and expect that the new system will give authors additional freedom in the preparation of their manuscripts. This development continues the commitment of the editors of the journal to the presentation of the most recent and exciting developments in analytical science in the most effective and comprehensive way, whatever the nature of the work. We hope that this reorganization will encourage both regular contributors and new authors to submit papers on all branches of analytical chemistry.

A. M. G. Macdonald
Harry L. Pardue
Alan Townshend
J. T. Clerc

Analytica Chimica Acta, 134 (1982) 3—11
Elsevier Scientific Publishing Company, Amsterdam — Printed in The Netherlands

DECOMPOSITION OF BIOLOGICAL MATERIALS, ROCKS AND SOILS WITH SIMULTANEOUS VOLATILIZATION OF TRACE ELEMENTS IN PURE OXYGEN UNDER DYNAMIC CONDITIONS

H. B. HAN[a], G. KAISER and G. TÖLG*

Max-Planck-Institut für Metallforschung, Institut für Werkstoffwissenschaften, Laboratorium für Reinststoffe, Stuttgart und Schwäbisch Gmünd (W. Germany)

(Received 7th July 1981)

SUMMARY

Cadmium, thallium, lead and bismuth are quantitatively liberated from rocks and soils after addition of various additives, by opening out in a stream of pure oxygen in a special combustion apparatus. The elements volatilize as oxides and/or halides and condense on a cold finger, whence they are dissolved with about 2 ml of hydrochloric acid (1 + 1) or nitric acid (65%) by boiling under reflux. Concomitant heavy metals remain in the slug which forms on the sample holder that is removed after combustion. Yield monitoring for cadmium, lead and bismuth was done by using radioactive nuclides and for thallium by a spectrophotometric method (rhodamine B). The recovery rates are over 95% for all matrices studied. Good agreement was found for thallium values with standard reference materials.

The determination of traces of elements at ng g^{-1} and lower levels in environmentally relevant materials assumes greater importance as more and more elements are recognized to exert adverse or beneficial effects to life. Consequently, the question of what may be a normal concentration in the pertinent matrices and what may be a toxic or deficient concentration is of the utmost relevance. In order for these inherently difficult analytical problems to be solved, new procedures have to be developed, or well-proven classical methods have to be matched to the new requirements, as regards high sensitivity, accuracy, ease of handling and economy.

The increasing work-load of routine analysis, e.g., in medicine, food chemistry and environmental analysis partly engendered by governmental regulations, calls for speedy analytical procedures with the requisite figures of merit. Indisputably a very economical path is direct analysis of the sample without any pretreatment such as has been proposed occasionally in connection with electrothermal atomic absorption spectrometry (a.a.s.) [1, 2]. This is certainly possible for some selected matrices and a few elements with precisely adjusted apparatus parameters by calibration with standard

[a]On leave from the Institute of Environmental Chemistry, Academia Sinica, Peking, China.

reference materials, but there is some danger in the tendency to apply such techniques generally on economical grounds. Electrothermal a.a.s. with the platform technique [3, 4] and Zeeman a.a.s. [5] have been proposed for the direct analysis of biological samples for trace elements, and certainly yield advantages in some special cases, but these techniques cannot be a panacea for all the problems involved. The same is true for inductively-coupled plasma emission spectrometry (i.c.p.e.s.) which normally allows the determination of multiple trace element concentrations in large numbers of samples on a real-time basis [6, 7]. But if the sample is complex, and this holds for nearly all biological materials, serious interferences can be encountered at ng g^{-1} levels and this often leads to higher detection limits. Therefore, a separation from the matrix is often indispensable [8, 9].

The problem is exemplified, for example, by the determination of thallium, which is of universal interest on account of its high toxicity. In natural waters and body fluids, thallium can be selectively determined by anodic stripping voltammetric methods [10, 11], but for solid samples the situation is much more complicated. The determination of this element in, for example, rocks by electrothermal a.a.s. is impossible even after its separation by ignition tube volatilization because the very low quantities of chloride that covolatilize interfere with the final determination [12]. Therefore, a laborious path via decomposition and separation is necessary [13, 14, 15].

For these reasons, a combined decomposition and separation technique has been developed in order to isolate some problematic elements, e.g., Tl, Cd, Pb and Bi, from biological materials, rocks and soils to allow or to facilitate their reliable determination. The apparatus used (Trace-O-Mat) is the same as described earlier [16] and the execution of the combustion is the same as for the volatilization of selenium [17].

In this study, the sample to be decomposed is blended with additives; in the case of biological materials, silicic acid and in some instances magnesium chloride are used. Rocks and soils are admixed with cellulose and silicic acid/cellulose respectively, and with magnesium chloride if thallium and lead are to be liberated. In the case of the evolution of cadmium from soils, lanthanum nitrate is necessary. As yet, arsenic and antimony cannot be quantitatively recovered even after addition of a range of auxiliary substances that should facilitate volatilization (see below). All investigations were done with radioactive nuclides with the exception of thallium for which no appropriate nuclide is available. In this case, yield monitoring was done by a photometric determination with rhodamine B [18].

EXPERIMENTAL

Apparatus

The decomposition apparatus used was a Trace-O-Mat [16] (H. Kürner, Neuberg 1, F.R.G.). The die for pelleting the samples was specially made from PTFE (teflon). The pressure decomposition apparatus consisted of PTFE vessels with a steel housing, an aluminium oven and electronically-controlled temperature setting [19] (H. Kürner, Neuberg 1, F.R.G.).

A multichannel analyzer type ND-60 with a well-type detector (3 × 3 in. NaI/Tl), a teletype TTY and a HP 7004B X—Y recorder (Nuclear Data GmbH, Frankfurt/M.) was used for radioactive measurements. For spectrophotometry, a Zeiss photometer (type PMQ II) with 1-cm quartz cells and stoppers (Carl Zeiss, Oberkochen, F.R.G.) was used. Automatic micropipettes and continuously adjustable pipettes were from Eppendorf (Hamburg, F.R.G.).

Reagents and standard solutions

For the dynamic combustion process, the oxygen was 99.995% pure. Silicic acid (Riedel de Haen) was heated to 1150°C for 2.5 h in a stream of oxygen to remove thallium blanks (>1 ng g^{-1}). All reagents were of analytical-reagent grade (Merck) unless stated otherwise. Quartz twice-distilled water was used for all solution preparations.

Cellulose (Merck; No. 2337) and lanthanum nitrate (No. 5326) were used as received. Magnesium chloride (No. 5833) was used after drying at 100°C for 2 h and then pulverizing. Hydrochloric acid (1 + 1) and nitric acid (65%) were used for boiling under reflux. For the pressure decomposition, hydrofluoric acid (48%), perchloric acid (60%), hydrochloric acid (1 + 1) and boric acid (No. 165) were used.

The thallium stock solution was prepared from a Titrisol ampoule and contained 2000 μg ml^{-1} in 0.1 M nitric acid. More dilute solutions were prepared daily using 0.1 M nitric acid.

Standard solutions of arsenic-74 were prepared by diluting $H_3{}^{74}AsO_4$ in 0.5 M hydrochloric acid (0.85 mCi ml^{-1} corresponding to 0.8 μg ^{74}As) with 0.5 M hydrochloric acid to give 0.086 μCi/10 μl corresponding to 0.08 ng ^{74}As/10 μl; inactive arsenic was added to give a final concentration of 1 ng μl^{-1}. The antimony-125 standard solution was prepared by diluting $H_3{}^{125}SbO_4$ in 0.5 M hydrochloric acid (0.52 mCi ml^{-1} corresponding to 100 μCi μg^{-1}) with 0.5 M hydrochloric acid to give 0.032 μCi/10 μl (about 0.2 μg antimony-125/10 μl).

The bismuth-207 standard solution was prepared by diluting bismuth-207 chloride in 1 M hydrochloric acid (2.0 μg Bi ml^{-1}, carrier-free) with 0.5 M hydrochloric acid to give 0.050 μCi/10 μl corresponding to 25 ng bismuth-207/10 μl. Cadmium-115 standard solution was prepared by diluting ^{115}Cd chloride in 0.5 M hydrochloric acid (500 μCi/5 ml, corresponding to 5 mg of cadmium) with 0.5 M hydrochloric acid to 0.05 μCi/5 μl, corresponding to 0.5 μg cadmium/5 μl. Lead-203 chloride in 1 M hydrochloric acid (5 mCi/5 ml with 20 ng of carrier) was diluted with 1 M hydrochloric acid to an activity of 0.5 μCi/5 μl. Inactive lead was added to give a final concentration of 20 ng/5 μl.

Optimization of the volatilization of the individual elements

For the individual matrices, various additives were employed which on one hand favour the volatilization of the element to be determined and on the other hand bind interfering heavy metals in the slug [17].

Silicic acid (about 20% of the sample weight) is mixed with biomaterials and some soils. Interfering elements are fixed in the slug which forms on the sample holder that is removed after combustion. Magnesium chloride (15—30% of the sample weight) enhances the volatilization of thallium (Fig. 1) and lead, mainly from rocks and soils. An addition of lanthanum nitrate proved to be effective for the liberation of cadmium from soils, probably because the phosphate present at higher levels in soils is bound (Table 1). Arsenic and antimony could not be recovered completely, even with addition of strong reducing agents; oxalate showed the greatest effect in this (Tables 2 and 3). Baking of the oxides in the prongs of the sample holder during combustion before the volatile compounds form, seems a likely explanation.

Recommended methods

Combustion in a stream of oxygen. The sample preparation and parameters for combustion are the same as described earlier [17] save that various auxiliary substances are added to the matrix.

Method for wet decomposition. For the determination of thallium, the geological sample (0.1—0.3 g) is weighed into a PTFE vessel to which 0.3—0.5 ml perchloric acid (60%) and 2—4 ml hydrofluoric acid (48%) are added; the treatment is as described elsewhere [19]. The decomposition solution is evaporated to 0.5 ml to which 0.1—0.3 g boric acid and 1 ml of nitric acid (65%) are added before further strong heating.

Determination of thallium. Thallium(III) is extracted from 0.5 M hydrobromic acid with di-isopropyl ether. After the organic phase has been washed with 2 M hydrobromic acid and aqueous 0.2% (w/v) hydroxylammonium-chloride solution to remove interfering gold and mercury, the aqueous phase is discarded and the organic layer is shaken with an aqueous solution (0.05%) of rhodamine B to form the Tl(III)-halide—rhodamine B complex which is photometrically evaluated at 555 nm [18].

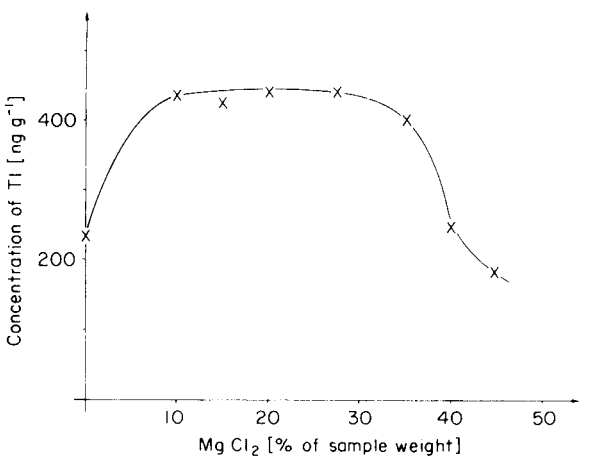

Fig. 1. Release of thallium from standard rock material (AGV 1) in dependence of magnesium chloride added and mixed.

TABLE 1

Recovery of cadmium-115 from spiked biological materials, rocks and soils after ashing in a stream of oxygen and refluxing with 2 ml of nitric acid (65%)

Matrix	Sample weight (mg)	Additive[a]	Recovery[b] (%)
Cellulose	300	Silicic acid	97.7
Milk powder	200	Silicic acid	97
Rice flour	300	Silicic acid	96.9
Orchard leaves	300	Silicic acid	96.5
Blood	200	Silicic acid	95.7
Gravel stone	50	Cellulose	100.6
	100	Cellulose	97.5
	150	Cellulose	96.7
	200	Cellulose	95.3
Soil (Ispra)[c]	250	Cellulose	80
	200	Cellulose	87.4
	150	Cellulose	90
	100	Cellulose	93
	100	Cellulose + $MgCl_2$	92
	100	Cellulose + NaH_2PO_4	81
	100	Cellulose + NaH_2PO_4 + $La(NO_3)_3$	94
	100	Cellulose + $La(NO_3)_3$	96.9
	100	Cellulose + $La(NO_3)_3$	97.1
	100	Cellulose + Silicic acid	94.8

[a]Sample—cellulose ratio 1:1; sample—other additive ratio 5:1. [b]Mean value from 3 repeat measurements. [c]Left to stand for 5 days after spiking.

TABLE 2

Recovery of arsenic-74 from spiked biomaterials, rocks and soils after ashing in a stream of oxygen and refluxing with 2 ml of nitric acid (65%)

Matrix	Sample weight (mg)	Additive[a]	Recovery[b] (%)
Cellulose	200[c]	—	95
	200[c]	Silicic acid	40
	200	—	81
Milk powder	300	—	72
Orchard leaves	300	—	60
Cellulose	200	Silicic acid + NaCl	20
	200	Iron powder	10
	200	Graphite powder	40
	200	Sodium oxalate	56
	200	Silicic acid + KNO_3	23
Rock (AGV-1)	200	Cellulose	20
Soil	200	Cellulose	10

[a]Sample—cellulose ratio 1:1; sample—other additive ratio 5:1. [b]Mean values of 3 repeat measurements. [c]Without separation of the ash.

TABLE 3

Recovery of antimony-125 from spiked biomaterials, rocks and soils after ashing in a stream of oxygen and refluxing with 2 ml of nitric acid (65%)

Matrix	Sample weight (mg)	Additive[a]	Recovery[b] (%)
Cellulose	300	—	81
	300	Silicic acid	63
	300	Silicic acid	21
	300	Silicic acid + NaCl	21
	300	Silicic acid + graphite powder	46
	300	Silicic acid + sodium oxalate	77
Orchard leaves	200	Silicic acid	61

[a]Sample—additive 5:1. [b]Mean values of 3 repeat measurements.

Radioactive monitoring

The pelleted samples were spiked with the respective radionuclide and ashed. The recoveries of the nuclides arsenic-74, antimony-125, cadmium-115, lead-203 and bismuth-207 were determined γ-spectrometrically in the total decomposition solution (2 ml) by comparison with corresponding standard solutions of the radioactive components, in the same test tube, under identical geometrical conditions.

RESULTS AND DISCUSSION

The applicability of the Trace-O-Mat to the destruction of biomaterials, rocks and soils with simultaneous volatilization of cadmium, arsenic, antimony, lead and bismuth was investigated by using radioactive isotopes (Tables 1—5). For the determination of thallium, for which there is no appropriate radionuclide, little attention was directed towards the development of a sensitive multistage procedure, and the work was concentrated primarily on an examination of the completeness of the volatilization (Table 6). The photometric rhodamine B method with an absolute detection limit of about 20 ng sufficed for many matrices. Cross-comparisons with different decomposition methods (e.g., pressurized destruction using acid mixtures, and ignition tube volatilization) showed excellent agreement with other data for standard reference materials (Table 7).

For the other elements, yield determinations were done radiochemically only. With cadmium, lead and bismuth, the recoveries were higher than 95% with a standard deviation of about 3%. Arsenic and antimony could not be volatilized completely. Better recoveries were obtained when the sample holder was left in the decomposition apparatus and leached with the acid used for refluxing, but this means that the advantage of a simultaneous separation from interfering elements is dropped.

TABLE 4

Recovery of lead-203 from spiked biomaterials, rocks and soils after ashing in a stream of oxygen and refluxing with 2 ml of nitric acid (65%)

Matrix	Sample weight (mg)	Additive	Recovery (%)
Cellulose	300	Silicic acid	96.1
	300	Silicic acid + $MgCl_2$	98
Milk powder	200	Silicic acid	96.4
	200	Silicic acid + $MgCl_2$	97.8
Wheat flour	200	Silicic acid	95.2
	200	Silicic acid + $MgCl_2$	98.8
	200	Silicic acid + $MgCl_2$	96
Orchard leaves	150	$MgCl_2$	99.7
Blood	200	Silicic acid	98.8
Gravel stone	200	Cellulose	98.1
	200	Cellulose + $MgCl_2$	97.5
Rock G-2	100	Cellulose + $MgCl_2$	97.4
	100	Cellulose	89
Soil	150	Cellulose	45
	150	Cellulose + $MgCl_2$	91
	150	Cellulose + $MgCl_2$	96
	100	Cellulose + $MgCl_2$	96.7
	100	Cellulose + $MgCl_2$	97.5

TABLE 5

Recovery of bismuth-207 from spiked biomaterials, rocks and soils after ashing in a stream of oxygen and refluxing with 2 ml of nitric acid (65%)

Matrix	Sample weight (mg)	Additive[a]	Recovery[b] (%)
Cellulose	300	—	96.6
	300	Silicic acid	97.1
Milk powder	300	Silicic acid	97
Rice flour	300	Silicic acid	96.3
Wheat flour	300	Silicic acid	96
Orchard leaves	300	—	95.9
	300	Silicic acid	96.1
Bovine liver	200	Silicic acid	96.6
(NBS 1577)	100	Silicic acid	99
	50	Silicic acid	103
Blood	200	Silicic acid	96
Gravel stone	200	Cellulose	98.4
	500	Cellulose	97.4
Soil (Ispra)	100	Cellulose	96.1
	100	Cellulose + $MgCl_2$	97.5

[a]Sample—cellulose ratio 1:1; sample—other additive ratio 5:1. [b]Mean values of 3 repeat measurements.

TABLE 6

Determination of thallium added to biomaterials

Matrix	Sample weight (mg)	Additive[a]	Amount of thallium[b] (ng)		Recovery (%)
			Added	Found	
Cellulose	226	—	80	80	100
	227	Silicic acid	80	75	94
	300	Silicic acid	216	220	102
	300	Silicic acid + $MgCl_2$	108	110	102
	300	Silicic acid + $MgCl_2$	432	420	97
Milk powder	300	—	80	85	103
	300	Silicic acid	216	220	102
Rice flour	300	—	216	210	95
	300	Silicic acid	216	206	95
Wheat flour	300	—	216	220	102
	300	Silicic acid	216	212	98
Orchard leaves	290	—	—	66	(212 ppb)[c]
Orchard leaves[d]	217	—	—	>2000	—

[a]The sample—additive ratio was always 5:1. [b]The concentration of thallium lies below the detection limit with the exception of orchard leaves. [c]Recommended value (NBS), 100 ppb. [d]Pressure decomposition fails because of interferences from undigested material.

TABLE 7

Determination of thallium in rocks and soils[a]

Matrix	Sample weight (mg)	Amount of thallium (ng)		Concentration of thallium (ng g^{-1})		Other data (ng g^{-1})
		Added	Found	Combustion	Pressure decomp.	
Rock G-2	150[b]	120	220	666		670—1800[c]
	30[b]	—	—	600		847[c]
	132	—	110	831		
	128	108	204	828		
	150	240	360	800		
	50—150				858 ± 35	
Rock GSP-1	87	216	372.5	1790		710—2100[c]
	80	—	148	1850		
	150	120	390	1800		
	70[b]	216	309	1330		
	70—200				1630 ± 50	
Rock AGV-1	180	216	296	444		424[d]
	190	—	66.5	350		224—1630[c]
	100	432	473	410		
	128	216	270	420		
	100—200				382 ± 58	
Soil	170	214	284	260	—	—

[a]Except where indicated, both cellulose and magnesium chloride were added. The sample—cellulose ratio was 1:1 and the sample—$MgCl_2$ ratio was 5:1. [b]Only cellulose was added. [c]Data have been reviewed [11]. [d]Ignition tube volatilization [10].

The problems encountered when samples, mainly rocks and sandy soils, are spiked with radionuclides for yield determinations, can be considerable because this technique takes no account of the different forms in which the element may exist in the sample, and the apparent recoveries of the tracer compounds will not necessarily represent the behaviour of the element that may, for example, be present in the lattice of the matrix. In this respect, conclusions can only be drawn from recent experience in the volatilization of selenium and thallium, and from studies under less drastic conditions [14, 20] as to the effectiveness of the techniques described here. Ultimately, only appropriate methods of determination for the individual elements will give clear-cut information, but at this stage of development, it seemed necessary first to provide an overview of what can be volatilized in this combustion apparatus, so that methods of determination compatible with the Trace-O-Mat can be sought. Multi-stage procedures universally applicable for sensitive and accurate determinations of the mentioned elements in the materials cited above should then be possible.

One of us (H.B.H.) is grateful to the Max-Planck Society for the award of a research fellowship. We thank S. Pahlke for his help in the radioactive measurements.

REFERENCES

1 J. A. Nichols, R. D. Jones and R. Woodriff, Anal. Chem., 50 (1978) 2071.
2 F. J. Langmyhr and S. Orre, Anal. Chim. Acta, 118 (1980) 307.
3 C. L. Chakrabarti, C. C. Wan and W. C. Li, Spectrochim. Acta, 35B (1980) 92.
4 C. L. Chakrabarti, C. C. Wan and W. C. Li, Spectrochim. Acta, 35B (1980) 547.
5 P. Frigieri and R. Truco, Spectrochim. Acta, 35B (1980) 113.
6 R. H. Scott and A. Strasheim, Anal. Chim. Acta, 76 (1975) 71.
7 R. L. Dahlquist and J. W. Knoll, Appl. Spectrosc., 32 (1978) 1.
8 J. M. Motooka, E. L. Mosier, S. J. Sutley and J. G. Viets, Appl. Spectrosc., 33 (1979) 456.
9 B. Pahlavanpour, M. Thompson and L. Thorne, Analyst, 105 (1980) 756.
10 J. E. Bonelli, H. E. Taylor and R. K. Skogerboe, Anal. Chim. Acta, 118 (1980) 243.
11 D. I. Levit, Anal. Chem., 45 (1973) 1291.
12 H. Sager and G. Tölg, unpublished work.
13 H. Berndt, J. Messerschmidt, F. Alt and D. Sommer, Fresenius Z. Anal. Chem., 306 (1981) 385.
14 H. Heinrichs, Fresenius Z. Anal. Chem., 294 (1979) 345.
15 R. C. Carpenter, Anal. Chim. Acta, 125 (1981) 209.
16 G. Knapp, S. Raptis, G. Kaiser, G. Tölg, P. Schramel and B. Schreiber, Fresenius Z. Anal. Chem., 308 (1981) 97.
17 H. B. Han, G. Kaiser and G. Tölg, Anal. Chim. Acta, 128 (1981) 9.
18 H. Sager and G. Tölg, Mikrochim. Acta, in press.
19 L. Kotz, G. Kaiser, P. Tschöpel and G. Tölg, Fresenius Z. Anal. Chem., 260 (1972) 207.
20 W. Geilmann and K.-H. Neeb, Fresenius Z. Anal. Chem., 165 (1959) 251.

Analytica Chimica Acta, 134 (1982) 13—19
Elsevier Scientific Publishing Company, Amsterdam — Printed in The Netherlands

A NEW INSTRUMENT FOR TIME-RESOLVED REDUCTION OF SCATTERED RADIATION IN FLUORESCENCE MEASUREMENTS

R. E. RUSSO and G. M. HIEFTJE*
Department of Chemistry, Indiana University, Bloomington, IN 47405 (U.S.A.)
(Received 30th June 1981)

SUMMARY

An opto-electronic cross-correlation system was employed to reduce the scattering influence in fluorescence measurements. A stable optical delay line incorporated into the instrument was positioned to yield detection at a fixed time after excitation; the optimal delay time was determined simply from the ratio of the fluorescence decay curve to a similar curve portraying scattering response. Signal-to-scattering background enhancements greater than two were measured for the very short-lived (τ = 0.7 ns) fluorophores whereas a six-fold increase was measured for fluorophores with longer lifetimes. The shortest lifetime which would benefit from time-resolution in this system is limited by the time-response of the photomultiplier tube (1.1 ns FWHM); the excitation pulses are on the order of 6 ps.

One of the main hindrances in fluorescence spectrometry is the scattering of excitation source radiation [1—4]. For condensed-phase samples, not all of the light passes through a solution or is absorbed; some is scattered by finely dispersed particles, part is reflected from the cuvette surfaces (if not coated with an anti-reflection coating), and a fraction is Rayleigh-scattered from the solvent [5]. The effect of scattering is to deflect a portion of the exciting radiation into the fluorescence detection optical path, causing erroneously high measured intensities. Generally, scattered radiation is not directly detected in molecular fluorimetry because of a wavelength shift of the fluorescence from the absorption region; spectral discrimination is therefore possible. However, in low-resolution dispersing systems such as those employing filters, scattering can be detected directly. Moreover, even in higher quality systems, scattering contributes to stray light which can limit sensitivity, precision, and accuracy in molecular fluorimetry.

Scattering is potentially an even more serious problem in atomic fluorescence spectrometry (a.f.s.) because resonance transitions are commonly employed. In a.f.s., scattering arises from refractive index inhomogeneities in the flame (Rayleigh scattering) and from incompletely atomized particles (Mie scattering); the greatest contribution is from Mie scattering [3, 6]. In fact, Mie scattering, which is the principal noise source in many atomic fluorescence measurements, limits accuracy, detection limits, and precision.

0003-2670/82/0000-0000/$02.75

Correction for, or elimination of, scattering is essential if atomic fluorescence spectrometry is to be used as a practical analytical technique [7—11].

Several methods have been proposed for reducing the deleterious effects of scattering in a.f.s. Among these methods are (a) the use of non-resonance transitions, (b) polarization discrimination, (c) wavelength modulation, and (d) time resolution. The use of non-resonance transitions is similar to molecular fluorimetry in that the fluorescence radiation is wavelength-shifted from that of the incident radiation, and can be spectrally isolated. However, non-resonance transitions are less probable than resonance ones, and are not commonly employed in routine determinations [12, 13]. In polarization discrimination, Rayleigh scattering, unlike fluorescence, exhibits a dependence on polarization and on direction of observation of the scattered light. By using linearly polarized light for excitation and by placing the detector at a right angle to the direction of the exciting light in the same plane as the polarization, one can minimize scatter while maintaining the fluorescence signal. However, this approach is effective only for reduction of Rayleigh scattering and is generally not applicable to flame atomic fluorescence where Mie scattering can be dominant [14]. With wavelength modulation, scattering intensity is essentially constant over small changes in excitation wavelength, whereas atomic fluorescence is highly sensitive to wavelength shifts. Electro-optically tuned c.w. dye lasers can provide 1-nm repetitive wavelength scans at MHz modulation frequencies [15, 16]. Wavelength modulation and gated detection also preserve the advantage of amplitude modulation in that background emission from the flame is minimized. Time-resolution involves a pulsed excitation source and gated detection system. Scattering is essentially instantaneous and is therefore of the same duration as the excitation pulse, whereas fluorescence exhibits a finite lifetime. Therefore, the detection of scattered radiation can be greatly reduced if one measures fluorescence only after a finite time beyond excitation, i.e., after the excitation pulse is finished but before complete decay of the fluorescence radiation [17].

In the present work, time resolution is explored. A variable, fixed-time delay spectrofluorimeter has been designed which is capable of eliminating most of the scattered radiation problem. Scatter is reduced by observing fluorescence a finite time after a light pulse excites the sample. This time-dependent observation is accomplished by means of a unique opto-electronic signal = gating scheme constructed to perform the cross-correlation between two photodetector response functions [18—21]. This arrangement is well suited for such studies because of the extremely narrow pulses provided by a synchronously pumped dye laser. In addition, an optical delay line is incorporated into the instrument and can be accurately positioned to measure fluorescence at any selected time after excitation, yet is free from triggering instability and drift.

EXPERIMENTAL

Instrumentation

The experimental arrangement includes a synchronously pumped dye laser and opto-electronic cross-correlation system described previously [18, 21]. Briefly, the pulses (6 ps FWHM) from a synchronously pumped dye laser (Model 171-06 Argon ion laser; Model 342 mode-locker with Model 452 mode-locker driver; Model 375 dye laser and Model 341 Synchronously Pumping Accessory Package, Spectra-Physics, Mountain View, CA) simultaneously irradiate a fast photodiode (Model 403B, Spectra-Physics) and sample cell (flame or cuvette) containing the fluorophore of interest. The fluorescence is detected by a fast response photomultiplier tube (Model 31024, RCA, Lancaster, PA), the output of which is connected to one input of a double-balanced microwave mixer (Model ZFM-4, Mini-Circuits, New York, NY). The second input to the mixer receives the pulse from the fast photodiode, and the mixer performs a multiplication between the two signals. Because the photodiode signal is zero except when the laser illuminates it, the signal serves as a "gate function" when it multiplies (in the mixer) the photomultiplier (PMT) output. Therefore, the photomultiplier output is sampled only during the time corresponding to the arrival of the laser pulse at the photodiode. Conveniently, the relative arrival time of the pulses at the two detectors (photodiode and photomultiplier) is easily varied by means of an optical delay line. Time-resolution of this delay line is 3 ps and its range of adjustment is approximately 12 ns. The delay is positioned so that the sample cell receives the laser pulse earlier than the photodiode. The time difference is chosen to be greater than the response time of the PMT under scattering conditions, but less than the lifetime of the fluorophore to be studied. When no fluorophore is present, the output of the mixer is approximately zero. However, when a fluorophore is placed in the sample cell, the pulse width from the PMT is increased because of the finite lifetime of the fluorophore. Measurements of fluorescence intensity are therefore obtained in the absence of scattered radiation.

Procedures

The actual procedure involves measuring the instrument response function (by directing scattered light toward the photomultiplier) and fluorescence decay curves (Fig. 1) and determining from them the optimal position of the delay line. Specifically, the ratio of fluorescence intensity (S) to scatter intensity (B) was calculated as a function of optical delay setting. The delay time at which S/B is greatest is used to perform the scattering elimination experiments. Ideally, the fixed position of the delay line is such that sampling by the photodiode gate occurs in a temporal region where only fluorescence and no scattering exists (cf. Fig. 1).

The influence of scatter was reduced in both atomic and molecular fluorescence measurements. Molecular fluorophores examined were rhodamine B (τ =

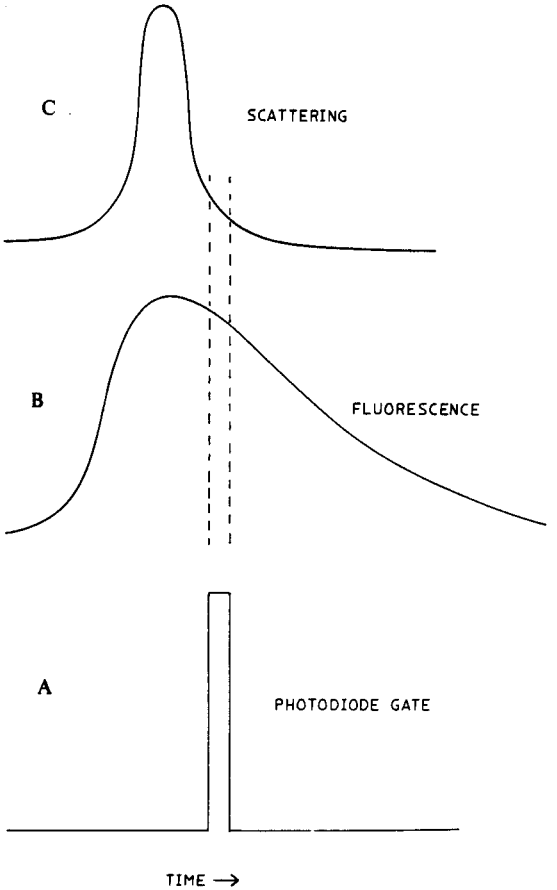

Fig. 1. Diagram showing ideal position of sampling gate (A) with respect to the fluorescence response (B) and impulse response (C) curves.

2.79 ns) and rose bengal (τ = 0.70 ns), each of which was prepared at a concentration of 1 μM (in ethanol) with a fixed amount of polystyrene scattering spheres (0.22 ± 0.006 μm diameter, Dow Chemical Co., Indianapolis, IN) added to the solution. Polystyrene sphere concentrations ranged from 0 to 40 μg ml^{-1} (6 solutions). Care was exercised in all measurements to ensure that the detected signal (fluorescence plus scatter) was within the linear range of the PMT response. Laser power was adjusted by using a variable neutral-density filter to give the maximum permissible signal (below PMT saturation) when the fluorophore sample contained the highest concentration of scattering spheres.

In the measurement of atomic fluorescence, sodium (τ = 0.72 ns) at a concentration of 10 μg/ml^{-1} (as NaCl solution) was mixed with four concentrations of aluminum chloride: 100, 500, 1000, and 5000 ppm. Each solution

was aspirated into a stoichiometric (F/O = 0.13) air—acetylene flame using a gas-dispersion-tube nebulizer. In the flame, aluminum is not significantly atomized, but is converted largely to desolvated particles which generate strong Mie scattering.

RESULTS AND DISCUSSION

The relationship between time delay and the ratio of fluorescence (S) to scatter (B) is shown in Fig. 2. The measured S/B ratio at zero-time delay is normalized to unity; all measurements at successive time delays are related to this value. For the rhodamine B solution with its relatively long lifetime (2.79 ns), a greater than six-fold increase in S/B is measured. However, for the shorter lifetime fluorophores rose bengal (0.70 ns) and sodium atoms (0.72 ns), the increase in S/B is not as great, but is still significant. Any such increase in S/B is valuable in that detection limits can be lowered and the precision of fluorescence measurements increased [2].

From the curves in Fig. 2, one can determine the optimum (best S/B) position of the optical delay line for the elimination of scatter. For rhodamine B, a delay of 3 ns was chosen, whereas for both rose bengal and sodium measurements a 1.6 ns delay was employed.

The degree to which scatter can be eliminated through time-resolution is revealed in Fig. 3, where the total measured signal (ostensibly from fluorescence alone) is plotted versus the concentration of scattering spheres. In conventional steady-state fluorimetry, the presence of a scattering substance in the fluorophore solution would cause erroneously high intensity levels (Fig. 3A). Of course, with a high-resolution spectrometer, little scattering would be detected directly and curve A would exhibit a lower slope. However, in the present measurement system, a broad-band (10 nm) interference filter was employed to effect the worst case.

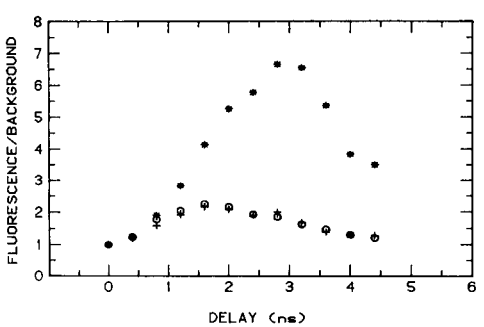

Fig. 2. Signal-to-background enhancement with time-delay sampling. (*) Rhodamine B, τ = 2.79 ns; (○) rose bengal, τ = 0.70 ns; (+) sodium, τ = 0.72 ns.

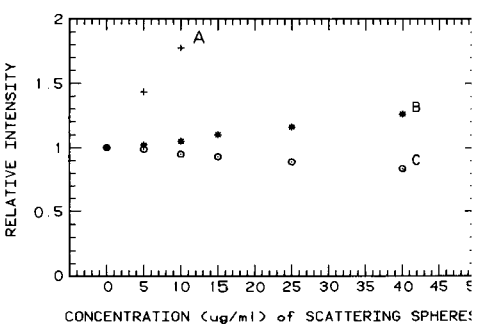

Fig. 3. Reduction of scatter by time resolution. A, rhodamine B (τ = 2.79 ns), delay line at 0.0 ns (conventional); B, rose bengal (τ = 0.70 ns), delay line at 1.6 ns; C, rhodamine B (τ = 2.79 ns), delay line at 3.0 ns.

The strong scatter/stray light signal in curve A is greatly reduced by measuring the fluorescence intensity at a finite delay after excitation (Fig. 3, B and C). As expected (cf., Fig. 2), the longer this delay time, the better the rejection of the scattering interference. The slight decrease in measured signal with scatterer concentration (cf., Fig. 3C) can be attributed to a reduction in source intensity in the observed sample volume caused by scattering-induced losses. This effect is similar to the inner-filter behavior [13] common in molecular fluorimetry. Specifically, as the concentration of scattering spheres is increased, the intensity of the exciting laser beam is attenuated by scattering losses as it traverses the sample cell. Concurrently, the fluorescence itself is scattered during its passage from the laser-beam location in the cell toward the detection system. For the relatively short lifetime of excited-state rose bengal in solution, the measured increase in relative fluorescence intensity results from an offset of this inner-filter effect by a relatively high scatter/stray signal. For this solution, the optical delay time (cf., Fig. 2) is so close to the scatter (instrument) response curve that a significant amount of scatter can still be detected. A longer delay time could be employed if further scattering reduction is necessary; however, a significant loss of fluorescence signal would result. It is expected that Fig. 3B would exhibit an even greater slope (more closely following the zero-time delay scatter, Fig. 3A) if inner-filter effects were absent.

Freedom from the effects of scattered radiation in sodium atomic fluorescence is displayed in curve B of Fig. 4, where a 1.6-ns time delay was employed between excitation and detection. In this experiment, added aluminum chloride increased the density of scattering sites in the flame, as seen in curve A. However, the use of time-delayed detection (curve B) eliminates most of the scattering error. There are at least three possible competing processes that affect the measured fluorescence signal in Fig. 3. These are the inner-filter effects from scattering by incompletely atomized aluminum particles, occlusion of the sodium by aluminum in solution, and detected scattered/stray light intensity. However, occlusion was found to be negligible in a separate experiment; equal emission intensity was measured for

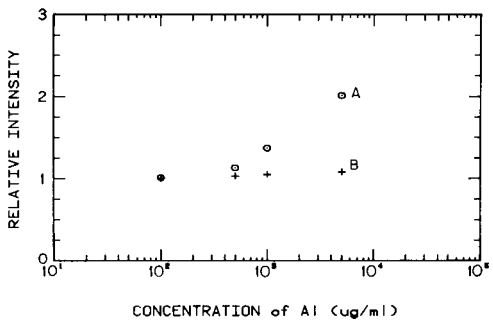

Fig. 4. Reduction of scattered radiation for sodium atomic fluorescence in an air—acetylene flame. A, conventional sampling, no time delay after excitation; B, sampling 1.6 ns after excitation.

sodium with 0 and 5000 ppm Al in solution. Similar to the rose bengal case (cf., Fig. 3), detection of scatter/stray light is expected at the 1.6-ns delay because the fluorescent decay overlaps the background (scatter) pulse.

This paper is taken in part from the doctoral thesis of R. E. Russo. The work was supported in part by the National Institutes of Health through grant PHS GM 24473, by the Office of Naval Research, and the National Science Foundation.

REFERENCES

1 P. L. Larkins and J. B. Willis, Spectrochim. Acta, 26B (1971) 491.
2 L. M. Fraser and J. D. Winefordner, Anal. Chem., 44 (1972) 8.
3 N. Omenetto, L. P. Hart and J. D. Winefordner, Appl. Spectrosc., 26 (1972) 612.
4 J. C. Van Loon, Anal. Chem., 52 (1980) 955A.
5 A. J. Pesce, C. G. Rosen and T. L. Pasby, Fluorescence Spectroscopy, M. Dekker, New York, 1971.
6 K. J. Doolan and L. E. Smythe, Spectrochim. Acta, 34B (1979) 187.
7 P. L. Larkins and J. B. Willis, Spectrochim. Acta, 29B (1974) 319.
8 M. S. Epstein, T. C. Rains and O. Menis, Can. J. Spectrosc., 20 (1975) 22.
9 J. P. S. Haarsma, J. Vlogtman and J. Agterdenbos, Spectrochim. Acta, 31B (1976) 129.
10 L. M. Fraser and J. D. Winefordner, Anal. Chem., 47 (1971) 1693.
11 L. M. Fraser and J. D. Winefordner, Anal. Chem., 44 (1972) 1444.
12 J. D. Winefordner, M. L. Parsons, J. M. Mansfield and W. J. McCarthy, Spectrochim. Acta, 23B (1967) 37.
13 D. R. DeOlivares, Ph.D. Thesis, Indiana University, 1976.
14 D. A. Goff and E. S. Yeung, Anal. Chem., 50 (1978) 625.
15 W. M. Fairbank, T. W. Hänsch and A. C. Schawlow, J. Opt. Soc. Am., 65 (1975) 199.
16 J. M. Telle and C. L. Tang, Appl. Phys. Lett., 15 (1974) 85.
17 G. D. Boutilier, J. D. Bradshaw, S. J. Weeks and J. D. Winefordner, Appl. Spectrosc., 31 (1977) 307.
18 J. M. Ramsey, G. M. Hieftje and G. R. Haugen, Appl. Opt., 18 (1979) 1913.
19 G. M. Hieftje and G. Horlick, Am. Lab., March (1981) 76.
20 G. M. Hieftje and G. R. Haugen, Anal. Chem., 53 (1981) 755A.
21 R. E. Russo and G. M. Hieftje, Appl. Spectrosc., June (1981), in press.

Analytica Chimica Acta, 134 (1982) 21—29
Elsevier Scientific Publishing Company, Amsterdam — Printed in The Netherlands

TIME DISCRIMINATION IN THE LASER FLUORIMETRY AND ULTRATRACE DETERMINATION OF EUROPIUM(III) AND SAMARIUM(III) WITH 4,4,4-TRIFLUORO-1-(2-THIENYL)-1,3-BUTANEDIONE

SUNAO YAMADA, KOJI KANO and TEIICHIRO OGAWA*
Department of Molecular Science and Technology, Kyushu University, Hakozaki, Fukuoka 812 (Japan)

(Received 1st July 1981)

SUMMARY

Efficient application of time discrimination has succeeded in substantial reduction of the detection limit of laser fluorimetry. A nitrogen laser and a pulse-gated photon counting method are combined. The detection limits for europium(III) and samarium(III) with 4,4,4-trifluoro-1-(2-thienyl)-1,3-butanedione in solution are 0.4 pg l^{-1} and 0.3 ng l^{-1}, respectively. The results are attributed to effective removal of the short-lived unwanted signals. This technique makes possible the ultratrace determination of a fluorescent molecule in a mixture with others by making the most of the difference of their emission lifetimes. The europium(III) complex can be determined with high selectivity and sensitivity in a large excess of the samarium(III) complex.

Direct identification and determination of chemical substances at an ultratrace level is of basic importance to environmental and health studies. Laser fluorimetry has greatly contributed to the ultratrace determination of fluorescent substances [1]. The pulsed nature of lasers has made the time-resolved fluorimetric technique possible. Pulsed laser excitation coupled with pulse-gated photon counting provides an extremely sensitive analytical tool, and has reduced detection limits substantially [2—4]; the detection limit of tris(4,4,4-trifluoro-1-(2-thienyl)-1,3-butanediono)europium(III), EuTTA, is 2 pg l^{-1} [4]. The time discrimination technique consisting of a pulsed laser and a gated detection system has also shown great efficiency in suppressing the fluorescence signals of coexisting compounds and impurities [3, 5].

The europium(III) and samarium(III) β-diketonates are strongly luminescent and their fluorimetric determinations have been widely studied by steady-state fluorimetry [6]. However, it is difficult to detect one component with high selectivity in a mixed sample of both complexes, because they have similar absorption spectra and their emission bands in the 500—700-nm region overlap [7].

Both europium(III) and samarium(III) β-diketonates have much longer emission lifetimes and larger Stokes shifts than those of organic molecules

0003-2670/82/0000-0000/$02.75

[7]. The successful utilization of these characteristics should increase the sensitivity and selectivity of their determinations.

In this paper, a simple and highly sensitive laser fluorimetric system is described, and the value of time discrimination for suppressing unwanted signals and decreasing the minimum detectable concentration is demonstrated. EuTTA can be determined in solution at the sub-pg l^{-1} level. Furthermore, a method for extremely selective determination of a trace amount of the europium complex in the samarium complex is discussed.

EXPERIMENTAL

Materials

Commercial $EuCl_3 \cdot 6H_2O$ (99.9%), $SmCl_3 \cdot 6H_2O$ (99.9%), and ethanol (analytical grade) from Kishida Chemicals, were used without further purification. 4,4,4-Trifluoro-1-(2-thienyl)-1,3-butanedione (HTTA) was obtained from Dojindo Laboratories.

The EuTTA complex [8] and the piperidinium salt of the octacoordinated Sm^{3+} complex, SmTTA [7], were prepared from the above chlorides by established procedures, and were identified by elemental analyses. No impurity was detected in the visible and ultraviolet spectra. An attempt was made to prepare the hexacoordinated samarium(III) complex from the corresponding piperidinium salt by heating in vacuo [7], but a pure product could not be obtained because of some thermal decomposition. The piperidinium salt, SmTTA, was therefore used as the sample for analysis.

Instrumentation

Basic components of the experimental apparatus for time-resolved spectrometry are a nitrogen laser as the excitation light source and a pulse-gated photon counter as the emission detecting equipment (Fig. 1). A Molectron UV12 nitrogen laser was operated at a repetition rate of 20 Hz with the use of a HP 214B pulse generator as an external trigger source. Its power and pulse width were nominally 2.5 mJ and 10 ns, respectively. Photoemission was focused onto the entrance slit of a JASCO CT-50 monochromator or onto an interference filter (for EuTTA: λ_{max} 614.5 nm, T_{max} 40.5%, $\Delta\lambda_{1/2}$ 15.5 nm; for SmTTA: λ_{max} 644.5 nm T_{max} 49.5%, $\Delta\lambda_{1/2}$ 15.5 nm). The photons were detected with a cooled photomultiplier (HTV R-649), and counted with a photon counter (NF PC-545A).

A typical sequence for the fluorimetric determination of EuTTA is illustrated in Fig. 2. On laser firing, a fluorescence signal appeared on the background signals. The background signals may consist of scattered light from the source radiation, electrical noise from the nitrogen laser, and source-independent backgrounds such as dark currents of the photomultiplier. The scattered light and electrical noise were effectively removed by a 2-μs delay of the sampling gate from the laser pulse. Both fluorescence and the other background signals were obtained at the sampling gate (1.5 ms); the latter

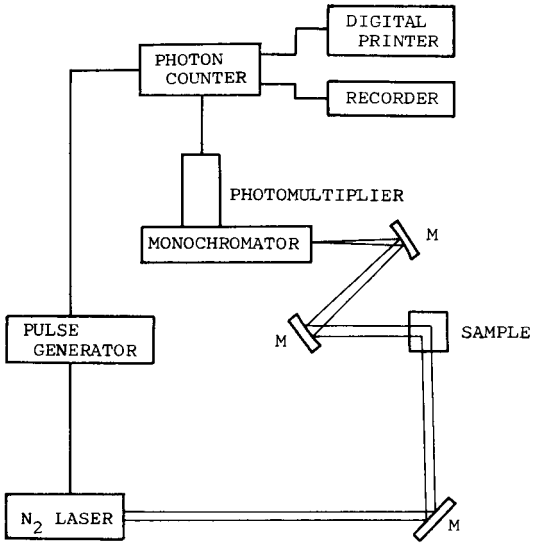

Fig. 1. Schematic diagram of the instrumentation.

was also obtained at the reference gate (1.5 ms), which was located 10 ms after the sampling gate. The fluorescence signal was selectively secured by taking the difference of signals at the two gates. The time delays of the sampling and reference gates were controlled by the pulse generator.

For SmTTA, 100 μs was chosen as the sampling gate time. The sampling and reference delay times were adjusted to 2 μs and 1 ms, respectively.

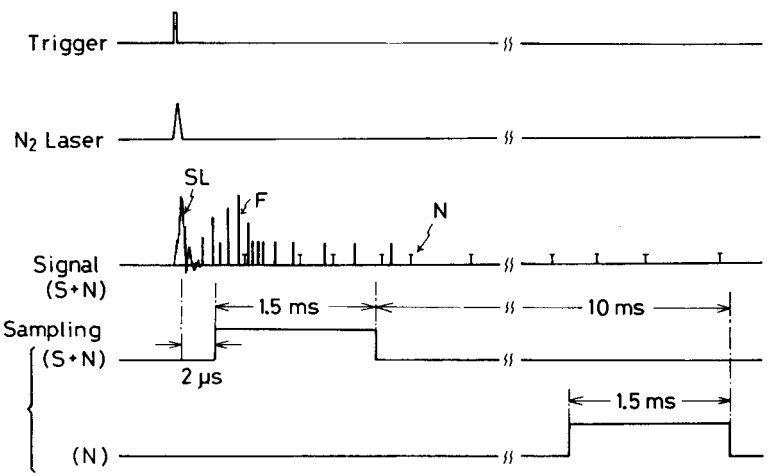

Fig. 2. Sequence for the time-resolved fluorimetric determination of EuTTA: F, fluorescence signal; N, noise; SL, scattered light and electrical noise.

Optical measurements

The absorption spectra were taken on a JASCO UVIDEC-505 spectrophotometer. The fluorescence spectra were measured with a Hitachi 650-10S spectrofluorimeter, using a Toshiba L-39 long-pass filter to cut off the scattered light of the source radiation. Stock solutions of 1.9×10^{-3} M EuTTA and 1.5×10^{-3} M SmTTA were used in all measurements. Stock solutions of HTTA containing an equimolar amount of piperidine (guaranteed reagent grade; Wako Pure Chemicals) were 10^{-3}—10^{-2} M. Diluted sample solutions were prepared from these stock solutions by successive dilutions.

The emission lifetimes of EuTTA and SmTTA were measured with sampling gate times of 100 and 10 μs, respectively. The sampling gates were delayed successively by 100 and 5 μs, respectively. The photons were counted over 100 laser pulses for each sampling delay time, and were plotted against the sampling delay time to obtain the emission lifetime.

In the case of time-resolved fluorimetry a Toshiba L-39 or O-55 long-pass filter was used to cut off the scattered light of the laser radiation. All sample solutions were deaerated by nitrogen gas (99.99%) before measurements. Time-resolved emission spectra covering the 600—660-nm region were obtained by integration over 200 laser pulses, and three runs measured under identical conditions were accumulated.

In the measurement of the analytical curves, an emission signal was counted over 100 laser pulses, and ten runs measured under identical conditions were accumulated. Three cells (A, B, C) were used in order to correct for variation in the laser power and the optical characteristics of the quartz cells. The signals for various concentrations of EuTTA from 0—2.5×10^{-14} M were measured in cell A, while the concentrations in cells B and C were constant, 1.3×10^{-14} M and 0 M, respectively. By reference to the signals of cells B and C, the ratio of emission signals was obtained. The detection limit is defined as the concentration giving $S/N = 2$.

In all measurements the standard quartz cell ($4 \times 1 \times 1$ cm^3) was used. The cell and glassware were thoroughly washed with fuming nitric acid and then water purified as described by Ishibashi et al. [9].

RESULTS

Steady-state fluorimetry

Absorption and emission spectra (excited at 337 nm) of EuTTA and SmTTA are shown in Fig. 3, and the corresponding spectral data are listed in Table 1. The wide absorption band in the 300—400-nm region is based on the π—π^* transitions of the ligand [6]. These complexes have several narrow emission bands arising from f^*—f transitions via intramolecular energy transfer processes [6]. The strongest emission bands are located at 614 nm for EuTTA and 644 nm for SmTTA. Therefore, it is preferable to establish the detection limits at these wavelengths.

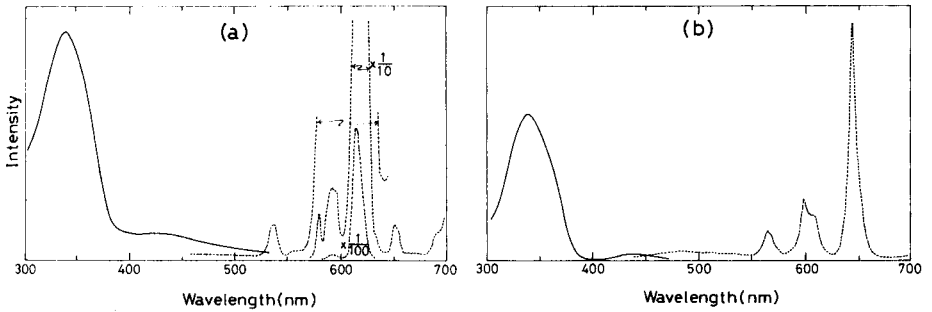

Fig. 3. Absorption (—) and emission (---) spectra of EuTTA (a) and SmTTA (b) in ethanol at room temperature.

The emission intensity of these complexes, however, tends to decrease with time, especially at lower concentrations. The intensity is restored immediately on addition of excess of ligand. This finding suggests that the coordinated ligands are dissociated at least partially in very dilute ethanolic solutions. Although no appreciable change in the emission spectrum of EuTTA (1.9×10^{-6} M) was observed on addition of an equimolar amount of ligand, the emission intensity of very dilute solutions was markedly dependent on the concentration of added ligand; it became constant when the concentration of ligand was in the 2×10^{-6}—1×10^{-5} M region. Thus, the spectra and the analytical curve for EuTTA were measured in the presence of excess of ligand (3×10^{-6} M). Alcohols appear not to be able to coordinate to EuTTA in carbon tetrachloride [10]. It can be concluded, therefore, that the most stable and dominant species present in the ethanolic solution containing excess of ligand is the hexacoordinated complex. Similar behavior of the emission spectra was observed for SmTTA.

The calibration graph for EuTTA was linear from 0 to 1×10^{-6} M and the detection limit with the use of the conventional spectrofluorimeter was 5×10^{-12} M (4 ng l^{-1}). The calibration graph for SmTTA in the presence of 1×10^{-5} M ligand was straight over a wide range (0—1×10^{-6} M) and the detection limit was 5×10^{-10} M (600 ng l^{-1}). Comparison of the results with literature values for other techniques is shown in Table 2.

TABLE 1

Spectroscopic data for EuTTA and SmTTA

Complex	Absorption maximum (nm)	Molar absorptivity (10^4 l mol^{-1} cm^{-1})	Emission maxima (nm)
EuTTA	339	8.2	540, 580, 593, 595, 614, 652, 690, 700
SmTTA	338	7.3	564, 567, 599, 608, 644, 707

TABLE 2

Detection limits for europium and samarium

Analytical method	Detection limit (ng l^{-1})		Ref.
	Europium	Samarium	
Flame atomic emission spectrometry	200	2×10^5	[11]
I.c.p. emission spectrometry	60	500	[12]
Fluorimetry			
Xe lamp—d.c. amplifier	4	600	This work
N_2 laser—pulse-gated photon counter	0.002	—	[4]
	0.0004	0.3	This work

Detection limits by the time-resolved photon counting method

The absorption spectra given in Fig. 3 show that a nitrogen laser is a very favourable excitation source for these complexes. The emission lifetime of EuTTA was found to be 420 μs in ethanol; thus, the sampling gate time was adjusted to 1.5 ms. The time-resolved emission spectrum of EuTTA could be measured with the present apparatus even at 5×10^{-15} M. For SmTTA, the sampling gate time was adjusted to 100 μs, because its emission lifetime was 21 μs in ethanol. The emission spectrum could be measured even at 1×10^{-12} M in a similar manner.

Stokes shifts of EuTTA and SmTTA in ethanol are more than 200 nm (Fig. 3 and Table 1). In such a case, an optical filter is preferable to a monochromator for ultratrace determinations [4, 9]. Accordingly, filters were used for establishing the detection limits.

In general, the fluctuation of fluorescence and background signals greatly affects the detection limit of such ultratrace methods. In the presence of a background signal, n_b (where n is the number of photoelectrons), the actual emission signal, n_f, can be obtained by subtracting n_b from the signal of the sample, n_s.

Then the S/N ratio is expressed [9] as $S/N = n_f/[\sigma^2_{n_s} + \sigma^2_{n_b}]^{1/2}$, where σ is the standard deviation. A typical calibration graph for EuTTA is shown in Fig. 4, together with the calculated line at which $S/N = 2$. The detection limit is the intersecting point of the two lines, and was evaluated as 5×10^{-16} M (0.4 pg l^{-1}); improvement of the apparatus reduced the detection limit compared with the previous result (2 pg l^{-1}) [4].

For SmTTA, the calibration graph was obtained in the 0—2.0×10^{-12} M region, and the detection limit was evaluated as 3×10^{-13} M (0.3 ng l^{-1}). These values are shown in Table 2.

Selective detection of each complex in the mixture

Although no impurity in SmTTA was detected by steady-state fluorimetry, time-resolved fluorimetry revealed that an extremely small amount of EuTTA was present in the sample solution of SmTTA. The time-resolved emission

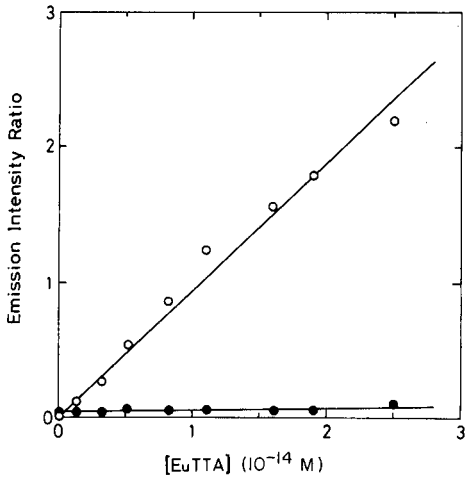

Fig. 4. The calibration graph for EuTTA: (○) observed value measured from the emission intensity ratio; (●) calculated value at which $S/N = 2$.

spectrum of 1×10^{-6} M SmTTA in ethanol was recorded in the 600—660-nm region (Fig. 5a). The sampling delay time was set to 150 μs so as to emphasize the signals of EuTTA if any. In addition to the signal of SmTTA around 640 nm, a weak emission signal appeared around 610 nm. Upon addition of 3.5×10^{-11} M EuTTA to this sample solution, the fluorescence intensity at 614 nm was markedly enhanced (Fig. 5b). These results suggest that the emission band at 614 nm is due to EuTTA. A calibration graph obtained by using a monochromator was satisfactorily linear for 0—3.5×10^{-11} M EuTTA in ethanolic 1×10^{-6} SmTTA solutions. The detection limit for

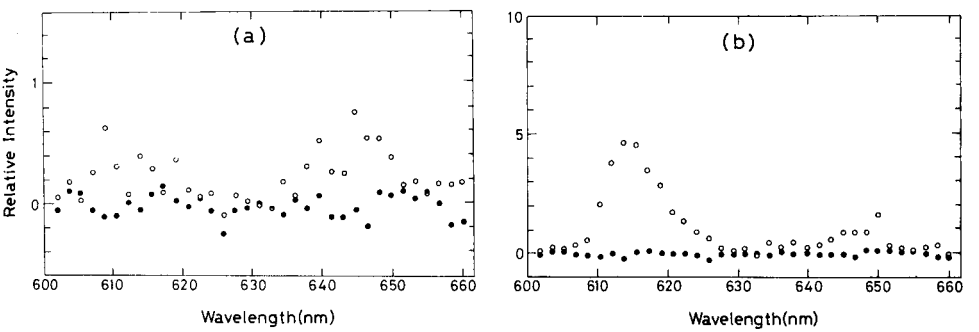

Fig. 5. Emission spectra of SmTTA and EuTTA by laser excitation in ethanol containing 1×10^{-5} M ligand at room temperature. Sampling gate time, 1.5 ms; sampling delay time, 0.15 ms; reference delay time, 10 ms. (a) Spectrum of SmTTA (1×10^{-6} M) (○) and background (●); (b) spectrum of a mixed solution of SmTTA (1×10^{-6} M) and EuTTA (3.5×10^{-11} M) (○) and background (●).

EuTTA in 1×10^{-6} SmTTA was 5×10^{-12} M (4 ng l^{-1}). The concentration of EuTTA present in the sample solution (Fig. 5a) was below the detection limit ($S/N = 2$). The above results show that EuTTA can be determined even in the presence of a 10^5-fold excess of SmTTA. The same measurements were examined for sample solutions containing 1.5×10^{-9} M SmTTA, and satisfactory reproducibility in the content of EuTTA was observed.

It is difficult, however, to detect a trace amount of SmTTA in a large excess of EuTTA by means of time-resolved fluorimetry, because the emission lifetime of SmTTA (21 μs) is much shorter than that of EuTTA (420 μs). Selective determination of SmTTA in the presence of excess of EuTTA can, however, be done by selecting an emission wavelength where the emission intensity of SmTTA is relatively strong compared with that of EuTTA. As Fig. 3 shows, 564 nm may be suitable for this purpose. The detection limits of EuTTA and SmTTA determined by steady-state fluorimetry were 12 and 5 μg l^{-1}, respectively, when the emissions from these complexes were monitored at 564 nm. When time-resolved fluorimetry was used with a monochromator and a sampling gate time of 100 μs, the detection limits were 4 μg l^{-1} for EuTTA and 0.2 μg l^{-1} for SmTTA. Most of the photons emitted from SmTTA can be counted within this sampling gate time, but only part of the photons from EuTTA can be counted. The ratios of the detection limit of SmTTA to that of EuTTA for steady-state and time-resolved fluorimetry were 0.4 and 0.05, respectively. Thus time-resolved fluorimetry is more sensitive for detecting residual SmTTA in EuTTA solution than steady-state fluorimetry.

DISCUSSION

Time-resolved fluorimetry is a highly sensitive and selective analytical method, because it can suppress not only dark noise but also unwanted signals by selecting an optimum sampling gate. The residual fluorescent organic molecules, Raman band of the solvent, and scattered light of the source radiation are major obstacles to ultratrace determinations of fluorescent organic molecules such as fluorescein [9] and pyrene [3], because these compounds have relatively short emission lifetimes compared with EuTTA and SmTTA. In the present study, these unwanted signals could be effectively removed by selecting the delay (2 μs) of the sampling gate from the laser pulse. Losses of the emission signals caused by the 2-μs delay are estimated to be only 0.5% for EuTTA and 9.1% for SmTTA.

Most organic molecules have fluorescence lifetimes of the order of nanoseconds. The time resolution of the instrument, therefore, should be about one nanosecond for successful application of time discrimination for ultratrace determinations of fluorescent organic molecules.

The detection limit of EuTTA in the present study is even lower than that of the previous report [4]. In the previous study, the nitrogen laser was laboratory-made and its electrical noise was much larger than that from the

Molectron nitrogen laser used now. The reduction of electrical noise provides the increase in the S/N ratio.

The extent of the reduction in the detection limit by altering the analytical means from steady-state fluorimetry to time-resolved fluorimetry is larger for EuTTA (at 614 nm) than for SmTTA (at 644 nm). This is attributed predominantly to the longer sampling gate time (1.5 ms) for EuTTA which must increase the S/N ratio.

Most (ca. 99%) of the emission signal of SmTTA in a mixture of both complexes is removed by the 150-μs delay of the sampling gate from the laser pulse, while ca. 70% of the emission signal must be detected for EuTTA. The intensity of the emission from EuTTA at 614 nm in ethanol is about 500-fold larger than that from the same concentration of SmTTA, so that EuTTA can be detected even in the presence of 10^4—10^5-fold amounts of SmTTA.

However, the selective detection of SmTTA in mixtures of SmTTA and EuTTA depends on the ratio of the fluorescence intensities of both complexes, because they are similarly excited by the nitrogen laser. The ratio of the detection limit for SmTTA to that for EuTTA at 564 nm is one order of magnitude smaller in time-resolved fluorimetry than in steady-state fluorimetry. Therefore, it can be said that time-resolved fluorimetry is also more selective for the determination of SmTTA in the presence of excess of EuTTA.

The present study confirms that time discrimination is very useful for the ultratrace determination of fluorescent compounds. This technique is especially successful with the combined use of a pulsed laser source and a pulse-gated photon counter, and for compounds having long emission lifetimes. Furthermore, a highly sensitive and selective detection of a compound in the presence of large amounts of others becomes possible by making the best use of the difference of their emission lifetimes.

This study was partly supported by a Grant-in-Aid for Special Project Research from the Ministry of Education.

REFERENCES

1 J. C. Wright and M. J. Wirth, Anal. Chem., 52 (1980) 988A.
2 K. Miyaishi, M. Kunitake, T. Imasaka, T. Ogawa and N. Ishibashi, Anal. Chim. Acta, 125 (1981) 161.
3 M. Kunitake, T. Imasaka and N. Ishibashi, Nippon Kagaku Kaishi, (1981) 55.
4 S. Yamada, F. Miyoshi, K. Kano and T. Ogawa, Anal. Chim. Acta, 127 (1981) 195.
5 J. H. Richardson, K. M. Larson, G. R. Haugen, D. C. Johnson and J. E. Clarkson, Anal. Chim. Acta, 116 (1980) 407.
6 See, e.g., H. G. Huang, K. Hiraki and Y. Nishikawa, Nippon Kagaku Kaishi, (1981) 66.
7 Y. Matsuda, S. Makishima and S. Shionoya, Bull. Chem. Soc. Jpn., 41 (1968) 1513; 42 (1969) 356, and references therein.
8 L. R. Melby, N. J. Rose, E. Abramson and J. C. Caris, J. Am. Chem. Soc., 86 (1964) 5117.
9 N. Ishibashi, T. Ogawa, T. Imasaka and M. Kunitake, Anal. Chem., 51 (1979) 2096.
10 H. G. Brittain, J. Chem. Soc. Dalton Trans., (1979) 1187.
11 H. Haraguchi, Kagaku No Ryoiki, 32 (1978) 313.
12 P. W. J. M. Boumans and R. M. Barnes, ICP Inf. Newsl., 3 (1978) 445.

Analytical Chimica Acta, 134 (1982) 31—38
Elsevier Scientific Publishing Company, Amsterdam — Printed in The Netherlands

FLUORESCENCE POLARIZATION STUDIES OF THE CONFORMATION OF SOIL FULVIC ACID

ANTHONY J. LAPEN and W. RUDOLF SEITZ*
Chemistry Department, University of New Hampshire, Durham, NH 03824 (U.S.A.)
(Received 20th January 1981)

SUMMARY

The conformation of soil fulvic acid was studied by fluorescence polarization as a function of pH, concentration, and ionic strength. Rotational relaxation times were measured from the slopes of plots of polarization vs. the ratio of temperature to viscosity. The rotational relaxation time did not change over the pH range 5—8 or over the concentration range 3.3×10^{-5}—3.3×10^{-4} M fulvic acid. This suggests that fulvic acid does not aggregate or change conformation. Changes in ionic strength also do not cause a measurable change in rotational relaxation time. A net rotational relaxation of 2.0 ns was calculated for fulvic acid. This value is based on a fluorescence lifetime of 2.1 ns which is the best single exponential fit to the observed fluorescence decay. A molecular weight of 2400 was calculated for fulvic acid assuming that fulvic acid is spherical. The discrepancy between this value and the true number-average molecular weight of 990 suggests that fulvic acid exists in a flat extended conformation.

The study of humic and fulvic acids is important because these materials interact not only with naturally occurring chemicals but also with chemicals introduced into the environment [1]. These interactions may be influenced by the macromolecular structure of the humic materials. The macromolecular structure of humic materials has been studied by a variety of methods including small angle x-ray scattering [2, 3], dialysis and ultrafiltration [4—10], and gel chromatography and viscosity measurements [11—12]. Although these studies generally report that the conformation and/or state of aggregation of fulvic acid varies with pH and concentration, the results are not consistent. Many of the methods require high concentrations which promote aggregation.

The work reported here was inspired by a study of copper complexation by fulvic acid which showed an increase in the number of binding sites for copper as pH increased from 4 to 6 [13]. This suggests a structural change that exposes more binding sites to metal ions at high pH.

Fluorescence polarization is an attractive method for studying the conformation of humic substances. Because fluorescence detection limits are low, it is possible to make measurements at naturally occurring concentration levels of fulvic acid. Because fulvic acid itself fluoresces, polarization measure-

ments are possible without requiring chemical modification. The fluorescence spectrum of fulvic acid is broad and featureless with a maximum between 390 and 540 nm [14]. Maximum emission shifts to longer wavelengths as the excitation wavelength is increased [15]. This is consistent with the fact that fulvic acid is an exceedingly complex mixture.

THEORY

Fluorescence polarization experiments are based on the measurement of the polarization of fluorescence emitted by a molecule which has been excited by a beam of plane polarized light. A molecule will absorb radiation and become excited only when its electronic transition vector is parallel with the plane of polarization of the excitation beam. When the excited chromophore relaxes to the ground state, the emitted photon is polarized in the plane of the transition moment vector for the emission process. The measured polarization, P, is defined as

$$P = (I_1 - I_2)/(I_1 + I_2) \tag{1}$$

where the measured intensities, I_1, and I_2, are the fluorescence intensities with emission polarizers orientated parallel to and perpendicular to the plane of polarization of the excitation beam, respectively. From theoretical considerations, the polarization can vary from $+1/2$ to $-1/3$ depending on the orientation of the transition moments for excitation and emission [16, 17].

In dilute solution, fluorescence is depolarized by rotation of the chromophore while in the excited state. This depolarization is affected by the size and shape of the molecule, the temperature and viscosity of the solution, and the fluorescence lifetime of the chromophore. These parameters are related for a rigid spherical molecule by the Perrin equation [18]

$$[1/P - 1/3] = [1/P_o - 1/3]\ [1 + (\tau\ R\ T/\eta\ V)] \tag{2}$$

where P_o is the intrinsic polarization of the molecule, τ is the fluorescence lifetime, R is the ideal gas constant, T is the temperature in K, η is the solution viscosity, and V is the partial molar volume of the molecule. A Perrin plot can be constructed by graphing $1/P$ vs. T/η. The intercept will be equal to $1/P_o$, and the slope will be proportional to the harmonic mean of the rotational relaxation time of the fluorophore [18].

EXPERIMENTAL

Instrumentation

The fluorescence polarization spectrophotometer is a two-detector instrument which has been described elsewhere [19]. The light source is a Sylvania 5000Q/CL 500-W tungsten—iodine lamp. The excitation wavelength is selected by an Aminco grating monochromator equipped with variable entrance and exit slits. The emission wavelength is selected by the use of

cutoff filters. Standard Type 1 Polaroid film polarizers are used for both the excitation and emission beams. The detectors are RCA 1P21 photomultiplier tubes mounted at right angles to the excitation beam. This arrangement allows the two signals, I_1 and I_2, to be measured simultaneously. The signals from the photomultiplier tubes are amplified by current to voltage operational amplifier circuits. The resulting signals are used to calculate the polarizations.

Reagents

Well-characterized soil fulvic acid was obtained from J. H. Weber. The material was prepared from the B_2 horizon of a podzol soil (Conway, NH, USA) [20]. A number average molecular weight of 990 was determined by cryoscopy [21]. Further characterization of the soil fulvic acid has been described elsewhere [13, 22].

Lifetime measurement

A 6.7×10^{-5} M solution of the fulvic acid at pH 6.0 was used for the fluorescence lifetime measurement. The time-correlated single photon method was used [23, 24]. A hydrogen flash lamp with a pulse width of 1.5 ns at half-maximum intensity operating at 10.37 kHz was used as the excitation source. Excitation wavelength was selected by a 350-nm wide-band filter and emission wavelength was selected by a Corning 420-nm cutoff glass filter. The fulvic acid count rate was 85 Hz and 93950 counts were made. Under the same experimental conditions, a water blank produced a count rate of 20 Hz. Experimental fluorescence decay curves were deconvoluted from the lamp pulse and then fitted to single and double exponential decay curves to obtain the lifetimes.

Procedure

The soil fulvic acid was dried at 100°C for 2 h prior to use. Solutions of 6.7×10^{-5} M fulvic acid were prepared in 0.10 M KNO_3. Potassium nitrate was employed to achieve the same medium as in the work of Bresnahan et al. [13] which initially inspired this study. The pH was adjusted with 0.010 M KOH in 0.10 M KNO_3. To obtain fluorescence polarization data, a cell filled with distilled water was placed in the cell compartment of the instrument and the amplifier offsets were adjusted to compensate for the photomultiplier dark currents of both channels. The sample was then placed in the cell compartment of the instrument with both emission polarizers oriented vertically. The gain of the I_1 channel was adjusted so that the outputs from both channels were equal. This compensates for any differences in the optical paths and photomultiplier tube responses. The I_2 polarizer was then rotated to the horizontal position and the fluorescent intensities I_1 and I_2 were measured. Data were collected by measuring the fluorescence intensities as the sample was heated from 15°C to 60°C. The excitation wavelength was 420 nm, and 475-nm cutoff filters were used for the emission. A microthermistor was inserted into the sample cell but out of the optical path to measure the temperature to ±0.1°C. Data were collected at pH 5.0, 6.0, 7.0, and 8.0.

Perrin plots were also obtained by varying the viscosity of the solutions. In this case, glycerin was added to produce solutions containing 10—50% (w/w) glycerin. This produced a change in viscosity of 1—10 centipoise. Polarization measurements were taken isothermally at 20°C. Because viscosity is a difficult parameter to measure accurately, the densities of the solutions were determined using a Westfall balance and the viscosity was obtained from standard tables.

As temperature increased, the observed fluorescence intensity decreased as expected. Higher temperatures typically cause an increase in the rate of internal conversion with a corresponding decrease in fluorescence efficiency and lifetime. Assuming that the intrinsic fluorescence lifetime is unaffected by temperature, then $\tau = \theta_f \tau_o$, where τ is the experimental lifetime, θ_f is the fluorescence quantum efficiency, and τ_o is the intrinsic fluorescence lifetime (observed only if there are no competing radiationless processes).

The values of P vs. temperature will be affected by changes in lifetime. This effect was corrected with the following relationship

$$I_f/I_{fr} = \theta_f/\theta_{fr} = \tau/\tau_r \qquad (3)$$

where τ is the lifetime and I_f is fluorescence intensity. The terms in the denominator with the subscript fr or r refer to pH 6 and 20°C, the reference point at which the experimental lifetime was determined. The fluorescence intensity I_f was calculated from the values of I_1 and I_2: $I_f = I_1 + 2I_2$. Equation (3) states that the relative intensities at two sets of temperatures and viscosities are a measure of the relative fluorescence efficiencies under these conditions. It follows from the equation $\tau = \theta_f \tau_o$ that the relative efficiencies are a measure of the relative fluorescence lifetimes. The values of T/η were accordingly multiplied by I_f/I_{fr} before plotting P vs. T/η (see Eqn. 2.).

A similar correction was applied for the Perrin plots obtained by varying viscosity. In this case, increasing viscosity caused an increase in fluorescence.

The experimental correction factors ranged from 0.78 to 1.05. It would, of course, be better to measure lifetime vs. temperature and viscosity directly but this was not practical because instrumentation for measuring fluorescence lifetimes is not available to us.

To investigate the effects of concentration and ionic strength, solutions of 3.3×10^{-5} M and 3.3×10^{-4} M soil fulvic acid were prepared in both distilled water and 1.0 M KNO_3, and adjusted to pH 6 with 0.01 M KOH. Perrin plots were then obtained by varying temperature.

RESULTS AND DISCUSSION

Lifetime measurement

The experimental fluorescence decay curve was fitted to a single exponential decay by a least-squares method. The best fit corresponded to a lifetime of 2.1 ns, but the fit was poor. The ratio of deviations to points was 0.20. The decay curve was also fitted to a double exponential decay. The lifetimes for

two components were calculated to be 1.0 ns and 6.0 ns. The ratio of the fluorescence intensities of the short-lifetime to the long-lifetime component is 4.8. The quality of the double exponential fit was considerably better than that for the single exponential. The ratio of the sum of squares of the deviations to the sum of the data points was 8.9×10^{-3}. In view of the known heterogeneity of fulvic acid [1], it is probable that the observed decay is actually the sum of many different decays. The fact that the double exponential fit is so good is not to be taken as an indication that fulvic acid has only two fluorescent components.

Perrin plots

The Perrin plots are presented in Figs. 1 and 2. The results of the linear regressions for the individual runs are summarized in Table 1. The harmonic mean of the rotational relaxation time, ρ_h, was calculated from the equation below which is a more general version of Eqn. (2) in that it applies to non-spherical molecules [17]

$$[1/P - 1/3] = [1/P_o - 1/3]\ [1 + 3\tau/\rho_h] \quad (4)$$

This calculation produced a rotational relaxation time of 2.0 ns at pH 8 and 25°C. There is no significant difference in the slopes of the lines in the Perrin plots obtained by varying temperature. This suggests that there is no pH-dependent conformational change in the pH 5—8 range. The data obtained by varying temperature at pH 5 through 8 were then pooled and a least-squares fit of $1/P = (a \pm s_a)\ T/\eta \pm b \pm s_b$ was calculated, with a and b the slope and intercept, and s_a and s_b, the standard deviations of the slope and

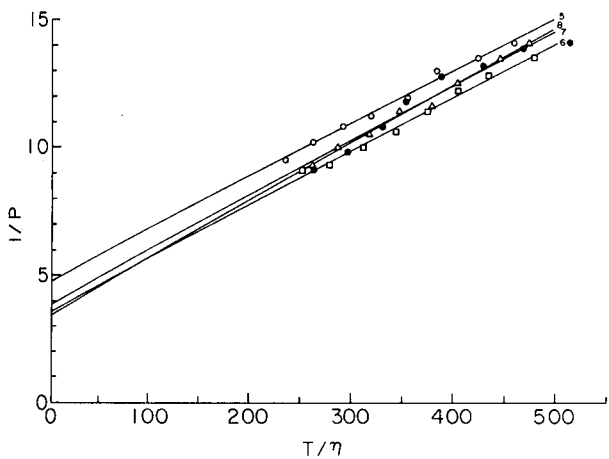

Fig. 1. Fluorescence polarization Perrin plots for 6.7×10^{-5} M fulvic acid produced by varying the temperature: (○) pH 5; (□) pH 6; (△) pH 7; (●) pH 8. The least-squares fit for the pooled data is $1/P = (0.0207 \pm 0.0011)\ T/\eta + 4.12 \pm 0.08$ with $s_{yx} = 0.465$. The x-axis units are K/centipoise.

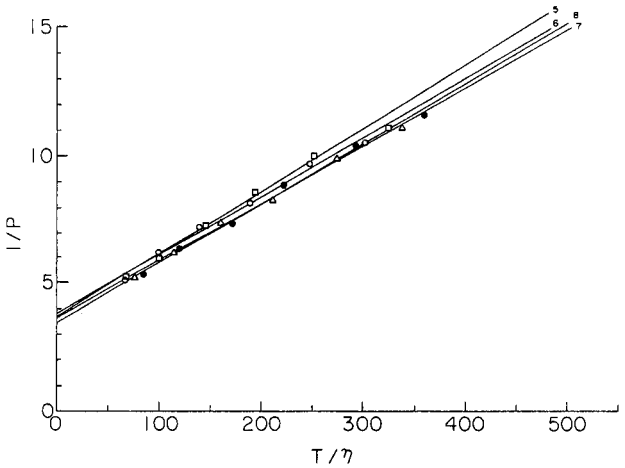

Fig. 2. Perrin plots for 6.7×10^{-5} M fulvic acid produced by varying the viscosity of the solutions: (○) pH 5; (□) pH 6; (△) pH 7; (●) pH 8. The least-squares fit for the pooled data is $1/P = (0.0228 \pm 0.00057)\ T/\eta + 3.70 \pm 0.05$ with $s_{yx} = 0.251$. The x-axis units are K/centipoise.

intercept, respectively. Similarly, the data obtained by varying viscosity at pH 5—8 were pooled. The difference between the pooled slopes of the temperature and viscosity data was statistically significant. This happens because the viscosity data were taken at lower values of T/η. Perrin plots are

TABLE 1

Summary of linear regression data

pH	Slope	Std. dev. slope	Intercept	Std. dev. intercept	Standard error
5[a]	0.0206	8.15×10^{-4}	4.71	0.0602	0.170
6[a]	0.0207	7.36×10^{-4}	3.65	0.0207	0.152
7[a]	0.0224	8.38×10^{-4}	3.41	0.0588	0.166
8[a]	0.0212	2.19×10^{-3}	3.86	0.1740	0.492
5[b]	0.0229	1.13×10^{-3}	3.82	0.0927	0.227
6[b]	0.0245	9.29×10^{-3}	3.66	0.0824	0.202
7[b]	0.0227	4.59×10^{-3}	3.54	0.0415	0.102
8[b]	0.0232	8.44×10^{-4}	3.47	0.0803	0.197
6[c]	0.0228	1.61×10^{-3}	3.38	0.0849	0.190
6[d]	0.0261	1.98×10^{-3}	3.09	0.0660	0.175
6[e]	0.0277	5.30×10^{-3}	3.16	0.0205	0.579
6[f]	0.0234	2.05×10^{-3}	2.99	0.0850	0.241

[a]Temperature varied between 15°C and 60°C; 6.7×10^{-5} M fulvic acid. [b]Viscosity varied by adding 10—50% glycerin; 6.7×10^{-5} M fulvic acid. [c]3.3×10^{-5} M fulvic acid, $\mu = 0.002$. [d]3.3×10^{-4} M fulvic acid, $\mu = 0.003$. [e]3.3×10^{-5} M fulvic acid, $\mu = 1.0$. [f]3.3×10^{-4} M fulvic acid, $\mu = 1.0$.

expected to have a negative curvature when the fluorescence lifetimes and/or rotational relaxation times differ among different components of the sample [17]. This is what is observed, with the viscosity data showing the larger slope. The agreement between the temperature and viscosity data also shows that thermally activated denaturation or chromophore rotations do not occur.

This failure to observe a conformational change between pH 5 and 8 is not inconsistent with the observed change in the number of metal binding sites because it has been shown that metal ions induce conformational changes which can account for the variation in binding [25]. Perrin plots obtained for 3.3×10^{-5} and 3.3×10^{-3} M fulvic acid at ionic strengths of 0.002 and 1.0 produced the pooled least-squares line $a = 0.0225$, $b = 4.08$, with $s_a = 0.00341$, $s_b = 0.145$, and $s_{yx} = 0.759$. These data are not significantly different from the data for 6.7×10^{-5} M fulvic acid. It was more difficult to obtain these measurements because fluorescence intensities were lower. At the high concentration of fulvic acid, there was a significant inner filter effect.

For a rigid, spherical molecule with uniformly distributed chromophores, a molecular weight can be calculated [16] from the rotational relaxation time by the equation $\rho = \text{m.w.}/1.23 \times 10^3$. This equation assumes that the molecular density is 0.8 g ml^{-1}, an average value for proteins, and that the chromophores are tightly bound and do not move independently of the molecule. The difference between the real molecular weight and the calculated molecular weight can be taken as a measure of the departure of the molecule from sphericity. A molecular weight of 2.4×10^3 was calculated for fulvic acid assuming that it is a sphere and its molecular density equals that of proteins. Even allowing for uncertainties in the calculations, the molecular weight is unquestionably much larger than that determined for the same material by cryoscopy. This suggests that fulvic acid exists in a flat extended conformation. If the conformation of fulvic acid were cylindrical or rodlike, then one would expect a much shorter rotational relaxation time.

The high calculated molecular weight could be interpreted as evidence for aggregation. We do not believe this is the case because the fluorescence polarization measurements were made at lower concentration than those used in determining the molecular weight. Also a change in rotational relaxation time with concentration would be expected if aggregation occurs because higher concentration will tend to favor aggregation equilibria.

Conclusions

It is shown that fluorescence polarization can be used to study conformation/aggregation of fulvic acid. It has been possible to study conformation at significantly lower concentrations than are possible by most other techniques. Measurements at fulvic acid levels below 3.3×10^{-5} M are possible, particularly if the sample can be excited in the ultraviolet region where the fulvic acid absorbs more strongly. Unfortunately, the instrument used did not have this capability, because neither the tungsten—iodine source nor the Polaroid film polarizers are suitable for ultraviolet radiation. Measure-

ments above pH 8 and below pH 5 are also possible. However, protonation or deprotonation may change the fluorescence lifetime of the fulvic acid. In order to establish reliably the rotational relaxation times in these ranges, one should measure the fluorescence lifetimes at these pH values because they may differ from the fluorescence lifetime at pH 6.

In applying fluorescence polarization to humic materials, it should be kept in mind that these materials are exceedingly complex mixtures. Because of this, the structures of the fluorophores in humic and fulvic acids are not known nor is it known what fraction of the material actually fluoresces. Because fluorescence methods respond only to the fluorescent component of humic substances, it is possible that measured characteristics of humic substances based on fluorescence may not accurately reflect the overall characteristics. The application of fluorescence methods to humic materials is discussed elsewhere [26].

We thank Dr. James H. Weber who generously contributed the fulvic acid and Dr. Charles Braun who determined the fluorescence lifetimes.

REFERENCES

1 M. Schnitzer and S. Khan, Humic Substances in the Environment, M. Dekker, New York, 1972.
2 R. L. Wershaw, P. J. Burcar, C. L. Suluta and B. J. Wiginton, Science, 157 (1967) 1429.
3 R. L. Wershaw, S. L. Heller and D. J. Pinckney, Adv. X-Ray Anal., 13 (1970) 609.
4 N. Ogura, Mar. Biol., 24 (1974) 305.
5 J. E. Schindler and J. J. Alberts, Arch. Hydrobiol., 74 (1974) 429.
6 R. Smith, Anal. Chem., 48 (1976) 74.
7 E. T. Gjessing, Schweiz. Z. Hydrol., 33 (1971) 592.
8 A. Wilander, Schweiz. Z. Hydrol., 34 (1972) 190.
9 J. C. T. Kwak and W. R. P. Nelson, Geochim. Cosmochim. Acta, 41 (1977) 993.
10 E. T. Gjessing, Environ. Sci. Technol., 4 (1970) 437.
11 J. H. Reuter, Geological Society of America, Abstracts, Vol. 9, 1977.
12 M. Schnitzer and S. I. M. Skinner, Isotopes and Radiation in Soil Organic Matter Studies, International Atomic Energy Agency, Vienna, 1968, p. 41.
13 W. T. Bresnahan, C. L. Grant and J. H. Weber, Anal. Chem., 50 (1978) 1675.
14 B. K. Seal, K. B. Roy and S. K. Mukherjee, J. Indian Chem. Soc., 41 (1964) 212.
15 M. Levesque, Soil Sci., 113 (1972) 346.
16 G. Weber, in D. M. Hercules (Ed.), Fluorescence and Phosphorescence Analysis, Interscience, New York, 1966, p. 217f.
17 G. Weber, Biochem. J., 51 (1952) 145.
18 F. Perrin, J. Phys. Radium, 7 (1926) 390; Ann. Phys. (Paris), 12 (1929) 169.
19 P. M. Roemelt, A. J. Lapen and W. R. Seitz, Anal. Chem., 52 (1980) 796.
20 J. H. Weber and S. A. Wilson, Water Res., 9 (1975) 1079.
21 J. H. Weber, personal communication, 1981.
22 S. A. Wilson and J. H. Weber, Anal. Lett., 10 (1977) 75.
23 L. M. Bollinger and G. E. Thomas, Rev. Sci. Instrum., 32 (1961) 1044.
24 L. J. Cline Love and L. A. Shaver, Anal. Chem., 48 (1976) 364A.
25 R. A. Saar and J. H. Weber, Environ. Sci. Technol., 14 (1980) 877.
26 W. R. Seitz, Trends in Analytical Chemistry, in press.

Analytica Chimica Acta, 134 (1982) 39—45
Elsevier Scientific Publishing Company, Amsterdam — Printed in The Netherlands

FLUORIMETRIC DETERMINATION OF AROMATIC ALDEHYDES WITH 4,5-DIMETHOXY-1,2-DIAMINOBENZENE

MASARU NAKAMURA, MITSUKO TODA and HIROKO SAITO

Faculty of Pharmaceutical Sciences, Fukuoka University, 11 Nanakuma, Nishi-ku, Fukuoka 814-01 (Japan)

YOSUKE OHKURA*

Faculty of Pharmaceutical Sciences, Kyushu University 62, Maidashi, Higashi-ku, Fukuoka 812 (Japan)

(Received 3rd August 1981)

SUMMARY

A sensitive fluorimetric method for the determination of aromatic aldehydes is described based on their reaction in dilute acid with 4,5-dimethoxy-1,2-diaminobenzene to give a compound which fluoresces intensely in alkaline solution. The fluorescence is stabilized by β-mercaptoethanol. The method is simple, selective for aromatic and arylaliphatic aldehydes, and sensitive; almost all the aldehydes can be determined at concentrations of 10^{-8}—10^{-7} M.

Many fluorimetric methods have been developed for the determination of aliphatic aldehydes. These include determinations of formaldehyde with acetylacetone and ammonia [1], J-acid [2], and dimedone [3], of acetaldehyde with *o*-phenylphenol [4], of acrolein with 1,3-diaminobenzene [5], of malonaldehyde with 4,4′-sulfonyldianiline, 4-aminobenzoic acid or its ethyl ester and 4-aminoacetophenone [6], of succindialdehyde with 1,2-diaminobenzene [7], of succinsemialdehyde with 3,5-diaminobenzoic acid [8], and of formaldehyde, acetaldehyde, propionaldehyde and butyraldehyde with 1,3-cyclohexanedione [9]. For the determination of aromatic aldehydes, however, only a few methods, based on reactions in acidic media with 2-aminothiophenol [10], 1,2-diaminonaphthalene [11], 2,2′-dithiobis-(1-aminonaphthalene) [12], and 1,2-diaminobenzene [13], have been proposed. Dansylhydrazine (1-dimethylaminonaphthalene-5-sulfonylhydrazine) [14], mansylhydrazine (*N*-methyl-2-anilino-6-naphthalenesulfonylhydrazine) [15], and 2-diphenylacetyl-1,3-indanedione-1-hydrazone [16] have also been utilized for the determination of carbonyl compounds. The photometric determination of aldehydes, including the use of the intrinsic fluorescence of aromatic aldehydes, has been reviewed by Sawicki and Sawicki [17].

It is shown in this paper that 4,5-dimethoxy-1,2-diaminobenzene reacts selectively in an acidic medium with aromatic aldehydes even at moderate temperatures, to give a compound which fluoresces intensely in alkaline

solution; the fluorescence is stabilized by β-mercaptoethanol. Benzaldehyde was employed as a model compound to establish suitable reaction conditions for a more general analytical method.

EXPERIMENTAL

Reagents and solutions

All chemicals were of analytical-reagent grade, unless otherwise specified. Double-distilled water was used throughout. Melting points were uncorrected.

4,5-Dimethoxy-1,2-diaminobenzene monohydrochloride. The reagent was synthesized from 4,5-dinitroveratrole [18] as follows. 4,5-Dinitroveratrole (5 g) was dissolved in 200 ml of benzene and 100 g of iron powder (60 mesh; Wako, Osaka, Japan) mixed with 20 ml of concentrated hydrochloric acid was added in small portions over 1 h under reflux. The mixture was then refluxed for 4 h, mixed with 10 ml of water and further refluxed for 2 h. After cooling, the mixture was made alkaline with 2.5 M sodium hydroxide and extracted several times with 200-ml portions of benzene. The extracts were combined and the solvent removed. The product 4,5-dimethoxy-1,2-diaminobenzene [19, 20] (m.p. 131°C; yield ca. 3 g) was mixed with ca. 10 ml of concentrated hydrochloric acid and the resulting salt was recrystallized from ethanol to yield very slightly pink needles of the monohydrochloride [19] (m.p. 240°C, decomp.; yield ca. 3 g). The reagent was stable for at least a year in a desiccator.

For the reagent solution (1.0 mM), the hydrochloride (204 mg) was dissolved in 10.0 ml of 4.0 M hydrochloric acid and diluted with water to 1 l. The solution was used within 3 h.

4,5-Dimethoxy-1,2-diaminobenzene sulfate. 4,5-Dimethoxy-1,2-diaminobenzene (2 g) was dissolved in 20 ml of ethanol and mixed with ca. 2 ml of concentrated sulfuric acid. The product was recrystallized from ethanol to almost colorless needles (m.p. 244°C, decomp.; yield ca. 2 g). Calculated for $C_8H_{14}O_6N_2S$: 36.1% C, 5.3% H, 10.5% N; found 35.85% C, 5.6% H, 10.4% N.

Aldehydes. Commercial aldehydes were purified just before use by distillation or recrystallization. Solutions were prepared in boiled water to minimize oxidation.

Procedures

Uncorrected fluorescence spectra and intensities were measured with a Hitachi MPF-2A spectrofluorimeter in 10 × 10 mm quartz cells; spectral bandwidths of 10 nm were used in both the excitation and emission monochromators.

To prepare fluorescent derivatives, aqueous test solutions (1.0 ml) and 2.0 ml of the 4,5-dimethoxy-1,2-diaminobenzene monohydrochloride solution were incubated in a glass-stoppered test tube at 37°C for 50 min, and 0.5 ml each of 0.8 M sodium hydroxide solution and 0.2 M β-mercaptoethanol solution were added. A reagent blank was prepared by treating 1.0 ml of water in the same manner. The fluorescence intensities of the test sample and blank were measured at the emission maximum wavelength with irradia-

tion at the excitation maximum (see Table 1). The concentration of aldehyde was read from a calibration curve prepared in the usual manner.

RESULTS AND DISCUSSION

Determination of benzaldehyde

The excitation and emission maxima for the product from benzaldehyde occurred at 338 and 402 nm, respectively (Fig. 1). On irradiation at 338 nm, the reagent blank fluoresced weakly (Fig. 1); the intensity was 5% of that given by 2×10^{-6} M benzaldehyde. Raman scattering of the solvent water was not observed under the recommended conditions. The background fluorescence may have been due to aldehydic contaminants. The 4,5-dimethoxy-1,2-diaminobenzene monohydrochloride (DDB·HCl) reacted with benzaldehyde in hydrochloric or sulfuric acid but not in alkaline and neutral solutions; dilute hydrochloric acid was used in the procedure. The concentration of the acid affected the fluorescence development (Fig. 2); acid concentrations of 25—50 mM gave maximum intensities and 40 mM was selected as optimum. Dilute sulfuric acid yielded a maximum fluorescence intensity (at 0.36 M) only 60% of that in dilute hydrochloric acid. The reason for this is unknown. The concentration of DDB·HCl also affected the fluorescence development (Fig. 3), a 1.0 mM solution giving the maximum intensity. DDB sulfate (0.75 mM) dissolved in 0.11 M hydrochloric acid gave a maximum intensity 75% of that given by the monohydrochloride solution.

The fluorescence reaction occurred even at 0° C; at higher temperatures, the fluorescence developed more rapidly, but heating at higher than 50° C for more than 10—20 min caused a decrease in its intensity (Fig. 4). At 37° C, which was selected for convenience, the fluorescence intensity reached a maximum after 45—60 min and then decreased slightly (Fig. 4); incubation for 50 min was chosen for the final procedure. Reaction at 80° C for 20 min

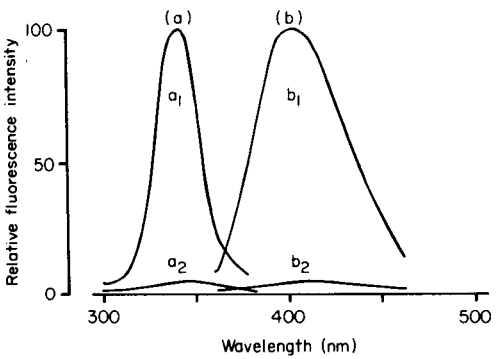

Fig. 1. Excitation (a) and emission (b) spectra of the reaction mixture of 2×10^{-6} M benzaldehyde (a_1, b_1) and the reagent blank (a_2, b_2).

TABLE 1

Excitation and emission maxima and limits of detection (LD) for fluorescent aldehyde derivatives

Aldehyde[a]	λ_{ex} (nm)	λ_{em} (nm)	LD[b] (M)	Aldehyde[a]	λ_{ex} (nm)	λ_{em} (nm)	LD[b] (M)
Benzaldehyde	338	402	1×10^{-7}	4-Chlorobenzaldehyde	340	424	2×10^{-7}
3-Tolualdehyde	334	420	1×10^{-7}	4-Dimethylaminobenzaldehyde	346	396	8×10^{-8}
2-Hydroxybenzaldehyde	358	406	2×10^{-7}	Vanillin	348	400	2×10^{-7}
3-Hydroxybenzaldehyde	342	394	4×10^{-7}	o-Vanillin	358	422	3×10^{-7}
4-Hydroxybenzaldehyde	342	386	2×10^{-7}	Piperonal	344	402	5×10^{-7}
2,4-Dihydroxybenzaldehyde	364	400	8×10^{-7}	2-Naphthaldehyde	348	466	6×10^{-7}
3,4-Dihydroxybenzaldehyde	348	402	3×10^{-7}	*o*-Phthalaldehyde	342	395	2×10^{-7}
2-Methoxybenzaldehyde	340	400	1×10^{-7}	Terephthalaldehyde	376	506	2×10^{-8}
3-Methoxybenzaldehyde	342	406	1×10^{-7}	Furfural	340	374	1×10^{-7}
4-Methoxybenzaldehyde	342	394	3×10^{-7}	Phenylacetaldehyde	348	400	4×10^{-7}
2,3-Dimethoxybenzaldehyde	338	398	2×10^{-7}	Cinnamaldehyde	364	478	1×10^{-7}
3,4-Dimethoxybenzaldehyde	346	400	2×10^{-7}	4-Dimethylaminocinnamaldehyde	346	400	3×10^{-6}
2-Chlorobenzaldehyde	328	428	2×10^{-7}				

[a]Portions (1.0 ml) of 1×10^{-6} or 5×10^{-6} M aldehyde solution were used. [b]The concentration giving a fluorescence intensity twice the blank.

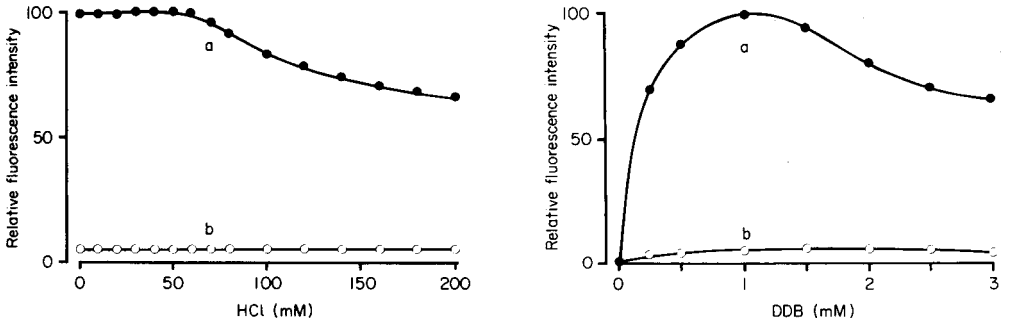

Fig. 2. Effect of the concentration of hydrochloric acid on the fluorescence. Benzaldehyde 2×10^{-6} M was treated with DDB·HCl dissolved in various hydrochloric acid concentrations: (a) benzaldehyde; (b) reagent blank.

Fig. 3. Effect of the concentration of DDB·HCl on the fluorescence. Benzaldehyde solution (2×10^{-6}M) was treated with various concentrations of DDB·HCl solutions: (a) benzaldehyde; (b) reagent blank.

could be used to save time, but the maximum fluorescence intensity was then only 95% of that obtained under the recommended conditions.

The reaction mixture fluoresced intensely only in alkaline solution and a maximum, constant signal obtained when the mixture was made more than ca. 0.05 M in sodium hydroxide. β-Mercaptoethanol stabilized the fluorescence in the final solution. In its absence, the signal decreased by ca. 30% h^{-1} in daylight at room temperature, and by ca. 20% h^{-1} in the dark. The addition of β-mercaptoethanol at concentrations exceeding 0.17 M prevented this; a 0.2 M solution was used in the procedure. The fluorescence developed under the prescribed conditions did not change on irradiation for 5 min at the excitation maximum of 338 nm, and was stable for at least 30 min in daylight and for

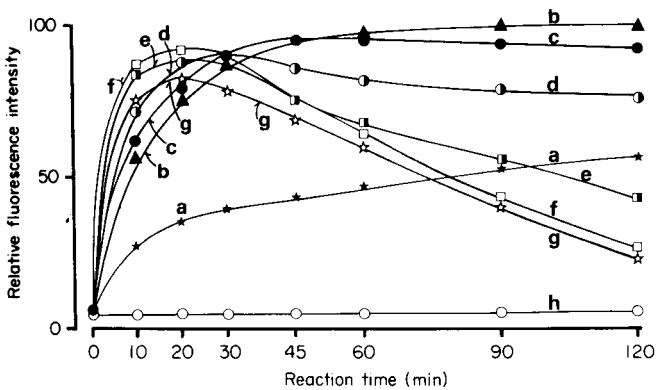

Fig. 4. Effects of reaction temperature and time. Benzaldehyde (2×10^{-6} M) solutions were treated for various times at different temperatures: (a) 0; (b) 23; (c) 37; (d) 50; (e) 70; (f) 80; (g) 100° C. Curve (h) is the reagent blank corresponding to a–g.

at least 2 h in the dark at room temperature. At β-mercaptoethanol concentrations of 0.3 M or greater, however, the fluorescence intensity was less than 70% of that obtained under the recommended conditions, and the intensity of the blank more than doubled.

The calibration graph for benzaldehyde was linear up to 5×10^{-5} M. The precision was established by performing 20 determinations on a 1×10^{-6} M benzaldehyde solution; the coefficient of variation was 1.7%.

Fluorescence from other aldehydes

Many aromatic aldehydes fluoresced under the conditions recommended. The excitation and emission maxima, and the limits of detection are shown in Table 1. The excitation and emission maximum wavelengths were not entirely characteristic of individual aldehydes, and substituent effects on the wavelengths and intensities of the fluorescence were not found. The limits of detection for most aldehydes were in the range 10^{-8}—10^{-7} M. The methods based on 2-aminothiophenol [10], 1,2-diaminonaphthalene [11], 2,2′-dithiobis-(1-aminonaphthalene) [12], and 1,2-diaminobenzene [13] gave similar results. However, some aromatic aldehydes did not fluoresce appreciably, even at a concentration of 1×10^{-5} M; when the present procedure was used, there was little or no reaction from 2,5-dihydroxybenzaldehyde, 3-nitro- and 4-nitrobenzaldehydes, 2-hydroxy-1-naphthaldehyde and terephthalaldehydic acid. Isovanillin gave a weak fluorescence; the intensity of a 1×10^{-5} M solution was only twice the blank value. Hydroxybenzaldehydes and 2-naphthaldehyde have been reported to fluoresce in water [17], but fluorescence was not observed in 1×10^{-6} M aqueous solutions in the present study.

Arylaliphatic aldehydes (e.g., phenylacetaldehyde and cinnamaldehydes) fluoresced under the conditions recommended, but aliphatic aldehydes (e.g., formaldehyde, acetaldehyde, propionaldehyde, isovaleraldehyde, *n*-butyraldehyde and crotonaldehyde) did not.

Reaction of other substances

Pyruvic and 2-oxoglutaric acids gave very weak responses with the reagent at a concentration of 1×10^{-5} M; the intensity was lower than that of 3×10^{-7} M benzaldehyde. All other substances examined did not fluoresce, even at concentrations of 1×10^{-5} M: D-glucose, D-fructose, D-xylose, D-glucuronolactone, D-galacturonic acid, L-ascorbic acid, methanol, ethanol, benzyl alcohol, formic acid, levulinic acid, 3-nitroaniline, 4-toluidine, acetone, acetylacetone, 1,4-benzoquinone, 3-nitrobenzenesulfonic acid, 2-chlorophenol, 3-nitrophenol, 2-aminothiophenol, glycine, 17 different L-α-amino acids, glutamine, glutathione, citrulline, creatine, creatinine, urea, allantoin, putrescine, dopa, tyramine, octopamine, thiamine hydrochloride, nicotinamide, cholesterol, dehydroepiandrosterone and cortisone. This suggests that the proposed method is very selective for aromatic and arylaliphatic aldehydes.

Studies on the mechanism of the fluorescence reaction are in progress. The reaction between 1,2-diamino-naphthalene and aldehyde gives a fluores-

cent naphthimidazole derivative [11] so that the reaction proposed here probably yields benzimidazole derivatives. The β-mercaptoethanol seems to protect the fluorescent product from oxidation by air.

The reported method with 2-aminothiophenol [10] is troublesome to carry out, and the method with 1,2-diaminonaphthalene [11] requires a carcinogenic reagent. The method with 1,2-diaminobenzene [13] cannot be applied to aqueous samples. The present method is as selective for aromatic aldehydes as the method with 2,2′-dithiobis-(1-aminonaphthalene) [12], more selective than the method with 1,2-diaminonaphthalene [11], and much more selective than the methods with dansylhydrazine [14] and mansylhydrazine [15]. It is sensitive, and should be useful for the determination of traces of aromatic aldehydes in complex samples.

REFERENCES

1 S. Belman, Anal. Chim. Acta, 29 (1963) 120.
2 E. Sawicki, T. W. Stanley and J. D. Pfaff, Anal. Chim. Acta, 28 (1963) 156.
3 E. Sawicki and R. A. Carnes, Mikrochim. Acta, (1968) 148.
4 Y. Asabe, S. Kojima, M. Suzuki and S. Takitani, Anal. Biochem., 79 (1977) 73.
5 S. A. Ipatova and E. V. Deyanova, USSR Patent 375,532; Chem. Abstr., 79 (1973) 38336h.
6 E. Sawicki, T. W. Stanley and H. Johnson, Anal. Chem., 35 (1963) 199.
7 E. Sawicki, J. D. Pfaff and R. A. Taft, Chemist—Analyst, 55 (1966) 6.
8 R. A. Salvador and R. W. Albers, J. Biol. Chem., 234 (1959) 922.
9 M. Pesez and J. Bartos, Talanta, 14 (1967) 1067.
10 T. Uno and H. Taniguchi, Bunseki Kagaku, 21 (1972) 76.
11 Y. Ohkura and K. Zaitsu, Talanta, 21 (1974) 547.
12 Y. Ohkura, K. Ohtsubo, K. Zaitsu and K. Kohashi, Anal. Chim. Acta, 99 (1978) 317.
13 T. Kaito, K. Sagara and K. Ikunaga, Chem. Pharm. Bull., 27 (1979) 3167.
14 R. Chayen, R. Dvir, S. Gould and A. Harell, Anal. Biochem., 42 (1971) 283.
15 H. Zeitler, Anal. Biochem., 88 (1978) 649.
16 D. J. Pietrzyk and E. P. Chan, Anal. Chem., 42 (1970) 37.
17 E. Sawicki and C. R. Sawicki, Aldehydes — Photometric Analysis, Vols. 1—5, Academic Press, London, 1975—1978.
18 N. L. Drake, H. D. Anspon, J. D. Draper, S. T. Haywood, J. van Hook, S. Melamed, R. M. Peck, J. Starling, Jr., E. W. Walton and A. Whiton, J. Am. Chem. Soc., 68 (1946) 1356.
19 W. Heinisch, Monatsh. Chem., 15 (1894) 233.
20 M. C. Mourew and M. H. Moissan, C. R. Acad. Sci., 125 (1897) 32.

Analytica Chimica Acta, 134 (1982) 47—53
Elsevier Scientific Publishing Company, Amsterdam — Printed in The Netherlands

SPECTROPHOTOMETRIC AND FLUORIMETRIC ENZYMATIC DETERMINATION OF SERUM CREATINE KINASE MB ISOENZYME BY USING IMMUNO-INHIBITION

CHANG-LI YUAN[a], SHIA S. KUAN[b] and GEORGE G. GUILBAULT*
Department of Chemistry, University of New Orleans, New Orleans, LA 70122 (U.S.A.)
(Received 30th July 1981)

SUMMARY

Two fully enzymatic methods, colorimetric and fluorimetric, are reported for the determination of creatine kinase (EC 2.7.3.2) MB isoenzyme after immuno-inhibition with the use of goat anti-human CK-M IgG antibodies. The residual creatine kinase activity is assayed by using hexokinase and glucose-6-phosphate dehydrogenase systems; the resulting NADPH is determined spectrophotometrically by reaction with *p*-iodonitrotetrazolium violet in the presence of diaphorase as an intermediate electron carrier, or fluorimetrically by coupling the NADPH with resazurin/diaphorase to form resorufin. Both assays take only 12 min and require only 100 or 25 μl of serum. The calibration plots of enzyme activities are linear up to 580 and 435 U l^{-1} of CK-MB in serum for the spectrophotometric and fluorimetric assays, respectively, the coefficients of variation being 2.3% and 4.6%, and the recovery values 103% and 100%, respectively. The results correlate very well with those obtained by the Helena electrophoresis—fluoridensitometric methods. As little as 4 U l^{-1} and 2 U l^{-1} CK-MB could be measured reproducibly.

Many methods have been proposed for the assay of creatine kinase (EC 2.7.3.2) MB isoenzyme, which is one of the earliest occurring, most reliable and most sensitive enzyme indicators of acute myocardial infarction [1—5]. Recently an immuno-inhibition method for CK-MB assay has been developed [6—10]. Being a type of homogeneous enzyme immuno-assay (EIA), the immuno-inhibition technique relies on inhibition of enzyme activity after the antibodies combine with an enzyme-labeled antigen, because of steric hindrance.

After immuno-inhibition, CK-MB is quantified by monitoring the increase in NADPH absorbance at 340 nm via two other consecutive enzyme reactions (Oliver—Rosalki system). The low sensitivity of this u.v. system, sold commercially as the Merck—Dade kit, is the major limitation of this CK—MB test [11]; this prompted a search for a better procedure for the determination of CK-MB after immuno-inhibition. Both spectrophotometric and fluorimetric approaches are described here. In the former, the reduction of $NADP^+$ is

[a]Present address: E. I. du Pont de Nemours & Company, La Place, LA 70068, U.S.A.
[b]Present address: 4298 Elysian Fields Ave., Food & Drug Administration, New Orleans, LA 70122, U.S.A.

coupled to the reaction of 2-*p*-iodophenyl-3-*p*-nitrophenyl-5-phenyltetrazolium salt, a NADPH-trapping agent, in the presence of diaphorase (EC 1.6.99-) as an intermediate electron carrier. In the fluorimetric assay, the NADPH produced is oxidized by resazurin to yield a highly fluorescent compound, resorufin [12], which is measured by monitoring the change in fluorescence at λ_{ex} 548 nm and λ_{em} 598 nm.

EXPERIMENTAL

Apparatus

A Cary 17 spectrophotometer (Varian Instrument Division, Palo Alto, CA) and a fluorimicrophotometer (American Instrument Company, Inc. Silver Springs, MD) were used to monitor the enzyme reactions. A laboratory immersion heater (Blue M Electric Company, Blue Island, IL) and a circulating pump (Brinkman IC-2, Brinkman, Westbury, NY) were used to maintain a constant temperature (±0.1°C) in the water bath. A strip-chart recorder A-25 (Varian Aerograph) was used to display the reaction rate and a Beckman Research pH meter was used for pH adjustments.

Autopipettes (Finnpipette, Helsinki, Finland) of 5—50, 50—200 and 200—1000 μl capacities were used to deliver sera, substrates and reagents.

Reagents and solutions

Cardiozyme CK-MB reagent kit (containing the Cardiozyme reagent with anti-human CK-M IgG antibody and the buffered substrate), control sera, Cardiozyme CK control level I and II, and Isozyme CK marker (used for standardization), were supplied by Dade Division, American Hospital Supply Corporation (Miami, FL 33152). This kit is now available from Harleco Inc., PA. The composition of all these reagents is given in the specification sheet from the maker.

p-Iodonitrotetrazolium violet [INT; (2-*p*-iodophenyl)-3-*p*-nitrophenyl-5-phenyltetrazolium chloride; No. I-8377, grade 1] was obtained from Sigma Chemical Co., and resazurin from Aldrich Chemical Co. Diaphorase (54 U mg^{-1} from *Clostridium kluyveri*) was a product of Worthington Biochemical Corp., Freehold, NJ 07728. Different concentrations of INT, resazurin and diaphorase were prepared by dissolution in 0.1 M triethanolamine buffer (pH 7). A 10^{-5} M solution of quinine sulfate in 0.05 M sulfuric acid was used to calibrate the fluorimeter.

Sample sera, non-hemolyzed, were obtained from Hotel Dieu and Charity Hospitals.

All stock solutions were made with double-distilled and deionized water.

Procedures

Spectrophotometric method. Add 2.0 ml of buffered substrate (Dade) to a vial of Cardiozyme lyophilized reagent containing the CK-MB antibody (Dade) and incubate at 37°C for 3 min in a constant-temperature water bath.

Into this vial, introduce a 0.1-ml aliquot of unknown serum or CK-MB control, followed by 0.1 ml of diaphorase solution (2.7 U per assay). Transfer the vial contents to a 1-cm cuvet and initiate the reaction by addition of 0.1 ml of INT (1.78 mg ml^{-1} or 3.5×10^{-3} M). Before the measurement, slightly swirl the cuvet and invert to mix. Record continuously the absorbance at 500 nm for 7 min. Instead of taking the initial burst (about 1 min; see Discussion), measure the most stable, linear portion of the recorded rate on the chart paper to determine the absorbance change per minute (ΔA min^{-1}). The calibration plot of $\Delta A/\Delta t$ vs. CK-MB activities is linear up to 580 U l^{-1}.

Fluorimetric method. Place 2.0 ml of buffered substrate (Dade) and 2.0 ml of triethanolamine buffer (pH 7.0, 0.1 M) into a vial containing lyophilized coenzyme—enzyme—antibody reagent. Swirl the solutions to mix and let stand for 2 min to equilibrate. Draw 1.0 ml of reaction mixture into a clean test tube (0.8 × 7.5 cm), then add 25 μl of diaphorase solution (1.35 U per assay in triethanolamine buffer) and incubate at 37°C in a water bath for 3 min. Into the test tube, introduce 25 μl of unknown serum or control, followed by 25 μl of resazurin solution (6×10^{-4} M in triethanolamine buffer). Gently swirl and invert the tube after sealing it with a piece of parafilm. Place the test tube in the preset temperature-controlled cell compartment and record continuously the change in fluorescence at 598 nm (λ_{ex} = 548 nm) for 5—7 min. Use the most stable, linear portion of the recorded reaction rate to determine the fluorescence change per minute (ΔF min^{-1}). The calibration plot of $\Delta F/\Delta t$ vs. CK-MB activity is linear up to 435 U l^{-1} with the 25-μl sample size.

RESULTS

Spectrophotometric method

Because the optimal pH for the CK reaction, which yields ATP and creatine, is 6.8, the compromise pH for this coupled reaction was 7.0. Among the buffers tried, triethanolamine was found to be the best. At high buffer concentrations, a slight inhibitory effect on the activity was observed. A 0.1 M buffer concentration was used to maintain a constant pH in the solution during the assay. The effect of ionic strength was tested by addition of sodium chloride; high ionic strength inhibited the enzymatic reactions, apparently because of distortion of the enzyme—substrate complex. To increase the sensitivity and shorten the lag phase, a temperature of 37°C was used during assay. One of the CK isoenzymes BB, if present, would be very labile at 37°C, thus providing a favorable factor for the CK-MB assay.

It was found that 2.7 U of diaphorase per assay and 1.45×10^{-4} M (or 71 μg ml^{-1}) INT solution were sufficient for the determination of CK-MB in the clinically significant range.

Fluorimetric method

The activity of CK decreased when the pH of the triethanolamine buffer (0.1 M) was increased from 6.8 to 8.0 in the fluorimetric resorufin system.

The pH effect in the fluorimetric NADPH system proves that the results obtained above in the spectrophotometric system were governed mainly by the CK—HK—GPD system. The optimal activity of diaphorase added was 1.35 U per assay. The effect of the fluorogenic dye resazurin on the relative acidity was studied. The plot of rate vs. dye concentration was linear up to 6.75×10^{-6} M, reached a peak, and decreased at 2.0×10^{-5} M. The compromise concentration chosen was 1.35×10^{-5} M, which makes the reaction zero-order in resazurin.

Performance characteristics

To test reproducibility and precision, two levels of sera (normal and abnormal values) were analyzed on three consecutive days. Table 1 shows the excellent run-to-run and day-to-day precision for both the spectrophotometric and fluorimetric methods.

On addition of control sera to a serum that had been previously assayed, the analytical recovery ranged from 98 to 108% for spectrophotometry and 98 to 102% for fluorimetry (Table 2). The blank value measured relative to a known 30 U l^{-1} solution of CK-MB was zero.

In the fluorimetric system, the amount of CK-MB giving a reproducible signal (relative standard deviation 0.7%) was 2 U l^{-1}, and in the spectrophotometric system as little as 4 U l^{-1} was measurable (relative standard deviation 1.0%).

Selectivity. Several interfering substances present in serum were examined for their effect on the accuracy of the assay. The interfering substances, at concentrations which were as much as ten times the normal concentrations in human serum (or blood), were added to a control serum (CK-MB, 34 U l^{-1}). No notable effect (less than 1% error) was found in either method for the following concentrations in serum: creatine (6.5 mg dl^{-1}), ascorbic acid (6.2 mg dl^{-1}), uric acid (44 mg dl^{-1}), bilirubin (1.8 mg dl^{-1}), hemoglobin (100.0 mg dl^{-1}).

Ascorbic acid in serum is oxidized easily but caused only a slight effect at concentrations higher than 6.2 mg dl^{-1}. As the serum samples which are used for CK-MB assay are not hemolyzed, hemoglobin will not be an interfering species. Also, because the whole serum sample is highly diluted (4%), the effect of possible interfering substances, even if present, will be negligible, their concentrations being below that at which less than 1% error occurs.

TABLE 1

Precision of the two methods for serum CK-MB[a]

	Spectrophotometry		Fluorimetry		Spectrophotometry		Fluorimetry	
	Normal	Abnormal	Normal	Abnormal	Normal	Abnormal	Normal	Abnormal
	Run-to-run				*Day-to-day*			
Mean (U l^{-1})	6.0	135.6	6.00	134.40	6.2	136.0	5.90	122.0
S.d. (U l^{-1})	0.12	4.20	0.16	7.70	0.03	2.72	0.03	6.71
C.v. (%)	2.0	3.1	2.70	5.90	0.48	2.0	0.55	5.50

[a]Each value is the average of 4 assays.

TABLE 2

Analytical recovery of serum CK-MB by the two methods

Spectrophotometry			Fluorimetry		
CK-MB (U l^{-1})		Recovery (%)	CK-MB (U l^{-1})		Recovery (%)
Amount added	Total found		Amount added	Total found	
0	34.0	—	0	27.7	—
12.0	46.2	102	4.20	31.8	98
24.0	59.0	104	8.50	36.2	100
48.0	86.0	108	34.0	62.5	102
96.0	128	98			Mean = 100
		Mean = 103			

Comparison studies

The CK-MB activities of 35 and 20 fresh sera were determined by the spectrophotometric and fluorimetric methods, respectively, and the results obtained were compared with those found by using the cellulose acetate electrophoresis—fluorescence scanning kit (Helena) used by the Hotel Dieu and Charity Hospitals. A linear regression analysis gave coefficients of correlation of 0.998 and 0.999 for the spectrophotometric and fluorimetric procedures, respectively. The regression equations for comparison were $(y) = 0.998x + 0.781$ U l^{-1} for spectrophotometry, and $(y) = 0.96x + 1.18$ U l^{-1} for fluorimetry. The standard deviations of the intercepts were 0.01 and 0.015 U l^{-1}, the standard deviations of the slopes were $0.004x$ and $0.01x$, respectively, for the spectrophotometric and fluorimetric procedures.

DISCUSSION

In an evaluation of commercial kits for CK assay by Pryce et al. [10], Dade's kit was graded as "very good". The only reported problem with this kit involves poor precision at low values because of lack of sensitivity [11]. As shown above, this low sensitivity of the ultraviolet method could be improved by use of a better chromogenic inductor reaction. The apparent molar absorptivity of reduced INT was found to be 1.7×10^4 l mol^{-1} cm^{-1} (using 7.85×10^{-5} M INT–formazan in 0.1 M triethanolamine buffer at pH 7.0). This is a higher value than that of NADPH (6.3×10^3 l mol^{-1} cm^{-1}) [13], and more sensitive results should give more certainty to the assay at normal CK-MB values.

Phenazine methosulfate (PMS) was tried as the electron carrier, but it is light-sensitive and a serious background occurred even when no creatine kinase was added. Therefore, diaphorase was used instead.

Usually, when the unstable reagents are added last into the assay mixture as the initiating reagent, a burst (sudden rise) in the reaction rate occurs

because of the accumulated NADPH triggered by the CK-B. Fortunately, the INT-coupled reaction gave a longer linear range which gave the true maximum rate for the reaction. It is better to use INT (spectrophotometry) or resazurin (fluorimetry) as the initiating reagent rather than diaphorase. If possible, the addition of creatine phosphate or $NADP^+$ to initiate the reaction would be the best approach.

The theory of this assay is based on the fact that the isoenzyme CK-BB does not occur in serum where the blood barrier is intact [6] and that during the assay the activity of CK-M subunits is completely blocked and the residual activity is measured as one half of the total MB activity. The pre-incubation of serum sample and antibody is generally preferred in order to obtain complete inhibition.

However, in many enzyme immuno-assays, the residual enzyme activity is measured after an incubated mixture of enzyme and antibody has been added to the substrate. This is done because the substrates or regulatory molecules may induce conformational changes of the enzyme, thus rendering some determinants unavailable for combination with antibody. This factor has been observed with most enzyme systems, but creatine kinase is one of the exceptions. The activity of CK can be measured when enzyme and antibody are not pre-incubated, but are mixed in the presence of substrate (simultaneous addition) [14, 15].

In conclusion, both the spectrophotometric and fluorimetric kinetic determinations of CK-MB with immuno-inhibition have provided reliable, sensitive and time-saving ways to diagnose myocardial infarction in the clinical laboratory. Because of the higher sensitivity resulting from the use of INT and resorufin, routine assays of CK-MB can be done with excellent precision and accuracy. Furthermore, because measurements are performed in the visible region, interferences originating from the presence of serum protein in the u.v. region can be avoided.

We thank Dr. Alfred Hew, Jr. (Hotel Dieu Hospital) for his generous supply of analyzed sera. Appreciation is expressed to Dr. Joe Giegel at the Dade Corporation (Div. of Am. Hospital, Miami, FL) for his kind provision of Cardiozyme Kits and the CK-MB kits, and the CK-M antibody.

REFERENCES

1 G. A. Moss, Creatine Kinase Isoenzymes: Methods and Clinical Significance, Worthington Biochemical Corp., Freehold, NJ 00728, 1976.
2 D. A. Nealon and H. R. Henderson, Clin. Chem., 21 (1975) 392.
3 S. M. Sax, J. J. More, J. L. Giegel and M. Welsh, Clin. Chem., 22 (1976) 87.
4 P. J. Kudirka, M. G. Busby, R. N. Carey and E. C. Toren, Jr., Clin. Chem., 21 (1975) 450.
5 P. Grande, C. Christiansen, A. Pedersen and M. S. Christensen, Circulation, 61 (1980) 723.
6 U. Wurzburg, N. Hennrich and H. Lang, Klin. Wochenschr., 54 (1976) 357.

7 D. Neumeier, W. Prellwitz, U. Würzburg, M. Brundobler, M. Olbermann, H. J. Just, M. Knedel and H. Lang, Clin. Chim. Acta, 73 (1976) 445.
8 P. C. P. Wong and A. F. Smith, Clin. Chim. Acta, 65 (1975) 99.
9 Dade, American Hospital Supply Corp., Cardiozyme—CK-MB Reagents for Quantitative Determination of Creatine Kinase MB Isoenzyme Activity, August 1978.
10 F. H. Pryce, E. K. Kim and J. E. Logan, Clin. Biochem., 10 (1977) 206.
11 J. Boone, E. J. Sampson, S. Lewis, V. Whitner, S. McKneally and B. Houston, Clin. Chem., 26 (1980) 513.
12 G. G. Guilbault and D. N. Kramer, Anal. Chem., 37 (1965) 1219.
13 H. U. Bergmeyer, Z. Klin. Chem. Klin. Biochem., 13 (1975) 507.
14 A. J. Samuels, Biophys. J., 1 (1961) 437.
15 B. Cinader, Ann. N. Y. Acad. Sci., 103 (1973) 495.

Analytica Chimica Acta, 134 (1982) 55—71
Elsevier Scientific Publishing Company, Amsterdam — Printed in The Netherlands

FLOW INJECTION ANALYZER FOR STUDENTS, TEACHING AND RESEARCH
Spectrophotometric Methods

J. RŮŽIČKA*, E. H. HANSEN and A. U. RAMSING

Chemistry Department A, The Technical University of Denmark, Building 207, 2800 Lyngby (Denmark)

(Received 15th July 1981)

SUMMARY

The flow streams in simple manifolds are propelled by controlled gas pressure; ancillary equipment consists of a small spectrophotometer or colorimeter and a chart recorder. The analytical result is available in less than 20 s after sample injection, with a reproducibility better than 1%, using microlitre volumes of sample and less than millilitre volumes of reagent per assay. These are the performance data of a simple, robust and inexpensive flow injection analyzer designed for use with a wide range of detectors. The application of spectrophotometry is illustrated by five exercises aimed at teaching instrumental analysis and intended for those who wish to introduce flow injection analysis in their laboratories.

The FIAstar[a] system (the name is an acronym from the title of this paper) has been developed with two purposes in mind: first to demonstrate that even with very simple means a flow injection analyzer capable of excellent performance may be constructed; and secondly to make flow injection analysis (f.i.a.) accessible to all those who cannot afford, or are not willing to invest the funds necessary, to purchase any of the first generation of commercially available f.i.a. instruments. The initial impulse to undertake this work, which turned out to be more difficult than anticipated, was the authors' rewarding experience in graduate courses in instrumental analysis, to which a simple flow injection system was introduced five years ago [1]. Further encouragement was given during numerous visits of colleagues who expressed their interest in acquiring a simple system which would allow them to initiate research in f.i.a. Several versions of the instrument were considered, constructed, and tested in this laboratory, at CENA at the University of São Paulo (Brasil), and at the University of Utah in Salt Lake City. The final version of the FIAstar system, suitable for both teaching and research purposes, and available for 1/10 of the cost of any commercial flow injection analyzer, is described below, together with five spectrophotometric exercises designed for teaching laboratories and for those who are not yet familiar

[a]The word FIAstar is a trade mark.

with f.i.a. methods. It is hoped that in this way not only students, but also skilled analysts will be able to experience the surprising features of f.i.a., its amazing speed of response and its reproducibility of measurement. While the latter quality may readily be estimated from the figures presented below (where all response curves were reproduced photographically from the recorder charts), the speed of response, simplicity of the setup and versatility of the method can be evaluated only through experiments.

Ideally, a flow injection analyzer should be constructed to have the following features: (1) the carrier stream must flow in a pulse-free manner through a narrow channel of strictly uniform diameter, including the injection and detector sections; (2) the microlitre volume of sample solution must be injected in a reproducible manner, as a plug, into the carrier stream without disturbing its flow; (3) the flow path should be easily reprogrammable to suit a wide variety of assays and therefore any side streams must be connected to the main stream in an easy, yet reproducible manner, and the volume of the injected sample must be adjustable at will; (4) the flow-through detector selected must yield instant reproducible response to the analyte content with maximum signal yield.

If these criteria are fulfilled, and the previously postulated rules [2] are followed, then such a well designed flow injection analyzer will: (a) yield the readout within 20 s after sample injection; (b) require totally a maximum of 100 μl of sample solution per assay (for injection of 20-μl samples, but proportionally more for larger injected volumes, which may be up to 200 μl); (c) use a maximum of 500 μl of reagent stream per assay (and even less reagent in the merging zones mode); (d) become filled with reagents, or washed out with water, in less than 3 min during the start-up or close-down routines because its total hold-up volume, including the connecting lines, does not exceed 1—2 ml; and (e) require no more bench space than a typewriter.

With these requirements to be met, the development of the FIAstar was undertaken; the design would have to be simple and inexpensive, yet sufficiently robust to withstand the usual treatment in a teaching laboratory. The concept on which the system is based is illustrated by Fig. 1(a), where the propulsion unit, reagent reservoirs, some manifold components, injection valve and the detector can be identified. Gas at very low pressure (up to 0.4 bar, i.e., 6 psi) is maintained at a constant, adjustable level by means of a gas regulator and then distributed into the reagent bottles from where the reagent streams can be released via open—shut valves to a T-connector and further to the sample injection valve where the sample, the volume of which can be varied by changing the sample loop length, is introduced. These components plus the reaction coils and the detector are situated on two working planes in such a way that they can be freely moved around, depending on the detector used and on which flow system is to be designed. In order to meet the previously mentioned criteria, it is imperative to situate the flow-through detector as close to or preferably directly on the board; otherwise

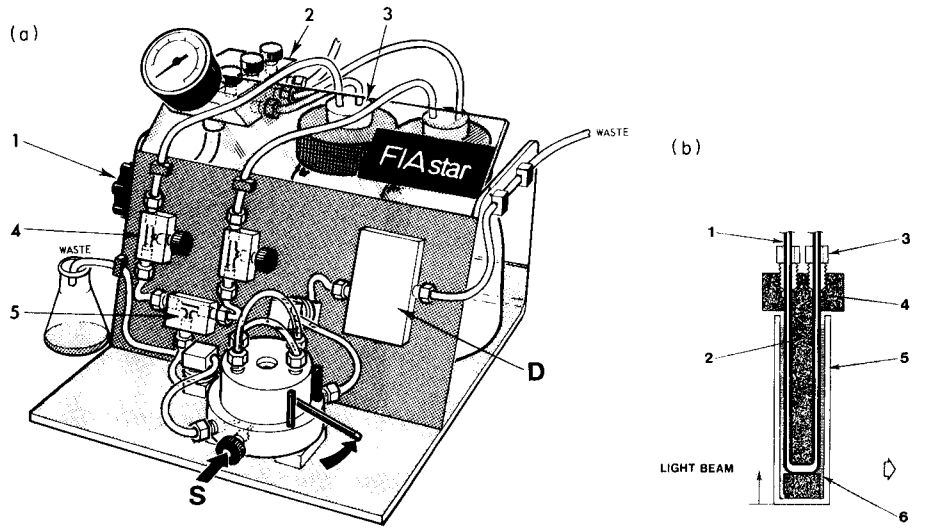

Fig. 1. FIAstar system. (a): (1) gas regulator; (2) distribution unit; (3) reagent reservoirs; (4) open—shut valves; (5) T-connector; (S) sample injection valve; (D) detector. (b): flow-through cell, see text.

any long connecting line to an outside bulky apparatus will spoil the performance characteristics of the microflow design of the FIAstar system. For spectrophotometric measurements, there are two alternatives: the use of light fibres, or the use of a miniaturized detection instrument. The first approach would allow the use of a bulky spectrophotometer of the conventional type, from which the light beam may be piped out to a flow-through cell situated on the board and back again to the meter. Yet it was found that this approach required experience and experimental skill to ensure that a sufficiently large amount of light energy passed through the fibres and the equally narrow (~1.5 mm i.d.) optical path of a flow-through cell, because older types of spectrophotometers operate with wide light beams. Therefore, a second approach was chosen, where a minispectrophotometer, equipped with a specially designed tube flow cell, was placed directly on the FIAstar board (Fig. 2). It can be seen that the components depicted in Figs. 1 and 2 are identical, yet in different geometrical arrangement. It is the use of Lego boards and building blocks, serving as support for individual manifold components, which readily allows the choice of any desired manifold in a stable configuration. Thus all five f.i.a. exercises, as well as further FIAstar applications (see Discussion), can be performed using the same components, rearranged according to the flow systems depicted in Fig. 3(a—d); the configuration in Figs. 1(a) and 2 corresponds to the flow system in Fig. 3(b).

The exercises are: (1) functional test and dispersion measurement; (2)

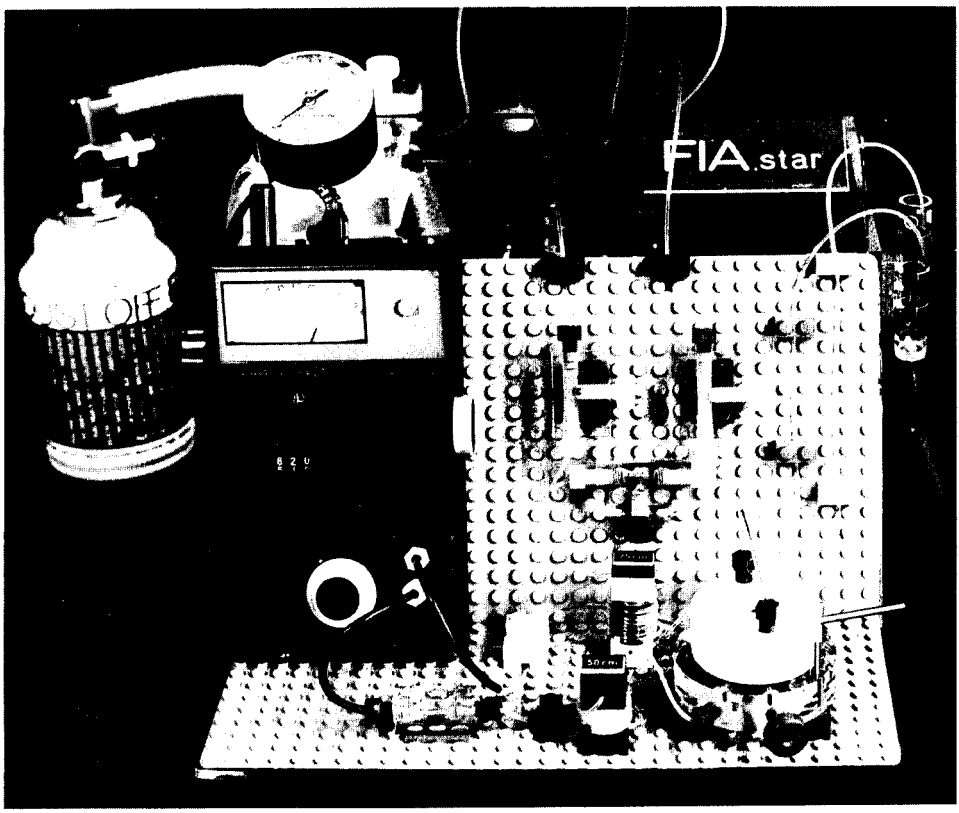

Fig. 2. FIAstar system furnished with a minispectrophotometer. (Note the gas container in the background.)

determination of chloride; (3) determination of calcium in the presence of magnesium; (4) determination of chromium(VI) by the merging zones technique; and (5) high-speed acid—base titration. These have been chosen to illustrate the important features of f.i.a., on simple well known chemical determinations based on colour formation. Of special f.i.a. techniques, the merging zone approach, used to save reagents, is demonstrated in Exercise 4, while the stopped-flow technique, applicable to all exercises, is explained in connection with Exercises 1, 3 and 4. These simple stopped-flow experiments, which allow an estimate of how far a colour development has progressed within 10—15 s after the sample has been injected into the reagent stream, may well convey the most surprising information, even to experienced analysts, considering that the literature recommends 5—15 min for full colour development when these assays are performed manually or even automatically in air-segmented continuous flow systems. Finally, it should be pointed out that each of the exercises should not be viewed alone, but rather in the context of the others, as, with modification, stopped flow may

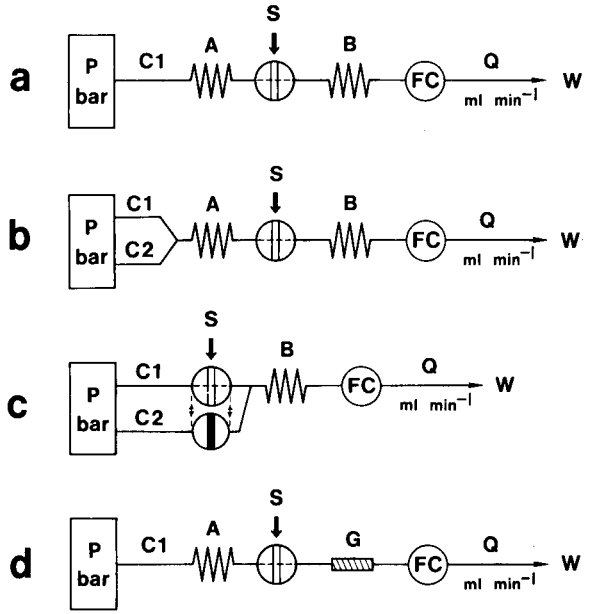

Fig. 3. Flow diagrams for Exercises 1 to 5. FC, flow cell; W, waste; for other details, see text.

be used even in Exercise 5, the interference test in Exercises 2 and 4, etc. The value of the first exercise should not be underestimated, although it does not involve any chemical reaction, because it serves not merely as a simple performance test. The measurement of dispersion offers a chance to gain better insight into what happens when a sample is injected and forced to flow, to stop and flow again. The magnitude of sample zone dispersion should therefore be considered as a quantitative term, providing insight into the physical processes which take place in the flow channel. Only then can the kinetics of mixing be distinguished from the chemical processes which take place during actual determinations, when the sample plug is being continuously mixed with the carrier stream while moving towards the detector.

EXPERIMENTAL

Apparatus

The FIAstar system for spectrophotometry (Figs. 1(a) and 2) has been designed as a complete solution handling system including a flow-through measuring cell of novel design which fits into the instruments specified below and very likely into most modern spectrophotometers. A detailed description of the injection valve and the specially designed flangeless connectors allowing a free flow of liquids propelled by a very low pressure, is available on request.

The flow-through cell (Fig. 1(b)) is constructed as follows. A transparent plastic tube (1) (such as Microline) of 0.5 mm i.d. has a widened section situated in the light beam of a spectrophotometer and held there axially by means of an opaque plastic holder (2), two screws (3) and elastomer gaskets (4). The whole assembly is placed into a cuvette (5) made of transparent plastic (such as acrylic). Silicone oil (6) is used to fill all interstices so that losses of light by reflection on the curved ends of the plastic tubing are minimized. In order to accommodate the flow cell in different spectrophotometers, which may have the light beam situated at various distances from the bottom of the cuvette (see the arrow), several holes may be drilled at various levels so that the plastic tubing may be axially placed at the desired level.

The FIAstar has to be complemented by a source of pressurized gas, by a spectrophotometer or a colorimeter, and by a recorder. Several alternatives are mentioned below so that the choice of instrumentation is not restricted.

The gas source must not have a pressure higher than 4 atm, as the pressure regulator of the FIAstar would otherwise be overloaded. Air from a sufficiently stable central supply or a pressurized tank, or an inert gas are all equally suitable. As the gas consumption is typically a few ml min^{-1}, even a small container of gas, such as Freon, as supplied by photographic shops (e.g., Dust-off, Falcon Safety Products Inc., N.J., U.S.A.) in a 12 oz. can (Fig. 2) will last for several weeks.

The spectrophotometer shown in Fig. 2 is a Bausch and Lomb Mini 20, which has a variable wavelength control (band width 20 nm). Alternatively a filter colorimeter, such as the Corning 252, can be used as it is so small that the flow cell compartment can be situated quite close to the manifold components. As both of these instruments provide the recorder output in transmittance units, a home-made logarithmic converter was used to convert the signal fed to the recorder and therefore all figures in this work show absorbance vs. time curves.

The strip chart recorder (such as a Radiometer Servograph REC 61 or REC 80) with a suitable input sensitivity must have sufficiently fast response (full scale deflection in 0.1 s) and a stepwise chart speed adjustable to about 2 s cm^{-1} (high speed) and 1 min cm^{-1} (low speed).

Reagents

The distilled or deionized water must be deaerated prior to use by vigorous stirring for 5 min under a slight vacuum, provided by, e.g., a water pump. If microbubbles of air still persist in being trapped in the flow-through cell, addition of 0.01—0.5% of a surfactant such as glycerol or Brij-35 will alleviate the problem.

EXERCISES

Prior to any exercise, the individual components must be assembled according to the selected flow diagram (Fig. 3), the containers filled with distilled water and a pressure of 0.4 bar applied to test all connectors and the injection valve for leaks. The streams should move freely through all lines; this may be tested by briefly inverting the filled containers and observing the movement of air bubbles.

Exercise 1. Functional tests and measurement of dispersion

By pumping a colourless buffer solution and injecting a suitable dye dissolved in the same buffer, it is possible to check the reproducibility of sample injection, of peak broadening on the way to the detector, and of the detector response. More quantitatively, it becomes easy to estimate the maximum sampling frequency beyond which intermixing of samples will occur, as well as the degree of mixing between the sample and carrier solution in that element of fluid which yields the analytical readout. The degree of mixing has been defined as the dispersion D [2]

$$D = C^{O}/C^{max} \text{ and } D_g = C^{O}/C \qquad (1)$$

where C^{O} is the original sample concentration, C^{max} is the concentration at peak maximum, D is the dispersion at peak maximum, and D_g is the dispersion along the sample zone gradient (of concentration C). The maximum sampling frequency is related to the standard deviation of the peak, $S_{max} = 3600/6\sigma_t$ where σ_t is expressed in seconds and S_{max} in samples per hour. The dispersion value D and the standard deviation are interrelated and are therefore influenced by the same parameters, i.e., flow geometry, pumping rate and sample volume [2, 3].

Carrier stream solution. Aqueous 1×10^{-2} M borax solution containing 0.01% Brij (C1) is used.

Dye solutions. The dye stock solution is prepared by dissolving 0.400 g of bromothymol blue in 25 ml of 96% ethanol, making the final volume up to 100 ml with the 1×10^{-2} M borax solution. The dye solution for injection is then prepared by mixing 1 ml of stock dye with 199 ml of the 1×10^{-2} M borax solution and is further referred to as 1/200 BTB. The absorbance of the 1/200 BTB solution at 620 nm is 1.2 in a 10-mm path length. (Note that the cheap tubular cell may be up to 40% shorter because of bending of the ends.)

Procedures. Assemble the FIAstar components according to the flow diagram given in Fig. 3(a), where A = 75 cm, B = 50 cm and the connection from coil B to the flow cell is 10 cm long. Insert a sample loop 25 cm long, corresponding to $S = 50$ μl (all tubing 0.5 mm i.d.). Fill the reagent bottle with the borax solution (C1). Set the detector at 620 nm. Apply a pressure of ca. 0.3 bar and measure the flow rate by collecting the effluent at waste

(W) for 1 min. If necessary, adjust the pressure P to obtain a final flow rate Q of ca. 1.2 ml min^{-1}. Prepare 1/400, 1/800, 1/1600 BTB solutions by further dilution of the 1/200 BTB with borax and inject these solutions successively, in triplicate, to check the reproducibility and linearity of the response, using the low recorder speed (cf. Fig. 4a). The standard error of estimate of these measurements should be equal to or better than 0.3% and the regression coefficient r^2 should be 0.998 or more.

Next, to estimate the maximum allowed sampling frequency, record at high chart speed (about 2 s cm^{-1}) a single peak by injecting 50 μl of 1/200 BTB and measure the peak width at 0.61 C^{max} (cf. Fig. 4b). For 2σ = 5 s, S_{max} = 240 samples per hour [2]. With this set-up, test the stopped flow function by injecting a sample and turning the injection valve to the middle position between the "inject" and "fill" positions immediately when the recorder pen starts to descend on the peak tail section. A horizontal line will be recorded as long as a fixed section of the dispersed dyed zone is held still in the flow cell.

Finally, investigate the influence of the sample volume on the peak height by injecting 25, 50, 100 and 200 μl of 1/400 BTB (cf. Fig. 4c). Note that, as in the previous experiment, the paper chart should be returned to the same starting position after each run. The injected volume is changed simply by changing the length of the sample loop, made of 0.5 mm i.d. tube, while the valve is turned to the middle position. Because of this change in the overall length of the analytical channel, the flow rate (which was initially adjusted to 1.2 ml min^{-1} for the 50-μl sample loop) changes slightly and therefore the leading edges of the upgoing curves do not coincide. (This observation is in contrast to previous experiments done with peristaltic pumps [2], the delivery rates of which are not affected by such small changes of the flow resistance.) Measure the peak heights and the peak widths at 0.61 C^{max}, and finally fill the flow cell with the 1/800 BTB solution

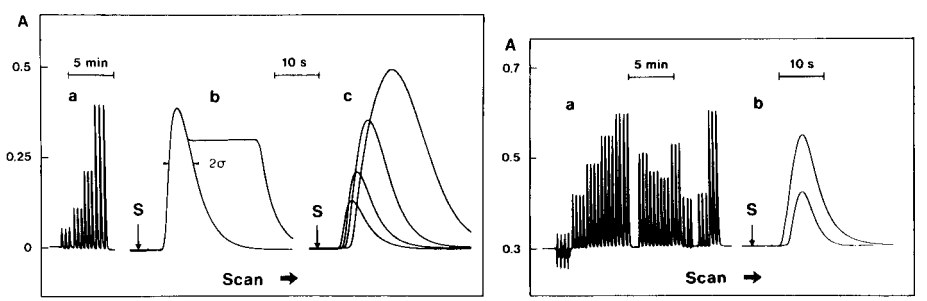

Fig. 4. Recordings obtained in Exercise 1 with the flow system shown in Fig. 3(a). For explanation, see text.

Fig. 5. Recordings obtained in the determination of chloride in Exercise 2 (Fig. 3(a)). Standards contained 10, 20, 30, 40 and 50 ppm of chloride; these are followed by triplicate injections of five samples and two standards.

for measurement. Compute C^0 and the D values for experiments a, b and c (Fig. 4). Much more advanced experiments along these lines may be aimed at the influence on the dispersion of the tube length, tube diameter, and packing with inert materials (e.g., the single-bead string reactor [4]), and the investigation of the tank-in-series model which leads to the size and position of a single mixing stage which is the theoretical basis of the high-speed f.i.a. titrations [3].

Exercise 2. Determination of chloride

This simple colorimetric procedure [5, 6], which is being widely used for determination of chloride in serum and other materials, has been adapted as an f.i.a. exercise for the determination of chloride in sea water in connection with an investigation of the mixing patterns between salt and fresh water at the mouth of a river [1]. The colour formation, monitored at 480 nm, is based on the reaction between chloride and thiocyanatomercury(II) ions and the subsequent formation of the red-brown thiocyanatoiron(III) complex [1, 5, 6].

Carrier stream solution. Dissolve 0.626 g of mercury(II) thiocyanate in ca. 500 ml of water, add 30.3 g of iron(III) nitrate, 4.72 g of concentrated nitric acid and 150 ml of methanol, and finally dilute the volume to 1 l with water.

Standard solutions. Prepare 10, 20, 30, 40 and 50 ppm chloride solutions by suitable dilutions of a 100 ppm chloride stock solution (1.648 g of NaCl in 1 l of water).

Procedure. Assemble the FIAstar components according to the flow diagram given in Fig. 3(a), where A = 100 cm, B = 50 cm, and the connection from coil B to FC is 10 cm long. Insert a sample loop 12.5 cm long (all tubes are 0.5 mm i.d.). Apply a pressure of about 0.3 bar to obtain Q = 1.3 ml min^{-1}, and set the low chart speed. Inject standard chloride solutions in quadruplicate (Fig. 5a), followed by samples to be assayed (e.g., "sea water") in triplicate and recheck the calibration thereafter by two standards, say, 20 ppm and 50 ppm in triplicate. Compute the standard error or estimate and the regression coefficient as well as the chloride content of the assayed samples.

In additional experiments, inject the 20 and 50 ppm standards and record the peaks at high chart speed to measure σ and S_{max} (Fig. 5b). Explain the reason for the negative peaks obtained for the 10 ppm chloride solution and support this by an experiment in which water is injected as a blank, or by repeating the calibration run using a carrier stream of reagent diluted 1:1 by water. Predict the interferences caused by formation of any undissociated mercury(II) compounds, and carry out tests by means of the interference procedure described in the next exercise. Further details on interferences are available [7], and additional applications of the colorimetric method in the analysis of waters [8, 9] and biological materials [10] may also be found in the literature.

Exercise 3. Determination of calcium in the presence of magnesium

In samples of biological and agricultural origin as well as in waters, the Ca/Mg ratio is usually 5:1 or more. Of the various colorimetric methods available, the *o*-cresolphthaleincomplexone method [2, 11—13] was adapted for a FIAstar exercise. This reagent (also called metalphthalein or phthaleincomplexone) is an acid—base as well as a metal indicator; it is colourless up to pH 7.8 and gradually changes colour with increasing alkalinity up to pH 11.4, where the colour starts to change from pink to red [14, 15]. This red or red—violet is similar to the colour of the indicator—metal complexes with magnesium, calcium, strontium or barium, the first two being the most stable ($\log K_{MgI} = 8.9$, $\log K_{CaI} = 7.8$). These relatively weak complexes are therefore formed in alkaline media, yet pH values above $pK_3 = 11.4$ should be avoided, because otherwise the free indicator would interfere by contributing its own colour to the colour of the calcium complex measured at the same wavelength (i.e., 580 nm). Hence, the pH, the excess of indicator and the reaction conditions must be exactly controlled, and even absorption of carbon dioxide, which might affect the pH of the solution, must be avoided. In the presence of 8-quinolinol, the interfering effect of magnesium is suppressed [12, 13].

Carrier stream solutions. These must be prepared fresh daily by diluting stock solutions with 1×10^{-2} M sodium tetraborate solution. The carrier solution (C1) is prepared by further diluting 1:20 a stock solution containing 150 ml of diethylamine already diluted with 1×10^{-2} M sodium tetraborate to 1 l. The stock solution for the carrier solution C2 is prepared by weighing out 200 mg of *o*-cresolphthaleincomplexone and adding it to 360 ml of dimethylsulfoxide, followed by 2.5 g of 8-quinolinol and about 500 ml of water; after vigorous mixing until dissolution is complete, 1 ml of Brij is added and the solution is diluted to 1 l with water. To obtain the C2 carrier reagent solution, this stock is diluted 1 + 1 with 1×10^{-2} M sodium tetraborate prior to use.

Standard solutions of calcium. The stock solution (100 ppm Ca) is prepared by dissolving 0.250 g of calcium carbonate in 1.4 ml of concentrated hydrochloric acid and diluting to exactly 1 l with water. This solution is then further diluted with water to give calcium standards in the range 2.5—15 ppm Ca. The calcium/magnesium solutions for the interference studies are made by mixing appropriate volumes of the 100 ppm Ca stock and a 500 ppm Mg stock solution (5.072 g of $MgSO_4 \cdot 7H_2O$ in 1 l of 0.1% sulfuric acid) and diluting with water.

Procedure. Assemble the FIAstar manifold as shown in Fig. 3(b) (cf. Figs. 1(a) and 2), where A = 50 cm, B = 100 cm, and the connection from B to the flow cell is 10 cm. Insert a sample loop 10 cm long, corresponding to $S = 20$ µl (all tubes are of 0.5 mm i.d.). Fill the reagent bottles with the carrier solutions C1 and C2 described above and apply a pressure of about 0.4 bar to obtain $Q = 1.7$ ml min^{-1}. Inject standard calcium solutions in the range 2.5—15 ppm Ca in duplicate (cf. Fig. 6a) and then perform the inter-

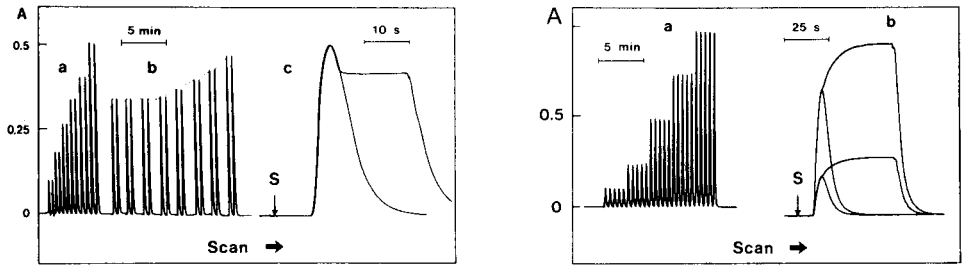

Fig. 6. Recordings obtained in Exercise 3 with the flow system shown in Fig. 3(b). Calibration run obtained by injection of 2.5, 5.0, 7.5, 10.0, 12.5 and 15.0 ppm Ca. Note a sudden increase of peak height in experiment (b) when solutions containing 10 ppm Ca and 0, 5, 10, 20, 40, 60, 80 and 100 ppm Mg were subsequently injected in duplicate.

Fig. 7. Recordings obtained in determining chromium(VI) in Exercise 4 by the merging zone technique (flow system Fig. 3(c)). Injected sample concentrations contained 1, 2.5, 5, 7.5 and 10 ppm Cr(VI). The stopped-flow experiment (b) shows that some colour continued to be formed when the sample zone was stopped in the flow cell.

ference test by injecting 10 ppm Ca solutions, containing progressively increasing amounts of magnesium (Fig. 6b). Finally, using the 15 ppm Ca standard, record a peak in the continuous flow mode, for the estimate of the maximum sampling frequency, and another peak in the stopped-flow mode, to learn how far the colour formation has progressed (Fig. 6c). The linearity of the calibration curve is limited to the range 2.5—15 ppm Ca, and therefore samples such as aqueous soil extracts or blood serum, must be prediluted to fall within this range.

Barium, strontium, iron and zinc interfere and their influence may be tested as described above. The use of alternative reagents, such as an ammonia buffer of pH 10—11 instead of diethylamine and borax, may be feasible [14, 16].

The calcium method described above may serve as a model system for developing a number of colorimetric procedures based on the use of reagents of the EDTA type into which a chromophoric framework has been introduced. Thus xylenol orange, which has a very similar structure to *o*-cresolphthalein but with a functional sulfonic acid group, is a very useful colorimetric reagent for a large number of metal ions [14, 15] which may be selectively determined by selecting proper pH-conditions and masking agents.

Exercise 4. Determination of chromium(VI) by the merging zones technique

The merging zones technique is a f.i.a. method in which the colour-forming reagent is consumed only when a sample is injected into the carrier stream [2]. In this exercise, the sample is injected into an inert carrier stream (C1, see Fig. 3c) to which the reagent stream (C2) is added intermittently by means of the specially constructed valve. This approach, allowing saving of reagent, is demonstrated on the determination of chromium(VI) by means

of 1,5-diphenylcarbazide. These two species form in acidic solution an intensely red—violet complex which can be measured photometrically at 540 nm. As the reaction is very sensitive, selective and fast when the pH is kept at 1—2, it is especially suitable for the determination of very small amounts of chromium(VI).

Carrier stream solution. The C1 stream (Fig. 3c) consists of 0.1 M sulfuric acid to which is added 10% of 96% ethanol and 0.01% Brij-35.

Reagent solution (C2). This is prepared by diluting a stock solution 1:4 with 0.1 M sulfuric acid to which is added 0.01% Brij-35. The stock solution is prepared by dissolving completely 250 mg of 1,5-diphenyl carbazide in 100 ml of 96% ethanol to which is added 100 ml of 0.2 M sulfuric acid. The stock solution should be stored in a dark bottle, in which case it will be stable for about a week.

Standard solutions. Solutions containing 1, 2.5, 5, 7.5 and 10 ppm Cr(VI) are made by suitable dilution of a 500 ppm Cr(VI) stock solution (1.415 g of potassium dichromate in 1 l of water).

Procedure. Assemble the FIAstar manifold as outlined in Fig. 3(c), where B = 100 cm and the connecting tubes from the injection valve to the merging point are ca. 10 cm each; the sample loop length is 12.7 cm of 0.5 mm i.d. tubing corresponding to 25 μl. In this procedure, the "extra set of holes" in the injection valve is used so that the reagent line (C2) is connected to that hole in the stator which communicates with the hole in the rotor only while the sample loop is in the inject position (the other hole in the stator being blocked by a dummy screw). Apply a pressure of 0.3 bar to obtain a pumping speed of 1.3 ml min^{-1}, and inject the standard solutions (see Fig. 7a) followed by the samples to be assayed; then repeat the calibration run. Because of the slight differences in refractive index of the two merging streams, a small peak is formed at the foot of the signal peaks. Therefore it is recommended to return the sample valve to the inject position immediately after the top of the peak of each sample has been recorded.

From the calibration record, the standard error of estimate and the regression coefficient can be computed. Further, by running one of the samples at high paper chart speed, the σ-value and thus the maximum sampling frequency may be determined. This in turn can be used to calculate the economy of the procedure, i.e., the reagent consumption per assay (calculated from the time elapsed from the injection to the appearance of the top of the peak measured on the chart or recorded on a watch) compared to the volume of reagent solution needed if the reagent were to be pumped continuously.

By stopping the carrier/reagent stream whenever the top of the peak is reached (Fig. 7b), the extent of the chemical reaction under the prevailing experimental conditions can be evaluated. The reaction between chromium(VI) and 1,5-diphenylcarbazide must take place in acidic medium, and the experiments can be extended by repeating the calibration run and stopped-flow measurement using carrier solutions C1 with decreasing con-

centrations of sulfuric acid and thus establishing how the rate of the chemical reaction is influenced by changing this parameter.

The practical use of the chromium(VI) assay may be demonstrated by the determination of chromium in soils [17]. Alternatively, one may consider as a sample material, acidified aqueous absorbates of welding fumes after appropriate collection times, where the level of chromium(VI) is being tested for health protection of welders. It should be appreciated, however, that the merging zones technique is merely demonstrated here on the chromium assay, as its main advantage of improved reagent economy becomes apparent only when expensive reagents are used, e.g., in enzymatic and in immuno assays. Unfortunately, the merging zones technique is difficult to use with strongly coloured reagent solutions.

Exercise 5. High-speed acid—base titrations

It follows from any f.i.a. response curve that each point on the ascending part of the curve with a dispersion value D_g corresponds to another point on the descending part of the peak with an identical dispersion D_g. Flow-injection titrations are based on relating the physical distance (i.e., the time span) between these two points to the concentration of analyte, the identification of these equivalence points being done by means of a suitable indicator. In order to obtain a simple mathematical relation between the time span (Δt), the concentration of analyte (C_A^o) and the concentration of the titrant carrier solution (C_B), a so-called single mixing stage must be identified [2, 3] which due to its dominating volume gives rise to an exponential concentration profile of the injected sample. Then it can be shown [2, 3] that

$$\Delta t = (V_m/Q) \ln 10 \log (C_A^o/C_B) + (V_m/Q) \ln 10 \log (S/V_m n) \qquad (2)$$

where S is the injected sample volume, V_m is the volume of the mixing stage, Q is the pumping rate, and n is the stoichiometric factor between the reacting components. As the last term is a constant for a defined set of experimental conditions, a plot of Δt versus log C_A^o, obtained by injecting a series of standards, will yield a straight line with a slope of V_m/Q (ln 10). Hence, on the basis of this calibration curve, measurement of Δt for a given sample enables its initial concentration C_A^o to be determined.

One of the ways to design a single mixing stage in f.i.a. systems is to inject an appropriate volume of sample into a gradient tube of defined geometry, which would yield titration times of the order of a few seconds. Yet, for such short Δt times, the data have to be collected at high frequency by a microcomputer in order to achieve sufficient precision of measurement [3]. If the Δt times are to be measured from the peak widths on a recorder chart, it is necessary to stretch the titration times to obtain longer Δt intervals. From Eqn. (2) it is obvious that this can be done by (a) increasing the volume of the gradient tube (V_m); (b) injecting a larger sample volume (S); (c) decreasing the pumping rate (Q); or (d) decreasing the concentration of the titrant carrier solution (C_B).

These parameters cannot, however, be varied completely independently at will. Thus, it has previously been found that a V_m/S ratio of approximately 2 is optimal [3], and for practical purposes excessively low pumping rates in the FIAstar should be avoided as they are difficult to control. Thus, the preferable parameter to vary is the concentration of the titrant, as will be demonstrated in the following exercise on the titration of acid (HCl) with base (NaOH).

Manifold. The flow system is shown in Fig. 3(d). The parameters are: P = 0.2 bar; A = 250 cm 0.5 mm i.d. tubing; S = 75 μl, i.e., both external loops of the injection port consist of 13 cm of 0.86 i.d. tubing; G = gradient tube of 150-μl volume (2.0 mm i.d.), the lengths of Microline tubing linking the gradient tube with the injection port and the flow cell being 5 and 10 cm, respectively; FC = 600 nm; and Q = 1 ml min^{-1}. The coil placed in front of the injection valve serves merely as a brake coil in this case. As the flow rate should be approximately 1 ml min^{-1}, a system without a brake coil would require such low pressure that it would be difficult to adjust and maintain it properly.

In order to obtain sufficient precision when reading off the peak widths on the recorder paper, the paper speed should be adjusted to at least ca. 2 mm s^{-1} (5 s cm^{-1}).

Carrier stream (C1). Sodium hydroxide solutions (5×10^{-4} M, 1×10^{-3} M, 5×10^{-3} M and 1×10^{-2} M) are prepared, to each of which are added 0.2 ml of bromothymol blue stock indicator solution (see Exercise 1) and 3 ml of 96% ethanol per 100 ml of titrant.

Standard acid solutions. Solutions in the range 5×10^{-3}—1×10^{-2} M are made by appropriate dilution of a 0.1 M hydrochloric acid stock solution.

Procedure. The FIAstar is first furnished with the 1×10^{-3} M NaOH titrant solution and a calibration curve is obtained by injecting each of the acid standards (in duplicate). Whether transmittance or, as here, absorbance is measured, the colour changes of the indicator during the titration cycle (from the blue base colour to the yellow acid colour and back to blue again) will be registered by the spectrophotometer as a "blue" or "no blue" signal; that is, all peaks will be of approximately the same height, but their widths will vary as a function of C_A^o (Eqn. 2, where n = 1).

In the calibration curve, Δt is plotted on the ordinate versus log C_A^o on the abscissa; Δt (s) is read directly off the recorder paper as the peak width b (mm), measuring the peak width of all peaks at the same level, approximately halfway between the baseline and the top of the peak, i.e., $b = \Delta t v_r$, where v_r is the recorder speed (mm s^{-1}). From this calibration curve, the concentration of any unknown hydrochloric acid sample may be determined.

From Eqn. (2) it is clear that Δt may be varied by changing the concentration of the titrant solution (C_B), i.e. the dynamic measuring range of the procedure may be shifted as a function of C_B. This is readily demonstrated by repeating the calibration run, and by adjusting the concentration levels of sodium hydroxide in the carrier stream. As seen in Fig. 8, the use of

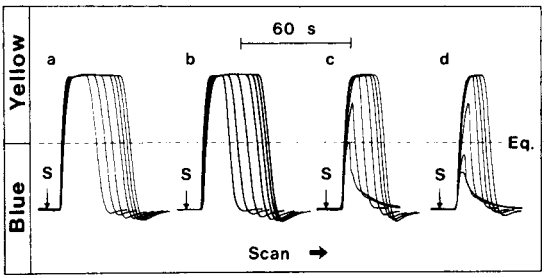

Fig. 8. Recordings obtained in Exercise 5 (flow system Fig. 3(d)) in the titration of hydrochloric acid (C_{HCl} = 5 × 10^{-3} M, 1 × 10^{-2} M, 2 × 10^{-2} M, 4 × 10^{-2} M, 6 × 10^{-2} M, 8 × 10^{-2} M and 1 × 10^{-1} M) with (a) 5 × 10^{-4} M NaOH; (b) 1 × 10^{-3} M NaOH; (c) 5 × 10^{-3} M NaOH; (d) 1 × 10^{-2} M NaOH. A decreasing concentration of the titrant in the carrier stream from 1 × 10^{-2} M to 1 × 10^{-3} M NaOH increases the limit of sensitivity of the measurement (d, c, b), but beyond the latter level it only increases the time needed to complete the titration cycle (a).

the most dilute titrant leads to longer Δt times (a) while increasing concentrations of titrant gradually reduce the peak widths (b—d). Yet the relative difference in the Δt distances between the individual standards remain constant, as all calibration curves are parallel (cf. Eqn. 2). It must be noted, however, that the more dilute acid samples cannot be determined with the high titrant concentrations. Therefore, varying the concentration of the titrant solution will not, per se, change the absolute precision of the titration procedure, but it may serve as a convenient means of adjusting the titration times for a series of samples to fall within a chosen time range, i.e., changing the dynamic measuring range of the procedure. It should also be added that as the gradient of the injected sample formed in the gradient tube cannot be expected to be strictly exponential over more than about two decades (any non-exponential dilution process will show in the calibration plot as a deviation from linearity according to Eqn. 2), the C_B concentration may be varied to yield a linear calibration curve in that range within which the samples to be assayed would fall.

Extensions of the exercise. As previously described [1], the exercise may be connected to a practical case by simulating the analysis of samples collected from a plant where the concentration of an acid process stream has to be checked as a function of time.

Furthermore, the following parameters can be determined: the limit of sensitivity (by extrapolating the individual calibration curves to Δt = 0); the apparent volume of the mixing stage (V_m in Eqn. 2) as derived from the slope when Q is known (determined) compared with the actual volume of the gradient tube (150 µl). Also, as it has recently been suggested [18] that only water with indicator be used as the carrier stream instead of sodium hydroxide with indicator, with the aim of increasing the sensitivity of titrations, tests with such a system will provide enough data to assess whether anything is to be gained by this approach.

In addition to acid—base titrations such as that described above, a number of complexime tric or redox titrations may be done with exactly the same set-up as that depicted in Fig. 3(d). Thus, for instance, the complexime tric titration of zinc(II) by EDTA, using xylenol orange as indicator, can be tried. The composition of the titrant carrier stream should be 1×10^{-3} M EDTA in 0.1 M acetate buffer (pH 4.69) to which is added aqueous 0.5% xylenol orange indicator stock solution. Standards are prepared from zinc sulfate in the concentration range 5×10^{-3} M to 1×10^{-1} M, and the wavelength of measurement is 575 nm. The peak widths are as usual read off at approximately half peak height.

DISCUSSION AND CONCLUSIONS

It is unfortunate that, despite their cost, most commercial flow injection analyzers presently available do not fulfill the performance criteria postulated in the Introduction and will therefore require more time, sample material and reagents per determination than the FIAstar instrument uses for any of the above-described exercises. It is, however, only fair to point out the drawbacks of the FIAstar construction, so that the trade-off between simplicity of design, cost and the extent of manual operations acceptable, can be evaluated.

Although the gas propulsion system of FIAstar provides a pulse-free flow, it is difficult to control so that it will provide an exact delivery of liquids through two or several parallel channels. The reason is that the flow resistances of parallel lines must be very carefully balanced, as otherwise the streams will not merge in 1:1 proportion. Furthermore, such malfunction is difficult to detect as only the combined outflow to waste can be monitored during the assay; this outflow will not much change even if one of the reagent lines becomes completely blocked because both reagent containers are propelled by the same gas pressure, and most of the flow resistance originates from the coils, injection valve and waste line. This limitation is manageable for two channels, but a peristaltic pump, though more expensive, is a far more suitable tool for simultaneous propulsion of several streams. Peristaltic pumps also allow a choice of different flow rates in individual channels, and aspiration of solutions for automated sampling.

The manually operated injection valve, without a bypass, precludes full automation of the system with active control of the analyzer functions by a microcomputer. As the sampling valve is not motorized and not furnished with a microswitch, it cannot be activated nor can it trigger pump or sampler functions. Therefore, the stopped-flow technique in the FIAstar system serves only as a means of testing how far the color development has progressed. It would require much skill and attention to use FIAstar for quantitative procedures based on reaction-rate monitoring [2]. For the same reason, the merging zones approach can be used only in its simplest version. Furthermore, the FIAstar instrument is not thermostated. It cannot be used for

solvent extraction, and columns longer than ca. 10 cm, even if very loosely packed, cannot be incorporated.

In spite of these limitations, the versatility and performance of the FIAstar system sets a high standard for the design of any flow injection analyzer. Though many may regard the simplicity of the present concept to be exaggerated, it should be kept in mind that this approach was deliberately chosen in order to make this analytical technique accessible to the widest possible academic and research community. Though the present paper has been limited to a description of simple spectrophotometric assays, it is hoped that these few examples will inspire further exploitation of this traditional analytical methodology, which has such an extensive literature containing a wealth of information on selective and sensitive assays of numerous species. The versatility of the FIAstar concept will be further illustrated in future work. The next paper, currently under preparation, deals with the use of FIAstar in potentiometry, for both ion-selective electrode measurements and titrations. Other analytical methods such as fluorescence, luminescence, flame methods and gas-diffusion techniques may also be handled by means of the FIAstar system. It is hoped that this versatility will win flow injection analysis the place in teaching and research which it truly deserves.

The authors express their gratitude to Drs. Joel Harris and Jiri Janata, University of Utah, for advice and critical comments, and to Dr. Marek Trojanowicz, University of Warsaw, for thorough scrutiny of the exercises.

REFERENCES

1 E. H. Hansen and J. Růžička, J. Chem. Educ., 56 (1979) 677.
2 J. Růžička and E. H. Hansen, Flow Injection Analysis, Wiley—Interscience, New York, 1981.
3 A. Ramsing, J. Růžička and E. H. Hansen, Anal. Chim. Acta, 129 (1981) 1.
4 J. M. Reijn, W. E. van der Linden and H. Poppe, Anal. Chim. Acta, 126 (1981) 1.
5 I. Iwasaki, S. Utsumi and T. Ozawa, Bull. Chem. Soc. Jpn., 25 (1952) 226; Chem. Abstr., 47 (1953) 10407 f.
6 I. Iwasaki, S. Utsumi, K. Hageno and T. Ozawa, Bull. Chem. Soc. Jpn., 29 (1956) 860; Analyt. Abstr., 4 (1957) 3954.
7 R. D. Rodabaugh and G. T. Upperman, Anal. Chim. Acta, 60 (1972) 434.
8 T. M. Florence and Y. J. Farrar, Anal. Chim. Acta, 54 (1971) 373.
9 British Standards 2690, Part 6 (1968).
10 V. Kulhánek and C. Fišer, Collect. Czech. Chem. Commun., 31 (1966) 1890.
11 G. Schwarzenbach, Analyst, 80 (1955) 713.
12 H. V. Connerty and A. R. Briggs, Am. J. Clin. Pathol., 45 (1966) 290.
13 B. Zak, J. Salancy, W. L. Clark, S. S. Marie and E. Baginski, Advances in Automated Analysis, Technicon International Congress 1972, Mediad Inc., New York, 1973.
14 R. Pribil, Analytical Applications of EDTA and Related Compounds, Pergamon, Oxford, 1972.
15 E. Bishop, Indicators, Pergamon, Oxford, 1972.
16 J. Körbl and R. Pribil, Collect. Czech. Chem. Commun., 23 (1958) 1213.
17 S. S. Jørgensen and M. B. B. Regitano, Analyst, 105 (1980) 292.
18 H. L. Pardue and B. Fields, Anal. Chim. Acta, 124 (1981) 39, 65.

Analytica Chimica Acta, 134 (1982) 73—80
Elsevier Scientific Publishing Company, Amsterdam — Printed in The Netherlands

EXTRACTION—SPECTROPHOTOMETRIC DETERMINATION OF BORON WITH 2,6-DIHYDROXYBENZOIC ACID AND 4-(4-DIETHYLAMINOPHENYLAZO)-*N*-METHYLPYRIDINIUM IODIDE, WITH APPLICATION TO STEELS

MITSUKO OSHIMA, KEIJI FUJIMOTO, SHOJI MOTOMIZU* and KYOJI TÔEI

Department of Chemistry, Faculty of Science, Okayama University, Tsushima-naka, Okayama-shi (Japan)

(Received 22nd May 1981)

SUMMARY

The sensitive and selective method reported is based on the reaction of boric acid with 2,6-dihydroxybenzoic acid in acidic aqueous solution to form a 1:2 complex anion which can be extracted into chloroform as an ion-pair with 4-(4-diethylaminophenylazo)-*N*-methylpyridinium ion. The ion-pair formed by the excess of reagents and co-extracted into chloroform, is removed by washing the organic phase with phosphate buffer solution (pH 7.0) and 0.025 M sulfuric acid solution. The absorbance of azo dye in chloroform is measured at 570 nm. Calibration graphs are linear in the range 0—1.5×10^{-5} M of boron. The molar absorptivity is 6.6×10^4 l mol^{-1} cm^{-1} and the absorbance of the reagent blank is 0.030. The method was applied to the determination of boron at the 0.001% level in steels.

The analytical chemistry of boron is very important in such fields as nuclear-reactor materials, industrial metallurgy, pharmacy and agriculture. Many spectrophotometric methods for boron have been reported; of these, methods based on extraction of tetrafluoroborate with methylene blue or on curcumin have probably been most widely used [1—3]. Methods based on 2,4-dinitro-1,8-naphthalenediol (DNNDO) with brilliant green [4] and on 1,8-dihydroxynaphthalene-4-sulfonic acid with tetradecyldimethylbenzylammonium chloride [5] have been reported from this laboratory. These procedures are relatively simple, sensitive and selective, their disadvantages being, that in the former method DNNDO reacted with boric acid only in an acetic acid solution, and in the latter method measurements had to be done at 341 nm. Further reagents were therefore sought. Vasilevskaya [6] determined boron with salicylic acid and rhodamine B, whereas Bassett and Matthews [7] used salicylic acid and ferroin. Though salicylic acid reacted with boric acid in aqueous medium, the conditions for reaction were severe (probably because of the low solubility of salicylic acid in water) and the ion-pair formed by borodisalicylate with the cation was not readily extractable. 2,6-Dihydroxybenzoic acid (DHBA), which possesses an additional hydroxyl group, ortho to the carboxyl group, is easily soluble in water and was found

to react readily with boric acid in an acidic aqueous medium to form a complex anion, which could be extracted into chloroform with cationic dyes. Suitable procedures are reported in this paper. The most appropriate cationic dye was found to be 4-(4-diethylaminophenylazo)-*N*-methyl-pyridinium iodide.

EXPERIMENTAL

Apparatus and reagents

A Hitachi Model 139 spectrophotometer and a Shimadzu UV 300 recording spectrophotometer were used with glass cells of 10-mm path length. An Iwaki Model V-S-KM shaker was used for horizontal shaking of the 18-ml stoppered polypropylene test tubes (Nalgene 3110).

Polypropylene, teflon or quartz vessels were used in all analytical operations.

4-(4-Diethylaminophenylazo)-N-methylpyridinium iodide. 4-(4-Diethylaminophenylazo)pyridine was synthesized as described by Faessiger and Brown [8]. The recrystallized product was dissolved in a benzene solution of methyl iodide, and the solution was refluxed for 3—5 h for alkylation. The products precipitated were filtered on paper and washed with fresh benzene until the filtrate was scarcely colored. This product (m.p. 163°C) was dissolved in deionized water.

2,6-Dihydroxybenzoic acid. Commercially available DHBA (Tokyo Kasei Kogyo Co.) was recrystallized twice from deionized water, giving white needles (m.p. 187—190°C, dec.). The recrystallized DHBA was dissolved in deionized water containing about equimolar sodium acetate.

Commercial spectroscopic-grade chloroform was used without further purification. Other reagents were of analytical-reagent grade.

Recommended procedure

Transfer the sample solution (up to 5 ml) into a stoppered polypropylene test tube and dilute to 5 ml with deionized water if necessary. Add 0.5 ml each of EDTA (0.02 M) and DHBA (0.25 M) aqueous solutions, followed by 1 ml of 1.2 M hydrochloric acid solution and 2 ml of a 2×10^{-3} M solution of the cationic azo dye. Mix thoroughly, leave for 5 min, and add 5 ml of chloroform. After shaking for 10 min, discard the aqueous phase. Wash the organic phase twice with 5-ml portions of phosphate buffer (0.2 M, pH 7) and then with 10 ml of 0.025 M sulfuric acid. After phase separation, measure the absorbance of the chloroform phase at 570 nm in a 10-mm glass cell.

Preliminary experiments

Extraction of the complex boron anion formed with DHBA was also examined by using 4-(4-diethylaminophenylazo)-*N*-ethylpyridinium iodide and 4-(4-diethylaminophenylazo)-*N*-propylpyridinium chloride (which were synthesized similarly to the methyl derivative), methylene blue, malachite

green, brilliant green, pararosaniline, crystal violet, ethyl violet and rhodamine B as the counter-ions at various pH values; 1,2-dichloroethane, isobutyl methyl ketone, chlorobenzene, 1,2-dichlorobenzene, benzene and toluene were tested as the solvents. None of these systems proved better than the system with 4-(4-diethylaminophenylazo)-*N*-methylpyridinium iodide and chloroform. When chloroform or 1,2-dichloroethane was used for extraction, the reagent blanks were very large and could not be decreased by back-washing the organic phase except for the methyl and ethyl derivatives of the above pyridinium compound. When benzene or toluene was used, the reagent blank was relatively small, but the complex boron anion was less effectively extracted.

Preparation of steel sample solutions

Weigh 0.1—1.0 g of steel sample into a quartz beaker. Add 5—15 ml of 4 M hydrochloric acid and then add 30% hydrogen peroxide solution in limited amounts until the steel sample is dissolved or the dissolution no longer proceeds. For 0.1-g and 1-g samples of steel, 5 ml and 15 ml of 4 M hydrochloric acid were added, respectively. After dissolution of the sample, heat the solution on a hot plate (40—50°C) until effervescence ceases (a few minutes); then boil it for about 5 min in order to complete the removal of the hydrogen peroxide. Adjust the solution to pH 1.5—2.0 by adding sodium hydroxide solution, and dilute it to an accurate volume with deionized water. Determine the boric acid in such solutions by the recommended procedure.

RESULTS AND DISCUSSION

Contamination from water, reagents and vessels

Contamination from water was tested by the above recommended procedure for three kinds of water: (1) water deionized in ordinary apparatus and distilled from commercial Pyrex glass apparatus; (2) deionized water; and (3) deionized water distilled in non-boiling quartz apparatus (Daiken Sekiei Garasu Co., Type DPB-5). The water distilled from Pyrex apparatus, not surprisingly, showed serious and variable contamination. The deionized water, whether or not distilled in quartz apparatus, gave only a small absorbance (0.03—0.04), and ordinary deionized water was therefore used.

When commercially available DHBA was used without purification, the absorbance of the reagent blank was about 0.1 because DHBA reacted easily with boron in glass. The DHBA was therefore purified in a quartz beaker, and teflon or polypropylene apparatus and storage bottles were used throughout. Silicone rubber stoppers became badly stained with the cationic azo dye, but polypropylene was satisfactory.

Reaction and extraction mechanisms

The reaction mechanism of boric acid with DHBA(H_3R) and the extraction mechanism of the ion-pair are considered to be as follows

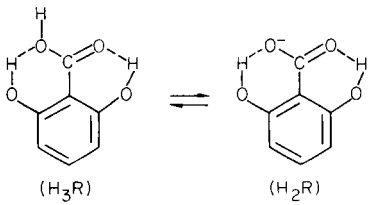

(1)

$$H_3R \text{ (or } nH_3R) \rightleftharpoons (H_3R)_{org} \text{ (or } [(H_3R)_n]_{org}) \quad (2)$$

$$Dye^+ + H^+ \rightleftharpoons H \cdot Dye^{2+} \quad (pK_a = 3.69\ [9]) \quad (3)$$

$$H_2R^- + Dye^+ \rightleftharpoons (Dye^+)(H_2R^-)_{org} \quad (4)$$

$$H_3R + H \cdot Dye^{2+} \rightleftharpoons (Dye^+)(H_2R^-)_{org} + 2\,H^+ \quad (5)$$

$$2\,H_3R + H_3BO_3 \rightleftharpoons B(HR)_2^- + 3\,H_2O + H^+ \quad (6)$$

$$B(HR)_2^- + H \cdot Dye^{2+} \rightleftharpoons (Dye^+)[B(HR)_2^-]_{org} + H^+ \quad (7)$$

$$B(HR)_2^- + Dye^+ \rightleftharpoons (Dye^+)[B(HR)_2^-]_{org} \quad (8)$$

Reactions (2), (4), (5) and (7) occur at acidic pH values, and reactions (4) and (8) in near neutral solutions. When the aqueous phase is acidic, the boron complex formation proceeds as in reaction (6) and the ion-pair formed with the cationic azo dye is extracted as in reaction (7). Some of the large excess of DHBA is co-extracted into the organic phase as the neutral species, H_3R or $(H_3R)_n$, and as an ion-pair with the azo dye. The boron complex anion, once formed in acidic medium, is very stable and does not decompose in neutral or alkaline medium (below pH 10); the boron-containing ion-pair is more readily extracted than the ion-pair of H_2R^- with the azo dye. When the organic phase is washed with phosphate solution (at about pH 7), the boron-containing ion-pair remains in the organic phase, but almost all the co-extracted DHBA removes into the aqueous phase as H_2R^-; the DHBA remaining in the organic phase as the ion-pair with the azo dye is then washed out with dilute acid in the form of H_3R and $H \cdot Dye^{2+}$. The absorbance of the reagent blank then becomes very small.

Effect of experimental variables

The effect of acidity on the formation of the boron complex is shown in Fig. 1A. The optimum range for the hydrochloric acid solution added is 1.0—1.4 M, the absorbance of the ion-pair being maximal and the reagent blank minimal. When sulfuric acid solutions are used, the optimum concentration of the acid is 0.4—0.7 M; the absorbance of the reagent blank is then about 0.08. From these results, 1 ml of 1.2 M hydrochloric acid solution was added to the 5 ml of sample solution.

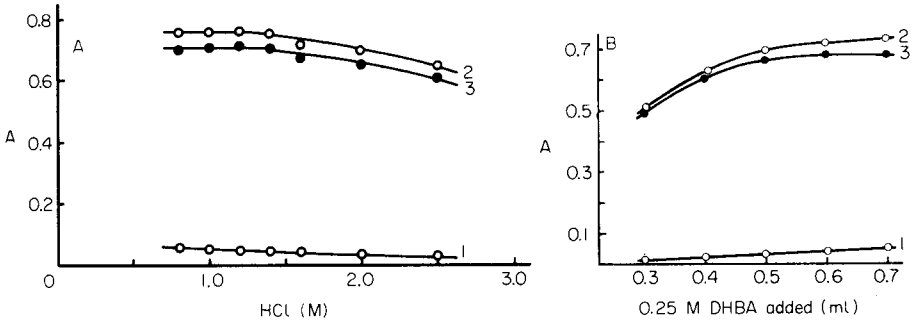

Fig. 1 (A). Effect of acidity on the complex formation; 1 ml of hydrochloric acid of the specified concentration was added. (B) Effect of the concentration of DHBA. (1) Reagent blank (solvent reference); (2) 1×10^{-5} M boron (solvent reference); (3) net absorbance.

As the amount of DHBA is increased, the absorbance of the reagent blank increases gradually (Fig. 1B), and 0.5 ml of 0.27 M DHBA solution is recommended. The effects of varying the added volume of the 2×10^{-3} M cationic azo dye solution from 1 ml to 3 ml proved to be very similar to those shown in Fig. 1B for DHBA. Addition of 2—3 ml of the dye solution provides constant maximal absorbance with low blanks; a volume of 2 ml was therefore selected.

Further tests showed that complete extraction of the boron complex into chloroform is achieved within 5 min when a mechanical shaker is used; for certainty, a shaking time of about 10 min is recommended. A time of 5 min is necessary for complete formation of the boron complex at room temperature (about 20°C).

The effect of the temperature is quite important. With solution temperatures below 15°C, the absorbance of the boron-containing ion-pair in chloroform varies significantly, because white precipitates of DHBA and EDTA form. There are no deposits at 25°C, and so the entire procedure should be used at 20—25°C.

The removal of the excess of DHBA from the organic phase is also important. The ion-pair of the azo dye and iodide is scarcely extracted into chloroform, but some of the excess of DHBA is extracted into chloroform as the neutral H_3R or $(H_3R)_n$ species and as the ion-pair with the azo dye ($Dye^+ \cdot H_2R^-$). Washing the organic phase twice with 5 ml of acetate buffer (pH 4—6) or phosphate buffer (pH 6—8) removes most of the DHBA to the aqueous phase. The pH of the wash solution is not vital but the phosphate buffer allows faster phase separation. To reduce the blank still further (to about 0.03 absorbance), the organic phase is washed finally with 10 ml of 0.025 M sulfuric acid.

Absorption spectra and calibration graph

Under the recommended conditions, the absorption spectrum for a 10^{-5} M boric acid solution (measured against the solvent) shows a single peak in the

range 400—700 nm with a clear maximum at 570 nm. In the wavelength range specified, the reagent blank shows only a broad low band of almost negligible significance. The calibration graph with the reagent blank as reference is a straight line through the origin over the range 0—1.5×10^{-5} M boron. The molar absorptivity calculated from the slope of the graph is 6.6×10^4 l mol^{-1} cm^{-1} at 570 nm. This is a little larger than the value 6.2×10^4 l mol^{-1} cm^{-1}, obtained in the extraction of the complex anion of nickel(II) ion and 4-chloro-2-nitroso-1-naphthol into chloroform [10].

Effect of co-existing ions

The interferences of co-existing ions (Table 1) were examined by using 5 ml of sample solution containing boric acid (1×10^{-5} M) and each co-existing ion in the absence and presence of EDTA. EDTA does not interfere at concentrations below 10^{-3} M, but causes negative errors above 10^{-2} M. In the presence of 0.02 M EDTA, the slope of the calibration graph becomes about 3% less than that in the absence of EDTA. When 0.5 ml of 0.2 M EDTA is added, iron(III) ion at a concentration of 2×10^{-2} M, and molybdenum(VI) ion at a concentration of 10^{-4} M do not interfere.

Determination of boron in steel samples

Steel samples were analyzed as described in the Experimental. Large amounts of hydrogen peroxide interfere with the determination because they oxidize the cationic dye and the DHBA. Although hydrogen peroxide can easily be decomposed by boiling the solution, this heating can volatilize boron from the acidic solution. However, tests showed that when the acidic solution of boric acid was heated, and boiled for about 10 min on a hot plate at about 200°C, the volatilization of boron was not significant.

TABLE 1

Effect of co-existing ions

Ion	Maximum tolerable concentration (M)
In the absence of EDTA	
Cl^-	5×10^{-1} [a]
Br^-	2×10^{-2} [a]
Co^{2+}, Ni^{2+}, EDTA	1×10^{-2}
I^-, NO_3^-, ClO_4^-, $H_2PO_4^-$, HCO_3^-	2×10^{-3} [a]
Ca^{2+}, Mg^{2+}, Cu^{2+}, Mn^{2+}, Cr^{3+}, Al^{3+}	1×10^{-3} [a]
Fe^{3+}, Zn^{2+}, Pb^{2+}	2×10^{-4}
V(V)	1×10^{-4}
Mo(VI)	1×10^{-5}
In the presence of EDTA (2×10^{-2} M)	
Fe^{3+}	2×10^{-2}
Mo(VI)	1×10^{-4}

[a]Maximum tested.

Standard steel samples (Japanese Standards, JSS, and NBS) were analyzed as described above. When EDTA was added to the sample solutions, large amounts of iron (below 0.02 M) did not interfere. Table 2 shows the results obtained. The boron contents obtained are in good agreement with the certified values, except for NBS 362. The standard deviation of the determination of boron in the JSS 159-3 steel was very good (see footnote to Table 2).

Conclusions

The boron complex formed with the 2,6-dihydroxybenzoic acid reagent is easily extracted with cationic azo dyes as an ion-pair into chloroform. Measurement of the absorbance of the ion-pair in the chloroform phase enables trace amounts of boron in steel samples to be determined. The advantages of this method are as follows: the boron complex is formed in aqueous solution and the sensitivity and selectivity for boron are high; the absorbance of the reagent blank is small. Finally, the complex-forming reagent is commercially available, and the counter-cation (azo dye) is easily synthesized in high yields.

TABLE 2

Determination of boron in steel samples

Sample[a]	Certified content (%)	Sample solution	Boron found[b] (μg)	Content (%)
JSS 161-3	0.012	0.1064 g/200 ml	0.339	0.0127
		0.1101 g/200 ml	0.348	0.0127
		0.1091 g/200 ml	0.353	0.0129
		0.1110 g/200 ml	0.361	0.0130
NBS 364	0.0106	0.0914 g/200 ml	0.247	0.0109
		0.0922 g/200 ml	0.248	0.0108
		0.0961 g/200 ml	0.261	0.0109
		0.0989 g/200 ml	0.263	0.0106
JSS 160-3	0.0063	0.1040 g/200 ml	0.166	0.00637
		0.1070 g/200 ml	0.169	0.00632
		0.1074 g/200 ml	0.172	0.00638
		0.1103 g/200 ml	0.172	0.00622
NBS 362	0.0025	0.1008 g/200 ml	0.078	0.00309
		0.1089 g/200 ml	0.082	0.00301
		0.1080 g/200 ml	0.084	0.00311
		0.1100 g/200 ml	0.078	0.00284
JSS 159-3	0.0013	0.5226 g/500 ml	0.072	0.00138
		0.5132 g/500 ml	0.065	0.00127
		0.5145 g/500 ml	0.073[c]	0.00136

[a]JSS: Japanese Standards of Iron and Steel. [b]Boron content in the 5 ml of sample solution used for the determination. [c]Measurements on ten 5-ml aliquots of this solution gave a standard deviation of ± 0.0009 μg.

REFERENCES

1 L. R. Uppström, Anal. Chim. Acta, 43 (1968) 475.
2 M. Miyamoto, Bunseki Kagaku, 11 (1962) 635.
3 H. Goto, Y. Kakita and K. Takada, Bunseki Kagaku, 18 (1969) 52.
4 K. Kuwada, S. Motomizu and K. Tôei, Anal. Chem., 50 (1978) 1788.
5 T. Korenaga, S. Motomizu and K. Tôei, Anal. Chim. Acta, 120 (1980) 321.
6 A. E. Vasilevskaya, Nauchn. Tr. Inst. Miner. Resur. (Ukr. SSR), (1971) 22; Anal. Abstr., 24 (1973) 55.
7 J. Bassett and P. J. Matthews, Analyst, 99 (1974) 1.
8 R. W. Faessiger and E. V. Brown, Trans. Kans. Acad. Sci., 24 (1963) 106.
9 K. Higuchi, S. Monya, Y. Shimoishi, H. Miyata and K. Tôei, Bunseki Kagaku, 29 (1980) 180.
10 S. Motomizu and K. Tôei, Anal. Chim. Acta, 120 (1980) 267.

Analytica Chimica Acta, 134 (1982) 81—92
Elsevier Scientific Publishing Company, Amsterdam — Printed in The Netherlands

ZUR ANALYTIK CHEMISCHER BINDUNGSFORMEN VON NICKELSPUREN IN KAFFEE, TEE UND ROTWEIN MIT CHROMATOGRAPHISCHEN UND SPEKTROSKOPISCHEN METHODEN

G. WEBER und G. SCHWEDT*

Anorganisch-Chemisches Institut der Universität, Tammannstr. 4, D-3400 Göttingen (W. Germany)

(Eingegangen den 1. Juli 1981)

SUMMARY

(The determination of traces of nickel and its chemical speciation in coffee, tea and red wine by chromatographic and spectroscopic methods)

Nickel is determined spectrophotometrically in coffee, tea and red wine with pyridine-2-aldehyde-2-quinolylhydrazone. The scheme outlined for establishing the distribution of the nickel relies on simple techniques: the total amount of nickel (about 100 ppb) is divided into different fractions by use of direct photometric analysis, filtration and liquid—liquid extraction. Further division of the ethyl acetate fraction is possible by means of thin-layer chromatography. Information about organic compounds obtained by chemical spray reactions and u.v.—visible and i.r. spectroscopy, is compared with the results of corresponding nickel determination (50—150 ng). Characteristic nickel patterns dependent on chemical groups (e.g., phenolic and amine) are obtained.

ZUSAMMENFASSUNG

In verschiedenen wäßrigen Getränken (Tee, Kaffee, Rotwein) wird die Nickelmenge spektrophotometrisch mit Pyridin-2-aldehyd-2-chinolylhydrazon bestimmt. Ein mit einfachen Methoden durchführbares Untersuchungsschema zur differenzierenden Nickelanalyse wird vorgestellt. Die Gesamtmenge (im Bereich von etwa 100 ppb) wird nach photometrischer Direktbestimmung, Filtration und Flüssig—flüssig-Extraktion in verschiedene Anteile aufgeteilt. Am Beispiel der Essigsäureethylester-Fraktion wird eine weitere Unterteilung mit Hilfe der Dünnschichtchromatographie erarbeitet. Durch Einsatz von Sprühreagenzien, UV—VIS- und IR-Spektroskopie werden Aussagen über die organischen Inhaltsstoffe gewonnen und mit den entsprechenden Nickelmengen (50—150 ng) verglichen. Es werden Nickelverteilungsmuster in Abhängigkeit von funktionellen Gruppen wie phenolische OH-Gruppen, NH-Gruppen, etc., erhalten.

In der Analytik von Elementspuren wurden bisher überwiegend Bestimmungen der Gesamtgehalte durchgeführt. Durch Angabe von Gesamtmengen ist aber eine sinnvolle Aussage über die Rolle des entsprechenden Elements in biologischen Systemen nicht möglich. So wird die Erforschung der Bindungsformen von Elementen in verschiedenen Materialien immer wichtiger. Dies um so mehr bei Elementen, die für die menschliche Ernährung entweder durch ihre Giftigkeit oder durch ihre Essentialität von größter Bedeutung sind. Sinnvolle Aussagen über Grenzwerte oder Bedarf können hier nur

aufgestellt werden, wenn differenzierte Analysen über Bindungsformen vorliegen; die dann Rückschlüsse auf Verfügbarkeit, Kontamination, etc. zulassen.

Entsprechende Methoden zur differentiellen Analyse von Elementspuren existieren zum Teil schon; als Beispiel sei hier die Arbeit von Fukai und Huynh-Ngoc über chemische Bindungsformen von Zink in Seewasser angeführt [1]. Die meisten Arbeiten befassen sich aber mit der Wasseranalytik [2], während über das Vorliegen in Lebensmitteln so gut wie nichts bekannt ist.

Dies gilt besonders für ein Element wie Nickel, das erst in den letzten Jahren als essentielles Spurenelement nachgewiesen wurde. Einige Nickelverbindungen spielen auch wegen ihrer tumorbildenden Eigenschaften für die menschliche Gesundheit eine Rolle. In dieser Arbeit wird versucht, mit möglichst einfachen Analysenmethoden wie Spektrophotometrie, Dünnschichtchromatographie (DC), etc., einige methodische Ansatzpunkte zu erarbeiten, die erste Aussagen über die vorliegenden Bindungsformen zulassen.

EXPERIMENTELLER TEIL

Geräte und Chemikalien

Geräte. Zeiss-Spektrophotometer PMQ II mit Mikroküvettenhalter; Shimadzu-Spektrophotometer UV-200 (nur für UV—Vis-Spektren); Flüssig—flüssig-Extraktoren mit regelbarem Heizpilz; DC-Elutionsgerät "Eluquick" (CAMAG); DC-Eluator (DESAGA); Aerosol-Sprühgerät (CAMAG); Membranfiltrationsapparatur (Schleicher & Schüll); pH-Meter (Knick 507).

Chemikalien. Alle Chemikalien Reinheitsgrad p.a. und alle Lösungen mit bidest. Wasser angesetzt. Pyridin-2-aldehyd-2-chinolylhydrazon (PAC; EGA-Chemie) DC-Plastikfolien Kieselgel 60, Schichtdicke 0,2 mm (Merck), Silica-Rapid-Glasplatten Woelm F 254 Schichtdicke 0,25 mm Benutzte Sprühreagenzien siehe Tabelle 1.

Angewandte Methodik

Photometrische Bestimmung von Nickel mit PAC (Verfahren 1). Nickel wird bei pH 10 mit PAC und Benzol aus dem wässrigen Medium ausgeschüttelt und bei 515 nm gegen Blindwert photometriert [3].

TABELLE 1

Verwendete Sprühreagenzien zur Dünnschichtchromatographie

Sprühreagenzien	Anfärbbare Verbindungen
α,α'-Dipyridyl/$FeCl_3$	Phenole, red. Verbindungen
Dragendorffs Reagenz	Alkaloide, *N*-haltige Verbindungen
Echtblausalz B/O, 1 M NaOH	Phenole, kupplungsfähige Amine
Ninhydrin/Cd-Acetat	Aminosäuren, Amine
Chloramin T/1 M HCl	Koffein
Vanillin/H_2SO_4	Phenole, Steroide, eth. Öle, Alkohole
Thymol/H_2SO_4	Zucker
o-Dianisidin	Aldehyde, Ketone

Mikroverfahren zur Nickelbestimmung mit Abtrennung des Reagenzieüberschusses (Verfahren 2). Nach Extraktion des Nickels mit PAC/Benzol wird durch DC (Kieselgel 60/Aceton) der Nickelkomplex von überschüssigem PAC und ev. gebildetem Eisen—PAC-Komplex abgetrennt und in Mikroküvetten bei 515 nm gegen Benzol photometriert [3].

Direktbestimmungen. Die Direktbestimmungen mit PAC/Benzol wurden nach Verfahren 1 durchgeführt, wobei allerdings zusätzlich eine Maskierung des überschüssigen Eisens durch 3—5 ml einer 5%igen KF—Lösung nötig war.

Bei einigen Materialien wurde auch das folgende Verfahren mit Pyridylazonaphthol (PAN) angewandt [4]. Zu ca. 10 ml Lösung gibt man 10 Tropfen 5%ige KF—Lösung und 2 ml methanolische PAN—Lösung (0,1%) und 1 ml Hexamminlösung. Es wird zweimal mit je 10 ml *o*-Dichlorbenzol ausgeschüttelt, auf 25 ml aufgefüllt und bei 575 nm gegen Blindwert gemessen.

Aufschlußverfahren (incl. Abtrennung überschüssigen Eisens; Gesamtbestimmung). Bis zu 1 g Material (Trockensubstanz) wird mit 4 ml konz. HNO_3 (65%) versetzt und in einem abgedeckten Glasgefäß langsam erhitzt und zur Trockene eingedampft. Nach Abkühlen wird mit einigen Tropfen konz. HNO_3 versetzt und wiederum erhitzt. Dies wird wiederholt, bis keine nitrosen Gase mehr entstehen und der Rückstand vollständig mineralisiert ist. Der Rückstand wird in 5 ml 1 M HCl gelöst, mit 2 ml 20%iger $KSCN^-$-Lösung versetzt und mit je 10 ml Isoamylalkohol/MIBK (1 + 3) extrahiert, bis der Extrakt nur noch schwach rot gefärbt ist. Die wäßrige Phase wird eingedampft, mit einigen Tropfen konz. HNO_3 erhitzt, um überschüssige Extraktionsmittel zu zerstören und nach dem Abkühlen in 5 ml Wasser (+ 5 Tropfen 1 M HCl) gelöst. Danach erfolgt die Nickelbestimmung nach Verfahren 1.

Filtrationen. Zur Ermittlung des an festen Teilchen gebundenen bzw. adsorbierten Nickelanteils wurden etwa 100 ml des entsprechenden Getränkes durch einen Membranfilter (0,45 μm) filtriert (ohne Nachwaschen). Die auf dem Filter befindliche Nickelmenge wurde durch Aufschluß (s. oben) ermittelt.

Flüssig—flüssig-Extraktionen. Eine Abbildung der benutzten Apparatur findet sich in [5]. Etwa 100 ml des Getränkes wurden eine Stunde (in Vorversuchen ermittelte Zeit für vollständige Extraktion) mit dem jeweiligen Extraktionsmittel (auch ca. 100 ml vorgegeben) extrahiert und danach das Extraktionsmittel am Rotationsverdampfer abdestilliert. Der Rückstand wurde dann entweder aufgeschlossen oder in einem geeigneten Lösungsmittel gelöst und weiteruntersucht.

Chromatographie nach Extraktion. Der Rückstand der Essigsäureethylesterextraktion wurde in 2 ml Aceton + 1 ml Methanol gelöst und etwa zur Hälfte auf eine DC-Folie (Kieselgel 60, 20 × 20 cm) strichförmig aufgetragen und in einer gesättigten DC-Kammer mit Essigsäureethylester chromatographiert (Laufstrecke ca. 17 cm). Die DC-Folie wurde danach in fünf R_f-Bereiche zerschnitten und von den fünf erhaltenen Teilen mit Methanol mittels des Eluquick-Gerätes die Substanz eluiert (25 Min Vorelution, 50 s

Durchmischung). Die erhaltenen methanolischen Lösungen können (ev. verdünnt) direkt zur Aufnahme von UV—VIS-Spektren benutzt werden (210—500 nm). Zur Nickelbestimmung werden die Lösungen eingedampft und mit 1—2 ml konz. HNO_3 (65%) aufgeschlossen. Die Nickelbestimmung erfolgt nach dem Mikroverfahren (Verfahren. 2), wobei die vorherige Abtrennung des Eisens nicht erforderlich ist. Zur Aufnahme von IR Spektren können die eingedampften Lösungen direkt verwendet werden, indem der feste Rückstand als KBr-Preßling gemessen wird.

Chemische Anfärbereaktionen von funktionellen Gruppen können direkt auf einem Chromatogramm durchgeführt werden. Über die verwendeten Sprühreagenzien gibt Tabelle 1 Auskunft (eine genaue Arbeitsanweisung zur Herstellung und zur Nachbehandlung findet sich in [6]).

ERGEBNISSE UND DISKUSSION

Die untersuchten Materialien sind in Tabelle 2 aufgeführt. Die Untersuchung des Materials wurde nach dem in Abb. 1 gezeigten Schema durchgeführt. Dieses Schema ist auf einfacher Methodik aufgebaut und führt zu einem groben Überlick über die Nickelverteilung und Bindung an bestimmte funktionelle Gruppen. Die Aussage über die chemische Struktur der Liganden läßt sich durch Kenntnisse über die Inhaltsstoffe des untersuchten Materials meist noch präzisieren. Für spezielle Fragestellungen läßt sich das Schema leicht erweitern bzw. modifizieren, so daß hiermit nur eine systematische Richtung gegeben ist, die sich je nach Anforderungen durch Hinzunahme anderer Techniken oder Methoden an das jeweilige Material anpassen läßt.

Tabelle 3 gibt einen Überblick über Gesamtgehalte, direkt (photometrisch) bestimmbaren Anteil, Filtrationsrückstand und Nickel in verschiedenen Lösungsmittelfraktionen. Die beiden Materialien "Jacobs Kaffee" und "Sir Winston Tea" wurden erst nachträglich zum Vergleich der Essigesterfraktionen verschiedener Tees und Kaffees hinzugenommen. Da es sich hierbei nicht um Instant-Getränke handelt (s. Tabelle 2), wurde der Nickelanteil in Kaffeepulver bzw. Teeblättern mit dem des Getränkes verglichen. Die Ergebnisse finden sich in Tabelle 4.

TABELLE 2

Untersuchte Materialien

Franz. Rotwein	Vin de pays de l'Herault, Vin de table 1978
Ital. Rotwein	Lambrusco Rubino (Perlwein), Großkellerei Girelli S.p.A., Trient
Instant-Tee	Meßmer Tee Gold "Ceylon Blend" gefriergetrocknet
Instant-Kaffee	Nescafé Gold Mocca gefriergetrocknet
Kaffee (Pulver)	Jacobs Kaffee "Krönung" (gemahlen)
Tee (Blätter)	Sir Winston Broken Orange Pekoe Tea

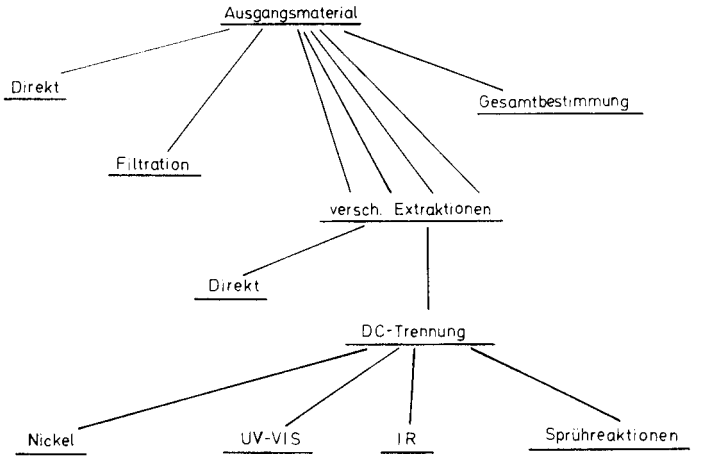

Abb. 1. Allgemeines Untersuchungsschema.

Gesamtgehalte

Vergleicht man die Gesamtgehalte mit Literaturwerten [7, 8], die meist mit anderen Bestimmungsverfahren erhalten wurden, so stellt man eine recht gute Übereinstimmung fest, wobei allerdings zu beachten ist, daß jedes Material je nach Anbaugebiet, Verarbeitungsprozeß und Lagerung unterschiedliche Nickelmengen enthält. Diese Unterschiede können unter Umständen mehrere Zehnerpotenzen ausmachen (z.B. bei Weinen). Die hier erhaltenen Werte stimmen aber größenordnungsmäßig gut mit den vergleichbaren Literaturwerten überein.

Direktbestimmungen

Da in den untersuchten Materialien ein großer Eisenüberschuß vorlag, mußte das photometrische Bestimmungsverfahren mit PAC/Benzol modifiziert

TABELLE 3

Nickel-Gesamtmengen und -Verteilungen in verschiedenen Fraktionen

Material	pH des Getränkes	Gesamt Ni (µg)	% der Gesamtnickelmenge		Extraktionen			
			Direkt	Filtr. Rst.	Essigester	Chloroform	MIBK	Dieth. Ether
Lambrusco	3,4	1,4 in 10 g Wein	54	7,1	36,4	12,1	8,6	(<5)
Fr. Wein	3,3	0,92 in 10 g Wein	82	20,4	6	9,7	9,2	(<5)
Nescafé	5,15	2,2 pro Tasse[a]	59,1	20,9	42,3	59	40	17,3
Meßmer Tee	5,1	3,35 pro Tasse[a]	20	23,2	41,8	41,2	11,6	(<5)

[a]1 Tasse = 1,8 g Kaffee bzw. 1/3 g Tee mit Wasser auf 150 ml aufgefüllt.

TABELLE 4

Nickel in Kaffee und Tee (Rohmaterial) und in den wäßrigen Getränken

Material	Ni in "Rohmaterial"	Ni im Getränk	Ni (EE) / Ni (Getränk) %
Jacobs Kaffee	5,47 μg in 5,4 g[a]	1,95 μg ≈ 35,6% pro Tasse[a]	40
Sir Winston Tea	17,83 μg in 4 g[a]	9,31 μg ≈ 52,2% pro Tasse[a]	12

[a]5,4 g Kaffee bzw. 4 g Tee entsprechen einer Tasse (150 ml).

werden (Maskierung des Eisens durch Fluorid). Ein Überschuß von Fluorid stört aber ebenfalls, so daß die zuzusetzende Fluoridmenge für jedes Material in Vorversuchen ermittelt werden muß (auf Kieselgel 60 mit Aceton als Laufmittel trennt sich überschüssiges PAC von gebildetem Nickelkomplex und bei Anwesenheit von überschüssigem Eisen tritt ein weiterer Fleck auf, so daß die vollständige Maskierung nachgeprüft werden kann; s. auch [3]).

Bei einigen Materialien ist die Anwendung des PAC-Verfahrens durch Bildung einer Emulsion nicht möglich. Hier läßt sich das Verfahren mit PAN/*o*-Dichlorbenzol anwenden. Durch Vergleich beider Verfahren an einem Material wurde festgestellt, daß jeweils der gleiche Wert für den Nickelgehalt gemessen wird. Die direkt bestimmbaren Werte geben den Nickelanteil an, der sich durch das entsprechende photometrische Verfahren in dem wäßrigen Getränk nachweisen läßt. Da hierbei ein Ligandenaustausch stattfindet, kann man auf die Stärke der Bindung des Nickels an organische Moleküle schließen. In Tabelle 5 sind die Bildungskonstanten der PAC— und PAN—Nickelkomplexe aufgeführt. Da beide Verfahren bei verschiedenen pH-Werten und mit verschiedenen Extraktionsmitteln arbeiten und trotzdem zu einheitlichen Werten führen, spielen diese Einflüsse und auch die Unterschiede der Konstanten offensichtlich keine große Rolle. Die direkt bestimmbare Nickelmenge muß wesentlich schwächer gebunden sein und die nicht direkt bestimmbare Nickelmenge wesentlich stärker als es den Bildungskonstanten der Komplexe entspricht. (Bei dieser Überlegung werden kinetische Effekte nicht berücksichtigt).

Vergleicht man die untersuchten Materialien miteinander, so fällt der franz. Wein auf, bei dem die Hauptmenge des Nickels mit 82% direkt bestimmbar und damit relativ schwach gebunden vorliegt, und der "Meßmer Tee", bei dem die Verhältnisse genau umgekehrt liegen.

Filtration und Extraktionen

Die verschiedenen Extraktionen überschneiden sich, so daß man eine Summierung auf 100% mit einer gewissen Berechtigung wohl nur beim franz. Wein durchführen kann, da sich die Werte der Direktbestimmung und der

TABELLE 5

Komplexbildungskonstanten von Nickel mit Pyridylazonaphthol (PAN) und Pyridinaldehydchinolylhydrazon (PAC)

L	log K_1 (für NiL)	log K_1K_2 (für NiL_2)
PAN	12,7	25,3
PAC	10,5	19,9

Filtration nicht wesentlich überschneiden dürften. Dieses Material wurde dann auch nicht weiteruntersucht.

Betrachtet man die Werte der anderen drei Materialien, so fällt auf, daß in der Reihenfolge Ester—Keton—Ether die Nickelmengen ziemlich rasch abfallen, was auf die Polarität der extrahierten Verbindungen schließen läßt. Zur weiteren Untersuchung der organischen Inhaltsstoffe wurde die Essigesterfraktion benutzt, die etwa 40% des Nickel erfaßt. Beim "Sir Winston Tea" beträgt dieser Anteil allerdings nur 12%. Drückt man den Nickelanteil aber nicht in Prozent aus, sondern vergleicht die Absolutwerte (Tabelle 6), so ergeben sich relative konstante Werte für Kaffee und Tee. Die Nickelmenge im Essigester wird also wohl nicht durch eine bestimmte Prozentzahl der Gesamtmenge, sondern durch die Menge der extrahierten organischen Substanz bestimmt, die zur Bindung von Nickel befähigt ist. Dieser Wert ist für Tee etwas höher als für Kaffee.

Direktbestimmung nach Extraktion

Nach Extraktion mit Essigsäureethylester und anschließendem Abdestillieren des Extraktionsmittels am Rotationsverdampfer wurde der Rückstand in Wasser gelöst und die direkt bestimmbare Nickelmenge festgestellt (PAC/Benzol). Die erhaltenen Werte sind in Tabelle 7 zusammengestellt. Bei den beiden Materialien, die in den Extrakten direkt bestimmbares Nickel enthalten ("Nescafé" und "Lambrusco") ergibt sich aus der Differenz von Nickel im Extrakt und direkt bestimmbarem Nickel die Menge der starken Nickelkomplexe. Addiert man diesen Wert zu gesamt direkt bestimmbarer Menge und zum Wert der Filtration, so ergibt sich beim "Nescafé" etwa 100%, d.h. bei diesem Material lassen sich alle nicht direkt bestimmbaren Nickelverbindungen mit Essigester extrahieren. Beim ital. Wein und beim "Meßmer

TABELLE 6

Nickel-Gesamtmengen in Essigsäureethylester-Extrakten von Kaffee und Tee[a]

	Nescafé	Jacobs K.	Meßmer Tee	Sir Winston Tee
Ni in EE (µg)	0,93	0,78	1,4	1,1

[a]Die angegebenen Nickelmengen beziehen sich auf je 150 ml des Getränkes (s. auch Tabellen 3 und 4).

TABELLE 7

Direkt bestimmbare Nickelanteile in Essigsäureethylester-Extrakten

Material	% der Gesamtnickelmenge			
	Ni in EE (gesamt)	davon direkt	Differenz (starke K.)	Σ [a]
Lambrusco	36,4	11,1	25,3	86,4
Fr. Wein	6	(<5)	6	108,4
Nescafé	42,3	19	23,3	105,5
Meßmer Tee	41,8	(<5)	41,8	85,0

[a] Σ = Gesamt-Direktbestimmung (s. Tabelle 3) + Filtrations-Rückstand (s. Tabelle 3) + starke Komplexe in EE.

Tee" bleibt eine Differenz von ca. 15%, die sich weder direkt bestimmen noch mit Essigester extrahieren läßt.

Chromatographie

Zur genaueren Bestimmung von funktionellen Gruppen, an die Nickel gebunden ist, wurde der Essigsäureethylesterextrakt chromatographiert, um dann nach weiterer Fraktionierung eine genauere Aussage über vorliegende Bindungsformen zu erhalten.

Sprühreagenzien. Die getrockneten Chromatogramme wurden mit den in Tabelle 1 aufgeführten Sprühreagenzien auf funktionelle Gruppen untersucht. Zusätzlich wurde die Fluoreszenz unter der UV-Lampe (366 nm) und die Fluoreszenzlöschung bei 254 nm beobachtet. Die Reagenzien wurden einmal nach Gruppen ausgewählt, von denen bekannt ist, daß sie Komplexbindungen zu Nickel bilden können wie —OH, —NH, $\rangle$C=O etc., andererseits wurden einige Reagenzien nach den bekannten Inhaltsstoffen der Materialien ausgewählt (z.B., Chloramin T für Koffein). Nicht alle Sprühreagenzien sind für jedes Material geeignet; andererseits treten auch einige Überschneidungen auf, was aber zu einer größeren Sicherheit der Aussage führt.

Mit Hilfe der Sprühreaktionen und der Fluoreszenz wurden die Chromatogramme in jeweils 5 Fraktionen eingeteilt, in denen dann später die Nickelmenge bestimmt wurde. Die Diagramme in Abb. 2 zeigen schematisch die Verteilung von funktionellen Gruppen in den Materialien und die Einteilung in Fraktionen. Die Diagramme geben zwar nur einen ersten Überblick, aber es treten doch charakteristische Verteilungsmuster auf, die bei den beiden Kaffees oder Tees ziemlich ähnlich sind, sich aber zwischen Kaffee, Tee und Rotwein unterscheiden. Bei allen Materialien ist Fraktion 5 nur wenig oder gar nicht anfärbbar, was auf wenige charakteristische Gruppen schließen läßt.

UV—VIS-Spektren. Zusätzliche Informationen über die organischen Substanzen kann man relativ einfach durch Aufnahme von UV—VIS-Spektren [9] (210—500 nm) erhalten. Hierfür können die methanolischen Lösungen, die beim Eluieren der Chromatogramme erhalten werden, direkt benutzt

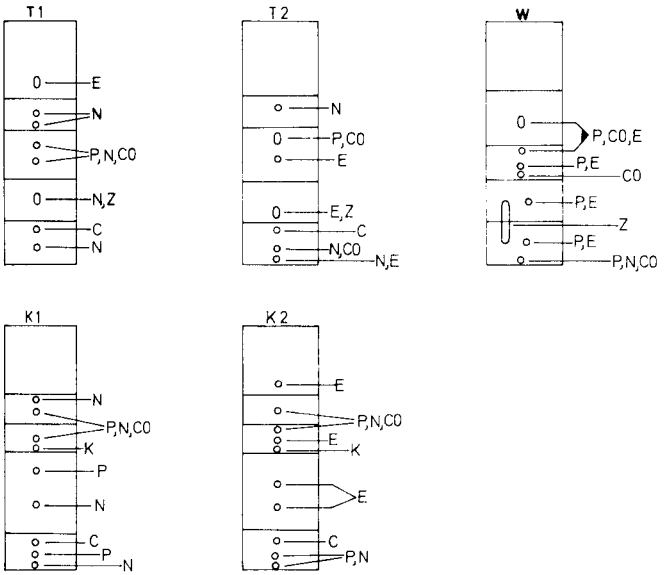

Abb. 2. Verteilung von Substanzen mit speziellen funktionellen Gruppen auf DC-Schichten (Kieselgel/Essigsäureethylester). T1, Meßmer Tee; T2, Sir Winston Tee; W, Lambrusco; K1, Nescafé; K2, Jacobs Kaffee; C, Koffein; CO, Carbonylgruppen; E, Höhere Alkohole, Steroide, eth. Öle; K, Kaffeesäure; N, stickstoffhaltige Subst. (Amine, Alkaloide, etc.); P, Phenole; Z, Zucker. Die Unterteilungen der Diagramme geben die Fraktionsgrenzen für die Elution an (s. experimenteller Teil).

werden. Aus den erhaltenen Spektren läßt sich zwar wenig über funktionelle Gruppen aussagen, aber einiges über die Art des Molekülgerüstes (aromatisch, konjugiert, etc.). Abbildung 3 gibt einen Überblick über die Absorptionsmaxima in den einzelnen Fraktionen (unabhängig von der jeweiligen Intensität). Aus den Lagen der Maxima sind Ähnlichkeiten und Unterschiede der einzelnen Materialien zu erkennen. Die hieraus gewonnenen Aussagen über aromatische Verbindungen, phenolische Gruppen, etc., decken sich weitgehend mit den Erkenntnissen aus den Sprühreaktion. Zusätzlich erkennt man in Fraktion 1 der Tees und Kaffees z.B. einen (sehr intensiven) Peak bei etwa 270 nm, der vom Koffein herrührt (s. auch unten). Wichtig ist die Auswertung der Spektren auch im Hinblock auf die Gesamtmenge an organischer Substanz, die man sonst wegen der kleinen Mengen auf den Chromatogrammen kaum bestimmen kann. Aus der Wasseranalytik ist bekannt, daß die gemessenen Extinktionen bei ca. 220 nm proportional zu CSB-Wert und totalem org. Kohlenstoffgehalt (TOC) ansteigen [10]. Eine graphische Darstellung der Verteilung der organischen Substanz in den verschiedenen Fraktionen ist in den Diagrammen der Abb. 4 zu sehen (s. unten).

IR-Spektroskopie. Eine zusätzliche Möglichkeit zur Beurteilung der organischen Substanzen ergibt sich durch die IR-Spektroskopie. Die Anwendung ist allerdings schwieriger, weil größere Mengen benötigt werden

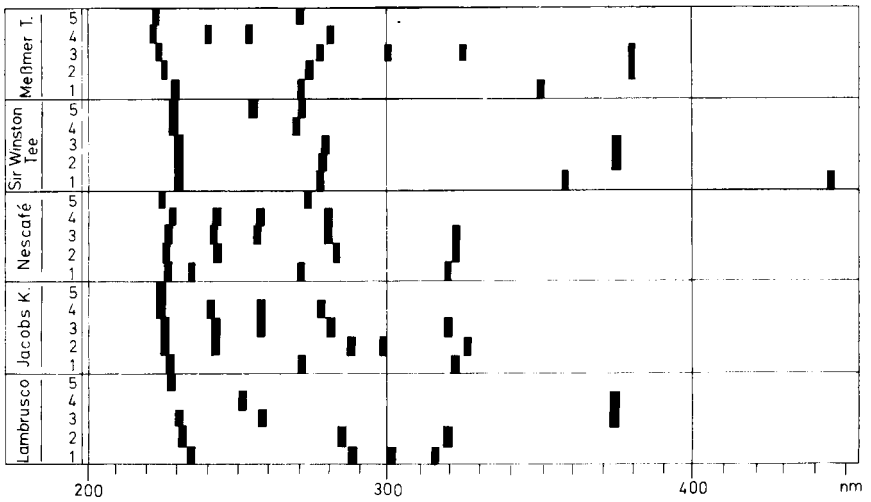

Abb. 3. UV—VIS Absorptionsmaxima in DC-Fraktionen der verschiedenen Materialien nach Essigsäureethylester-Extraktion. Die Ziffern 1—5 geben die Fraktionen aus der DC an (s. auch Abb. 2).

und bei Spektren von ganzen Fraktionen die Interpretation durch Überlagerungen erschwert wird. (Auch Restspuren von Kieselgel oder Wasser stören). Anhand des "Jacobs Kaffees" wurde die Verwendbarkeit von IR Spektren überprüft. Man findet phenolische OH Gruppen, charakteristische Banden für Aromaten und Doppelbindungen, C=O Gruppen, etc. Bei Vorliegen von Vergleichsspektren können auch ganze Substanzen oder Substanzgruppen festgestellt werden (in Fraktion 1 läßt sich das Koffein-Spektrum ziemlich deutlich wiederfinden). Die IR-Spektroskopie ist also gut für gezielte Nachforschungen geeignet, während die Anwendung auf größere Fraktionen ohne Anhaltspunkte wenig bringt.

Nickelmengen (Vergleich mit organischen Substanzen)

Um die gewonnenen Aussagen über die organischen Substanzen mit Nickelmengen zu vergleichen, wurde in den einzelnen Fraktionen nach Verfahren 2 der Nickelgehalt bestimmt. Das Ergebnis ist in Abb. 4 graphisch dargestellt. (Beim Vergleich von Nickelmenge und organischer Gesamtmenge ist zu beachten, daß keine Absolutwerte dargestellt sind, sondern Prozent der jeweiligen Gesamtmenge.) Eine eindeutige Korrelation von Nickelmenge und organischer Gesamtmenge läßt sich nicht feststellen. Diagramm 6 (Abb. 4) zeigt die Nickelverteilung im "Jacobs Kaffee" nach Zusatz von etwa 150% ($\approx$3 μg) Nickel. Absolut gesehen haben alle Fraktionen zugenommen, allerdings die Fraktionen 1, 3 und 4 überproportional stark.

Vergleicht man die Verteilungsmuster (in Bezug auf Nickel) der einzelnen Materialien, so erkennt man bei den drei Gruppen Kaffee, Tee und Wein je ein charakteristisches Muster in den Fraktionen 2—5. Innerhalb einer Gruppe

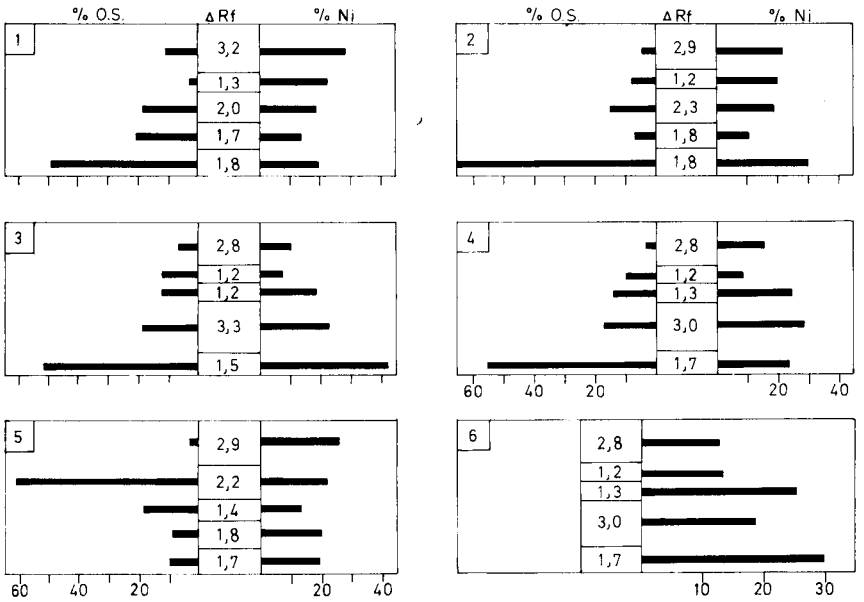

Abb. 4. Darstellung der prozentualen Verteilungen von Nickel (Ni) und organischer Substanzen (O.S.) auf die DC-Fraktionen für verschiedene Materialien. ΔR_f, Höhe der Fraktionen in R_f-Einheiten (×10). (1) Meßmer Tee; (2) Sir Winston Tee; (3) Nescafé; (4) Jacobs K.; (5) Lambrusco; (6) Jacobs K. + 150% Ni (Zusatz von 3 µg Ni; Probe wie 4).

treten Unterschiede außer in den Gesamtmengen hauptsächlich in Fraktion 1 auf (Fraktion mit den polarsten Substanzen).

Aus einer Kombination der gewonnenen Aussagen über organische Liganden und Nickelkonzentrationen ergibt sich die Feststellung, daß das Nickel über den gesamten R_f-Bereich verteilt ist; es treten aber je nach Material doch gewisse Unterschiede auf. So ist die Nickelverteilung beim Wein relativ gleichmäßig, während bei Kaffee und Tee die Fraktionen 1 und 3 + 4 überproportional viel Nickel enthalten. Dies sind auch die Fraktionen, die bei Zugabe eines Nickelüberschusses am meisten zunehmen. Diese Fraktionen sind hauptsächlich durch viele phenolische OH-Gruppen, aromatische NH-Gruppen und C=O-Gruppen charakterisiert. Solche Gruppierungen treten in Tee und Kaffee verstärkt in Form von Gerbstoffen wie Catechinen, Chlorogensäuren, Flavonolen, Kaffeesäure, Chinasäure, etc., auf. Diese Moleküle scheinen bei der Bindung von Nickelspuren eine wichtige Rolle zu spielen. Zusätzlich fällt auf (vor allem beim Tee), daß in Fraktion 5, die sich kaum anfärben läßt und auch wenig organische Substanzen enthält, doch relativ viel Nickel gebunden ist. Nach den Daten aus UV- und IR-Spektren kann diese Fraktion nur aus größeren aliphatischen Molekülen mit einigen Doppelbindungen und/oder Substituenten wie —OH, R—OH—, etc. bestehen (Steroide, Terpene, u.ä.).

Mit den hier angewandten einfachen Untersuchungsmethoden ist eine trendmäßige Aussage über Nickelbindungsformen möglich. Bei Vorliegen von mehr Vergleichsdaten wäre es durchaus denkbar, Aussagen über eventuelle Kontaminationen machen zu können (s. Änderung des Ni-Verteilungsmusters im Kaffee bei zugesetztem Nickelüberschuß).

LITERATUR

1 R. Fukai und L. Huynh-Ngoc, J. Oceanogr. Soc. Jpn., 31 (1975) 179.
2 T. M. Florence und G. E. Batley, Crit. Rev. Anal. Chem., 9 (1980) 219.
3 G. Weber, G. Schwedt, Fresenius Z. Anal. Chem., 1981, in Druck.
4 K. L. Cheng und B. L. Goydish, Microchem. J., 7 (1963) 166.
5 Organikum, 15. Auflage, VEB Deutscher Verlag der Wissenschaften, Berlin, 1977, S. 80.
6 E. Merck (Herausgeber), Aufärbereagenzien für Dünnschicht-und Papierchromatographie, Darmstatt, 1980.
7 H. Eschnauer, Spurenelemente in Wein und anderen Getränken, Verlag Chemie, Weinheim, 1974.
8 D. Schlettwein-Gsell und S. Mommsen-Straub, Spurenelemente in Lebensmitteln (Beiheft Nr. 13 zur Internationalen Zeitschrift für Vitamin- und Ernährungsforschung), Verlag H. Huber, Bern, 1973, S. 62—70.
9 A. I. Scott, Interpretation of the Ultraviolet Spectra of Natural Products, Pergamon, Oxford, 1964.
10 N. Ogura und T. Hanja, J. Water Pollut. Contr. Fed., 40 (1968) 464.

Analytica Chimica Acta, 134 (1982) 93—100
Elsevier Scientific Publishing Company, Amsterdam — Printed in The Netherlands

A PHOSPHORUS-SENSITIVE MOLECULAR EMISSION CAVITY ANALYSIS DETECTOR FOR HIGH-PERFORMANCE LIQUID CHROMATOGRAPHY

M. J. COPE[a] and ALAN TOWNSHEND*[b]

Chemistry Department, Birmingham University, P.O. Box 363, Birmingham, B15 2TT (Gt. Britain)

(Received 30th July 1981)

SUMMARY

Molecular emission cavity analysis is adapted to monitor organophosphorus compounds emerging from both normal-phase and reversed-phase columns. Reproducibility of detection was ca. 3% (using peak area measurements) and sub-microgram quantities were easily detectable. The detector consists of a water-cooled duralumin disc with 40 cavities drilled into its circumference. Eluent is collected in the cavities and rotated stepwise into a H_2—N_2—air flame where the HPO emission is monitored at 528 nm. During rotation, the bulk mobile phase is completely evaporated. Examples are given of separations of phosphate esters, phosphonates, pyrophosphonates, phosphonic acids and pesticides. The detector also operates as a sulphur-selective detector at 384 nm.

Very little work has been reported on the high-performance liquid-chromatography (h.p.l.c.) of organophosphorus compounds. This has probably been due to the lack of a suitably sensitive and selective detector. In 1976 Szalontai [1] described the successful separation of a number of phosphorus esters using h.p.l.c., employing a non-selective flame-ionization detector. Julin et al. [2] reported the coupling of an h.p.l.c. system to a flame spectrophotometer via a modified nebuliser arrangement. The detector was sensitive to phosphorus and sulphur compounds in aqueous solvents, but not readily usable with organic eluents, because many organic solvents quench HPO and S_2 emissions [3]. More recently, Chester [4] described a dual flame photometric detector aimed at decreasing these solvent interferences and McGuffin and Novotny [5] have designed a single burner system which can accommodate solvents containing up to 50% of certain organic liquids. As solvents play such a large part in the quenching of molecular emissions, it seemed expedient to completely evaporate the solvent prior to detection.

---

[a]Present address: Department of Instrumentation and Analytical Science, UMIST, P.O. Box 88, Sackville Street, Manchester M60 1QD.

[b]Present address: Department of Chemistry, University of Hull, Hull HU6 7RX.

Developments in flame emission spectrometry led, in 1973, to the introduction of molecular emission cavity analysis (m.e.c.a.) [6]. A few microlitres of sample are placed within a small cavity and introduced, after solvent evaporation, into a premixed hydrogen—nitrogen—air flame. A molecular emission is stimulated within the cavity (e.g., HPO from phosphorus compounds) which is enhanced by the cool cavity walls (the so-called Salet phenomenon). The technique has already been successfully employed for the determination of nanogram-amounts of organophosphorus compounds, based on their HPO emission [7], and it seemed promising to adapt the technique to the detection of organophosphorus compounds in an h.p.l.c. eluent. To do this, three main problems had to be overcome [8]: firstly, evaporation of the bulk solvent prior to introduction of the sample into the flame; secondly, preservation of the resolution of the separated organophosphorus compounds between the column outlet and the detection site; thirdly, continuous m.e.c.a. detection of the eluent as it emerges from the h.p.l.c. column.

EXPERIMENTAL

Detector design

The m.e.c.a. detector consists of a duralumin disc (10-cm diameter) with 40 cylindrical cavities (6-mm diameter, 6-mm depth) drilled into its circumference. The disc is powered by a stepper motor and rotated in an anticlockwise direction (Fig. 1). The stepper motor is controlled by a Digitical Indexer

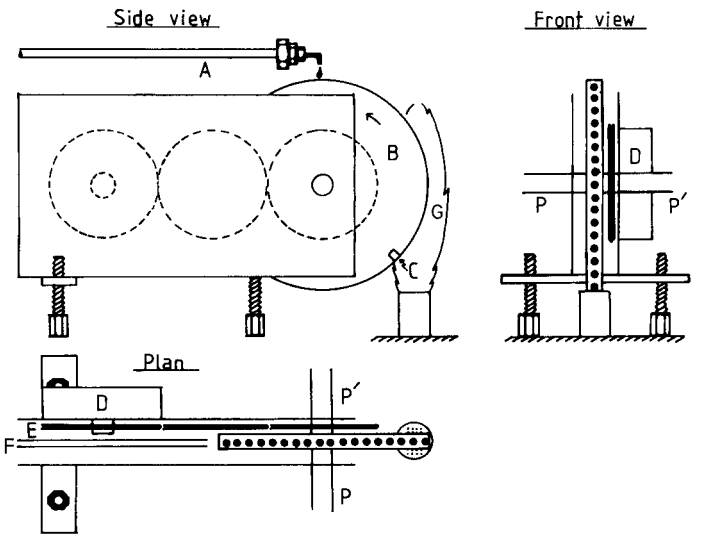

Fig. 1. Detector based on m.e.c.a. (A) H.p.l.c. column; (B) duralumin disc with 40 cylindrical cavities drilled into its circumference; (C) cavity position for measuring emission; (D) stepper motor; (E) gears connecting stepper motor to disc; (F) tube from air pump to aid in solvent evaporation; (G) flame; (P,P') inlet and outlet pipes for water.

(Unimatic Engineers Ltd., 122 Granville Road, London) and a custom-built timer unit. Usually one drop of eluent is collected per cavity, as shown. This cavity then steps on and the following drop is collected in the next cavity, and so on. The index time of the stepper motor (time between steps) is set to a value between 1 and 3 s so as to be synchronized with the drop time. The delay must also be sufficient to allow HPO emission to be generated in the cavity entering the flame (see below) because maximum emission occurs a few seconds after the cavity has entered the flame.

Because the disc is positioned in a hydrogen flame it normally requires constant cooling. Water is pumped from a thermostatted bath, through the inner brass cooling chamber of the disc (Fig. 2), so that the surface temperature of the disc always remains constant. During rotation of the disc, solvent evaporation takes place. This is accomplished by adjusting the temperature of the disc to an appropriate value, and by using a small air inlet positioned as shown. After solvent evaporation, the sample band, which is usually distributed between about 7 cavities, is carried round into the flame. The green HPO emission is most intense at the flame edge when the cavity enters the flame at 45° below the horizontal. After emission measurement, the cavities pass through the bulk of the flame where most residual phosphorus compound is removed, and step round to the vertical position where they collect more eluent.

The detector was placed within a modified Evans Electroselenium (EEL) 240 atomic absorption spectrometer, operated in the emission mode. An EEL emission burner head (diameter 2.5 cm) was used throughout. The emission is detected at 528 nm with the slit set to collect a spectral bandwidth of 3 nm. The signal is registered on a Servoscribe 1S chart recorder (response time 0.5 s) connected to the 10-mV output of the detector.

Chromatographic instrumentation

The pump used was an Altex model 100, dual-position reciprocating pump. An Altex injection valve was also used, with a 20-μl sample loop;

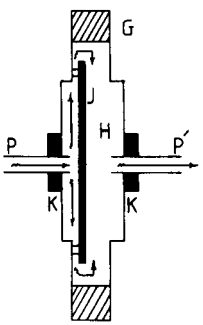

Fig. 2. Front-view section of the m.e.c.a. detector illustrating its water-cooling system. The disc rotates around the stationary inlet and outlet pipes (P,P'); (G) outer aluminium ring (containing cavities); (H) inner brass cooling chamber; (J) deflector plate; (K) water seals.

however, the loop was only partly filled with a 10-μl slug of the sample. The columns and eluents used will be mentioned in particular examples later. Stainless steel pipework (0.25 mm i.d.) with low dead volume was used between the column outlet and the detector. A few cm of such pipework was connected to the column outlet and bent at right angles about 5 mm from its end, as shown in Fig. 1. Eluent flowing from the column was broken up into drops at this point, for introduction into the cavities.

Reagents

Analytical-grade reagents were used in the case of the phosphate esters (BDH Ltd.). The phosphonates, pyrophosphonates and phosphonic acids were synthesised at the Chemical Defence Establishment, Porton Down. Sample solutions were mostly made up in water; in some cases, methanol was used. Analytically pure solvents were used for the h.p.l.c. mobile phase.

RESULTS AND DISCUSSION

Reproducibility and optimization of the response

The typical m.e.c.a. HPO response from a single cavity is an emission—time peak, the height or area of which is proportional to the concentration of the phosphorus compound. The sensitivity changes with the identity of an organic phosphorus compound, so that a different calibration graph is required for each compound [7]. The sensitivity also depends on the size and shape of the cavity, its position in the flame, and the condition and reflectivity of the cavity surface. Thus in order to achieve reproducible signals from a sequence of 40 cavities drilled into the circumference of a disc, it is essential that the cavities are all drilled to the same dimensions, to a tolerance of ca. 0.125 mm, or better. The disc must rotate exactly symmetrically. When this was achieved, the freshly drilled cavities gave emissions differing in peak height by less than 5%. During use, the surface properties of the cavities change, thus decreasing the intensity, but to different extents for each cavity. This is partly the result of reflectance changes. However, a cavity can be restored to its original performance by adding a few drops of 1 M sodium hydroxide, allowing to react for 1 min, and then washing well with water.

Before the disc was used for chromatographic detection, the performance of a single cavity for phosphorus detection was optimized by injection of 5-μl aliquots of a 100 mg P l^{-1} solution of triethyl phosphate. The flame composition which gave greatest intensity was 4.0 l H_2 min^{-1}, 1.8 l N_2 min^{-1} and 2.75 l air min^{-1}; this was used in all the following work. The greatest intensity was achieved when the cavity entered the edge of the flame at a position of 45° below the horizontal (Fig. 1). The detector was adjusted to view the emission from the cavity in this position. Under these conditions, triethyl phosphate gave a linear calibration graph (peak height) for 10—100 ng of phosphorus, with a 2σ detection limit of 5 ng of phosphorus.

Applications to high-performance liquid chromatography

The performance of the disc for h.p.l.c. detection was next tested. Six identical injections of 8 μg of triethyl phosphate onto an adsorption column gave the responses shown in Fig. 3. The relative standard deviation was 22% by peak height, but only 3% by peak area. It can be seen that the shape of the responses varies considerably. This arises because the eluent stream is broken into drops prior to detection. Each drop gives a characteristic m.e.c.a. peak, so that the overall chromatographic "peak" is a sequence of m.e.c.a. peaks, the relative heights of which depend on the concentration in each drop. The distribution of the sample band over several cavities is not exactly reproducible for each run, so that the distribution of peak heights also varies. Thus peak area is a more suitable quantity to measure than peak height when this detection is used, as the total emission intensity is proportional to total phosphorus concentration, irrespective of the distribution amongst cavities.

Figure 4(a) shows the separation of three phosphate esters. It was possible to separate these closely-related homologues by adsorption chromatography. The member of the series with the least molecular weight was retained the longest and less retention occurred as the series was ascended. This is probably because the specific interaction between the P—O groups and the adsorbent is sterically hindered as the size of the alkyl group increases.

Because many organophosphorus compounds are difficult to remove from surfaces, after these compounds have passed through the flame, small amounts sometimes remain in the cavities. As these cavities revolve into the flame for a second time they re-emit, giving a smaller, memory peak. Examples are shown in Fig. 4. Memory effects may be decreased by increasing the surface temperature of the disc (water-bath temperature); however, this

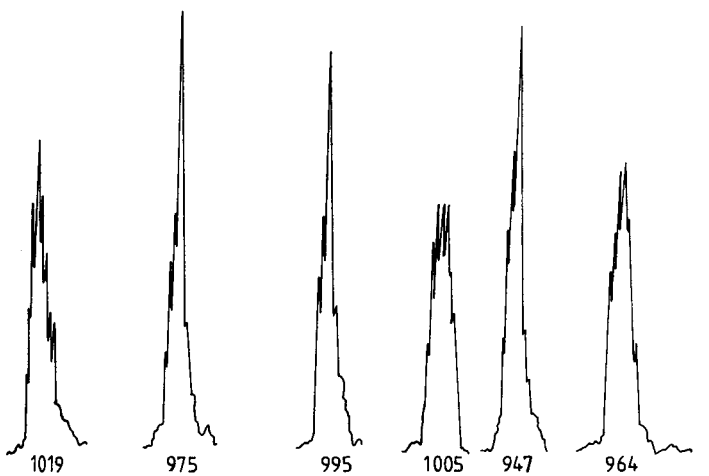

Fig. 3. Chromatograms from six identical injections of 8 μg of triethyl phosphate. Retention time 8.5 min. Lichrosorb 10-μm adsorption column (25 cm × 3.2 mm i.d.); mobile phase, methanol at 0.2 ml min^{-1}; 400 psi; water-bath temperature, 30°C; chart speed, 30 mm min^{-1}. The numbers below the peaks denote their relative peak areas.

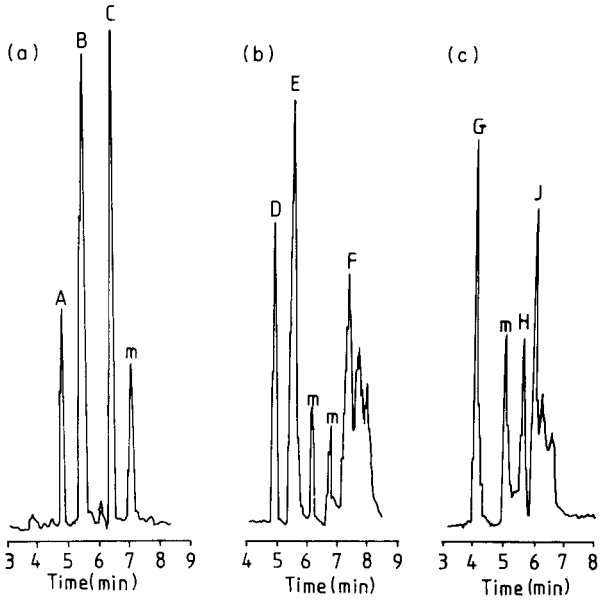

Fig. 4. Phosphorus-selective chromatograms from Partisil 5-μm adsorption columns (25 cm × 4.6 mm i.d.). (a) Chromatogram of (A) tributyl phosphate (3.15 μg P), (B) tripropyl phosphate (3.13 μg P) and (C) triethyl phosphate (1.67 μg P); hexane/isopropanol (80:20) mobile phase at 0.9 ml min^{-1}, 430 psi, index time 2.2 s, water-bath temperature 36°C. (b) Chromatogram of (D) dibutyl methylphosphonate (2.13 μg P), (E) diisopropyl methylphosphonate (2.8 μg P) and (F) diethyl methylphosphate (5.09 μg P); hexane/ethanol (80:20) mobile phase at 0.9 ml min^{-1}, 460 psi, index time 1.9 s, water-bath temperature 40°C. (c) Chromatogram of (G) diethyl dimethylpyrophosphonate (2.74 μg P), (H) dipinacolyl dimethylpyrophosphonate (3.6 μg P) and (J) dibutyl dimethylpyrophosphonate (1.86 μg P); mobile phase as for (b), index time 1.36 s, water-bath temperature 37.5°C. Peaks marked (m) are memory effects.

is sometimes achieved at the expense of sensitivity, as in the case of these esters, owing to the lesser effect of the Salet phenomenon at higher temperatures. A future solution to this problem appears to lie in the positioning of an intense flame jet between the hydrogen flame and the eluent collection point. This will remove any traces of organophosphorus compounds not burnt out by the hydrogen flame. In the present studies, care was taken to adjust the chromatographic conditions so that memory peaks usually fell between the true sample peaks. For a three-component mixture this was reasonably simply achieved.

Figure 4(b) depicts the separation of three methyl phosphonates. Their order of retention is similar to that of the phosphate esters in Fig. 4(a). However, a mobile phase of greater polarity is necessary to remove them from the column, because their dipole moment is greater than that of the phosphate esters. As retention in adsorption chromatography is largely the

result of hydrogen bonding, the larger the dipole moment, the greater the retention.

Pyrophosphonates are difficult to separate by gas chromatography because of their involatility; if they are heated until they become volatile, they begin to decompose. Consequently, h.p.l.c. should be a more favourable means of separation. Figure 4(c) shows the separation of three pyrophosphonates by adsorption chromatography. In general, their order of retention was found to be in the order of increasing molecular weight, but dipinacolyl dimethylpyrophosphonate eluted earlier than would be expected from its molecular weight (Table 1).

Figure 5 shows the separation of two phosphonic acids by reversed-phase chromatography. Formic acid (0.1 M, pH 2.55) was used as the mobile phase. With acids, a higher m.e.c.a. sensitivity is obtained when the disc temperature is greater than 90°C. For this reason, the rotating disc was operated without water cooling, so as to find its own equilibrium temperature (ca. 95°C). When water is dropped onto such a hot metal surface, normal evaporation does not occur because the liquid does not wet the surface, and becomes partially insulated from it by a layer of vapour which retards evaporation (the Leidenfrost phenomenon) [9]. In such cases, it is necessary to increase the eluent flow rate so that eluent is sprayed onto the disc surface rather than falling in drops. The eluent is thus forced to wet the cavity surface and sensible evaporation of the solvent occurs.

The m.e.c.a. detector may also be made selective for sulphur compounds. Figure 6 shows the separation of three common pesticides containing both phosphorus and sulphur. In this case the molecular emissions are measured at 384 nm. The detector could also be used to monitor other elements which produce molecular emissions in hydrogen flames (selenium, halides, etc.) [10]. It might also find use as a detector for other flow methods of analysis, and the concept of a rotating metal disc might also be considered as a transport device for the flame ionization detector, thus eliminating solvent effects.

TABLE 1

Retention times of some dimethylpyrophosphonates with various mobile phases (Lichrosorb 10-μm column, 25 cm × 3.2 mm i.d.; flow rate, 1.3 ml min^{-1}; pressure 330 psi.)

Mobile phase		Retention time[a] (s)				
		DiEt	$DiPr_n$	$DiPr_i$	$DiBu_n$	DiPin
Dichloromethane—isopropanol	(95:5)	135	205	—	205	200
	(90:10)	125	230	225	220	210
Dichloromethane—methanol	(95:5)	125	175	180	180	135
	(90:10)	125	150	150	145	135

[a]Et = ethyl, etc.; Pin = pinacolyl.

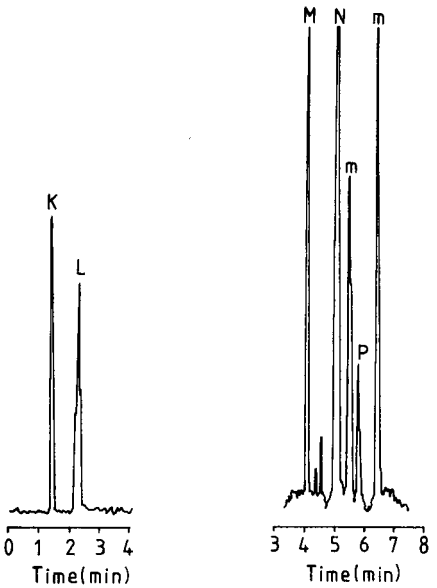

Fig. 5. Phosphorus-sensitive chromatogram of (K) methylphosphonothionic acid (10.8 μg P) and (L) ethyl methylphosphonic acid (15.7 μg P). Conditions: Partisil 10-μm reversed-phase ODS column (10 cm × 5 mm, i.d.); 0.1 M formic acid mobile phase at 2.0 ml min^{-1}, 1040 psi; no water cooling.

Fig. 6. Sulphur-selective chromatogram of three pesticides: (M) phorate (723 ng S), (N) malathion (2.75 μg S) and (P) guthion (5.77 μg S); (m) memory effects. Conditions: Partisil 5-μm adsorption column (25 cm × 4.6 mm i.d.); cyclohexane/isopropanol (95:5) mobile phase at 0.9 ml min^{-1}, 850 psi; detector 384 nm; index time 1.9 s; water-bath temperature 60° C.

This work was supported by an SRC CASE award in collaboration with the Chemical Defence Establishment, Porton Down. The authors thank Mr. S. Travers for constructing the device.

REFERENCES

1 G. Szalontai, J. Chromatogr., 124 (1976) 9.
2 B. G. Julin, H. W. Vandenborn and J. J. Kirkland, J. Chromatogr., 112 (1975) 443.
3 T. L. Chester, Anal. Chem., 52 (1980) 638.
4 T. L. Chester, Anal. Chem., 52 (1980) 1621.
5 V. L. McGuffin and M. Novotny, Anal. Chem., 53 (1981) 946.
6 R. Belcher, S. L. Bogdanski and A. Townshend, Anal. Chim. Acta, 67 (1973) 1.
7 R. Belcher, S. L. Bogdanski, O. Osibanjo and A. Townshend, Anal. Chim. Acta, 84 (1976) 1.
8 M. J. Cope, Anal. Proc., 17 (1980) 273.
9 K. J. Baumeister, R. C. Hendricks and T. D. Hamill, NASA TN D-3226, 1966.
10 S. L. Bogdanski, M. Burguera and A. Townshend, CRC Crit. Rev. Anal. Chem., 10 (1981) 185.

Analytica Chimica Acta, 134 (1982) 101—109
Elsevier Scientific Publishing Company, Amsterdam — Printed in The Netherlands

TEMPERATURE DEPENDENCE OF ELECTROCHEMICAL DETECTION FOR LIQUID CHROMATOGRAPHY

DAVID J. MINER
Lilly Research Laboratories, Indianapolis, IN 46285 (U.S.A.)
(Received 9th July 1981)

SUMMARY

The temperature dependence of amperometric response to compounds commonly assayed by liquid chromatography with electrochemical detection is reported. Temperature dependence ranges from 1.5 to 9% change in response per degree. Both diffusion and heterogeneous electron transfer contribute to temperature-induced variability. Controlling the temperature of the chromatographic column markedly reduces the effect of ambient temperature on the electrochemical detector. The efficiency of using different internal standards to compensate for temperature effects is shown to depend on the electrochemical similarity of the standard and the analyte. Several additional approaches to minimization of temperature dependence are discussed. Alteration of detector temperature for the enhancement of signal-to-noise ratio has little advantage.

Numerous factors affect the precision and accuracy of liquid chromatographic (l.c.) measurements. Although the importance of factors such as precise delivery of eluent by the l.c. pump are widely recognized [1], others are not. The impetus for the work described here came from observations made during the determination of enviroxime and zinviroxime in biological media by liquid chromatography with electrochemical detection (l.c./e.c.) [2]. When lengthy unattended l.c. runs were made, the peak heights of standards were observed to decrease 5—15% during the late evening and then return to their initial heights the following day. This behavior could not be explained by changes in chromatographic retention time but paralleled the cycle of the room temperature. The effect which temperature has on traditional electrochemical determinations is well known, but the importance of controlling detector temperature in l.c./e.c. has not been thoroughly explored [3, 4]. This paper describes detailed investigations of the influence of temperature on an amperometric electrochemical detector for liquid chromatography.

EXPERIMENTAL

Equipment and reagents

The liquid chromatograph was assembled from a Waters Associates model 6000A pump, a Rheodyne 7120 injection valve and 20-μl loop, and a 25 cm ×

0003-2670/82/0000-0000/$02.75

4.6 mm DuPont column packed with 6 μm Zorbax C8 material. The column was thermostatted using a Bioanalytical Systems LC-22/23 block heater. A 24-cm section of 0.3-mm i.d. teflon tubing joined the column to the detector cell. A conventional thin-layer amperometric detector cell [5], constructed of Kel-F (Bioanalytical Systems TL-5) was employed. The glassy carbon working electrode was repolished between experiments using a suspension of 0.05-μm alumina on a Texmet polishing pad (Buehler). The cell was equipped with a 127-μm spacer gasket and a Ag/AgCl/3 M NaCl reference. The pin which provided electrical contact to the working electrode was sealed at the cell block with epoxy. For most experiments, the cell was immersed in a small bath of hexane, mounted in a water bath thermostatted by an immersion circulator (Polytemp, Polyscience). A Bioanalytical Systems LC-4 cell controller was connected to the cell, to a Perkin Elmer model 56 recorder and to a central chromatographic data acquisition system. This data system measured retention times, peak heights and peak areas.

Mobile phases were prepared with distilled deionized water, analytical reagent-grade chemicals and chromatographic methanol (Tedia). Prior to use, mobile phases were filtered through 0.2-μm Nylon filters (Ultipor, Pall) and degassed by refluxing. Most of the compounds tested were obtained commercially. *N*-(4-Hydroxyphenyl)propionamide and *N*-(4-hydroxy-3-methylphenyl)acetamide were a gift from Dr. P. T. Kissinger, Purdue University.

Procedures

Chromatography. Acetaminophen and its analogs were chromatographed with 0.1 M citrate buffer (pH 4.0) and methanol (86:14) as the mobile phase. The flow rate was 1.0 ml min^{-1} and the column temperature was 30°C. Approximately 25 ng of each compound was injected. Enviroxime, zinviroxime and the stilbestrols were chromatographed with 0.1 M sodium acetate/methanol (34:66) plus 6 mg of disodium-EDTA per liter as the mobile phase. The flow rate was 0.9 ml min^{-1} and the column temperature 29°C. Approximately 60 ng of each compound was injected. The catecholamines were chromatographed with 1.4% monochloroacetate (pH 3.0) and methanol (95:5) as the mobile phase. Sodium octyl sulfonate (25 mg l^{-1}) and disodium-EDTA (0.38 g l^{-1}) were also added to this solution. The flow rate was 1.0 ml min^{-1} and the column temperature 28°C. Approximately 40 ng of each compound was injected.

Hydrodynamic voltammetry. The voltammetric characteristics of the compounds were determined under their chromatographic conditions by making repetitive injections of the same sample at different working electrode potentials. The initial injection was made at a potential high enough to give diffusion-limited response. Before each subsequent injection, the potential was lowered and the background current allowed to stabilize. Peak heights were then ratioed to the height at the initial potential. The equation for Nernstian response was fitted to the potential vs. peak height data using a non-linear least-squares estimation. The fit generated estimates of the half-wave potential and apparent reversibility ($E_{3/4} - E_{1/4}$).

Temperature dependences. Temperature dependences were estimated by repetitive injection of a single sample. For all runs, the initial temperature was near 0° and data were taken up to 45°C. A second-order polynomial was fitted to the temperature vs. response data using a least-squares computation. The resulting polynomial was used to calculate the temperature dependence at 22°C. All data reported in this paper were calculated from peak heights, but use of peak areas gave essentially the same results.

Alternative configurations. The effect of configuration on the observed temperature dependences was studied by comparing the setup detailed above to two others. In the first, the e.c. cell was mounted in a chamber of air in the thermostatted bath, instead of being immersed in hexane. For the other, a 58-cm length of small-bore stainless steel tubing was used to connect the column to the cell (immersed in hexane). Most of this tubing was submerged in the thermostatted bath.

RESULTS AND DISCUSSION

The importance of the temperature dependence of amperometric l.c./e.c. response was initially established by estimating the effect for several sets of analytes commonly determined by l.c./e.c. Typical curves obtained are depicted in Fig. 1. Response was linearly related to temperature for some of the systems studied (e.g., *cis*-DES), while others such as hexestrol exhibited upward curvature. The slope of each curve at 22° was taken as the temperature dependence. The results of a series of these experiments are summarized in Table 1. It is evident that for any of these systems, a change of several degrees in laboratory temperature can have a significant effect.

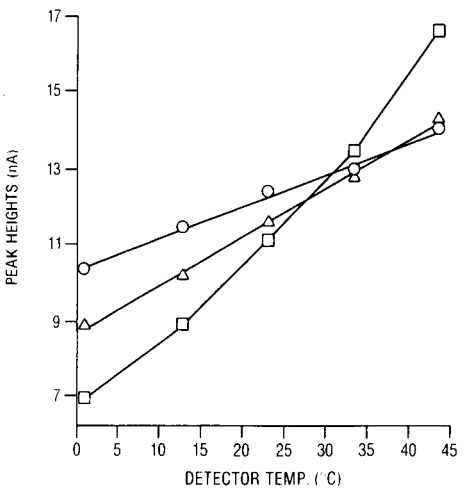

Fig. 1. Typical temperature dependence: (△) diethylstilbestrol; (□) hexestrol; (○) *cis*-diethylstilbestrol.

TABLE 1

Temperature dependences under common assay conditions

Compound	E_{cell}(V)	Temperature dependence (% $^{\circ}C^{-1}$ at 22° C)
Enviroxime	+0.85	2.7
Zinviroxime		4.1
Hexestrol		2.1
Diethylstilbestrol	+0.85	1.1
Cis-Diethylstilbestrol		0.7
Benzestrol		1.1
Acetaminophen	+0.66	1.5
N-(2-Hydroxyphenyl)acetamide		5.0
N-(4-Hydroxy-3-methylphenyl)acetamide		0.8
N-(4-Hydroxyphenyl)propionamide		1.2
Hydroquinone		0.7
Methylhydroquinone		0.6
Uric acid	+0.65	0.7
Norepinephrine		0.9
Dopa		0.8
Epinephrine		0.9
3,4-Dihydroxybenzylamine		0.9
Dopamine		0.9

The experimental configuration used in obtaining the data in Table 1, namely a short length of tubing joining a thermostatted column to the cell mounted in independently thermostatted hexane, represents a compromise between the two most representative configurations. Data obtained for acetaminophen and its analogs with all three configurations are given in Table 2. Different dependences were observed with the three cell geometries, because of the dynamics of heat transfer between the mobile phase, the cell block, and the environment. The configuration used for all other experiments (hexane bath/short tubing) is shown in the second column. The configuration with the cell in air, simulates the real situation in which column temperature is controlled and the cell is at ambient temperature. Dependences for this configuration are roughly half that of the hexane bath/short tubing configuration. For the last setup, a length of tubing immersed in the bath was used to connect the column to the cell. This served to adjust the mobile phase from column temperature to cell temperature, prior to arrival at the cell. This setup simulates the temperature dependence of electrochemical response when both the column and the cell are at ambient temperature. Dependences for this configuration are just over twice those of the hexane bath/short tubing setup. When column temperature is not controlled, fluctuations in peak heights caused by changes in retention times will of course add to the response changes arising from the electrochemical detection alone.

TABLE 2

Influence of chromatographic configuration on temperature dependence[a]

Compound	Temperature dependence (% °C^{-1} at 22° C)		
	Cell in air	Cell in hexane with short tubing	Cell in hexane with preequilibration coi
Acetaminophen	0.3	0.7	1.6
N-(2-Hydroxyphenyl)acetamide	0.4	0.8	1.9
N-(4-Hydroxyphenyl)propionamide	0.4	0.7	1.5
Hydroquinone	0.4	0.7	1.5
Methylhydroquinone	0.3	0.7	1.5

[a] E = +0.91 V.

Causes of temperature dependence

Temperature affects the response of amperometric detectors because of its influence on the rate of diffusion of molecules to the electrode surface and its influence upon the rate of reaction of molecules reaching the surface. Both factors result in a change in the fraction of the molecules passing through the cell which are oxidized or reduced. Coulometric detectors should not exhibit temperature-sensitive responses.

The contribution of diffusion was measured by estimating temperature dependences under limiting-current conditions. For example, the detector electrode potential given in Table 1 for the stilbestrols and benzestrol is sufficiently high to ensure diffusion-limited response. When acetaminophen and its analogs were assayed under diffusion-limited conditions (E = +0.91 V), their temperature dependences averaged 0.68 ± 0.06% per °C at 22° C.

Hannekamp and Van Nieuwkerk [6] have recently described a generalized equation for the limiting current in solid-electrode flow-through electrochemical cells. Limiting currents for thin-layer, tubular, disk, and wall-jet electrodes all were shown to be functions of various geometric factors and the two-thirds power of the diffusion coefficient. Thus, temperature dependences for all solid electrode cells may be expected to be similar to those found for the thin-layer cell used in this study. Limiting current for the common dropping mercury detectors is a function of the square root of the diffusion coefficient. As a result, these detectors may be somewhat less sensitive to diffusional variability, but lack of temperature control of the mercury reservoir may lead to more serious variability [3].

The second major cause of temperature-induced variability in l.c./e.c. is the effect that temperature may have on the electrode reaction. Figure 2 illustrates the importance of detector potential. Temperature dependences for acetaminophen and its five analogs were estimated at three potentials. The resulting dependences are plotted as a function of the difference between the detector potential and the half-wave potential for the individual compound. Seventy millivolts or more above the half-wave potential, where

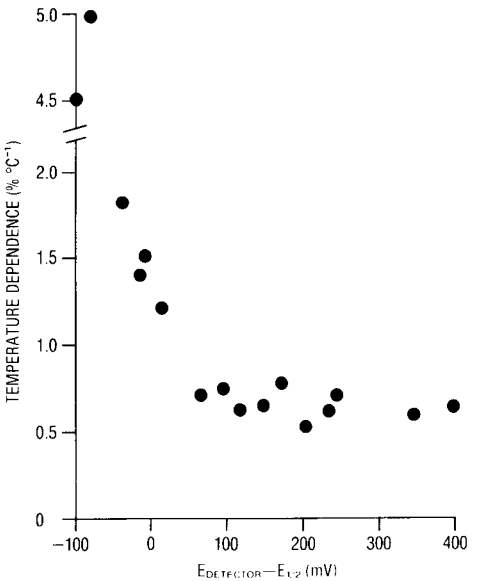

Fig. 2. Effect of detector potential on temperature dependence of acetaminophen and five analogs; detector potentials are referenced to the half-wave potential for the individual compound.

diffusional variability alone contributes, the dependence is relatively constant. At or below the half-wave potential, dependences rise sharply. This trend is consistent with that which would be calculated with the Nernst equation, but the magnitude is greater than would be expected for a two-electron oxidation like that of acetaminophen.

One reason that actual dependences are larger than might be expected is slow heterogeneous electron transfer. Very few organic analytes exhibit ideal electrochemical behaviour at solid electrodes or in typical chromatographic eluents. To study the effect of temperature on electrode reactions, hydrodynamic voltammograms were obtained at 1°C and then a second set done at 25°C on the same electrode. The results are listed in Table 3. At lower temperatures, the half-wave potentials were greater and the waves were more drawn out, as measured by the parameter $(E_{3/4} - E_{1/4})$, for all five compounds. To confirm these effects, the experiment was repeated in a different fashion. Measurements were made at two temperatures each time the detector electrode potential was changed. Results of this experiment were consistent with those listed in Table 3. Although the changes in the properties of the electrode appear to be real, they are not particularly large, given the 24°C change in temperature. The half-wave potential changes approximately 1 mV/°C.

TABLE 3

Effect of temperature on hydrodynamic voltammograms

Compound	$E_{1/2}$ (mV)		$E_{3/4} - E_{1/4}$ (mV)	
	1°C	25°C	1°C	25°C
Hydroquinone	540	510	136	120
Acetaminophen	700	670	99	85
Methylhydroquinone	440	430	122	118
N-(4-Hydroxyphenyl)propionamide	670	640	97	84
N-(2-Hydroxyphenyl)acetamide	770	740	71	65

Minimization of temperature effects

The information presented above suggests several possible approaches to minimization of temperature-induced variability in l.c./e.c. measurements. The most obvious solution, to thermostat the entire chromatograph, is not normally practical. When the chromatograph used has an oven for maintenance of column temperature, it is sometimes possible to mount the detector cell in the oven. However, when the column is operated at elevated temperatures, this approach may not be desirable, as the subsequent section on signal-to-noise ratios indicates.

The column temperature should at least be controlled, because the temperature of the chromatographic eluent influences the temperature of the cell. Because the cell exists in a dynamic state of heat transfer, increasing the flow rate through a system in which column temperature is controlled, decreases temperature swings at the detector. For example, the regression equation obtained by averaging the temperature dependences (TD) of hydroquinone, acetaminophen, and methylhydroquinone at an applied potential of +0.91 V and flow rates of 0.5, 1.0, 1.5 and 2.0 ml min^{-1} was TD (% $°C^{-1}$) = 0.732 ± 0.003 − 0.247 ± 0.002 (ml min^{-1}) with standard error of 0.003% $°C^{-1}$ and $r > 0.999$. Increasing the flow rate is not always possible, because of pressure limitations, and it may not be desirable when detecting analytes with unfavourable electrode kinetics. A third approach to minimization of temperature-induced variability is to operate the detector on the limiting current region of the analyte. For many compounds, this is not possible, because of interferences or because they would require potentials greater than those required for solvent breakdown.

Perhaps the best way to minimize temperature-induced variability is through use of a proper internal standard. The ideal internal standard will, in addition to compensating for variability in other portions of the assay, minimize temperature variability by virtue of its diffusional and electrochemical similarity to the analyte. For example, three analogs of acetaminophen (Table 1) that could be used as internal standards are *N*-(2-hydroxyphenyl)-acetamide, *N*-(4-hydroxy-3-methylphenyl)acetamide and *N*-(4-hydroxyphenyl)propionamide. All are structurally very similar to acetaminophen.

The potential used in this determination (E = +0.66 V) is close to the half-wave potential of acetaminophen under these conditions ($E_{1/2}$ = 0.67 V). In the event of an extreme change in temperature, such as from 23 to 30° C, without an internal standard the acetaminophen response increased by 12%. Because *N*-(4-hydroxy-3-methylphenyl)acetamide is more readily oxidized than acetaminophen ($E_{1/2}$ = 0.56 V), the response is not as temperature-dependent. Ratioing the responses of acetaminophen and *N*-(4-hydroxy-3-methylphenyl)-acetamide reduced the change to +6%. Because *N*-(2-hydroxyphenyl)acetamide ($E_{1/2}$ = 0.74 V) is more difficult to oxidize than acetaminophen, there was overcompensation; ratioing acetaminophen to *N*-(2-hydroxyphenyl)acetamide caused a —22% change in results. With an $E_{1/2}$ of 0.64 V, *N*-(4-hydroxyphenyl)-propionamide is more nearly an ideal internal standard. The ratio of the responses of acetaminophen to *N*-(4-hydroxyphenyl)propionamide changed only +1.7% after the 7° C change in cell temperature.

The other internal standards listed in Table 1, hexestrol, benzestrol, and 3,4-dihydroxybenzylamine lessen temperature-induced variability in their respective assays with varying degrees of effectiveness. Some measure of this can be seen by comparing the temperature dependence of the internal standard to that of the analytes.

Temperature dependence of detector noise

The effect of temperature on the background current and noise at the glassy carbon electrode was also evaluated. In order to minimize non-instrumental contributions to the noise, the experiments were performed when the rest of the laboratory was not operating. Typical results are depicted in Fig. 3.

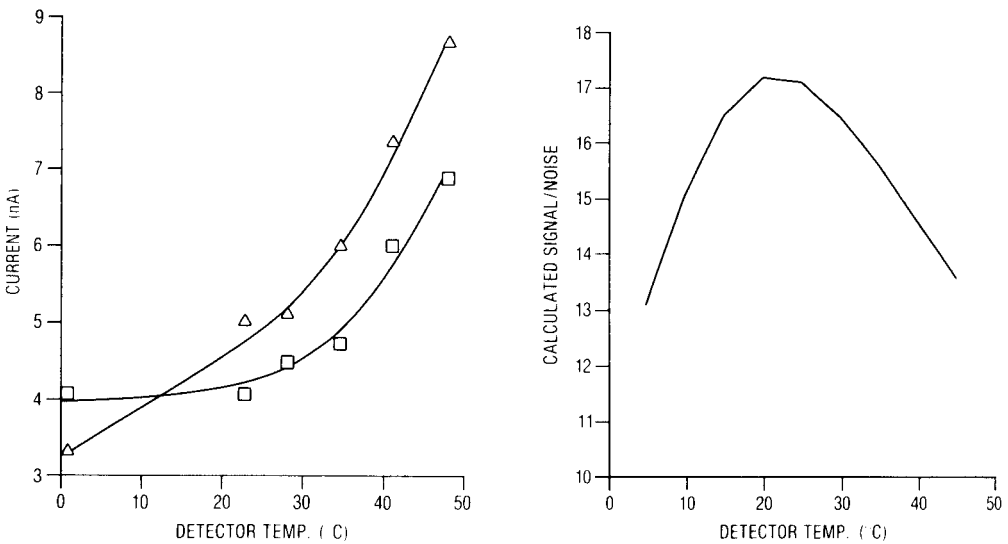

Fig. 3. Influence of temperature on detector background current and noise: (□) peak-to-peak noise × 8; (△) background. Conditions: E = +0.75 V vs. (Ag/AgCl/3M NaCl), mobile phase 34% 0.1 M sodium acetate/66% methanol at 0.9 ml min^{-1}.

Fig. 4. Calculated signal-to-noise ratios for hexestrol. Chromatographic conditions as in text.

The shape of the temperature dependence of the background current appeared to be similar to that of the analytes examined previously. However, the dependence of peak-to-peak noise was relatively constant over the range 0—20° and then it increased rapidly.

The empirical equations relating cell response and temperature for several analytes (the top two groups in Table 1) and an equation fitted to the noise under the same chromatographic conditions were used to calculate signal-to-noise ratio as a function of temperature. One such calculated dependence is depicted in Fig. 4. All dependences calculated exhibited a peak, the location of which varied from 15°C for an analyte with relatively small temperature-dependence (*cis*-diethylstilbestrol) to 50°C for zinviroxime, a highly temperature-sensitive analyte. The maximum change in S/N over the range 0—50° was only a factor of 2, however. Although the assays examined here represent only a small fraction of those possible by l.c./e.c., there appears to be little advantage to alteration of detector temperature for enhancement of signal-to-noise ratio.

This paper was presented in part at the 32nd Pittsburgh Conference, Atlantic City, NJ, 9th March 1981. The assistance of Dr. J. F. Nash, Dr. F. W. Rockhold, Dr. R. J. Bopp, Mr. D. Crozier, Dr. J. W. Becker, Mr. K. W. Perry and Mrs. K. Z. Farid is gratefully acknowledged.

REFERENCES

1 S. R. Bakalyar and R. A. Henry, J. Chromatogr., 126 (1976) 327.
2 R. J. Bopp, C. L. Gries, C. J. Parli and J. F. Quay, 1980 LCEC Symposium, Abstract 15, Indianapolis, IN, 12th May, 1980.
3 U. Baltensperger and R. Eggli, Anal. Chim. Acta, 123 (1981) 107.
4 L. R. Snyder and J. J. Kirkland, Introduction to Modern Liquid Chromatography (2nd edn.), Wiley—Interscience, NY, 1979, p. 162.
5 P. T. Kissinger, Anal. Chem., 49 (1977) 447A.
6 H. B. Hanekamp and H. J. Van Nieuwkerk, Anal. Chim. Acta, 121 (1980) 13.

Analytica Chimica Acta, 134 (1982) 111—118
Elsevier Scientific Publishing Company, Amsterdam — Printed in The Netherlands

CLASSIFICATION OF MONOSUBSTITUTED PHENYL RINGS BY PARAMETRIC METHODS APPLIED TO INFRARED AND RAMAN PEAK HEIGHTS

RUSHUNG TSAO and WILLIAM L. SWITZER*
Department of Chemistry, North Carolina State University, Raleigh, NC 27650 (U.S.A.)
(Received 12th February 1981)

SUMMARY

A statistical linear discriminant method is used to determine if a carbon, nitrogen or oxygen atom is bonded to a monosubstituted phenyl ring. A pattern vector is developed using peak heights of each of the seventeen active infrared and sixteen active Raman bands characteristic of the ring vibration. The Sadtler Standard Raman Spectra, which includes infrared spectra, served as the data base. The success rate is compared for the use of infrared data only, Raman data only and combined infrared and Raman data normalized by several possible methods.

Since the late 1960s, many different pattern recognition methods have been applied in the field of chemistry. The majority of these applications used digitized chemical data such as from mass spectrometry, infrared (i.r.) spectroscopy, nuclear magnetic resonance spectrometry, stationary electrode polarography, etc. These methods were used to elucidate molecular structure [1—4], to find relationships between chemical structure and biological activity [5—8], to identify the source of oil spills [9—14], etc.

Pattern recognition, an application of multivariate data analysis, is a data interpretation process which empirically explores relationships among physically measurable properties of samples belonging to a finite number of groups. When the properties that distinguish a group are highly correlated with the selected properties, unknown samples can be assigned to groups which most closely exhibit the same physical properties.

This paper describes an attempt to correlate measurable properties of both i.r. and Raman spectra to the identity of the next atom attached to a moiety that is known to be present. Traditionally, the characteristic group frequencies are found by visual examination of vibrational spectra. The transition energy, relative intensity, and sometimes the shape of the vibrational band, are three factors that might be used to determine molecular structure. For example, in an infrared spectrum, a strong and broad band near 3000 cm^{-1} with satellite bands near 2650 and 2550 cm^{-1} could be a carboxylic dimer; in a Raman spectrum a strong band near 2100 cm^{-1} with a strong band between 355 and 335 cm^{-1} may be a monosubstituted alkyl acetylene, etc.

0003-2670/82/0000-0000/$02.75

However, to correlate structure visually with more than two or three parameters becomes increasingly difficult and increasingly less successful. The computer combined with applied mathematical methods can be used to aid in interpreting multivariate data.

Drozdov-Tikhomirov [15] first utilized i.r. data to classify carbonyl compounds, using a learning machine method. After that, i.r. and Raman data were tested by using various pattern recognition techniques. For example, the ASTM binary i.r. data were taken to identify functional groups by a probability discriminant method [16]; digitized i.r. and Raman spectra were classified by a linear learning method [17]; and digitized i.r. spectra of oils were used to characterize unknown petroleum products by a statistical discriminant analysis method [12—14].

In studying integrated i.r. peak areas of the ring vibrations of monosubstituted benzenes, Brownlee et al. [18] discovered that the areas of the ν_8 and ν_{19} vibrations were highly correlated to the Hammett σ values of the substituent group. The correlation results from electronic interactions between the substituent group and the phenyl ring. This discovery led us to investigate whether the substituent group on a monosubstituted benzene might be identified from the peak heights of the bands associated with the phenyl ring vibrations in these compounds. In particular, an attempt is made to correlate normalized peak heights to the atom bonded to the phenyl ring in order to identify that atom as a carbon, nitrogen or oxygen.

The Sadtler Infrared and Raman Spec-Finder [19] was used exclusively as the data base for this study. Bands characteristic of monosubstituted phenyl rings are easily recognized from these spectra whereas small variations in the transition energies are difficult to recognize. Even more difficult to detect are changes in the peak shape. However, variation in relative peak heights within groups is large compared to the readability error. Therefore, the present attempt to correlate variation in peak heights to structure of the molecule should not be biased either by the choice of data base or by errors in reading peak heights from this data base.

EXPERIMENTAL

Data set

A set of 158 spectra of liquid, monosubstituted benzenes was chosen as the sample; only compounds with a C, N, or O bonded to the phenyl ring were selected. The ph-C~ group contained 124 sample spectra, whereas the ph-N~ group contained 10 spectra and the ph-O— group contained 24 sample spectra. A set of peak heights for characteristic vibrational bands of the phenyl ring was used as component for the pattern vector. There are 17 active bands in each infrared spectrum and 16 bands in each Raman spectrum. Table 1 lists the active bands by their Wilson's mode classification with their nominal frequency range [20]. From the reference spectrum of each sample, a vector of net i.r. and Raman peak heights for the active modes was

TABLE 1

Characteristic vibrational bands of monosubstituted derivatives of benzene

Wilson's mode number	Infrared ν (cm^{-1})	Raman ν(cm^{-1})	Wilson's mode number	Infrared ν(cm^{-1})	Raman ν(cm^{-1})
8a	1605 ± 7	1607 ± 10	18a	1030 ± 4	1028 ± 3
8b	1588 ± 9	1585 ± 6	12	1000 ± 4	1000 ± 5
19a	1500 ± 5	1500 ± 2	17a	970 ± 10	970 ± 10
19b	1450 ± 10	1445 ± 6	17b	904 ± 8	—
14	1310 ± 7	1315 ± 10	10a	839 ± 8	838 ± 10
3	1285 ± 10	1280 ± 5	10b	750 ± 15	740 ± 11
9a	1178 ± 3	1180 ± 4	4	695 ± 5	—
9b	1156 ± 4	1156 ± 5	6b	620 ± 3	618 ± 4
18b	1070 ± 10	1070 ± 5	16a	—	406 ± 8

created. The net peak heights were expressed in absorbance units for the i.r. spectra and in arbitrary units for the parallel polarized Raman spectra. The net i.r. peak heights were determined as the differences between baseline and peak absorbances. This method is similar to that used by Lynch and Brown [21]. Raman peak heights were determined by subtracting baseline levels from peak levels. A table of the raw data will be supplied on request.

Both the net i.r. and Raman peak heights were then normalized by three methods: (1) ratioing each peak height to that for one chosen band; (2) ratioing each peak height to the sum of all peak heights; (3) ratioing each possible pair of peak heights. Each of these normalization methods used some feature of the spectrum as an internal reference. Normalizing net i.r. peak heights is necessary to compensate for different sample thicknesses; normalizing net Raman peak heights is necessary to compensate for different source intensities and collection efficiencies. Three additional data sets with 5%, 10%, and 15% random variations in the initial data were generated and tested to see if random error gave different classification results.

Linear pattern classifiers

A linear discriminant function analysis, which has been discussed in detail [22], was used for the pattern classification. The classification criterion is based on the generalized square distance which is calculated from the inverse pooled covariance matrix of pattern vectors. An unknown sample is classified into the group which gives the smallest general square distance.

A feature selection technique is used to determine the best subset of predictors. Predictors are chosen by a stepwise procedure that selects the predictors giving the maximum separability among the specified groups. Predictors are added until the increase in separability ceases to be statistically significant.

The stepwise linear discriminant analysis from the Biomedical Computer Program Package (BMDP) [23] was run on the Triangle Universities Com-

puting Center IBM 370/168. The BMDP07M program package adopts the jack-knife method which excludes each sample pattern, one at a time, uses the rest to develop classifiers, and then treats the excluded sample as an unknown. Therefore, there is no need to separate limited samples into training and testing sets like most learning machine methods do.

RESULTS AND DISCUSSION

A three-group classification (ph-C~, ph-N~ and ph-O~) was considered using i.r. and Raman peak heights normalized by ratioing the bands in each sample spectrum to one of the other bands in the same spectrum. The five strongest i.r. peaks, which fall nominally at 1605, 1500, 1450, 750, and 695 cm^{-1} and the six strongest Raman peaks, which fall nominally at 1607, 1180, 1156, 1028, 1000, and 618 cm^{-1}, were chosen as possible internal reference bands. The results were judged based on the success rate, defined as the percent of correct classifications.

For the i.r. data, only a 39.2% success rate was found when the 1500 cm^{-1} band was used as the internal reference; only one predictor was entered using this band. However, for each of the other four bands used, the success rates were considerably higher and 4—8 bands were entered. Figure 1 shows the success rates as a function of the number of predictors added by the stepwise procedure. In all the studies described below the same stepwise procedure was used and gave results similar to those shown in Fig. 1. In each case, the success rate reaches a plateau after 3—6 bands have been entered.

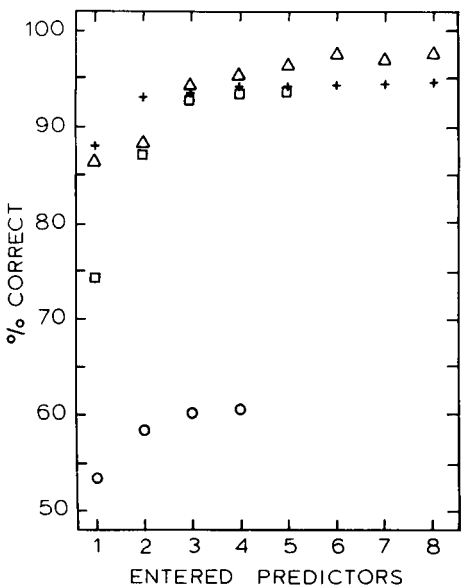

Fig. 1. The success rate as a function of the number of entered predictors for the i.r. data where each peak height is normalized with (○) 1605 cm^{-1} band, (+) 1450 cm^{-1} band, (□) 750 cm^{-1} band and (△) 695 cm^{-1} band.

TABLE 2

Percent of correct classifications by normalizing each peak height to that of one chosen band

Data set	Reference band (cm^{-1}) and correct classifications (%)					
Infrared	1605	1500	1450	750	695	
	60.1[a](58.9)[b]	39.2(39.2)	94.3(93.0)	93.7(93.7)	97.5(96.2)	
Raman	1607	1180	1156	1028	1000	618
	70.3(67.7)	89.2(86.7)	76.6(74.7)	80.4(79.1)	90.5(87.3)	93.0(89.2)

[a]Success rate using the complete data set. [b]Success rate using the jack-knife method.

Table 2 gives the final results for both the i.r. and Raman normalizations relative to each of the internal reference bands indicated above. Values not enclosed in parentheses are the success rates using the complete data set, whereas those enclosed in parentheses are the success rates using the jack-knife method.

The highest success rates were obtained using internal reference bands at 695 cm^{-1} for the i.r. spectra and at 618 cm^{-1} for the Raman spectra. The 97.5% success rate using the i.r. data resulted from 4 misclassifications of the 158 samples; two samples in the ph-O— group and one sample in each of the other two groups were misclassified. The 93.0% success rate using the Raman data resulted from nine misclassifications of samples belonging to the ph-C~ group and two belonging to the ph-O— group. Using the combined i.r. and Raman data, the success rate was 99.4%; only one of the 124 ph-C~ samples was misclassified into the ph-N~ group and all of the ph-N~ and ph-O— samples were correctly classified. These results are summarized in Table 3 (Method 1). When the jack-knife method was used, again the combined data gave the highest success rate of 98.7%. Only two of the ph-C~ samples were misclassified. The success rates with the jack-knife method are again shown in parentheses.

TABLE 3

Percent of correct classifications using three different normalization methods

Data	Normalization method		
	1[a]	2[b]	3[c]
I.r.	97.5[d](96.2)[e]	98.7(96.2)	99.4(97.5)
Raman	93.0(89.2)	91.8(86.7)	99.4(92.4)
I.r. + Raman	99.4(98.7)	99.4(97.5)	100.0(99.4)

[a]The i.r. bands are normalized relative to the 695 cm^{-1} band and the Raman bands relative to the 618 cm^{-1} band. [b]The i.r. and Raman bands are normalized relative to the sum of all bands in the respective spectra. [c]The i.r. and Raman bands are normalized by taking all possible ratios of i.r. bands and of Raman bands. [d]Success rate using the complete data set. [e]Success rate using the jack-knife method.

The second normalization method calculated the ratio of each sample peak to the sum of all peak heights in the sample spectrum. This normalization introduced a singularity into the subsequent matrix calculations because the sum of the normalized bands was unity. To eliminate this singularity, a weak band at nominally 620 cm^{-1} was deleted from each i.r. spectrum and a weak band at nominally 406 cm^{-1} was deleted from each Raman spectrum. The results for this method of normalization are summarized in Table 3 (Method 2) along with the results obtained by the jack-knife method. Again the combined i.r. and Raman data gave the best results with a success rate of 99.4% when the complete data set was used and 97.5% by the jack-knife method.

For the third normalization method by ratioing each possible pair of peak heights, there are 139 possible combinations of i.r. bands (17 × 16/2) and 120 combinations of Raman bands (16 × 15/2). The results of the third method of normalization are shown in the last column of Table 3. The combined i.r. and Raman data gave the highest success rate. When the complete data set was used, all 158 samples were correctly classified and only one sample was misclassified by the jack-knife method.

Data sets with 5%, 10%, and 15% random variation of the initial peak heights were tested to determine if the results were sensitive to errors in reading the peak heights. Only the third normalization was tested. Even with

TABLE 4

Entered predictors with their corresponding *F* values using the i.r. and Raman combined data[a]

I.r./695 cm^{-1} Raman/618 cm^{-1}	*F* value	I.r./Σ i.r. Raman/Σ Raman	*F* value	$I.r._i/i.r._j$ $Raman_i/Raman_j$	*F* value
1450_i	45.99	1605_i	86.13	$1500/695_i$	112.94
1500_i	43.36	1450_i	50.10	$1607/1585_r$	59.52
1607_r	43.27	1156_r	26.37	$1588/1450_i$	36.53
1585_r	42.91	1607_r	21.92	$1028/618_r$	20.41
1588_i	38.42	1588_i	19.20	$1310/1178_i$	16.61
1178_i	16.68	1500i	12.96	$1605/1588_i$	15.56
1605_i	15.02	1310_i	10.87	$1588/1000_i$	13.76
839_i	12.03	1178_i	8.96	$1500/750_i$	13.69
1028_r	11.82	839_i	7.71	$1178/970_i$	13.53
1310_i	11.01	1280_r	7.54	$1607/618_r$	10.52
1070_i	10.92	750_i	5.62	$1450/695_i$	10.06
1180_r	9.49	1000_r	5.43	$1500/1070_i$	9.41
1156_r	5.78	1315_r	5.05	$1605/1450_i$	9.29
904_i	3.45	1180_r	4.59	$1585/618_r$	9.15
		1585_r	3.07	$1180/618_r$	8.26
				$1500/1000_i$	7.81
				$1280/1156_r$	6.54
				$1585/1445_r$	6.22

[a] i = i.r. band, r = Raman band.

15% random variation from the peak heights initially read, a 100% success rate was observed when the complete data set was used. When the jack-knife method was applied, the success rates dropped from 99.4% to 98.7%, 97.5%, and 97.5%, respectively, for the three levels of random noise.

Table 4 lists the bands that are entered by the stepwise procedure. The *F*-statistic indicates the significance with which the entered predictors help to separate the samples among the specified groups. The larger the value, the more important the predictor is in the classification. Bands are listed in order of decreasing *F* values. The ν_{8a}, ν_{8b}, ν_{19a} and ν_{19b} bands, which were studied by Brownlee et al. [18], show consistently large *F* values indicating their importance in the classification. Only the results for the combined i.r. and Raman data sets are shown. Tables for the i.r.-only and Raman-only data are available on request.

Table 5 identifies the samples which were misclassified. Only the combined i.r. and Raman results are shown and these only for the jack-knife method. Both of the failures by the first method of normalization are also failures by the second method. However, one of the ph-C~ samples is classified into the ph-O— group by the first normalization and into the ph-N~ group by the second normalization. The single misclassification by the third normalization was not seen by either of the first two methods.

Conclusions

From a set of peak heights for the characteristic vibrational modes of the monosubstituted phenyl rings, linear discriminant analysis has a high probability of identifying which one of three atoms (C, N, or O) is attached to the phenyl ring. The results do not significantly depend on errors of up to 15% in measuring the net peak heights. Thus, the method should be relatively insensitive to choice of spectrometer and sampling conditions. No clear choice is demonstrated for any of the three different normalization methods described above. The first normalization involving the ratio of each peak

TABLE 5

Misclassifications by the jack-knife method with combined i.r./Raman data

Normalized peak heights	Classification expected	Classification found	—R
I.r./695 cm^{-1} and	C	N	$—CC(CH_2)_5CH_3$
Raman/618 cm^{-1}	C	O	$—COCH_2OH$
I.r./Σ i.r. and	C	O	—COH
Raman/Σ Raman	C	O	$—COOSn(n\text{-}Bu)_3$
	C	N	$—CC(CH_2)_5CH_3$
	C	N	$—COCH_2OH$
$I.r._i/i.r._j$ and	N	C	$—NO_2$
$Raman_i/Raman_j$			

height to one chosen band suffers from the time-consuming test needed to select the best band for the internal reference. The second method of normalizing each peak height to the sum of all peak heights takes the least computing time but gives slightly lower success rates. The last method of ratioing each possible pair of peak heights gives the highest success rates, but it requires both the most computer storage and the longest computing time.

REFERENCES

1 T. L. Isenhour, B. R. Kowalski and P. C. Jur, Crit. Rev. Anal. Chem., 4 (1974) 1.
2 W. S. Meisel, M. Jolly, S. R. Heller and G. W. A. Milne, Anal. Chim. Acta, 112 (1976) 407.
3 H. Rotter and K. Varmuza, Anal. Chim. Acta, 103 (1978) 61.
4 L. A. Gribov and M. E. Elyashberg, Crit. Rev. Anal. Chem., 8 (1979) 111.
5 H. T. Haili, R. C. T. Lee, M. Shapiro and A. M. Guarino, Science, 180 (1973) 417.
6 B. R. Kowalski and C. F. Bender, J. Am. Chem. Soc., 96 (1974) 916.
7 S. Schiffman, Science, 185 (1974) 112.
8 H. Abe and P. C. Jur, Anal. Chem., 47 (1975) 1829.
9 H. A. Clark and P. C. Jur, Anal. Chem., 47 (1975) 374.
10 D. L. Duewer, B. R. Kowalski and T. F. Schatski, Anal. Chem., 47 (1975) 1573.
11 J. S. Mattson, Natl. Tech. Inf. Serv. AD/PB Rep., AD-039387 (1976) 48.
12 F. K. Kawahara and Y. Y. Yang, Anal. Chem., 48 (1977) 651.
13 J. S. Mattson, C. S. Mattson, M. J. Spencer and F. W. Spencer, Anal. Chem., 49 (1977) 297.
14 J. S. Mattson, C. S. Mattson, M. J. Spencer and F. W. Spencer, Anal. Chem., 49 (1977) 500.
15 L. N. Drozdov-Tikhomirov, Opt. Spectrosc., 27 (1968) 77.
16 S. R. Lowry, H. B. Woodruff, G. L. Titter and T. L. Isenhour, Anal. Chem., 47 (1975) 1126.
17 J. M. Comerford, P. G. Anderson, W. H. Snyder and H. S. Kimmel, Spectrochim. Acta, 33 (1976) 651.
18 R. T. C. Brownlee, A. R. Katritzky and R. D. Topsom, J. Am. Chem. Soc., 88 (1966) 1413.
19 The Sadtler Standard Raman Spectra, Sadtler Research Laboratories, Philadelphia, PA, 1973.
20 R. R. Randle and D. H. Whiffen, Molecular Spectroscopy, Institute of Petroleum, London, 1955, p. 111.
21 P. F. Lynch and C. W. Brown, Environ. Sci. Technol., 7 (1973) 1123.
22 W. J. Dixon (Ed.), BMD Biomedical Computer Programs, University of California Press, Berkeley, CA, 1974, p. 221.
23 W. J. Dixon and M. B. Brown (Eds.), BMDP-79 Biomedical Computer Programs P-series, University of California Press, Berkeley, CA, 1979.

Analytica Chimica Acta, 134 (1982) 119—127
Elsevier Scientific Publishing Company, Amsterdam — Printed in The Netherlands

THE GENERALIZED STANDARD ADDITION METHOD: INTERMETALLIC INTERFERENCES IN ANODIC STRIPPING VOLTAMMETRY

R. W. GERLACH[a] and B. R. KOWALSKI*

Laboratory for Chemometrics, Department of Chemistry BG-10, University of Washington, Seattle, WA 98195 (U.S.A.)

(Received 21st July 1981)

SUMMARY

A barrier to routine application of anodic stripping voltammetry is the possible formation of intermetallic compounds which can lead to significant errors in the estimated analyte concentrations. As the method of standard additions can correct only for matrix effects, it is powerless to correct for intermetallic interferences which are not matrix effects. By changing the experimental design, the new generalized standard addition method can simultaneously characterize and correct for this type of interference as well as matrix effects expected for real samples. The method is tested on the Cu—Zn—Hg system and error estimates are provided for calculated linear response constants and analyte concentrations.

The formation of intermetallic compounds in amalgams is a well known phenomenon and numerous examples have been documented [1—11]. Much interest has been generated in these compounds because of their tendency to cause interference effects in electrochemical studies in methods such as polarography [12] or anodic stripping voltammetry (a.s.v.) [13—15]. Kemula and coworkers were the first to recognize their effect on a.s.v. [6, 7, 16]. Their presence usually caused a reduction in the height of the dissolution wave of one metal and occasionally the production of a new peak. Ficker and Meites [17] and Hovsepian and Shain [9] suggested that compounds such as Zn_2 also formed in mercury. Later work by Rogers [11] showed that, at most, only a small fraction of the amalgamated zinc was in the form of a dimer.

Most of the recent work on intermetallics has focused on the Cu—Zn—Hg system. The interaction of zinc with copper in mercury has been investigated several times with respect to its behavior in a.s.v. [18—20]. These recent investigations have been inspired mainly by the increased use of a.s.v. in trace metal analysis of environmental samples [21—22], for in many cases the most abundant trace metals are copper and zinc and the interference effect can hinder their determination.

[a]Present address: Center for Analytical Chemistry, National Measurement Laboratory, National Bureau of Standards, Washington, DC 20234, U.S.A.

Though the formation of Cu—Zn compounds in a.s.v. is agreed upon, there are contrasting reports with regard to their stability. A decrease in the zinc peak in the presence of copper is the most notable feature. Stromberg and Gorodovykh [12] monitored stripping currents as a function of the Cu/Zn ratio and attributed their results to the formation of an insoluble 1:1 Cu—Zn compound having a solubility product of 5×10^{-8}. Stromberg et al. [23] and Mesyats et al. [24] monitored stripping currents as a function of pre-electrolysis time and concluded that a slightly soluble 1:1 Cu—Zn compound with solubility product 1×10^{-6} was present. Other investigations have also concluded that the intermetallic Cu—Zn stoichiometry is 1:1 [25—26]. Solubility product values have been reported from 1×10^{-5} [26] to 5×10^{-8} [12] with numerous values spanning this range [27].

In contrast to the often reported depression of the zinc peak, the effect of Cu—Zn intermetallic formation on the copper peak is very small. This has been attributed to another peak from the oxidation of the intermetallic compound at a potential very close to the potential at which copper is removed [20].

The wide range of solubility products reported demonstrates that the amalgamated Cu—Zn intermetallic system is not easily studied. Shuman and Woodman [20] suggested that not only is there a 1:1 Cu—Zn intermetallic present, but also 1:2 and 1:3 species, and that the 1:3 species is insoluble. Their analysis was based on attempts to fit solubility schemes involving a variety of intermetallic species. What can be concluded from the above is the lack of sound information necessary for correction of the Cu—Zn interference during a chemical analysis.

As an alternative, Copeland et al. [18] discovered that by addition of gallium the Cu—Zn intermetallic interference of the zinc peak could be suppressed. It had previously been shown that gallium forms a Cu—Ga intermetallic [28, 29] and this compound is formed in preference to the Cu—Zn species. This allows zinc to be determined unambiguously, but has the undesired effect of interfering with copper determinations.

The present approach to the simultaneous determination of copper and zinc with anodic stripping voltammetry, outlined below, involves a mathematical analysis scheme designed not only to correct for interference effects in general, but to use them to advantage. The methodology involved is applicable to the entire range of problems having to do with interference effects.

THE GENERALIZED STANDARD ADDITION METHOD

Standard addition is a well known technique for circumventing the problems associated with matrix effects common to many analytical methods. It assumes a linear response and requires the measurement of the analytical signal before and after one or more standard additions have been made to the sample. The initial concentration is found from a regres-

sion of the measured signals, or responses as they will be referred to hereafter, to the known concentration change increments. The intercept of this regression line on the concentration axis corresponds to the initial concentration. In general, the response is given by

$$R_l = ck_l = (\Delta c + c_0)k_l \tag{1}$$

where Δc is the concentration change after any standard addition, c_0 is the initial concentration of the analyte and k_l is the linear response constant. The real value of the method of standard additions is that calibration is performed in the sample. Matrix effects that would cause k_l to be different from calibration solutions to sample are not a problem.

Equation (1) can be used only under certain conditions. It requires the response to be zeroed, the functional relationship to be linear, and the absence of interferences from other components in the sample.

The applicability of Eqn. (1) in the analysis of multicomponent systems requires the responses to be fully selective [30]. Each response must be a function of only one analyte. However, it is not unusual to find examples where the response function is a function of more than one analyte (the interference effect problem). If the interference effects are linear, the total response can be modelled by extending Eqn. (1) to include contributions from each analyte as given by

$$R_l = \sum_{s=1}^{r} c_s k_{sl} \tag{2}$$

where c_s is the concentration of the sth component and k_{sl} is the corresponding response constant. Analogous to the expansion in Eqn. (1), Eqn. (2) can be expressed as

$$R_l = \sum_{s=1}^{r} \Delta c_s k_{sl} + \sum_{s=1}^{r} {}_0c_s k_s \tag{3}$$

In order to make use of Eqn. (3), the generalized standard addition method, g.s.a.m. [31, 32], was developed. It requires that the number of analytical signals, p, be greater than or equal to the number of analytes, r. Then, it is necessary to measure each response R_l ($l = 1, p$) before and after the addition of standards. Each standard must, of course, be added at least once; the total number of additions, n, must be greater than or equal to the number of analytes, r. Each response is allowed to depend on any combination of analytes, the only requirement being that every analyte must perturb at least one response.

The preceding equation can be expressed more succinctly as $\mathbf{R} = \mathbf{CK}$, where $\mathbf{R}$ is an $n \times p$ matrix of p measured responses, $\mathbf{C}$ is an $n \times r$ matrix whose rows correspond to the total concentration, $\Delta c + c_0$, of each of the r analytes at that particular standard addition, and $\mathbf{K}$ is an $r \times p$ matrix whose columns represent sets of response constants for individual sensors. Obvi-

ously, **C** is initially unknown, for the initial concentrations are unknown, and matrix **K** is also unknown. It may also be pointed out that the absence of a particular interference effect will merely result in a zero value at the corresponding element of **K**.

In order to solve for **K** and the original concentrations, $\mathbf{R} = \mathbf{CK}$ must be rewritten. If the volume changes associated with the standard additions are negligible, as is often the case when very small volumes of highly concentrated standards are added to a relatively large sample volume, it is possible to separate **C** as $\mathbf{C} = \Delta\mathbf{C} + \mathbf{C}_0$, where $\Delta\mathbf{C}$ is the known matrix of total concentration changes arising from the standard additions and $\mathbf{C}_0$ is a matrix with identical rows. Since $\Delta\mathbf{C}$ is a matrix of effective concentration changes at some place during the multiple standard addition procedure, any substantial change in volume will invalidate the definition of $\mathbf{C}_0$ above as concentrations are not additive. Fortunately, this is not a problem because a simple volume correction can be made if standard additions cause volume changes [32]. Just as **C** can be separated, **R** can also be separated to give a matrix of $\mathbf{R}_0$ with all rows equal to the initial responses and a matrix $\Delta\mathbf{R}$ of response changes caused by n successive standard additions: $\mathbf{R} = \Delta\mathbf{R} + \mathbf{R}_0$. Now, the g.s.a.m. solves for **K** beginning with

$$\Delta\mathbf{R} = \Delta\mathbf{CK} \tag{4}$$

and then uses **K** to find the initial concentrations from the vector of initial responses via

$$\mathbf{C}_0^{\mathrm{T}} = \mathbf{R}_0^{\mathrm{T}}\mathbf{K}^{-1} \tag{5}$$

The experimental designs, the complete derivation of the solution for **K** and $\mathbf{C}_0$, and a treatment of deterministic error bounds can be found in the literature [31, 32]. The g.s.a.m. is a multivariate generalization of the method of standard additions. Responses are recorded before and after known standard additions are made for each analyte. It is the only method that can correct for both matrix effects and interferences. In this study, the g.s.a.m. was used to overcome the interference effects caused by the formation of intermetallic compounds during the determination of copper and zinc by anodic stripping voltammetry.

EXPERIMENTAL

Apparatus

The computer-controlled potentiostat, rotator, glassy carbon electrode, reference electrode, counter electrode, and cell assembly have been described [33]. The glassy carbon disk electrode was polished prior to each set of runs with 0.5-μm alumina to provide uniform surface conditions for each run. Electrical contact between the reference electrode and the test solution was made through a bridge of saturated potassium chloride.

The potentiostat and rotator were controlled by a Digital Equipment Corporation PDP-11/05 minicomputer and a custom-built general-purpose

interface [34]. Cell potentials could be set with a resolution of 1.22 mV, and a maximum scan rate of 5000 mV s^{-1} was available with a resolution of 1.22 mV s^{-1}. Rotation rates up to 10000 rpm could be chosen with a resolution of 2.44 rpm. Voltammograms consisted of 256 data points equally spaced between the initial and final voltages of the scan.

Reagents

Hydrochloric and nitric acids and potassium chloride were Ultrex grade (J. T. Baker Co.); potassium nitrate, sodium acetate and acetic acid were Baker Analyzed Reagent grade. Standard copper and zinc solutions were prepared by dissolving ultrapure copper powder and zinc oxide (Alfa Products) in a minimum of nitric acid, followed by dilution with distilled water. The mercury(II) plating solution was prepared by dissolving mercury (Baker Instrumental Grade) in a minimum of nitric acid and diluting to give 0.01 M $Hg(NO_3)_2$.

Airco Prepurified nitrogen (Airco) was further purified by passage through a washing bottle containing a vanadium(II) solution and then through a second washing bottle containing supporting electrolyte before being used to purge oxygen from the cell solution. All water for this study was purified by passage through a high-capacity demineralizing cartridge (Corning 3508-B) and then distilled in a Corning AG-2 quartz still before collection in pre-leached linear polyethylene containers. All polyethylene bottles and laboratory glassware were leached for one week in 6 M HNO_3 (Baker Analyzed Reagent) and then with distilled water to ensure that contamination of the system was minimized [35—38]. The cell and electrodes were stored in 6 M HNO_3 between runs. Standard additions were made using an Eppendorf 100-μl pipette with disposable tips.

Procedure

Plating of the electrode and the background-subtracted linear-scan a.s.v. runs were all done under computer control after the run parameters were selected. The procedure used was essentially the same as described elsewhere [33]. A mercury film thickness of 300 nm was selected to ensure maximum sensitivity. Film thicknesses below 200 nm give reduced sensitivities to both copper and zinc [33, 39].

In this study, the two analytes were copper metal and zinc metal. The two signals used were the background-corrected currents at the stripping potentials of copper and zinc. With reference to Eqn. (4), the ΔC matrix consisted of the changes in concentration resulting from standard additions of copper and zinc. The ΔR matrix contains the resultant response changes.

For this study, the initial concentrations of copper and zinc were equal to the change in concentration caused by their respective standard additions. Runs were started with initial concentrations of 5.3 ppb Cu and 13.3 ppb Zn. All standard additions of zinc were made first and then all standard additions of copper were done. This method was chosen for two reasons. When

run at the maximum sensitivities, the additional copper would create peaks larger than the capabilities of the system because of the larger capacitive current at the position of the copper peak. In addition, the coverage of the response surface for subsequent measurement is maximized when all additions of one component are carried out sequentially. If copper and zinc additions had been added alternately, the response surface coverage would be limited to a narrow zone of points, and information relevant to the 2-dimensional nature of the problem would be difficult to recover.

Fortran IV computer programs used for the g.s.a.m. calculation are available from Informetrix, Inc., P.O. Box 25808, Seattle, WA 98125.

RESULTS AND DISCUSSION

A sample consisting of 13.3 ppb Zn and 5.30 ppb Cu was analyzed first by the simple method of standard additions ignoring interference effects, and then by the g.s.a.m. In each case, four additions of zinc were made, each changing the concentration by 13.3 ppb and seven additions of copper were made, each changing the concentration by 5.30 ppb. The size and number of additions were chosen to minimize the total error in the analysis. The results for the g.s.a.m. were calculated three different ways: the TDC-g.s.a.m., with unscaled and scaled data and the IDC-g.s.a.m. For each row of ΔR in Eqn. (4), the TDC-g.s.a.m. uses the total response changes from the initial responses. Correspondingly, for ΔC it uses the total effective concentration change for each analyte. The IDC-g.s.a.m. uses the respective incremental changes from one step in the multiple standard addition procedure to the next step. Scaling involves making the resulting rows of the ΔR matrix have a vector norm equal to one. This scaling forces every concentration change term in ΔR to the same vector length on the multi-dimensional response surface. Its effect in this case is to remove any bias from the different magnitudes of the responses.

The final analytical results are shown in Table 1. The initial concentrations using the simple method of standard additions are predictably low because of the interference caused by intermetallic formation. The results for the various calculation variations of the g.s.a.m. are substantially the same and amount to a considerable improvement over the results obtained by the method of standard additions.

TABLE 1

Estimated initial concentrations (ppb)

	$[Zn]_0$	Error (%)	$[Cu]_0$	Error (%)
True	13.30	—	5.30	—
Simple standard addition	10.37	22.0	4.82	9.0
TDC-g.s.a.m.	13.38	0.6	5.02	5.3
TDC-g.s.a.m. (scaled)	13.41	0.8	5.02	5.3
IDC-g.s.a.m.	13.17	1.0	5.01	5.5

Table 2 contains the K matrix of linear response constants calculated by using the IDC-g.s.a.m. The results obtained by the other g.s.a.m. variations are essentially the same. The individual values show the effect of each metal on each signal. The relative size of $k_{Zn,Zn}$ to $k_{Cu,Cu}$ is an indication of the sensitivity of the method to the two analytes. The interference coefficients are both negative as is expected when an intermetallic compound is formed. The small negative value for $k_{Cu,Zn}$ is consistent with the previously mentioned report that the Cu—Zn intermetallic species is oxidized at a potential very near to where copper is removed.

Using the g.s.a.m. readily allows accurate results for the determination of copper in the presence of zinc by a.s.v. The g.s.a.m. is used routinely in this laboratory, as it is simple and provides accurate results.

The interference of copper on the determination of zinc can be compensated for but not without paying a price. The theory of multicomponent analysis in the presence of interferences [32] states that when interferences are large, measurement errors actually can be amplified to produce larger uncertainties in the estimates of the response constants and initial analyte concentrations. An upper bound to this error amplification is the condition number of the matrix K. The cond(K) for K in Table 2 is 2.68 meaning that, in the worst case, the relative error in measuring the responses can be multiplied by 2.68 to give the relative error in final concentration estimates. However, it should be remembered that this is a worst-case upper bound.

When one considers all of the possible sources of error, propagation becomes much more complicated [32]. In fact, given a cond(K) of 2.68 and an estimated 1% error in making standard additions, and taking into account response errors and errors in the estimated response constants, upper-bound relative error estimates are 7% for zinc and 13% for copper.

Because the error bounds are truly only bounds, a further error propagation analysis was undertaken. Ten response matrices were calculated by perturbing the measured response matrix with a random normal error with mean zero and standard deviation equal to the measured errors in the responses. The g.s.a.m. calculations were carried out on all sets. The mean and standard deviation of these ten sets of g.s.a.m. results were then calculated (Table 3) and can be compared to those presented in Tables 1 and 2. Though the condition of K is large, the resulting relative precision in C_0 is less than 2% for zinc and less than 4% for copper. These error values are much more realistic than the mathematical bounds generated previously.

TABLE 2

Linear response constraints

	Zn peak	Cu peak
Zn	60.55	−0.47
Cu	−13.66	24.06

TABLE 3

Uncertainty perturbation results (IDC-g.s.a.m.) (mean values of ten calculations with standard deviations in parentheses)

K matrix	Zn peak	Cu peak
Zn	60.57 (0.18)	−0.50 (0.19)
Cu	−13.68 (0.10)	24.07 (0.11)
Initial concentrations (ppb)		
	$[Zn]_0$ = 13.15 (0.23)	$[Cu]_0$ = 5.01 (0.20)

Finally, it should be noted that the true values fit well within the 95% confidence internal about the mean values (Table 3) or the calculated values from the g.s.a.m. (Table 1). Zinc at 13.3 ppb is within one standard deviation of the estimated concentration and copper is within two standard deviations.

CONCLUSION

The ability to compensate for intermetallic interference effects in anodic stripping voltammetry has been demonstrated. The often reported effect of copper interfering with zinc can be eliminated and the ability to monitor copper simultaneously has been substantially improved. Three possible methods of approaching the analysis of the data were used with no results clearly favoring the use of any particular method. Though the conditions associated with any chosen experimental design will favor one variant of g.s.a.m. over another, it is presently unclear how an *a priori* choice of one design over another may be made.

In addition, an error analysis was undertaken. Error bounds found through the application of advanced numerical methods appear to be overly broad. Until further studies are made with improved error estimates, a more reasonable approach is to rely on the results from the solution of several perturbed data sets. However, this does not diminish the value of the error-bound calculation for demonstrating how the overall experimental design may be improved.

The generalized standard addition method should be useful for eliminating not only the interference effects of intermetallic compounds in a.s.v., but interference effects and matrix effects in many other methods, and of other origins (spectral, chemical, physical), as well. Its application depends only on the ability to obtain the required number of responses while making standard additions.

The authors thank S. D. Brown for constructing the a.s.v. system. C. Jochum and Maynard du Koven deserve special thanks for many helpful discussions. This research was supported in part by the Office of Naval Research.

REFERENCES

1 Z. Galus, CRC Crit. Rev. Anal. Chem., 4 (1974) 359.
2 G. Tammann and W. Jander, Z. Anorg. Allg. Chem., 124 (1922) 105.
3 A. S. Russell, P. V. F. Cazalet and N. M. Irving, J. Chem. Soc., (1932) 852.
4 W. Kemula and Z. Galus, Bull. Acad. Pol. Sci. Ser. Sci. Chim., 7 (1959) 553.
5 W. Kemula, Z. Galus and Z. Kublik, Bull. Acad. Pol. Sci. Ser. Sci. Chim., 7 (1959) 613.
6 W. Kemula, A. Galus and Z. Kublik, Bull. Acad. Pol. Sci. Ser. Sci. Chim., 7 (1959) 723.
7 W. Kemula and Z. Galus, Bull. Acad. Pol. Sci. Ser. Sci. Chim., 7 (1959) 729.
8 W. Kemula, Z. Galus and Z. Kublik, Ann. Chem., 33 (1959) 139.
9 B. K. Hovsepian and I. Shain, J. Electroanal. Chem., 14 (1967) 1.
10 M. Kopanica and F. Vydra, J. Electroanal. Chem., 31 (1971) 175.
11 R. S. Rogers, Ph.D. Thesis, Clarkson College of Technology, Potsdam, New York, 1970.
12 A. G. Stromberg and V. E. Gorodovykh, Zh. Neorg. Khim., 8 (1963) 2355.
13 S. T. Crosman, J. A. Dean and J. R. Stokey, Anal. Chim. Acta, 75 (1975) 421.
14 E. Barendrecht, in A. J. Bard (Ed.), Electroanalytical Chemistry, Vol. 2, M. Dekker, New York, 1967, p. 53.
15 E. M. Roizenblat and K. Z. Brainina, Elektrokhimiya, 5 (1969) 396.
16 W. Kemula and Z. Kublik, Nature (London), 182 (1958) 1228.
17 H. K. Ficker and L. Meites, Anal. Chim. Acta, 26 (1962) 172.
18 T. R. Copeland, R. A. Osteryoung and R. K. Skogerboe, Anal. Chem., 46 (1974) 2093.
19 A. A. Kaplin, N. K. Dzhabarova and A. G. Stromberg, J. Anal. Chem. USSR, 30 (1975) 308.
20 M. S. Shuman and G. P. Woodman, Jr., Anal. Chem., 48 (1976) 1979.
21 T. M. Florence, J. Electroanal. Chem., 35 (1972) 237.
22 M. I. Abdullah, B. Reuschberg and R. Klimek, Anal. Chim. Acta, 84 (1976) 307.
23 A. G. Stromberg, M. S. Zakharov and N. A. Mesyats, Elektrokhimiya, 3 (1967) 1440.
24 N. A. Mesyats, A. G. Stromberg and M. S. Zakharov, Elektrokhimiya, 4 (1968) 987.
25 R. G. Rudolph, Ph.D. Thesis, University of Nebraska, Lincoln, Nebraska, 1969.
26 W. L. Bradford, Chesapeake Bay Institute Report No. 76, Johns Hopkins University, Baltimore, Maryland, 1972.
27 M. Kozlovsky and A. Zebreva, in P. Zuman and I. M. Kolthoff (Eds.), Progress in Polarography, Vol. III, Interscience, New York, 1972.
28 M. S. Zakharov, Zh. Anal. Khim., 18 (1963) 450.
29 O. S. Stepanova, Izv. Tomsk. Politekh. Inst., 151 (1966) 14; Chem. Abstr., 67 (1967) 87214.
30 H. Kaiser, Pure Appl. Chem., 34 (1973) 35.
31 B. E. H. Saxberg and B. R. Kowalski, Anal. Chem., 51 (1979) 1031.
32 C. Jochum, P. Jochum and B. R. Kowalski, Anal. Chem., 53 (1981) 85.
33 S. D. Brown and B. R. Kowalski, Anal. Chim. Acta, 107 (1979) 13.
34 J. D. S. Danielson, S. D. Brown, C. J. Appellof and B. R. Kowalski, Chem. Biomed. Environ. Instrum., 9 (1979) 29.
35 D. E. Robertson, in M. Zief and R. Speights (Eds.), Ultrapurity Methods and Techniques, M. Dekker, New York, 1972, p. 207.
36 M. Zief and J. W. Mitchell, Contamination Control in Trace Element Analysis, J. Wiley, New York, 1976.
37 J. R. Moody and R. M. Linstrom, Anal. Chem., 49 (1977) 2264.
38 G. E. Batley and D. Gardner, Water Res., 11 (1977) 745.
39 M. J. Pinchin and J. Newham, Anal. Chim. Acta, 90 (1977) 91.

Analytica Chimica Acta, 134 (1982) 129—137
Elsevier Scientific Publishing Company, Amsterdam — Printed in The Netherlands

OBTAINING THE KEY SET OF TYPICAL VECTORS BY FACTOR ANALYSIS AND SUBSEQUENT ISOLATION OF COMPONENT SPECTRA

EDMUND R. MALINOWSKI

Department of Chemistry and Chemical Engineering, Stevens Institute of Technology, Hoboken, NJ 07030 (U.S.A.)

(Received 21st July 1981)

SUMMARY

The key set of typical rows (or typical columns), used to reproduce a data matrix, are obtained by finding the set of rows (or set of columns) most orthogonal to each other. If the data matrix consists of the spectra of a series of related mixtures, and there exists at least one data point unique to each of the components, the spectra of the pure components can be isolated. The method is applied to problems in nuclear magnetic resonance, gas—liquid chromatography and mass spectrometry.

One of the objectives of factor analysis is to express a data matrix in terms of a minimum number of factors. A key set of typical rows or typical columns, taken from the data matrix itself, is often used for this purpose when the real underlying factors have not been deduced or when one simply wishes to correlate the data [1]. This modeling technique has been successfully employed in a variety of chemical applications involving areas such as nuclear magnetic resonance [2], mass spectroscopy [3], biological activity [4] and gas—liquid chromatography [5, 6].

For a data matrix lying in an n-dimensional factor space, any arbitrary set of n rows or n columns (called typical vectors) will not necessarily span the factor space. The problem is to select that set of rows or columns which best reproduces the data. Finding the key set poses little difficulty when the data matrix is small because all possible combinations of typical (row or column) vectors can be tested in the "combination step" [1]. For large data matrices that lie in a factor space greater than three-dimensional, testing every possible combination becomes impractical. For example, if c were the number of data columns and n the number of factors, there would be $c!/(c - n)!n!$ combinations of typical columns; hence for a 35 × 35 data matrix involving six factors there would be $35!/(35 - 6)!6! = 1{,}623{,}160$ combinations to be tested, a costly and time-consuming task even for large computers. There is, therefore, a need to develop efficient methods for obtaining the key set of typical vectors. Selzer and Howery [6] suggested using chemical insight to select a trial set of key vectors, substituting new vectors, one at a time, tabulating the improvement and eventually generating an acceptable solution using a greatly reduced set of combination tests.

This procedure, although more efficient, is also time-consuming. A rapid, automatic method for obtaining the key set of typical vectors is developed herein and is applied to several chemical problems.

BASIS OF THE METHOD

The strategy of the method is based on the investigation of Knorr and Futrell [7] involving the separation of the mass spectra of pure components from the spectra of mixtures by factor analysis. They isolated the real component spectra by searching for "pure masses", i.e., unique to each component. The pure masses were located as follows. First, the abstract mass-cofactor matrix (i.e., the row-factor matrix resulting from principal factor analysis) was normalized so that the sum of squares across each row was unity. The first "pure mass" point (a key point) was chosen to be that containing the least amount of the first principal eigenvector. The second "pure mass" was selected to be that having the greatest difference in the second eigenvector contributions between it and the first "pure mass". The third "pure mass" was that with the greatest difference in the third eigenvector contributions between it and the average of the previously chosen "pure masses". This process of averaging the next eigenvector contributions of the previously chosen "pure masses", then finding the mass with the greatest difference in its corresponding eigenvector contribution was continued until all n "pure mass" points (i.e., all key points) were obtained. An $n \times n$ non-orthogonal rotation matrix, constructed from the chosen set of "pure mass" vectors, was then used to transform the abstract row matrix into component spectra.

This procedure works well when the factor space is three-dimensional or less, but will fail when the factor space is greater than three and there is a mass point that lies close to the first, second or third "pure masses", a situation which is likely to occur with large data matrices. A better procedure, outlined below, is to find the mass point (key point) whose component vector representation is most orthogonal to the resultant component vector representation of the previously chosen "pure mass" points (key points) in their corresponding subspace. This method can be used not only to isolate pure component spectra but also to select the key set of typical rows or columns.

METHOD

Principal factor analysis [1], also known as principal component analysis, is used to decompose a data matrix, **D**, into an abstract row matrix, **R**, and abstract column matrix, **C**, such that $\mathbf{D} = \mathbf{RC}$ within experimental error. These matrices are called abstract because they constitute mathematical solutions, devoid of any chemical meaning. It is often desirable to express the data in terms of a key set of typical data rows, $\mathbf{D}_{key}$, chosen from the

data matrix itself. To achieve this, a transformation matrix T must be found so that

$$D = RTT^{-1}C = D_{key}\bar{C} \tag{1}$$

where $D_{key} = RT$ and $\bar{C} = T^{-1}C$. Any arbitrary set of data columns chosen from the data matrix will not necessarily span the factor space nor satisfy Eqn. (1).

It is proposed here that the key set of typical rows is that which has the most unique behavior, recognizable as those with relative mixtures of eigenvectors least like the first principal eigenvector and least like each other, i.e., most orthogonal to each other. Accordingly, after the size of the factor space is deduced, each row of the abstract row-factor matrix, viewed as a vector composed of n elements, is normalized to unit length. This normalization places each row point on the surface of an n-dimensional hypersphere in factor space. The coordinates of the factor space are the primary set of eigenvectors that constitute the rows of the abstract column-factor matrix. Normalization provides a method for comparing the vector directions of the row points in factor space in relation to the eigenvector axes.

If $V_i = (v_{i1}, v_{i2}, \ldots, v_{in})$ is the ith row vector of the abstract row-factor matrix after normalization, v_{ik} would represent the relative importance of the kth eigenvector on the direction of the ith row. The first key row is that row which contains the least relative amount of the first eigenvector (i.e., the row with v_{i1} closest to zero). Because the first eigenvector accounts for a maximum of the variation in the data and lies in a direction passing through the highest density of row points, this row will have a direction least like the most important eigenvector.

Each eigenvector which emerges from factor analysis successively accounts for a maximum variation in the residual data. Thus this first eigenvector is most important, the second eigenvector is next most important, and so on. To obtain the second key row, only the first two components of each normalized row vector are considered because these components are associated with the two most important eigenvectors. Hence the jth row with $V_j = (v_{j1}, v_{j2})$ most orthogonal to the first chosen row vector, V_i, in two-dimensional space will be the second key row point. In other words, the dot product between V_i and V_j should be a minimum in the two-dimensional subspace.

To obtain the third key row, only the first three components of the normalized row vectors are considered. The third key row will be that which is most orthogonal to the plane defined by the first two chosen row vectors, expressed in three-dimensional space. This is accomplished by recognizing that the cross product between the first two chosen row vectors is a vector perpendicular to the plane, hence the dot product between this vector and the most orthogonal row vector will be farthest from zero. If $V_k = (v_{k_1}, v_{k2}, v_{k3})$ represents the third key row then mathematically

$$(\mathbf{V}_i \times \mathbf{V}_j)\cdot\mathbf{V}_k = \begin{vmatrix} v_{i1} & v_{i2} & v_{i3} \\ v_{j1} & v_{j2} & v_{j3} \\ v_{k1} & v_{k2} & v_{k3} \end{vmatrix} \quad (2)$$

The third key row is that row which makes the value of the determinant expressed in Eqn. (2) farthest from zero.

In a similar manner, each successive key row can be extracted from the normalized row matrix. In general, the mth key row is that row vector which makes the value of the determinant constructed from itself and the previously chosen key rows farthest from zero in mth space, i.e.,

$$\det \begin{vmatrix} v_{i1} & v_{i2} & \cdots & v_{im} \\ v_{j1} & v_{j2} & \cdots & v_{jm} \\ \vdots & \vdots & & \vdots \\ v_{m1} & v_{m2} & \cdots & v_{mm} \end{vmatrix}$$

is farthest from zero. The key set of typical columns is obtained by subjecting the transposed data matrix to the same procedure described above.

A computer program called KEYSET, written in FORTRAN IV, will locate the key sets of typical rows and typical columns of a 35 × 35 data matrix within a few seconds with a Digital Equipment Corporation DEC-SYSTEM-10 computer. Another program called KEYSET SPECTRAL ISOLATION, also written in FORTRAN IV, is designed to isolate the spectra of the pure components when the data matrix consists of the spectra of related mixtures and there are data points unique to each component. This program incorporates the KEYSET program in the initial stages, prints out a matrix of pure spectra and a corresponding matrix of relative concentrations. It also incorporates concepts based upon the theory of error for target factor analysis [1, 8], yielding errors associated with the intensities of each isolated spectra and errors in the relative concentration of each component. Copies of these programs with input instructions can be obtained from the author.

APPLICATIONS

Nuclear magnetic resonance

Weiner et al. [2] found that the effect of solvent on the proton magnetic resonance shifts of a series of simple substituted methanes required three factors. Based on some experience, they selected acetonitrile, carbon tetrachloride and dibromomethane to represent the three key solvents from which all other solvent shifts in the scheme could be predicted. The resulting equations, based on covariance, reproduced the original data with a root-mean-square difference of 0.79 Hz (see Table 1). This was judged to be excellent because this value was very close to the experimental error, ±0.5 Hz.

The KEYSET program, operating on the same data matrix, identified the three key solvents to be acetonitrile, carbon tetrachloride and diiodomethane, in excellent accord with the original choice of Weiner et al. [2], differing only in the selection of diiodomethane in place of dibromomethane. The

TABLE 1

Comparison of root-mean-square differences in predicting proton shifts obtained with various combinations of three solvents and the key set (first row) obtained by the KEYSET program

Solvent combination			RMS[a]	Solvent combination			RMS[a]
CH_3CN	CCl_4	CH_2I_2	0.673[b]	$CHCl_3$	CCl_4	CS_2	4.034
CH_3CN	CCl_4	CH_2Br_2	0.790[c]	CH_2Cl_2	CCl_4	CH_2Br_2	4.470
CH_3CN	CS_2	CH_2I_2	0.878	CH_3CN	CH_2Cl_2	$CHCl_3$	10.006
CH_2Br_2	CH_3I	CH_2I_2	0.972	CH_3CN	CH_3I	CH_2I_2	14.060
$CHBr_3$	CH_3I	CH_2I_2	1.410				

[a]Root-mean-square error of data reproduction (see Appendix). [b]Key set found by the KEYSET program. [c]Key set chosen intuitively by Weiner et al. [2].

RMS difference, 0.67 Hz (Table 1) was slightly greater than 0.5 Hz, showing that the KEYSET program selected an acceptable set of key solvents. When compared to all other arbitrary combinations of three solvents (a small selection of which is shown in Table 1), the KEYSET program choice was confirmed to be the best.

The three key solutes were identified by KEYSET to be methane, iodoform and chlorocyanomethane. The final equations, resulting from covariance-about-the-origin, were as follows:

$$S(CH_3CN, k) = 3.20\,f_1 - 0.09\,f_2 + 0.42\,f_3$$
$$S(CH_3Cl, k) = 2.62\,f_1 + 0.32\,f_2 + 0.21\,f_3$$
$$S(CH_2Cl_2, k) = 1.32\,f_1 + 0.56\,f_2 + 0.55\,f_3$$
$$S(CHCl_3, k) = -1.49\,f_1 + 0.69\,f_2 + 1.02\,f_3$$
$$S(CH_3Br, k) = 2.20\,f_1 + 0.23\,f_2 + 0.25\,f_3$$
$$S(CH_2Br_2, k) = 0.80\,f_1 + 0.51\,f_2 + 0.55\,f_3$$
$$S(CHBr_3, k) = -0.57\,f_1 + 0.91\,f_2 + 0.61\,f_3$$
$$S(CH_3I, k) = 2.21\,f_1 + 0.16\,f_2 + 0.22\,f_3$$
$$S(CH_2I_2, k) = 1.23\,f_1 + 0.54\,f_2 + 0.23\,f_3$$
$$S(CH_2ClBr, k) = 1.24\,f_1 + 0.53\,f_2 + 0.55\,f_3$$
$$S(CHBrCl_2, k) = 1.43\,f_1 + 0.77\,f_2 + 0.91\,f_3$$

where $f_1 = S(CH_4, k)$, $f_2 = S(CHI_3, k)$, and $f_3 = S(CH_2ClCN, k)$. In these equations $S(i, k)$ represents the proton shift of solute i, at very low concentration in solvent k, measured in Hz at 60 MHz with a trace of tetramethylsilane as an internal standard. These equations reproduce the data with an RMS difference of ±1.2 Hz. All other possible combinations yielded RMS differences that were larger than this value.

Gas—liquid chromatography

Correlating and predicting retention behavior in gas—liquid chromatography is difficult because of the large number of yet unknown factors involved. Using principal factor analysis, Selzer and Howery [6] found that

six abstract factors were required to regenerate the retention indices of some 18 ethers on 25 stationary phases. Because it was too time-consuming to examine every possible combination, they attempted to find the key set of typical ethers and the key set of typical stationary phases by the following procedure. An arbitrary number of combination sets of typical vectors was employed in data reproduction and the results were tabulated carefully. Those typical vectors which appeared most frequently in the better data reproductions were selected to constitute the key set of typical vectors. The results obtained by this method are shown in Table 2.

When the same data were subjected to the KEYSET program, the key sets shown in Table 2 were obtained within a few seconds. The root-mean-square error in data reproduction using these key sets were very close to those obtained by the key sets of Selzer and Howery. This demonstrates how efficiently the KEYSET program can find an acceptable combination of typical vectors.

It is interesting to note that the first three typical vectors chosen by the method of Knorr and Futrell [7] are identical to those selected by KEYSET, but then reached an impasse because the fourth vector was identical to the third. Thus only three of the six key vectors could be found by the Knorr–Futrell method.

Mass spectrometry

The KEYSET SPECTRAL ISOLATION program extracted from each of the mass spectral data matrices of Ritter et al. [9] the same "pure" masses as those obtained by Knorr and Futrell [7]. This was expected because each series of mixtures contained no more than three components, a situation for which the Knorr–Futrell method should be successful because no redundancies appear. The KEYSET SPECTRAL ISOLATION program has no such limitations. To learn specific details of how the key masses are used to isolate the spectra of the pure components, readers are referred to the publication of Knorr and Futrell [7].

TABLE 2

Key sets of typical ethers and typical stationary phases obtained by the KEYSET program compared to those obtained by Selzer and Howery [6]

Key set of typical ethers		Key set of typical stationary phases	
KEYSET program	Selzer and Howery	KEYSET program	Selzer and Howery
Dimethyl ether	Dimethyl ether	Hyprose SP80	Hyprose SP80
t-Butyl methyl ether	*t*-Butyl methyl ether	Zonyl E7	Zonyl E7
Isopropyl propyl ether	Butyl ethyl ether	Carbowax 20M	Carbowax 20M
t-Butyl isopropyl ether	Diisopropyl ether	Diglycerol	Diglycerol
Ethyl vinyl ether	Diisopentyl ether	Dow Corning FS1265	SE-52
Butyl vinyl ether	Isobutyl vinyl ether	Apiezon L	Flexol 8N8
3.9[a]	4.0[a]	4.2[a]	2.9[a]

[a]Root-mean-square error of data reproduction (see Appendix).

To test further the KEYSET SPECTRAL ISOLATION method, an artificial data matrix, generated by randomly mixing mass spectral data of five pure components [10] (see Table 3), was investigated. The line intensities of each of ten mixed mass spectra were normalized so that the base peaks were 100. Random round-off was applied, thus introducing an average error of approximately 0.5 intensity units. When this data matrix (see Table 4) was subjected to abstract factor analysis [1, 11], the results shown in Table 5 were obtained. As seen in the table, all three error criteria clearly indicate the presence of five components (factors). The real error equals 0.51 when five abstract factors are employed; the imbedded error levels off after five factors, and the indicator function reaches a minimum at five factors. With five factors, the KEYSET program chose, chronologically, *m/z* 103, 138, 91, 120 and 70 to constitute the key set. With this key set, the spectra of each of the five hypothetically unknown components were isolated. The results are shown in Table 3 so that each point can be compared to its true

TABLE 3

Mass spectra of pure components compared to spectra isolated by the KEYSET SPECTRAL ISOLATION method

m/z	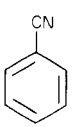		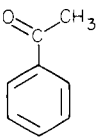		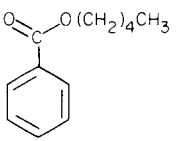		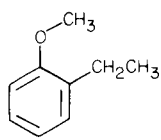		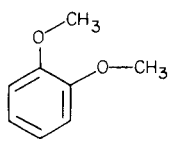	
	a	b	a	b	a	b	a	b	a	b
63	3	2	4	3	0	1	10	10	7	8
65	0	−1	4	5	0	0	20	20	23	23
70	0	0	3	0	85	87	1	0	0	0
76	32	32	5	5	8	9	1	−2	0	1
77	5	5	74	74	48	49	25	22	52	53
78	0	0	10	11	5	6	14	13	5	5
91	0	0	0	0	0	0	90	90	0	0
92	0	−1	4	5	0	0	9	9	5	5
93	0	0	3	4	0	0	9	9	4	4
95	0	−1	3	3	0	0	0	1	64	64
103	100	100	0	0	0	0	5	0	0	0
104	8	7	0	0	0	1	4	4	0	−1
105	0	0	100	100	100	100	8	4	0	0
106	0	1	1	11	8	8	2	1	0	0
120	0	0	29	31	0	0	1	0	0	0
121	0	0	0	0	0	1	100	100	1	0
122	0	0	0	−1	6	6	9	8	1	1
123	0	−1	0	−1	27	27	2	3	50	50
136	0	0	0	0	0	0	46	46	0	0
138	0	0	0	0	0	0	0	0	100	100
EFL[c]	—	±0.5	—	±0.5	—	±0.7	—	±0.5	—	±0.5

[a]Taken from graphs shown in reference [10]. [b]Obtained from KEYSET SPECTRAL ISOLATION. [c]Error in the factor loading.

TABLE 4

Simulated mass spectral data of ten mixtures of the five components listed in Table 3 (round-off error ±0.5)

m/z	Mixture number									
	1	2	3	4	5	6	7	8	9	10
63	9	10	5	14	10	7	16	14	6	11
65	13	22	6	29	25	8	30	28	10	26
70	29	11	64	24	31	28	20	52	49	16
76	36	7	21	5	12	28	25	37	14	6
77	61	100	62	67	100	74	81	100	72	100
78	11	15	10	18	13	13	20	15	13	17
91	40	25	22	89	8	24	90	41	31	40
92	5	9	3	11	8	5	13	8	6	10
93	6	7	3	11	6	5	11	8	5	9
95	11	37	0	24	59	2	23	53	7	41
103	100	11	42	11	20	71	72	100	27	2
104	10	1	5	5	2	7	9	9	4	2
105	63	92	100	48	80	100	64	78	100	87
106	7	10	10	5	7	10	7	8	9	10
120	8	24	8	4	13	20	12	5	13	21
121	44	27	25	100	10	28	100	46	34	45
122	6	3	6	10	4	4	10	9	7	5
123	18	31	21	28	55	8	25	58	19	35
136	21	13	12	46	4	13	45	21	15	21
138	17	54	0	36	90	0	33	82	8	60

value. The bottom line of the table lists the errors in the factor loadings, EFL, estimated from the key set target transformation matrix and the real error [1, 8]. These values are in complete agreement with the round-off error, ±0.5, that was purposely introduced.

In spite of the fact that two rows (*m/z* 103 and *m/z* 70) of the data matrix did not contain perfectly "pure" mass points, the spectral isolation was

TABLE 5

Results of abstract factor analysis of the data matrix shown in Table 4

n	Eigenvalue	Real error (RE)	Imbedded error (IE)	Indicator function (IND)
1	256164.15	16.92	5.35	0.209
2	21191.68	13.77	6.16	0.215
3	17665.59	9.52	5.21	0.194
4	10231.84	4.52	2.86	0.125
5	2421.77	0.51	0.36	0.020
6	10.00	0.45	0.35	0.028
7	5.87	0.41	0.34	0.046
8	5.20	0.35	0.31	0.088
9	3.58	0.26	0.24	0.258
10	1.33	—	—	—

successful. Inspection of other data sets containing "almost pure" masses often produced erroneous results. To be reliable, the method requires at least one relatively "pure" mass point for each component. Because mixtures containing isomers will rarely meet this stringent requirement, the method is not recommended when isomers are suspected to be present.

Appendix

When the root-mean-square (RMS) difference between the raw data and the reproduced data is computed using typical vectors it is important to take into account the correct number of degrees of freedom. If r is the number of rows, c the number of columns and n the number of factors, there are $r(c-n)$ degrees of freedom when typical columns are used and $(r-n)c$ degrees of freedom when typical rows are used. Hence, for typical columns

$$\text{RMS} = \{[\sum(d_{ik} - d_{ik}^{\ddagger})^2]/[r(c-n)]\}^{1/2}$$

and for typical rows

$$\text{RMS} = \{[\sum(d_{ik} - d_{ik}^{\ddagger})^2]/[(r-n)c]\}^{1/2}$$

where d_{ik} is a raw data point and $d_{ik}^{\ddagger}$ is a reproduced data point.

REFERENCES

1 E. R. Malinowski and D. G. Howery, Factor Analysis in Chemistry, J. Wiley, New York, 1980.
2 P. H. Weiner, E. R. Malinowski and A. R. Levinstone, J. Phys. Chem., 74 (1970) 4537.
3 R. W. Rozett and E. McLaughlin Petersen, Anal. Chem., 47 (1975) 2377; 48 (1976) 817.
4 M. L. Weiner and P. H. Weiner, J. Med. Chem., 16 (1973) 655.
5 D. G. Howery, P. H. Weiner and J. F. Blinder, J. Chromatogr. Sci., 12 (1974) 366.
6 R. B. Selzer and D. G. Howery, J. Chromatogr., 115 (1975) 139.
7 F. J. Knorr and J. H. Futrell, Anal. Chem., 51 (1979) 1236.
8 E. R. Malinowski, Anal. Chim. Acta, 103 (1978) 339.
9 G. L. Ritter, S. R. Lowry, T. L. Isenhour and C. L. Wilkins, Anal. Chem., 48 (1976) 591.
10 H. Budzikiewicz, C. Djerassi and D. H. Williams, Interpretation of Mass Spectra of Organic Compounds, Holden—Day, San Francisco, 1964.
11 E. R. Malinowski, Anal. Chem., 49 (1977) 612.

Analytica Chimica Acta, 134 (1982) 139—151
Elsevier Scientific Publishing Company, Amsterdam — Printed in The Netherlands

POTENTIAL METHODS IN PATTERN RECOGNITION
Part 5. ALLOC, Action-orientated Decision Making

D. COOMANS and D. L. MASSART*

Farmaceutisch Instituut, Vrije Universiteit Brussel, Laarbeeklaan 103, B-1090 Brussels (Belgium)

I. BROECKAERT

Dienst Gastro-Enterologie, Sint Pieter Hospitaal, Hoogstraat 322, B-1000 Brussels (Belgium)

(Received 20th July 1981)

SUMMARY

The possibilities of action-orientated pattern recognition with the supervised pattern recognition technique, ALLOC, are discussed. The emphasis is on the importance of the definition of overlapping regions between classes as a way for obtaining more information about the separation between classes. Action-orientated classification and feature selection with ALLOC are discussed using the results obtained for two data bases concerning the characterization of the functional state of the thyroid and the determination of the origin of milk samples.

In a previous article of this series [1], classification of objects with the supervised pattern recognition method, ALLOC, of Hermans and Habbema [2] was discussed. A single boundary between each pair of related classes is then needed in the pattern space. The boundary corresponds with the minimum *a posteriori* probability of error [1, 2]. This means that an object is classified in the class to which it seems to belong with the largest *a posteriori* probability (as obtained with the Bayes equation). The use of the minimum *a posteriori* probability of error rule is based on the assumption that it is not worse to misclassify an object from one class than to misclassify an object from another class. The usual way to evaluate the performance of such a classification rule is to calculate the correct classification rate.

Such a classification problem is often called an identification problem [2]. In analytical chemistry, classification problems are often pure identification problems. For identification problems, one often uses non-probabilistic methods such as KNN (k-nearest neighbour rule) [3—5] and LLM (linear learning machine) [3, 4, 6, 7]. In the related domain of medical decision-making based on the results of laboratory tests, however, non-probabilistic methods seldom find application. The reason is that a medical decision is never related to a simple identification but to an action which may have important consequences. For instance, a physician will not consider a patient

0003-2670/82/0000-0000/$02.75

as healthy when the probability that he is healthy is only slightly larger than the probability that he is not; more certain diagnosis is needed because of the risk associated with a misclassification. Such a risk is usually not equal for the classification of an ill patient as normal and a healthy one as ill. All this leads to the use of action-orientated decision boundaries and the construction of overlapping regions (regions of doubt) between the diagnostic classes. Moreover, it is often seen that patients belonging to the overlapping regions require an action distinct from those where the diagnosis has been established with a high degree of certainty.

On the same basis, some classification problems encountered in non-clinical analytical chemistry may also need an action-orientated approach. For instance, the determination of the origin of milk samples [8, 9] may be considered action-orientated. This happens when the decisions are associated with food quality control where for instance pure samples have to be differentiated from adulterated samples.

The aim of this paper is to discuss the action-orientated possibilities of ALLOC on the basis of the THYROID (1, 10-12) and MILK (8, 9) examples used in previous papers. It is also shown that, even for identification problems, an action-orientated approach, and more especially the evaluation of the amount of overlap between classes, gives rise to a more complete picture of the performance of a probabilistic classification technique.

ACTION-ORIENTATED PROCEDURES

Action-orientated classification

An action-orientated classification procedure starts with the determination of the *a posteriori* probabilities of class membership. This is done on the basis of the Bayes equation [13, 14]. In a previous article of this series [1], it was seen that ALLOC differs from other probabilistic techniques in the way in which the probability densities in the Bayes equation are estimated.

Action-orientated classification with ALLOC can be carried out according to two different philosophies. First, the minimum probability of error classification rule is replaced by the minimum overall risk rule. This means that the boundary between two classes is displaced so that it is closer to the class with smaller misclassification risk (meaning that it is considered a smaller risk that a patient who belongs in reality to this class is classified into another one). Alternatively, a region containing doubtful cases is defined, which means that the boundary is now a zone instead of a line.

The minimum overall risk rule. The minimum overall risk classification corresponds with the classification of an object in the class with the smallest conditional risk. The conditional risk of an object i with measurements $\mathbf{x}_i$ for a class ω_p out of K classes is given by the equation

$$R(\omega_p/\mathbf{x}_i) = \sum_{q=1}^{K} l_{pq} P(\omega_q/\mathbf{x}_i) \qquad (1)$$

$P(\omega_q/\mathbf{x}_i)$ is the *a posteriori* probability that an object with measurement vector $\mathbf{x}_i$ belongs to class ω_q and l_{pq} is the loss which quantifies the risk for an object i belonging to ω_q being allocated in ω_p. The l_{pq} values are the elements of the so-called loss matrix L, i.e.,

$$\mathbf{L} = \begin{bmatrix} l_{11} \ldots l_{p1} \ldots l_{K1} \\ \vdots \\ l_{1q} \ldots l_{pq} \ldots l_{Kq} \\ \vdots \\ l_{1K} \ldots l_{pK} \ldots l_{KK} \end{bmatrix} \tag{2}$$

The diagonal elements of the loss matrix are the losses associated with a correct classification. In this study, they are considered to be zero. For two-class problems, Eqn. (1) reduces to

$$R(\omega_1/\mathbf{x}_i) = l_{11}P(\omega_1/\mathbf{x}_i) + l_{12}P(\omega_2/\mathbf{x}_i) \tag{3}$$

$$R(\omega_2/\mathbf{x}_i) = l_{21}P(\omega_1/\mathbf{x}_i) + l_{22}P(\omega_2/\mathbf{x}_i) \tag{4}$$

An object i is classified in ω_1 if

$$R(\omega_1/\mathbf{x}_i) < R(\omega_2/\mathbf{x}_i) \tag{5}$$

otherwise it is classified in ω_2.

The most difficult point in this approach is the quantification of the risks in terms of loss values. Many authors have considered this problem in medical decision-making and concluded that in this field much more work has to be done before accurate loss values will be available. A review is given in the book by Patrick [15]. However, this action-orientated approach appears to be of great interest for screening purposes in medical decision-making as well as in analytical chemistry, i.e., the decision boundary is placed in the pattern space in such a way that almost no members of a given class are misclassified which means that one is screening for possible members of that class. In this situation, the value for the losses for the misclassification of members of the screened class are made large with respect to the losses for other misclassifications.

The boundary region approach. The simplest way to implement this approach is to separate each pair of adjoining classes (say they are ω_1 and ω_2) by two boundaries instead of one. The first boundary defines the separation between ω_1 and the overlapping region ω_{12} and the second separates ω_2 from ω_{12}.

For a two-class problem the loss matrix of Eqn. (2) becomes

$$\mathbf{L} = \begin{bmatrix} 0 & a \\ b & 0 \end{bmatrix} \tag{6}$$

where a is the loss associated with a misclassification of an object of ω_2 in ω_1, and b is the loss associated with a misclassification of an object of ω_1 in ω_2.

If a equals b, then

$$\mathbf{L} = \begin{bmatrix} 0 & 1 \\ 1 & 0 \end{bmatrix} \tag{7}$$

The minimum conditional risk classification rule reduces to the minimum *a posteriori* probability of error rule or in other words the action-orientated approach reduces to the identification approach. If one assumes that the prior probabilities in the Bayes equation are the same, the decision boundary between the classes is situated in the position where the two probability density curves cross each other in Fig. 1.

A boundary region can be obtained by considering two different ratios a/b. The boundary which is closest to the ω_2 class is determined by considering $b > a$. This means that a misclassification of an object belonging to class ω_1 is considered to be worse than a misclassification of an object belonging to ω_2. Therefore the decision boundary with this loss matrix (III in Fig. 1) is displaced to the right of the identification boundary II. The second boundary can be obtained by taking $b < a$. This boundary, I, is closer to ω_1 than the identification boundary II. The region between boundaries I and III is the overlapping region ω_{12}. On the basis of these boundaries, it is possible to obtain an estimate of the degree of overlap of classes ω_1 and ω_2. The number of objects situated in the boundary region is counted and the correct classification rate is calculated. This refers to objects which are classified in the correct class (not in the overlapping region). A more complete picture is obtained when the degree of overlap is explored in a dynamic way by varying the boundaries I and III. Up to now only two adjoining learning classes have been considered. However, the concept of overlapping regions can be extended to more adjoining classes and to the multivariate case.

ALLOC defines for the boundaries I and III of the two-class problem of Fig. 1 a threshold value δ for the *a posteriori* probabilities. The decision rule for a K-class problem then becomes: classify i in class ω_p if

$$P(\omega_p/\mathbf{x}_i) = \max\,[P(\omega_q/\mathbf{x}_i)]\,;\; q = 1, \ldots, K \tag{8}$$

and

$$P\,(\omega_p/\mathbf{x}_i) > \delta \tag{9}$$

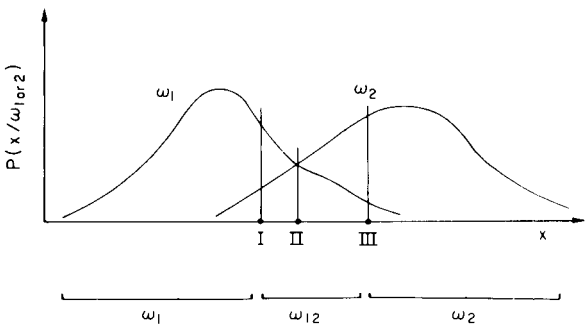

Fig. 1. Classification boundaries between two classes ω_1 and ω_2 according to the loss matrix given by Eqn. (6). Boundaries: I, $a > b$; II, $a = b$; III, $a < b$.

If object i is not classified in any class by application of expressions (8) and (9), it is a boundary zone case.

A close relationship exists between the loss matrix and δ. It can be shown for the binary decision problem that the relationship between a, b and δ is given by

$$\delta = b/(a + b) \text{ for } P(\omega_1/\mathbf{x}_i) \tag{10}$$

and

$$\delta = a/(a + b) \text{ for } P(\omega_2/\mathbf{x}_i) \tag{11}$$

When symmetrical overlap regions are used, two boundaries are considered so that for the first boundary the loss matrix of Eqn. (6) is used (loss matrix $\mathbf{L}$ with $b > a$) and for the second boundary a loss matrix where a is replaced by b and b by a (loss matrix $\bar{\mathbf{L}}$ with $a > b$). In this situation the decision rule as formulated in expressions (8) and (9) for two classes is equivalent to: classify i in class ω_1 if

$$R(\omega_1/\mathbf{x}_i) < R(\omega_2/\mathbf{x}_i) \tag{12}$$

and in class ω_2 if

$$\bar{R}(\omega_2/\mathbf{x}_i) < \bar{R}(\omega_1/\mathbf{x}_i) \tag{13}$$

If object i is not classified, it is a boundary zone case. R and $\bar{R}$ indicate that the loss matrices $\mathbf{L}$ and $\bar{\mathbf{L}}$, respectively, are used. The latter decision rule (expressions 12 and 13) can be considered as an extension of the rule given by expression (5).

Further extensions of the concept of overlapping regions have been discussed by Habbema et al. [16] and Hermans et al. [17], but they have not been implemented in ALLOC.

Action-orientated feature selection

It has already been shown [9] that the forward feature selection procedure of ALLOC is directly based on classification rates. An accurate way to express a classification rate in an identification problem is the probability of error estimated by means of the leave-one-out classification of the members of the learning set. The probability of error is then given by

$$P(\text{error}) = \sum_{q=1}^{K} P(\omega_q)\, n_q(\text{error})/n_q \tag{14}$$

where for ω_q, $q = 1, \ldots, K$ (the K learning classes), $P(\omega_q)$ is the prior probability of ω_q (for explanation, see [9]), n_q(error) is the number of objects belonging to ω_q, misclassified on the basis of the leave-one-out procedure, and n_q is the total number of objects belonging to ω_q.

The feature selection procedure described earlier [9] may be applied also in action-orientated feature selection on the condition that P be replaced by

R, the overall conditional risk estimated by means of the leave-one-out classification of the members of the learning set. The overall conditional risk is given by

$$R = \sum_{p=1}^{K} \sum_{q=1}^{K} P(\omega_q)\, l_{pq}\, n_{pq}(\text{error})/n_q \qquad (15)$$

where n_{pq}(error) indicates the number of objects belonging to ω_q but which are misclassified in ω_p.

The selection procedure of ALLOC proceeds until a subset of variables is selected that gives rise to a decrease of R which is smaller than a threshold value T. However, the selection of the subset that minimizes R seems to be a better choice (see also [9]).

DATA BASES

Differentiation of pure milk from different species and mixtures (MILK)

Statistical linear discriminant analysis was applied to these data by Smeyers-Verbeke et al. [8] and the same data were used earlier [9] for discussion of the feature selection procedure of ALLOC. The data base consists of different milk classes, each of which has 20 samples characterized by 15 gas chromatographic peak measurements. Besides the three pure milk classes — cow (C), goat (G) and sheep (S) — synthetic binary mixtures are also considered. In the present study, the same binary differentiations as studied earlier [9] are investigated, i.e., the differentiation between a pure milk class and another pure milk class or a related 9/1 mixture class.

The MILK differentiation problem is a typical example in analytical chemistry where an action-orientated approach may be of interest in practice.

Functional state of the thyroid gland (THYROID)

This data base consists of three learning classes : EU, HYPER and HYPO. For each patient (blood sample), five laboratory results (RT3U, T4, T3, TSH, ΔTSH) are available. From the clinical point of view, the differentiation EU/HYPER and EU/HYPO is of interest. Studies on this data base have been reported earlier (1, 10—12).

RESULTS AND DISCUSSION

Evaluation of the overlap between classes

For this purpose, symmetrical overlap regions are used. For symmetrical overlap regions, the methods discussed above under Action-orientated procedures are the same, and so the method corresponding to expressions (8) and (9) is used. The threshold probability δ defines the symmetrical overlap region. In the MILK example as well as in the THYROID example, the overlaps are evaluated on the basis of the percentage of objects which are correctly classified with a δ degree of certainty, i.e., objects that are classified

in the correct class (not in the overlapping region). In a binary decision problem, the first value (0.500) corresponds to a single identification boundary.

For the milk example, the optimal subset of variables selected by the ALLOC selection procedure [9, 18] was used initially. Table 1 shows the number of samples which are correctly classified with a δ degree of certainty as a function of δ. It can be seen that more information can be obtained about the separation of the classes by considering different δ values instead of one single identification boundary with $\delta = 0.500$. For instance, although the pure milk classes seem to be separated completely from each other on the basis of $\delta = 0.500$, a further comparison can be made on the basis of the degree of certainty of the classification; for the differentiation S/G (sheep/goat), no overlap is observed up to a δ value equal to 0.950 but for the other differentiations C/S (cow/sheep) and C/G (cow/goat) the separation is not so clear-cut. It can be concluded that S/G can be better distinguished than C/G and C/S, and C/S better than C/G. Furthermore, it can be seen that differentiation of the mixture C9G1 from C is not so obvious as indicated by the straightforward identification results. Moreover, the results obtained with large δ values show that the separation C/C9G1 is somewhat more difficult than the separation C/G. Although this was expected, it could not be observed from the classification rate of the simple identification approach. When a safe overlap region is created by taking, e.g., $\delta = 0.95$, then Table 1 shows that very few, if any, samples can be identified with certainty for the differentiations C/C9S1, S/C1S9 and G/S1G9. This means that, although a relatively good classification rate is obtained for $\delta = 0.500$, in practice predictions are very difficult and doubtful in these situations.

The THYROID example also shows clearly that the evaluation of overlap regions gives more complete information about the separability of the

TABLE 1

MILK differentiations showing the number of samples (the maximum, i.e., 100% correct classification is 40) correctly classified with δ degree of certainty

δ	C/G (1)[a]	C/S (1)	S/G (1)	C/C9S1 (3)	S/C1S9 (3)	C/C9G1 (3)	G/S1G9 (2)
0.500	40	40	40	37	32	40	32
0.600	39	40	40	29	22	39	26
0.750	38	40	40	20	12	37	10
0.800	38	40	40	15	6	35	4
0.900	37	39	40	7	2	27	1
0.950	37	38	40	2	1	18	1
0.975	35	37	39	2	1	12	1
0.990	32	32	39	2	0	6	1
0.999	19	20	37	0	0	4	0

[a]The number in brackets is the number of variables used in the particular differentiation problem.

learning classes and about the confidence that one may have in the classification of new objects. For the ALLOC classification on the basis of the original set of 5 laboratory tests, Table 2 reveals that a better classification rate is obtained with $\delta = 0.500$ and with the 5 original laboratory tests for the differentiation EU/HYPER than for the differentiation EU/HYPO. However, as the δ values are increased, it can be seen that for the HYPO class, in contrast to the HYPER and EU classes, there is no decrease of the correct classification rate. This means that a larger number of HYPO cases can be detected with a higher degree of certainty (see $\delta > 0.95$).

This way of presenting results is much more useful in (medical) decision-making. In fact, non-probabilistic pattern recognition techniques such as the linear learning machine (LLM) are not useful at all in medical decision making and in many problems in analytical chemistry where a degree of certainty is required for a decision, even when excellent classification results are obtained, such as have been shown earlier [1].

Another example concerns the difference between an ALLOC classification on original data or after preprocessing by statistical linear discriminant analysis (SLDA + ALLOC); the latter has been discussed [12]. Table 2 shows that on the basis of a simple leave-one-out classification of the learning classes ($\delta = 0.500$), no important difference is obtained between ALLOC and SLDA + ALLOC for both the EU/HYPER and EU/HYPO differentiations. However, SLDA + ALLOC performs less well than ALLOC does, because the correct classification rate decreases with increasing δ value faster for SLDA + ALLOC; the EU cases are usually not detected with a high degree of certainty on the basis of SLDA + ALLOC. A reason for the worse results of SLDA + ALLOC is certainly the loss of information. In the case of binary decision problems, the SLDA + ALLOC procedure supposes that the different probability levels (chosen by means of the δ values) are parallel hyperplanes in the pattern space. In reality, this is seldom the case. The original ALLOC classification procedure, however, is able to discover the real form of the decision boundaries. For the examples given in Table 2, the loss of information was observed only when higher δ values were considered instead of simply 0.500. The loss for EU/HYPO is larger than for EU/HYPER. For practical reasons and in situations discussed earlier [12], however, SLDA + ALLOC may still be preferred to ALLOC applied on the original variables although the performance is somewhat less good.

Feature selection in the case of symmetrical overlapping regions

The feature selection procedure discussed earlier [9] was based on the maximum correct classification rate without considering overlapping regions. The criterion for the selection of the optimal subset of variables is given above by Eqn. (11). The question whether the selected optimal subset of variables also minimizes the overlap between the classes, i.e., maximizes the correct classification rate according to "classification with δ degree of certainty", is of some importance. In the MILK example this was evaluated by calculating

TABLE 2

THYROID example showing the classification rates with δ degree of certainty

δ	EU/HYPER						δ	EU/HYPO					
	ALLOC (original variables)			SLDA + ALLOC				ALLOC (original variables)			SLDA + ALLOC		
	EU	HYPER	Mean	EU	HYPER	Mean		EU	HYPO	Mean	EU	HYPO	Mean
0.500	99	97	98	97	97	97	0.500	99	87	93	97	93	95
0.600	99	97	98	97	97	97	0.600	99	83	91	97	93	95
0.750	99	94	96.5	96	94	95	0.750	99	83	91	95	93	94
0.800	98	94	96	94	91	92.5	0.800	99	83	91	91	93	92
0.900	97	89	93	88	91	89.5	0.900	98	83	91	79	90	84.5
0.950	93	77	85	84	89	86.5	0.950	97	83	90	67	87	77
0.975	92	71	81.5	81	89	85	0.975	95	83	89	58	80	69
0.990	90	69	79.5	71	74	72.5	0.990	89	83	86	41	80	60.5
0.999	86	63	74.5	47	63	55	0.999	71	83	77	8	77	42.5

at each step of the feature selection procedure the number of samples which were correctly classified with δ degree of certainty for δ = 0.500, 0.750, 0.950 and 0.999. Figure 2 shows the diagrams for the binary differentiation of the pure milk samples C/G, C/S and S/G, and Fig. 3 shows the diagrams for binary differentiations between mixtures and the related pure milk class. Figure 2 shows that the pure milk classes are completely distinguishable for each degree of overlap, but higher δ values require more variables than considered in the optimal subsets of Table 2. This is clearest for the differentiation C/S. For a simple classification, one variable suffices, but at least 4 and 8 variables are respectively necessary in order to obtain certainties of 0.950 and 0.999. For the differentiation between a pure milk and a mixture (Fig. 3) the behaviour of the curves is more complicated. When the four binary differentiations are observed the following conclusions can be reached. First, an important overlap is observed between the classes, in each step of the selection procedure; even where a complete separation is obtained with δ = 0.500 (see C/C9G1), the number of samples which are classified with a high degree of certainty is rather small. Secondly, in order to optimize the classification rate for a higher degree of certainty than 0.5, more variables are needed, i.e., more information is required. Thirdly, the negative influence observed on the classification rate for low δ levels when the number of variables used for ALLOC classification is increased up to the original set of 15 variables, is not observed for higher δ levels. This means that lower δ level classifications are more sensitive to noise, possibly because the more doubtful (i.e., closer to the borderline) the objects are, the more sensitive they are to noise.

The feature selection in the THYROID example was done in the same way as in the MILK example. Figure 4 shows for the EU/HYPER and EU/HYPO differentiation the relationship for δ = 0.500, 0.750, 0.950 and 0.999 between the percentage of correctly classified patients (leave-one-out procedure) and the number of selected variables in each step of the procedure. It can be seen for the EU/HYPER differentiation that at all levels of certainty, a set of 3 variables (i.e., T4, ΔTSH and T3) is the most appropriate choice. No important change was obtained when the other variables were added to the selected set. The separation is very acceptable : on the basis of the three vari-

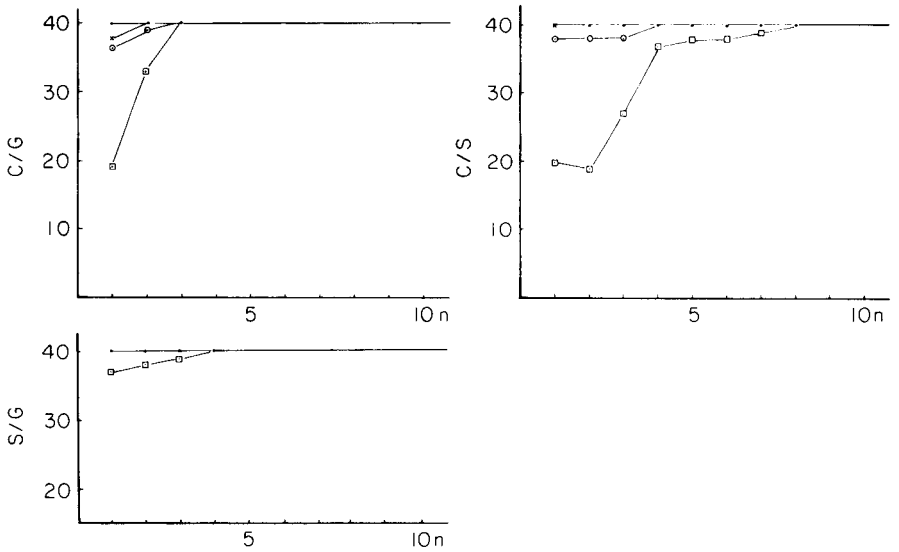

Fig. 2. Differentiation between pure MILK classes showing the relationship between the number of correctly classified samples with δ degree of certainty and the number of variables (n) selected by the ALLOC feature selection procedure according to Eqn. (14). (•)δ = 0.500; (×)δ = 0.750; (⊙)δ = 0.950; (⊡)δ = 0.999. The final lines shown up to n = 10 continue to n = 15.

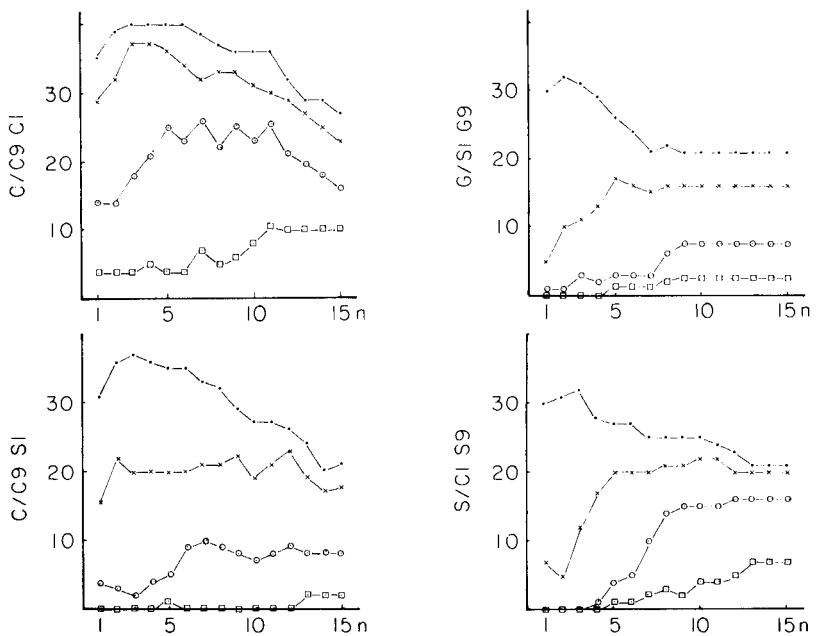

Fig. 3. Differentiation between a pure MILK class and a 9/1 mixture class showing the relationship between the number of correctly classified samples with δ degree of certainty and the number of variables (n) selected by the ALLOC feature selection procedure according to Eqn. (14). (•)δ = 0.500; (×)δ = 0.750; (⊙)δ = 0.950; (⊡)δ = 0.999.

ables 74% of the cases can be diagnosed with a certainty of 0.999. For the EU/HYPO differentiation, it was concluded in previous papers [9, 10] that the combination of two variables (T4 + ΔTSH) provides the best classification rate and that a further addition of variables causes a slight decrease of the classification rate. This is true for the simple identification (δ = 0.500) or with δ values such as δ = 0.750. However, Fig. 4 shows that for the larger δ values, a slight increase of the classification rate is observed when more variables are added to the proposed set of two. It can therefore be concluded that the first two variables are essential for a good separation between the classes; further addition of variables produces greater certainty about the classification. This may not be trivial for medical diagnosis. In this respect, the set of five variables is theoretically the most appropriate choice because 77% of the cases can be diagnosed with a certainty of 0.999. As in the MILK example, a decrease of the classification rate for small δ values together with an increase for the larger δ values is observed in the EU/HYPO differentiation. However this phenomenon is here less pronounced.

Action-orientated feature selection

In the previous section, the feature selection procedure for simple classification given by Eqn. (14) was evaluated in view of minimizing the amount of overlap between classes. In this section the action-orientated feature selection procedure given by Eqn. (15) is discussed on the basis of the THYROID example. It is assumed in this case that the losses associated with a correct diagnosis are zero. Five different ratios between a and b of the loss matrix of Eqn. (6) were considered, i.e., a/b = 100/1, 20/1, 1/1, 1/20 and 1/100. The value b is the loss associated with classifying an individual of the EU class in the pathological class and the value a is the loss associated with the inverse situation. In this way, five single boundaries are assumed. For the ratio 1/1, the feature selection is equivalent to the simple classification by Eqn. (14), the ratios 100/1 and 20/1 correspond to a selection of variables which are essential for screening pathological cases, and the ratios 1/20 and

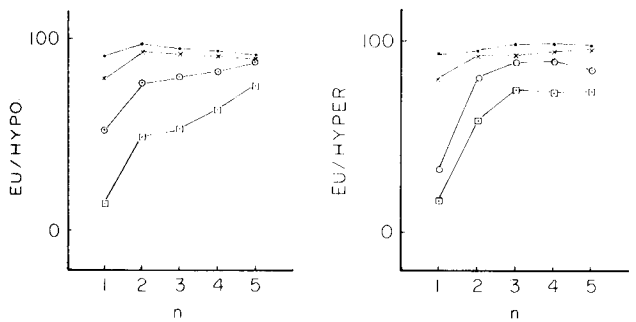

Fig. 4. EU/HYPO and EU/HYPER differentiation of the THYROID example showing the relationship between % correct classification with δ degree of certainty and the number of variables selected by the ALLOC feature selection procedure according to Eqn. (14). (•)δ = 0.500; (×)δ = 0.750; (⊙)δ = 0.950; (⊡)δ = 0.999.

TABLE 3

Action-orientated selection of features for the EU/HYPO differentiation according to different loss ratios a/b

Step	a/b				
	100	20	1	0.05	0.01
1	T4(0.026)[a]	T4(0.213)	T4(0.087)	TSH(0.183)	TSH(0.012)
2	TSH(0.015)	TSH(0.057)	ΔTSH(0.027)	T4(0.167)	T4(0.010)
3	ΔTSH(0.005)	RT3U(0.050)	T3(0.040)	ΔTSH(0.150)	T3(0.010)
4	RT3U(0.005)	T3(0.060)	RT3U(0.053)	RT3U(0.150)	RT3U(0.010)
5	T3(0.005)	ΔTSH(0.677)	TSH(0.073)	T3(0.150)	ΔTSH(0.042)

[a]Numbers in brackets are the overall conditional risks obtained in the particular step of the selection (see Eqn. 15).

1/100 correspond to a selection of variables essential for screening the EU-cases. Table 3 shows the sequence in which the variables were selected for the EU/HYPO differentiation according to the different loss ratios; the appropriate subset of variables is shown separated from the superfluous variables by underlines. It can be seen that the optimal subset of variables differs according to the ratio a/b. This means that screening of HYPO cases is preferentially done by measuring the variables T4, TSH and ΔTSH (a/b = 100) or T4, TSH and RT3U (a/b = 20). For screening of EU cases, only TSH and T4 are needed. It is surprising that T4 is most important for the HYPO screening while TSH is most important for the EU screening. These results can be explained on a biochemical basis, but this is outside the scope of this paper. Furthermore, it is possible to define overlapping regions on the basis of two screening boundaries (e.g., the ratios 100/1 and 1/100 which in fact correspond to δ = 0.99). However, this approach differs from the one discussed in the previous section because this leads to a classification based on two different subsets of variables, one for each boundary. However, with this approach the classification ratio found was only slightly better than with the single optimal set of variables proposed above (see Fig. 4). For the EU/HYPER differentiation, the influence of the loss ratio on the selection of variables was similar.

CONCLUSIONS

The action-orientated approach can be utilized in two ways involving either the construction of a decision boundary which takes different risks associated with the decision into account or the construction of overlapping regions. Even in identification problems, a more detailed picture will be obtained about the separability of the classes when overlapping regions are taken into account. In this respect, ALLOC is a very attractive software package for

pattern recognition. It combines an accurate method for probability estimation with the possibility of action-orientated classification and feature selection. A disadvantage, however, is the absence of criteria for the detection of outliers.

REFERENCES

1 D. Coomans, I. Broeckaert, A. Tassin and D. L. Massart, Anal. Chim. Acta, 133 (1981) 215.
2 J. Hermans and J. D. F. Habbema, Manual for the ALLOC-discriminant analysis program, Department of Medical Statistics, University of Leiden, P.O. Box 2060, Leiden, Netherlands, 1976.
3 D. L. Duewer, J. R. Koskinen and B. R. Kowalski, ARTHUR (available from B. R. Kowalski, University of Washington, Seattle).
4 A. M. Harper, D. L. Duewer and B. R. Kowalski, in B. R. Kowalski (Ed.), Chemometrics, Theory and Practice, Am. Chem. Soc. Symp. Ser., No. 52, 1977.
5 B. R. Kowalski and C. F. Bender, Pattern Recognition, 8 (1976) 1.
6 N. J. Nilsson, Learning Machines, McGraw-Hill, New York, 1965.
7 D. R. Preuss and P. C. Jurs, Anal. Chem., 46 (1974) 520.
8 J. Smeyers-Verbeke, D. L. Massart and D. Coomans, J. Assoc. Off. Anal. Chem., 60 (1977) 1382.
9 D. Coomans, M. P. Derde, I. Broeckaert and D. L. Massart, Anal. Chim. Acta, 133 (1981) 241.
10 D. Coomans, I. Broeckaert, M. Jonckheer, P. Blockx and D. L. Massart, Anal. Chim. Acta, 103 (1978) 409.
11 D. Coomans, L. Kaufman and D. L. Massart, Anal. Chim. Acta, 112 (1979) 97.
12 D. Coomans, I. Broeckaert and D. L. Massart, Anal. Chim. Acta, 132 (1981) 69.
13 G. F. Box and G. C. Tiao, Bayesian Inference in Statistical Analysis, Addison-Wesley, New York, 1973.
14 R. O. Duda and P. E. Hart, Pattern Classification and Scene Analysis, Wiley—Interscience, New York, 1973.
15 E. A. Patrick, Decision Analysis in Medicine: Methods and Applications, CRC Press, Boca Raton, Florida, 1979.
16 J. D. F. Habbema, J. Hermans and A. T. van der Burgt, Biometrika, 61 (1974) 313.
17 J. Hermans, J. D. F. Habbema and A. T. van der Burgt, Bull. I.S.I., 45 (1973) 523.
18 J. D. F. Habbema and J. Hermans, Technometrics, 19 (1977) 487.

Analytica Chimica Acta, 134 (1982) 153—165
Elsevier Scientific Publishing Company, Amsterdam — Printed in The Netherlands

AUTOMATED STANDARDIZATION TECHNIQUE FOR AN INDUCTIVELY-COUPLED PLASMA EMISSION SPECTROMETER

J. R. GARBARINO* and H. E. TAYLOR

U.S. Geological Survey, MS 407, P.O. Box 25046, Denver Federal Center, Lakewood, CO 80225 (U.S.A.)

(Received 12th May 1981)

SUMMARY

The manifold assembly subsystem described permits real-time computer-controlled standardization and quality control of a commercial inductively-coupled plasma atomic emission spectrometer. The manifold assembly consists of a branch-structured glass manifold, a series of microcomputer-controlled solenoid valves, and a reservoir for each standard. Automated standardization involves selective actuation of each solenoid valve that permits a specific mixed standard solution to be pumped to the nebulizer of the spectrometer. Quality control is based on the evaluation of results obtained for a mixed standard containing 17 analytes, that is measured periodically with unknown samples. An inaccurate standard evaluation triggers restandardization of the instrument according to a predetermined protocol. Interaction of the computer-controlled manifold assembly hardware with the spectrometer system is outlined. Evaluation of the automated standardization system with respect to reliability, simplicity, flexibility, and efficiency is compared to the manual procedure.

Inductively-coupled plasma (i.c.p.) atomic emission spectrometry offers the capability for simultaneous multi-element determinations of trace and major constituents in a variety of aqueous samples. The use of i.c.p. techniques for routine chemical analysis inherently requires some degree of data management and automated instrumentation, when large volumes of raw analytical data are produced in a laboratory environment. Currently, the U.S. Geological Survey uses an external minicomputer system for i.c.p. data acquisition, processing, and storage. Instrument automation consists of a minicomputer-controlled sampler subsystem that permits unattended sample introduction [1]. Unfortunately, the i.c.p. spectrometer in conjunction with the automatic sampler subsystem still has substantial disadvantages because of numerous operator-intensive activities. The operator is required to standardize the instrument frequently by means of a reagent blank and a series of four mixed-analyte standard solutions, and to periodically make judgements concerning quality control based on results obtained for a standard solution containing 17 analytes, dispersed among sample unknowns in the sampler tray.

0003-2670/82/0000-0000/$02.75

To minimize these disadvantages, a procedure was devised to facilitate computer-controlled standardization and on-line quality control [2]. Standardization is achieved by using a microcomputer-controlled assembly that consists of a manifold, a series of solenoid valves, and separate holding reservoirs for the reagent blank and each mixed-analyte standard solution. Each solenoid valve is actuated under computer control to allow the standard solution to be pumped to the nebulizer. During instrument standardization, the microcomputer disables the automatic sampler, actuates each solenoid valve in a specific order, transmits commands to the spectrometer to trigger initiation of a spectrometer integration period, and identifies each standard to the data acquisition system.

On-line quality control is achieved through software that tests results obtained for check standards. Normally, such standards, containing 17 analytes, are measured every five unknown samples. The results of all measurements whether for unknown samples or standards, are transmitted to the minicomputer for data processing. The sequence in which these standards and samples are measured needs to be entered into the minicomputer prior to the start of a series of measurements. This enables the minicomputer to distinguish between sample and standard data, so that the quality of the measurements can be assessed. If results for the standard are satisfactory, the automatic sampler continues to process samples. However, when results are unsatisfactory, the sample processing is halted, and the restandardization procedure is initiated. This real-time standardization procedure emulates the steps of the manual procedure except that the assembly of microcomputer and manifold eliminates standard manipulations and manual entry of spectrometer software commands.

This paper describes the manifold assembly, driver electronics, computer interface, and control software that makes automated standardization possible. This automated standardization system is evaluated with respect to its versatility and efficiency. The accuracy and precision of results obtained with this new system are compared with those from the manual standardization procedure.

EXPERIMENTAL

Instrumentation

The spectrometer used was the Jarrell-Ash Plasma AtomComp Model 975 provided with a Digital Equipment Corporation (DEC) PDP-8 minicomputer as the dedicated controller. The Jarrell-Ash Mark II Operating System provided software commands to control spectrometer functions. Minor modifications to the AtomComp hardware were made to implement control of the automatic sampler [1]. Because the PDP-8 is dedicated to controlling the spectrometer through Jarrell-Ash software, it was impractical to make software modifications to facilitate data management. Therefore, a DEC PDP-11 was interfaced with the PDP-8 to perform the following tasks:

(1) acquisition, processing, and storage of spectrometric data; (2) on-line quality control; and (3) initiation of standardization system software.

A Heathkit H-11, a microcomputer based on the DEC LSI-11 processor, was dedicated to control the standardization procedures. The standardization system required H-11 control of manifold operations and transmission of standardization commands to the AtomComp. This procedure was initiated by the PDP-11 through a hardware interface between the PDP-11 and H-11. All software needed to control the manifold assembly and provide real-time standardization was written in assembly coding.

The automated sampler subsystem consisted of a Technicon AutoAnalyzer II sampler modified to permit computer control of the sampler by the PDP-8 minicomputer [1].

A Gilson Minipuls II peristaltic pump was used to pump solutions from the sampler and manifold assembly to the nebulizer. Any pulsations caused by the pump had negligible effects on the precision and accuracy of individual determinations [3].

Reagents and solutions

All standards were prepared from ultra-high purity metals or metal salts, deionized water, and transistor-grade acids (Baker).

Single-element stock solutions (100 mg l^{-1}) were made in 1% (v/v) nitric acid. Four mixed-analyte working standards were prepared on a weekly basis by diluting aliquots of stock solutions to a final concentration of 10.0 mg l^{-1} for each analyte. Each mixed-analyte working solution was stored in a nitric acid-washed polytetrafluoroethylene (teflon) bottle. The composition of each mixed working standard solution is shown in Table 1.

A reagent blank was prepared by diluting 1 ml of concentrated nitric acid to 1 l with deionized water. This solution also was stored in an acid-washed teflon bottle. A mixed-analyte check standard containing every analyte present in the four mixed-analyte working standards, was prepared by diluting aliquots of stock solutions to a final concentration of 5.00 mg l^{-1} for each analyte.

Manifold assembly

The manifold assembly consisted of a branched glass-tubing manifold, four two-way miniature solenoid valves, two three-way miniature solenoid valves, and five solution reservoirs. Control of the manifold assembly required

TABLE 1

Composition of mixed working standard solutions

Standard number	Analytes	Standard number	Analytes
I	Cd, Fe, Pb, Mn, Zn	III	Ba, Li, Mo, SiO_2
II	Be, Co, Cu, Sr, V	IV	Ca, Mg, Na

solenoid-valve driver electronics in conjunction with a computer interface. The manifold was constructed from pyrex tubing (4-mm o.d.) with four branches offset from the main channel as shown in Fig. 1. Each branch inlet was connected to a solenoid valve via teflon tubing. The solenoid valve inlet was routed to one of the solution reservoirs via teflon tubing. All wetted components of the miniature solenoid valves used were constructed of teflon to eliminate corrosion and contamination. In addition, solenoid valves having small dead volumes were used to minimize rinse-out time.

The configuration of the automated standardization system also is shown in Fig. 1. The three-way solenoid valve V6 determined from which source the solution would be drawn, either the automatic sampler or the manifold. During standardization, valve V6 was actuated simultaneously with one of the other valves, V1 to V5. Actuation of a wave corresponding to one of the standards permitted the selected standard to be pumped to the nebulizer. The configuration of the reagent blank valve with respect to the manifold is significant. Reagent blank was pumped to the nebulizer through three-way solenoid valve V5 without passing through the manifold. This configuration eliminated the possibility of blank contamination from finite amounts of standard solution trapped in adjacent branch inlets when the blank solution passed other manifold branch inlets. The possibility of standard cross-contamination and dilution within the branched manifold is discussed later. Materials and components used in the construction of the manifold assembly are listed in Table 2.

Solenoid valve decoder/driver and interface description

The solenoid-valve decoder/driver electronics were designed and built to implement control of the manifold assembly. The microcomputer interface provides the signals to control the solenoid valves through the decoder/driver circuits.

Each solenoid valve, V1 through V5, is assigned a unique binary code that is used to actuate it selectively. The decimal representations of these binary codes for valves V1 through V5 are 1 through 5, respectively. Valve V6 is

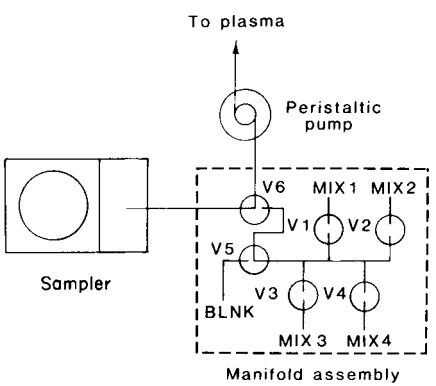

Fig. 1. Configuration of automated standardization system.

TABLE 2

Parts list for manifold assembly

Quantity	Item
15 cm	4-mm o.d. pyrex tubing for branched manifold.
4 ea.	Two-way miniature teflon solenoid valves, with 1/4-28 ports and teflon nut and ferrule, +12 V d.c., 20 lb in^{-2}.
2 ea.	Three-way miniature teflon solenoid valves, with 1/4-28 ports and teflon nut and ferrule, +12 V d.c., 20 lb in^{-2}.
0.5 m	1/8-in. o.d. flexible teflon tubing.
5 ea.	250-ml teflon bottles.

de-energized during operation of the sampler so that sample solution can be pumped to the nebulizer. Operation of the manifold assembly requires that valve V6 be energized to permit solution flow from the manifold assembly. The reservoir from which solution is pumped is chosen by actuating one of the valves V1 through V5. To accomplish these operations, the microcomputer transmits one of the American Standard Code for Information Interchange (ASCII) valve codes to the decoder/driver circuitry through a serial interface. For example, when it is desired to pump standard MIX1 to the nebulizer during standardization procedures, an ASCII 1, octal 61, is sent to the serial interface. When this code is received by the decoder/driver circuit, it is translated into binary format and decoded, resulting in the actuation of valves V1 and V6. At the conclusion of manifold functions transmission of an ASCII 0, octal 60 de-energizes valves V1 and V6 to allow sampler solution to be pumped to the nebulizer.

A standard Electronic Industries Association (EIA) RS-232C serial interface is used for communication between the microcomputer and manifold assembly. A universal asynchronous receiver transmitter (UART) and baud (bits s^{-1}) rate generator circuit is used to translate ASCII code received from the serial interface into its 8-bit binary representation. This UART-baud rate generator board is available in kit form (Electronic Designs, San Jose, CA). However, the serial interface could easily be replaced by a parallel interface eliminating the need for the UART-baud rate generator board. The data transmission rate from the microcomputer to manifold assembly is set at 110 baud, because speed is not important. The signal level of the "receive-data" line, pin 3 of a standard RS-232C 25-pin connector, needs to be conditioned to transistor-transistor-logic (TTL) levels prior to entering the UART. This is accomplished by using a line receiver chip. IC 1489 (Fig. 2). The TTL level is then connected to the serial input, pin 18, of the UART-baud rate generator board.

The decoder/driver circuit is shown in Fig. 3. Bits 0 through 2, B0, B1 and B2, respectively, are decoded using a 4-line to 16-line decoder chip (IC1). For example, the 3-bit binary representation 101 would be decoded to equal decimal 5, and, consequently, force pin 6 of IC1 LOW. This signal is inverted

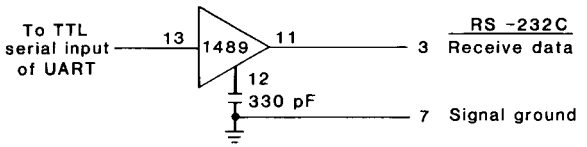

Fig. 2. EIA to TTL conversion circuit.

to drive transistor Q5 which actuates valve V5; the actuation of valve V6 is coincident with this operation. Because pin 1 of IC1 is HIGH during this period, the signal present at the NAND gate input is LOW. The second NAND gate input corresponds to the value of bit 4, B4, which is HIGH. Therefore, the output of the NAND gate is HIGH, forcing transistor Q6 to

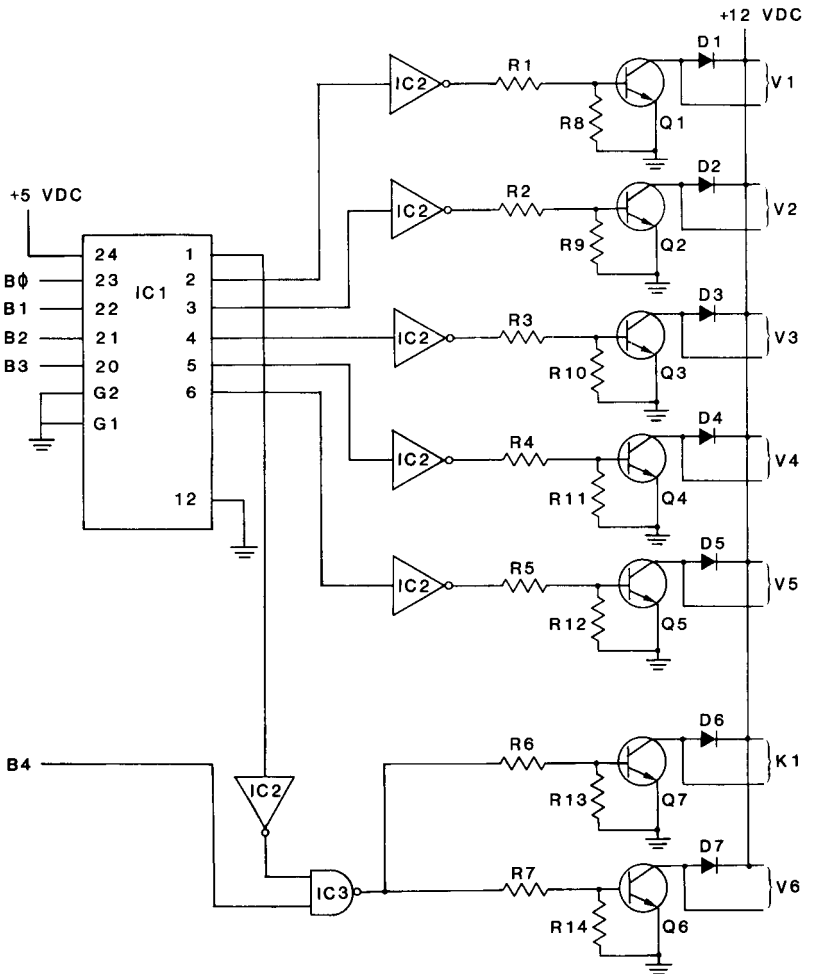

Fig. 3. Decoder/driver circuit.

actuate valve V6. If an ASCII 0 is transmitted to the decoder/driver, pin 1 of IC1 will be LOW; on inversion this forces the output of the NAND gate LOW, to deactivate valve V6. At this point, solution will be pumped from the automatic sampler.

In addition to controlling the standardization manifold, the decoder/driver circuit is also used to enable and disable the sampler. Whenever quality control indicates standardization is necessary, bit B4 is set HIGH. Consequently, the output of the NAND gate is high, forcing transistor Q7 to actuate a normally-closed relay, K1, which disables the timing circuits of the sampler [1]. When standardization is complete, the microcomputer transmits on ASCII 0, octal 60, to the decoder/driver circuit which deactivates relay K1 to re-enable the automatic sampler.

The truth table for the 4-bit binary decoder (IC1) is Table 3. Components used in the construction of the decoder/driver circuit are listed in Table 4. A power supply was built to provide +5 and −12 V d.c. power for the UART-baud rate generator board and the decoder/driver circuit (Fig. 4). The +12 V d.c. required to drive the miniature solenoid valves is available from the AtomComp power supply.

Software description

The H-11 microcomputer is dedicated to controlling the manifold assembly and the AtomComp during any standardization operation. The PDP-11 minicomputer provides on-line quality control, data acquisition and management, and is responsible for starting H-11 software routines. Configuration of the total system in block form is shown in Fig. 5. The H-11 is interfaced with the AtomComp PDP-8, manifold assembly, and data acquisition/H-11 controller PDP-11. The PDP-11 is interfaced with the H-11 microcomputer and AtomComp PDP-8. The AtomComp PDP-8 is interfaced with the H-11, PDP-11, and sampler subsystem. The interface, through terminal T1, between the PDP-8 and H-11 permits hard-copy output from the AtomComp. However, all AtomComp commands must pass through the

TABLE 3

Truth table[a]

Solenoid valve	Solution reservoir	ASCII/ octal	Binary bits 0-2	Decoder pin output 1	2	3	4	5	6	7	8
V1	MIX1	1/61	001	—	L	—	—	—	—	—	—
V2	MIX2	2/62	010	—	—	L	—	—	—	—	—
V3	MIX3	3/63	011	—	—	—	L	—	—	—	—
V4	MIX4	4/64	100	—	—	—	—	L	—	—	—
V5	BLNK	5/65	101	—	—	—	—	—	L	—	—
V6	N.A.	0/60	000	L	—	—	—	—	—	—	—

[a]—is HIGH, L is LOW, N.A. = not applicable; selects manifold assembly or sampler.

TABLE 4

Component list for decoder/driver circuit

Quantity	Item
1	IC1: 74154 4-line to 16-line decoder/demultiplexer
7	Q1—Q7: NPN transistors, 2N2222
7	R1—R7: 200 Ω 1/4-W carbon film resistors
7	R8—R14: 1000 Ω 1/4-W resistors
7	D1—D7: 1N914 diodes
1	IC2: 7404 Hex inverter
1	IC3: 7400 Quad 2-input NAND gate

H-11, either via the terminal keyboard or via H-11 software. Flow charts of the software used with the H-11 and the PDP-11 are shown in Figs. 6 and 7, respectively. The information in Figs. 5—7 describes the interaction between microcomputer and minicomputer hardware and software.

The first step in the measurement procedure is the entry of the sequence of samples and check standards into the PDP-11 minicomputer, so that the software can distinguish between results received from the AtomComp; this enables the minicomputer to perform on-line quality control. The minicomputer then commands the microcomputer to standardize the instrument. This standardization procedure uses exactly the same AtomComp commands as the manual procedure. Applicable commands are shown in Table 5. The methodology requires that each sample and standard result be based on the average of two sequential measurements [3]. Therefore, the command Q-strings used for samples and standards are QE[G]GAC and QEGGAIN, respectively. Commands [and] are used for control of the sampler [1]. Q-strings can be recalled by using the single letter command O.

Standardization begins with the microcomputer disabling the sampler and setting the Q-string to QEGGAIN. The standardization procedure requires the following steps for each standard: (a) actuation of the appropriate manifold solenoid valves, (b) transmission of commands to the AtomComp,

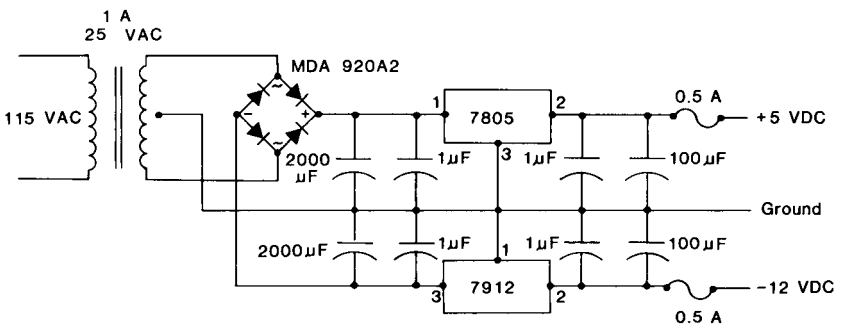

Fig. 4. Power supply.

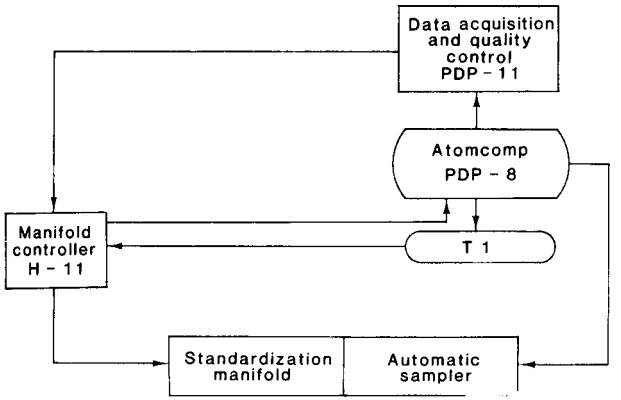

Fig. 5. System configuration.

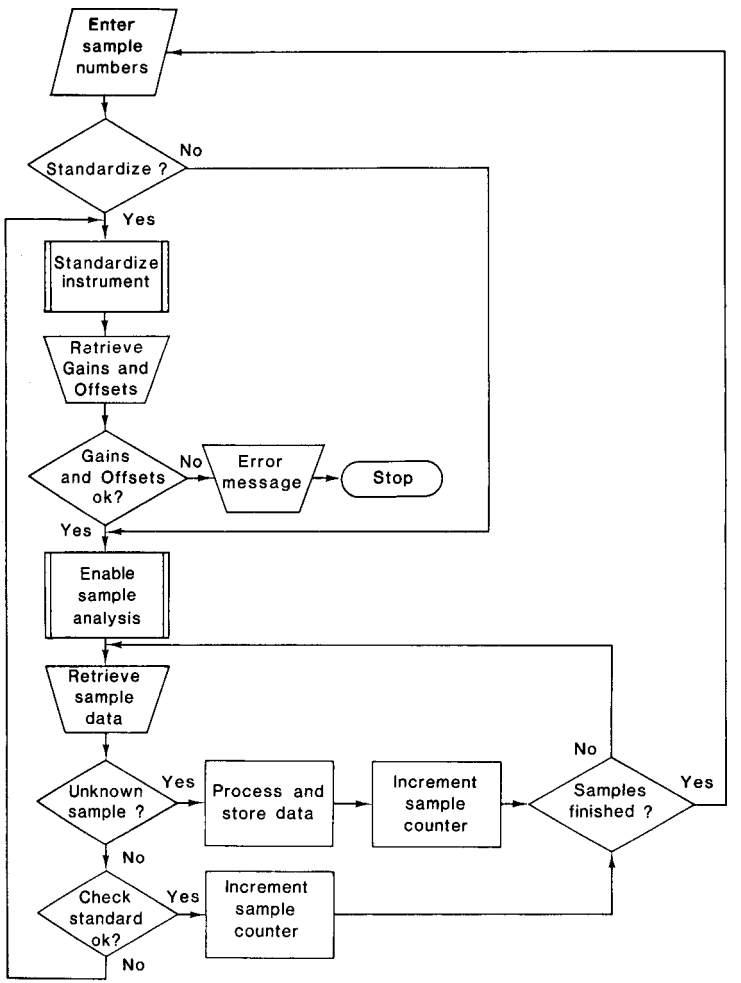

Fig. 6. Interactive software flow chart: minicomputer data retrieval software in BASIC.

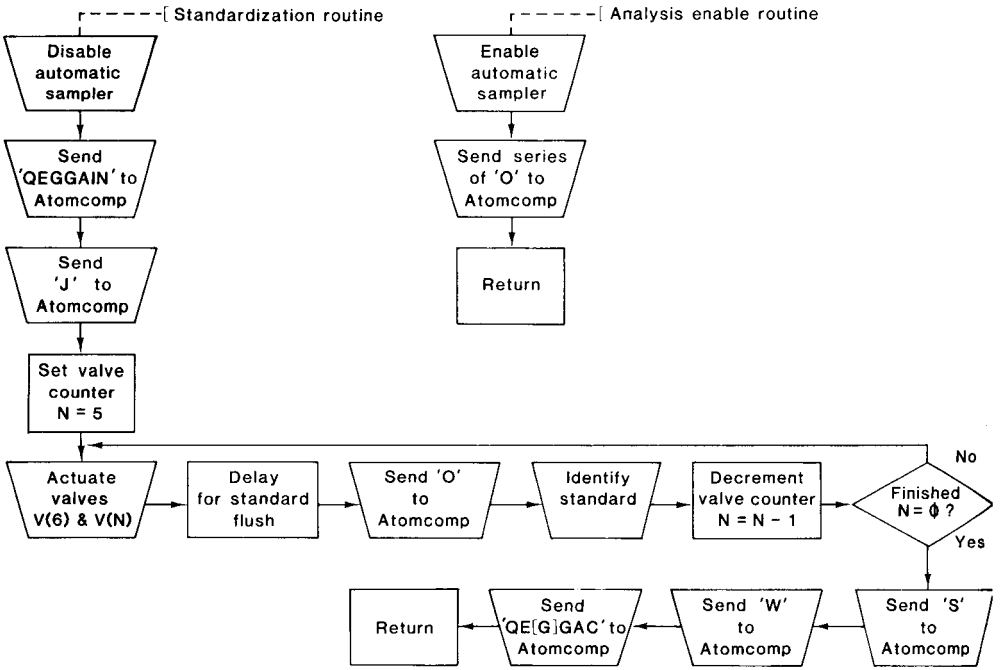

Fig. 7. Interactive software flow chart: microcomputer standardization routine in assembly coding.

and (c) identification of each standard following its measurement. For example, standardization starts with measurement of the reagent blank. The reagent blank is pumped to the nebulizer by energizing valves V6 and V5. Following a delay period that allows the standard to flush the system, an O command is transmitted to the AtomComp to begin the measurements. On completion, the AtomComp cues the microcomputer for the name of the standard used. In this case, the reagent blank is identified by BLNK. Standardization using the other four multi-analyte standards follows the same procedure in the sequence: MIX1, MIX2, MIX3, and MIX4. Following analysis of all five standards, the S command is transmitted to the AtomComp to complete the standardization procedure.

Gain and Offset values, which are mathematically related to the slope and intercept of the analytical curve, respectively, are calculated for every element by AtomComp software; therefore these two parameters can be used to determine the acceptability of a standardization. Execution of the W command by the AtomComp prints the Gains and Offsets at the terminal/printer and transmits them to the minicomputer. The minicomputer compares these values to stored mean values. If the new values are outside the acceptable range, a message is sent to the minicomputer console terminal indicating that an instrument problem exists. Otherwise, the minicomputer

TABLE 5

AtomComp operating system commands

Command	Result
Q	Store following command string: Q-string
E	Erase data buffers
G	Perform all measurements on a sample or standard
A	Average data in storage buffers
C	Print concentrations
I	Print absolute intensities
N	Average standardization data and request standard identification
J	Use standardization data buffers for subsequent measurements
S	Standardize elemental channels
W	Print current Gains and Offsets
O	Recall current Q-string
[and]	Controls the automatic sampler subsystem; door switch function

commands the microcomputer to engage the sampler, change the Q-string to QE[G]GAC, and transmit a series of O commands, one for each sample up to 24, to the AtomComp to begin the sample measurements.

When measurements on a sample have been completed, the results are sent to the terminal/printer and transmitted to the minicomputer. If the stored sampler sequence indicates that the data received from the AtomComp corresponds to an unknown sample, the results are processed and stored. However, when results correspond to the check standard, they are evaluated for accuracy. The results for all elements must be within 2% of the corresponding mean. Failure of this test indicates that restandardization of the instrument is appropriate. Unsatisfactory accuracy is assumed to result from instrument drift, not instrumental malfunction; in the latter case, restandardization would be inappropriate. Normally, the AtomComp requires only two or three standardizations per day, depending on the environment in which the instrument is operated and type of samples analyzed. When restandardization is necessary, the minicomputer commands the microcomputer to start the same standardization procedure described earlier. If the resultant Gains and Offsets are within their prescribed ranges, processing of unknown samples is resumed. Unknown samples that were measured between the last good check standard and the check standard that failed evaluation, must be reprocessed.

RESULTS AND CONCLUSION

Tests were conducted to evaluate the automated standardization procedure for precision and accuracy, operational stability, and potentiality for standard cross-contamination in the manifold. The use of a branched manifold of this type, where all branches lead into a common channel, suggested

TABLE 6

Accuracy comparison between automated standardization and manual standardization

Element	Gains		Offsets	
	Automated	Manual	Automated	Manual
Ba	0.4	0.4	−0.02	−0.006
Ca	0.9	0.9	−0.003	−0.009
Cd	0.03	0.03	0.0004	−0.0006
Cu	0.5	0.5	−0.0005	0.002
Fe	0.3	0.3	−0.003	−0.003
Na	3	3	−2	−2
Sr	0.2	0.2	−0.0002	−0.0002
Zn	0.1	0.1	−0.0005	−0.004

the possibility of standard cross-contamination resulting from the finite amounts of standard solution trapped in adjacent branch inlets. Because standards MIX1, MIX2, MIX3, and MIX4 contain only specific analytes at 10 mg l^{-1}, any cross-contamination theoretically would be negligible. In addition, at these concentrations, any dilution effects also would be negligible. Experiments showed that if the reagent blank was located on a manifold branch, sufficient contamination from other standards could occur, thereby biasing the analytical results. For this reason, the reagent blank was separated from the manifold through three-way solenoid valve V5.

Accuracy of results obtained while employing this real-time standardization procedure is indicated by comparing the Gains and Offsets resulting from the automated and manual procedures. The Gains and Offsets for selected elements resulting from both procedures (Table 6) are, in general, very similar. Data obtained from four replicate standardizations of several elements using both procedures are presented in Table 7. Correlation of the mean Gains

TABLE 7

Multiple standardizations using automated and manual standardization

Element	Manual Gains		Automated Gains	
	Mean	Standard deviation[a]	Mean	Standard deviation[a]
Ba	0.4	0.002	0.4	0.002
Ca	0.9	0.007	0.9	0.006
Cd	0.03	0.0004	0.03	0.0001
Cu	0.5	0.006	0.5	0.0002
Fe	0.3	0.005	0.3	0.003
Na	3	0.03	3	0.02
Sr	0.2	0.003	0.2	0.0008
Zn	0.1	0.002	0.1	0.0002

[a]Based on four replicates.

between automated and manual procedures is excellent, but precision data generally indicate superior performance by the automated procedure.

The computer-controlled real-time standardization system has proven to be versatile and efficient in addition to increasing sample throughput. The system has freed the operator of tedious instrumental monitoring and has increased the precision of the standardization process. The possibility of errors during standardization and contamination of standard solutions has been reduced. No modifications to AtomComp software were necessary and modifications to AtomComp hardware were only minor and had no effect on stand-alone AtomComp operation.

The system described was configured to operate under control of two separate processor units, one to acquire and manage data and another to control manifold hardware and real-time standardization. However, one dedicated minicomputer could easily be implemented to control both phases of operation.

REFERENCES

1 J. R. Garbarino and H. E. Taylor, Chem. Biomed. Environ. Instr., 11, No. 4 (1981) 289.
2 J. R. Garbarino and H. E. Taylor, presented in part at the Pittsburgh Conference on Analytical Chemistry and Applied Spectrometry, Paper 239, Atlantic City, NJ, 1980.
3 J. R. Garbarino and H. E. Taylor, Appl. Spectrosc., 33(3) (1979) 220.

Analytica Chimica Acta, 134 (1982) 167—178
Elsevier Scientific Publishing Company, Amsterdam — Printed in The Netherlands

A SEMI-HIERARCHIC COMPUTER NETWORK FOR DATA ACQUISITION AND CONTROL IN STAIRCASE VOLTAMMETRY

CHIA-YU LI*, THOMAS H. BARRETT, JR.[a], DAVID LUNNEY and ALGER SALT
Department of Chemistry, East Carolina University, Greenville, NC 27834 (U.S.A.)
(Received 3rd June 1981)

SUMMARY

A simple computer system designed for controlling voltammetric experiments has been implemented. The system connects a Hewlett-Packard 2100A minicomputer with a Texas Instruments 9900 microcomputer by means of a bidirectional serial transmission link. Experimental parameters are down-loaded from the host to the satellite which supervises the experiments at a remote location. The data collected are transmitted back to the host at 2400 baud for reduction and plotting. Through this division of labor, each system is used to its best advantage. Although the software developed is specifically for staircase voltammetry, the system hardware is of general-purpose design which is suited for other types of pulse experiment.

Staircase voltammetry has been successfully demonstrated as a useful method in both equilibrium and kinetic studies. It has been shown that the detection limit of staircase voltammetry is in the order of 10^{-7} M [1], which matches that of pulse polarography. In heterogeneous kinetic work, staircase voltammetry is superior to conventional cyclic voltammetry because of its ability to minimize charging current interferences [2]. Some rate data for coordination complexes have been collected by using this technique [3]. In spite of these developments, staircase voltammetry has not been widely used since its initial introduction by Mann in 1961 [4]. This is in part due to the complex analog circuitry required for waveform generation and current sampling in staircase voltammetry.

In Mann's early design which required photography of the oscilloscope screen [4], data acquisition was cumbersome. Schroeder and coworkers [5] later made improvements by using a transient recorder to provide a continuous display of data. Both systems lacked flexibility in data manipulations and were rather difficult to operate. With the advent of modern integrated circuit technology, computers have become a logical choice for use in this computer-compatible technique. Recent developments include the minicomputer system of Perone and coworkers [1, 6] and the microcomputer system of Barrett et al. [7]. In the former design, a dedicated minicomputer was used

[a]Present address: Custom Terminals Inc., Raleigh, NC 27604, U.S.A.

0003-2670/82/0000-0000/$02.75

to control the experiment and a second independent minicomputer was employed for data processing, such as ensemble averaging and curve-smoothing. The software used was highly sophisticated but the hardware arrangement was not economical because it tied down an expensive minicomputer for the sole purpose of direct on-line control. Barrett et al. [7] replaced the minicomputer with a low-cost microcomputer for both control and data acquisition. Although it is a cost-effective system, it lacks the versatility that a minicomputer normally offers, and it is inconvenient to use because the voltammograms have to be plotted by hand from the video monitor display. This report presents an alternative approach which takes advantage of the power of both mini- and micro-computers.

A microprocessor-based satellite computer is used as a dedicated device for controlling the electrochemical instrumentation. The satellite microcomputer communicates directly with a host minicomputer via a bidirectional asynchronous serial data path. This semi-hierarchic network allows a rapid on-line transfer of commands and data. The voltammetric experiments are supervised by the microcomputer while the minicomputer does what it is best suited for, namely data processing, storage, and plotting. With the use of a real-time software system, the microcomputer merely acts as a peripheral device to the host computer. This arrangement also frees the minicomputer to perform other tasks while the measurements are run.

SYSTEM DESCRIPTION

Electrochemical apparatus

The complete cell assembly fitted with a K0020 hanging mercury drop electrode (HMDE), a K77 saturated calomel electrode, and a platinum wire auxiliary electrode was obtained from Princeton Applied Research Corp. (Princeton, NJ). The custom-built, fast settling three-electrode potentiostat used here has been described [8]. Its link with a general-purpose interface and the micro/minicomputer is represented by the block diagram in Fig. 1. A current follower (TP 1340) was used to track the current. The analog voltage was monitored by a Fluka 8000 digital multimeter at the output of the voltage follower.

General-purpose interface

This interface includes a 12-bit successive approximation analog-to-digital converter (ADC) (Datel HZ12BGC), a 12-bit digital-to-analog converter (DAC) (Burr Brown DAC 80), a programmable real-time clock (Monitor Products Type 850), and an autoranging amplifier. The autoranging amplifier has been described [9]. The general-purpose interface was a wire-wrapped design constructed on four separate perforated boards and housed in an aluminum card enclosure.

The DAC provides the voltage signal for the potentiostat through a 140-kHz low-pass filter. Its output range is ±2.5 V with a resolution of 1.22 mV/step

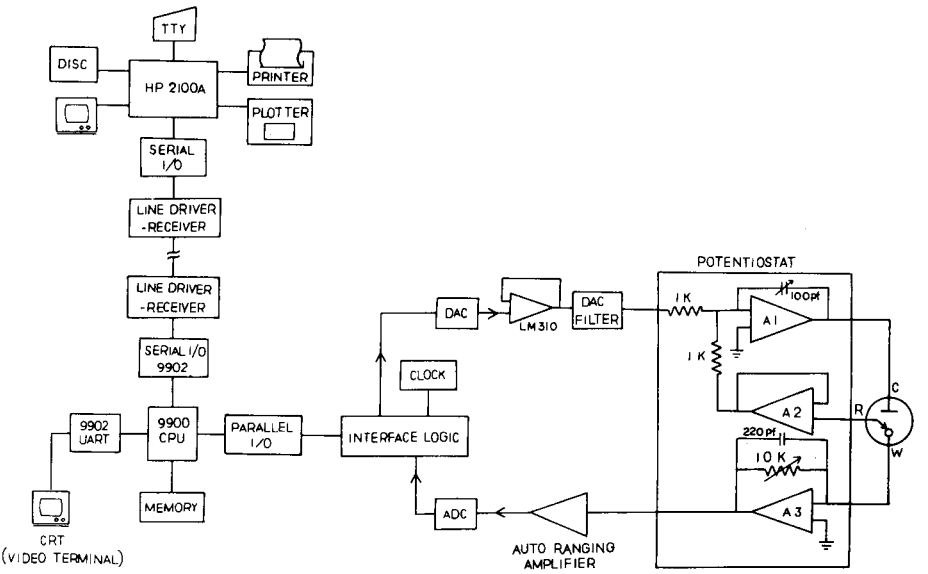

Fig. 1. Block diagram of mini/microcomputer controlled voltammetric system. A1 is Analog Devices 120A, A2 is Burr Brown 3013/15, and A3 is Burr Brown 3064/15. For clarity, circuit detail is not shown.

and a settling time of 3 μs (to $\pm 0.01\%$ of full scale range). The DAC is updated by placing the digital value on the output lines of the general interface bus (GIB) and latching it through three 4-bit bistable latches (74LS75). A voltage follower (LM 310) was used to provide high input impedance.

Schematic and timing diagrams of analog-to-digital conversion are presented in Figs. 2 and 3. An analog-to-digital conversion is initiated by a negative transition on the ADC convert bit of the GIB (pin 20, Fig. 2). This transition triggers one-shot #1 which clears the flip-flop, and through it, the end-of-convert bit. If the autorange feature is not selected, one-shot #2 is triggered directly by the ADC convert bit. If the autorange is selected, a 5 μs delay is introduced by one-shot #1 to allow the multiplexer on the autoranger to settle. One-shot #2 produces a 5-μs negative pulse which controls the sampling of the sample-and-hold (S & H) amplifier. With a 30-nF hold capacitor, the S & H gives a 5-μs acquisition time to $\pm 0.01\%$ for a 10-V change and a droop rate of 7 mV s^{-1}. The S & H acquires input voltage when the digital control is at a logic low and holds the voltage constant when the digital control returns to the logic high at the end of the 5-μs pulse. This transition triggers one-shot #3 to generate a 500-ns positive pulse, which in turn triggers a conversion on the ADC. The ADC achieves a 12-bit conversion in 20 μs, and sets the flip-flop on completion of the conversion. This sets the end-of-convert bit (pin 19) on the GIB, which is the signal to the microcomputer that valid data are available.

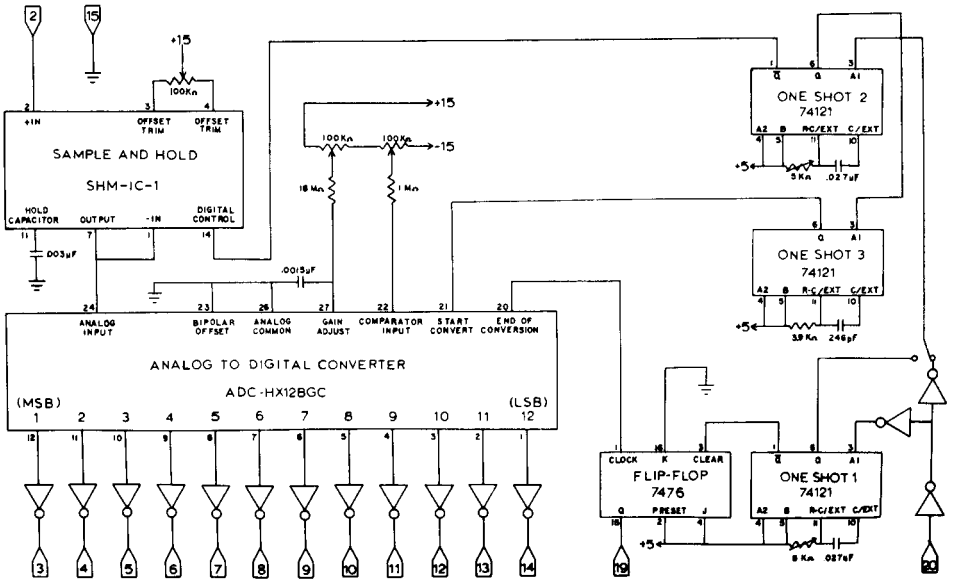

Fig. 2. Schematic diagram of analog-to-digital converter circuitry.

Serial data transmission hardware

A line driver/receiver system was developed to provide serial, bidirectional data transmission between the host and the satellite computers, which were separated by a distance of approximately 50 m. Standard, shielded, twisted pair transmission cables were used. No signal degradation or crosstalk was observed. Although the unit can handle a data rate up to 4800 baud, 2400 baud was used because this was the upper limit configured on the HP2100 serial interface card used.

The line driver—receiver are configured around the Texas Instruments SN-75114/SN75115 integrated circuit set. The SN75114 converts a single-ended TTL level signal to a differential TTL signal, while the SN75115 does the

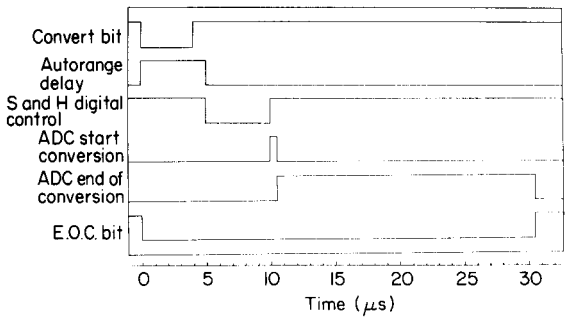

Fig. 3. Timing of events during analog-to-digital conversion.

reverse translation. The differential TTL signal is sent over the twisted pair in a balanced line transmission system, making it compatible with the EIA RS-422 standard. The schematic diagram of one of the line driver/receiver circuits is shown in Fig. 4. Since part of the transmission line is exposed outside the building, isolation is necessary to protect the computer system from high-voltage transients that could be imposed on the line (e.g., by lightning). Optical couplers with Darlington output transistors (Texas Instruments TIL-113) were used to isolate the transmission line electrically from the computer systems. The inputs to the line driver and the outputs from the line receiver are compatible with RS-232-C standard to allow communication between computers or between a terminal and a computer.

Computer hardware

The host system used in this work was a Hewlett-Packard 2100A minicomputer with 64 kbytes of memory (Fabri-Tek, Inc.) and a 2.5 Mbytes of hard disc storage (Hewlett-Packard 7900A). The associated peripheral devices consist of a Centronics Model 101 line printer, a Hewlett-Packard 7210A digital plotter, a Lear-Siegler ADM-3A video terminal, and two teletypes (ASR 33 and 35). The satellite microcomputer used was the Technico SS9900 system, which is based on the TMS 9900 microprocessor, an advanced 16-bit LSI central processor with minicomputer-like architecture and instruction set. It is supported by 34 kbytes of random access memory (RAM), 2 kbytes of read only memory (ROM), and 2 kbytes of erasable, programmable read only memory (EPROM). Thirty-two bits of parallel I/O were provided to interface the system to the electrochemical instrumentation. In addition, two serial channels (based on the TMS 9902 asynchronous communications controller) were used. One channel supports a Lear-Siegler ADM-3A terminal and the other links the microcomputer with the host system.

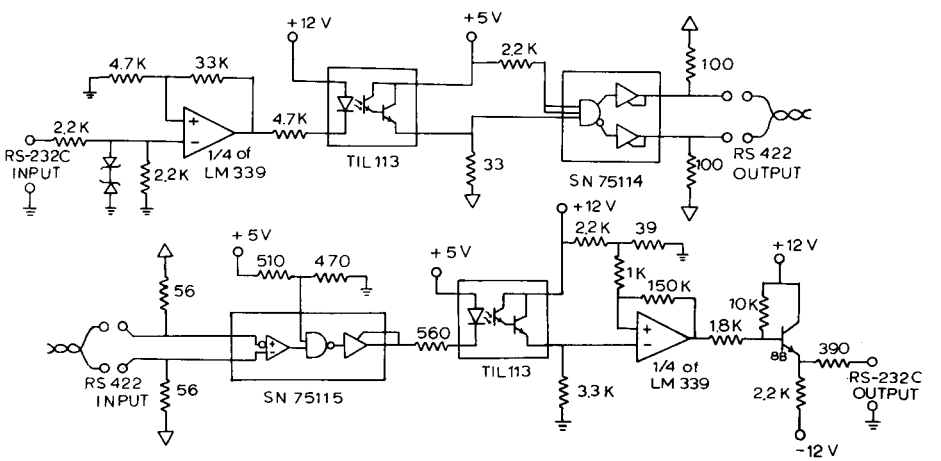

Fig. 4. One channel of line driver/receiver circuitry.

Computer software

Communication package. Three modes of communication developed in the system were the satellite-terminal mode, the satellite-host mode and the pass-through mode. The communication programs make direct dialogue between the host and the satellite computers possible. They were semi-permanently loaded in the EPROM. In addition, the Technico built-in ROM monitor program was available for program control and manipulation.

The satellite-terminal mode provides access to the satellite microcomputer through the video terminal. In this mode, the characters generated by the terminal are interpreted as information for the satellite and all responses are routed to the terminal for display. This mode is required for microprocessor program development and to gain control of the satellite system upon initial satellite start up.

The satellite-host mode is used to transfer control information from the host to the satellite and transfer data from the satellite to the host. A software handshake protocol was used to prevent unsolicited characters from disrupting the program and causing loss of data. Several characters were designated in the driver program to coordinate data flow between the two computers. A prompt character (a dollar sign) is transmitted by the host when it is prepared to receive a line of data from the satellite. The satellite receives the character, pauses for several milliseconds to allow for the read operation on the host to initiate, and then transmits one line of characters terminated by a pound sign (#) and a carriage return. All further transmission is suspended until receipt of another prompt character which forces the satellite to re-enter the monitor and to issue a monitor prompt (a question mark). The line feed and null characters are ignored when received by the satellite and are deleted from all transmission from the satellite.

The pass-through mode acts as a transparent link between the host and the satellite. In this mode, characters passed from the terminal to the host and vice versa are not interpreted as satellite commands. This mode is entered by a "G" (go to program) command from either the satellite-terminal mode or the satellite-host mode. The escape character is used to signal an exit from the pass-through mode to another mode. If the escape character is sent by the terminal, then the satellite-terminal mode is entered; if it is sent by the host, the satellite-host mode is entered.

Real-time interpreter. The real-time interpreter (RTI) is a program which allows complex series of data acquisition and control functions to be executed at a speed much higher than that which could be attained in high-level languages. Event timing is inherent in the language and is provided by synchronizing the events with the programmable timer. Like the communication programs, the RTI is contained in EPROM. The RTI executes the instructions stored in sequential memory addresses. Each instruction requires one word of memory, which is divided into the command field and the argument field. The command field is composed of the four most significant bits. It functions as the operand code and defines which of five operations is to be performed.

These five operations are: return to monitor, wait, A/D conversion with wait, D/A conversion, A/D conversion followed by D/A conversion. The twelve least significant bits constitute the argument field, in which specific functions are stored. Two registers were used in the RTI. The first register was used as the program counter and the second one, which acts as an index register, was used as the data pointer.

The RTI is composed of several software routines. A "DAC/Clock Set-Up" routine initializes the DAC and clock to the desired voltage and period. A "Run Data Acquisition" routine initializes the program counter and data pointer, then starts the experiment. A central routine called "Instruction Interpreter" interprets each instruction to be executed and calls a service routine, which performs a unique operation as defined by the machine code command. The sequence of events in executing RTI routines is depicted in Fig. 5. The data acquisition is terminated when the command field is equal to zero.

Host system software. Four programs residing in the host computer were used for experimental initiation, data acquisition, data manipulation, and

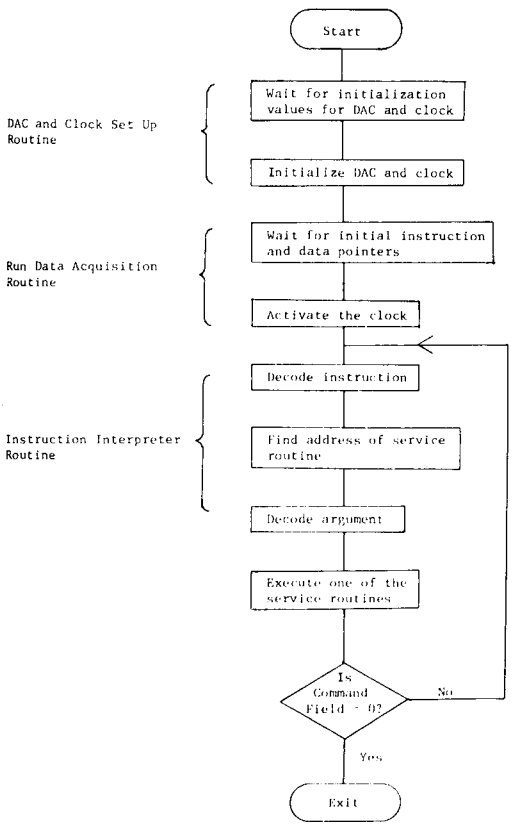

Fig. 5. Real-time interpreter execution sequence flow chart.

plotting. The programs were written in FORTRAN IV and run under the control of the Hewlett-Packard Real Time Executive II operating system. Each program in the family is linked to the others through a common file on which experimental data are stored. Complete listings of these programs are available upon request.

A program, STPIT, allows the operator to enter the parameters that define the staircase voltammetry experiment. The parameters used to generate the staircase waveform are the initial potential, E_i (in V), the step size, ΔE (in mV), the step duration, τ (in ms), and the final potential, E_f (in V). The program rounds the ΔE value entered to the nearest integral of 1.22 mV (the resolution of the 12-bit DAC) and calculates the number of required potential steps based on E_i and E_f. The form of data acquisition to be used is described by the number of sampling points per step and their corresponding sampling times, t_m. Options were provided for the user to save, abort, or regenerate the files that have been initiated.

A program, DATA, supervises actual information transfer and data acquisition. Information describing the experiment is read from the disc files created by STPIT. The experimental parameters are translated into a form which is compatible with the programs on the satellite system. The restructured parameters are then down-loaded to the satellite from the host. When the user is ready, the program initiates the experiment and waits for the satellite to complete it. Upon completion, the data collected are uploaded to the host system where they are stored on the disc for future use.

A program, STPGP, reproduces the voltammograms with scale information and annotation on a digital plotter. The voltammograms are scaled to take full advantage of all the available area in which they can be plotted. Captions such as sample name and experimental notes are printed over the voltammograms.

A program, STPRP, processes the raw data in the disc file and generates a report. This report provides a summary of the experimental conditions, the key experimental results (peak current height, peak potential position, t_m/τ ratio, and peak current ratio at t_m and τ) and optionally, a complete listing of voltage and current values for each voltammogram.

Real-time data acquisition and control

The staircase voltammetry experiment is started by creating a disc file using program STPIT. The file can be generated either through the video terminal on the host system or through the lab video terminal using the pass-through communication mode. After initial start-up, the program DATA is used to take over the experiment by controlling the data flow between the two computers.

The system first enters the satellite-host communication mode. A command is issued by the host computer to the satellite to execute the "DAC/Clock Set-Up" routine, which sets the DAC to desired initial voltage and clock frequency. This is followed by down-loading the machine code command list into the satellite memory from the host. These commands define the number of data points to be sampled per step and the time between

adjacent data points. The system then enters the pass-through communication mode to inform the user on the video terminal that the preparation for the experiment is completed. The user can respond by typing a GO command on the keyboard to start executing the experiment. This action causes the system to re-enter the satellite-host communication mode. At the command of the host, the satellite enters the "Run Data Acquisition" routine and assigns values to the instruction and data pointers. After the experiment is completed, the satellite prompts the host with a monitor prompt and the system enters the pass-through mode to inform the user that the data have been collected and are about to be transmitted to the host. At this juncture, no user interaction is required. The system automatically enters the satellite-host communication mode for the third and final time. The host issues a memory dump command and the satellite begins to upload the section of memory containing the raw experimental data to the host. When the data transfer has been completed, the host directs the satellite to enter the pass-through mode again to inform the user about the completion of the experiment and terminates the program DATA. For a typical experiment that requires a waveform of 60—100 voltage steps and four current sampling times per step, the whole handshake process takes less than 2 min to complete. The actual execution time of the experiment depends on the step duration τ and is normally between 200 ms and 3 s.

PERFORMANCE TESTS

A typical staircase voltammogram for the reduction of cadmium ion at the HMDE is shown in Fig. 6. The experimental parameters chosen were: ΔE = 10 mV, τ = 2 ms, t_m = 1 ms (approximately 20 cell constants), E_i = —0.400 V, and E_f = —1.00 V. A least-squares fit of peak currents, I_p, sampled near the end of each step versus $\tau^{-1/2}$ for τ between 1 and 20 ms at constant ΔE gave the equation $I_p = (273 \pm 11)\tau^{-1/2} + (20.3 \pm 0.8)\ \mu A$ with standard error of 6.1 μA and a correlation coefficient of 0.9923. The linear relationship given by these data (Fig. 7a) is in agreement with the prediction of Zipper and Perone [1]. The slope of this plot, 273 μA ms$^{1/2}$ agrees well with the theoretical slope of 257 μA ms$^{1/2}$ calculated for C^* = 2.9 mM Cd^{+2}, $D_o = 7.0 \times 10^{-6}$ cm^2 s^{-1}, and A = 0.0184 cm^2. The deviation is attributed to the difference between the spherical diffusion of the HMDE used in this work and the planar diffusion from which the theoretical equation was originally derived [10]. As expected from theory [1, 2], at constant ΔE and τ, I_p was also found to be linear with concentration (Fig. 7b). The correlation coefficient of this plot is 0.9993 for a concentration range between 0.01 and 10 mM. Below 0.01 mM, the current measurement was affected by the noise generated by the DAC as well as by the microprocessor and its support chips. The noise problem from the computer was also experienced by other workers [11]. The DAC noise can be reduced somewhat by more careful choice of RC filtering. However, real improvement can probably be achieved through software modification, such as ensemble averaging.

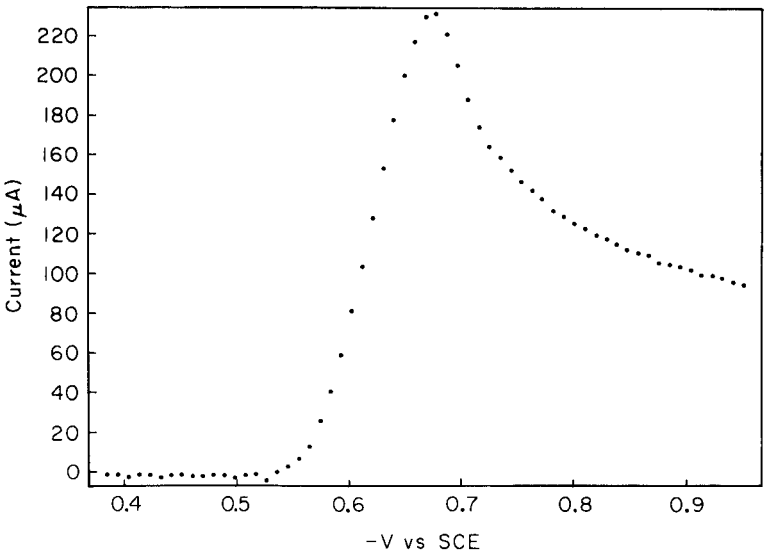

Fig. 6. A typical staircase voltammogram for the reduction of 2.9 mM of Cd^{2+} in 0.1 M KCl at the HMDE.

The performance of the system is further demonstrated by the reduction of *N*-(4-aminoantipyryl)-*p*-benzoquinoneimine in a methanol (70% v/v)/phosphate buffer (pH 8.3) mixture. Like all quinoneimines [12, 13], this compound is reduced reversibly to the corresponding aminophenol in a $2e^- - 2H^+$ reaction. Figure 8 shows its staircase voltammograms at a fixed τ of 5 ms and ΔE of 10 mV. The set of curves represents four individual voltammograms obtained at four different current sampling times within a single run from $E_i = +0.050$ V to $E_f = -0.700$ V. It can be seen that for constant ΔE, the peak current decreases as the current sampling time, t_m, increases. A

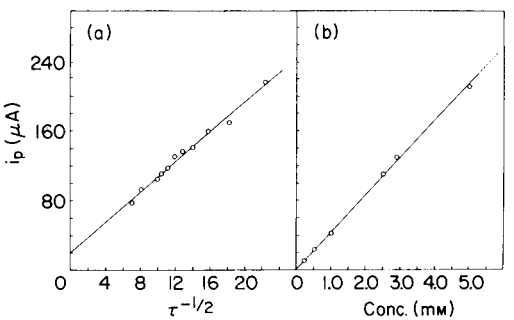

Fig. 7. (a) Current $-\tau^{-1/2}$ response for the reduction of Cd^{2+} at $\Delta E = 10$ mV. (b) Current–concentration response for the reduction of Cd^{2+} at $\Delta E = 10$ mV and $\tau = 5$ ms. The currents are the average of at least four runs.

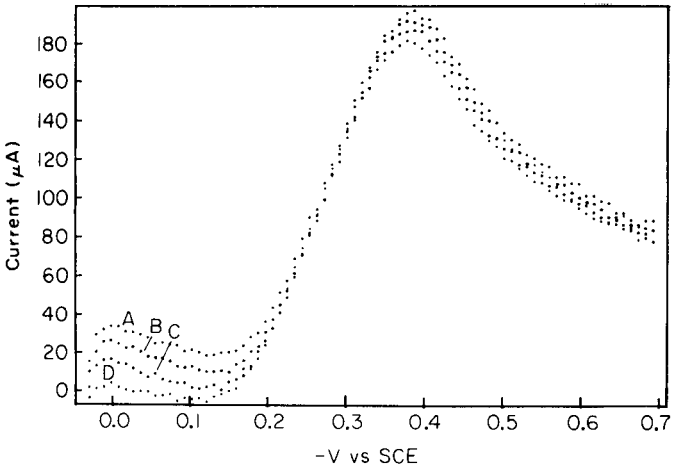

Fig. 8. Staircase voltammograms for the reduction of 1.0 mM *N*-(4-aminoantipyryl)-*p*-benzoquinoneimine in methanol/phosphate buffer at the HMDE. ΔE = 10 mV and τ = 5 ms. Curves: (A) t_m = 0.5 ms; (B) t_m = 1.0 ms; (C) t_m = 2.0 ms; (D) t_m = 5.0 ms.

similar set of voltammograms obtained at τ = 5 ms and ΔE = 5 mV showed that, for constant t_m, the peak current increases as ΔE increases. These two observations are in agreement with the theoretical predictions [1, 2]. Furthermore, the ability of this system to plot simultaneously several voltammograms at different t_m values has great utility in the determination of heterogeneous electron-transfer rate constants [2, 5].

DISCUSSION

The microcomputer system developed here is an outgrowth of one of Dessy's computer networking concepts [14]. In principle, it is somewhat similar to his point-to-point network arrangement. Although the minicomputer in the present system is presently serving one electrochemical station, it could be expanded to add other laboratory stations under time-sharing software control without altering the microcomputer hardware structure. The number of additional stations is, of course, limited by the number of I/O channels available on the host system.

The TMS 9900 microprocessor chosen in this work possesses several features which lend themselves to the real-time environment of the laboratory. Efficient interrupt processing is made possible throughout the sixteen levels of vectored and prioritized interrupts which allow bits to be accessed singly or in groups of variable length High-speed calculations are made possible by hardware multiply and divide instructions, while data can be handled conveniently by the varied addressing modes available.

One important advantage of the present system is its flexibility and ease of developing types of voltammetry experiments other than staircase voltam-

metry. By modifying the STPIT and DATA programs, the user could generate waveforms suitable to run normal or derivative pulse polarography. This is because the sequence of executing the machine code commands which determines the waveform shapes is down-loaded from the host to the satellites. The EPROM-resident RTI routines which supervise actual execution would therefore not need to be rewritten for each different type of experiment. A user who has experience in FORTRAN but not in assembly language would find this feature convenient.

Because the logic required to control the ADC and DAC circuits is largely software-based, it inevitably introduces some timing error. This error originates from uncertainty in the length of the waiting period for clock pulses to appear for performing an analog-to-digital or digital-to-analog conversion. It is also in part due to the finite time required for such conversion processes to take place. The timing error was estimated to be on the order of 10—50 μs. Thus, a step of 1 ms or shorter would suffer an error of approximately 3%, but the error would be insignificant when longer step times are used. It also appears that timing control is improved somewhat ($\sim$5 μs) if the autorange feature is not used. It should be noted that, however, the step width is always the same because the same amount of "error" (or really the time offset) is reproducible for each step.

More complete software details will be provided to interested readers.

This work was supported in part by grants from the East Carolina University Research Committee and Burroughs Wellcome Co. gift-matching fund. We thank Marc Walter for constructing the programmable timer and Elizabeth Whalen for providing organic samples. This paper was presented in part at the J. Heyrovsky Memorial Congress on Polarography, Prague, Czechoslovakia, August, 1980.

REFERENCES

1 J. J. Zipper and S. P. Perone, Anal. Chem., 45 (1973) 452.
2 D. R. Ferrier and R. R. Schroeder, J. Electroanal. Chem., 45 (1973) 343.
3 J. F. Endicott, R. R. Schroeder, D. H. Chidester and D. R. Ferrier, J. Phys. Chem., 77 (1973) 2579.
4 C. K. Mann, Anal. Chem., 33 (1961) 1484.
5 D. R. Ferrier, D. H. Chidester and R. R. Schroeder, J. Electroanal. Chem., 45 (1973) 361.
6 L. L. Miaw, P. A. Boudreau, M. A. Pichler and S. P. Perone, Anal. Chem., 50 (1978) 1988.
7 P. Barrett, L. J. Davidowski and T. R. Copeland, Anal. Chim. Acta, 122 (1980) 67.
8 C.-Y. Li, M. L. Caspar and D. W. Dixon, Electrochim. Acta, 25 (1980) 1135.
9 A. D. Salt and D. Lunney, Anal. Chem., 52 (1980) 2237.
10 J. H. Christie and P. J. Lingane, J. Electroanal. Chem., 10 (1965) 176.
11 E. T. Gray, Jr. and H. J. Workman, in P. Lykos (Ed.), Personal Computers in Chemistry, Wiley—Interscience, New York, 1981, Chap. 5.
12 R. S. Nicholson and I. Shain, Anal. Chem., 37 (1965) 190.
13 D. W. Leedy and R. N. Adams, J. Am. Chem. Soc., 92 (1970) 1646.
14 R. E. Dessy, Anal. Chem., 49 (1977) 1100A.

Analytica Chimica Acta, 134 (1982) 179—188
Elsevier Scientific Publishing Company, Amsterdam — Printed in The Netherlands

AIDS TO SOFTWARE DEVELOPMENT FOR SINGLE-BOARD MICROCOMPUTERS

ISRAEL R. BONNELL, RICHARD J. DALLE-MOLLE, and JAMES D. DEFREESE*
Department of Chemistry, The University of Kansas, Lawrence, KS 66045 (U.S.A.)
(Received 30th June 1981)

SUMMARY

A general-purpose microcomputer running the CP/M disk operating system is used to develop software for minimum-configuration microcomputers. The implementation of the minimum system software is facilitated by a software development package that runs in the general-purpose computer, a powerful monitor that resides in the minimum system, and an erasable programmable read-only memory programmer based on a single-board computer. With this development system, programs can be entered, edited, and assembled and the resulting object code transferred to the small computer for testing interactively via the terminal of the main computer.

Several reports from this laboratory have described the application of minimum configuration microcomputer systems in data acquisition and control functions in chemical instrumentation [1—3]. The use of microcomputers in dedicated control and measurement is well documented [4], and a large proportion of commercial chemical instrumentation contains dedicated microcomputers. These computers perform repetitive, pre-programmed calculations and may be responsible for the control of certain instrument parameters. Although the inherent power of the microcomputers is not fully exploited in many of these dedicated applications, they are attractive for routine use because of their low cost, ease of implementation, and programmability. Of these factors, programmability is perhaps the most important. This means that one basic design of the computer itself should suffice for a large variety of applications. With minimal or no change in interface hardware and a new program, it is easy to use the same hardware system to control the wavelength of a monochromator, applied potential in electrochemistry, synchronization of external events in a variety of circumstances, and the acquisition and reduction of data from various chemical and physical transducers. Performing these functions with non-programmable hardware systems is of course possible, but each system would be permanently dedicated to its single function with little potential for subsequent evolution.

It is possible today to buy commercial single-board computers at a moderate cost. These computers contain a small amount of read-write memory (RAM), a few kilobytes of erasable programmable read-only memory

0003-2670/82/0000-0000/$02.75

(EPROM), digital input/output (I/O) capability, and some form of keypad and display for user interaction. The single-board computer is fully functional for use in dedicated control, measurement, and computational applications. With very little formal training, a researcher can learn to implement moderately sophisticated programs.

Although the low cost and small size of the minimum-configuration microcomputer system are desirable features when one is considering a computer which will be used for performing one or a limited number of tasks, it begins to exhibit drawbacks when one considers its use in applications which require more than 100—200 program statements. Single-board computers generally have only a minimal monitor program to act as an interface to the user. The monitor lacks an assembler and, therefore, the user must manually code and key-in the program. Because the small system has no disk or tape storage, the keying-in process must be repeated each time the system is turned on. For programs of any substantial length, these processes are extremely tedious and prone to error. Moreover, the inevitable task of debugging software becomes very difficult because the single-board computer provides no breakpoint capability [5] and only limited access to programs during execution. Finally, for the same reasons as above, changing programs to accommodate new parameters is also difficult. Thus, if one becomes even moderately involved in the use of microcomputers for dedicated applications, it soon becomes clear that for the efficient development of minimum-configuration systems, it is necessary to have the facilities of a larger computer system with its hardware and software support.

A computer system that includes the facilities necessary for the development and implementation of programs that run on a minimum-configuration microcomputer system is termed a development system. A development system should have at its disposal a number of peripherals and programs in order to be effective. These include a cathode ray tube (CRT) terminal or teletypewriter for easy entry of programs and commands, disk or tape storage for saving and retrieving programs, text editing facilities for the entry and correction of programs, a line printer for producing hard copies of entered programs, an assembler for generating machine code from assembly language mnemonics, debugging capability, and an EPROM programmer for permanently storing developed code for use in the minimum-configuration system. The system must also have hardware and software that allow communication between the development system and the minimum system under development. A development system can be purchased from the manufacturer of the microprocessor, but the cost may be too high to justify in terms of its ultimate utility for a chemistry laboratory.

In this paper, facilities for the efficient development of software for minimum-configuration microcomputer systems are described. These consist of a relatively inexpensive, general hardware system (~$6000) and the software necessary to use this system in the development of code for single-board, minimum-configuration microcomputers.

HARDWARE

A block diagram of the system is shown in Fig. 1. The general-purpose laboratory microcomputer system consists of a Z-2 mainframe (Cromemco, Mountain View, CA) with 56 kbyte of RAM, dual Thinkertoys (Morrow Designs, Richmond CA) eight-inch floppy disk drives, CRT terminal (Lear Siegler ADM 3A) and line printer (Centronics 306C). A Cromemco TUART digital interface board provides an RS-232C-compatible communication link with the minimum system under development.

Although different types of minimum-configuration microcomputers are used in this laboratory [2, 3, 6], only the SDK-85 (Intel, Santa Clara, CA) single-board computer will be considered in this paper. The SDK-85 microcomputer has an 8085 central processing unit (CPU), two 8755 EPROMs with I/O ports (4 kbyte EPROM and 32 I/O lines), two 8155 RAM with I/O ports and timer (512 byte RAM, two 14-bit programmable timers and 44 I/O lines), 8279 keyboard display interface, keypad, six-digit seven-segment LED display, and 20-mA current loop serial interface. The RS-232C interface was wired in the breadboard area according to directions given in the manual [7]. This microcomputer is used extensively in this laboratory because of its low cost ($250), high degree of hardware integration, and the extensive soft-

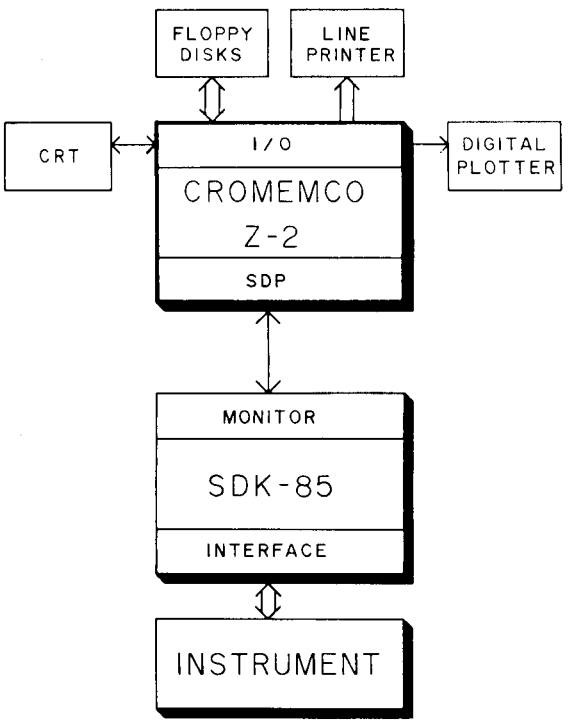

Fig. 1. Block diagram of development system.

ware support available for the 8080/8085 family of microprocessors. There is also ample breadboard area in which to wire the interface circuits.

When a program is developed, it is necessarily tested in RAM before storage in EPROM. The SDK-85 does not have enough RAM to hold even moderately sized programs and one might wire additional memory in the breadboard area. This has been avoided by designing a 2-kbyte RAM board which plugs into an 8755 socket, giving RAM in place of EPROM to test programs. It consists of two 8185 1-kbyte RAMs and a 7404 inverter. Construction techniques similar to those described by Swayne [8] were used. Once the program has been tested, it is stored in EPROM which then replaces the RAM module in the SDK-85. One limitation of this approach is that the I/O lines of the second 8755 cannot be used during testing. However, the SDK-85 has 60 other I/O lines, a sufficient number for most applications. The interface circuits can easily be designed not to use the I/O lines of the second 8755.

The EPROM programmer used in this laboratory is also based on the SDK-85 microcomputer. It can program 2716, 8755, and 2732 EPROMs. A block diagram of the unit is shown in Fig. 2. The SDK-85 communicates with the EPROM being programmed through the I/O ports of the first 8755 and 8155. The control circuitry is wired on the breadboard area. With a few minor additions, 2764 EPROMs can also be programmed. The RAM board is plugged into the second 8755 socket to provide 2 kbyte of buffer memory. Detailed schematics of the programmer can be sent to interested readers upon request.

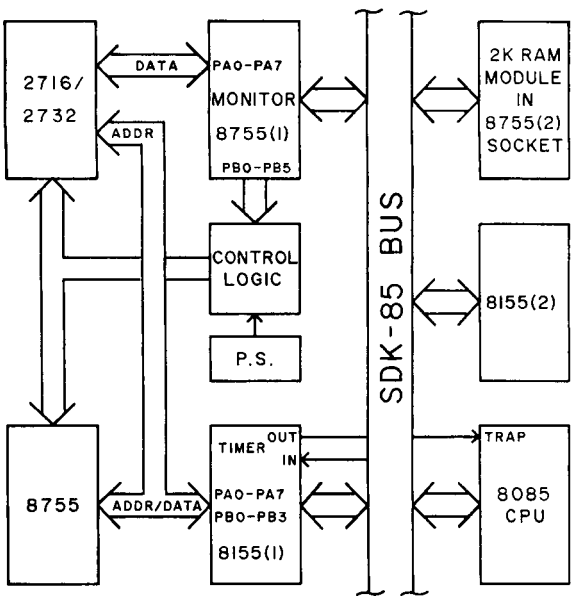

Fig. 2. Block diagram of SDK-85-based EPROM programmer.

SOFTWARE

The microcomputer systems in this laboratory run the CP/M (Digital Research, Pacific Grove, CA) disk operating system [9]. CP/M is available configured and ready to run for a wide variety of microcomputer hardware at a moderate cost ($150). It is so widely used that it can be considered the *de facto* standard for microcomputer operating systems. CP/M supports a text editor, assembler, debugger, and utilities for transferring files between peripheral devices such as disks and printers. In addition, a variety of vendor-supplied software such as text editors, macro assemblers, and high-level languages (PASCAL, BASIC, FORTRAN, etc.) that run under the CP/M operating system are available at a reasonable cost. Because of these facilities, writing programs to run in a microcomputer with the CP/M operating system is quite straightforward. The same facilities can be used to develop programs for minimum-configuration microcomputers such as the SDK-85. Two programs, SDP (Software Development Package) and MONITOR, provide a convenient means to extend the capabilities of a microcomputer running the CP/M operating system to the development of programs for minimum-configuration microcomputers.

Software development package (SDP)

The SDP program runs in the Z-2 computer. The SDP commands and functions, listed in Table 1, can be classified into four groups: (1) disk access commands that load object files created by the assembler or linking loader into the memory buffer of SDP; (2) communication commands that transmit a file in the memory buffer of SDP to a minimum system or vice versa at any convenient communication speed; (3) terminal mode command that allows the user to communicate directly with the minimum system from the terminal of the Z-2; and (4) status commands that print the starting and ending addresses of the memory buffer and of the most recently loaded program.

With these commands, it is possible to read an object file from the disk

TABLE 1

SDP commands

Command	Function
L	Load HEX or COM file from disk and store in memory buffer of Z-2
B	Program communication speed (baud)
S	Send program/data to minimum system
R	Receive program/data from minimum system
I	Interact directly with minimum system (exit with '@')
M	Print SDP memory buffer limits
F	Print starting and ending addresses of file in buffer
Q	Exit SDP (Quit)

into the memory buffer of SDP, transfer it to the minimum system, and test it interactively under the control of the minimum system monitor.

The SDP program is designed to be hardware independent to the greatest extent possible. All interactions with the terminal and disks are performed via CP/M function calls [10]. Only the sections of the program that access the TUART are specific to the hardware used, and they can easily be modified to suit any serial I/O board. Also, SDP automatically determines the amount of memory available in which to buffer programs. The buffer extends from the last address used by SDP to the starting address of the CP/M operating system. Consequently, SDP can run under any size of CP/M operating system with no possibility that the program loaded from the disks or received from the minimum system will overwrite SDP or CP/M.

Monitor program (MONITOR)

The monitor program developed in this laboratory is used in all our microcomputers. The monitor source program has conditional assembly [11] directives which enable it to be assembled for six hardware configurations, including the SDK-85, Z-2, and the SDK-85-based EPROM programmer. All the versions of MONITOR have the same set of basic commands, as well as a few commands which are specific to a particular version. This method effectively hides the hardware differences from the user who always works with nearly the same set of commands on all the microcomputers. In addition, updating and maintaining MONITOR is easy, as only one source file is required. The object code for any version of MONITOR is less than two kilobytes long and fits in one 2716 or 8755 EPROM. A source listing is available upon request.

A list of MONITOR commands and their functions is given in Table 2. The commands can be classified into four groups: (1) program entry and debugging commands that execute a program, set breakpoints, display registers, program memory or registers, and dump memory in hexadecimal, ASCII, or decimal; (2) communication commands that transfer contents of blocks of memory to another computer or vice versa and that punch or read Intel hex format paper tapes [12]; (3) system diagnostic command that tests memory; and (4) hardware specific commands that are implemented only in a particular version of MONITOR. For example, those commands that program EPROMs are contained only in the SDK-85 EPROM programmer version.

For a stand-alone minimum system, MONITOR provides a means to interact with a terminal and to enter, test, and execute small programs. However, for larger programs, it is easier to write in assembly language on a disk-based computer. In this case, it is necessary to transfer the program to the minimum system. A simple protocol is used for communication between the two computers. For example, to transfer the contents of a block of memory from the Z-2 to the SDK-85, SDP outputs the command 'R' (receive) followed by the starting and ending addresses for storing the data. MONITOR tests for

TABLE 2

MONITOR commands

Command	Version[a]	Function
G	1	Execute program with optional breakpoint
C	1	Continue program with optional new breakpoint
X	1	Display/substitute CPU registers
P	1	Program memory
D, A, B	1	Display memory in hexadecimal, ASCII, or decimal
F	1	Fill RAM with a constant
M	1	Move contents of memory
V	2	Compare two areas of memory
T	1	Test memory
U	2	Dump memory to paper tape
Y	1	Read paper tape
R	3	Receive program/data from another computer
S	3	Send program/data to another computer
E	4	Program 2708 EPROM using BYTESAVER board
W	5	Program 2716, 8755, or 2732 EPROM
L	5	Load contents of EPROM into RAM
V	5	Compare contents of RAM with EPROM

[a]1 = all, 2 = all except EPROM programmer, 3 = SDK-85 and ADD8080, 4 = Cromemco Z-2 and Altair 8800B, and 5 = EPROM programmer.

RAM at the two addresses and outputs the character 'O' (OK) if it is ready to accept the data or 'N' if there is no RAM. After an 'O' is received, SDP transmits the data as 8-bit binary numbers in serial format. MONITOR receives the data bytes and stores them. When the required number of bytes have been received, the calculated checksum is sent back. The SDP program compares this checksum with the checksum calculated before transmission and outputs an error message if they are not equal. Most of the communication takes place via cables less than 25 m long. Therefore, the probability of transmission errors is extremely low and this simple error checking technique is adequate. The integrity of the communication system has been confirmed by repeated transfers of a large block of data from the Z-2 to the SDK-85 and then back, followed by a byte-by-byte comparison of the original data with the data returned by the SDK-85.

Thus, the combination of CP/M, SDP, and MONITOR provides the facilities needed to develop software for the SDK-85 or similar systems efficiently. The use of the system is illustrated by the example shown in Table 3. The program TEST.HEX (Table 4) sets up the programmable counter of the second 8155 on the SDK-85 to divide the system clock frequency of 3.072 MHz by 3072 and produce a 1-kHz square wave. Here, no program errors were detected, but longer programs invariably will have errors. If these are minor, object code changes can be made directly with MONITOR. However, if major changes must be made in the source program, then the steps shown

TABLE 3

Program development example using SDP and MONITOR

Dialogue[a]	Explanation
A > SDP	Load and execute SDP
STARTING ADDRESS OF BUFFER = OAE7 ENDING ADDRESS OF BUFFER = C506	SDP sign on message
^B 4800 1	4800 baud, 1 stop bit
^I	Enter terminal mode (Press space bar for baud identification and SDK-85 signs on with '*')
*@	Exit terminal mode
^L B:TEST.HEX 1000	Load program from disk into memory buffer of SDP with 1000H offset
STARTING ADDRESS OF FILE = 1800 ENDING ADDRESS OF FILE = 180C	
^S 1800 180C 800	Send program to SDK-85
^I	Re-enter terminal mode
*D 0800 080C	Display memory to check for program
0800 3E 00 D3 2C 3E 4C D3 2D 3E C0 D3 28 C9	
*G 0800	Execute program (Observe 1-kHz square wave on oscilloscope)
*@	Exit terminal mode
^Q	Exit SDP
A>	Back in CP/M

[a]User inputs are underlined.

TABLE 4

Listing of program TEST.HEX

```
;
;EXAMPLE PROGRAM TO SET UP THE SECOND 8155 COUNTER OF THE SDK-85
;TO DIVIDE THE SYSTEM CLOCK (3.072 MHZ) BY 3072 AND PRODUCE
;A 1-KHZ SQUARE WAVE
;
;
;
TSTART EQU    0C0H                  ;CODE FOR START TIMER
TMODE  EQU    40H                   ;TIMER MODE — SQUARE WAVE GENERATOR
LOBYTE EQU    3072 MOD 256          ;LEAST SIGNIFICANT BYTE
HIBYTE EQU    (3072/256) + TMODE    ;MOST SIGNIFICANT BYTE
       ORG    0800H
       MVI    A,LOBYTE              ;LOAD LEAST SIGNIFICANT BYTE
       OUT    2CH
       MVI    A,HIBYTE              ;LOAD MOST SIGNIFICANT BYTE
       OUT    2DH
       MVI    A,TSTART              ;START TIMER
       OUT    28H
       RET                          ;RETURN TO MONITOR
```

in Table 3 must be repeated after the edit and assembly. Large programs, which are usually developed in stages, often need considerable debugging. In this case, the steps in Table 3 will be repeated several times, enhancing the value of SDP and MONITOR in terms of reduced program development time.

EPROM programming

When the program has been tested successfully in RAM, it is permanently stored in EPROM in the dedicated minimum system. A version of MONITOR is used in the SDK-85-based EPROM programmer also. It receives the object code to be programmed into the EPROM from another computer running SDP or from Intel hex format paper tapes via a teletypewriter connected directly to the programmer. This version of MONITOR is augmented with three commands to program (W), verify (V), and read (L) the contents of EPROMs (see Table 2).

Because MONITOR and SDP are used with the EPROM programmer, the steps involved in transferring a program from the disks of the Z-2 to RAM in the EPROM programmer are identical to those in Table 3. After transferring the program, the command, W 8755 0800 080C 0000, will program the 8755 (or 2716 or 2732) EPROM and verify the results. In the command line, 0800 and 080D are the starting and ending addresses of the program in RAM and 0000 is the starting address in the EPROM.

Conclusion

This system has been used to develop software for all minimum-configuration microcomputers used in this laboratory. One such example is a versatile microprocessor ratemeter for kinetic determinations [13]. The program, the object code of which is over 2 kbyte long, is a software project of such complexity that it would not have been attempted without this development system. Because of the program length, it was developed in stages. The SDP and MONITOR programs were used during the entire design process to test and debug the program at each stage.

Even with software development facilities, implementing programs in assembly language for applications involving extensive computations is relatively difficult, error-prone, and time-consuming. An attractive option is the production of object code for minimum-configuration microcomputers directly from high-level languages such as FORTRAN, PASCAL, or BASIC. In fact, this is rapidly becoming a necessity as more sophisticated computation and control are being applied in instrumentation for characterization of complex chemical systems [14, 15]. The problem of increased object code length compared to that produced from assembly language has been alleviated by the availability of high density EPROMs (2732 and 2764) at moderate cost. Therefore, greater emphasis on writing application programs in high-level languages for small dedicated computers is expected. The only adaptation needed for the aids described in this paper to support this mode of

program development is the addition of appropriate I/O interface routines to the library of the high-level language.

This paper was presented in part at the 16th Midwest Regional Meeting of the American Chemical Society, Lincoln, Nebraska, November 1980. Acknowledgement is made to the donors of The Petroleum Research Fund (administered by the American Chemical Society), the University of Kansas (General Research Allocation 3330-XO-0038), and Research Corporation for partial support. Financial support to I. R. B. by a Phillips Petroleum Company fellowship and to R. J. D-M. by the Stauffer Chemical Company is gratefully acknowledged.

REFERENCES

1 R. Dalle-Molle and J. D. Defreese, Anal. Chem., 51 (1979) 1755.
2 I. R. Bonnell and J. D. Defreese, Anal. Chem., 52 (1980) 139.
3 R. Dalle-Molle and J. D. Defreese, J. Automatic Chem., 2 (1980) 76.
4 D. Betteridge and T. B. Goad, Analyst, 106 (1981) 257.
5 T. P. Hughes and D. H. Sawin III, Comput. Des., 17(11) (1978) 99.
6 J. Avery and D. Lovse, The ADD-8080 Microprocessor Manual, Department of Chemistry, University of Illinois, Urbana, IL, 1977.
7 SDK-85 System Design Kit User's Manual, Intel Corp., Santa Clara, CA, 1978, p. 5—8.
8 P. Swayne, Kilobaud Microcomp., October (1980) 50.
9 R. Zaks, The CP/M Handbook with MP/M, Sybex, Berkeley, CA, 1979.
10 CP/M 2.0 Interface Guide, Digital Research, Pacific Grove, CA, 1979.
11 8080/8085 Assembly Language Programming Manual, Intel Corp., Santa Clara, CA, 1977, p. 4—8.
12 A. R. Miller, Interfaceage, 3(3) (1978) 158.
13 I. R. Bonnell and J. D. Defreese, Anal. Chim. Acta, 134 (1982) 189.
14 J. W. Frazer, Anal. Chem., 52 (1980) 1205A.
15 J. W. Frazer, Am. Lab., 13(4) (1981) 60.

Analytica Chimica Acta, 134 (1982) 189—200
Elsevier Scientific Publishing Company, Amsterdam — Printed in The Netherlands

MICROPROCESSOR RATEMETER FOR KINETIC DETERMINATIONS

ISRAEL R. BONNELL and JAMES D. DEFREESE*
Department of Chemistry, The University of Kansas, Lawrence, KS 66045 (U.S.A.)
(Received 30th June 1981)

SUMMARY

A simple, compact, easy-to-implement microprocessor ratemeter for kinetic determinations based on initial rate, fixed time, and variable time is presented. The hardware and software are such that the ratemeter can be used with almost any transducer or instrument to monitor reactions in a wide variety of chemical systems. The performance of the ratemeter is demonstrated by its application to the determination of phosphorus by stopped-flow spectrometry, glucose by amperometry, and alkaline phosphatase activity in control sera by visible spectrophotometry.

Determinations based on chemical kinetics quantify the analyte either via its rate of reaction with an added reagent or its catalytic effect on another reaction [1, 2]. Compared to equilibrium methods, kinetic methods offer greater speed, relative freedom from interfering side reactions, ability to analyze mixtures of closely related compounds without physical separation, and very high sensitivity in the case of catalytic reactions. In determinations of enzyme activity, it is the rate itself which is the quantity sought. In addition, instrument offsets, imperfect cuvettes, turbid samples, etc., do not introduce significant error because of the relative nature of the measurement.

Kinetic methods are used extensively in clinical laboratories where enzyme assays are performed on a routine basis. Several types of rate-measuring systems are available and have been reviewed by Pardue [3], Crouch et al. [4, 5], and Malmstadt et al. [6, 7]. They can be broadly classified as hardwired systems and computer-controlled systems. Hardwired systems using digital and analog circuitry have been described for kinetic methods based on fixed time, variable time, and initial rate. However, each hardwired system is suitable only for a particular type of kinetic determination and has limited data-processing capability and dynamic range.

In contrast, computer-controlled systems are versatile for any method of kinetic data processing, often have a high degree of automation in sample handling, and are very well-suited for fundamental kinetic studies and analytical method development. However, these systems are relatively expensive, bulky, and complex, and many of their features may be unnecessary for routine applications. With the availability of microprocessors, high-density semiconductor memories, and versatile interface circuits, it is now

possible to build powerful, compact, dedicated laboratory data acquisition, control, and computation systems for a moderate cost. This paper describes one such system, a versatile microprocessor-based ratemeter for kinetic determinations, which is easy to build, compact, keyboard programmable, and capable of acquiring rate data from a variety of transducers and instruments and of calculating rates by different methods.

INSTRUMENTATION

A block diagram of the ratemeter is shown in Fig. 1. It is based on the SDK-85 single-board microcomputer (Intel, Santa Clara, CA). The SDK-85 microcomputer has an 8085 central processing unit (CPU), two 8755 erasable programmable read only memories (EPROM) with input/output (I/O) ports (4k EPROM and 32 I/O lines), two 8155 read-write memories (RAM) with I/O ports and timer (512 bytes RAM, two 14-bit programmable timers, and 44 I/O lines), 8279 keyboard display interface, keypad, six-digit LED display, and a 20-mA serial interface. This microcomputer was chosen because of its low cost ($250), its high degree of integration, and the extensive software support available for the 8080/8085 family of microprocessors. The

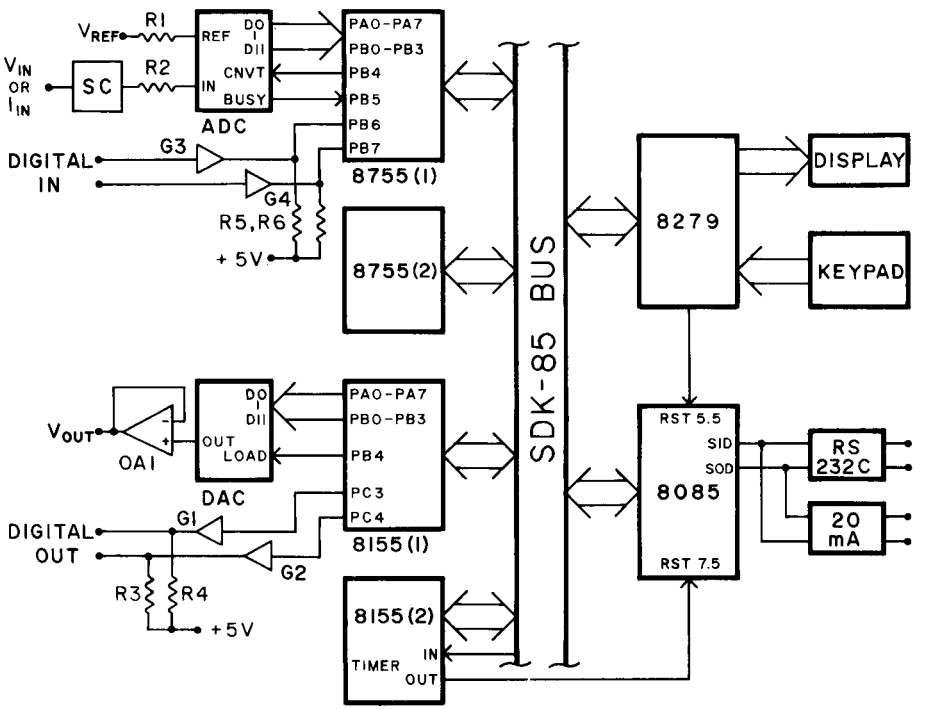

Fig. 1. Block diagram of microprocessor ratemeter. R1, 500 kΩ, 1%; R2, 1 MΩ, 1%; R3—R6, 2.2 kΩ; G1—G4, 7407 I.C.; OA1, 1/4 of 4136 operational amplifier; V_{ref}, Precision Monolithics REF-01; SC, signal conditioner (see Fig. 2); ADC and DAC (see text).

analog-to-digital converter (ADC), digital-to-analog converter (DAC), and signal preconditioning and instrument interface circuits are wire-wrapped on the breadboard area of the SDK-85. They are connected to the bus of the SDK-85 through the I/O ports of the 8755s and 8155s.

The data acquisition interface consists of an integrating 12-bit ADC (Datel EK12B) and signal-conditioning circuitry. The integrating nature of the ADC results in a high signal-to-noise ratio at the expense of conversion time (24 ms). The ADC is wired to operate in the 0 to +10 V range as recommended by the manufacturer. The eight least significant bits (LSB) of the ADC output are connected to port A of 8755 (1) and the four most significant bits (MSB) are connected to port B, bits 0 through 3. The START CONVERT input and BUSY output are connected to bits 4 and 5 of port B, respectively. An AD conversion is initiated by pulsing the START CONVERT bit HI. The BUSY output of the ADC remains HI while a conversion is in progress.

The signal conditioning circuitry, shown in detail in Fig. 2, consists of two operational amplifiers and a switch network. It is designed to present a 0 to +10 V signal to the input of the ADC. Operational amplifier, OAl, functions as a variable gain voltage or current amplifier and OA2 functions as an inverter. The different settings of the eight miniature switches allow the types of signals shown in Table 1 to be transformed to the ADC input range for most applications, but any other circuit can be used so long as a 0 to +10 V signal is presented to the ADC input.

The analog output (Fig. 1) consists of a 12-bit DAC with input latches (Datel DAC-HK12BGC) that is wired to operate in the −5 V to +5 V range as recommended by the manufacturer. The eight LSBs of the DAC are con-

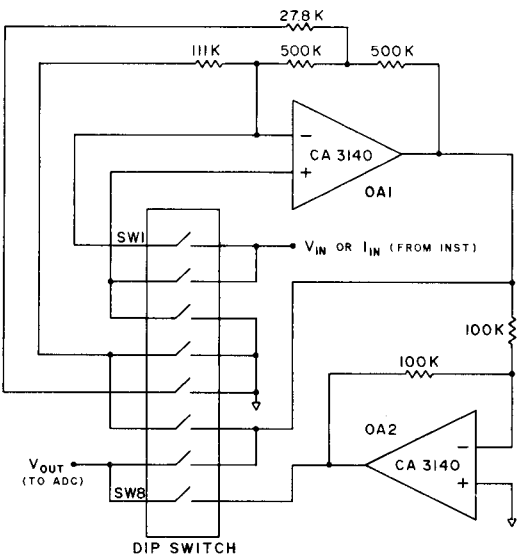

Fig. 2. Signal conditioning circuit.

TABLE 1

Switch settings of the signal conditioning circuit for different types of input signals

Range	SW1	SW2	SW3	SW4	SW5	SW6	SW7	SW8
0 to +10 V	OFF	ON	OFF	OFF	OFF	OFF	ON	OFF
0 to −10 V	OFF	ON	OFF	OFF	OFF	OFF	OFF	ON
0 to +1 V	OFF	ON	OFF	ON	OFF	OFF	ON	OFF
0 to −1 V	OFF	ON	OFF	ON	OFF	OFF	OFF	ON
0 to −1 μA	ON	OFF	ON	OFF	ON	OFF	ON	OFF
0 to +1 μA	ON	OFF	ON	OFF	ON	OFF	OFF	ON
0 to −10 μA	ON	OFF	ON	OFF	OFF	OFF	ON	OFF
0 to +10 μA	ON	OFF	ON	OFF	OFF	OFF	OFF	ON
0 to −100 μA	ON	OFF	ON	OFF	OFF	ON	ON	OFF
0 to +100 μA	ON	OFF	ON	OFF	OFF	ON	OFF	ON

nected to port A of 8155 (1) and the four MSBs are connected to bits 0 through 3 of port B. Bit 4 of port B is connected to the LOAD DATA input of the latches of the DAC.

The ratemeter has two digital output and two digital input lines to allow interfacing with nearly any instrument. The output lines are connected to bits 3 and 4 of 8155 (1) port C and the input lines are connected to bits 6 and 7 of port B of 8755 (1). Both the output and input lines are buffered with 7407 gates. The current version of the software however uses only one output and one input line.

Timing for the ratemeter is provided by the 14-bit programmable counter/timer in 8155 (2). The input to the timer is the 3.072 MHz system clock of the SDK-85. The timer is programmed in mode 2 [8] to divide the input frequency by 15360 to produce a 200-Hz square wave. The output of the timer is connected to the RST 7.5 interrupt input of the CPU to generate an interrupt on every rising edge of the output clock pulse. The timekeeping and data acquisition functions are performed by interrupt service routines that are described in detail in the software section.

SOFTWARE

The hardware of the ratemeter is simple and general. The function and versatility of the ratemeter derive from the software. Consequently, a significant portion of the design effort was spent on software. The software development methods and facilities have been described [9].

The major components of the ratemeter program are: (1) method selection and parameter entry routines, (2) rate measurement and computation routines, (3) instrument interface routines, (4) RST 7.5 interrupt service routines, and (5) input/output routines. The program is written in Intel 8080 assembly language. Macro assembler MACRO-80 and LINK-80 linking loader (Microsoft, Bellevue, WA) were used to assemble, link, and load the ratemeter program. Two versions of the program are currently in use. Version 1 is about two kilobytes long and fits in one 8755 EPROM. Version 2 is about

three kilobytes long and requires two 8755 EPROMs for storage. The latter version includes routines to output the results of rate computations to a printer at 30 or 10 characters per second via the 20-mA serial interface.

The following sections describe the features of these routines and how they contribute to the versatility of the ratemeter in different types of kinetic determinations. Descriptions of specific details of implementation are kept to a minimum here, but are contained in the ratemeter source program listing which is available on request.

Method selection and parameter entry routines

The ratemeter can analyze kinetic data by (1) initial rate, (2) fixed time, and (3) variable time methods. Upon pressing the SUBST MEM key, the message TECH is output on the display and the ratemeter waits for the method (key 1, 2, or 3) to be entered. Once the method has been selected, the parameters necessary for making the measurement must be entered. The prompt messages for these parameters and the acceptable range of values are shown in Table 2. All parameters are decimal numbers in the range of 0.001 to 9999. Entry is terminated by the NEXT key. The entered parameters are converted to a form that is convenient for computation: millivolts are converted to 12-bit binary numbers to be compatible with a 12-bit ADC, delay times are converted to number of clock periods, and integration times are converted to number of AD conversions. Once parameters within acceptable ranges have been entered, a flag is set in memory and rate measurements based on the preset method and parameters can be made any number of times by simply pressing the GO key.

Rate measurement and computation routines

Initial rate. The integration slope method [6] is used to compute the slope of the initial rate curve. The signal is integrated for two consecutive fixed intervals of time. These integrals are computed by summing the required number of AD conversions (0.025 s per conversion). The difference between

TABLE 2

User inputs for different methods

Method	Prompt	Meaning	Range of values
(1) Initial rate	dt	Premeasurement delay time	0.005—328 s
	it	Integration time	0.025—1638 s
(2) Fixed time	dt	Premeasurement delay time	0.005—328 s
	tc	Integration time	0.025—1638 s
	td	Time delay between two integrations	0.005—328 s
(3) Variable time	dt	Premeasurement delay time	0.005—328 s
	tc	Signal averaging time	0.025—3.0 s
	S1	Signal level for starting timer	0—9999 mV
	S2	Signal level for stopping timer	0—9999 mV

the integrals (which is proportional to the slope of the input signal) is calculated, converted to a six-digit decimal number, and output to the display.

Fixed time method. The computation is identical to the initial rate method except that there is a delay time between the two integrations.

Variable time method. The direction in which the signal will change is determined from signal threshold levels entered during method selection. During the measurement, the program monitors the input signal until it crosses the first signal threshold level (S1) from the proper direction, at which time the software timer in the RST 7.5 interrupt service routine is started. The timer is stopped when the signal crosses the second threshold level (S2). The reciprocal of the elapsed time is then calculated and displayed.

The precision of the results by the variable time method is very sensitive to noise on the input signal [6]. To minimize the effects of noise in signal comparison, a real-time modification of the sliding window smoothing algorithm [10] is used to average the input signal before comparison. The width of the window is selected by the user and can range from 25 ms to 3 s. Initially, the number of AD conversions corresponding to the duration of the window (25 ms per conversion) is acquired. These values are stored in a table in memory and their average is compared to S1. After each subsequent conversion, the first value in the table is discarded, the others are moved up, the new value is stored at the end of the table, and the new average is compared to the appropriate signal level (S1 or S2). Because the comparison is performed after each conversion, the resolution for measurement of time is the same, irrespective of the width of the window. The characteristics of this type of filter have been discussed in detail by O'Haver [11].

Instrument interface routines

To start data acquisition, the ratemeter can send a TTL level trigger signal to an instrument and/or wait for a trigger signal to come from the instrument. For example, the stopped-flow spectrophotometer (730S, McPherson Instruments, Acton, MA) [12] needs a 1 → 0 (HI → LO) pulse at the CYCLE input to start the cycle. When the flow stops, the ready output undergoes a 1 → 0 transition. The necessary trigger signals can be easily programmed from the keypad. Pressing the EXAM REG key will allow the type of output pulse (1 → 0 or 0 → 1) to be set. Pressing the F key will allow the type of input pulse (1 → 0 or 0 → 1) to be set. The user inputs for different pulse types are shown in Table 3. Once the pulse types have been programmed, they are automatically generated and/or waited for before making each rate measurement. However, on power up or after a reset, the ratemeter is set to the default mode (no trigger pulses).

RST 7.5 interrupt service routine

When the 8155 (2) timer generates an interrupt (every 5 ms), the interrupt service routine may perform any of several functions depending on whether or not a rate measurement is in progress. The ratemeter functions as a digital

TABLE 3

Interface trigger signal selection

User input	Signal out[a]	Signal in
00	no pulse	no pulse
01	⎍	⎍
10	⎍	⎍

[a]Output pulsewidth, 100 μs.

volt/current meter (DVM) at all times. Because the conversion time of the ADC is ⩽24 ms, its output is read and a new conversion is triggered on every fifth interrupt. Ten AD conversions are averaged, converted to millivolts, and output to the four-digit address field of the display if it is not being used by the main program. Therefore, the signal averaging time is 250 ms in the DVM mode.

When a rate measurement is made, the main program enables desired functions by setting flags and loading numbers in predetermined memory locations. The software time-delay generator is started by loading the time delay (as number of interrupts) and setting a flag byte. The delay time is decremented after each interrupt and the flag is reset when the contents of the counter equal zero. Counting can be stopped at any time by resetting the flag. The counter can thus be used to measure elapsed time by subtracting its contents from the initial value loaded. Data acquisition is initiated by setting the number of points to be acquired, the number of AD conversions to skip before storing one, and the address for storing the data points. The number of data points will be decremented after each data point has been acquired and will be set to zero when data acquisition is complete. A third function is a call to any subroutine (e.g., integration of signal) which is enabled by setting a flag and loading the address of the subroutine.

Input-output routines

The keypad and display of the SDK-85 are interfaced to the bus by the 8279 keyboard display integrated circuit (Fig. 1). Whenever a key is pressed, its corresponding code is stored in the 8279 and a RST 5.5 interrupt is generated. The RST 5.5 interrupt service routine reads the code from the 8279 and stores it in a pre-assigned memory location to be read by the main program. Inputs from two keys are interpreted by the interrupt service routine itself. The SSTEP key causes the display busy flag to be cleared so that the display is available for the DVM routines. The A key will interrupt whatever operation the ratemeter is performing and cause it to wait for commands from the keypad. Data are output to the display by writing to specified addresses in the 8279. Output to the printer is provided via the Serial Out Data (SOD) line of the 8085 using routines supplied by Intel [8].

RESULTS AND DISCUSSION

The combined hardware and software features of the ratemeter enable it to be coupled with almost any transducer or instrument used for monitoring a reaction. The ratemeter allows the user to select different kinetic methods and their corresponding parameters by simple entries from the keypad. The selection of a particular technique for maximum accuracy and dynamic range is determined by the nature of the analyte (catalyst or reactant), species being monitored (reactant or product), response characteristics of the transducer (linear or nonlinear with concentration), and kinetics of the reaction (zero-order or first-order). These considerations have been discussed in detail by Pardue [3] and by Ingle and Crouch [13].

Measurement times can range from 25 ms to 1600 s so that a wide variety of reactions can be used with this ratemeter. Premeasurement delay times ranging from 5 ms to 325 s can be used to avoid making rate measurements during the lag phase of a reaction or during temperature equilibration.

The software can automatically compute the rates of signals which increase or decrease with time. Examples of the first type are product concentration monitored by absorbance or amperometry, and reactant concentration monitored by transmittance. Signals decreasing with time include reactant concentration monitored by absorbance or amperometry, and product concentration monitored by transmittance.

The following sections illustrate the use and performance of the ratemeter for several types of determination using different types of instruments.

Determination of phosphorus

The determination of phosphorus is based on the method of Javier et al. [14]. Phosphate reacts with 0.1 M molybdenum(VI) in 0.4 M nitric acid to form 12-molybdophosphoric acid which absorbs at 400 nm. The reaction is pseudo-first-order in phosphate with a half-life of about 600 ms. A stopped-flow spectrophotometer [12] is used for monitoring this reaction. The experimental setup is shown in Fig. 3(a). The photomultiplier tube (PMT) current, which is proportional to the transmittance of the reaction mixture, is fed into the ratemeter set to accept current signals in the range of 0 to -10 μA. The PMT output is nonlinearly related to the concentration of 12-molybdophosphoric acid and, therefore, the variable time method would seem to be the method of choice. However, large variations in initial transmittance are observed when phosphate and molybdenum(VI) solutions are mixed. This results in a different initial transmittance reading for each concentration of phosphate, preventing the use of the variable time method. Hence, the initial rate method is used.

The ratemeter is programmed to provide a $1 \rightarrow 0$ pulse to start the stopped flow cycle and wait for a $1 \rightarrow 0$ transition at the READY output before acquiring data. When the GO key is pressed, the ratemeter cycles the stopped-flow, acquires the data, calculates the rate, and displays the result. Calibration

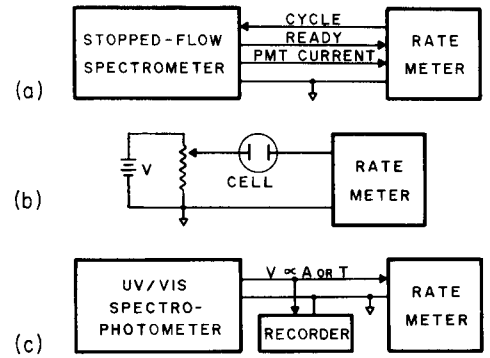

Fig. 3. Instrument/ratemeter combinations for determination of (a) phosphorus, (b) glucose, and (c) alkaline phosphatase activity.

data for the determination of phosphorus in the 0.5—4 μg ml^{-1} range are given in Table 4. The slope, intercept, correlation coefficient, and standard error of estimate are 69 ± 1, 29 ± 3, 0.9995, and 3.3, respectively. Because the molar absorptivity of 12-molybdophosphoric acid is low, the transmittance change during the measurement interval is very small. The precision of the measurements is therefore limited by the reproducibility of the stopped-flow mixing system. The ratemeter was tested with synthetic ramps and the precision of the slope measurements was 0.1% or better.

Enzymatic determination of glucose

The enzymatic determination of glucose is based on the method of Pardue [15]. Glucose is oxidized to gluconic acid and hydrogen peroxide in the presence of glucose oxidase. The hydrogen peroxide oxidizes excess iodide present in the reaction medium to iodine at a rate which is very much faster than that of the oxidation of glucose. The concentrations of the reagents are such that the reaction is first-order with respect to glucose. The iodine formed by the reaction is monitored biamperometrically using a rotated (600 rpm) platinum electrode and a stationary platinum wire electrode. The experimental arrangement is shown in Fig. 3(b). The polarizing voltage across the electrodes is 200 mV and is derived from a 1.5-V battery

TABLE 4

Determination of phosphorus[a]

Conc. (μg P ml^{-1})	0.5	1.0	1.5	2.0	3.0	4.0
Rate	62	97	133	173	237	303
RSD (%)	7.0	4.3	3.3	1.8	2.5	2.1

[a]Ratemeter settings: method = initial rate (1); delay time = 0.5 s; integration time = 0.1 s. Relative standard deviation relates to 10 determinations. The regression equation is Rate = (69 ± 1)C° + 29 ± 3 with standard error = 3.3 and r = 0.9995.

and 1000-ohm potentiometer. The anode is connected to the voltage source and the cathode is connected to the ratemeter input which is arranged to accept current signals in the range of 0 to +10 μA.

The fixed-time method is best suited for reactions which follow first-order kinetics and is used in this case. In the measurement step, 5 ml of the composite reagent is pipetted into the thermostatted reaction cell and the rotating platinum electrode is turned on. Then 1 ml of the glucose solution is pipetted into the cell and the GO key on the ratemeter is pressed simultaneously. The rate is displayed at the end of the measurement period. Calibration data for the determination of glucose in the range 1—100 μg ml^{-1} are given in Table 5. The slope, intercept, correlation coefficient, and standard error of estimate are 14.7 ± 0.2, −8 ± 8, 0.9996, and 16, respectively. The precision of the measurements depended on the reproducible positioning of the electrodes with respect to each other and with respect to the center of the reaction cell. Consequently, the electrodes and cell were firmly clamped and an aspirator was used to remove the waste reagents from the reaction cell.

Determination of alkaline phosphatase activity

The determination of alkaline phosphatase activity in serum is based on the method of Bowers and McComb [16]. The enzyme catalyzes the hydrolysis of *p*-nitrophenyl phosphate to *p*-nitrophenol which is monitored spectrophotometrically at 410 nm. The concentration of the substrate is sufficiently high that rate measurements are made under pseudo-zero-order conditions. The ratemeter is connected in parallel with the stripchart recorder of a UV/VIS spectrophotometer (721D, McPherson Instruments) as shown in Fig. 3(c). The ratemeter input is set to accept signals in the range 0 to +10 V.

The variable time method is used for the determination as the enzyme activity can then be calculated directly without the use of an enzyme standard. For the assay, 2.7 ml of pH 10.3 buffer, 0.2 ml of substrate, and 0.1 ml of serum are mixed in the cuvette and the GO key is pressed on the ratemeter. The ratemeter measures the time required for the input signal to change from S1 to S2 (50 mV difference) and displays $10000/\Delta t$. The spectrometer—

TABLE 5

Determination of glucose[a]

Glucose (μg ml^{-1})	1	5	10	15	25	35	45	75	100
Rate	10.9	60.3	136	207	363	523	656	1061	1478
RSD (%)	9.0	1.2	3.2	1.6	2.6	1.1	0.9	1.3	0.2

[a]Ratemeter settings: method = fixed time (2); delay time = 10 s; Δt = 15 s; signal averaging = 5 s. Relative standard deviation is for 4 determinations. The regression equation is Rate = (14.7 ± 0.2)C° − 8 ± 8 with standard error = 16 and r = 0.9996.

ratemeter combination is calibrated with standard *p*-nitrophenol solutions in pH 10.3 buffer. The 50-mV signal change corresponds to a concentration change of 1.35 μmol l^{-1}. The results of the determination of alkaline phosphatase activity in dilutions of Enzatrol control serum (Dade Division, American Hospital Supply Corp., Miami, FL) are given in Table 6.

CONCLUSION

The ratemeter hardware is very general and easy to duplicate. Because a commercial single-board computer is used, wiring the ADC and DAC circuits should not take more than a few days. Detailed circuit and component layout diagrams can be sent to interested readers on request. However, developing the necessary software which is versatile, reliable, and easy to modify is extremely time-consuming. Published flow charts or structure diagrams may not be of too much help in implementing the software. Source program listings are too long to be published and are a nuisance to type into a computer. In order to facilitate the duplication of the ratemeter system with minimum effort, EPROMs supplied by interested readers will be programmed with the object code on request. However, for those readers who have appropriate facilities, the source program can be supplied on an 8-inch, single-density, CP/M (Digital Research, Pacific Grove, CA) compatible floppy disk. The support software necessary for implementing and modifying the ratemeter program will also be included on the disk [9].

Most of the computations performed on the data by the ratemeter are very simple in nature, i.e., calculation of slopes, averages, and differences. More sophisticated manipulations of the data would be desirable [12, 17], e.g., calculations of slopes by least-squares techniques, multiple slope computations, and multicomponent computations. Such programs are difficult to code in assembly language directly. A high-level language such as PASCAL, FORTRAN, or BASIC is desirable for generating the object code for such applications. Work in this direction is currently in progress in this laboratory [9].

TABLE 6

Determination of alkaline phosphatase activity[a]

Dilution factor	Activity[b] (μmol l^{-1} min^{-1})	Normalized activity	RSD (%)
0.25	116	463	1.5
0.50	229	458	2.5
0.75	363	484	2.0
1.00	483	483	2.1

[a]Ratemeter settings; method = variable time (3); delay time = 10 s; signal averaging = 3 s; S1 = 500 mV; S2 = 550 mV. Relative standard deviation is for 4 determinations. [b]Temperature, 30.0 ± 0.02°C.

This paper was presented in part at the 16th Midwest Regional Meeting, American Chemical Society, Lincoln, Nebraska, November 1980. Acknowledgement is made to the donors of The Petroleum Research Fund (administered by the American Chemical Society), the University of Kansas (General Research Allocation 3330-X0-0038), and the Research Corporation for research support. Financial support provided to I. R. B. by a Phillips Petroleum Company fellowship is gratefully acknowledged.

REFERENCES

1 H. V. Malmstadt, E. A. Cordos and C. J. Delaney, Anal. Chem., 44 (1972) 26A.
2 H. B. Mark, Jr., in H. H. Bauer, G. D. Christian and J. E. O'Reilly (Eds.), Instrumental Analysis, Allyn and Bacon, Boston, 1978, Chap. 18.
3 H. L. Pardue, in C. N. Reilley and F. W. McLafferty (Eds.), Advances in Analytical Chemistry and Instrumentation, Vol. 7, Wiley—Interscience, New York, 1969, pp. 141—207.
4 S. R. Crouch, in J. S. Mattson, H. B. Mark, Jr. and H. C. MacDonald, Jr. (Eds.), Computers in Chemistry and Instrumentation, Vol. 3, M. Dekker, New York, 1973, Chap. 3.
5 S. R. Crouch, F. J. Holler, P. K. Notz and P. M. Beckwith, Appl. Spectrosc. Rev., 13 (1977) 165.
6 H. V. Malmstadt, C. J. Delaney and E. A. Cordos, Anal. Chem., 44 (1972) 79A.
7 H. V. Malmstadt, Analyst, 105 (1980) 1018.
8 MCS-80/85 Family User's Manual, Intel Corp., Santa Clara, CA, USA, 1979, p. 6—17; A1—32.
9 I. R. Bonnell, R. J. Dalle-Molle and J. D. Defreese, Anal. Chim. Acta., 134 (1982) 179.
10 A. Savitsky and M. J. E. Golay, Anal. Chem., 36 (1964) 1627.
11 T. C. O'Haver, Anal. Chem., 50 (1978) 676.
12 I. R. Bonnell and J. D. Defreese, Anal. Chem., 52 (1980) 139.
13 J. D. Ingle, Jr. and S. R. Crouch, Anal. Chem., 43 (1971) 697.
14 A. C. Javier, S. R. Crouch and H. V. Malmstadt, Anal. Chem., 41 (1969) 239.
15 H. L. Pardue, Anal. Chem., 35 (1963) 1241.
16 G. N. Bowers, Jr. and R. B. McComb, Clin. Chem., 12 (1966) 70.
17 H. L. Pardue, Clin. Chem., 23 (1977) 2189.

Analytica Chimica Acta, 134 (1982) 201—209
Elsevier Scientific Publishing Company, Amsterdam — Printed in The Netherlands

APPLICATION OF POTENTIOMETRIC STRIPPING ANALYSIS TO COMPLEXIMETRIC TITRATIONS

DANIEL JAGNER* and KERSTIN ÅRÉN

Department of Analytical and Marine Chemistry, Chalmers University of Technology and University of Göteborg S-412 96 Göteborg (Sweden)

(Received 3rd July 1981)

SUMMARY

Samples that are 0.1—10 mM in lead(II) or 0.025—0.25 mM in bismuth(III) can be titrated with EDTA and the titrations monitored by means of computerized potentiometric stripping analysis. The coefficients of variation are 0.12—0.40%; systematic errors are estimated from computer-calculated titration curves using conditional constants obtained from the titration curves. The conditional stability constants for calcium(II), manganese(II) and lanthanum(II) in 0.5 M sodium chloride are determined from the exchange reaction with the lead—EDTA complex.

In previous applications of potentiometric stripping analysis, total trace metal concentrations have been determined. In order to ensure that the trace metal analytes exist in an electrochemically reversible form, hydrochloric acid was added to the sample prior to analysis [1—5]. By proper choice of potentiostatic deposition potentials, however, it is possible to discriminate between different chemical forms of the trace metal analytes by potentiometric stripping analysis. This is particularly simple if one fraction of the trace metal analyte is in the form of easily reducible aquo- or chloro-complexes and the other fraction is in the form of, e.g., a stable EDTA complex. Thus potentiometric stripping analysis can be used to monitor complexiметric titration.

Potentiometric monitoring of complexiметric titrations with membrane ion-selective electrodes as sensors has been reported by several authors and the results have been summarized by Moody and Thomas [6]. For the titration of divalent heavy metal ions, solid membranes of mixed sulphides have been used. These membranes respond to the activity of the uncomplexed heavy metal ion. If, however, several elements forming highly insoluble sulphides are present in the sample at the same time, the electrode will respond to the heavy metal ion which has the lowest value for $K_{MS} \times [M^{2+}]^{-1}$, where K_{MS} is the solubility product for MS(s). Thus interference with the sensor potential is possible even if the interfering ions are present in concentrations very much lower than that of the ion to be monitored. In this respect, potentiometric stripping analysis has the advantage of being less vulnerable to sensor interference. Furthermore, the technique is capable of

measuring very low concentrations of reducible ionic species, which means that it is possible to monitor the titration in the immediate vicinity of the equivalence point thus increasing accuracy and precision.

The purpose of this work is to illustrate how potentiometric stripping analysis can be used to monitor complexiметric titration. Although the technique can be used for all elements which are measurable by potentiometric stripping analysis [7], it will be illustrated here only by the titration of two elements, lead(II) and bismuth(III). In order to illustrate the large concentration range within which the technique can be used, lead(II) samples in the mM concentration range and bismuth(III) in the μM concentration range have been titrated. The use of potentiometric stripping analysis for the determination of conditional stability constants will also be illustrated.

THEORY

Complexiметric titration

If v_0 ml of a sample containing M^{n+} is titrated with v ml of t M EDTA (H_4Y) according to the reaction

$$M' + Y' \rightleftharpoons MY \tag{1}$$

where M' denotes $M' = \Sigma_{i=0}^{q} ML_i$, L denotes all ligands, except Y^{4-}, present in the sample, and Y' is $Y' = \Sigma_{n=0}^{4} H_nY$, then $[MY]/[M'][Y'] = K'_{MY}$, where K'_{MY} is the conditional constant [8].

If K'_{MY} is greater than approximately 10^4, then

$$[MY]_{eq} \approx [M]_{tot} \cdot v_0(v_0 + v_{eq})^{-1} \tag{2}$$

where $[MY]_{eq}$ denotes the concentration of MY at the equivalence point v_{eq}, and $[M]_{tot}$ is the total concentration of M^{n+} prior to the commencement of the titration. Consequently

$$[M']_{eq} = [M_{tot} \cdot v_0(v_0 + v_{eq})^{-1}(K'_{MY})^{-1}]^{1/2} \tag{3}$$

where $[M']_{eq}$ denotes the concentration of M' at the equivalence point.

Assuming that the reaction in Eqn. (1) dominates, then for $v < v_{eq}$

$$(v_0 + v)v_0^{-1}[M'] \propto v_{eq} - v \tag{4}$$

i.e., if $F_1 = (v_0 + v)v_0^{-1}[M']$ is plotted against v ml of titrant added, a straight line will be obtained for $v < v_{eq}$ which on extrapolation to zero will intersect the v-axis at $v = v_{eq}$.

If the titration is monitored by means of potentiometric stripping analysis, the stripping time for M(Hg), $t_{M,strip}$, at a given potential for potentiostatic deposition is proportional [8] to

$$t_{M,strip} \propto t_{dep} \times \sum_{i=0}^{q} k_i[ML_i] \tag{5}$$

where t_{dep} is the time of potentiostatic deposition and the constants k_i depend on the diffusion constants for ML_i and the kinetics in the reduction of ML_i to M(Hg). Thus at constant [L] and a given time for potentiostatic deposition, $t_{M,strip} \propto [M']$. Combination of this expression with relation (4) gives

$$F_2 \equiv (v_0 + v)v_0^{-1} t_{M,strip} \propto v_{eq} - v \quad (6)$$

The assumption made in the derivation of expression (4) that the reaction $M' + Y' \rightarrow MY$ is quantitative obviously does not hold in the whole volume range $v < v_{eq}$. The completeness of the reaction depends on $[M]_{tot} \times K'_{MY}$: the higher this value, the more complete the reaction. Furthermore, the reaction is not as quantitative close to the equivalence point as it is in the beginning of the titration. In order to test the accuracy of expression (4), and thus also of expression (6), theoretical titration curves with different values for $[M]_{tot} \times K'_{MY}$ were generated by means of the computer program HALTAFALL [9]. The relative accuracy in the calculations was 10^{-6}% in the total concentrations of $[M]_{tot}$ and $[Y]_{tot}$. From these calculations, it was concluded that the maximum systematic error in F_1 and F_2 was less than 0.05% for $[M]_{tot} \times K'_{MY}$ values greater than 10^5 if [M'] values in the concentration range $30[M']_{eq} > [M'] > 10[M']_{eq}$ were used to evaluate v_{eq}. For $[M]_{tot} \times K'_{MY}$ values greater than 10^6, concentration data above $3[M']_{eq}$ could be exploited without introduction of relative systematic errors exceeding 0.05%.

In a complexiметric titration an approximate value for $[M]_{tot}$ is normally known and an approximate value for K'_{MY} can either be obtained from the literature or estimated experimentally from a preliminary titration, e.g., by calculating

$$(t_{M,strip})^2_{[M']=[M]_{tot}} (t_{M,strip})^{-2}_{[M']=[M']_{eq}} [M]^{-1}_{tot} v_0(v_0 + v_{eq})^{-1} \approx K'_{MY} \quad (7)$$

Determination of relative conditional constants

If v_0 ml of a sample containing M_I (where M_I is a metal ion which can be measured by potentiometric stripping analysis) is titrated with v ml of t M EDTA until the equivalence point is reached and a known concentration of M_{II} is added to the sample, the equilibrium

$$M_IY + M'_{II} \rightleftharpoons M'_I + M_{II}Y \quad (8)$$

will be established. The addition of M_{II} will increase the potentiometric stripping signal for M_I as is indicated schematically in Fig. 1. The concentration of all species in Eqn. (8) can then be calculated (cf. Fig. 1) as

$$[M_IY] = v_1 t(v_0 + v)^{-1} \quad (9)$$

$$[M'_I] = [M_{II}Y] = t(v_{eq} - v_1)(v_0 + v)^{-1} \quad (10)$$

$$[M'_{II}] = [M_{II}]_{tot} - t(v_{eq} - v_1)(v_0 + v)^{-1} \quad (11)$$

provided that v_1 is on the linear part of the plot $t_{M_I,strip}$ vs. v ml of EDTA added (cf. Fig. 1). Since

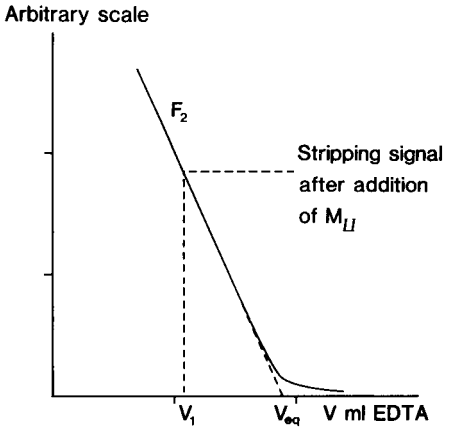

Fig. 1. Determination of relative conditional constants according to Eqns. (9—12).

$$[M_IY]\,[M'_{II}]\,/[M'_I]\,[M_{II}Y] = K'_{M_IY}/K'_{M_{II}Y} \qquad (12)$$

relative conditional constants can be determined by combining Eqns. (9—12) provided that $K'_{M_{II}Y} < K'_{M_IY}$. If this criterion is not fulfilled, $[M'_{II}]$ cannot be determined experimentally by Eqn. (11).

EXPERIMENTAL

Instrumentation and chemicals

The Potentiometric Stripping Analyzer (Radiometer ISS820) was supplemented with a laboratory-constructed microcomputer system [10]. The glassy carbon working electrode had a total surface area of 2 mm^2 and was rotated at 1200 rpm. The platinum counter electrode was separated from the sample by a 0.5 M KCl salt bridge in order to prevent the reaction Pb—EDTA → PbO_2(s) from occurring when large concentrations of Pb—EDTA were present in the sample. The EDTA solution was added with a motor syringe burette (Radiometer, ABU80) with a total syringe volume of 2.5 ml.

An approximately 0.1 M stock solution of Na_4—EDTA was prepared by adding sodium hydroxide to Titriplex III (Merck) in a calibrated volumetric flask. Approximately 0.0025 mol kg^{-1} bismuth(III) and 0.1 mol kg^{-1} lead(II) stock solutions were prepared by dissolving the nitrates in accurately weighed amounts of 0.2 M hydrochloric acid and distilled water, respectively. Hydrochloric acid, sodium chloride and sodium acetate were of Suprapur grade (Merck).

Mercury pre-plating of the glassy carbon electrode

The glassy carbon electrode was pre-plated with mercury by potentiostatic deposition at —0.60 V vs. SCE for two minutes prior to stripping in a solution which was 2 mM in Hg(II), and 0.1 M in hydrochloric acid. The working

electrode was rotated both during potentiostatic deposition and stripping. The potentiostatic deposition/stripping cycle was repeated at —0.70 and —0.80 V vs. SCE. The working electrode was removed from the pre-plating solution in order to prevent the reaction $Hg(s) + Hg(II) + 2\ Cl^- \rightarrow Hg_2Cl_2(s)$ from occurring, and rinsed in distilled water. Once mercury-coated, the electrode could be used for several days provided that it was stored in distilled water.

Titration procedure for lead(II)

An accurately weighed amount of lead(II) stock solution (0.5—5 g) was transferred to 45 ml of a solution which was 0.5 M sodium chloride and 0.25 mM in mercury(II) and buffered with 0.40 M sodium acetate and 0.1 M acetic acid (pH ≈5.0). Approximately 90% of the EDTA required for equivalence was added prior to recording of the potentiometric stripping signals. The potentiometric stripping signal was recorded after one minute of potentiostatic deposition at —0.65 V vs. SCE. The equivalence point was evaluated by means of straight line regression of the plot F_2 vs. v ml of titrant. In this evaluation, only experimental data having F_2 values ten times greater than the value of $F_{2,eq}$ were used.

Titration procedure for bismuth(III)

An accurately weighed amount of bismuth(III) stock solution (0.5—5 g) was transferred to 45 ml of a solution which was 0.5 M in sodium chloride and 0.25 mM in mercury(II) and buffered with hydrochloric acid to pH 2.3. The potentiometric stripping curve was recorded after potentiostatic deposition at —0.23 V vs. SCE for one minute. The equivalence point was evaluated by means of linear regression of F_2, using only data with F_2 more than ten times greater than $F_{2,eq}$.

RESULTS AND DISCUSSION

Choice of potentiostatic deposition potential

Potentiostatic deposition for one minute at potentials between 0.0 and 0.8 V vs. SCE was done in a sample which was 10 μM in Bi(III), 500 μM in Bi—EDTA and 0.5 M in sodium chloride at pH 2.3. Reduction of Bi(III) commenced at —0.12 V vs. SCE, and at potentials below —0.20 V vs. SCE a constant stripping signal for bismuth was obtained. Reduction of Bi—EDTA started at —0.58 V vs. SCE.

The experiment was repeated in the potential range —0.50 to —1.10 V vs. SCE in a sample which was 10 μM in lead(II), 500 μM in Pb—EDTA and 0.5 M in sodium chloride at pH 5.0. In this sample, reduction of Pb(II) commenced at —0.52 V vs. SCE, a constant lead stripping signal was obtained at potentials below —0.62 V vs. SCE, and reduction of Pb—EDTA started at potentials below —0.88 V vs. SCE. Consequently, it can be concluded that Bi(III) and Pb(II) can be determined in the presence of their EDTA com-

plexes within a wide potential range, the optimum potential for Bi(III) being chosen as −0.23 and that for Pb(II) as −0.65 V vs. SCE.

Based on results obtained by anodic stripping voltammetry, Florence [11] concluded that the Pb—EDTA complex dissociates at the mercury film/glassy carbon electrode at potentials below −0.70 V vs. SCE. These results were obtained after in situ plating of a very thin mercury film on the glassy carbon substrate. On such an electrode, only part of the surface may be covered by mercury and potentiometric stripping experiments showed that Pb—EDTA dissociates much more readily on glassy carbon than it does on mercury. The glassy carbon electrode was therefore pre-coated with mercury in a separate solution in the potentiometric stripping experiments. Furthermore, mercury(II) ions were added to the sample prior to titration so that the mercury film was continuously renewed during potentiostatic deposition. In order to avoid interference of mercury(II) with the main titration reaction, chloride ions were added to the sample prior to titration. Because of the high stability of the mercury(II) chloride complexes (log β_{HgCl_4} = 15.1 [12]), interference from mercury(II) was eliminated. Moreover, the chloride ions ensured that changes in ionic strength during the titration were negligible. Some titrations were, however, done without mercury(II) ions present. This did not affect the form of the titration curves for lead(II) or for bismuth(III). Mercury pre-plating was, however, necessary after five to ten titrations, whereas in samples containing mercury(II) ions the same mercury film could be used for a large number of titrations.

Titration of lead(II)

Figure 2 shows the titration of 0.2049 mmol of lead(II), dissolved in 45 ml of 0.5 M sodium chloride at pH 5.0, with v ml of 0.1000 M EDTA. From

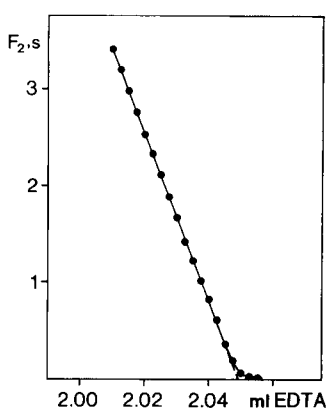

Fig. 2. Titration of 0.2049 mmol of lead(II) in 45 ml of 0.5 M sodium chloride at pH 5.0.

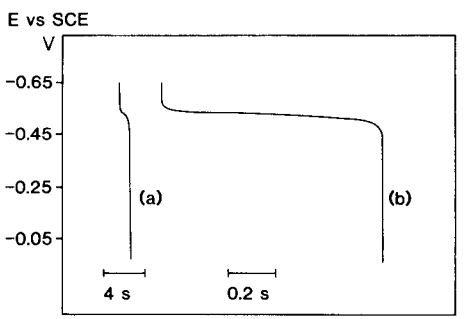

Fig. 3. Potentiometric stripping curve for lead(II) recorded after one minute of potentiostatic deposition at −0.65 V vs. SCE at v = 2.039 ml EDTA in Fig. 2. For explanation, see text.

the linear portion of F_2 in Fig. 2 a value for log K'_{PbY} equal to 9.7 can be estimated. This is in good agreement with the value 11.2 given by Ringbom [8] when the lead(II)—chloride complexes (log β_{PbCl} = 1.2 and log β_{PbCl_2} = 1.7 [12]) are taken into account.

Figure 3 shows the potentiometric stripping curve for lead obtained at v = 2.039 ml of 0.1000 M EDTA in Fig. 2. Curve (a) of Fig. 3 shows the primary potentiometric stripping curve and curve (b) shows the background-corrected curve displayed by the microcomputer at a rate approximately twenty times slower than the real time event.

Titration of forty 0.5—5-g portions of a sample containing 0.09989 mol kg^{-1} lead and diluted with 45 ml of titration medium yielded a mean value of 0.09981 mol kg^{-1} if it was assumed that the titre of the EDTA solution used as primary standard was correct. The coefficient of variation was 0.09%. Twenty titrations of 0.05—0.5-g portions of the same solution diluted with 45 ml of titration medium yielded an average value of 0.09988 mol kg^{-1} with a coefficient of variation of 0.21%. The difference in the results obtained in the two concentration ranges was mainly attributable to systematic errors inherent in the F_2 plot and to a minor extent to trace impurities of lead in the titration medium.

The reproducibility of the potentiometric stripping measurements was estimated by ten consecutive measurements of the potentiometric stripping curve shown in Fig. 3. The mean value for the stripping time when evaluated from the computer background-corrected curve (curve b in Fig. 3) was 0.992 s with a standard deviation of 0.006 s. This corresponds to a standard deviation of 0.07 mV for a lead(II)-selective electrode.

Titration of bismuth(III)

Figure 4 shows the titration of 1.223 μmol of bismuth(III) in 45 ml of 0.5 M sodium chloride at pH 2.3. From the titration curve, log K'_{BiY} can be estimated as 7.1, which is approximately one order of magnitude higher than the value given by Ringbom [8] if the stability constants of bismuth(III)—chloride complexes are assumed to be log β_1 = 2.4, log β_2 = 3.5 and log β_3 = 5.4 [12]. Twenty titrations of 0.5—5-g portions of a sample containing 0.002390 mol kg^{-1} bismuth(III) in 45 ml of titration medium yielded a mean value for this sample of 0.02401 mol kg^{-1} and a coefficient of variation equal to 0.38%. In these calculations, it was assumed that the titre of the EDTA titrant was correct, as well as that of the bismuth(III) nitrate stock solution.

Determination of relative stability constants

Aliquots of the 0.09989 mol kg^{-1} lead(II) stock solution were diluted with 45 ml of 0.5 M sodium chloride at pH 5.0 and titrated to the equivalence point (cf. Fig. 2). Known amounts of calcium(II), manganese(II) and lanthanum(III), respectively, were added to the sample until a constant potentiometric stripping signal of about 0.1 s (cf. Figs. 1 and 2) was obtained. The ratio between K'_{PbY} and the conditional constant for the particular element

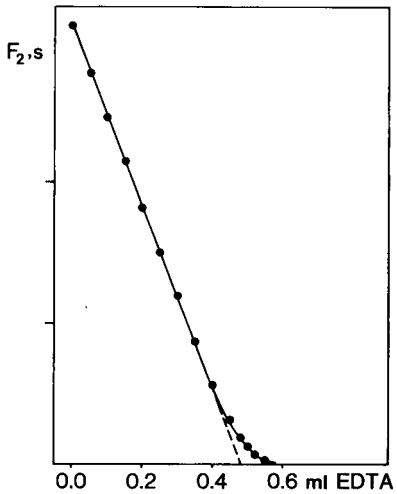

Fig. 4. Titration of 1.223 μmol of bismuth(III) in 45 ml of 0.5 M sodium chloride at pH 2.3.

under investigation was calculated by Eqns. (9—12) and the results are summarized in Table 1. The conditional constants in Table 1 were calculated by assuming that $\log K'_{PbY} = 9.7$ and that the chloride complexes for calcium(II), manganese(II) and lanthanum(III) can be neglected. The agreement between the results obtained by potentiometric stripping analysis and those known from the literature [8] is quite satisfactory.

CONCLUSIONS

It has been shown that the concentrations of aquo and chloro complexes of metal ions can be monitored by means of potentiometric stripping analysis in the presence of a 10^5-fold excess of the metal—EDTA complex, provided that the potentiostatic deposition potential is properly adjusted. Because of the high reproducibility which can be obtained with the rotated glassy carbon electrode, potentiometric stripping analysis seems to be better suited for monitoring high-precision complexiметric titration than, for example, ion-selective membrane electrodes. The accuracy of the titrations depends on the stability constant for the main titration reaction and is thus independent of the sensor used to monitor the titration. Although only a few elements, e.g., Cu(II), Cd(II), Zn(II), Hg(II), can be monitored directly by potentiometric stripping analysis, these ions can be used for the indirect monitoring of many other elements according to the well-known principles of complexiметric titration theory [8].

Since computerized potentiometric stripping analysis can measure metal ion concentrations down to 10^{-9} M, conditional stability constants within a wide logarithmic range can be measured. The conditional constants for those elements which cannot be measured directly by potentiometric stripping analysis have to be estimated indirectly according to the principles

TABLE 1

Conditional stability constants for the EDTA complexes of Ca(II), Mn(II) and La(III) in 0.5 M sodium chloride at pH 5 determined by potentiometric stripping analyses

Element	$\log K'_{MY}$ This work	$\log K'_{MY}$ Ringbom [8]
Ca(II)	3.5	3.2
Mn(II)	7.1	7.4
La(III)	8.1	8.7

described above. It is, however, necessary that the conditional constant for the EDTA complex of the metal ion monitored by potentiometric stripping analysis be at least one order of magnitude greater than the stability constant of the EDTA complex of the element under investigation. Of those elements which can be monitored by potentiometric stripping analysis, bismuth(III) forms the strongest EDTA complex. Consequently, stability constants for elements forming EDTA complexes more stable than Bi—EDTA, e.g. iron(III) and thorium(IV), cannot be measured.

The time required for the recording of one titration curve by means of potentiometric stripping analysis is approximately one hour. Most of this time is ascribed to the one minute of potentiostatic deposition needed for each titration point. As can be seen from Figs. 2 and 3, the potentiostatic deposition time could be decreased considerably without significant loss of precision, but one minute was the minimum potentiostatic deposition time possible with the instrumental set-up used in this investigation. It is also apparent from Figs. 2 and 3 that non-computerized instrumentation could be used for monitoring complexiметric titrations but potentiostatic deposition times of the order of magnitude of 4—16 min would then be necessary in the immediate vicinity of the equivalence point.

REFERENCES

1 D. Jagner and A. Granéli, Anal. Chim. Acta, 83 (1976) 19.
2 D. Jagner and K. Årén, Anal. Chim. Acta, 100 (1978) 375.
3 D. Jagner, Anal. Chem., 51 (1979) 342.
4 D. Jagner, L.-G. Danielsson and K. Årén, Anal. Chim. Acta, 106 (1979) 15.
5 D. Jagner and K. Årén, Anal. Chim. Acta, 107 (1979) 29.
6 G. J. Moody and J. D. R. Thomas, in H. Freiser (Ed.), Ion-Selective Electrodes in Analytical Chemistry, Plenum Press, New York, 1978.
7 D. Jagner, Proceedings of the Analytical Division of the Royal Society of Chemistry, in press.
8 A. Ringbom, Complexation in Analytical Chemistry, Interscience, New York, 1963.
9 N. Ingri, W. Kakotowicz, L. G. Sillén and B. Warnqvist, Talanta, 14 (1967) 1261.
10 A. Granéli, D. Jagner and M. Josefson, Anal. Chem., 52 (1980) 568.
11 T. M. Florence, Electroanal. Chem., 26 (1970) 293.
12 R. M. Smith and A. E. Martell, Critical Stability Constants, Plenum Press, New York, 1976.

Analytica Chimica Acta, 134 (1982) 211—218
Elsevier Scientific Publishing Company, Amsterdam — Printed in The Netherlands

AMPEROMETRIC DETECTION OF AMINES AND AMINO ACIDS IN FLOW INJECTION SYSTEMS WITH A NICKEL OXIDE ELECTRODE

BEN S. HUI and C. O. HUBER*

Department of Chemistry, University of Wisconsin-Milwaukee, Milwaukee, WI 53201 (U.S.A.)

(Received 16th March 1981)

SUMMARY

The use and characteristics of a nickel oxide electrode as a detector for amines in a flow injection system are described. The anodic electrode reaction mechanism involves a higher oxidation state of nickel maintained by the applied potential (+0.49 V vs. SCE). The electroanalytical parameters are investigated and the currents for a series of amines and amino acids are compared. Two electrode configurations are compared. The flow injection technique is shown to be suitable for buffered 25-μl samples of pH as low as 3. The linear range for glycine is 10^{-6}—10^{-3} M with detection limits of a few nanograms.

Fleischmann et. al. [1] reported that alcohols and amines are oxidised at a nickel anode in aqueous alkaline solution. They showed that the rate-determining step (r.d.s.) is oxidation of the substrate by an oxide species formed anodically on the surface of the nickel

$$\mathrm{Ni} \underset{-2e^-}{\overset{2OH^-}{\longrightarrow}} \mathrm{Ni(OH)_2} \underset{}{\overset{-e^-,\,OH^-}{\rightleftharpoons}} \mathrm{NiOOH} + \mathrm{H_2O} \qquad (1)$$

$$\mathrm{NiOOH} + \text{analyte (adsorbed)} \xrightarrow{\text{r.d.s.}} \mathrm{Ni(OH)_2} + \text{radical} \qquad (2)$$

$$\text{radical} \longrightarrow \text{products.} \qquad (3)$$

The electrode reaction has been applied to ethanol determinations with the flow injection technique [2]. The present report describes application of the nickel oxide electrode with the flow injection technique to the determination of amines. In addition, the reactions of amino acids at the nickel oxide electrode are characterized and parameters that influence electrode response are examined.

Previous applications of the nickel oxide electrode have used samples adjusted to the high pH at which the electrode is most active, whereas this report describes the application to samples buffered at lower pH.

Advantages of the flow injection technique have been reviewed [3]. In the application reported here, the additional advantages of maintenance and reproducible restoration of an active electrode surface are shown.

EXPERIMENTAL

Apparatus

The flow injection apparatus was constructed by using 0.5 mm i.d. PTFE tubing and standard high-performance liquid chromatographic type fittings. A 4-l plastic reservoir of background electrolyte positioned 1 m above the injection valve was used to maintain the desired constant flow of background electrolyte through the cell. Flow rate was regulated from 0.5 to 3.0 ml per minute by a stopcock located 30 cm below the reservoir. A Rheodyne Model 50 injection valve with a 25-μl sample loop was used.

The detector cell was a three-electrode system consisting of a nickel oxide working electrode, platinum counter electrode, and a mercury/mercury(II) oxide reference electrode. Two types of working electrode were examined. The first type, a tubular electrode, was prepared by drilling a 0.8 mm hole through 1.3 mm thick nickel sheet. The nominal surface area was 0.03 cm^2. The nickel sheet was embedded in a cast epoxy block (2 × 3 × 2 cm) which was machined to accept the necessary fittings. The other type of working electrode consisted of a randomly coiled nickel wire (12 cm long, 0.1 mm diameter). The coiled wire was positioned in a 2 mm i.d. tube. The nominal working electrode area was 0.5 cm^2. The counter electrode was a 1 × 10 mm platinum wire positioned in the exit tube of the detector. The reference electrode consisted of a pool of mercury covered with a paste made by grinding mercury and red mercury(II) oxide moistened with 0.1 M NaOH together in a mortar. The filling solution was 0.1 M NaOH. Unless otherwise stated, all applied voltages are referred to the mercury/mercury(II) oxide electrode with an observed potential of −0.06 V vs. the saturated calomel electrode.

A potentiostat capable of measuring nanoampere currents was constructed. The potentiostat consisted of voltage controller, current-to-voltage converter, and inverter amplifier for off-set adjustment. The three operational amplifiers were an RCA 3140, and an RCA 3240 dual unit, respectively. The potentiostat was housed in a small aluminum box, and was powered by a 15 V d.c. power supply. A potentiometric recorder was used for read-out.

Reagents and samples

All reagent solutions were prepared with distilled water. Unless otherwise specified, all materials were reagent grade. Background electrolyte was 0.1 M NaOH to which nickel sulfate (1×10^{-4} M) had been added. In this solution, the nickel is virtually all insoluble nickel hydroxide.

Procedure

After the flow rate has been set, the baseline level is adjusted via the circuit offset control. The 25-μl sample loop is filled, the sample is introduced into the flow stream, and the resulting signal is recorded. Peak height is used as the analytical signal.

RESULTS AND DISCUSSION

To investigate the nature of the electrode reaction for amino acids, chronoamperometric data were obtained. The current after stepping the potential from 0.26 to 0.46 V was observed. The results are shown in Fig. 1. These results indicate a steady-state current when oxidation of amino acid is occurring. This suggests that the mechanism proposed by Fleischmann [1] for alcohols and amines is also applicable for amino acids.

To examine the effects of the applied potential at the working electrode, the potential was changed in 20 mV increments between 0.44 V and 0.64 V. Both background and analyte currents were determined. The background current increased with increasing applied potential (Fig. 2). The increases in background current with applied potential may be due to the increased rate of oxidation of water. The optimum potential, defined as that which produces the largest analyte signal, is about 0.55 V for both amines and amino acids. Apparently, at potentials more anodic than 0.55 V, solvent oxidation increasingly competes with analyte oxidation.

The effects of hydroxide concentration at an applied potential of 0.55 V are shown in Fig. 3. At the lowest concentration, the formation of the higher oxide on the surface is limited whereas at concentrations greater than 0.1 M, solvent oxidation probably becomes competitive with that of the analyte. Analyte signals were observed to increase with ionic strength (Fig. 4). The increase in signal shows a consistent trend, but is not large.

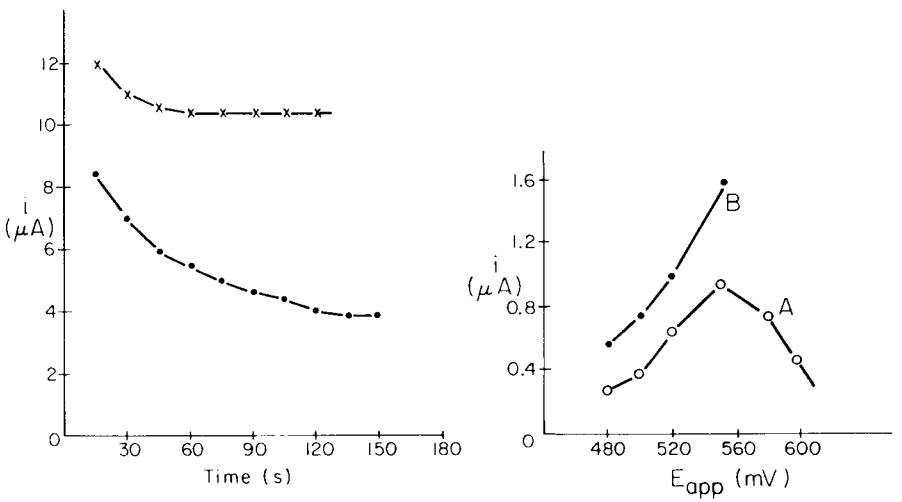

Fig. 1. Chronoamperometry after stepping the potential from 0.20 to 0.40 V. (×) 1 mM glycine; (•) background electrolyte only.

Fig. 2. Signal dependence upon applied potential (vs. Hg/HgO): (A) peak height; (B) background baseline current.

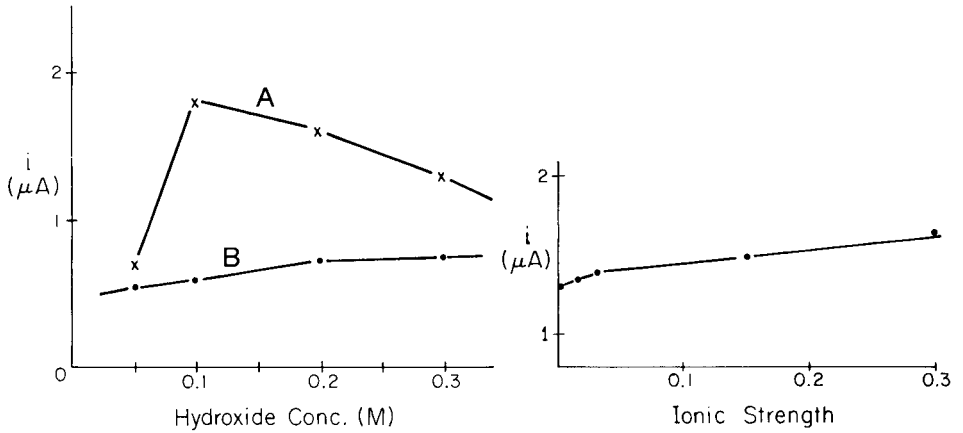

Fig. 3. Current dependence on hydroxide concentration at an applied potential of 0.55 V vs. Hg/HgO: (A) peak current; (B) background current.

Fig. 4. Effect of ionic strength on serine (1×10^{-4} M) using sodium nitrate.

Effects of flow rate were examined. Peak currents for 0.1 mM serine increase with flow rate up to 1.5 ml min^{-1} with no further increases for flow rates up to 3 ml min^{-1}. At flow rates up to 1.5 ml min^{-1}, dependence on flow rate can be attributed to increasing convective mass transport at the electrode. Limitation of the analyte signal with increasing flow rates can be attributed to the rate-limiting step for electron transfer at the electrode, which is independent of mass transport (see reaction 2).

Analyte currents for a series of simple amines and common amino acids were determined. All were prepared in background electrolyte and determined at the conditions indicated above. Typical signals for 25 μl of 1.0×10^{-3} M samples are summarized in Table 1.

The factors affecting oxidation rates are steric effects on adsorption and stoichiometry, i.e., number of oxidizable sites such as amino and hydroxyl groups. The stereochemical control of the oxidation rates can be observed. Propylamine yields a larger signal than butylamine and primary amines yield much larger currents than secondary and tertiary amines. For the amino acids, increases in molecular weight correspond to decreases in peak current. As examples, serine vs. tyrosine, serine vs. lysine, alanine vs. phenylalanine, and alanine vs. valine can be noted. Stoichiometry effects are shown by comparing serine with alanine and tyrosine with phenylalanine. Both serine and lysine contain 3 hydrogens with 2 active groups, yet the more bulky lysine yields a current only 6% of that for serine. This indicates that the effect of steric hinderance exceeds that of stoichiometry.

Relating the amine and amino acid structures and oxidation currents, it may be suggested that the rate of oxidation increases with the number of α-hydrogens and the number of active sites, and with decreasing size of

TABLE 1

Peak currents for 1 mM amines and amino acids

Compound	Formula	Peak current (μA)	Compound	Formula	Peak current (μA)
Propylamine		3.1	Tryptophan	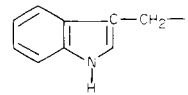	0.64
Butylamine		2.9			
Diisopropylamine		0.03			
Triethylamine		0.04	Valine		0.58
Glycine	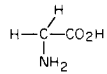	12.0	Histidine	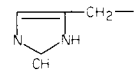	0.55
Serine		7.2			
Tyrosine	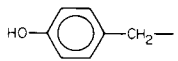	6.6	Threonine		0.47
Asparagine		4.9	Lysine	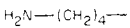	0.44
Cysteine	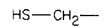	4.2	Methionine	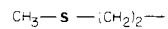	0.30
			Isoleucine		0.17
Alanine		1.9			
Arginine	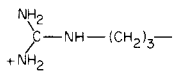	1.3	Proline	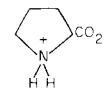	0.14
Glutamic Acid		1.2			
Phenylalanine	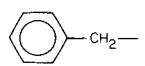	0.85			
Leucine	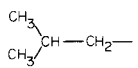	0.77			

the substrate molecule. These observations are consistent with the reaction mechanism described.

In chromatography, as well as in other applications, samples are often in a buffered medium at pH values considerably lower than that of the carrier electrolyte used here. Thus, it was necessary to study pH effects on the detection signal from the nickel oxide electrode. Glycine at pH 5.1 in 0.1 M acetate buffer and at pH 3.5 in 0.1 M formate buffer was used with the nickel tubular electrode. A negative peak precedes the positive peak used to quantify each component (Figs. 5 and 6). The negative peak height depends on pH and on buffer concentration. Simply injecting buffered blank samples also produces negative and positive peaks and the peak heights increase with buffer concentration as shown in Table 2.

The time profiles at the working electrode shown in Fig. 5 can be used to propose a mechanism for the signals obtained. When the sample reaches the detector, a maximum in sample concentration and a minimum in hydroxide concentration occur simultaneously. The decrease in pH and buffering capacity result in reduction of the higher, active nickel oxide, i.e., decrease in the surface coverage, θ, of the Ni(III) oxide. The reduction of NiOOH is experimentally evidenced by the sharp negative peak obtained when a low pH buffer solution segment is injected (see Fig. 6). Pourbaix [4] shows that the oxidizing nickel(III) species when held at +0.55 V vs. Hg/HgO will be reduced to a nonoxidizing form at pH values lower than 9. As the hydroxide concentration begins to increase during the tail of the passing sample zone, the active higher

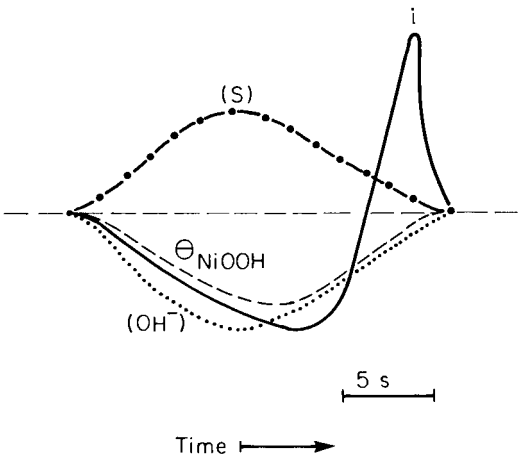

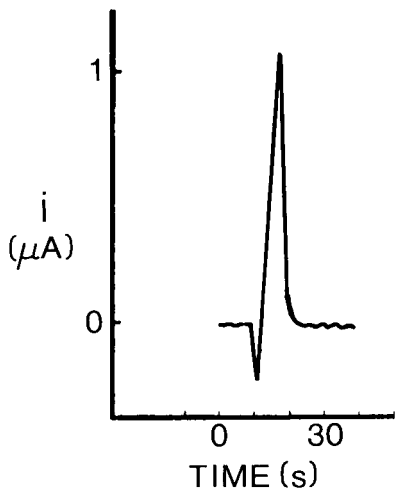

Fig. 5. Profiles passing electrode: (i) analyte current; (S) sample concentration; (θ) surface coverage by higher oxide; (OH^-) hydroxide concentration.

Fig. 6. Analytical signal for low pH sample.

TABLE 2

Peak height dependence on solution composition

Glycine (M)	Buffer (M)	Negative peak (μA)	Positive peak (μA)
1×10^{-4}	0.1	0.21	1.45
0.0	0.01	0.14	0.57
0.0	0.05	0.18	0.70
0.0	0.10	0.24	0.90

oxide surface is renewed. The amino acid sample is oxidized by the newly formed disordered nickel oxide surface containing relatively many active sites. In support of this mechanism, current—voltage curves for $Ni(OH)_2$ surface electrodes were experimentally observed here to show anodic NiOOH formation beginning at +0.4 V, in agreement with earlier reports [1, 5]. The high rate of this process conforms to Fleischmann's report [1] showing that the layer of NiOOH initially formed is only a few monolayers in thickness and follows Langmuir (i.e., equilibrium) adsorption behavior [1].

Analyte signals were observed to be enhanced as much as two-fold over those obtained for pH-matched samples. This apparent greater activity of the freshly deposited NiOOH corresponds to reports of anodization of $Ni(OH)_2$ electrodes in aqueous hydroxide solutions to yield formation of active forms of nickel(III) with subsequent "aging" properties [6]. Precision was examined for five replicate determinations at each sample pH value for pH 11, 7.5, 5.1 and 3.5. The estimated relative standard deviations were between 1 and 2% for all of the sample pH values. Such consistent precision suggests a reproducible higher oxide layer formed after its temporary removal by the lower pH of the mid-portion of the sample zone. It should be noted that these results point up the special advantage of the flow injection technique in reproducing surface exposure conditions when active electrode materials are used in voltammetry.

Analyte signal characteristics for pH-matched samples are summarized in Table 3. Plots of the means for triplicate determinations of currents were used. Reduced sensitivity at higher concentrations is presumably due to saturation of available sites on the electrode surface. For glycine samples in pH 7.4 and pH 3.5 buffers, the positive signals were generally slightly greater than for pH-matched samples while the linearity was similar over the concentration range 10^{-5}—10^{-3} M.

The effects on the signal of the coiled wire electrode can be attributed to (a) increased turbulance of the sample solution at the electrode surface, (b) increased area of the electrode, and (c) increased dispersion of the sample plug. The third effect decreases the signal whereas the first two enhance it. Thus, although the nominal area of the coiled wire electrode is fifteen times that of the tubular electrode, the net enhancement of sensitivity observed is

TABLE 3

Linearity data for selected compounds

Compound	Electrode	Linear range (M)	n	Slope (μA mM^{-1})	Intercept (μA)	Standard error of the estimate (μA)	Dete limit (μg)
Propylamine	Tubular	10^{-5}—10^{-2}	10	2.2	0.05	0.01	0.02
Butylamine	Tubular	10^{-5}—10^{-2}	8	2.2	0.05	0.09	0.2
Diisopropyl-amine	Tubular	10^{-3}—10^{-1}	9	2.2	0.03	0.09	0.2
Triethylamine	Tubular	10^{2}^{3}—10^{-1}	7	2.2	0.04	0.09	0.2
Glycine	Tubular	5×10^{-6}—10^{-3}	9	12.0	0.0	0.6	0.3
Glycine	Coiled	$5 \doteq 10^{-7}$—10^{-4}	10	72	0.3	0.2	0.16

typically only six-fold. Limits of detection are given as absolute masses by using the sample volume injected, 25 μl. The limit of detection (in μg) is computed as (0.025) (3) s' (m.w.)/m, where s' is the standard error of the estimate, and m is the slope for the regression line.

While the coiled wire electrode had a lower limit of detection, its effective volume was about 25 μl, whereas the effective volume of the tubular electrode was less than 1 μl.

Other amines or amino acids would yield somewhat higher limits of detection and lower sensitivity as indicated in Table 1.

REFERENCES

1 M. Fleischmann, K. Korinek and D. Pletcher, J. Chem. Soc. Perkin Trans. 2, (1972) 1396.
2 T. N. Morrison, K. G. Schick and C. O. Huber, Anal. Chim. Acta, 120 (1980) 75.
3 J. Růžička and E. H. Hansen, Flow Injection Analysis, Wiley, New York, 1981.
4 M. Pourbaix, Atlas of Electrochemical Equilibria, Pergamon, Brussels, 1966, pp. 330—341.
5 G. W. D. Briggs, E. Jones, and W. F. K. Wynne-Jones, Trans. Faraday Soc., 51 (1966) 1433.
6 R. S. Schrebler Guzman, J. R. Vilche and A. J. Arvia, J. Electrochem. Soc., 125 (1978) 1578.

Analytica Chimica Acta, 134 (1982) 219—226
Elsevier Scientific Publishing Company, Amsterdam — Printed in The Netherlands

FAST-SCAN DIFFERENTIAL PULSE POLAROGRAPHY AT A DROPPING MERCURY ELECTRODE

V. GAJDA* and K. HORÁK

Laboratorní přístroje, 162 03-Prague-6 (Czechoslovakia)

(Received 14th July 1981)

SUMMARY

A fast-scan modification of differential pulse polarography (d.p.p.) is described, in which a dropping mercury electrode with a drop lifetime of 50 s is polarized by 100-ms pulses with a 100-ms interval between pulses; sampling and treatment of the current data are the same as in d.p.p. The method can be used to determine amalgam-forming metals at concentrations above 1×10^{-8} mol l^{-1} with good reproducibility. The technique permits a ten-fold decrease in the measuring time compared to conventional d.p.p. The method can be used for direct polarographic determinations and also advantageously replaces d.p.p. in anodic stripping.

Pulse polarographic methods exhibit high sensitivity and good reproducibility because of the practically complete elimination of the charging current. Among these techniques, differential pulse polarography (d.p.p.) has become the most widely applied. The main disadvantage of d.p.p. is the long time required for each measurement, because slow potential scan rates are required. Each potential pulse is imposed only once during the drop lifetime, which leads to an optimum scan rate of about 1 mV s^{-1}. The use of short, controlled drop times permits an increase in the scan rate, but sloping baselines are obtained [1, 2] and the sensitivity is decreased, as follows from the theoretical study by Christie and Osteryoung [3]. Attention has therefore been given to the application of stationary electrodes in d.p.p. [4—6]. The results obtained with these electrodes have shown that the shortening of the delay between individual pulses does not influence the sensitivity and accuracy of the data obtained [4, 5, 7, 8]. These findings have been verified by the results obtained with the fully computerized polarographic system described by Bond and Grabaric [8].

For fast-scan d.p.p. as described in this paper, the mercury electrode with an extended drop lifetime described by Novotný [9] was used. This type of electrode, applied in synchronization with the differential pulse mode, provides results which are extremely reproducible and sensitive, and there is a considerable decrease in the time required for the measurement.

EXPERIMENTAL

The polarograph used was developed by Laboratorní přístroje, Prague. It makes the following types of measurements: d.c., sampled d.c., d.p.p. and fast-scan d.p.p. on a slowly growing or static mercury drop electrode. The construction of the intrument includes a combination of analog circuits (polarization current generator, sample-and-hold circuits, current amplifier) and fixed hardware with TTL logic which comprises the polarization pulse generator, generator of pulses controlling the sample-and-hold circuits, automatic measurement cycle for the d.c., sampled d.c. and d.p.p. methods, the increase of the polarization voltage being synchronized with the falling of the mercury drop. The polarization voltage generator is connected as a servo device which allows adjustment of the initial voltage within a range of 2 V, to which is added a linearly varying voltage range of up to 3 V. The scan rate can be adjusted in the range 0.5—500 mV s^{-1}. The potentiostat operates with an input impedence of 10^{12} ohm. The current samples are recorded and differentiated by the sample-and-hold circuit block. This block contains two systems, one with a time constant of 100 ms, the other of 10 ms. The polarization pulse generator, trigger block and drop hammer are synchronized by the mains frequency.

Because the polarization voltage in fast-scan d.p.p. cannot be triggered manually, it must be synchronized with the increase in the size of the electrode drop. The time program generator controls the measuring cycle which is composed of the following steps: after turning the instrument on at any point during the growth of the mercury drop, the drop is detached after 16 s, during which time the applied voltage changes in the required direction at a preset rate. After 20 s, the polarization voltage changes stepwise to the previously chosen value of the initial potential E_i; after 56 s, the drop is detached. After 59 s, the polarization voltage begins to change from the initial value E_i in the preset direction at the predetermined rate. This lasts for 36 s and the polarographic curve is recorded during this time. The sequence of these steps is shown graphically in Fig. 1. The base electrolyte response is automatically subtracted from the sample curve by the recording polarographic terminal RPT-1 digital apparatus (Laboratorní přístroje, Prague).

A spindle-shaped capillary, prepared as described by Novotný [9] was used for the slowly growing dropping mercury electrode. This electrode gives increased stability and drop reproducibility combined with the possibility of changing the flow rate and drop time over a wide range. The drop lifetime for the capillary used was 63 s. A saturated calomel reference and platinum auxiliary electrode were also used.

Water was distilled twice from a quartz apparatus. Oxygen dissolved in the measured solutions was removed with purified nitrogen.

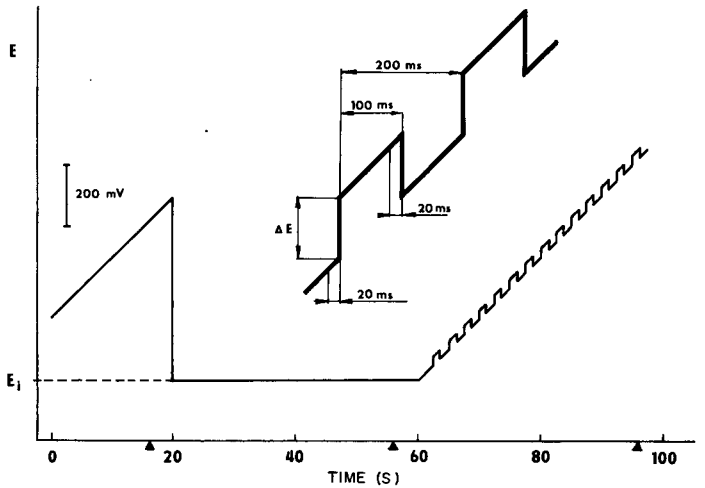

Fig. 1. Synchronization of recording of the fast-scan d.p.p. response with drop growth. At time zero, the trigger circuit is activated; the arrows indicate the instant of drop detachment.

RESULTS

Choice of wave-form

Because measurement with a slowly growing mercury drop electrode allows the use of relatively long pulses, a pulse width of 100 ms was chosen. This is sufficient for the charging current resulting from pulse application, $i_{c,p}$, to decrease to less than 1 pA, as follows from the relationship [10] $i_{c,p} = (\Delta E/R)\exp(-\tau/RC)$, where ΔE is the pulse amplitude, R is the solution resistance and τ is the pulse length. According to this equation, at ΔE = 25 mV, $C = 4\ \mu$F and $\tau = 100$ ms, $i_{c,p} \ll 1$ pA, which is negligible for measurements under normal conditions. On the basis of the results obtained with a computerized polarograph, Bond and Grabaric [8] demonstrated that, even under conditions where the pulse time is comparable with the gap between pulses, analytically useful results can be obtained. Consequently, the time between pulses was also set at 100 ms. In this pulse arrangement and with a voltage sweep of 20 mV s^{-1}, one pulse plus the intervening time corresponds to a change in the polarization voltage of 4 mV. As the sampling is done in the same manner as in d.p.p., one measurement of current is obtained for every 4 mV change in the polarization voltage. The resultant data-point density is thus the same as in d.p.p. for a drop time of 2 s and polarization rate of 2 mV s^{-1}.

In measurements at a single mercury drop, the instant in the drop lifetime when the measurement commences is important. Synchronization of the measurement with the growth of the drop is possible by using the timing

program described above. In this program, the pre-sweep delay is set at 4 s. Under these conditions, the electrode can be polarized for 36 s, i.e. over a range of 720 mV.

Figure 2 depicts the polarograms obtained by fast-scan d.p.p. measurements on a 6×10^{-7} mol l^{-1} Cd^{2+} solution in 0.1 M KCl. These curves do not differ from those obtained by d.p.p. except that in the reverse-sweep mode the fast-scan d.p.p. peak is higher because of the stripping effect. The high sensitivity of fast-scan d.p.p. is indicated by the fact that at a depolarizer concentration of 10^{-7} mol l^{-1}, background current correction is not necessary.

Fast-scan d.p.p. at a dropping mercury electrode

The following equation was derived [5] for a d.p.p. response at a stationary electrode:

$$i_{max} = n F A c D (1 - \sigma)/(1 + \sigma)\pi\tau \quad (1)$$

where A is the electrode area, c is the depolarizer concentration, σ is defined by the relationship $\sigma = \exp[(nF/2RT)\Delta E]$, and the other symbols correspond to the usual electrochemical quantities. In this work the electrode area changes with time according to

$$A = 0.00853 m^{2/3} [\tau_0 + (E_p - E_i)/v]^{2/3} \quad (2)$$

where m is the mercury flow rate, τ_0 is the pre-sweep delay and v is the polarization rate. Equation (1) was derived assuming that the pulse duration is much shorter than the interval between pulses [5]. Nevertheless, the validity of Eqn. (1) was tested for measurements with the described fast-scan technique. The results indicated that the dependence of Δi_{max} on the de-

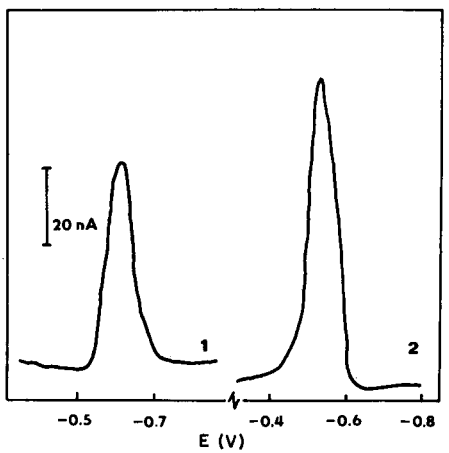

Fig. 2. Fast scan d.p.p. response for 6×10^{-7} mol l^{-1} Cd^{2+} in 0.1 M KCl. $\Delta E = 50$ mV; $\tau_0 = 4$ s. (1) Forward sweep; (2) reverse sweep (anodic stripping).

polarizer concentration is linear in the range 3×10^{-8}—1 mol l^{-1}, as required by Eqn. (1). The dependence of Δi_{max} on the $(1 - \sigma)/(1 + \sigma)$ value is depicted in Fig. 3. This dependence is linear up to ΔE values of about 30 mV; virtually the same dependence was obtained for d.p.p. measurements [11]. The peak potential E_p is also changed by a change in ΔE, given by $E_p = E_{1/2} - \Delta E/2$, where $E_{1/2}$ is the polarographic half-wave potential of the particular depolarizer. The results obtained by fast-scan d.p.p. do not correspond exactly to this equation; the corresponding data are given in Table 1. The differences can be attributed to instrumental artefacts, as in d.p.p. measurements [11].

The dependence of Δi_{max} on the electrode surface area can be found by changing the pre-sweep delay or the mercury flow-rate. As the τ_0 value cannot be changed in the construction described, the Δi_{max} vs. A dependence was verified both by changing the initial potential E_i (see Eqn. 2) and also by changing the mercury flow rate. A linear dependence of Δi_{max} on the electrode surface area was obtained in both cases.

It follows from the results obtained that Eqn. (1) is valid for the fast-scan d.p.p. method described with deviations which, similar to conventional d.p.p., result from instrumental artefacts.

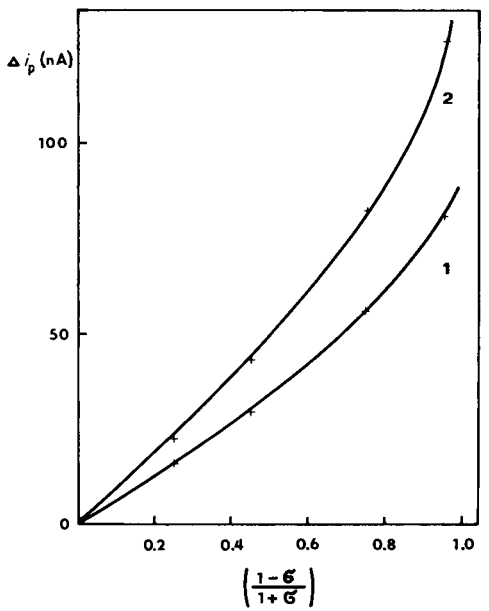

Fig. 3. Dependence of peak current Δi_p on $(1 - \sigma)/(1 + \sigma)$ for 6×10^{-7} mol l^{-1} Cd^{2+} in 0.1 M KCl. (1) Forward sweep; (2) reverse sweep.

TABLE 1

The dependence of E_p on the pulse amplitude ΔE in fast-scan d.p.p. for 6×10^{-7} mol l^{-1} Cd^{2+} in 0.1 M KCl

ΔE (mV)	E_p(V) calc.[a]	E_p(V) found
12.5	0.629	0.63
25	0.616	0.62
50	0.571	0.61
100	0.541	0.59

[a]Calculated from $E_p = E_{1/2} - \Delta E/2$.

Synchronization of the fast-scan d.p.p. measurement with the growth of the dropping mercury electrode

Synchronization of the d.p.p. measurement with the growth of the mercury drop as described above leads to an overall measurement time of 100 s. The drop is detached mechanically at any given moment during its growth, depending on the instant in the drop lifetime at which the measuring cycle is activated. If the drop is detached at the beginning of its growth, the size of the subsequent drop is not very reproducible and the measurements must then be done during the growth of the following drop, as depicted in Fig. 1. Very reproducible results were obtained under these conditions.

Another synchronization method depends on regular drop detachment every 40 s; the measurement is initiated by a controlling pulse from the drop hammer with an adjustable (5, 10 and 15-s) pre-sweep delay. Both methods yield the same results; an advantage of the latter is the possibility of changing the pre-sweep delay.

Sensitivity and reproducibility of fast-scan d.p.p. determinations

The precision of current measurement at low depolarizer concentrations will be affected by the magnitude of the background current. The background current does not affect the precision of measuring i_{max} at a depolarizer concentration of 10^{-7} mol l^{-1}. At lower concentrations (10^{-8} mol l^{-1}), the magnitude of the background current must be considered (see Fig. 4). The interference of the background current under these conditions can partly be eliminated by increasing the interval between pulses [7] or by increasing the pre-sweep delay. In both cases, however, the interval in which the electrode can be polarized is decreased. Thus it is preferable to employ an apparatus for automatic subtraction of the base electrolyte response from the sample response.

The reproducibility of measurement was tested by a ten-fold repetition of the determination of cadmium(II) and thallium(I) ions in 0.1 M KCl and KNO_3, respectively, without background current correction. The results indicated that the peak height standard deviation was 0.2% at a metal ion concentration of 5×10^{-5} mol l^{-1}, 0.8% at 6×10^{-7} mol l^{-1} and 1.5% at

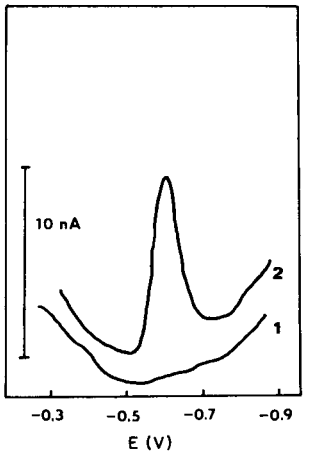

Fig. 4. Fast-scan d.p.p. responses for 5×10^{-8} mol l^{-1} Cd^{2+} in 0.1 M KCl. $\Delta E = 50$ mV, $\tau_0 = 4$ s. (1) Electrolyte; (2) electrolyte + 5×10^{-8} mol l^{-1} Cd^{2+}.

5×10^{-8} mol l^{-1}. This reproducibility is better than that obtained by Bond and Grabaric [8] with a computerized polarograph in measurements with a dropping electrode with a lifetime of 10 s and a polarization rate of 50 mV $s.^{-1}$.

The reproducibility also depends on the characteristics of the electrode used. Under the conditions described, the surface area of the electrode changes with time (Eqn. 2). However, if a static electrode, in which the mercury flow is stopped mechanically, is used, the electrode has a constant surface area but the measuring reproducibility is not as great as for a dropping electrode; this was shown by comparing the results obtained by fast-scan d.p.p. on a home-made static electrode (the mercury flow was opened and closed with a needle valve [9]) and on the dropping electrode described.

In the determination of small concentrations of a depolarizer which forms an amalgam, it is preferable to polarize the electrode toward positive potentials, the anodic stripping approach, in fast-scan d.p.p. The pre-sweep delay should be lengthened to 10 s, yielding satisfactory results for $\geqslant 10^{-8}$ mol l^{-1} concentrations.

Conclusions

The results described indicate that fast-scan d.p.p. at a slowly dropping mercury electrode yields very reproducible results. Higher sensitivity is obtained than with conventional d.p.p. and the measurement is ten times as fast. This technique has been used successfully for the determination of copper, cadmium and zinc in industrial waste-waters [12] and for the determination of cyanide based on measurement of a catalytic current [13]. Fast-scan d.p.p. can also be used in electrochemical stripping analysis [14]. Differential-pulse anodic stripping has a very low detection limit (10 ng l^{-1}) but the time

required for recording the stripping curve is long, frequently more than the initial electrolysis period. Application of fast-scan d.p.p. to stripping determinations considerably shortens the total time required. The instrumentation and electrode used are not expensive and the measurement can be automated with simple analog elements.

REFERENCES

1 A. M. Bond and R. J. O'Halloran, J. Electroanal. Chem., 68 (1976) 257.
2 A. M. Bond, J. Electroanal. Chem. Soc., 118 (1971) 1588.
3 J. H. Christie and R. A. Osteryoung, J. Electroanal. Chem., 49 (1974) 301.
4 K. F. Drake, R. P. van Duyne and A. M. Bond, J. Electroanal. Chem., 89 (1978) 231.
5 H. E. Keller and R. A. Osteryoung, Anal. Chem., 43 (1971) 342.
6 C. K. Burrows, M. P. Brindle and M. C. Hughes, Anal. Chem., 49 (1977) 1459.
7 H. Blutstein and A. M. Bono, Anal. Chem., 48 (1976) 248.
A. M. Bond and B. S. Grabaric, Anal. Chem., 51 (1971) 126.
9 L. Novotný, Proceedings II, J. Heyrovský Memorial Congress on Polarography, Prague, 1980, p. 129.
10 R. Kalvoda, J. Macků and K. Micka, Z. Phys. Chem., Sonderheft (1958) 66.
11 J. H. Christie, J. Osteryoung and R. A. Osteryoung, Anal. Chem., 45 (1973) 210.
12 J. Vorlicek and M. Kopanica, Rudy, in press.
13 V. Stará and M. Kopanica, Collect. Szech. Chem. Commun., in press.
14 M. Kopanica and V. Stará, J. Electroanal. Chem., 127 (1981) 255.

Analytica Chimica Acta, 134 (1982) 227—238
Elsevier Scientific Publishing Company, Amsterdam — Printed in The Netherlands

A POLAROGRAPHIC STUDY OF THE HYDROLYSIS OF 1,4-BENZODIAZEPINES AND ITS ANALYTICAL APPLICATIONS

W. FRANKLIN SMYTH*
Chemistry Department, University College, Cork (Eire)
J. A. GROVES
Health and Safety Executive, Brunell House, Cardiff (Gt. Britain)
(Received 6th May 1981)

SUMMARY

The mechanism of hydrolysis of flurazepam (Dalmane) and six of its metabolites was investigated in mildly acidic solution (pH 0—2) by differential pulse polarography. Simultaneous determinations of the "parent" compound(s) and hydrolytic degradation product(s) are possible because of the different reduction potentials. The kinetic results can be explained if the hydrolytic reaction is considered reversible; this is important for evaluation of the hydrolysis and absorption of 5-(*o*-fluorophenyl)-1,4-benzodiazepines in the stomach. The rate constants and the pK_a values corresponding to protonation of the azomethine groups are shown to be correlated. Appropriate kinetic data for other 1,4-benzodiazepines make it possible to evaluate the effects of certain substituents on the rate of hydrolysis and on the peak potentials of the "parent" compounds and their hydrolytic degradation products. The results of the kinetic investigations can be used for the identification of an isolated 5-(*o*-fluorophenyl)-1,4-benzodiazepine or identification of any 1,4-benzodiazepine studied here which exhibits some degree of acid hydrolysis within 24 h.

Most of the 1,4-benzodiazepines are unstable in acidic solution and undergo hydrolysis to some extent, in common with many Schiff bases of simpler molecular structure [1–4]. Many benzodiazepines are hydrolysed at room temperature but some require elevated temperatures and concentrated acidic solutions to initiate the reaction. Some information on the mechanism of hydrolysis of chlordiazepoxide and diazepam has been reported but this has mostly been concerned with the degradation products of formulations containing these active ingredients at elevated temperatures [5—7]. There has been no systematic study of the hydrolysis of 1,4-benzodiazepines, either generally or within a structural class such as for flurazepam (I) and its metabolites (II—VII). Hydrolysis reactions have been mentioned in a report on the determination of 1,4-benzodiazepines in blood and urine [8], and the rapid hydrolysis of bromazepam and flunitrazepam has been used in a scheme for the identification of 1,4-benzodiazepines based on exploitation of their acid—base properties [9]. The present polarographic study of the hydrolysis of 5-(*o*-fluorophenyl)-1,4-benzodiazepines and other 1,4-benzodiazepines

was carried out to clarify the mechanism of hydrolysis in dilute acidic solution with particular reference to the kinetics of the reaction, and to evaluate the resulting analytical applications.

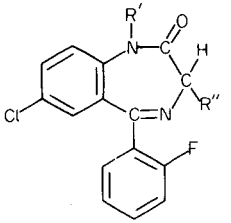

(I) Flurazepam; $R' = -CH_2 \cdot CH_2 \cdot N(C_2H_5)_2$, $R'' = -H$
(II) Monodesethylflurazepam, $R' = -CH_2 \cdot CH_2 \cdot NH(C_2H_5)$, $R'' = -H$
(III) Didesethylflurazepam; $R' = -CH_2 \cdot CH_2 \cdot NH_2$, $R'' = -H$
(IV) Hydroxyethylflurazepam, $R' = -CH_2 \cdot CH_2OH$, $R'' = -H$
(V) Acetic acid metabolite of flurazepam; $R' = -CH_2COOH$, $R'' = -H$
(VI) Desalkylflurazepam; $R' = -H$, $R'' = -H$
(VII) Desalkyl-3-hydroxyflurazepam; $R' = -H$, $R'' = -OH$

EXPERIMENTAL

Apparatus and reagents

A thermostatted cell of 25-ml capacity and a three-electrode system involving a dropping mercury electrode (d.m.e.), Radiometer K401 calomel reference (s.c.e.) and platinum wire counter electrode were employed for the polarographic measurements which were done with a PAR-174 Analyzer and a Bryans X-t recorder.

Flurazepam, six of its metabolites (II—VII) and other 1,4-benzodiazepines (Ro 5-4781, Ro 5-6728, potassium chlorazepate, medazepam, diazepam, Ro 5-2180, nitrazepam, Ro 5-4435, clonazepam and flunitrazepam) were received from Roche, Nutley, NJ. Stock solutions of each compound were freshly prepared in analytical-grade methanol such that the addition of 0.2 ml of solution to 10 ml of acid in the thermostatted cell would produce a working concentration of about 2.5×10^{-5} M. This final concentration was chosen with regard to the small quantities of each compound available; it also resulted in a relatively low concentration of methanol (ca. 2%) in the solution used for polarography. The acidic solutions were prepared from Volucon ampoules; polarographic backgrounds were acceptable at the current ranges employed.

The hydrolysis of each compound was recorded in 1 M, 0.1 M and 0.01 M hydrochloric acid as well as in 0.5 and 0.05 M sulphuric acid. This scheme provided a range of pH and also allowed for the possibility of specific anion catalysis and ion-pairing effects.

Procedures

An aliquot (10 ml) of the appropriate acid solution was pipetted into the thermostatted cell and the oxygen was removed by bubbling nitrogen for

15 min. During this time, the solution attained the required temperature. Nitrogen was then passed over the solution, and the s.c.e., platinum counter and d.m.e. were positioned in the cell. The polarographic curve of the acid alone was recorded under the polarographic conditions set out below. Subsequently, 0.2 ml of the methanolic stock solution was introduced into the cell by means of an auto-zero pipette inserted into the cell after partially removing the platinum electrode. Timing was begun when about 0.1 ml of the solution had been added. The solutions were thoroughly mixed by bubbling nitrogen for about 1 min. The polarograms were then recorded at convenient time intervals. When the reaction had substantially slowed down or if it proceeded only slowly, the plug of mercury which had accumulated in the cell was drawn off through the tap, and the remaining solution was run into a 25-ml conical flask, stoppered and placed in a water bath until a further polarogram could be recorded. This applied only to reactions at 25°C; at higher temperatures, the temperature differential between the cell and the water bath became too large for constant temperature conditions to be maintained. However, the reactions at the higher temperatures were completed quite quickly in the cell.

The use of 2.5×10^{-5} M concentrations of electroactive species, precluded the use of d.c. polarography, as the waves were diffuse and the half-wave potentials of some reactants and products were too close for adequate resolution. Differential pulse polarography (d.p.p.) provided the required sensitivity and good resolution in most cases. The d.p.p. conditions were as follows: initial potential −0.30 V for 1 or 0.5 M acids, −0.34 V for 0.1 or 0.05 M acids, −0.42 V for 0.01 M acids; scan rate 5 mV s^{-1}; potential scan 3.0 V; low pass filter 0.3 s; chart speed 20 cm s^{-1}; modulation amplitude 50 mV; 1 s drop time; current range 5 μA. The polarographic peak heights were measured in the usual way. In some cases, the waves of the reactant and product overlapped considerably; the usual method of measurement was still applied but it is noted in the text where this problem arose.

The time measurements used to construct concentration (or a function of concentration) vs. time plots, were not the times at which the recordings began but the times at which the peak related to the electroactive substance was reached in the differential pulse polarogram, calculated from the chart speed and the time at which each recording was begun.

POLAROGRAPHIC STUDY OF THE HYDROLYSIS OF COMPOUNDS I–VII

Differential pulse polarograms were obtained for 2.46×10^{-5} M flurazepam in 0.1 M hydrochloric acid over a period of ca. 240 min. Graphs of current vs. time were then plotted for this concentration and for 4.93×10^{-5} M and 0.99×10^{-5} M flurazepam. Tangents were drawn to the resulting curves at $t = 0$ to provide the initial rates of the reaction. The slope of a plot of $\log dx/dt$ vs. $\log a_0$ was 1.09 suggesting a first-order reaction for flurazepam in 0.1 M hydrochloric acid; here a_0 is the initial concentration and x is the

concentration of the product after time t. Further evidence for a first-order process came from a consideration of the fractional lives of the reaction. The times taken for the polarographic current to decay by 1/4 and 1/2 of its initial value were measured at the three concentrations listed above. These values, $t_{1/4}$ and $t_{1/2}$, were independent of concentration, indicating first-order reactions.

Tangents to the current—time curve were then drawn at various times and the values of log dx/dt were plotted against log $(a_0 - x)$. These plots showed curvature in both 0.1 M and 1 M hydrochloric acid solutions, which indicated a change in the order of the reaction. Indeed, the first-order rate constants corresponding to the hydrolysis of flurazepam in 1 M and 0.1 M hydrochloric acid as calculated from the linear portions of the log dx/dt vs. log $(a_0 - x)$ graph and from the equation $k = 0.693/t_{1/2}$ differed, which invalidates simple first-order kinetics when applied to this reaction.

One of the most likely causes of the deviation from first-order kinetics is that the back-reaction is significant. This is also suggested by the fact that the reaction does not go to completion, ca. 30% of the starting material remaining unhydrolysed at the end of the reaction. The equation representing the reaction rate where both forward and reverse reactions are first-order is $dx/dt = k_1(a_0 - x) - k_{-1}x$, where k_1 and k_{-1} are the rate constants for the forward and reverse reactions, respectively. This equation can be computed to

$$\log_{10}(a_t - a_\infty) = -(k_1 + k_{-1})t/2.303 + \log_{10}(a_0 - a_\infty) \quad (1)$$

where a_t is the reactant concentration after time t, and a_∞ is the reactant concentration at equilibrium.

From the slope of a graph of $\log_{10}(a_t - a_\infty)$ vs. t (which proved to be linear for flurazepam in 1 M and 0.1 M HCl) and the equation

$$a_\infty/a_0 = k_1/(k_1 + k_{-1}) \quad (2)$$

the following rate constants were calculated: $k_1 = 2.00 \times 10^{-4}$ and $k_{-1} = 0.83 \times 10^{-4}$ s^{-1} in 1 M HCl, and $k_1 = 5.75 \times 10^{-4}$ and $k_{-1} = 2.48 \times 10^{-4}$ s^{-1} in 0.1 M HCl. These values of k_1 are in reasonable agreement with those obtained by using the initial slope of the first-order plot of log dx/dt vs. log a_0. Correction for the back-reaction must be made to gain a more complete picture.

Deviation from first-order kinetics can also be explained by postulation of second-order kinetics and, in fact, graphs of a_t^{-1} vs. t for concentrations of 0.99×10^{-5} M, 2.46×10^{-5} M and 4.93×10^{-5} M flurazepam were linear. According to Laidler [10], postulation of such a second-order reaction is not at variance with the earlier treatment of a reversible reaction. The integrated rate equation (1) applies equally well to second- and first-order processes. As the second-order process does not become significant until the back-reaction has begun, it is probable that the second-order description of the reaction is due to a combination of the forward and back reactions. The hydrolysis is actually first-order, but the reversibility of the reaction produces second-order kinetics after a short period of time. The reaction then

continues under second-order kinetics until the back-reaction becomes significant and an equilibrium position is reached. At equilibrium, the ratio k_1/k_{-1} is numerically equal to the equilibrium constant K. The values of this constant for flurazepam in 1 M and 0.1 M HCl are 2.40 and 2.32, respectively.

The rate constants for the reaction of flurazepam and its metabolites in the five acidic solutions are shown in Table 1. The constants were evaluated from the simple first-order equation, which, as shown earlier, produces results in reasonable agreement with those that take into account the back-reaction. The half-life reported is that which would apply if first-order kinetics were valid for the entire reaction. The percentage reaction was estimated from the ratio of the final concentration of reactant to its initial concentration.

Flurazepam hydrolyses at a measurable rate in all five acidic solutions used. In 0.01 M HCl, the half-wave potentials of the reactant and product are separated by only 60 mV, causing considerable overlapping and making quantification of peaks difficult; only an estimate of $t_{1/2}$ was therefore possible. The extent of reaction in the remaining solutions was about 70%. The rate constants in 0.1 M HCl and 0.05 M H_2SO_4 were similar but hydrolysis took place half as fast again in 0.5 M sulphuric acid as in 1 M hydrochloric acid. This may be due to some form of specific anion catalysis. The main feature of these results is that reaction is faster in the less concentrated acid.

The removal of one of the ethyl groups in the 1-substituent to produce monodesethylflurazepam resulted in marked changes in the rate of hydrolysis. By the time the first polarogram has been recorded for this metabolite in 1, 0.1, and 0.01 M HCl, a two-wave pattern of product and reactant had already emerged. The wave heights indicated that 60—80% of the metabolite had reacted within 2 min of addition to the acidic solution. There was little subsequent change in the limiting current, signifying that equilibrium had been achieved. The reaction was somewhat slower in the sulphuric acid solutions, the rate constants again being in the ratio 2:1 for the 0.05 and 0.5 M acid, as for flurazepam.

TABLE 1

Kinetic data for flurazepam and its metabolites
(k is in units of 10^{-4} μA s^{-1} and $t_{1/2}$ is in min)

Compound	1M HCl			0.1 M HCl			0.01 M HCl			0.5 M H_2SO_4			0.05 M H_2SO_4		
	k	$t_{1/2}$	%	k	$t_{1/2}$	%	k	$t_{1/2}$	%	k	$t_{1/2}$	%	k	$t_{1/2}$	%
I	1.93	60	70	5.38	21	70	—	63[a]	—	2.72	43	72	5.47	21	69
II	—	2	83	—	2	70	—	2	—	1.97	59	68	3.85	30	71
III	—	2	78	—	2	75	—[b]	—	—	1.30	88	74	—	2	78
IV	0.14[c]	825	60	0.45	225	55[e]	0.52	222	45	0.20[c]	577	60	0.55	211	55
V	0.15	750	39	0.90	128	36	1.62	71	40	0.34[c]	337	56	0.91	126	32
VI	0.06	1838	70[e]	0.28	408	89[d]	0.54	215	87[e]	0.09	1330	79[e]	0.31	372	88[e]
VII	0.11[a]	1020	74[f]	0.04	2730	61[f]	0.01[a]	8849	—	0.14[a]	806	74[f]	0.07	1687	49[f]

[a]Estimated value as product and reactant waves overlapped. [b]Waves overlapped too much to allow measurement. [c]Estimated value. [d]Using polarographic current after 4 days. [e]Using polarographic current after 2 days. [f]Using polarographic current after 24 h.

Didesethylflurazepam showed some characteristics similar to the monodesethyl metabolite in that an initial fast reaction seemed to be followed by a much slower move towards equilibrium. Only in 0.5 M H_2SO_4 could the reaction be followed completely, but even here, 41% reaction had taken place by the time the first polarogram could be recorded. A further, slower reaction took place as the process approached equilibrium. The corresponding reaction of the monodesethyl compound showed only 14% reaction at the time of the first recording. Thus the rate of the initial reaction increases as the ethyl groups are successively removed from the basic 1-substituent — to such an extent that in most acidic solutions, the reaction is essentially complete after about 2 min.

The change in value of the rate constants brought about by the alteration of the 1-substituent suggests some involvement of this group in the rate-determining step of hydrolysis. It has been proposed [11] that this bulky group in flurazepam could interact with the azomethine group. If the 4,5-double bond is the centre of attack in the hydrolysis reaction, the above discussion confirms that steric interaction occurs. The apparent increase in the reaction rate in hydrochloric acid solutions upon removing the ethyl groups may indicate decreased physical shielding of the site of attack from the reacting water molecules. This interpretation applies only to those compounds having a nitrogen atom in the substituent at position 1 because complete removal of the basic portion of the side-chain, resulting in *N*-1-hydroxyethylflurazepam, again changes the pattern of hydrolysis. The reaction is more like that of flurazepam itself, but it takes place at only a tenth of the rate of the parent compound. Again, decreasing the pH decreases the rate of hydrolysis (Table 1).

Similarly, the acetic acid metabolite reacts faster, the higher the pH. The rate constant is twice that of the previous metabolite in 0.1 M HCl and three times the value in 0.01 HCl. The situation for *N*-1-desalkylflurazepam is similar to that of the acetic acid metabolite except that the rate constants are three times smaller. The trend is reversed with the 3-hydroxy metabolite, the reaction becoming slower as the pH is increased.

The first-order rate constants in Table 1 can be arranged in descending order of magnitude as follows:

1 M HCl. Monodesethyl = didesethyl > flurazepam > acetic = hydroxyethyl > desalkyl-3-OH > desalkyl;

0.1 M HCl. Monodesethyl = didesethyl > flurazepam > acetic > hydroxyethyl > desalkyl > desalkyl-3-OH;

0.01 M HCl. Monodesethyl = didesethyl > flurazepam > acetic > desalkyl = hydroxyethyl > desalkyl-3-OH;

0.5 M H_2SO_4. Flurazepam > monodesethyl > didesethyl > acetic > hydroxyethyl > desalkyl-3-OH > desalkyl;

0.05 M H_2SO_4. Didesethyl > flurazepam > monodesethyl > acetic > hydroxyethyl > desalkyl > desalkyl-3-OH.

It has been shown [11] that the order of ascending values of the available pK_a values, relating to the =C=N— groups, is: (VII) −1.02; (I) −1.42;

(V) −2.10; (IV) −2.26; (VI) −2.57. If the *N*-1-desalkyl-3-hydroxyflurazepam (VII) is omitted, then the order of the rate constants listed above in 1 and 0.1 M HCl and in sulphuric acid exactly matches the series of pK_a values (pK_a data are not available for the mono- and di-desethyl metabolites owing to their rapid hydrolysis in acid). This suggests that the reaction rate at a given pH depends to some extent on the pK_a of the reactant. Because the rate of hydrolysis tends to decrease with increasing hydrogen ion concentration, acid catalysis of the protonated compound does not appear to be responsible for the reaction in the pH range 0—2. As the pH approaches pK_a, there is a corresponding increase in the rate of reaction. At pH 4, however, where all the azomethine groups in the present series of compounds are unprotonated, no detectable hydrolysis takes place, although the reaction occurs to a small extent at pH 3. Accordingly, a pH between 3 and 4 seems to be the highest pH for acid catalysis of the reaction. In the pH range 0—2, acid-catalysed hydrolysis of the unprotonated benzodiazepine appears to account for the reaction. ("Unprotonated" refers only to the azomethine group.) While hydrolysis of the protonated species does take place, it is much slower than that of the unprotonated form.

Table 2 presents the peak potentials (vs. s.c.e.) for all seven compounds and their hydrolysis products in the five acid solutions employed. Taking into account the scan rate at which the polarograms were recorded, these potentials are correct to ±5 mV. In nearly all solutions, the peak potentials of flurazepam and its metabolites are quite close together but the range of potentials of the hydrolysis products is much larger.

The two most probable products of hydrolysis in dilute acid are structures VIII and IX, structure VIII being the more likely. Any attempt at recovery of these compounds must take into account their acid—base properties

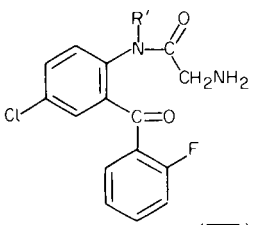

(VIII)

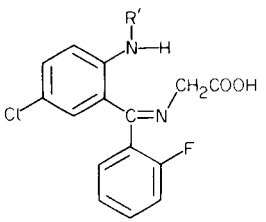

(IX)

in order that a suitable solvent extraction scheme can be devised. This was simplified by using *N*-1-desalkylflurazepam as the starting material for the hydrolysis so that there would be no additional equilibria arising from the substituent in position 1 which might complicate the acid—base behaviour of the hydrolysis product. In addition, it has been shown above that this metabolite reacts quite slowly in dilute acid. Because the reaction is thought to be reversible in alkali, it might also be suspected that this back-reaction would be correspondingly slow, thus providing sufficient time to recover the hydrolysis product from aqueous solution before the reverse reaction took place to any great extent. Attempts by De Silva et al. [8] to recover

TABLE 2

Peak potentials of flurazepam and its metabolites (R) and their acid hydrolysis products (P) (Potentials in V vs. s.c.e.)

Compound	1 M HCl		0.1 M HCl		0.01 M HCl		0.5 M H_2SO_4		0.05 M H_2SO_4	
	R	P	R	P	R	P	R	P	R	P
I	−0.515	−0.643	−0.565	−0.672	−0.634	−0.693	−0.520	−0.649	−0.575	−0.672
II	−0.515	−0.643	−0.560	−0.678	−0.629	−0.720	−0.531	−0.665	−0.575	−0.683
III	−0.515	−0.643	−0.571	−0.672	−0.677	−0.720	−0.525	−0.654	−0.581	−0.683
IV	−0.541	−0.675	−0.581	−0.705	−0.645	−0.763	−0.547	−0.675	−0.592	−0.715
V	−0.531	−0.665	−0.576	−0.699	−0.634	−0.742	−0.541	−0.665	−0.581	−0.705
VI	−0.515	−0.686	−0.566	−0.727	−0.613	−0.779	−0.525	−0.686	−0.571	−0.737
VII	−0.504	−0.675	−0.560	−0.742	−0.624	−0.795	−0.515	−0.654 −0.708	−0.571	−0.758

the hydrolysis product of flurazepam failed mainly because the back-reaction in alkali had taken place to such an extent that almost all of the starting material had been regenerated by the time solvent extraction was complete.

The amine function in structure VIII would be expected to contribute to a large extent to the acid—base properties of the molecule. It would be protonated below pH 9—10, and would therefore not be expected to extract into organic solvents. Ion-pairing effects may, however, alter this simple interpretation. Above a pH of about 10, the amine should no longer be protonated and would then be in a state amenable to extraction. The hydrogen of the amide function will not be affected by this pH because its pK_a value is <0. Structure VIII above should therefore be recoverable with a suitable organic solvent from an aqueous phase above pH 10.

Compound IX approximates to a substituted aniline. Aniline itself has a pK_a of 4.6 [12]. Thus, notwithstanding ion-pairing, structure IX should not be extractable below approximately this pH. At a pH greater than about 5, the carboxylic acid function will be ionized as in acetic acid, and the resulting charged species should again not be extracted by organic solvents.

On the grounds of pK_a data, it seems that compound IX should not be recoverable into an organic solvent at pH 10 whereas compound VIII should. These considerations form the basis of the recovery scheme. The peak potential of the starting material in the pH 10 solution was −0.620 V (vs s.c.e.) and that of the reaction product was −0.770 V. The hydrolysis product in 4 M HCl had a peak potential of −0.755 V in the same solution. This difference along with differences in R_f values and the intense yellow colour of the reaction product in concentrated acid, prove that structure X is not the product of reaction in dilute acid.

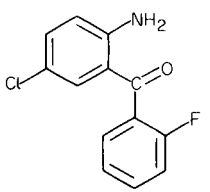

(X)

The reversibility of the reaction in dilute acid was shown in the earlier treatment of the kinetic results. This was demonstrated further when the *N*-1-desalkyl metabolite was extracted into diethyl ether from 0.01 M HCl leaving the reaction product in the aqueous phase. Polarographic measurements establishing that all of the starting material was extracted in this step. When the solution was made alkaline before extraction with diethyl ether, the starting material was extracted along with the hydrolysis product. The compounds were identified by means of polarography and thin-layer chromatography. The most probable structure of the hydrolysis product is compound VIII, which agrees with the findings of De Silva et al. [8].

POLAROGRAPHIC STUDY OF THE HYDROLYSIS OF OTHER 1,4-BENZODIAZEPINES

The first-order rate constants of the compounds included in this section were calculated in the same way as for flurazepam and its metabolites, and are given in Table 3. These compounds were chosen for study because they differ in such a way that it becomes possible to evaluate the effect of certain substituents on the rate of hydrolysis and the polarographic peak potentials. The compounds can be conveniently divided into groups for the purposes of discussion.

Flurazepam, Ro 5-4781 and Ro 5-6728

Flurazepam is included here because these three compounds form a series wherein the 5-*o*-phenyl substituent is altered. Thus, Ro 5-4781 possesses a 5-phenyl substituent, Ro 5-6728 a 5-*o*-chlorophenyl and flurazepam a 5-*o*-fluorophenyl. In 0.1 M HCl, the fluorinated compound reacts twice as

TABLE 3

Kinetic data for the benzodiazepines
(k is in units of 10^{-4} μA s^{-1} and $t_{1/2}$ is in min)

Benzodiazepine	1 M HCl					0.1 M HCl					
	k	$t_{1/2}$	%	E_p (R)[a]	E_p (P)[a]	k	$t_{1/2}$	%	E_p (R)[a]	E_p (P)[a]	E_p (NO_2)
Ro 5-4781	0.39	299	ND[b]	−0.573	−0.702	2.62	44	63	−0.597	−0.726	—
Ro 5-6728	0.28	415	64[c]	−0.525	−0.645	0.82	141	61[c]	−0.578	−0.662	—
K chlorazepate	—	>24 h[d]	19[c]	−0.568	−0.665	0.05[c]	2402	27[c]	−0.619	−0.780	—
Medazepam	—[e]	—	—	−0.611	—	—[e]	—	—	−0.688	—	—
Diazepam	—	>24 h	5[c]	−0.584	—	—	>24 h	24[c]	−0.630	−0.774 −0.817	—
Ro 5-2180	—	>24 h	13[c]	−0.579	−0.665	—	>24 h	12	−0.624	−0.785	—
Nitrazepam	0.17	672	86	−0.552	−0.665	0.18	652	ND	−0.589	−0.755	−0.069
Ro 5-4435	0.52	224	63[g]	−0.509	−0.649	3.03	38	98[c] [f]	−0.546	−0.685	−0.074
Clonazepam	0.11	1069	66	−0.520	−0.654	0.41	285	94[f]	−0.562	−0.701	−0.069
Flunitrazepam	0.49	237	61[c]	−0.547	−0.675	4.66	25	50[c]	−0.584	−0.723	−0.069

[a]R = reactant; P = product. [b]ND, not determined. [c]Measured after 24 h. [d]Estimated value. [e]No detectable reaction. [f]93% reaction after 3 h. [g]Measured after 5 h.

fast as the unsubstituted compound and some 6.5 times faster than the chlorinated analogue. In 1 M HCl, the unsubstituted compound hydrolyses only 1.5 times as fast as the *o*-chloro molecule, but flurazepam is about five times faster again. In both acid solutions, the descending order of rate constants is F > H > Cl.

The halogen atoms also affect the peak potentials of the compounds. The order of increasingly more negative potentials in both acid solutions is F > Cl > H. It should also be noted that flurazepam has a lower pK_a value than the unsubstituted analogue. The simple interpretation here is that the fluorine withdraws electronic charge from the azomethine group, resulting in a relatively positively-charged nitrogen, which would account for the lower pK_a value. The peak potentials of the hydrolysed halogenated compounds are very similar whilst that of the unsubstituted hydrolysis product is some 60 mV more negative.

Potassium chlorazepate, medazepam, diazepam and desmethyldiazepam

Medazepam and potassium chlorazepate were included in order that the influence of the 2-carbonyl group on the rate of hydrolysis might be determined. In most of the 1,4-benzodiazepines, the carbonyl at the 2-position provides a spatial arrangement of atoms which can be described as sp^2. The same position in potassium chlorazepate and medazepam is sp^3 hybridized. This alters the conformation of the seven-membered ring slightly, and might reasonably be expected to change some properties of the molecules.

Medazepam did not react at all in either 0.1 or 1 M HCl. Potassium chlorazepate has previously been shown to hydrolyse rapidly to desmethyldiazepam under the conditions of these experiments [13, 14]. The polarographic peak potentials of potassium chlorazepate and desmethyldiazepam (Ro 5-2180) are quite close together, so this reaction can not be observed by means of polarography. Table 3 shows the peak potentials of the final hydrolysis products to be the same in each case. Thus because of the rapid hydrolysis of potassium chlorazepate to desmethyldiazepam, the hydrolysis of the former to the benzophenone is effectively the reaction of the latter. Ring opening of potassium chlorazepate in acidic solution has been found to be negligible, the reaction proceeding almost entirely to the diazepam metabolite [14]. The hydrolyses of diazepam and its metabolite in 1 and 0.1 M HCl are slow, but unlike medazepam, they do take place at a significant rate.

The influence of the 5-*o*-fluorine atom is again evident from a comparison of the rate constants of desmethyldiazepam with *N*-1-desalkylflurazepam. The hydrolysis of both compounds proceeds slowly, but the fluorinated compound reacts several times faster than the diazepam metabolite. A difference in the peak potentials is also observed, the flurazepam metabolite being reduced some 64 mV more positively in both acid solutions, than the corresponding non-fluorinated compound.

Nitrazepam, flunitrazepam, desmethylflunitrazepam and clonazepam

These four compounds were grouped together because they each possess a 7-nitro group. In some ways, nitrazepam, clonazepam and desmethylflunitrazepam form a series analogous to Ro 5-4781 flurazepam, and Ro 5-6728 because there are H, Cl, F substituents in the 5-*o*-phenyl position. Once again, the fluorinated compound hydrolyses most quickly in both concentrations of acid used, with the unsubstituted compound second and the chlorinated drug third in 1 M HCl. The order of the last two compounds is reversed in 0.1 M HCl. The peak potentials are of the same order as in the flurazepam series, the order of increasingly negative potentials being F > Cl > H.

Flunitrazepam differs from its metabolite in that it bears a methyl substituent at the 1-position. The rate constant reported in Table 3 is that of the initial reaction. This fast rate slows to a more modest pace after about 15 min. The overall reaction of the metabolite Ro 5-4435 is faster than that of flunitrazepam itself. It is interesting to note that the reaction of Ro 5-4435 in 0.1 M HCl proceeds almost to completion, the reaction having consumed 93% of the starting material after only 3 h. The back-reaction is obviously not very significant for this compound, so this might be a better substance to use in the identification of the reaction product than was *N*-1-desalkylflurazepam, for which the back-reaction did not allow recovery of the product for identification. The reaction of clonazepam is not very fast, but it too proceeds almost to completion after 24 h in 0.1 M HCl.

The peak potentials of the nitro group in all four compounds in 0.1 M HCl are almost identical. Hydrolysis of the drugs does not alter these potentials, but the limitlng current increases steadily, though not at the same rate of decay as the current derived from the reduction of the azomethine group. This could indicate that the hydrolysis product has a slightly greater diffusion coefficient than the benzodiazepine.

Analytical application of hydrolysis reactions

The results in Table 1 indicate that within the 5-(*o*-fluorophenyl)-1,4-benzodiazepine series, there are notable differences in the rates of hydrolysis which could be used to identify the particular molecule isolated, as in a pharmaceutical preparation or after its separation from a biological fluid by solvent extraction or thin-layer chromatography. It would be possible, with 0.5 M H_2SO_4 or 0.05 M H_2SO_4 as the medium of hydrolysis, to identify any one of compounds I—VII by using the rate constant, k or the half-life $t_{1/2}$. Values of the peak potentials of the hydrolysis products (Table 2) would be of considerably less value in such identification procedures.

When a wider range of 1,4-benzodiazepines is evaluated, as shown in Table 3, values of k and $t_{1/2}$ could be used to identify all of the listed 1,4-benzodiazepines with the exception of medazepam, diazepam and desmethyldiazepam (Ro 5-2180) which are resistant to acid-catalysed hydrolysis within a 24-h time scale.

REFERENCES

1 E. H. Cordes and W. P. Jencks, J. Am. Chem. Soc., 84 (1962) 832.
2 E. H. Cordes and W. P. Jencks, J. Am. Chem. Soc., 85 (1963) 2843.
3 B. Kastening, Z. Elektrochem., 60 (1956) 130.
4 J. B. Culbertson, J. Am. Chem. Soc., 73 (1951) 4818.
5 J. T. Cartstensen, K. S. E. Su, P. Maddrell, J. B. Johnson and H. N. Newmark, Bull. Parenter. Drug Ass., 25 (1971) 193.
6 H. V. Maudling, J. P. Nazareno, J. E. Pearson and A. F. Michaelis, J. Pharm. Sci., 64 (1975) 278.
7 W. Mayer, S. Erbe, G. Wolf and R. Voigt, Pharmazie, 29 (1974) 700.
8 J. A. F. de Silva, C. V. Puglisi, M. A. Brooks and M. R. Hackman, J. Chromatogr., 99 (1974) 461.
9 W. Franklin Smyth, M. R. Smyth, J. A. Groves and S. B. Tan, Analyst, 103 (1978) 497.
10 K. J. Laidler, Chemical Kinetics, McGraw-Hill, New York, 1965, p. 16.
11 J. A. Groves and W. Franklin Smyth, Spectrochim. Acta, 35A (1979) 603.
12 A. Albert and E. P. Serjeant, Ionization Constants of Acids and Bases, Methuen and Co. Ltd., London, 1962.
13 A. MacDonald, A. R. Michaelis and B. Z. Senkowski, in K. Florey (Ed.), Analytical Profiles of Drug Substances, Vol. 1, Academic Press, NY, 1972.

Analytica Chimica Acta, 134 (1982) 239—245
Elsevier Scientific Publishing Company, Amsterdam — Printed in The Netherlands

STOPPED-FLOW SENSOR FOR DISSOLVED OXYGEN

JOSEPH WANG* and LALIT SARIN
Department of Chemistry, New Mexico State University, Las Cruces, NM 88003 (U.S.A.)
(Received 8th June 1981)

SUMMARY

Stopped-flow hydrodynamic modulation voltammetry is applied to membrane electrodes to minimize some of the problems that characterize steady-state dissolved oxygen probes. Mass-transport properties, sensitivity, precision, and linearity of response are reported. The low stopped-flow background current allows a limit of detection for dissolved oxygen near 36 $\mu g\ l^{-1}$. The relative standard deviation at the $mg\ l^{-1}$ level is 3% Glassy carbon electrodes are used, replacing the commonly used metal cathodes, to minimize passivation effects. The method is sensitive, reproducible, and simple.

The quantification of low concentrations of dissolved oxygen is a problem of widespread interest [1, 2]. Most commercial probes follow the type first described by Clark et al. [3], in which a semipermeable membrane separates the working cathode and the reference anode from the sample. Solution motion provides the convection required for transporting oxygen to the electrode. Oxygen diffuses across the membrane and is reduced to hydroxyl ions, producing a current, which reflects the combined solution and membrane mass transport resistance.

In spite of the widespread use of these probes, they suffer from some disadvantages, especially when they are used to quantify very low oxygen concentrations. Errors arise from changes in the convection rate, drift or slow response, low sensitivity, and lack of reproducibility [4—6]. Various approaches to reduce one or more of these disadvantages include an extremely small cathode [7] or a two-layer membrane [5] for reducing convection dependence, a potential pulse operation [6] for improving the sensitivity and reducing the convection dependence, or a non-membrane flow-through sensor [8] for obtaining a faster response.

This report describes the stopped-flow operation of a dissolved-oxygen flow cell that minimizes most of the limitations of probes described above, and seems well suited for the monitoring of trace quantities of oxygen. Stopped-flow voltammetry involves measurement of the current difference between zero and high flow rates. The flow pulsing produces a pulsation only in the convection-dependent current and thus it is free from most background interferences. Such a flow modulation has been exploited for trace determinations using various bare solid electrode (without membranes)

0003-2670/82/0000-0000/$02.75

flow cells [9—11]. Although the present state of the art of hydrodynamic modulation voltammetry (h.m.v.) has been reviewed [12], hydrodynamic modulation operation of membrane-covered electrodes has not been described yet. The hydrodynamically modulated current of a membrane-covered dissolved-oxygen electrode represents the change in flux of oxygen into the electrode caused by variations, at different convection rates, of the thickness of the diffusion boundary layer outside the membrane. The extent of convection, and therefore, the feasibility of a successful h.m.v. operation, depends upon the relative contributions by the membrane and the solution to the total mass-transport resistance. A highly permeable membrane, covering a relatively large surface area cathode, is preferable for sensitive modulation measurements. Because the background current of membrane-covered electrodes is non-convective in nature [4], h.m.v. provides highly efficient background correction. The resulting low limit of detection is of great importance for the monitoring of oxygen levels in essentially anaerobic systems.

A glassy carbon cathode is used in place of the metallic materials commonly employed, to minimize the effects of surface passivation. At platinum electrodes, oxygen may undergo simultaneous side-reactions, resulting in formation of a platinum oxide surface complex that partially inhibits the reduction process of interest [4]. Carbon does not suffer from this limitation and thus provides a more stable response. Primarily, this paper is a study of the characteristics of a stopped-flow membrane-covered glassy-carbon sensor used to monitor dissolved oxygen. Preliminary experiments, which include the modification of a commercial batch probe to a pulsed-stirring modulation procedure, are also described.

EXPERIMENTAL

Construction of sensor

A schematic diagram of the cell is shown in Fig. 1. The body consists of a Kel-F block (4 × 3.5 × 2 cm). A solution flow channel, drilled through the Kel-F body, has a 1.8-mm solution inlet, widened to 8.3-mm to accept the combined working and reference electrode assembly. The working electrode is a 2.5-mm diameter glassy carbon disk (Tokai Electrode Mfg., Japan) attached with epoxy cement inside an appropriate glass tube (2.6-mm i.d., 6-mm o.d., 7-cm long). Electrical contact to the glassy carbon disk is made by filling a portion of the glass sleeve with mercury and dipping a copper lead into it. The glassy carbon face is first roughly polished with silicon carbide papers (No. 400 and 600), followed by a 0.1-μm alumina slurry, until a mirror-like surface is obtained. The reference electrode, a silver wire coated with silver chloride, is wound around the glass sleeve. The resulting 7-mm diameter reference spiral also serves as a support for the membrane (B-05979-B; Yellow Springs Instruments). A section of the membrane is stretched over this coil and is held in place with a rubber O-ring. This results

in the formation of a containment region that is filled with a 0.1 M potassium chloride solution. The membrane-covered electrode assembly is centered in the flow channel with a rubber O-ring which provides a leak-proof seal. Solution outflow is maintained through a 1.6-mm diameter channel branching from the flow channel at a right angle. The two electrodes were connected to a Sargent-Welch 3001 polarograph.

Procedures

The deionized water sample solution (0.1 M in KCl) was stored in a 300-ml BOD bottle, fitted with a rubber cork containing two holes, one for the sample inlet and another for a gas delivery tube. Solution flows from the bottle to the cell via a glass tube (2-mm i.d., 9-cm long). Stopped-flow measurements were performed by turning on and off a stopcock that was placed at the cell outlet. The flow rates were calibrated and checked volumetrically. Changes in the oxygen concentration level were provided by bubbling oxygen or argon gases through the solution.

The working electrode was preconditioned at the beginning of each experiment at +0.9 V, −0.9 V and +0.9 V, for 3 min at each potential. Such conditioning served to put the glassy carbon surface into a clean and reproducible state prior to the experiment. The measurement potential, −0.80 V, was subsequently applied and ample time allowed for the system to reach steady-state before the stopped-flow current difference was recorded. Electrode calibration was made by comparing the current amplitude of the unknown to that recorded for air-saturated water, and deriving the oxygen concentration for 100% saturation from tables of solubility of oxygen in

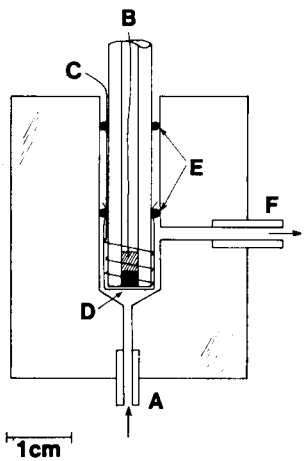

Fig. 1. Schematic diagram of the cell. A, Sample solution inlet; B, lead to working electrode; C, lead to reference electrode; D, membrane; E, O-rings; F, sample solution outlet.

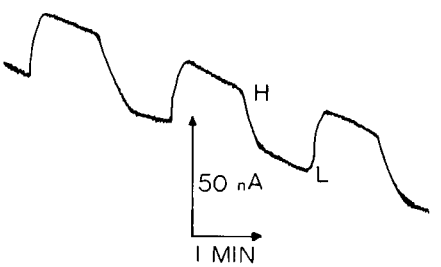

Fig. 2. Pulsed-stirring response of the Orion electrode for 1.5 ppm oxygen. Pulsing data: stirrer settings of 10 (H) and 2 (L) for 1 min.

water. All hydrodynamic modulation results were compared with steady-state results of an Orion oxygen electrode (Model 97-08, Orion Research).

RESULTS AND DISCUSSION

Modification of a commercial electrode to pulsed-stirring operation

Preliminary experiments were undertaken with an Orion 97-08 oxygen electrode that was modified for hydrodynamic modulation operation, based upon pulsing the stirring rate of the solution between two values and measuring the corresponding current difference. Pulsed-stirring voltammetry, which is a new h.m.v. procedure [13], can be easily incorporated with various probes. The Orion electrode [14] is based on Clark's design described earlier; a built-in stirrer bar (on the electrode accessory funnel), driven by an external magnetic field, provides the convective transport of oxygen to the electrode compartment. Stirring pulses were applied by switching the stirrer speed controller (Sargent—Welch, No. 76490) between low and high values. The electrode output was interfaced to a chart-recorder via a potentiometer and a 6-V battery, required to offset the steady-state signal and thus bring the modulated response into the recorder scale. Figure 2 is a reproduction of a pulsed-stirring chart-record for 1.5 ppm oxygen. The noise level (mainly from stirring) is near 1.5 nA. For a signal-to-noise ratio of 2, the limit of detection is about 0.14 ppm. The response times for the pulsed-stirring mode are about 10 s (high) and 25 s (low). The pulsed-stirring current is a small fraction of the total steady-state current. The drift in the steady-state current, which is a problem associated with some probes, does not affect the pulsed-stirring current amplitude; this is probably due to the non-convective nature of the drift component of the total steady-state current. This drift is usually larger at the beginning of a measurement when the potential difference is first applied between the two electrodes. While a waiting period is required in the steady-state operation in order to obtain a stable reading, this is not the case with the pulsed-stirring operation.

Four separate experiments were performed on different days during a month to examine the dependence of the pulsed-stirring current amplitude on dissolved oxygen concentration. For five concentration increments, from 2.5 to 12.5 ppm, calibration graphs showed good linearity (conditions: stirring settings, 10 (high) for 30 s, 2 (low) for 1 min). Least-squares treatment of the calibration data yielded slopes of 21 ± 0.5, 28 ± 0.9, 29 ± 1.3 and 38 ± 0.8 nA ppm^{-1} with standard errors of 3.7, 6.9, 10.2, and 6.5 nA respectively. These variations in the sensitivity are due to aging effects [4], changes in the membrane permeability, membrane irregularities, or changes in the membrane/electrolyte compartment. At higher concentrations (>14 ppm) deviation from linearity was observed, as expected from the dynamic range of the steady-state operation of this electrode indicated by the manufacturer [14].

The precision of results was estimated by ten repeated measurements of 7.4 ppm oxygen (conditions: stirring settings, 8 (high) for 30 s, 2 (low)

for 1 min). The mean pulsed-stirring current amplitude was 66.9 nA, with a standard deviation of 2.5 nA.

Evaluation of the stopped-flow sensor

Stopped-flow current—time responses for 4.1 ppm oxygen with different cycling times are shown in Fig. 3(A—C). The time required to reach the flow "on" steady-state is about 65 s. Such a response time is longer than that reported for non-membrane flow sensors operated in the stopped-flow procedure [9, 10], and it probably includes the lag time caused by diffusion through the membrane. The "off" current constantly decays (in a reproducible manner), representing the expansion with time of the diffusion layer thickness outside the membrane as the flow is stopped. This current does not attain a steady-state, probably because of a flux of oxygen outside the membrane (natural convection and semi-infinite linear diffusion) which exists even at zero flow rate (analogous to the Cottrell behavior at bare solid electrodes). The current spikes on both sides of the principal peaks are due to abrupt changes in the system as the stopcock is being turned on and off. The measurement cycle time can be shortened by making measurements before the flow "on" steady-state is achieved (Fig. 3, B and C). As the pulsing period is decreased, the stopped-flow current amplitude decreases. The 50% and 75% reductions in the cycling period (curves B and C vs. A) result in current diminutions of only 19% and 50%, respectively. Similar cut-off of the pulsed current amplitude with increased frequency has been reported for

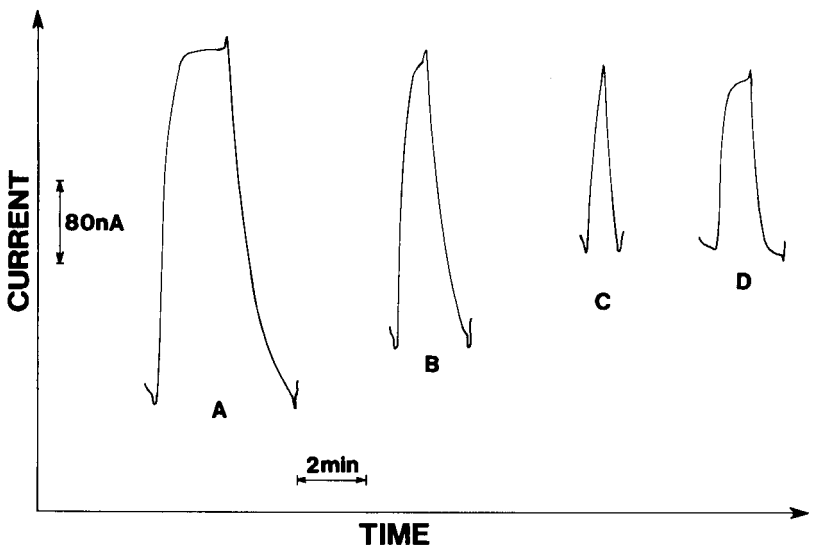

Fig. 3. Stopped-flow (A—C) and pulsed-flow (D) response for 4.1 ppm oxygen. Flow rates, 1.1 ml min^{-1} (on, A—C), 1.1 (low) and 2.0 (high) ml min^{-1} (D). Cycling times, 2 (on) and 2 (off) min (A); 1 (on) and 1 (off) min (B); 30 (on) and 30 (off) s (C); 1 (high) and 1 (low) min (D).

stopped-stirring [13] and stopped-rotation [15] studies at bare (non-membrane) solid electrodes. Analogous to these cases, the cut-off of the flow "on" steady-state may be due to the slow adjustment of the concentration profile adjacent to the membrane to changes in the convection rate, compared to the fast adjustment of the hydrodynamic regime. Based on these data, cycling times of 1 min "on" and "off" were used throughout as a compromise between sensitivity and speed.

Also shown in Fig. 3 is the pulsed-flow response of the same solution (curve D). In this case, "low" and "high" steady-states are achieved within about 40 s. However, the pulsed-flow current amplitude is usually smaller than that of the stopped-flow operation, because a larger portion of the steady-state response (that of the "low" current state) is not exploited for the quantification. In addition, stopped-flow operation is much simpler (on-off vs. level changes), and thus lends itself easily to automation.

A linear correlation was obtained between the nonsteady-state stopped-flow current and oxygen concentration. Eight concentration increments from 1 to 8 ppm yielded a linear plot (conditions: flow rate (on), 1.0 ml min^{-1}, 1 min on and off). A least-squares fit of the data gave the equation $I(nA) = (51.4 \pm 0.36)\, C_{(ppm)} + 0.79 \pm 1.9$ nA with a standard error of 2.3 nA.

The dependence of the stopped-flow current amplitude upon the "on" flow rate was studied under the cycling period (1 min on and off) chosen above. For a 6.02 ppm solution, the "on" flow rates of 0.5, 0.8, 1.65, 2.2 and 2.8 ml min^{-1} produced current amplitudes of 246, 292, 517, 602 and 672 nA, respectively. These data indicate that forced mass-transport through the solution adjacent to the membrane has a significant effect on the size of the modulated current. Higher "on" flow rates are thus preferable for achieving higher sensitivity.

Figure 4 is a reproduction of a stopped-flow chart record for 0.7 ppm oxygen. The noise level is very low, only around 0.7 nA. A detection limit of about 36 ppb oxygen is estimated for a signal-to-noise ratio of 2. This level is

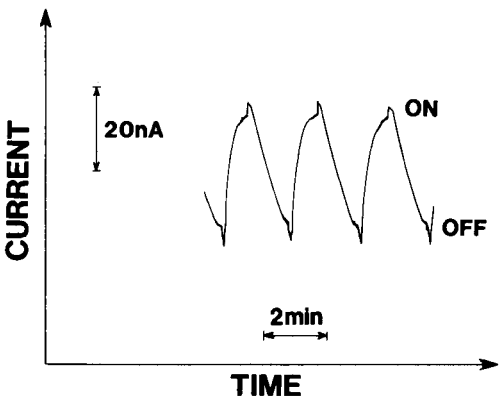

Fig. 4. Stopped-flow response for 0.7 ppm oxygen. Conditions as in Fig. 3B.

below the range of applicability of most oxygen probes employed presently. The precision of the results was further estimated by ten successive stopped-flow measurements of 4.1 ppm oxygen during a time period of 20 min (conditions as in Fig. 3B). The mean current amplitude found was 245 nA with a range of 237—259 nA and a relative standard deviation of 7.4 nA. The precision of the results depends on reproducible on-off timing because of the continuing decay of the "off" current with time.

Because steady-state and non-steady-state currents at forced-convective membrane-covered electrodes represent mixed membrane and solution control, membranes with different representative permeabilities are expected to demonstrate characteristic stopped-flow response. Other parameters that may affect the stopped-flow current amplitude (i.e., the flow sensitivity) are the membrane thickness, the surface area of the cathode, the temperature, or the viscosity of the sample. The characteristic parameters such as flow rate and cycle time, must therefore be adjusted to suit the requirements of each particular membrane-electrode combination or sample solution viscosity. Overall, the improved sensitivity and the simple instrumentation and procedure indicate considerable promise for the stopped-flow approach as a method of monitoring trace quantities of dissolved oxygen.

The authors thank Gordon Ewing for the use of the Orion oxygen electrode.

REFERENCES

1 I. Fatt, Polarographic Oxygen Sensors, CRC Press, Cleveland, OH, 1976.
2 M. L. Hitchman, Measurement of Dissolved Oxygen, J. Wiley, New York, NY, 1978.
3 L. C. Clark, Jr., R. Wolf, D. Granger and Z. Taylor, J. Appl. Physiol., 6 (1953) 189.
4 D. A. Gough and J. K. Leypoldt, Anal. Chem., 52 (1980) 1126.
5 S. Ben-Yaakov and E. Ruth, Talanta, 27 (1980) 391.
6 K. D. Wise, R. B. Smart and K. H. Mancy, Anal. Chim. Acta, 116 (1980) 297.
7 R. A. Butler, J. F. Nunn and S. Askill, Nature, 196 (1962) 781.
8 C. M. Wolff and H. A. Mottola, Anal. Chem., 49 (1977) 2118.
9 W. J. Blaedel and S. L. Boyer, Anal. Chem., 43 (1971) 1538.
10 W. J. Blaedel and J. Wang, Anal. Chem., 51 (1979) 799.
11 W. J. Blaedel and J. Wang, Anal. Chem., 53 (1981) 78.
12 J. Wang, Talanta, 26 (1981) 369.
13 J. Wang, Anal. Chim. Acta, 129 (1981) 253.
14 Instruction Manual, Model 97-08 Oxygen Electrode, Orion Research Inc., Cambridge, MA, 1979.
15 J. Wang, Anal. Chem., 53 (1981) 1528.

Analytica Chimica Acta, 134 (1982) 247—262
Elsevier Scientific Publishing Company, Amsterdam — Printed in The Netherlands

USE OF HALF-CELL BARRIERS TO ELIMINATE JUNCTION CLOGGING AND THERMAL HYSTERESIS IN SILVER/SILVER CHLORIDE REFERENCE ELECTRODES

DONALD P. BREZINSKI*

Research and Development Division, Sullivan Science Park, Corning Glass Works, Corning, NY 14831 (U.S.A.)

(Received 16th April 1981)

SUMMARY

The junctions of Ag/AgCl electrodes rapidly become clogged with precipitated silver chloride during use. This causes loss of flow and slow response with thick junctions and may cause offset and stirring error with thin junctions. This problem can be eliminated by using a pure potassium chloride junction electrolyte, together with suitable barriers to impede migration of silver chloride from the half-cell. Diffusional transport through a mechanical barrier is inversely proportional to its electrical resistance when filled with electrolyte. Based on this principle, very effective barriers to half-cell diffusion and flow were fabricated from microporous glass. Alternatively, a cation-selective membrane was used to block soluble silver chloride complexes without a significant increase in electrode resistance. Thermal drift and hysteresis are not inherent features of the Ag/Cl couple and are eliminated by proper design of the half-cell.

The reference electrode is frequently at fault when poor results are obtained in measurements with ion-selective electrodes. Events at the reference junction are responsible for performance problems such as slow response to changes in ionic strength and transference, offset errors at equilibrium, and stirring potentials. However, some aspects of reference electrode performance are determined by the half-cell. An adequate outward flux of KCl, provided by diffusion or flow of electrolyte, is generally required for optimal junction performance [1]. Precipitates formed by half-cell species can clog the junction, thereby degrading potentiometric performance. In particular, the Ag/AgCl electrode is widely regarded as less accurate and more likely to clog than certain other types (e.g., calomel), though this performance difference and its causes have remained unsubstantiated. Half-cell species may also cause problems by contaminating the measured sample. For example, mercury(I) ion from calomel electrodes has been found to cause marked inhibition in assays for creating kinase and certain other enzymes [2]. Finally, problems with thermal drift and hysteresis originate at the half-cell. The calomel electrode exhibits significant thermal hysteresis and a limited temperature range (80°C maximum) because of disproportionation of Hg^+

*Correspondence to: 54798—CR653, Paw Paw, MI 49079, U.S.A.

0003-2670/82/0000-0000/$02.75

ions. Thermal hysteresis in Ag/AgCl electrodes has also been reported [1, 3], but the reasons for its occurrence have remained uncertain.

That no one type of half-cell is totally free of problems is reflected in the fact that several different types are in widespread use. Among these, however, the Ag/AgCl half-cell offers a combination of practical advantages including ease of manufacture, relatively high stability and reproducibility, low toxicity, isopotential compatibility with ion-selective electrodes, and extended temperature range. Therefore, the purpose of this study was to determine and correct the functional deficiencies of the Ag/AgCl reference electrode. Junction problems caused by half-cell species could be eliminated by using a pure 4 M KCl junction electrolyte in conventional double-junction electrodes, but such electrodes are not optimally designed; present technology typically does not recognize the relationship between electrical conductance and diffusional transport through porous barriers, nor does it utilize barrier materials that are very effective in inhibiting flow transport caused by changes in ambient pressure and temperature. An optimized double-junction electrode incorporating a diffusion barrier of microporous Vycor glass was therefore developed. A non-specific diffusion barrier necessarily increases the electrical resistance of an electrode, which increases its noise sensitivity. Therefore, an ion-selective half-cell barrier was also developed that effectively blocks silver ions but adds negligible resistance. In the course of this work, half-cell dehydration, inhomogeneity, and species-depletion were found to be the principal causes of thermal drift and hysteresis in Ag/AgCl electrodes, and these problems were essentially eliminated in prototype electrodes.

Diffusion barrier theory

One approach to keeping silver chloride out of the junction is to place a mechanical diffusion barrier (e.g., a porous ceramic plug) between the half-cell compartment and the junction electrolyte. Since the plug also inhibits electrical conductivity, knowledge of the relationship between the diffusional and electrical properties of the barrier is important. One might wonder if a particular barrier configuration (e.g., elaborate interlocked baffles) would be particularly effective in inhibiting diffusion. However, the following analysis shows that steady-state diffusional transport is directly related to the overall electrolytic conductance of the barrier, and is otherwise independent of geometric factors such as size, shape, and pore structure.

Consider the following model. A minor soluble species (AgCl) is diffusing through a physical barrier of undefined geometry that is permeated with concentrated electrolyte (4 M KCl). At every point in the barrier, material flux is given by Fick's law, $\mathbf{f} = -D\ \mathbf{grad}\ C$, where $\mathbf{f}$ is the flux vector, D the diffusion coefficient, and C the concentration of the minor species. Also, the steady-state condition and conservation of mass require $\mathrm{div}\ \mathbf{f} = 0$. Ionic current in a voltage gradient, however, is governed by identical equations, with current density $\mathbf{j}$, electrolyte conductivity σ, and electric potential U, substituted for $\mathbf{f}$, D, and C, respectively. Because the steady-state differential

equations for mass and current transport are equivalent locally and subject to the same boundary conditions, the overall relationship between mass and current transport is independent of the detailed geometry. Thus, to determine the effectiveness of a diffusion barrier, one need only measure its electrical resistance when saturated with a known electrolyte. The quantitative relationship can be determined from the simplest case, a cylindrical column. When concentration C is maintained at one end of the column and zero at the other, the steady-state gradient is linear and the total transport rate is given by $Af = ADC/L$, where A and L are the cross-sectional area and length of the column, respectively. This transport rate is equivalent to an exchange of volumes of bulk solution, where $dV/dt \equiv Af/C = AD/L$. This "volume exchange" rate is independent of the concentration. Assuming a −electrolyte, letting $R_0 = A/\sigma L$ be the resistance of the column when filled with electrolyte at concentration C_0, substituting the Nernst relationship [4] between σ and D, and eliminating L/A, one obtains

$$dV/dt = RT/2F^2R_0C_0 \tag{1}$$

More generally, it can be shown that the volume exchange rate for diffusion of a binary electrolyte across a porous barrier is given by

$$dV/dt = (n_+^{-1} + n_-^{-1})\,\mu_+\mu_-\,(\mu_+z_+ + \mu_-|z_-|)^{-2}\,RT\,(F^2R_0C_0)^{-1} \tag{2}$$

where n_+ and n_- are the numbers of cations and anions per "molecule" of the electrolyte, μ_+ and μ_- are the relative mobilities of the cation and anion, z_+ and z_- are their valencies, and R_0 is the resistance of the barrier when filled with the electrolyte at concentration C_0. The diffusion potential caused by unbalanced transference is taken into account in Eqn. (2).

Equations (1) and (2) can be used to predict diffusion rates from barrier resistance measurements involving the same electrolyte species. Because resistivity and concentration are inversely related, the product R_0C_0 in these equations is roughly constant for a given strong electrolyte, yielding a comparably fixed value for dV/dt. With C_0 = 4 M and T = 25°C, Eqn. (1) yields

$$dV/dt = (0.12 \text{ ohm cm}^3 \text{ h}^{-1})/R_0 \tag{3}$$

Furthermore, except for H^+ and OH^-, diffusion constants are rather similar for most small electrolytes, so that barrier resistances measured in 4 M KCl should allow rough prediction of transport rates for silver complex and other minor species.

EXPERIMENTAL

Methods

Membrane transport rates were measured by dialysis. Membranes were glued to the ends of glass tubes, filled with a volume of inner fluid (e.g., AgCl-saturated 4 M KCl) and immersed in a test tube containing a volume

of outer fluid (e.g., pure 4 M KCl). Hydrostatic heads were minimized unless otherwise indicated. After a fixed time, concentrations of K^+ and Cl^- in the solutions were determined with ion-selective electrodes. Total silver ion in 4 M KCl solutions was determined by drying and fusion with sodium hydrogen sulfate, followed by the colorimetric dithiazone method for silver [5]. Potassium chloride in the samples appeared to compete for the silver during the fusion step, leading to low values and poor linearity. Thus, to provide meaningful results, standard curves were generated by using AgCl-saturated 4 M KCl stock solution diluted with pure 4 M KCl, and dialysis conditions were adjusted to give samples falling within the dynamic range of the assay (0—25 μg Ag ml^{-1}). Because dialysis data were analyzed in terms of "volume transport" and consequent dilution, accurate determination of absolute silver content was unnecessary. However, the results should be regarded as only semiquantitative.

Membrane (barrier) resistances were measured by applying a constant-current pulse, noting the resulting shift in membrane potential (measured with a pair of reference electrodes) and applying Ohm's law. Resistances as low as one ohm could be determined by removing the membrane and subtracting the measured background resistance of the electrolyte.

Flow rate of 4 M KCl through porous barriers was determined by applying a positive pressure head by means of a column of electrolyte, immersing the far end of the barrier in a volume of distilled water, and later measuring the KCl concentration in the water by means of a chloride-selective electrode. With microporous barriers, e.g., porous Vycor, it was necessary to account for the much larger background caused by diffusional transport by pre-exposing the pressurized barrier to pure water to allow formation of a steady-state diffusional profile, and then determining the flow-transport component from the slope of a plot of total transport versus applied pressure.

Reference electrodes were evaluated for thermally induced drift and hysteresis, which required a stable high-temperature reference. This was provided by using a 4 M KCl salt bridge to connect ambient ($\approx$23°C) and hot ($\approx$90°C) reservoirs of 4 M KCl electrolyte. A newly equilibrated and sealed Ag/AgCl electrode in the cold reservoir provided the reference potential.

Reference electrode response to changes in ionic strength and transference was determined by transfers between various solutions containing stationary 4 M KCl references.

Membranes and junctions

Celgard 3501 microporous polypropylene film (Celanese Corporation, Greer, SC) and unplasticized polyvinyl alcohol film (Type 1-0015-0; Monosol Division, Chris-Craft Industries) were used. Reverse osmosis membranes were obtained from UOP, Fluid Systems Division, San Diego, CA, and from Osmonics, Hopkins, MN.

DuPont Nafion perfluorosulfonic acid membrane sheet (Type 125) and tubing (Type 815) were obtained from E. I. DuPont de Nemours & Co., Polymer Products Department, Wilmington, Delaware. Nafion membrane was cemented to assemblies with Dow-Corning 734 RTV silicone Silastic, which adhered extremely well to the Nafion. Nafion membrane resistance was found to vary greatly with hydration conditions, so Nafion assemblies were stabilized prior to all testing by soaking them in 4 M KCl for 10 min at 95°C, followed by two days at room temperature.

Porous Vycor was fabricated from the parent borosilicate glass by phase separation at elevated temperatures, followed by acid leaching [6]. The Vycor was cemented to assemblies by using Wet-surface Patching Epoxy (Hardman, Belleville, NJ).

Unless otherwise specified, experiments with ceramic junctions employed a silica-based ceramic of 15% porosity, 1 mm diameter, and about 5 mm length, clad in glass and ground flat at the exterior surface.

RESULTS AND DISCUSSION

Junction clogging by silver chloride

The effects of silver chloride on flow rate, resistance and response time of a porous ceramic junction were determined in an experiment with several electrode bodies, some filled with pure 4 M KCl and some filled with AgCl-saturated 4 M KCl. Typical junction flow as a function of time in distilled water is shown in Fig. 1. With pure 4 M KCl, flow continued unabated for over a month, while the junction resistance decreased from 1.37 to 1.33 kΩ over this period. With AgCl in the electrolyte, flow decreased three-fold overnight and 20-fold in one week; junction resistance increased only very slightly (from 1.25 to 1.40 kΩ) in spite of the near total loss of flow, indicating an increase in the surface-to-volume ratio of the pores rather than

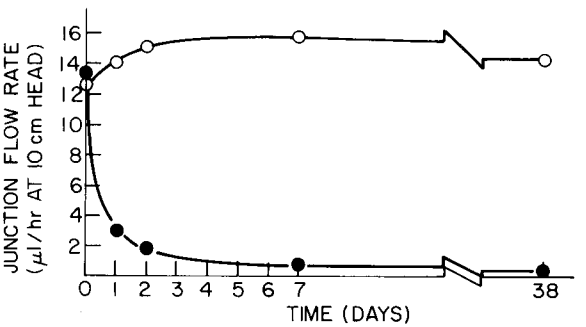

Fig. 1. Effect of AgCl on flow of electrolyte through reference junctions. The data points indicate measured transport of KCl electrolyte, with (•) and without (○) AgCl, through ceramic junctions immersed in distilled water.

complete blockage. Thus, the silver chloride is probably deposited as a finely-divided precipitate or as crystals that do not quite fit the pores. This clogging behavior was highly reproducible, with electrodes in each group giving virtually identical results. At the end of the flow experiment (38 days), the electrode bodies were equipped with half-cells and tested for response time (Fig. 2). The electrodes with silver chloride in the electrolyte showed the slow response usually observed with commercial Ag/AgCl electrodes. At 5 min after transfer, most of the potentials were still significantly in error. The junctions without silver chloride gave very fast response and the final results were accurate (the small offsets between solutions are mostly due to offsets in the stationary references).

Junction clogging occurs because the solubility of silver chloride is positively related to the KCl concentration. (In 0, 1, 2, 3, and 4 M KCl, dissolved AgCl is 0.01, 0.1, 0.6, 2.2, and ≈8 mM, respectively [7, 8]). This increase is due to the formation of various negatively-charged ionic complexes between Ag^+ and Cl^-, e.g., $(Ag_nCl_{n+1})^-$, $Ag^+(Cl^-)_n$. Within the junction, chloride concentration is reduced by diffusion, and the excess of silver chloride precipitates.

Absence of flow causes slow response by allowing species in the measured solution to diffuse deep into the junction, replacing 4 M KCl. During the subsequent measurement, this entrapped layer serves as the junction electrolyte, causing anomalous potentials until it is removed by diffusion.

In theory, clogging by silver chloride should also aggravate offset and stirring errors of a junction by increasing the surface-to-volume ratio of its pores, which would increase the ionic-strength threshold for boundary

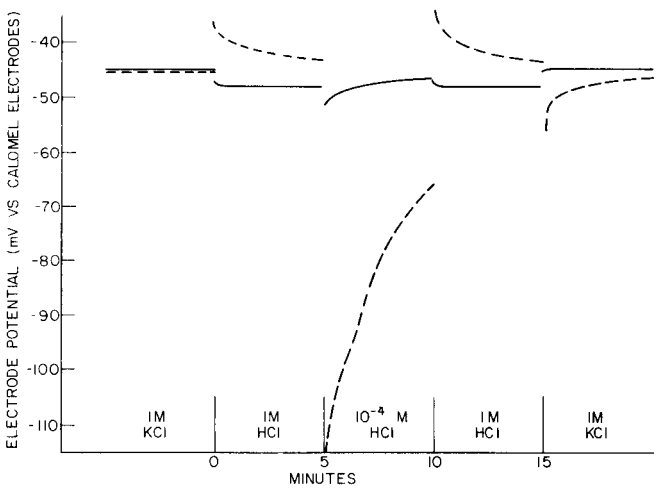

Fig. 2. Effect of AgCl clogging on a reference junction response time. Electrodes were stored 38 days in water prior to testing with a 10-cm head. (---) With AgCl; (—) without AgCl.

potentials arising from pore surface charge. Also, silver chloride would probably contribute some surface charge of its own. Nevertheless, silver chloride clogging was observed to have little direct effect on the offset and stirring error of the ceramic junctions, probably because the deposits occur in the interior of the junction where the KCl concentration remains quite high. With thin membrane junctions, however, the results were quite different. For example, Fig. 3 compares results obtained upon transferring an AgCl-clogged Celgard (porous polypropylene) membrane junction from 1 M HCl to 10^{-4} M HCl, before and after partial removal of silver chloride by brief exposure of the membrane to boiling 4 M KCl. In both cases, the electrode responded quite quickly without the large negative transient usually seen with thick junctions. However, with silver chloride present in the membrane, the steady-state reading in the dilute hydrochloric acid was offset by about −17 mV (0.3 pH). Also, this static error was accompanied by a correspondingly greater shift in potential when the solution was stirred. The stirred result is more accurate, because it is closer to the value given by the less clogged membrane and the value of −45 mV expected against calomel. The bimodal decay of the stirring potential suggests that more than one mechanism was operative. The silver chloride deposit was black, indicating the presence of photoreduced silver, which could introduce effects via chloride sensitivity as well as surface charge. Whatever the mechanism, the significant findings are that silver chloride clogging may substantially increase static and stirring error in membrane junctions, and that stirring can sometimes decrease the overall error, whereas more typically it increases the error.

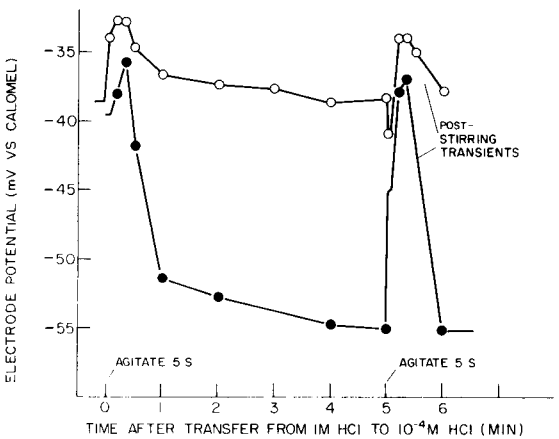

Fig. 3. Effect of AgCl clogging on static and stirring errors of Celgard membrane junction stored one week in pH 7 phosphate buffer. (•) Membrane partially clogged with AgCl; (○) membrane after treatment with hot 4 M KCl.

Diffusional transport of potassium chloride and transport of silver chloride

Equation (1) was confirmed by measurement of KCl diffusion through porous barriers. The observed diffusion rate of KCl through porous Vycor was 12% higher than predicted (Table 1). Equation (1) appears to provide a slight underestimate, probably because ionic mobilities are increased slightly by dilution in the diffusion gradient.

The performance of a specific silver chloride barrier is indicated by its "barrier efficiency", defined as the ratio of the transport rate predicted by Eqn. (3), divided by the transport rate actually observed. Thus, a barrier efficiency of ten indicates that the tested material was roughly ten-fold more effective at blocking silver transport than an electrolyte-saturated mechanical barrier of the same resistance.

Table 1 shows transport data for silver chloride for several tested barriers. The observed transport through a porous glass frit corresponded to a barrier efficiency factor of 1.3, indicating a close correspondence between observed and predicted diffusion rates. A factor somewhat above one would be expected, because the large silver complexes are likely to diffuse somewhat

TABLE 1

Diffusional transport through barriers.
(In measuring KCl transport, the inner (donor) solution was 4 M KCl, and the outer (recipient) solution was initially pure water. In measuring AgCl transport, the inner solution was AgCl-saturated 4 M KCl, and the outer was initially pure 4 M KCl)

Barrier	Resistance in 4 M KCl (Ω)	Dialysis conditions			Final relative concentration[c]	Observed transport constant[d] (Ω ml h^{-1})	Barrier efficien
		Head[a] (cm)	Volume[b] (ml)	Time (h)			
KCl transport							
Porous Vycor[f]	3050	0	5	72	2.55×10^{-3}M/4 M	0.135	0.89
	3050	290	5	24	0.88×10^{-3}M/4 M	0.140	—
AgCl transport							
Porous glass frit[g]	54	0	3.5	68	3.3% sat.	0.09	1.3
Polyvinyl alcohol[h] 1	200	0	1.7	72	0.8% sat.	0.04	3
2	74	0	3.0	89	3.5% sat.	0.09	1.3
Nafion 125[i]	13	0.7	3	400	0.6% sat.	6×10^{-4}	200

[a]Surface height of inner solution above outer solution. [b]Volume of recipient solution. [c]Fractional contamination of outer solution by inner species. [d]Observed transport constant = (resistance) (volume) (final relative concentration)/(time). [e]Barrier efficiency = (0.12 Ω cm^3 h^{-1})/(observed transport constant). In theory, this should equal 1 for free diffusion of KCl. [f]5 mm thick, 0.8 mm diameter. [g]2 mm thick, 1.6 mm diameter. [h]0.04 mm thick, 6 mm diameter. [i]0.13 mm thick, 21 mm diameter.

more slowly than KCl. Data are also shown for transport of silver chloride through 38-μm polyvinyl alcohol films rendered insoluble by baking overnight at 150°C. These membranes varied in resistance because of different degrees of charring. The less compact 74-ohm PVA membrane had a barrier efficiency close to that of the glass frit, even though the membrane was porous on a molecular rather than macroscopic level. However, because the assay was imprecise, this correspondence may be somewhat fortuitous.

Efforts to use common reverse-osmosis membranes to discriminate against AgCl complexes on the basis of size were unsuccessful because of problems with the materials; poly-ether/amide membrane (Fluid Systems RC100) quickly lost resistance in AgCl-saturated 4 M KCl because of oxidation by Ag^+, while cellulose acetate membrane (Osmonics SEPA-97) was very brittle when dry, and thermally unstable.

The ion-exchange barrier concept was tested by using DuPont Nafion perfluorosulfonic acid membrane, a cation exchanger. Extremely good results were obtained (Table 1). Silver ion transport through the membrane was over 100-fold less than predicted for a diffusion barrier of the same resistance. Large membrane diameters and long dialysis times were required to yield a detectable amount of silver.

It is somewhat surprising that the Nafion membrane is so effective as a silver ion barrier. According to published data, the permselectivity of Nafion is markedly reduced at high KCl concentrations, indicating significant penetration by chloride ion [9]. For example, at 2 M KCl, the permselectivity is roughly 70%, indicating that 15% of ionic conduction is due to chloride ion. Measurement of chloride diffusion through Nafion (from 4 M KCl into distilled water) showed a chloride barrier efficiency factor of only 9. This suggests that the high impermeability to silver complex of the membrane may be due not only to anion exclusion, but also to other factors such as ion size and solvation.

Barrier reference electrodes

Given the idiosyncracies and possible clogging problems of other types of half-cells, the most attractive solution to the clogging problem is to provide an Ag/AgCl electrode with a pure 4 M KCl electrolyte. However, silver chloride cannot be omitted from the electrolyte without further changes in electrode design. Saturation with silver chloride at the silver contact is required for electrode stability. Half-cells which contain little silver chloride, such as the electrolytic type, are readily stripped by pure potassium chloride solutions, causing a negative shift in potential. However, diffusion from half-cells equipped with ample silver chloride would typically saturate a pure filling solution within a matter of days. Deliberate confinement is required.

One approach is to place a porous diffusion barrier on the half-cell. Equation (3) gave good prediction of measured potassium chloride and silver complex diffusion rates, and can be used to determine how much

barrier resistance is required to adequately inhibit diffusional mixing between given volumes of half-cell and junction electrolyte. For example, to limit the silver chloride level in 3 ml of electrolyte to 4% of saturation at the end of one year, the required barrier resistance in 4 M KCl is R = (0.12 Ω cm^3 h^{-1})/(0.04 × 3 cm^3/y) = 8.7 kohm. Similarly, the drift rate when the electrode is filled with non-KCl junction electrolyte can be predicted. Diffusional loss of chloride from the half-cell compartment causes the electrode potential to drift upward at a constant rate

$$dE/dt = -58.16 \text{ dlog Cl}/dt = (3/R_0V_0)\Omega \text{cm}^3 \text{ mV h}^{-1} \quad (4)$$

where V_0 is the volume of half-cell electrolyte and R_0 is the junction resistance when saturated with 4 M KCl.

However, attempts to use conventional porous ceramics as diffusion barriers for permanently sealed half-cells proved disappointing. The available ceramics were too permeable to flow to prevent substantial solution exchange under expected variations in ambient pressure. For example, with a differential pressure of only 10 cm of water, which can be expected from fluctuations in atmospheric pressure, the low-flow junction ceramic of Table 2 gives about 30-fold more exchange by flow than by diffusion. To inhibit flow adequately, a 240-kohm barrier would have been required. More significantly, when a prototype with a 10 kohm barrier was heated for 5 days at 90°C, half of the electrolyte in the half-cell compartment was lost, presumably driven out through the junction by internal vapor pressure. Gelling of the internal electrolyte with aqueous polymers led to fabrication difficulties and still was not very effective in cutting down flow, particularly at high temperatures. Also, the thickeners commonly used (agar and sodium carboxymethylcellulose) are subject to bacterial, thermal, and chemical degradation, and also could conceivably clog the inner junction. Because such thickeners also generally bear fixed ionic groups, such clogging could cause erratic electrode potentials if the junction electrolyte were low in ionic strength.

TABLE 2

Comparison of flow and resistance properties of porous Vycor and typical junction ceramics

	High flow ceramic (15% void volume)	Low flow ceramic (1% void volume)	Porous Vycor (≈50% void volume)
Electrical resistivity in 4 M KCl (Ω cm)	49	816	96
Flow permeability (μl h^{-1} cm^{-2} H_2O)	81	0.4	0.034
Resistance × flow (Ω μl h^{-1} cm^{-1} H_2O)	4000	330	3.3

A preferable approach is to increase the ratio of flow resistance to electrical resistance by reducing the dimensions of the pore structure while retaining the same void volume. Porous Vycor, a continuous network of 96% silica, has a very fine pore structure (4—8 nm) that is extremely effective in blocking flow under pressure (Table 2). Diffusion-limited transport is obtained even with very large applied pressures, which minimizes the barrier resistance required for effective blocking. Though the surface-to-volume ratio of the Vycor pores was high, junction boundary potentials caused by space charge were absent down to reasonably low ionic strengths; electrode offset with 0.01 M KCl filling solution was below 1 mV. Thus, the Vycor barrier should be suitable for use with dilute and non-KCl filling solutions, as well as with concentrated KCl electrolytes.

A prototype of a Vycor barrier electrode is shown in Fig. 4A; the half-cell configuration is similar to a sealed double-junction electrode except for the materials employed. As discussed below, the electrode was exceptionally stable when filled with pure 4 M KCl electrolyte. Long-term drift with non-KCl filling solutions was roughly as predicted by Eqn. (4), though small fluctuations in potential were observed for a while after changing to non-KCl electrolytes. No photopotential was observed even with intense u.v. illumination (Mineralight S-52).

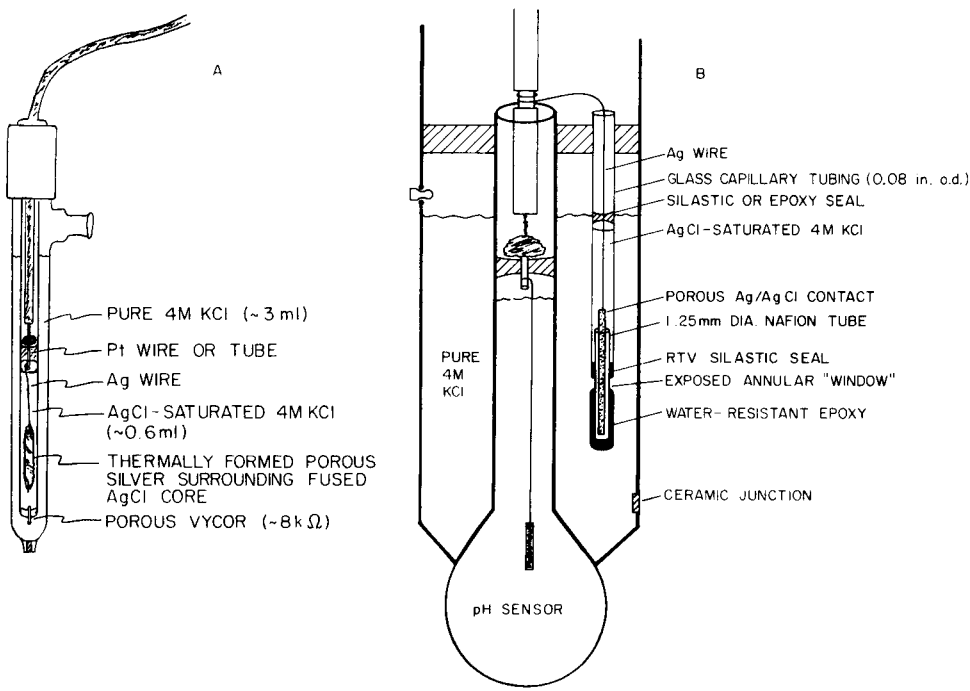

Fig. 4. A, Ag/AgCl reference electrode with Vycor diffusion barrier. B, Combination pH electrode with Nafion cation-exchange barrier on reference half-cell.

The diffusion barrier approach is suitable for most applications. However, the extra resistance introduced by the barrier is undesirable in applications requiring great immunity to electrical noise. The noise sensitivity of a well-shielded electrode circuit is often determined primarily by the impedance of the reference electrode, rather than the ion-selective electrode (i.s.e.). This arises from the fact that spurious currents from external sources pass primarily through the reference input of the electrometer, which provides a sink of relatively low impedance, rather than through the high-impedance i.s.e. input, which admits no current. Also, for some applications it is desirable to have particularly high barrier efficiency, e.g., in miniature electrodes with little electrolyte and easily depleted half-cells, electrodes for high temperatures, etc. However, with diffusion barriers, high blocking implies high resistance, because all species are retarded equally.

The required barrier resistance can be lowered by specific blocking. Nafion membrane was over 100-fold more effective in blocking silver transport than non-specific barriers of the same resistance. Here, the membrane blocks the negatively charged silver chloride complex, while allowing conduction via potassium ion transport. This approach could be extended to other types of half-cells, e.g., anion-exchange membranes could be used to block mercury(I) or thallium(I) ions while allowing conduction via chloride, or membranes narrowly selective for potassium ion or chloride could be used. However, the Nafion-blocked Ag/AgCl half-cell is a particularly attractive combination. Nafion, being a fluorocarbon polymer with sulfonic acid groups, has excellent thermal, physical, and chemical stability, while the Ag/AgCl half-cell is excellent aside from its tendency to clog the junction.

Figure 4B shows a prototype of a Nafion-blocked internal electrode intended for use in pH combined electrodes. A short length of DuPont Nafion 815 tubing surrounds a thermally formed porous Ag/AgCl contact [10]. Contact between the Nafion and external electrolyte is limited to a small annular window having a resistance of about 300 ohms.

Because of the charge-selective nature of the Nafion, a potential develops across the membrane in response to a concentration difference of the transported ions on the two sides of the membrane. Changing the concentration of the KCl electrolyte resulted in an abrupt shift in potential, whereas switching to a different type of electrolyte resulted in substantial drift. Thus, this type of internal is primarily suited for pH-type applications where the same junction electrolyte is always used.

Porous Vycor and ion-exchange membranes have been used previously as external reference junctions [11], but are ill-suitable to that application. The flow impermeability and high conductivity of porous Vycor preclude fast response in either thick or thin junctions, respectively, while Nernst-like response to admitted ions precludes the potentiometric use of ion-selective junctions in unknown solutions.

Thermal response of reference electrodes

A number of prototype and commercial electrode configurations were evaluated for stability in potential. Drift was studied at about 90°C in order to speed up the processes leading to changes in potential. At various times during thermal "ageing", electrodes were cycled between ambient and hot solutions to determine how quickly and reproducibly they would respond to changes in temperature. Some electrodes proved very unstable, showing drifts, fluctuations and hysteresis measurable in tens of millivolts. These problems were found to be caused by a variety of mechanisms that are rather obvious but not discussed in the literature. Insufficient silver chloride in the half-cell was found to be one major cause of instability; the solubility of silver chloride in 4 M KCl increases markedly with temperature [7], so that half-cells containing little silver chloride are readily stripped by large increases or fluctuations in temperature. Inhomogeneous distribution of solid KCl and AgCl with respect to the silver contact was another cause of hysteresis, as the additional material dissolved at higher temperatures is only slowly redistributed by convection or diffusion. Convectional fluctuations in KCl concentration, caused for example by a water evaporation—condensation cycle in the electrode barrel, caused thermal instability in electrodes with exposed half-cell contacts. Inhomogeneous temperature along the silver contact caused hot areas to become anodic and corrode, while silver crystals were deposited on the coldest, most cathodic portion of the contact. Similarly, solid silver chloride is transported to colder parts of the electrolyte where it is less soluble. The latter two processes caused drift and physical deterioration in non-uniformly heated half-cells.

These problems are largely eliminated in the granular column type of half-cell, which consists of a large downward-opening tube filled with an electron-conductive mixture of silver and silver chloride granules wetted with electrolyte. Such half-cells contain more than ample silver chloride, are physically homogeneous and are well isolated from the bulk electrolyte. Commercial Ag/AgCl electrodes of this design were among the most stable: typical results for Corning's version, the 476029, are shown in Fig. 5. With a new electrode, a change in temperature caused a rapid, asymptotic shift in potential (5.0 mV higher at 90°C than 25°C), and repeatability was very good through several thermal cycles (Fig. 5, curve a). However, even this half-cell design exhibited problems upon prolonged heating, showing a slow but significant drift (—0.4 mV/day) and failure to return to the initial potential upon cooling (Fig. 6, curve b). After high-temperature ageing, the electrode showed an erratic bimodal response to shifts in temperature, with poor reproducibility and little net change in potential (Fig. 5, curve b). In order to eludicate the mechanism behind this ageing effect, attempts were made to restore the original electrode performance. The half-cell column appeared to have lost some electrolyte. Vacuum cycling to flush and refill the Ag/AgCl column with electrolyte had virtually no effect, but when the column was evacuated, thoroughly rinsed with distilled water, dried, and refilled with fresh electrolyte, the

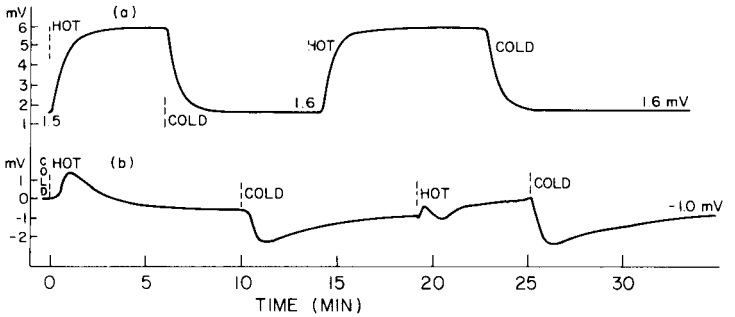

Fig. 5. Thermal response of new and aged reference electrodes. Corning 476029 Ag/AgCl electrode with granular column half-cell, transferred between baths of 4 M KCl at approximately 25 and 85°C. Potential vs. fixed Ag/AgCl electrode at ≈25°C. (a) New 476029 reference electrode; (b) 476029 electrode aged 5 days at 90°C.

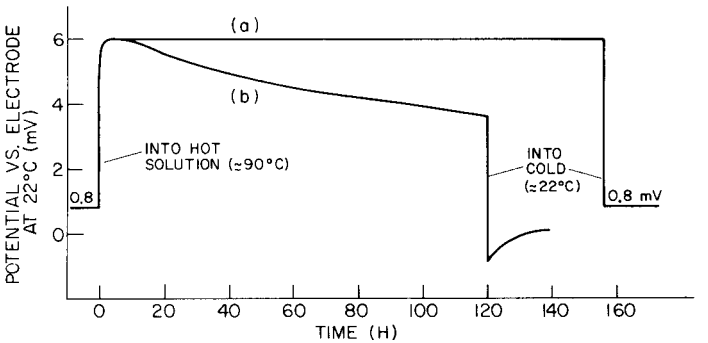

Fig. 6. Thermal drift of Vycor barrier (a) and granular column (476029) (b) reference electrodes.

electrode responded like new (as in Fig. 5, curve a). This suggests that the drift and hysteresis was caused by solid potassium chloride deposited in the column by dehydration of electrolyte, which would have converted the electrode from the 4 M KCl type to a saturated KCl type. The increased solubility of potassium chloride with temperature should result in a negative shift that opposes the primary, positive shift in potential. If precipitation and dissolution of potassium chloride is slow or inhomogeneous, a bimodal drift and hysteresis would occur, as observed. Other evidence favoring this mechanism is that new and aged electrodes had similar potentials at room temperature, but differed significantly (up to 10 mV) at 80°C. This shift in isopotential point is not consistent with a moderate fixed change in chloride concentration, but is readily explained by the increase in KCl solubility with temperature.

By preventing dehydration and other changes, half-cell barriers can pro-

vide enhanced thermal stability. In particular, the Vycor barrier electrode in Fig. 4A proved to be extremely stable at elevated temperatures, showing no drift (±0.1 mV; Fig. 6, curve a) and no evidence of thermal hysteresis before or after prolonged high-temperature ageing.

Because of the potassium-sensing aspect of Nafion membrane, considerable effort was required to arrive at a Nafion barrier configuration which was stable when the electrode was heated. Planar membrane configurations tended to drift, because of hydration and concentration inhomogeneities at the membrane surface. However, the configuration in Fig. 4B was quite stable, probably because the annular window and other construction details allow a more uniform contact to both electrolytes than is afforded by a planar membrane. This electrode drifted only 1.5 mV in 10 days at 90°C, and showed good short-term stability.

Thermal hysteresis in Ag/AgCl electrodes has traditionally been attributed to slow redistribution of the various chloride-complexed silver species after a thermal shift. But this hypothesis is untenable, because it should also apply to new granular column electrodes, which do not show hysteresis. Also, this hypothesis cannot explain hysteresis in aged electrodes, because the quick thermal response of new electrodes shows that the step $AgCl \rightleftharpoons Ag^+ + Cl^-$ is not rate-limiting, and the amount of chloride bound in complexes is insignificant compared to 4 M Cl^-, so that silver ion should remain constant even if the complexes are slow in redistributing. Thus, unlike the case of the calomel electrode, the sometimes poor thermal characteristics of Ag/AgCl electrodes must not be an inherent deficiency of the half-cell.

In conclusion, clogging with silver chloride appears to be a significant factor reducing the performance of Ag/AgCl electrodes. Because junction resistance does not increase appreciably, this clogging is not manifested by increased sensitivity to electrical noise. Most of the flow is lost within a matter of hours in dilute solution. This implies that even refillable Ag/AgCl electrodes are essentially no-flow electrodes. Junction electrolyte must therefore be lost primarily by evaporation through the filling hole rather than by flow out of the junction. This suggests that most "flow-type" Ag/AgCl electrodes would not need filling holes if they did not have them. Junction clogging may also explain why there may be little difference in the kinetic performance of commercial gel and flow-type Ag/AgCl electrodes. Storage of conventional Ag/AgCl electrodes in 4 M KCl is probably advisable as a means of inhibiting the clogging process and optimizing response.

Electrodes with well-designed half-cell barriers can eliminate the problems caused by half-cell species at the junction, and offer other benefits such as enhanced stability and utilizability with non-KCl electrolytes. Conversely, some electrodes which appear to use a pure KCl electrolyte really do not. For example, most calomel half-cells are bridged to the junction electrolyte by fiber connections having a resistance that is too low (typically $<50\ \Omega$) to provide effective diffusional isolation.

Thermal hysteresis can be eliminated in the Ag/AgCl reference. Undoubtedly, the interior half-cells of i.s.e.'s are subject to similar thermal problems. This situation warrants correction, as the erratic thermal response of electrodes may be partly responsible for the widespread lack of confidence in temperature-compensated measurements.

These findings correct most of the deficiencies of the Ag/AgCl half-cell and confine the major remaining problems of practical reference electrodes to the external junction.

REFERENCES

1 A. K. Covington, in R. A. Durst (Ed.), Reference Electrodes in Ion Selective Electrodes, NBS Special Publication 314, National Bureau of Standards, Washington, DC, 1969, pp. 126, 128.
2 K. J. Ellis, Anal. Biochem., 91 (1978) 224.
3 Jenaer Glaswerk Schott und Gen., Mainz, British Patent 894289, 1962.
4 R. C. Weast (Ed.), Diffusion Coefficients in Aqueous Solutions at 25°C, Handbook of Chemistry and Physics, 53rd edn., CRC Press, Cleveland, 1972, p. F47.
5 E. B. Sandell, Colorimetric Determination of Traces of Metals, 3rd edn., Interscience, New York, 1959, p. 816.
6 T. H. Elmer, M. E. Nordberg, G. B. Carrier and E. J. Korda, J. Am. Ceram. Soc., 53 (1970) 171.
7 G. S. Forbes, J. Am. Chem. Soc., 33 (1911) 1937.
8 A. Pinkus and A. M. Timmermans, Bull. Soc. Chim. Belg., 46 (1937) 46.
9 W. G. F. Grot, G. E. Munn and P. N. Walmsley, Perfluorinated Ion Exchange Membranes, presented at 141st National Meeting of the Electrochemical Society, 1975.
10 C. K. Rule and V. K. LaMer, J. Am. Chem. Soc., 58 (1936) 2339.
11 W. N. Carson, Jr., C. E. Michelson and K. Koyama, Anal. Chem., 27 (1955) 472.

Analytica Chimica Acta, 134 (1982) 263—269
Elsevier Scientific Publishing Company, Amsterdam — Printed in The Netherlands

COMPARATIVE STUDY OF DIFFERENT CYANIDE-SELECTIVE AIR-GAP ELECTRODES

J. FLIGIER*, M. GRATZL, G. NAGY and E. PUNGOR

Institute for General and Analytical Chemistry, Technical University, 1502 Budapest (Hungary)

(Received 6th August 1981)

SUMMARY

The characteristics of four solid-state cyanide-selective air-gap electrodes are described. When a minute volume of dicyanoargentate(I) solution was used as electrolyte, the double-Nernstian response to cyanide concentration was obtained only with the sensors based on silver or silver sulphide. Sensors based on silver iodide or a silver sulphide/iodide mixture displayed the normal Nernstian character shown by cyanide-selective electrodes dipped in solution. A theoretical explanation of the results involves the relevant equilibrium equations and the mass balance.

Solid-state cyanide electrodes are well known and commonly used [1—3]. Another kind of cyanide electrode was described by Frant et al. [4]; this is a gas sensor and its operation is based on the reaction $Ag(CN)_2^- \rightleftharpoons Ag^+ + 2CN^-$ with a response of about 118 mV/decade. Recently a very simple version of such a sensor has been reported [5]. Based on the air-gap concept [6], with its advantage of higher selectivity, this sensor consists of an ordinary calomel electrode, a silver wire as indicator electrode, and a minute volume of dicyanoargentate(I) solution as electrolyte. This air-gap sensor has been successfully used for the indirect determination of mercury(II) [7].

The above-mentioned sensors are based on either silver or silver sulphide as the indicator electrode. Because of the different constructions (polymer membrane and air-gap) as well as the different shapes of the indicator electrodes and different membrane materials, it is impossible to estimate and compare their behaviour in gas-sensing systems without suitable experimentation. For this reason, it was decided to test air-gap cyanide sensors based on silver and silver sulphide as well as silver iodide and silver sulphide—silver iodide mixtures. Selection of the same shape of pellets and the same geometrical conditions made it possible to compare these electrodes with respect to reproducibility, drift, calibration characteristics and response time.

*Present address: Institute of Analytical and General Chemistry, Silesian Polytechnical University, 44-101 Gliwice, Poland.

0003-2670/82/0000-0000/$02.75

EXPERIMENTAL

Reagents

Analytical-grade reagents and deionized water were used. A 10^{-3} M potassium cyanide stock solution was standardized potentiometrically with 10^{-2} M silver nitrate solution. The 10^{-4} M dicyanoargentate(I) electrolyte was adjusted to pH 9.3 with 0.1 M sodium tetraborate solution, and 1%(w/w) methyl cellulose was added. The standard solutions were acidified with 1 M tartaric acid.

Apparatus

Radiometer PHM 84 and Radelkis OP-205 pH/mV meters were used with a potentiometric Radelkis OH-814/1 recorder. The calibration graphs were calculated with a Hewlett-Packard 85 desk-top computer.

The silver sulphide, silver iodide and silver sulphide—silver iodide pellets (7-mm diameter) were prepared as described previously [8]. The silver disc was cut from a silver rod (99.99% pure). A hole (2-mm diameter) was drilled excentrically in each pellet and silver disc, which were then mounted on the end of glass tubes by means of epoxy resin.

The air-gap sensors (Fig. 1) consisted of a glass tube (1) closed at one end by the pellet or disc (2). Through the drilled hole was mounted a narrow glass tube (3) partly filled with 1 M potassium chloride solution gelled with agar—agar (4). The Ag/AgCl reference electrode (5) in 1 M potassium chloride solution (6) and the silver wire (7) joined to the pellet by silver-epoxy (8), were connected to the pH/mV meter. A ground-glass joint (9) was mounted at the end of the sensor. A glass conical flask of about 7-cm^3 capacity with a ground-glass joint served as measuring flask, and a piece of sponge soaked in electrolyte served as the electrolyte reservoir. Before use, the surfaces of the pellets were gently polished with Orion abrasive paper.

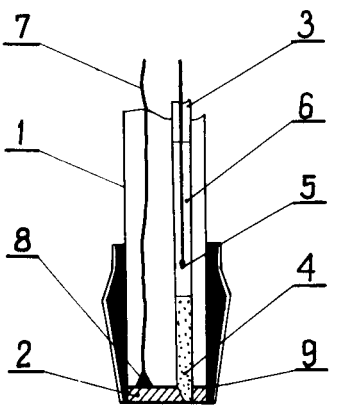

Fig. 1. Construction of the cyanide sensors. For details, see text.

Measuring technique

The electrolyte layer was applied to the electrodes by touching the sponge to the active part of the sensor. Then 5.0 ml of standard solution was pipetted into the measuring flask and 1.0 ml of 1 M tartaric acid was added. The flask was then immediately closed with the sensor and magnetic stirring was started. Steady potentials were read off after 3 min with a precision of 0.01 mV. After each measurement, the electrolyte layer was removed with distilled water, the electrode was dried with paper tissue and a fresh layer of electrolyte was applied. The sensor was stored above 1 M KCl solution in a closed system in order to prevent drying of the agar—agar bridge.

The sensors were used also as common dipped cyanide electrodes in standard cyanide solutions and in titrations of cyanide with silver nitrate solutions.

RESULTS AND DISCUSSION

The four types of solid-state cyanide air-gap electrode investigated were based on silver, silver sulphide, silver iodide, and a silver sulphide—silver iodide mixture. The reproducibility, drift, calibration characteristics and response time found experimentally for each sensor are summarized in Table 1.

The chemical equilibria taking place at the electrode surfaces are as follows. The reaction

$$Ag(CN)_2^- \rightleftharpoons Ag^+ + 2\ CN^-;\ K = [Ag(CN)_2^-]/[Ag^+]\,[CN^-]^2 \qquad (1)$$

with stability constant K, holds for each sensor tested whereas the dissociation (with solubility product K_{so})

TABLE 1

Experimental data characterizing the four different types of cyanide air-gap sensors

		Ag metal	Ag_2S	AgI	Ag_2S/AgI
Reproducibility[a] (mV)		1.75	4.65	1.25	2.69
Drift[b] (% min^{-1})		0.2—0.3	0.2—0.3	0.08—0.1	0.17—0.25
Slope[c] (mV/decade)		−115.9	−103.3	−50.3	−55.9
Linearity[c]		0.999	0.999	0.988	0.986
Standard deviation[c] (mV)		4.8	4.3	6.3	7.5
Response time[d] (s)	95%	6—12	54—84	24—30	24—48
	99%	15—30	96—126	66—84	42—80

[a]Standard deviation for 10 measurements of a 10^{-5} M CN^- solution. [b]% potential decrease of the $E_{max} - E_{baseline}$ value during 1 min. Representative range for 5 measurements with each electrode above a 10^{-4} M CN^- solution. [c]The slope, linearity and standard deviation of the calibration graphs were calculated on the basis of measurements above 10^{-3}, 10^{-4}, 10^{-5} and 10^{-6} M CN^- solutions. Each sensor was calibrated 10 times. [d]10^{-4} M CN^- solution was used. The given time range is a representative value obtained from 10 measurements for each electrode.

$$AgI \rightleftharpoons Ag^+ + I^-; K_{so} = [Ag^+][I^-] \quad (2)$$

holds only for the silver iodide-containing sensors. For both the latter types of sensor, the equilibrium

$$AgI + 2\,CN^- \rightleftharpoons Ag(CN)_2^- + I^- \quad (3)$$

should also be considered. Reaction (3) is, however, the simple algebraic sum of the first two reactions and so expresses no more information than reactions (1) and (2).

The potential of each sensor investigated can be expressed by

$$E = E^0_{el/Ag^+} + S \ln [Ag^+] \quad (4)$$

where E^0_{el/Ag^+} is the standard potential of the respective electrode against silver ion activity, and S is the Nernst factor.

According to reactions (1) and (3), only a double-Nernstian electrode function against cyanide concentration can be interpreted for each sensor. Table 1 shows, however, that this is true only for the sensors that were constructed without silver iodide; the silver iodide-containing sensors gave only a nearly normal Nernstian response.

For the usual, i.e., dipped, type of cyanide electrode based on silver iodide or the silver sulphide—silver iodide mixture, only the normal Nernstian response for monovalent anions was reported [2, 3]. This was interpreted [3, 9] on the basis of the assumptions that there is perfect equilibrium on the membrane surface [1—3], and that linear diffusion of the components takes place in chemical reactions (1) and (2) between surface and electrolyte bulk. These assumptions result [9] is the following expression

$$E = E^0_{el/Ag^+} + S \ln (2K_{so}D_I/D_{CN}) - S \ln [CN^-] \quad (5)$$

where D signifies diffusion coefficient.

In the case of air-gap electrodes, such an explanation of the normal Nernstian response would theoretically also be possible. Thus, because of reaction (3), the silver iodide surface is corroded and diffusion of cyanide to, and of iodide and dicyanoargentate(I) from the membrane surface can occur when the membrane contains silver iodide. Such diffusion does not occur with the silver or silver sulphide electrode. It might be concluded that equilibrium conditions are found with the silver and silver sulphide electrodes and so double-Nernstian response is obtained (reactions 1 and 3), whereas with sensors containing silver iodide, diffusion control predominates and so normal Nernstian response (Eqn. 4) is obtained. This interpretation would, however, be false for the following reasons. First, the response times are of the same order of magnitude in all cases (Table 1). Secondly, a diffusion-controlled response could not be proved by experiments with silver iodide-containing sensors; the electrolyte layer thickness or volume had no effect on the character of the responses. Thirdly, there is also a theoretical argument against this interpretation; the volume of the applied electrolyte was so small

(about 20 μl), that in all cases diffusion should have reached equilibrium after a few minutes, and so the measured steady potentials must correspond in all cases not to almost stationary diffusion but to a complete equilibrium state.

The interpretation must therefore be based solely on equilibria (1—3), and on the laws governing the volatilization of hydrogencyanide from the sample into the air-gap, and the absorption of this gas from the air-gap into the electrolyte. If the Henry law is valid, then for the final volatilization—absorption equilibrium,

$$[CN^-] = k_{vol}k_{abs}[CN^-]_s \qquad (6)$$

where k_{vol} and k_{abs} are the Henry constants corresponding to the volatilization and absorption, respectively, and $[CN^-]_s$ signifies the analytical cyanide concentration in the sample.

In the case of sensors based on silver and silver sulphide, the activity of the dicyanoargentate(I) complex in the electrolyte can be considered as constant, independent of the amount of cyanide absorbed. Thus, from the stability constant of the dicyanoargentate(I) ion with Eqns. (4) and (6)

$$E = E^0_{el/Ag^+} + S \ln \{[Ag(CN)_2^-]/K(k_{vol}k_{abs})^2\} - 2S \ln [CN^-]_s \qquad (7)$$

where the sum of the first two terms gives the standard potential of the air-gap sensor, E^0_{el/CN^-}, its value being constant. This explains the observed double-Nernstian character of the sensors based on silver or silver sulphide.

Equation (7) is, of course, also valid for silver iodide-containing sensors, but in these cases the approximation that the dicyanoargentate(I) complex activity is constant cannot be accepted. Because of reaction (3), the absorbed cyanide can significantly change this activity. In order to calculate this change, it is necessary to establish the complete equilibrium model of the electrode/electrolyte system, where the electrode contains silver iodide.

The mass balance for silver ion is

$$[Ag(CN)_2^-] + [Ag^+] = T + [I^-] \qquad (8)$$

where T is the concentration of dicyanoargentate(I) originally present in the applied electrolyte and $[I^-]$ is equivalent to the amount of silver ion that entered the electrolyte by dissolution of material from the silver iodide membrane.

The complete equilibrium model consists then of Eqn. (8) with the appropriate stability and solubility constants, expressed by the activities corresponding to the equilibrium reached. The unknown variables are $[Ag^+]$, $[I^-]$ and $[Ag(CN)_2^-]$. As three independent equations are available, $[Ag^+]$ can be calculated from them as a function of $[CN^-]$, which is given by Eqn. (6). Insertion of the appropriate constants into Eqn. (8) gives

$$(K[CN^-]^2 + 1)[Ag^+]^2 - T[Ag^+] - K_{so} = 0$$

hence

$$[Ag^+] = T \pm \{T^2 + 4K_{so}(K[CN^-]^2 + 1)\}^{1/2}/2(K[CN^-]^2 + 1)$$

As the pH of the electrolyte is much more alkaline than that of the acidified sample, the absorption of cyanide is favoured and so $[CN^-]$ is at least comparable to $[CN^-]_s$. Thus, $K[CN^-]^2 \gg 1$. Furthermore, $K \gg 1/K_{so}$, and T is also comparable to $[CN^-]_s$. Thus, $T^2 \ll 4K_{so}K[CN^-]^2$, and finally

$$[Ag^+] \approx (K_{so}/K)^{1/2}/[CN^-] \tag{9}$$

Insertion of Eqns. (6) and (9) into Eqn. (4) gives the equilibrium potential, E_{eq}

$$E_{eq} \approx E^0_{el/Ag^+} + S \ln (K_{so}^{1/2}/K^{1/2}k_{vol}k_{abs}) - S \ln [CN^-]_s \tag{10}$$

This means that the absorption of cyanide alters the complex activity in such a way that its effect compensates the double-Nernstian character and transforms it to a nearly normal Nernstian response. By inserting $[Ag(CN)_2^-] = T$ = constant into Eqn. (7), the double-Nernstian function of the tested air-gap sensors containing no silver iodide can be interpreted, whereas by inserting $[Ag(CN)_2^-] \approx (K_{so}K)^{1/2}[CN^-]$, a consequence of Eqn. (9), the nearly Nernstian function of silver iodide-based sensors can be understood.

On the basis of the above explanation, it becomes possible to interpret not only the differences in slope of the calibration graphs, but also the other experimental trends summarized in Table 1. For example, the worse linearity of the calibration graphs for the silver iodide-containing sensors may be due to their non-theoretical mechanisms (see the approximations in the derivation of Eqn. 10), while the very good linearity of the other electrodes is explained by their theoretical behaviour. The greater standard deviations of the silver iodide-based sensors are probably also due to their worse linearity.

As shown in Table 1, the reproducibility is worse for silver sulphide-containing sensors than for the other sensors. This is probably because the sulphide ion activity is not well buffered in the electrolyte layer covering the electrode surface, with the indirect result that the electrode potential is less well defined. Table 1 shows that the drift of the pure silver iodide-based sensor is significantly better than that for any of the other sensors. Like the reproducibility, this again can be interpreted on the basis of buffering effects; in the case of the pure silver iodide membrane, each ionic component of the electrolyte layer is well buffered after the sensor has reached the equilibrium state, whereas with the sulphide-containing membranes the sulphide activity is not well buffered and on the silver electrode the silver ion activity is also not well buffered. This interpretation is strengthened by the fact that the silver iodide-based sensor is best with regard to reproducibility. Such buffering effects have been discussed by Cammann [10].

The response times shown in Table 1 are significantly greater for precipitate-based sensors than for the silver-based sensor. This happens because with the silver-based sensor practically no cyanide is consumed by the dicyano-

argentate(I) complex, whereas with the silver iodide-containing sensors an important amount of cyanide is bound by the silver ions dissolving from the membrane material. Consequently, with nearly similar fluxes and final activities, equilibrium can be reached sooner with the silver-based sensor. This interpretation does not hold for the silver sulphide-based sensor, and its large response times must be due to other unknown effects.

Conclusions

It is well known that cyanide-selective electrodes based on silver iodide respond in the normal Nernstian way because of the non-equilibrium character of the measurement. It was tacitly assumed earlier [3, 9] that if such measurements were possible in the equilibrium state, the double-Nernstian electrode response should be obtained. The air-gap sensors presented here realize this equilibrium type of measurement, but surprisingly they also show the normal Nernstian character. This is easily interpreted if not only the equilibrium law but also the respective mass balance is taken into account.

The experimental results show the superiority of silver metal over the membranes tested as the indicator electrode in such sensors. With silver, the practically unlimited lifetime [5], the ease of forming any shape, and accessibility, are further advantages.

The authors thank Drs. K. Tóth and G. Horvai for advice and valuable discussion during this study.

REFERENCES

1 E. Pungor and K. Tóth, Analyst, 95 (1970) 1132.
2 W. Jaenicke, Z. Elektrochem., 55 (1951) 648.
3 G. P. Bound, B. Fleet, H. von Storp and D. H. Evans, Anal. Chem., 45 (1973) 788.
4 M. S. Frant, J. M. Riseman and J. A. Krueger, U.S. Patent 3950231, April 13, 1976.
5 J. Fligier, P. Czichon and Z. Gregorowicz, Anal. Chim. Acta, 118 (1980) 145.
6 J. Růžička and E. H. Hansen, Anal. Chim. Acta, 69 (1974) 129.
7 P. Czichon, J. Fligier and Z. Gregorowicz, Anal. Chim. Acta, 126 (1981) 221.
8 E. Pungor, J. Havas, K. Tóth and G. Madarász, Hungarian Patent 152106, 1964.
9 A. Hulanicki and A. Lewenstam, Talanta, 24 (1977) 171.
10 K. Cammann, Das Arbeiten mit Ionenselektiven Elektroden, Springer Verlag, Berlin, 1977, pp. 62—64.

Analytica Chimica Acta, 134 (1982) 271—281
Elsevier Scientific Publishing Company, Amsterdam — Printed in The Netherlands

ATOM-TRAPPING ABSORPTION SPECTROMETRY WITH WATER-COOLED METAL COLLECTOR TUBES

J. KHALIGHIE, A. M. URE and T. S. WEST*

The Macaulay Institute for Soil Research, Craigiebuckler, Aberdeen AB9 2QJ (Gt. Britain)

(Received 31st July 1981)

SUMMARY

Water-cooled metal collector tubes for atom-trapping atomic absorption spectrometry in air—acetylene flames are discussed, particularly for the more volatile elements such as cadmium and selenium which may be less efficiently trapped at the hotter surface of a silica tube. It was found that a nickel tube gave 3 times greater sensitivity than silica for the determination of cadmium but was only half as sensitive for the determination of selenium. No atomic absorption signal for copper could be obtained with a nickel collector tube. A copper tube was 3—4 times more sensitive than nickel for cadmium and selenium. Similar effects were observed for cadmium solutions containing 1000 ppm copper or nickel, and for selenium solutions containing 1000 ppm copper, with silica atom-trap tubes, but in both cases better results were obtained when the analyte solution of cadmium or selenium contained the co-element (1000 ppm) than when the cadmium or selenium was measured with a silica tube previously metallized with the co-element.

In previous papers [1—3] the use of a water-cooled silica tube has been described as an atom-trap for different elements in measurements by atomic absorption spectrometry (a.a.s.). Gains of 60, 18, 50, 48, 3 and 80-fold were obtained in the sensitivities (characteristic concentrations) of As, Cd, Cu, Pb, Se and Zn respectively [1, 3].

The work reported in this paper describes the use of titanium, nickel and copper tubes as collectors in place of silica. These were investigated because it was anticipated that the surface temperature of a water-cooled metal tube in an air—acetylene flame would be lower during the collection cycle of atom-trapping a.a.s. because of the higher thermal conductivity of metals relative to silica. It was expected that this could improve the trapping of elements with low melting or vaporization temperatures, e.g. cadmium. But, for the same reason, it was expected that the release of trapped species during the second cycle would be slower and would probably result in broader as well as later peaks. Additionally, complications might be expected from the formation of inter-metallic compounds between the metals deposited from the flame and the metal of the tube.

EXPERIMENTAL

Measurements were made with the same equipment described in the previous papers [1—3]. The position of the 4-mm (o.d.) metallic collectors was the same as that used with the silica tube, i.e., 5 mm above the primary reaction zone of the air—acetylene flame burning on the adapted burner head of a Varian-Techtron AA6 spectrometer. Slits were not used in these experiments to restrict the optical beam to the region of highest atomic density, though this would have resulted in greater sensitivity as noted previously [3].

RESULTS AND DISCUSSION

Use of titanium and nickel tubes as collectors

Titanium and nickel were chosen because of their inert nature, their availability and their relatively high melting and boiling points (for nickel, m.p. = 1453°C, b.p. = 2732°C; for titanium, m.p. = 1675°C, b.p. = 3260°C). Nickel has been used widely in the Delves cup a.a.s. technique [4] and has been shown to have a reasonably long life in air—acetylene flames.

The use of a titanium tube (4 mm o.d.) proved to be unsatisfactory because it distorted after only one or two trapping/release cycles in the flame and rapidly became too deformed for further use. Its sensitivity for copper was less than that obtained with a silica tube.

A nickel tube (4 mm o.d.) also became somewhat deformed in the flame but the effect was not serious enough to prevent repetitive measurements.

Determination of copper. Attempts to determine copper with a nickel tube were not successful. No atomic absorption signal was obtained after collection of copper and when concentrations $\geqslant$1000 ppm were used for 1 min, a rusty brown deposit appeared on the surface of the nickel tube. This disappeared when the tube was heated in the flame but, even so, no atomic absorption signal for copper was obtained.

Difficulties have been reported during the determination of copper in the presence of large amounts of some other metals using flame-assisted methods [5, 6]. Lund et al. [5], for example, used an electrochemical pre-concentration technique in which the copper was deposited electrolytically on a thin platinum wire which was then heated in an air—acetylene flame. They were not able to detect copper and reached the conclusion that this could be due to slow vaporization of the metal from the filament rather than poor atomization in the gas phase. They supported their conclusion by reference to the ease with which copper may be determined in an air—acetylene flame in the normal a.a.s. technique; yet it is well known that copper forms a low melting alloy with platinum. Ward et al. [6], using a micro-sampling nickel cup, reported that this method was insensitive for copper when an air—acetylene flame was used, but it became quite sensitive with the hotter and more strongly reducing nitrous oxide—acetylene flame.

To test the effect of interferences of nickel on copper in atom-trapping, a mixture from 1 ppm Cu and 1000 ppm Ni was collected on a silica tube, but no atomic absorption signal arising from release of copper atoms was obtained. Similarly when 1 ppm Cu was collected on a silica tube already coated with nickel, there was again no copper signal. It should be mentioned, however, that excess of nickel (1000 ppm) does not interfere with copper signals in conventional a.a.s.

Determination of cadmium. The nickel tube proved to be a sensitive collecting and releasing surface for cadmium and an enhancement of 83—132% relative to silica was obtained when 0.1 ppm Cd was collected on a nickel tube for different lengths of time. Figure 1 (A and B) shows high-speed (600 mm min^{-1}) recorder traces of cadmium absorbance peaks obtained

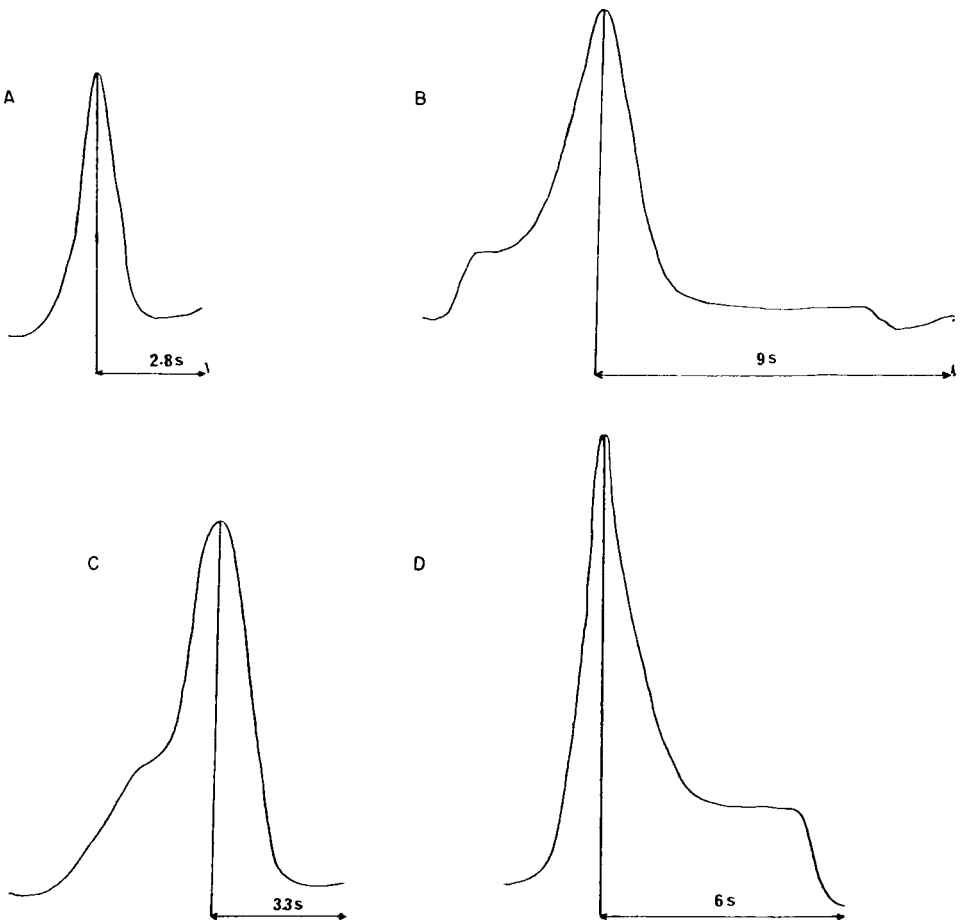

Fig. 1. Cadmium signals showing peak signal time t_P (in seconds): A, with silica tube; B, with nickel tube; C, with nickel-coated silica tube; D, when Cd is collected in presence of 1000 ppm Ni on a nickel-coated silica tube.

upon release from silica and nickel tubes. It can be seen that the peak signal time, t_P, for cadmium occurs at 9 s when the nickel tube is used, whereas for silica it occurs at 2.8 s.

Cadmium has fairly low melting and boiling points, and its trapping efficiency must, therefore, depend on keeping the surface temperature of the collector tube fairly low. It would be expected that in the flame the surface temperature of the water-cooled nickel tube would be considerably lower than that of a silica tube because of the better thermal conductivity of the metal. This was confirmed by the observation that the temperature of the water emerging from a silica tube in an air—acetylene flame rose by 1—2°C whilst for the nickel tube there was an increase of 4°C. This may also explain the slower release of cadmium from the nickel tube.

To investigate the effect of the presence of nickel on cadmium during collection and/or release, 0.1 ppm Cd was collected for 0.5—2 min on the silica tube (step 1), then a mixture containing 0.1 ppm Cd and 1000 ppm Ni was collected for the same time (step 2), and finally 0.1 ppm Cd was collected on the nickel-coated silica tube (step 3). After each step the cadmium was released and the absorbance measured. The results (Table 1) show that the best signal is obtained when the 0.1 ppm Cd—1000 ppm Ni mixture is used. Under the conditions used in step 2, the silica tube is effectively a nickel-coated tube after a short time. It has been shown [3] that large amounts of vanadium and copper also enhance the sensitivity for cadmium in the atom-trapping technique by a similar factor of 2—3.

The nature of the nickel species on the surface of the silica tube was examined by x-ray diffraction. The results showed the existence of Ni, NiO, and, possibly, some NiSi.

Figure 1 (C and D) shows high-speed (600 mm min^{-1}) recorder traces of the absorbance peaks obtained for 0.1 ppm Cd alone and for the 0.1 ppm Cd—1000 ppm Ni mixture released from the nickel-coated silica tube. Table 2 compares peak signal times, t_P, for cadmium with the normal silica tube and the nickel-coated silica tube, and for the Cd—1000 ppm Ni mixture

TABLE 1

Collection of 0.1 ppm Cd as a function of time with and without 1000 ppm Ni

Collection time (min)	Peak absorbance (228.8 nm)				
	0.1 ppm Cd on silica tube (step 1)	0.1 ppm Cd + 1000 ppm Ni on silica tube (step 2)	Enhancement factor[a]	0.1 ppm Cd on Ni-coated silica tube (step 3)	Enhancement factor[a]
0.5	0.090	0.270	3	0.220	2.4
1.0	0.150	0.460	3	0.340	2.3
2.0	0.225	0.800	3.5	0.500	2.2

[a]Relative to step 1, i.e., 0.1 ppm Cd on silica tube.

also on a nickel-coated silica tube. When the data in Tables 1 and 2 are arranged in order of decreasing peak signal time, t_p, and sensitivity for cadmium, the sequence is as follows: 0.1 ppm Cd—1000 ppm Ni (silica tube) > 0.1 ppm Cd (Ni-coated silica tube) > 0.1 ppm Cd (silica tube). These results suggest that excess of nickel probably interacts with the volatile cadmium species to form a more easily trapped, less volatile, Cd—Ni species with a longer release time and (or alternatively) that metallization of the silica surface by nickel alters the thermal characteristics of the tube—flame interface. It should be mentioned that excess of nickel (1000 ppm) does not affect cadmium (0.1 ppm) signals in conventional a.a.s.

Determination of lead, selenium and zinc. The nickel tube appeared to be less sensitive than a silica tube for determinations of lead, selenium and zinc; depressions of ca. 30%, 50% and 20% in sensitivity were obtained, respectively. The interference of nickel on selenium has been reported in carbon-furnace a.a.s. [7]; the addition of nickel solution to a sample containing selenium converted the latter to a much less volatile nickel selenide in the furnace. In the present work, the effects of excess of nickel (1000 ppm) on 10 ppm Se were studied with a silica tube collector: only small irreproducible signals were obtained which did not increase with increasing collection time.

Use of a copper tube

Determination of selenium. The thermal stabilization effect of nickel on selenium is not unusual, and the presence of copper results in the formation of a copper selenide which is less volatile than selenium [8]. Accordingly, a copper tube (4 mm o.d.) was used as a collector for selenium and the results were compared with those obtained with silica and nickel tubes. Figure 2A shows that the copper tube is much more sensitive than nickel and silica tubes for selenium. High-speed recorder traces (Fig. 2B, C) of the absorbance peaks obtained for 10 ppm Se with copper or nickel collector tubes show that the copper tube takes longer to release the selenium species than the nickel tube; the latter releases a rather small amount of selenium almost immediately. These results suggest that in the formation of inter-metallic compounds (Se—Cu or Se—Ni), the order of volatility is Se > Se—Cu > Se—Ni, and that the Se—Ni adduct is so involatile that the small initial

TABLE 2

Comparison of peak signal time, t_p, for cadmium with a silica tube and a nickel-coated silica tube in the absence and presence of 1000 ppm Ni

Cd solution	Collector	t_p(s)
0.1 ppm Cd	Normal silica tube	2.8
0.1 ppm Cd	Ni-coated silica tube	3.3
0.1 ppm Cd + 1000 ppm Ni	Silica tube	6.0

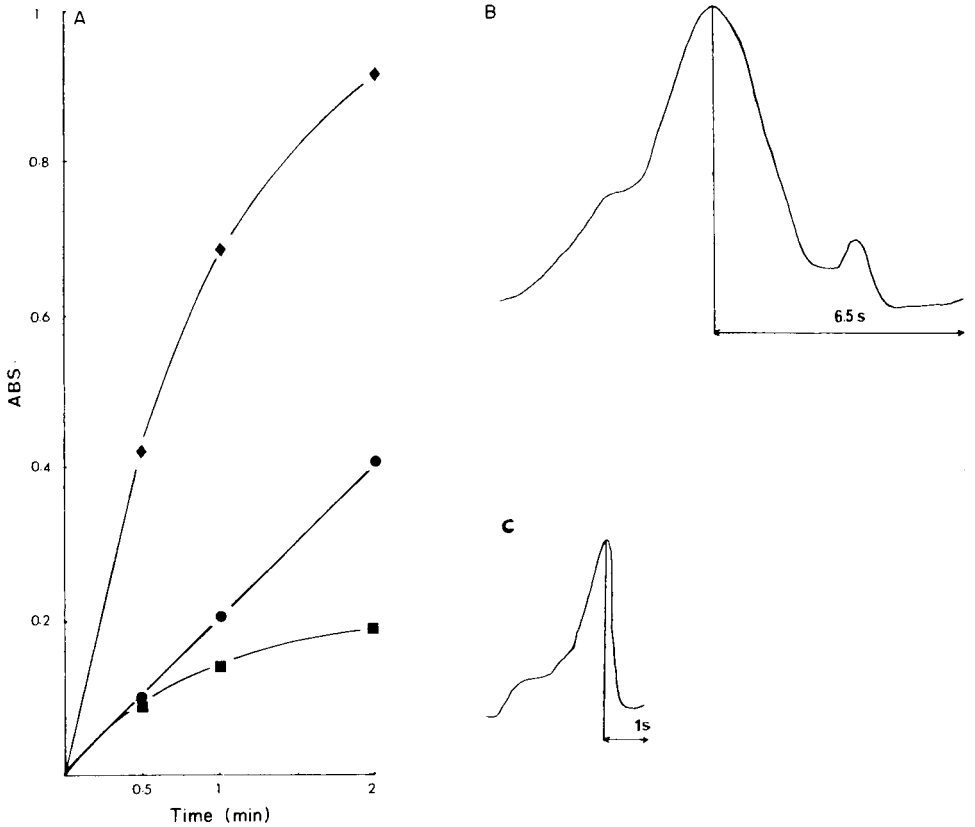

Fig. 2. A, Variation of signal for 10 ppm Se with collection time on copper (♦), silica (●), and nickel (■) tubes. B, Se signal with copper tube. C, Se signal with nickel tube.

signal obtained for selenium (with the nickel tube) is probably due only to free selenium trapped near the cool flame edges of the nickel tube and released on heating the bulk of the tube. It should again be noted that neither 1000 ppm Ni nor 1000 ppm Cu affects the signal for 10 ppm Se in conventional a.a.s.

Determination of cadmium. A copper tube appeared to be equally as sensitive as nickel for the collection and/or release of cadmium. The peak signal time, t_P, for cadmium with the copper tube occurs at 6.5 s which is later than that obtained with the silica tube (2.8 s). A disadvantage of the copper tube is that it tends to bend more than nickel on being successively heated and cooled.

The effect of a cold nickel tube in the flame

In view of earlier observations [3] on the effect of a cold silica tube on the a.a.s. of As, Cd and Se, further experiments were carried out to investi-

gate the effect of a cold nickel tube on the population of the free atoms in the flame gases. Table 3 shows the results obtained for measurements of absorption of the incident light beam by the free atoms [1] of different elements above and below the cold nickel and silica tubes in an air—acetylene flame using the following standards: 10 ppm As, 0.1 ppm Cd, 1 ppm Cu, 2 ppm Pb, 10 ppm Se and 0.1 ppm Zn. It can be seen that the behaviour of most elements is similar for the two collector tubes.

The effects of a cold copper tube and nickel interference on the distribution of free selenium atoms in the air—acetylene flame

A copper tube is very sensitive as a collecting and releasing surface for selenium (compared with nickel or silica tubes), as shown above. It was decided, therefore, to study the behaviour of free selenium above a cold copper tube and compare it with the results obtained with nickel and silica tubes. A 10 ppm Se solution was used as the standard. Figure 3 shows that the population of free selenium atoms is much less in the presence of a cold copper tube than with a nickel or a silica tube (especially just above the cold tube), i.e., the efficiency of trapping is greatest with copper.

It was mentioned above that no absorption signal arising from the release of atomic selenium was obtained when selenium was collected in the presence of excess of nickel on a silica tube. The effect of excess of nickel on the distribution of selenium atoms in the flame gases around a collector tube was therefore tested as follows. First, a 10 ppm Se solution was aspirated into the flame in the presence of a cold silica tube and the atomic absorption signal of selenium was measured at different burner heights (step 1), then a mixture containing 10 ppm Se and 1000 ppm Ni was aspirated (step 2) and finally 10 ppm Se was aspirated again with the nickel-coated silica tube (step 3). Figure 4 shows that the density of selenium atoms decreases in the presence of the nickel-coated silica tube (step 3) and that the effect is most marked just above the cold tube. But, when excess of nickel is present in the

TABLE 3

The absorbance of free atomic species above and below cold nickel and silica tubes

Burner assembly height scale setting (mm)	Nickel tube						Silica tube					
	As 193.7 (nm)	Se 196.0 (nm)	Cu 324.8 (nm)	Zn 213.9 (nm)	Pb 217.0 (nm)	Cd 228.8 (nm)	As 193.7 (nm)	Se 196.0 (nm)	Cu 324.8 (nm)	Zn 213.9 (nm)	Pb 217.0 (nm)	Cd 228.8 (nm)
0 Above tube	0.015	0.044	0.047	0.040	0.035	0.014	0.020	0.090	0.047	0.027	0.042	0.025
5 Above tube	0.042	0.056	0.051	0.042	0.038	0.017	0.052	0.130	0.045	0.030	0.047	0.030
7 Above tube	0.065	0.069	0.053	0.042	0.038	0.018	0.105	0.160	0.037	0.030	0.055	0.032
	Zone of obscuration											
15 Below tube	0.055		0.085	0.052	0.060		0.035	0.050	0.080	0.042	0.060	0.025
16 Below tube		0.042	0.080	0.047	0.060	0.018						
17 Below tube	0.040		0.070	0.047	0.050	0.016	0.030	0.040	0.065	0.038	0.045	0.025

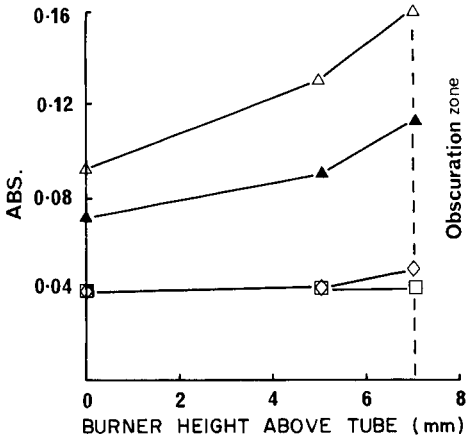

Fig. 3. Population of selenium atoms at different burner heights with cold silica (△), nickel (▲) and copper (□) tubes. These results are compared to those obtained in conventional a.a.s. (◇).

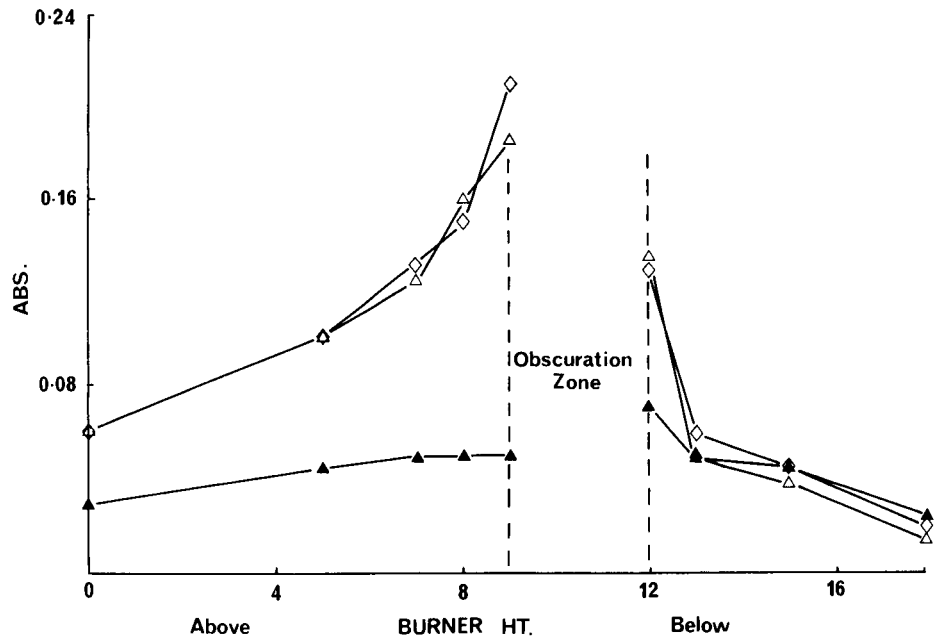

Fig. 4. The effect of excess of nickel on the population of selenium atoms using a cold silica tube: (△) 10 ppm Se with the silica tube; (◇) 10 ppm Se + 1000 ppm Ni with the nickel-coated silica tube; (▲) 10 ppm Se with the nickel-coated silica tube.

selenium standard (step 2), despite the silica tube being coated with nickel, the distribution of atoms is more or less the same as that obtained for selenium alone with the normal silica tube (step 1).

The above results indicate that when 10 ppm Se alone is aspirated into the flame in the presence of a cold nickel-coated silica tube, the nickel species deposited on the tube probably trap a high proportion of the selenium species in the flame gases passing around the tube and that when excess of nickel is present in the selenium solution (step 2) the resultant Se—Ni mixture behaves differently from selenium alone toward the nickel-coated tube. This suggests that either the trapping efficiency of the Se—Ni adduct is less than that obtained for selenium alone or that the presence of nickel in the selenium solution enhances the atomization of selenium. This second possibility may largely be discounted because excess of nickel does not affect the sensitivity of selenium in conventional a.a.s.

The effects of excess of copper, nickel and vanadium on the distribution of free cadmium atoms around a cold silica tube in an air—acetylene flame

Investigations on the effects of copper, nickel and vanadium on the cadmium signal showed that these elements enhance the sensitivity of cadmium in the collection technique. Similar experiments were carried out to examine the effects of 1000 ppm Cu, Ni and V on the distribution of cadmium in the flame gases. It may be seen from Figs. 5—7 that when cadmium alone is aspirated around the normal silica tube, the population

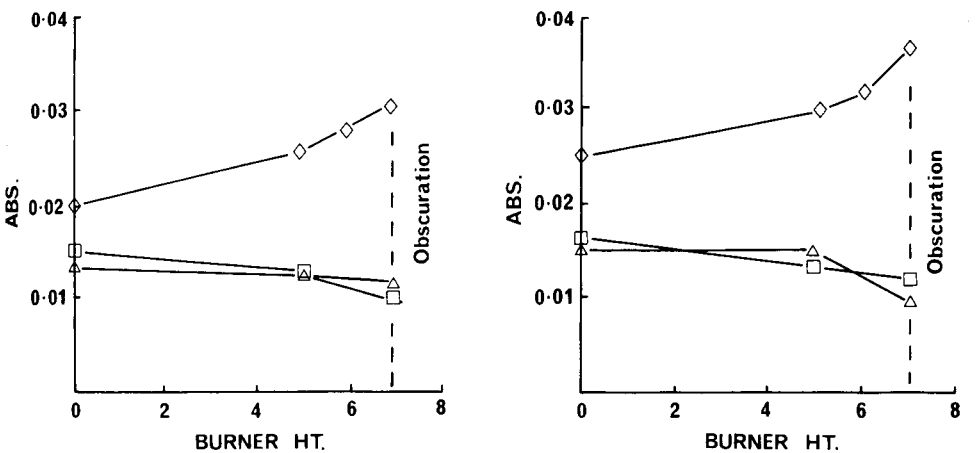

Fig. 5. The effect of excess of nickel on the population of cadmium atoms with a cold silica tube: (◇) 0.1 ppm Cd with the normal silica tube; (△) 0.1 ppm Cd + 1000 ppm Ni with the nickel-coated silica tube; (□) 0.1 ppm Cd with the nickel-coated silica tube.

Fig. 6. The effect of excess of copper on the population of cadmium atoms with a cold silica tube: (◇) 0.1 ppm Cd on the silica tube; (□) 0.1 ppm Cd + 1000 ppm Cu on the copper-coated silica tube; (△) 0.1 ppm Cd on the copper-coated silica tube.

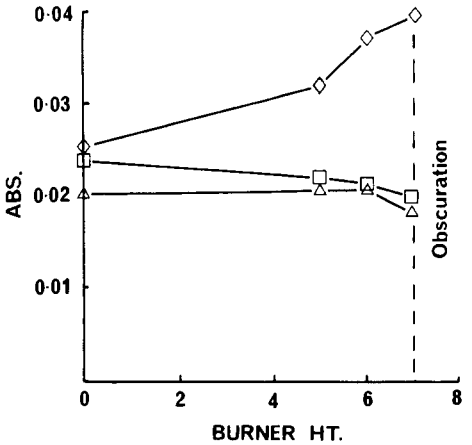

Fig. 7. The effect of excess of vanadium on the population of cadmium atoms with a cold silica tube: (◇) 0.1 ppm Cd on the silica tube; (△) 0.1 ppm Cd + 1000 ppm V on the V_2O_3-coated silica tube; (□) 0.1 ppm Cd on the V_2O_3-coated silica tube.

of free cadmium increases as the light beam approaches the top of the cold tube, but once the tube is coated with Cu, Ni or V species, free cadmium apparently behaves in a different manner, i.e., the population of free cadmium decreases with increasing proximity to the top of the collector tube.

This indicates that more cadmium atoms are trapped by a Cu, Ni or V_2O_3-coated silica tube than by an untreated one. It is probable that during the collection cycle, trapped atoms of some volatile elements such as cadmium are liberated to some extent and provide an appreciable signal in the flame gases just above the cold tube. But, if the tube is coated with, for example, nickel, an intermediate Cd—Ni compound is probably formed around the tube and this retains most of the cadmium atoms during collection but liberates them during the release cycle.

Conclusions

Nickel or copper collector tubes may be used in place of silica for atom-trapping a.a.s. A nickel tube provides ca. 3 times better sensitivity than silica for the determination of cadmium and the signal peaks at a later time. A silica tube precoated with nickel by flame deposition is almost equally effective and exhibits an earlier peak signal time close to that of an uncoated silica tube. The nickel tube gives poor sensitivity for selenium and is less sensitive than silica for lead and zinc. However, a copper collector tube also provides 3—4 times better sensitivity for cadmium than a silica tube and about 4 times better sensitivity for selenium. A copper-coated silica tube behaves in an equally suitable manner and gives quicker release times. It may be concluded that copper and nickel metal collector tubes or the correspondingly metallized silica tubes, prepared by pre-aspiration of 1000 ppm

solutions of copper or nickel, have advantages for the collection and release of volatile elements such as cadmium or selenium for measurement by atom-trapping a.a.s., but attention must be paid to their ability to trap some other species in forms which do not subsequently yield free atoms in the release cycle.

REFERENCES

1 J. Khalighie, A. M. Ure and T. S. West, Anal. Chim. Acta, 107 (1979) 191.
2 J. Khalighie, A. M. Ure and T. S. West, Anal. Chim. Acta, 117 (1980) 257.
3 J. Khalighie, A. M. Ure and T. S. West, Anal. Chim. Acta, 131 (1981) 27.
4 H. T. Delves, Analyst, 95 (1970) 431.
5 W. Lund, Y. Thomasson and P. Davie, Anal. Chim. Acta, 93 (1977) 53.
6 A. F. Ward, D. G. Mitchell and K. M. Aldous, Anal. Chem., 47 (1975) 1656.
7 R. D. Ediger, Perkin-Elmer Atomic Absorption Study No. 550 (1973), presented at the Easter Analytical Symposium, New York, November 1973.
8 R. D. Ediger, At. Absorpt. Newsl., 14 (1975) 127.

Analytical Chimica Acta, 134 (1982) 283—291
Elsevier Scientific Publishing Company, Amsterdam — Printed in The Netherlands

DETERMINATION OF TRACE METALS IN ESTUARINE SEDIMENTS BY GRAPHITE-FURNACE ATOMIC ABSORPTION SPECTROMETRY

R. E. STURGEON*, J. A. H. DESAULNIERS, S. S. BERMAN and D. S. RUSSELL

Division of Chemistry, National Research Council of Canada, Montreal Road, Ottawa, Ont. K1A OR9 (Canada)

(Received 16th June 1981)

SUMMARY

A simple and rapid acid digestion method for the decomposition of estuarine sediments is described. Quantitative recovery of Cd, Pb, Cu, Ni, Co, Be and Co is demonstrated. Sensitive, precise and accurate determination of these trace metals by graphite-furnace atomic absorption spectrometry in combination with the L'vov Platform provides an interference-free technique that permits calibration with simple aqueous solutions of metal standards. The accuracy of the method has been confirmed by analysis of two marine sediment reference materials, MESS-1 and BCSS-1.

Restricted disposal of sediments containing unacceptable materials is required by current regulations of the Department of the Environment in Canada [1]. Of particular environmental significance are toxic organic compounds (organohalogens) and trace heavy metals (notably cadmium and mercury). Sediments form a sink for soluble trace metals that parallels the pollution history and may reflect the trace metal content of the overlying water [2—6].

Of the myriad trace metal determinations carried out on sediments each year, little is known about the accuracy of the data, largely because of a lack of a sufficient number of well-characterized and representative standard reference materials. This problem was particularly evident in a recent interlaboratory quality control study [7] in which six out of eleven research and commercial laboratories produced unacceptable cadmium data, with levels being an order of magnitude greater than the accepted values for the test samples in some cases. As part of the National Research Council of Canada Marine Analytical Standards Program, this laboratory recently prepared two near-shore marine sediment reference materials, MESS-1 and BCSS-1. The sediments were obtained from the Gulf of St. Lawrence; MESS-1 was obtained from the Miramichi River estuary and BCSS-1 was obtained from the Baie des Chaleurs. Reliable results for twelve major and minor constituents as well as thirteen trace metals are available (Marine Analytical Chemistry Standards Program, marine sediment reference materials MESS-1 and BCSS-1, available from Division of Chemistry, National Research Council of Canada). These

reference materials are primarily intended for use in the calibration of procedures and the development of methods for use in analyses of marine sediments and other materials of similar matrix composition. Graphite-furnace atomic absorption spectrometry (g.f.a.a.s.) played a significant role in this project because its high sensitivity allowed the facile determination of cadmium, lead, and beryllium amongst other elements.

In this work, several approaches were used to evaluate the accuracy and precision of the results obtained by g.f.a.a.s. procedures. Three approaches to the analysis of dissolved sediments by g.f.a.a.s. were taken: (1) trace metals were determined by the method of standard additions after their extraction from a solution of the dissolved sediment with ammonium pyrrolidine dithiocarbamate/methyl isobutyl ketone (APDC/MIBK); (2) standard addition analyses were also made by injecting aliquots directly into the furnace; and (3) by direct comparison of the signals from the sediment solution with those from a calibration curve prepared from metal standards in deionized water. Results obtained by g.f.a.a.s. were intercomputed to assess precision and also compared to the accepted values for these sediments to assess the accuracy of these approaches. This report presents a detailed description of the procedures which permitted the accurate determination of Cd, Pb, Co, Cu, Cr, Ni, and Be in these sediments by g.f.a.a.s.

EXPERIMENTAL

Apparatus and reagents

A Varian-Techtron atomic absorption spectrometer, model AA-5, fitted with a Perkin-Elmer HGA-2200 graphite furnace and temperature ramp accessory, was used. Simultaneous continuum-source background correction was made on all signals. Sample solutions were delivered to the furnace using a Perkin-Elmer AS-1 autosampler. Absorbance peaks were recorded on a fast-response Speed Servo II strip-chart recorder (Esterline Corp.) and a digital storage oscilloscope (Gould Advance). Pyrolytically coated graphite tubes were used. The L'vov Platform (Perkin-Elmer) was used in conjunction with Perkin-Elmer pyrolytic graphite-coated tracked tubes.

Standard solutions of the elements of interest were prepared by dissolution of the pure metals or their salts. Distilled, deionized water was used for all dilutions as well as wetting and washing steps.

All reagents were purified prior to use. High-purity mineral acids and MIBK were prepared by sub-boiling distillation [8]. Fresh, aqueous 5% (w/v) solutions of APDC were filtered through 0.45-μm membrane filters to remove insoluble material and stripped free of metal impurities by repeated extraction with MIBK.

After their collection from two sites in the Gulf of St. Lawrence, the sediments were freeze-dried, sieved to pass through a No. 120 stainless steel screen (125 μm), blended, and bottled after verification of homogeneity. After bottling, the sediments were irradiated (γ-rays) to minimize effects of bacterial action.

Procedure

All sample preparations were done in a clean laboratory equipped with laminar flow benches and fume cupboards providing a class 100 working environment.

Randomly selected bottles were used for the determinations. Sediment samples (0.5 g), dried to constant weight at 105°C, were placed in 100-ml PTFE beakers and wetted with 4 ml of water. To each was added 5 ml of concentrated hydrochloric acid, 2 ml of concentrated nitric acid and 5 ml of concentrated hydrofluoric acid. The beakers were covered with polypropylene covers and heated for about 2 h at 90° C on a hot plate to effect dissolution. The covers were then removed and the solutions allowed to evaporate slowly to dryness. A further 5 ml of concentrated nitric acid and 2 ml of concentrated perchloric acid were added and the solutions were again evaporated to dryness on a low-temperature hot-plate to complete oxidation of the organic matter. The residues were dissolved in 20 ml of warm 1 M hydrochloric acid. The solutions were filtered through a 0.45-μm membrane filter and diluted to 50.0 ml with water. Total residues were less than 1 mg. Blanks were carried through all steps.

For the g.f.a.a.s. measurements, standard additions and direct comparison with aqueous standards in dilute acids were used. When standard additions were used, the samples were presented to the graphite furnace after chelation and extraction (to remove the trace metals from interfering matrix species), or by direct injection of the diluted sample (to which were added successively larger metal spikes).

For the extraction method, 8-ml aliquots of the dissolved sediment solution were diluted with 30 ml of 10 M HCl. Iron was removed from this solution by extraction of the chloro complex into MIBK [9]. The acidity of the aqueous phase was reduced by evaporation to near dryness and the sample was diluted to 100 ml with water. Aliquots (10 ml) of this solution, diluted to 50 ml with water, were used to prepare a standard additions plot by extracting the samples with APDC/MIBK as described by Sturgeon et al. [10]. After extraction into MIBK, the trace metals were back-extracted into 5.0 ml of 1 M HNO_3. Two blanks were run concurrently with each extraction. The results were subjected to regression procedures to obtain the intercepts.

Standard additions graphs were also prepared by direct injection of the dissolved sediment solution after dilution (by factors of 3—200 depending on the element), and additions of successively larger metal spikes.

For direct g.f.a.a.s., diluted aliquots of the sediment solution were injected and calibration graphs were prepared from aqueous standards with concentration ranges bracketing those of the sample. The L'vov Platform and tracked graphite tube were used for such direct measurements.

Peak heights were used for evaluation in all cases. Scale expansion (5X) was used for the Cr and Co signals when standard additions were used. Scale expansion was also used for the measurements of Cd, Cu, Ni, Co, and Be after direct injections onto the L'vov Platform. Optimum parameters for furnace operation and sample dilution are given in Table 1.

TABLE 1

Conditions for g.f.a.a.s.[a]

Element	λ(nm)	Char temp./time[b]	Atomize temp./time[b]	Sample dilution	
				Standard additions	Direct method[c]
Cd	228.8	450/25	2600/5	3×	10×
Pb	217.0	750/25	2600/5	10×	10×
Cu	324.8	1000/25	2500/5	10×	5×
Ni	232.0	1000/25	2700/5	10×	10×
Co	240.7	1000/25	2700/5	10×	25×
Be	234.9	1000/25	2700/5	25×	25×
Cr	357.9	1000/25	2700/5	100—200×	ND[d]

[a]Continuum-source background correction; 10-μl sample volumes, 100° C drying temperature (130° C for platform); maximum power heating used for Ni, Co, Be and Cr. [b]Temperature is given in °C and time in s. [c]L'vov Platform mounted in tracked tube. Maximum power heating used for Ni, Co and Be. [d]Not determined.

RESULTS AND DISCUSSION

Sediment dissolution

Trace elements in sediments and soils are frequently determined by atomic absorption spectrometry. Such materials have been examined by direct solid-sampling techniques [11] but prior solubilization of representative subsamples is generally undertaken. Solubilization is most frequently effected by either fusion or acid digestion, the latter being preferred for the determination of trace metals in sediments [2, 3, 12—17]. Mineral acids can be obtained sufficiently pure [8] that their use does not introduce any appreciable impurities, and acid decomposition methods, unlike fusion techniques, do not introduce large amounts of salts which can lead to instability as well as result in high instrument background readings.

The matrix and minor constituents of the two sediments are presented in Table 2. Appreciable amounts of aluminum, iron, and titanium as well as organic carbon are present. The acid decomposition procedure resulted in essentially complete dissolution of the sediment (residues <1 mg) with quantitative recovery of all trace metals of interest.

Care was taken to ensure complete oxidation of organic matter during acid dissolution (with perchloric acid) as the organic fraction of marine sediments has been shown to contain significant portions of the total Cd, Pb, and Zn [18]. Following destruction of carbonaceous matter, the sample was taken to dryness in order to remove perchloric acid from the solutions, as its presence has recently been shown to be responsible for many interference effects noted in g.f.a.a.s. [19].

TABLE 2

Matrix and minor constituents of the MESS-1 and BCSS-1 standards

Constituent	Concentration (%)[a]		Constituent	Concentration (%)[a]	
	MESS-1	BCSS-1		MESS-1	BCSS-1
C	2.99 ± 0.09	2.19 ± 0.09	S	0.72 ± 0.05	0.36 ± 0.05
Na_2O	2.50 ± 0.15	2.72 ± 0.21	Cl	0.82 ± 0.07	1.12 ± 0.05
MgO	1.44 ± 0.09	2.44 ± 0.23	K_2O	2.24 ± 0.04	2.17 ± 0.04
Al_2O_3	11.03 ± 0.38	11.83 ± 0.41	CaO	0.674 ± 0.064	0.760 ± 0.074
SiO_2	67.5 ± 1.9	66.1 ± 1.0	TiO_2	0.905 ± 0.028	0.734 ± 0.024
P_2O_5	0.146 ± 0.014	0.154 ± 0.016	Fe_2O_3	4.36 ± 0.25	4.70 ± 0.14

[a]Precision expressed as the 95% confidence interval for an individual result.

The results of blank measurements are given in Table 3. Blanks based on direct injection of a diluted sediment solution by either the method of additions or against a calibration graph prepared from aqueous standards are negligible for all elements. Those arising from extraction procedures are larger by factors of 3—10 for Cd, Pb, and Cu. Extraction blanks are significant only for cadmium and copper, for which they constitute 30% and 10% of the respective indigenous contents of these two elements in the sediment. No attempt was made to extract chromium and beryllium from these samples.

Matrix interferences

The effect of the dissolved sediment matrix on the analytical response for different experimental conditions is shown in Table 4. The response is calculated from the ratio of the signals obtained from metal spikes added to the sediment solution to those given by metal standards in dilute nitric acid. With the exception of lead, the dissolved sediment matrix significantly

TABLE 3

Blank measurements

Element	Direct injection		Chelation—extraction	
	$\mu g\ g^{-1}$	% of total	$\mu g\ g^{-1}$	% of total
Cd	0.008 ± 0.002[a]	3	0.08 ± 0.03[a]	30
Pb	0.23 ± 0.05	1	0.60 ± 0.02	3
Cu	0.15 ± 0.06	0.5	2.0 ± 0.3	10
Ni	<0.05	<0.1	<0.05	⩽0.1
Co	<0.02	<0.2	<0.02	⩽0.2
Be	<0.003	<0.3	ND[b]	—
Cr	<0.003	<0.03	ND	—

[a]Standard deviation (n = 8). [b]Not determined.

TABLE 4

Analytical response

Element	Response ratio (%)[a]		Element	Response ratio (%)[a]	
	Tube wall	L'vov Platform		Tube wall	L'vov Platform
Cd	120 ± 19 (6)[b]	101 ± 9 (11)	Co	128 ± 16 (10)	94 ± 8 (3)
Pb	67 ± 12 (6)	98 ± 10 (15)	Be	133 ± 6 (7)	100 ± 2 (3)
Cu	124 ± 5 (5)	97 ± 2 (3)	Cr	146 ± 19 (10)	ND[c]
Ni	130 ± 10 (7)	97 ± 5 (3)			

[a]Defined as the ratio of the absorbance peak height obtained for a given analyte concentration in the sediment solution to that obtained in dilute nitric acid. [b]Precision expressed as standard deviation, (n) = number of determinations. [c]Not determined.

enhances analyte response when atomization occurs from the tube wall, thereby giving positive interferences. In contrast to this, atomization of samples from the L'vov Platform produces a quantitative response for each analyte with the significant result that sample solutions may be analyzed by direct comparison to simple, aqueous standards. The use of the L'vov Platform provides a definite advantage over atomization from the tube wall in that use of the method of additions (with all its attendant risks and inherent imprecision) may be abandoned. Calibration of sediment solution against aqueous standards is more rapid and inherently more precise.

The L'vov Platform has recently been shown to be capable of significantly reducing matrix interferences in g.f.a.a.s. [20—23]. Because the analyte-vapor experiences greater effective temperatures when atomized from the platform [20], the extent of dissociation of the analyte species as well as matrix components is generally greater with the result that background absorption is also often reduced. The performance characteristics of the L'vov Platform (in the context of its use with these sediment solutions) are given in Table 5. In addition to quantitative response, signals for the volatile elements (Cd and Pb) in the sediment solutions were enhanced in sensitivity when atomized

TABLE 5

Performance characteristics with the L'vov Platform

Element	Sensitivity enhancement	Reduction of background	Element	Sensitivity enhancement	Reduction of background
Cd	3×	1×	Co	1×	3×
Pb	6×	3×	Be	0.2×	3×
Cu	0.3×	1×	Cr	1×	0.2×[a]
Ni	0.5×	15×			

[a]Background arising from continuum emission.

from the L'vov Platform. Copper, nickel and beryllium, however, suffered loss in sensitivity as a result of the slower rate of heating as compared to atomization from the tube wall [22].

Maximum background absorption was generally decreased when the platform was used. However, even in the case of nickel, where a 15-fold reduction was obtained, the background when the sample was atomized from the tube wall did not exceed 0.35 absorbance. Only chromium exhibited more severe background correction problems when the platform was used. This is a result of increased continuum emission from the incandescent platform. For this reason, no attempt was made to determine chromium using platform atomization.

Results for the sediment standards

Tables 6 and 7 show results for the determination of Cd, Pb, Cu, Ni, Co, Be, and Cr in MESS-1 and BCSS-1, respectively. Data obtained by g.f.a.a.s. procedures compare well with the accepted values.

Accepted values have been derived following an extensive analysis by a variety of techniques, including instrumental photonuclear activation analysis, x-ray fluorescence spectrometry, instrumental neutron activation analysis, isotope dilution spark source mass spectrometry, inductively-coupled plasma atomic emission spectrometry as well as flame atomic absorption and graphite-furnace atomic absorption spectrometry. The great majority of the results were obtained in-house with the cooperation of a small number of reliable laboratories.

Statistical analyses of the pooled results from all techniques permitted the calculation of reliable concentrations for major, minor, and trace constituents.

Data presented in Tables 6 and 7 reveal no statistical difference between results obtained by g.f.a.a.s. procedures and accepted values at the 95%

TABLE 6

Comparison of g.f.a.a.s. results with accepted values for MESS-1

Element	Concn. ($\mu g\ g^{-1}$)[a] by different methods			Accepted value
	Standard additions		L'vov Platform	
	Direct injection	Chelation—extraction	Direct injection	
Cd	0.54 ± 0.06 (9)	0.58 ± 0.11 (9)	0.65 ± 0.13 (3)	0.59 ± 0.1
Pb	26.4 ± 2.7 (9)	28.2 ± 6.5 (9)	27.3 ± 1.6 (3)	34.0 ± 6.1[b]
Cu	21.9 ± 2.3 (8)	25.4 ± 3.0 (10)	21.3 ± 1.6 (3)	25.1 ± 3.8
Ni	28.7 ± 2.9 (10)	31.2 ± 4.1 (11)	28.6 ± 4.8 (3)	29.5 ± 2.7
Co	11.7 ± 1.8 (14)	12.2 ± 2.7 (11)	11.7 ± 2.9 (3)	10.8 ± 1.9
Be	1.8 ± 0.2 (8)	ND[c]	1.8 ± 0.1 (3)	1.9 ± 0.2
Cr	70.3 ± 5.0 (6)	ND	ND	71 ± 11

[a]Precision expressed as the 95% confidence interval for a single result. (n) = number of determinations. [b]Accepted value excludes results from g.f.a.a.s. [c]Not determined.

TABLE 7

Comparison of g.f.a.a.s. results with accepted values for BCSS-1

Element	Concn. ($\mu g\ g^{-1}$)[a] by different methods			Accepted value
	Standard additions		L'vov Platform	
	Direct injection	Chelation—extraction	Direct injection	
Cd	0.24 ± 0.04 (9)	0.26 ± 0.10 (3)	0.23 ± 0.03 (3)	0.25 ± 0.04
Pb	22.0 ± 3.0 (6)	22.0 ± 10.1 (3)	20.0 ± 5.4 (3)	22.7 ± 3.4
Cu	15.0 ± 3.4 (3)	16.2 ± 2.2 (4)	14.6 ± 2.5 (3)	18.5 ± 2.7[b]
Ni	54.7 ± 5.1 (7)	56.6 ± 5.0 (5)	53.0 ± 2.2 (3)	55.3 ± 3.6
Co	12.7 ± 3.6 (3)	11.9 ± 6.9 (3)	10.7 ± 1.3 (3)	11.4 ± 2.1
Be	1.1 ± 0.2 (8)	ND[c]	1.1 ± 0.1 (3)	1.3 ± 0.3
Cr	122 ± 7 (6)	ND	ND	123 ± 14

[a, b, c] See footnotes to Table 6.

probability level. The method of additions thus provides an effective approach to sediment analysis in that compensation for all physicochemical interferences can be achieved. More significant, however, is that use of the L'vov Platform completely eliminates such interferences and allows direct calibration against simple aqueous standards.

Results reported for the chelation—extraction analyses of cadmium were corrected upwards by 10% to account for the loss of cadmium, as a chloro complex, during removal of iron from the sediment solution [9].

Dilution of the sediment solution, as outlined in Table 1, was essential for the accurate determination of beryllium and chromium by direct injection techniques using the method of standard additions. Failure to dilute the solution produced low results for these two elements. Dilution of samples for the determination of Cd, Pb, Cu, Ni, and Co was necessary only to reduce the analyte concentration to levels acceptable for g.f.a.a.s. For direct measurements with the L'vov Platform, a further dilution was required for cobalt (Table 1), otherwise high analytical results were obtained for this element. In this instance, the solutions were only diluted 5-fold for copper determinations in an effort to compensate for the reduction in sensitivity which occurred with atomization from the platform (Table 5).

Results for lead in MESS-1 and copper in BCSS-1 obtained by g.f.a.a.s. procedures appear to be biased on the low side of acceptability. (As a consequence, g.f.a.a.s. results for these two elements did not form part of the data pool used to calculate accepted values for these elements.) No systematic error is in evidence, however, as good agreement with accepted values is obtained for lead in BCSS-1 and copper in MESS-1.

Quantitative dissolution and recovery of chromium in both sediments is evident, indicating that complete dissolution of chromium-bearing minerals was achieved and that no significant loss of volatile $CrOCl_2$ species, possibly

formed during sediment digestion in the open beakers [12], occurred. Unfortunately, direct determination of chromium using the L'vov Platform was precluded by high levels of background emission intensity.

Precision of determination, expressed in Tables 6 and 7 as the 95% confidence interval for a single result, reflects the uncertainty involved in the method of decomposition as well as instrument calibration. For g.f.a.a.s. procedures, precision is greatest for direct solution calibrations and least for the chelation-extraction approach. This is not unexpected because of the increased sample manipulation as well as blank correction encountered with extraction procedures. No individual element can be singled out as having consistently poor precision of determination. Precision compares favorably with that reported by others [2, 5, 15, 24] for the determination of these trace metals in sediments.

The proposed method of acid decomposition of sediment is simple, rapid and yields essentially complete dissolution with quantitative recovery of the trace metals Cd, Pb, Cu, Ni, Co, Be, and Cr. Solutions of dissolved sediments, stored at room temperature in polypropylene bottles, were found to be stable for more than 16 months.

REFERENCES

1 Ocean Dumping Control Act, Canada Gazette, Part III, Vol. 1, Queen's Printer for Canada, 1975, Chap. 55.
2 A. J. Coggins, K. D. Tuckwell and R. E. Byrne, Environ. Sci. Technol., 13 (1979) 1281.
3 K. W. Bruland, K. Bertine, M. Koide and E. D. Goldberg, Environ. Sci. Technol., 8 (1974) 425.
4 E. D. Goldberg, E. Gamble, J. J. Griffin and M. Koide, Estuarine Coastal Mar. Sci., 5 (1977) 549.
5 J. Hamilton-Taylor, Environ. Sci. Technol., 13 (1979) 693.
6 J. C. S. Lu and K. Y. Chen, Environ. Sci. Technol., 11 (1977) 144.
7 H. S. Samant, D. H. Loring and S. Ray, Laboratory Evaluation Program First Quality Control Round Robin, Technology Development Report, EPS-4-AR-79-1, Department of Environment, Canada, 1979.
8 R. W. Dabeka, A. Mykytiuk, S. S. Berman and D. S. Russell, Anal. Chem., 48 (1976) 1203.
9 G. H. Morrison and H. Freiser, Solvent Extraction in Analytical Chemistry, J. Wiley, New York, 1957.
10 R. E. Sturgeon, S. S. Berman, J. A. H. Desaulniers and D. S. Russell, Talanta, 27 (1980) 85.
11 F. J. Langmyhr, Analyst (London), 104 (1979) 993.
12 H. Agemian and A. S. Y. Chau, Analyst (London), 101 (1976) 761.
13 H. Agemian and A. S. Y. Chau, Anal. Chim. Acta, 80 (1975) 61.
14 R. T. T. Rantala and D. H. Loring, At. Spectrosc., 1 (1980) 163.
15 S. A. Sinex, A. Y. Cantillo and G. R. Hetz, Anal. Chem., 52 (1980) 2342.
16 H. Heinrichs and J. Lange, Z. Anal. Chem., 265 (1973) 256.
17 H. Uchida, T. Uchida and C. Iida, Anal. Chim. Acta, 116 (1980) 433.
18 E. S. Pilkington and L. J. Warren, Environ. Sci. Technol., 13 (1979) 295.
19 S. R. Koirtyohann, E. D. Glass and F. E. Lichte, Appl. Spectrosc., 35 (1981) 22.
20 B. V. L'vov, Spectrochim. Acta, 33B (1978) 153.
21 W. Slavin and D. C. Manning, Spectrochim. Acta, 35B (1980) 701.
22 D. C. Gregoire and C. L. Chakrabarti, Anal. Chem., 49 (1977) 2018.
23 C. L. Chakrabarti, C. C. Wan and W. C. Li, Spectrochim. Acta, 35B (1980) 547.
24 K. Ohta and M. Suzuki, Talanta, 22 (1975) 465.

Analytica Chimica Acta, 134 (1982) 293—300
Elsevier Scientific Publishing Company, Amsterdam — Printed in The Netherlands

SOLVENT EXTRACTION--FLAME SPECTROMETRIC METHODS FOR THE DETERMINATION OF INDIUM IN ALUMINIUM ALLOYS

A. J. ALLER*
Analytical Chemistry Department, University of Valladolid, Valladolid (Spain)
(Received 13th March 1981)

SUMMARY

Atomic absorption and atomic emission methods for determining trace and minor amounts of indium in aluminium alloys are described. They involve the separation of indium from the aluminium matrix by extraction of indium diethyldithiocarbamate from hydrochloric acid at pH 3, and determination by emission at 451.13 nm or absorption at 303.9 nm in the extract; a nitrous oxide—acetylene or air—acetylene flame is used.

The detection limit for indium by atomic absorption spectrometry (0.05 ppm) [1] is greater than that for atomic emission spectrometry (a.e.s.) with the nitrous oxide—acetylene flame (0.002 ppm); the latter provides a very sensitive and selective determination of indium. However, combinations of a.e.s. and solvent extraction have seldom been used. Gotô and Sudô [2] extracted the indium 8-quinolinolate complex into 4-methylpentan-2-one (MIBK) at pH 4—12 to increase considerably the sensitivity of the indium a.e.s. determination. Potassium or ammonium iodide and 2—2.5 M sulphuric acid solutions and 0.2 M trioctylamine in *o*-xylene or 4-methylpentan-2-one as extractant have been used for indium in steel samples [3]. The iodide complex has been extracted into cyclohexanone from ore solutions [4]. Indium has been extracted from rock and soil samples at pH 1 with hexahydroazepiniumhexamethylenedithiocarbamate [5], and from industrial solutions [6] adjusted to 4.5 M hydrobromic or 1.5 M hydriodic acid. 4-Methylpentan-2-one over the range pH 2—9 may be used to extract indium tetramethylenedithiocarbamate [7].

There are several other papers of interest from the view-point of the extraction processes. Portman and Riley [8] extracted indium diethyldithiocarbamate into ethyl acetate at pH 3—10; others have preferred chloroform [9] and carbon tetrachloride [10]. Indium may be extracted from 5—6 M hydrochloric acid or 4 M hydrobromic acid with mesityl oxide as solvent [11]. Diethyldithiocarbamate (DDTC) has frequently been used as a chelating agent for the determination of heavy metals [12]. The complexed metal ions are extracted into an organic solvent and subsequently

*Present address: Research Laboratory, Polmetasa S.A., Mondragón, Guipuzcoa, Spain.

0003-2670/82/0000-0000/$02.75

determined by atomic absorption spectrometry (a.a.s.). The pH of the aqueous phase influences the extraction, so that pH control is necessary for both complexation and extraction. Diethyldithiocarbamate is unstable in acidic aqueous solutions. Decomposition is favoured when the pH is less than the pK value of the diethylammonium ion. The half-life for decomposition is independent of pH when the solution pH is much less than the pK_a of dithiocarbamic acid (pK_a = 4 for HDDTC) [13]. The half-life is of the order of seconds for HDDTC under acidic conditions [14, 15]. Contradictory reports have appeared concerning the usefulness of DDTC for extractions in the pH range 2—4 [16, 17]. From a practical point of view, the time stability of the various metal complexes after extraction is more important than the decomposition of pure dithiocarbamic acid in aqueous solution.

A need arose here for a reliable atomic absorption and/or emission method for determining traces of indium in a wide range of aluminium alloys. Sodium diethyldithiocarbamate was selected for the separation of indium because it shows no visible reaction with aluminium; 4-methylpentan-2-one and *n*-butyl acetate were selected because of their high extraction capacity and their well-known suitability for aspiration into flames. The proposed methods offer the advantages of high sensitivity and reasonable selectivity.

EXPERIMENTAL

Apparatus, solutions and reagents

A Pye-Unicam SP1900 flame spectrometer was used with the instrumental settings given in Table 1.

Standard indium solution (1000 ppm). Dissolve 0.5000 g of pure indium metal in 20 ml of concentrated hydrochloric acid (d. 1.19), cool and dilute

TABLE 1

Instrumental settings

Parameters	A.e.s.	A.a.s.
Grating	Visible	Ultraviolet
Wavelength (nm)	451.13	303.9
Slit (mm)	0.2	0.2
Burner slit (cm)	N—A (5)[a]; A—A (Meker)[a]	N—A (5)[a]; A—A (10)[a]
Lamp current (mA)	—	5
Burner height (cm)	1	1
Integration time (s)	1	4
Nitrous oxide pressure (kg cm^{-2})	5	5
Acetylene pressure (kg cm^{-2})	0.75	0.62
Nitrous oxide flow (l min^{-1})	5	5
Acetylene flow (l min^{-1})	3.5 (N—A); 0.8 (A—A)	3.5 (N—A); 1.3 (A—A)
Air flow (l min^{-1})	5	5

[a]N—A = nitrous oxide—acetylene; A—A = air—acetylene.

the solution to 500 ml with water. Prepare a 100 ppm solution by suitable dilution just before use.

Sodium-DDTC solution. Prepare an aqueous 1% (w/v) solution freshly as required.

4-Methylpentan-2-one (MIBK) and *n*-butyl acetate were analytical-reagent grade.

Calibration procedure

Into a 250-ml separatory funnel, pipette 5.0 ml of solution containing 0—10 ppm of indium. Add 5 ml of the sodium—DDTC solution and adjust the pH to 3—3.5 with hydrochloric acid or sodium hydroxide. Mix well and adjust the volume to 50 ml with water. Add exactly 20 ml of MIBK or *n*-butyl acetate and shake vigorously for 1 min. Discard the aqueous phase, and spray the organic phase into the flame for measurement of indium by a.e.s. or a.a.s. under the conditions given in Table 1. These solutions are not stable on prolonged standing.

Recommended procedure

Depending on the expected indium content, transfer an accurately weighed (0.2—0.5 g) sample to a 400-ml beaker, cover and add 20 ml of (1 + 1) hydrochloric acid. (If the sample contains little or no acid-insoluble material, it can be decomposed in a teflon beaker by adding 10 ml of hydrofluoric acid and 5 ml of concentrated nitric acid; after complete dissolution, dilute to 50 ml.) After heating to complete dissolution, rinse the beaker well with water, cool to room temperature, and adjust the pH to 3—3.5 with 50% (w/v) sodium hydroxide solution or hydrochloric acid. Transfer the solution to a 250-ml separatory funnel, add 5 ml of the sodium-DDTC solution, dilute to 50 ml if necessary, mix, add 20 ml of MIBK or *n*-butyl acetate, stopper and shake for 1 min. Complete the determination as in the calibration procedure.

RESULTS AND DISCUSSION

Extraction of reagent

Sodium—DDTC solution (50 ml of 1%, diluting to 50 ml) at different pH values was extracted with 20 ml of MIBK or *n*-butyl acetate. After phase separation, the organic phase was shaken with 50 ml of aqueous 5 ppm indium solution for 1 min to allow DDTC to react with the added indium. Atomic absorption and emission measurements of indium were made on portions of each solvent layer. The indium contents indicate the percentage of reagent extracted at the different pH values of the starting sodium—DDTC solution. Table 2 summarizes the results obtained. Some diethyldithiocarbamate is obviously extracted along with the indium—DDTC complex, and the amount extracted is roughly inversely proportional to the hydrogen ion concentration. The effect of excess of DDTC on emission measurements is a minor factor and

TABLE 2

Effect of pH on partition of excess of diethyldithiocarbamate between aqueous and organic phases

pH of aqueous solution	DDTC extracted[a] (%)		pH of aqueous solution	DDTC extracted[a] (%)	
	MIBK	*n*-Butyl acetate		MIBK	*n*-Butyl acetate
1	1.2	1.0	4	4.3	3.7
2	Trace	Trace	5	10.1	8.9
3	Trace	Trace	6	16.0	14.8

[a]Percentage of the amount of DDTC added originally. The values given were obtained by a.e.s. (mean of nine measurements). The results obtained with a.a.s. were similar.

the dependence found represents primarily its effect on the stability of the indium—DDTC complex and on the extraction.

Distribution coefficients and stability of the indium—DDTC complex

The indium method depends on the use of fairly large water-to-solvent ratios in order to achieve concentration as well as separation from bulk constituents. The percentage extraction decreases as the volume ratio increases. Some preliminary tests showed that a water-to-solvent ratio of 5:2 was satisfactory. Approximate distribution coefficients for the indium—DDTC complex were determined by measurements of successive extracts from water spiked with 5 ppm of indium, by means of the recommended procedure. Provided that the distribution coefficient exceeds 10, the ratio of the concentration in any two successive extracts is an approximate measure of the distribution coefficient. The values obtained are shown in Table 3. These values correspond to 99% extraction (*n*-butyl acetate) and to 95% extraction (MIBK).

To study the stability of the complex, a solution containing 5 ppm of indium at pH 3—3.5 was mixed with 5 ml of the 1% (w/v) sodium—DDTC solution, the volume was adjusted to 50 ml with water, and the indium—DDTC complex formed was extracted with 20 ml of MIBK or *n*-butyl acetate. The stability of the complex in the organic solvent was measured by comparing the atomic absorption and emission of these phases with the values for stable solutions of indium in dilute acid at increasing intervals of time. The complex was stable for several hours (Table 3), with slower decomposition in *n*-butyl acetate.

The stability of the indium—DDTC complex at pH 3—3.5 in aqueous solutions was studied by allowing indium solutions (5 ppm) to react with 5 ml of the sodium—DDTC solution (1%), diluting to 50 ml if necessary, and extracting the complex formed into *n*-butyl acetate after various periods of time, for measurements of atomic absorption and emission of indium. The results are shown in Table 4. It is clear that if samples are extracted within 5 min of complex formation and measurements are done within a few hours, no difficulty should be encountered.

TABLE 3

Analytical parameters for the recommended procedures, with extraction into 4-methylpentan-2-one (MIBK) and *n*-butyl acetate

Parameter		MIBK		*n*-Butyl acetate	
		A.e.s.	A.a.s.	A.e.s.	A.a.s.
Distribution coefficient (pH 3.0)		1920	1920	2500	2500
Minimum time for which complex is stable (h)		12	12	72	72
Sensitivity (ppm)	A—A[a]	0.021	0.010	0.015	0.013
	N—A[a]	0.013	0.016	0.009	0.032
Limit of detection[b] (ppm)	A—A[a]	0.16	0.20	0.12	0.22
	N—A[a]	0.11	0.10	0.08	0.10
Standard deviation[c] (ppm)	A—A[a]	0.13	0.08	0.12	0.09
	N—A[a]	0.12	0.11	0.09	0.10
R.s.d.[c] (%)	A—A[a]	2.45	1.59	2.38	1.73
	N—A[a]	2.38	2.18	1.78	1.96
Linear range (ppm)	A—A[a]	0—20		0—10	
	N—A[a]	0—20		0—5	0—10

[a]As in Table 1. [b]The concentration producing a signal equal to twice the background noise. [c]Calculated from 9 results; see text.

Influence of pH on extraction of the indium—DDTC complex

Indium (5 ppm) was extracted from 50 ml of solution adjusted to pH values in the range 2—12 with hydrochloric acid or sodium hydroxide and containing 5 ml of DDTC reagent (i.e., a theoretical 100% excess of reagent) by shaking for 1 min with 20 ml of organic solvent. A portion of the separated organic layer was removed from each funnel, its indium atomic absorption and emission were measured, and the indium concentrations were obtained from a calibration curve prepared from aqueous indium solutions. Figure 1 shows the results obtained by a.e.s.; results by a.a.s. were similar. The reagent was added to the metal ion solution to ensure that any effect of decomposition of the reagent was minimal. It can be seen that maximum extraction is obtained at pH 3—8.

Interferences

The interference of various ions (up to 2 mg ml^{-1}) were tested in the determination of 1 ppm of indium in solutions containing 20 mg ml^{-1} aluminium

TABLE 4

Effect of time on the stability of the indium—DDTC complex in aqueous solution at pH 3

Reaction time (min)	0	1	3	5	8	15	30	60
Indium lost[a] (%)	0.1	0.1	0.2	0.2	1.5	2.4	3.6	6.0

[a]Results obtained by a.e.s.

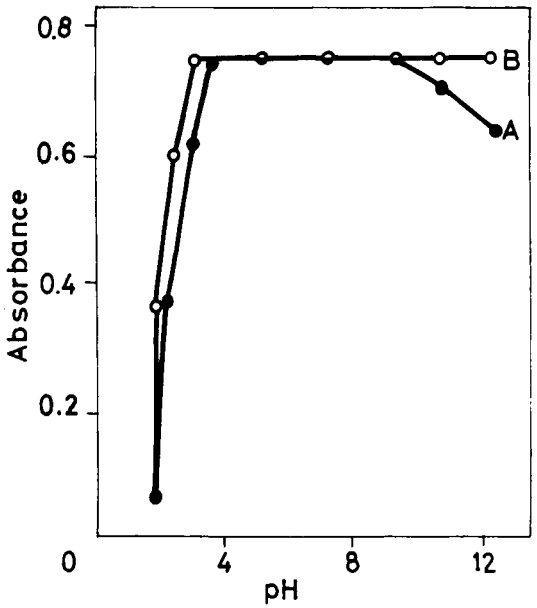

Fig. 1. Effect of pH on the extraction of 5 ppm indium from 50 ml of aqueous phase containing 5 ml of 1% sodium—DDTC solution with 20 ml of organic solvent: (A) MIBK; (B) *n*-butyl acetate.

by the recommended procedure. Hydrogen peroxide interfered with the extraction because of decomposition of the dithiocarbamate. The dithiocarbamates are generally inselective reagents [18] forming complexes with many metal ions, particularly heavy metals. However, Cu(II), Mn(II), Fe(III), Be(II), Tl(I), Ga(III), Si(IV), Bi(III), Cd(II), Ce(III), Co(II), Cr(III), Hg(II), Mg(II), Mo(VI), W(VI), Nb(V), Pb(II), Ni(II), Sb(III), Sn(II), Ti(IV), V(V), Ba(II), Ca(II), Sr(II), La(III) or Zn(II), at 2 mg ml^{-1} concentrations had no effect (<5%) on the indium absorbance in the air—acetylene or nitrous oxide—acetylene flame when *n*-butyl acetate was used. Larger amounts of Fe(III), Zn(II), Sb(III), W(VI) or Mo(VI) caused slightly low results for indium absorbance in the air—acetylene flame when MIBK was used. When the nitrous oxide—acetylene flame was used with MIBK as extractant, only W(VI) interfered.

In the atomic emission of indium, the above-cited elements again did not interfere (up to 2 mg ml^{-1}) in either flame, except for V(V), Mo(VI) and W(VI), which increased the emission of indium when MIBK was used as extractant. The interferences of these elements were less when *n*-butyl acetate was employed. The use of the nitrous oxide—acetylene flame with both extractants is preferable because interfering effects are smaller.

Applications

Under the recommended conditions, the limits of detection and sensitivities (concentrations for 1% absorption or emission) were satisfactory (Table 3).

To test the reliability of the proposed methods, they were applied in the analysis of certified aluminium samples and compared with emission spectrometry. The results (Table 5) are in excellent agreement when done by atomic absorption and emission, and agree well with the certified values and with the results obtained by emission spectrometry. The aluminium samples (Table 5) were certified by Pechiney; for the comparison, a Phillips Quantometer was kindly lent by the National Aluminium Company.

The precision of the method was tested by replicate (nine) determinations on 50 ml of aluminium alloy (L-3710/2) solution containing 5 ppm of indium. The standard deviation and relative standard deviation from the mean are shown in Table 3. The standard deviations in both a.a.s. and a.e.s. are of the same order and close to the intrinsic precision of the employed techniques.

Conclusions

Table 3 shows the parameters obtained in the determination of indium by the recommended a.a.s. and a.e.s. procedures. The a.a.s. sensitivity is improved when an air—acetylene flame is used, whereas the a.e.s. sensitivity is better with the nitrous oxide—acetylene flame. The latter flame is also preferable because there is less interference. The a.a.s. method provides better precision and more freedom from interferences, but the a.e.s. method provides slightly better detection limits. The wider linear calibration range available with MIBK as extractant is probably due to the smaller distribution coefficient. In general, the data given in Table 3 and the results obtained in the interference study indicate that *n*-butyl acetate is the more useful solvent. However, the choice of technique, flame and solvent is not really critical, because there are few aspects in which one choice is clearly superior to the other.

TABLE 5

Determination of indium in aluminium alloys

Designation	Certified value(%) In	Quantometer method	In found (%)[a]			
			A.e.s.		A.a.s.	
			A—A	N—A	A—A	N—A
L-3710/1	0.0280	0.0279	0.0283	0.0281	0.0296	0.0280
L-3710/2	0.0260	0.0264	0.0257	0.0261	0.0263	0.0260
L-3721/1	0.0410	0.0411	0.0400	0.0421	0.0411	0.0418
L-3721/2	0.0375	0.0379	0.0368	0.0370	0.0390	0.0378
L-3731/1	0.0057	0.0062	0.0050	0.0051	0.0061	0.0059
L-3731/2	0.0068	0.0070	0.0071	0.0066	0.0066	0.0068
L-3741/1	0.0372	0.0372	0.0375	0.0371	0.0370	0.0373
L-3741/2	0.0335	0.0336	0.0339	0.0342	0.0338	0.0336
L-3751/1	0.0008	0.0010	0.0009	0.0009	0.0011	0.0007
L-3751/2	0.0021	0.0020	0.0020	0.0022	0.0024	0.0019

[a]0.5-g samples taken; *n*-butyl acetate used as solvent with air—acetylene (A—A) and nitrous oxide—acetylene (N—A) flames.

DDTC is not a selective reagent but when the recommended conditions for pH values and spectrometric parameters are used, selective determinations are possible because any ions extracted into the organic phase do not interfere in the spectrometric measurement. It is possible to improve the extraction by increasing the amount of DDTC, for the absorbance or emission background caused by a large excess of DDTC is not appreciable. The nature of the acids employed in the decomposition of the aluminium matrix, before the extraction of the indium—DDTC complex, does not affect the final results.

The proposed methods are suitable for samples containing $\geqslant 0.0005\%$ of indium. The advantages of the methods lie in their speed, relative freedom from interferences, relatively good precision and high sensitivity.

The author gratefully acknowledges the assistance of Dr. D. Mariano de Andrés of E.N.D.A.S.A. (Valladolid) for his assistance in the collection of the aluminium alloys.

REFERENCES

1 G. F. Kirkbright and M. Sargent, Atomic Absorption and Fluorescence Spectroscopy, Academic Press, London, 1974.
2 H. Gotô and E. Sudô, Jpn. Analyst, 10 (1961) 456.
3 B. Y. Spivakov, V. I. Lebadev, V. M. Shkinev, N. P. Krivenkova, T. S. Plotnikova, I. P. Kharlamov and Yu. A. Zolotov, Z. Anal. Khim., 31 (1976) 757.
4 H. Spitzer and G. Tesik, Erzmetall, 22 (1969) 383.
5 N. I. Tarasevich, G. V. Kosyreva and Z. P. Portugal'Skaya, Vestn. Mosk. Univ. Khim., 16 (1975) 241.
6 N. I. Tarasevich, G. V. Kozyreva, N. P. Ivanov and G. L. Korienco, Vestn. Mosk. Univ. Khim., 12 (1971) 461.
7 C. E. Mulford, At. Absorpt. Newsl., 5 (1966) 88.
8 J. E. Portman and J. P. Riley, Anal. Chim. Acta, 35 (1966) 35.
9 A. Wyttenbach and S. Bajo, Anal. Chem., 47 (1975) 1813.
10 J. Starý and K. Kratzer, Anal. Chim. Acta, 40 (1968) 93.
11 M. B. Chavan and V. M. Shinde, Sep. Sci., 8 (1973) 285.
12 K. Burger, Organic Reagents in Metal Analysis, Pergamon, Oxford, 1973, p. 124.
13 A. Hulanicki, Talanta, 14 (1967) 1371.
14 R. J. Everson and H. E. Parker, Anal. Chem., 46 (1974) 1966.
15 K. I. Aspila, V. S. Sastri and C. L. Chakrabarti, Talanta, 16 (1969) 1099.
16 T. N. Tweeten and J. W. Knoeck, Anal. Chem., 48 (1976) 64.
17 P. Hannaker and T. C. Hughes, Anal. Chem., 49 (1971) 1485.
18 G. D. Thorn and K. A. Ludwig, Dithiocarbamates and Related Compounds, Elsevier, Amsterdam, 1962.

Analytica Chimica Acta, 134 (1982) 301—311
Elsevier Scientific Publishing Company, Amsterdam — Printed in The Netherlands

A RAPID SCREENING PROCEDURE FOR 2-AMINONAPHTHALENE IN NATURAL, SYNTHETIC, AND REFINED CRUDES

BRUCE A. TOMKINS*, VANESSA H. OSTRUM[a], and JOHN E. CATON

Analytical Chemistry Division, Oak Ridge National Laboratory, P.O. Box X, Oak Ridge, TN 37830 (U.S.A.)

(Received 26th June 1981)

SUMMARY

The mutagen, 2-aminonaphthalene, which is the dominant aromatic amine species in several fossil fuels, may be isolated readily by using a sequential high-performance liquid chromatographic procedure. An initial isolation is achieved on a semi-preparative scale aminosilane column and the final separation is completed with a nonpolar stationary phase column on an analytical scale with a pH-adjusted solvent. The use of fluorescence detection permits discrimination (at least 100-fold) against the nonmutagenic isomer, 1-aminonaphthalene. The overall recovery of 2-aminonaphthalene, as determined by scintillation counting of a radioactive 1-aminonaphthalene tracer, typically exceeds 50% and can reach 92% depending on both the sample matrix and the solubility of the isolate in acetonitrile. The minimum detectable quantity is 0.06 $\mu g\ g^{-1}$ of crude sample.

Several authors [1—3] have reported the presence of polycyclic aromatic amines (PAA) in synthetic fuels. These compounds, while usually present in trace quantities, are significantly more mutagenic [1, 4] on a weight to weight basis than the often-studied polycyclic aromatic hydrocarbons (PAH), and represent the determinant mutagens in some coal-derived materials. Consequently, there is a pressing need for valid but facile methods to determine routinely PAA in synthetic, natural, and refined fossil fuels.

In the quantification of PAA in energy-related materials, the sample may present handling difficulties, the individual components are typically present at trace levels, and there may be over one hundred amine species in a typical sample. For these reasons, it is advantageous to determine representative "marker" amines, which may represent the PAA in general and allow samples to be selected for more detailed study.

Recent papers, which described the determination of individual amines in coal-, shale oil-, and petroleum-derived products [5, 6] suggested that 2-aminonaphthalene would be an appropriate PAA marker. This species was a reasonable choice because of its well-known mutagenicity and carcinogenicity, its occurrence in all samples tested (within the detection limit of the method),

---

[a]Present address: University of Tennessee, U.S.A.

0003-2670/82/0000-0000/$02.75

and its presence as the major PAA species in these samples. The biological effects of 2-aminonaphthalene have been extensively documented [7].

2-Aminonaphthalene has been determined successfully in a variety of samples by turbidimetry [8], thin-layer chromatography on alumina which has been impregnated with metal ions [9, 10], derivatization followed by spectrophotometry [11—13], chemiluminescence [14], complexation with copper(II) ion followed by indirect atomic absorption spectrometry [15], anodic differential pulse voltammetry [16], and high performance liquid chromatography with electrochemical detectors [17—19]. These procedures are unsuitable for determining 2-aminonaphthalene in fossil fuels for one or more reasons that include the facts that aqueous media are required, the samples must be essentially free of interfering species, the sensitivity of the method is insufficient, and no estimate of the recovery of 2-aminonaphthalene is possible. Three papers which describe procedures for profiling amines present in synthetic fuels [2, 5, 6] overcame these objections, but these methods are extremely time-consuming and require considerable technical skill to achieve reproducible results with a wide variety of sample types. For these reasons, it was desirable to develop a new method for 2-aminonaphthalene which would be applicable to complex, nonaqueous matrices such as coal-derived oils, and which would be sufficiently accurate and rapid for use as a screening procedure.

In this paper, a procedure is described in which the 2-aminonaphthalene-enriched fraction of a synthetic fuel is isolated by using a semi-preparative scale bonded-phase high performance liquid chromatographic (h.p.l.c.) column. This isolated fraction is then eluted from an analytical-scale nonpolar stationary (reversed) phase h.p.l.c. column by using a pH-adjusted eluent. A fluorescence detector is used to detect 2-aminonaphthalene selectively. The procedure is rapid, applicable to most synthetic fuel materials, exhibits greater sensitivity than other procedures [2, 5, 6] and provides a means of calculating the overall recovery of analyte.

EXPERIMENTAL

Solvents and chemicals

Pentane, dichloromethane, and acetonitrile were of "distilled-in-glass" grade (Burdick & Jackson Laboratories, Muskegon, MI). The aminonaphthalenes were obtained in 99% purity (RFR, Hope, RI; and Sigma Chemical Co., St. Louis, MO). 3-Methyl-2-naphthylamine was procured from the National Cancer Institute Chemical Repository, Illinois Institute of Technology Research Institute, Chicago, (Chem. no. 424, lot no. CR71-9-1). The remaining PAA were obtained in 95% or better purity (Pfaltz & Bauer, Stamford, CT; K & K Laboratories, Plainview, NY; RFR; Aldrich Chemical Company, Milwaukee, WI). Methanol was reagent-grade (Fisher Scientific, Fairlawn, NJ). All chemicals and solvents were used as received.

The radiolabeled tracer, (1-^{14}C)-1-aminonaphthalene hydrochloride, specific activity 4.75 mCi mmol^{-1}, was custom-prepared (California Bionuclear Corp., Sun Valley, CA). Upon receipt, the tracer was dissolved in benzene and extracted three times with 1 M sodium hydroxide. After the solvent had been removed from the organic layer, the residue (the free base (1-^{14}C)-1-aminonaphthalene) was redissolved in toluene to yield a radiotracer spiking solution with an activity of approximately 2×10^6 dpm ml^{-1}.

Samples

All samples except the gasifier tar, standard shale oil, SRC-II coal oil, and Wilmington Petroleum Crude oil were obtained through the U.S. Environmental Protection Agency/Department of Energy Fossil Fuel Research Materials Facility [20, 21]. The latter included three Comparative Research Materials (CRMs) which are available [21] for biological assay and research and development of analytical methods. The SRC-II coal oil and Wilmington Petroleum Crude were obtained from the National Bureau of Standards (Washington, DC) through the joint NBS/DOE-sponsored Analytical Characterization Group. The gasifier tar, which was collected at the low BTU coal gasifier at the University of Minnesota, Duluth, was supplied by B. R. Clark, Oak Ridge National Laboratory. A certified shale oil standard (SRM 1580; purchased from the National Bureau of Standards) was also used.

Special glassware. The inert atmosphere—reduced pressure concentration device used to remove solvent from the extracts collected was that reported by Higgins and Guerin [22], and was fabricated in house. Volumetric flasks with capacities of 0.1, 0.3, or 0.5 ml (SGA Scientific, Bloomfield, NJ) were used.

Equipment

Preliminary isolation system. The isolation system was arranged as shown in Fig. 1. The solvent was pumped through a low-pressure solvent filter (Alltech Associates, Deerfield, IL) and 3.2-mm o.d. teflon tubing by a duplex reciprocating pump (Laboratory Data Control Division, Milton Roy Co., Riviera Beach, FL), which was connected to a pulse-dampening unit (Laboratory Data Control), and adjusted to deliver 2 ml min^{-1} at 1.72×10^6—3.44×10^6 Pa (250—500 psig). The solvent inlet line was connected in turn to the loop injector.

The sample was injected, using a 2.5-ml syringe, into a loop filler port (model 7011, Rheodyne Corp., Cotati, CA) connected to a six-port high-pressure loop injector (Valco Instrument Co., Houston, TX) which was equipped with a 250-μl stainless steel sampling loop. The sample passed from the loop to an MPLC Guard Column with an "Amino" MPLC cartridge (Brownlee Labs, Santa Clara, CA).

The guard column was connected to a semi-preparative scale (10 mm i.d. $\times$ 25 cm) aminosilane h.p.l.c. column packed with 10-μm Lichrosorb NH_2 (Altex Associates, Berkeley, CA). The eluted peaks were detected by using

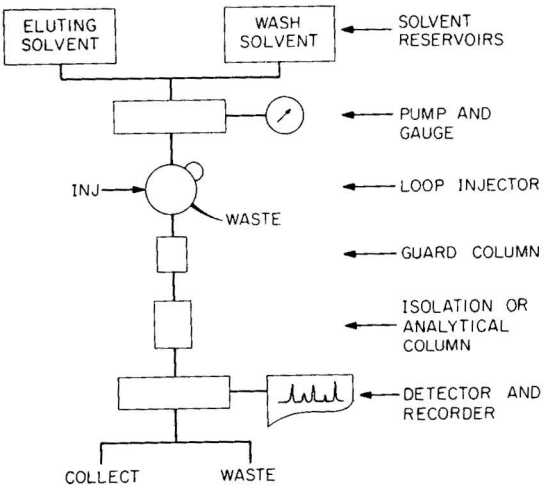

Fig. 1. Diagram of the h.p.l.c. instruments.

a fixed wavelength (254 nm) u.v. detector (model 1285, Laboratory Data Control). The eluant was either collected or shunted to waste.

All connections were made with 3.2-mm o.d. teflon tubing or 1.6-mm o.d. stainless steel tubing.

Quantitative system. The general form of the quantitative system is similar to that described above and depicted in Fig. 1. Solvent was pumped through a low-pressure solvent filter and 3.2-mm o.d. teflon tubing by a simplex reciprocating pump (Laboratory Data Control) which was adjusted to deliver 1 ml min^{-1} at 1.38×10^7—1.72×10^7 Pa (2000—2500 psig). The solvent line was connected to the loop injector.

Samples were injected by using a loop filler port (model 7011) and a loop injector (model 7010, Rheodyne Corp.) equipped with a 20-μl sampling loop. The sample was then flushed through the loop onto an MPLC Guard Column equipped with an "RP-18" cartridge (Brownlee Labs). The analytical column, which was connected to the guard column, was a 4.6 mm i.d. × 25 cm reversed-phase (C_{18}) column packed with 10-μm particles (Alltech Associates, Deerfield, IL).

The emerging peaks were monitored with a Model 203 fluorescence spectrophotometer (Perkin-Elmer Corp., Norwalk, CT) which contained a 20-μl volume, fused-silica flow-cell (Precision Cells, Hicksville, NY). The excitation monochromator was set at 270 nm and the emission monochromator was set at 405 nm.

All connecting tubing used in the quantitative system was capillary-bore stainless steel tubing (0.2 mm i.d., 1.6 mm o.d.).

Recovery measurement

Aliquots (10 μl) of the original spiked sample solution and the corresponding isolated fraction were added to 20 ml of scintillation solution,

prepared by dissolving 4 g of Omnifluor (New England Nuclear, Boston, MA) in 1 l of toluene.

Liquid scintillation counting of the 1-aminonaphthalene tracer was done for 2 min at room temperature with the carbon-14 counting channel of a Tri-Carb Liquid Scintillation Counter (model C-2425, Packard Instrument Co., Inc., Downers Grove, IL). All sample counts were corrected for scintillation quenching with the calibrated automatic external standard option of the instrument.

Procedure

Isolation of the 2-aminonaphthalene-bearing fraction. Neat dichloromethane and 50% (v/v) pentane in dichloromethane were degassed with vacuum for 15 min before use.

A standard containing approximately 100 μg ml^{-1} each of 1- and 2-aminonaphthalene in dichloromethane was eluted daily through the isolation system with 50% (v/v) pentane in dichloromethane. The retention time of 2-aminonaphthalene was noted, and the volume of solvent eluting between either 5 or 10 min prior to and after this time was taken as the 2-aminonaphthalene fraction.

The sample (1—4 g) and 1 ml of the tracer solution were dissolved in dichloromethane and diluted to a final volume of 10 ml. (Undissolved solid particles were removed with a medium-porosity fritted funnel.) A 250-μl aliquot of the sample solution was injected onto the isolation h.p.l.c. system. The 2-aminonaphthalene fraction was taken to dryness using vacuum and dry, flowing nitrogen. The fraction was then redissolved in exactly 0.1 ml of acetonitrile.

After an isolation was completed, the column was washed with neat dichloromethane until the u.v. absorbance at 254 nm was restored to its baseline value (typically, 20—60 min were required, depending upon the complexity of the sample). The column was re-equilibrated with 50% (v/v) pentane in dichloromethane for 20 min before processing another sample.

Determination of 2-aminonaphthalene. The h.p.l.c. mobile phase, 50/40/10% (v/v) methanol/water/acetonitrile was rendered basic by the addition of 4 ml of aqueous 7.4 M ammonia to 1 l of mobile phase. The final solution, which was 0.06 M (pH $\approx$ 11) in aqueous ammonia, was then degassed under vacuum for 30 min before use. The wash solvent, 20% (v/v) water in methanol, was degassed similarly.

A series of four 2-aminonaphthalene standards, ranging from 0.7 to 5.0 μg ml^{-1} in acetonitrile, was prepared weekly and processed before each fraction. Under the usual analytical conditions employed (flow rate of 1 ml min^{-1}, pressure of 1.38×10^7 Pa (2000 psig)), 2-aminonaphthalene eluted between 8 and 9 min.

Immediately after 2-aminonaphthalene was eluted, the column was washed with the methanol/water solvent for approximately 2 h. The column was reconditioned with the basic mobile phase for 20 min before processing another fraction.

Because solutions of high (>11) pH slowly dissolve the silica support of a reversed-phase column, a replaceable guard column was employed and the column was always flushed with the methanol wash solvent at the end of each day.

Calculations

Peak heights for the four 2-aminonaphthalene standards were fitted to a standard linear regression equation, thus yielding $f(h)$, the concentration of 2-aminonaphthalene ($\mu g\ ml^{-1}$) as a function of the peak height, h. (The correlation coefficient of $f(h)$ typically exceeded 0.995.) The concentration of 2-aminonaphthalene in the original crude is then given by the equation $C_{2\text{-AN}}$ ($\mu g\ g^{-1}$) = $4f\ (h)/wy$, where w is the mass (g) of the total sample, y is the overall recovery of 2-aminonaphthalene determined by liquid scintillation counting of the tracer in the final fraction, and the factor of 4 takes account of all volumes used. No correction is needed for the mass of the radioactive tracer unless 1-aminonaphthalene is the desired analyte.

RESULTS AND DISCUSSION

The determination of 2-aminonaphthalene in fossil fuels is complicated by the comparative instability of the analyte because 2-aminonaphthalene slowly degrades in the presence of light and air [23, 24], and will decompose even on standing in solution in the dark at 4°C. As a result, the more rapid the procedure, the greater the likelihood of good accuracy and precision. The slow degradation of PAA with time is probably one reason for the lack of precision shown in prior methods [5, 6]. Fresh standard solutions should be prepared at least weekly, and preferably more often, to preserve the integrity of the standards.

The recovery of 2-aminonaphthalene is determined by scintillation counting of the radioactive tracer (1-^{14}C)-1-aminonaphthalene. The cut points which define the aminonaphthalene-enriched fraction taken from the aminosilane column are sufficiently wide to insure that both 1- and 2-aminonaphthalene (hence, the tracer as well) are present in the isolated fraction. The tracer thus serves as a measure of the recovery for both species.

The pH of the analytical system eluant was sufficiently basic to permit separation of amine species on a reversed-phase column. The methanol/water/acetonitrile/aqueous ammonia solvent had an additional unexpected advantage: this medium rendered the fluorescence excitation spectra of 1- and 2-aminonaphthalene sufficiently different to permit spectroscopic resolution of the two isomers. This effect has been observed in other solvent systems as well [25]. It should be noted that these isomers may be partially resolved chromatographically by using an analytical-scale aminosilane column, but that a selective spectroscopic detector is still required to permit the proper quantification of 2-aminonaphthalene in the presence of 1-aminonaphthalene.

The fluorescence h.p.l.c. detector employed in this procedure enabled either 1- or 2-aminonaphthalene to be quantified independently in a given fraction. The excitation/emission wavelength pair 270/405 nm is very selective for 2-aminonaphthalene; the response of 2-aminonaphthalene is not changed even in the presence of an equimolar excess of 1-aminonaphthalene. If desired, 1-aminonaphthalene, the noncarcinogenic isomer, can be readily quantified as well, by using the wavelength pair 310/500 nm, which discriminates against 2-aminonaphthalene.

The effect of interferences was determined with 1-aminonaphthalene, 1- and 2-aminoanthracene, 1-aminopyrene, 2-aminochrysene, quinoline, acridine, and benz(a)acridine. The compounds 1-aminopyrene, 2-aminochrysene, and benz(a)acridine exhibited a significant fluorescence response at λ_{ex} = 270 nm/λ_{em} = 405 nm, and they were present in the 20-min cut used for some of the samples examined. These three compounds are not expected to present any significant interference because they are present in quantities at least one-fiftieth that expected for 2-aminonaphthalene [5, 6] and because they are chromatographically resolved from 2-aminonaphthalene. There is the possibility that an alkylaminonaphthalene species would coelute and yield a fluorescence response at the wavelengths chosen. The test interferent, 3-methyl-2-naphthylamine, did produce a fluorescence response under the conditions specified, but was chromatographically resolved from 2-aminonaphthalene.

The same set of compounds was used to determine the effect of interferences on the determinations of 1-aminonaphthalene in fossil fuel samples. In this case, only 2-aminoanthracene, 1-aminopyrene, and 2-aminochrysene displayed a fluorescence response at λ_{ex} = 310 nm/λ_{em} = 500 nm. These compounds are not likely to interfere in the determination of 1-aminonaphthalene for the same reasons that they do not interfere in the determination of the 2-isomer.

The overall recovery of (1-^{14}C)-1-aminonaphthalene typically exceeded 80% in samples which dissolved readily in acetonitrile. Isolates of PAA which did not dissolve well in this solvent showed a significant decrease in overall recovery. It should be noted that the tracer solution, like any other aminonaphthalene solution, will decompose with time, even if stored in the dark at 4°C. It is strongly recommended that the chromatographic purity of the tracer be checked monthly.

The accuracy of the h.p.l.c. procedure was tested by spiking a coal oil (CRM-1) with known quantities of 2-aminonaphthalene and calculating the recovery of the nonradioactive ("cold") spike. The data presented in Table 1 show a nominal recovery of 92% at the levels tested. Furthermore, when the total observed concentration of 2-aminonaphthalene was plotted against the concentration of spike, a straight line was observed (intercept = 90.3 $\mu g\ g^{-1}$, slope = 0.948, correlation coefficient = 0.991).

The 2-aminonaphthalene concentrations of several samples were determined, as shown in Table 2, using a 10-min collection time for the 2-amino-

TABLE 1

Accuracy and recovery studies for coal oil CRM-1 spiked with 2-aminonaphthalene (2-AN)

Spike level ($\mu g\ g^{-1}$)	Recovery of tracer (%)	Total 2-AN measured ($\mu g\ g^{-1}$)	Spike recovered[a] ($\mu g\ g^{-1}$)	Recovery of spike (%)
0	92	97	—	—
	78	89	—	—
12.27	70	101	11	85
	70	102	12	93
30.82	83	119	29	92
	74	114	24	76
60.80	73	156	66	108
	63	145	55	90
72.45	56	161	71	97
	81	152	62	85
92.18	79	177	87	94
	78	182	92	99
			Overall recovery	92

2-AN ($\mu g\ g^{-1}$) = 0.9470 (spike level) + 90.53

[a]Determined by subtracting intercept of regression line from each measured value of total 2-aminonaphthalene.

naphthalene fraction. This procedure yielded acceptable recoveries of the radioactive tracer and reproducible results. A typical chromatogram of the isolated fraction of NBS SRC-II coal oil is shown in Fig. 2.

The 10-min collection time did not work equally well with all samples. Low yields of radioactive tracer were observed for the crude and hydrotreated shale oil samples (4601, 4602, 4607). The yields improved significantly when a 20-min collection was used to define the 2-aminonaphthalene fraction.

TABLE 2

Concentration of 2-aminonaphthalene in various natural and synthetic crude samples determined by h.p.l.c. screening procedure[a]

Sample description	Recovery of tracer (%)[b]	Concentration of 2-aminonaphthalene[c] ($\mu g\ g^{-1}$)	
		H.p.l.c.	Reference[d]
Gasifier tar 83	77	24 ± 3	19 ± 6
NBS coal liquid oil (SRC-II)	65	87 ± 5	117[e]
Shale oil A[f]	77	5 ±1[g]	2.9 ± 1

[a]10-min cut unless noted otherwise. [b]Mean of 4 replicates. [c]Mean ± standard deviation. [d]Taken from reference [5]. [e]One determination. [f]Repository number, CRM-2 [21]. [g]20-min cut used.

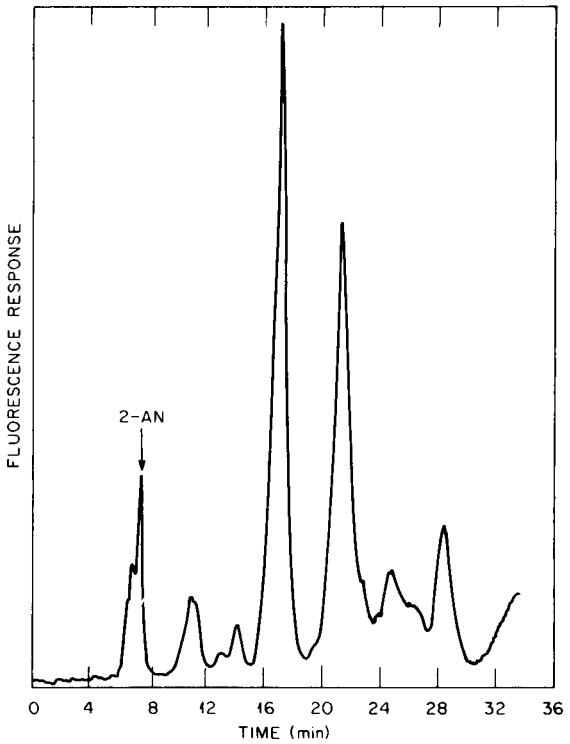

Fig. 2. Chromatogram of the isolated fraction of NBS SRC-II coal oil. Experimental conditions described in the text. The indicated peak, 2-AN, is 2-aminonaphthalene.

This observation suggested that certain samples would change the retention behavior of the column. Under these circumstances, the procedure was modified to include a longer collection time for 2-aminonaphthalene and the use of a "cold" 2-aminonaphthalene spike to verify that the cut-points were reasonable. In cases for which the 20-min collection time was used for the 2-aminonaphthalene fraction, three independent determinations were run, viz. one with and two without a 2-aminonaphthalene cold spike. The radioactive tracer was added to all samples. A summary of results for coal oil, shale oil, and petroleum-derived materials is given in Table 3.

The data in Tables 1—3 demonstrate the versatility of this method, which is readily applicable to coal oils, shale oils, petroleum crudes, and gasifier tars. Some of the results shown in Table 2 are compared with reference values generated using a more laborious and specific conventional isolation procedure [5, 6]. The precision (relative standard deviation) of the h.p.l.c. procedure is typically ± 20%.

It is apparent that the values determined in the screening procedure track those of the reference procedure, but the screening procedure values are consistently higher than the reference procedure data. The effect is probably due to the presence of small quantities of alkylated 2-aminonaphthalene

TABLE 3

Concentration of 2-aminonaphthalene in various natural and synthetic crude samples determined by h.p.l.c. screening procedure[a]

Repository No.[b]	Sample description	Recovery of tracer (%)	Concentration of 2-aminonaphthalene[c] ($\mu g\ g^{-1}$)
CRM-1	Coal oil A	76[d]	82 ± 4
CRM-3	Petroleum crude A	66[d]	2 ± 1
4601	Crude shale oil	73[d]	12 ± 3
4602	Hydrotreated shale oil	52[d]	6 ± 0.3
4607	Hydrotreated shale oil residue	75[e]	7 ± 2
1308	Atmospheric still, overhead	59[e]	18 ± 7
1309	Atmospheric still, bottom	75[e]	13 ± 2
1310	Vacuum still, overhead	80[e]	18 ± 5
1311	Vacuum still, bottom	75[d]	5 ± 2
—	NBS SRM 1580 shale oil[f]	75[e]	11 ± 3
—	NBS Wilmington petroleum[f]	54[d]	0.4 ± 0.2

[a]20-min cut unless noted otherwise. [b]See reference [21]. [c]Mean ± standard deviation. [d]Mean of 3 replicates. [e]Mean of 4 replicates. [f]10-min cut.

analogs which are not chromatographically resolved from 2-aminonaphthalene and yield a fluorescence response at the wavelengths employed for 2-aminonaphthalene. It should be evident, however, that the agreement between the two procedures is sufficient to allow the h.l.p.c. procedure to be used at least for quick selection of samples for further study.

The minimum detectable quantity of 2-aminonaphthalene in a given fossil fuel sample was estimated to be 0.06 $\mu g\ g^{-1}$, based on twice the noise level of the fluorimetric detector. The detection limit may be decreased by using a larger sample loop in the isolation procedure, by concentrating the isolated fraction further, or by using a fluorescence detector with improved signal to-noise ratio. The choice of the Perkin-Elmer 203 fluorescence spectrophotometer, rather than a commercial fluorescence h.p.l.c. detector, was dictated by the need for a narrow spectral bandpass in the detector. Filter fluorimeters would not possess the necessary bandpass; the spectrophotometer, which uses standard grating monochromators, does, and is sufficiently selective for this application.

Normally, it is feasible to generate four 2-aminonaphthalene-enriched fractions per person-day and to process two of these isolates per person-day on an independent instrument. The resulting overall sample turnaround time, two aliquots per person-day, is markedly superior to that of the more laborious procedure [5, 6], which is four aliquots per two person-weeks. The turnaround time could be shortened further, at the expense of additional sample handling, by precleaning the sample with either column chromatography or acid/base extraction.

The authors express their thanks to C. K. Bayne for his assistance in the statistical analysis of the data presented in this paper, and to R. R. Reagan for her assistance with the interference study. This work was funded by the U.S. Department of Energy, Office of Health and Evironmental Research, contract no. W-7405-eng-26 with the Union Carbide Corporation.

REFERENCES

1 M. R. Guerin, C.-h. Ho, T. K. Rao, B. R. Clark and J. L. Epler, Environ. Res., 23 (1980) 42.
2 C.-h. Ho, B. R. Clark, M. R. Guerin, C. Y. Ma and T. K. Rao, Am. Chem. Soc. Div. Fuel Chem. Prep., 24 (1979) 281.
3 M. V. Buchanan, C.-h. Ho, M. R. Guerin and B. R. Clark, in M. Cooke and A. J. Dennis (Eds.), Chemical Analysis and Biological Fate: Polynuclear Aromatic Hydrocarbons, Columbus, OH, Battelle Press, 1981, pp. 133—145.
4 M. R. Guerin, I. B. Rubin, T. K. Rao, B. R. Clark and J. L. Epler, Fuel, 60 (1981) 282.
5 B. A. Tomkins and C.-H. Ho, Anal. Chem., in press.
6 B. A. Tomkins, Analytical Chemistry Division Research and Development Summary, October 1980, Bio/Organic Analysis Section, Oak Ridge National Laboratory Central Files Number ORNL/CF-80/314, p. 6.
7 D. B. Clayson and R. C. Garner, in C. E. Searle (Ed.), Chemical Carcinogens, ACS Monograph 173, Washington, DC, American Chemical Society, 1976, pp. 366—461.
8 T. Akiyama and S. Kaiju, Kyoto Yakka Diagaku Gakuho, 14 (1966) 40.
9 K. Shimomura and H. F. Walton, Sep. Sci., 3 (1968) 493.
10 K. Yasuda, J. Chromatogr., 60 (1971) 144.
11 M. El-Dib, M. O. Abdel-Rahman and O. A. Aly, Water Res., 9 (1975) 513.
12 E. J. Dixon and D. M. Groffman, Analyst, 100 (1975) 476.
13 I. M. Korenman and L. N. Karyakina, Tr. Khim. Tecknol., 2 (1967) 114.
14 G. A. Rose, Br. J. Urol., 48 (1976) 61.
15 T. Mitsui and Y. Fujimura, Bunseki Kagaku, 23 (1974) 1309.
16 W. M. Chey, R. N. Adams and M. S. Yllo, J. Electroanal. Chem., 75 (1977) 731.
17 J. R. Rice and P. T. Kissinger, J. Anal. Toxicol., 3 (1979) 64.
18 R. M. Riggin and C. C. Howard, Anal. Chem., 51 (1979) 210.
19 I. Mefford, R. W. Keller, R. N. Adams, L. A. Sternson and M. S. Yllo, Anal. Chem., 49 (1977) 683.
20 D. L. Coffin, M. R. Guerin and W. H. Griest, Proceedings of the Symposium on the Potential Health and Environmental Effects of Fossil Fuel Technologies, Gatlinburg, TN, Sept. 25—28, 1978; CONF-780903, Oak Ridge National Laboratory, Oak Ridge, TN, 1979, p. 153.
21 W. H. Griest, D. L. Coffin and M. R. Guerin, Fossil Fuels Matrix Program, ORNL/TM-7346, Oak Ridge, TN, Oak Ridge National Laboratory, June 1980.
22 C. E. Higgins and M. R. Guerin, Anal. Chem., 52 (1980) 1984.
23 The Merck Index, 9th Edition, Entries #6225 and 6226, in M. Windholtz, S. Buavari, L. Y. Stroumtsos and M. N. Fertig (Eds.), Merck, Rahway, NJ, 1976.
24 A. F. Osteen, The Photosensitizing Action of 2-Naphthylamine on *Escherichia coli* K-12, U.S. NTIS PB Rep. 242340, Springfield, VA, 1973, pp. 35—41.
25 C. L. Holder, J. R. King and M. C. Bowman, J. Toxicol. Environ. Health, 2 (1976) 111.

Analytica Chimica Acta, 134 (1982) 313—320
Elsevier Scientific Publishing Company, Amsterdam — Printed in The Netherlands

THE SEPARATION OF PALLADIUM AND PLATINUM BY ION FLOTATION

EUGENE W. BERG*
Chemistry Department, Louisiana State University, Baton Rouge, LA 70803 (U.S.A.)
DANIEL M. DOWNEY
Chemistry Department, West Virginia University, Morgantown, WV 26506 (U.S.A.)
(Received 9th July 1981)

SUMMARY

Differences in the ion flotation properties of palladium(II) and platinum(IV) chloro complexes in aqueous solutions are used to achieve separations of these metals. The anionic chloro complex $PtCl_6^{2-}$ is floated selectively with cationic surfactants of the type, RNR'_3Br, from solutions of $PdCl_4^{2-}$ and various concentrations of hydrochloric acid. The palladium(II) does not float from solutions of ≥ 3.0 M HCl and the platinum(IV) floated from these solutions can be recovered free of palladium. However, the separation is incomplete as much of the platinum(IV) is also unfloated from these solutions. Quantitative separations are obtained by conversion of the palladium(II) to the cationic ammine, $Pd(NH_3)_4^{2+}$, with aqueous ammonia prior to flotation. The anionic chloro complex of platinum(IV) is unaffected by the presence of ammonia and is floated quantitatively with the surfactant *n*-hexadecyltri-*n*-propylammonium bromide from 0.01 M ammonia solutions.

As a result of observations made during a systematic study of the flotation properties of chloro complex anions of platinum group metals [1], Berg and Downey developed ion-flotation separation procedures for binary mixtures of rhodium(III) and iridium(IV) [2] and iridium(III) and platinum(IV) [3]. The initial study [1] also indicated that mixtures of platinum(IV) and palladium(II) might be separated by ion flotation.

In initial general study [1] of the flotation properties of the chloro complexes of the platinum group metals showed a significant difference in the floatability of the Pd(II) and Pt(IV) complexes as a function of hydrochloric acid concentration. As the acid concentration was varied from 0.01—3.0 M, the amount of floated Pt(IV) decreased to about two-thirds of the initial value while the amount of floated Pd(II) decreased to zero. These data indicated that the adjustment of the hydrochloric acid concentration in the sample might provide a simple means of separating the metal chloro complexes by ion flotation.

The present paper describes two separation procedures for platinum and palladium which evolved from the earlier study. The first involves the selective flotation of $PtCl_6^{2-}$ from $PdCl_4^{2-}$ in hydrochloric acid solutions with

0003-2670/82/0000-0000/$02.75

surfactants of the quaternary ammonium type. The second makes use of the charge selectivity of quaternary ammonium surfactants to achieve separation. The cationic ammine, $Pd(NH_3)_4^{2+}$, may be prepared in the presence of $PtCl_6^{2-}$, with the latter being selectively floated from the mixture with cationic quaternary ammonium surfactants. Both procedures are termed ion flotation because the metal complexes are initially ions in true solutions.

EXPERIMENTAL

Reagents and apparatus

Tetrachloropalladate(II) and hexachloroplatinate(IV) stock solutions were prepared by dissolving the high-purity palladium and platinum metals (A. D. Mackay, Inc.) in aqua regia, fuming the solution to dryness with hydrochloric acid, and making up to volume in 2 M HCl. Aliquots of these stock solutions were activated by thermal neutrons from ^{252}Cf in the LSU Nuclear Science Center to produce the radiotracers used to follow flotation. The predominant radionuclides produced were ^{109}Pd ($t_{1/2}$ 13.5 h) and ^{197}Pt ($t_{1/2}$ 20 h). The radioactive solutions were allowed to decay for six hours prior to use to eliminate activity from ^{38}Cl ($t_{1/2}$ 37.3 min).

Surfactants used for flotation were hexadecyltrimethylammonium bromide (HTMAB), hexadecyltriethylammonium bromide (HTEAB), hexadecyltripropylammonium bromide (HTPAB) and hexadecyltributylammonium bromide (HTBAB). The preparation and purification of these surfactants was described earlier [1]. All surfactant stock solutions were prepared in absolute ethanol.

A 2 M ammonia solution was prepared by diluting 138 ml of reagent-grade 27% ammonia liquor to 1 l. All other reagents were analytical-reagent grade.

A flotation system similar to that of Rubin and Johnson [4] was used. The flotation cell was a fine sintered (4—5.5 μm) glass Buchner funnel lengthened to 30 cm. A port was drilled 1 cm above the frit and fitted with a rubber septum for sample removal by a syringe. The flotation cell was positioned above a deep tray to contain any spilled radioactive solutions.

Samples were counted with a 2 × 2-inch NaI(Tl) well crystal detector in conjunction with a TMC 401A multichannel analyzer. Spectrophotometric measurements were made with a Beckman DB spectrophotometer and matched quartz cuvettes.

General flotation procedure

Solutions were prepared for flotation for the first series of studies by pipetting aliquots of the Pt(IV) and Pd(II) stock solutions into a 200-ml volumetric flask. The aliquots of each metal stock solution were calculated to give a final metal chloro complex concentration of 5×10^{-5} M. The concentration of 5×10^{-5} M corresponds to 0.975 mg of platinum and 0.532 mg of palladium per 100 ml. Enough surfactant was then added in 2 ml of absolute ethanol to give a concentration of 2×10^{-4} M after solution. The

hydrochloric acid content of the solution was adjusted by adding a calculated volume of 6 M HCl stock solution. After dilution of the mixture to 200 ml, the solution was stirred for 10 min and 100 ml was transferred to the cell for flotation.

The preparation of sample solutions for the second series of studies differed from the first only in that aliquots of the ammonia stock solution were added instead of 6 M hydrochloric acid. The cationic palladium ammine complex was prepared directly in the 200-ml volumetric flask. The stirring time of 10 min was sufficient for the complete formation of the ammine.

The samples were then subjected to flotation by passing humidified nitrogen through the solution with a controlled flow rate of 10 cm^3 min^{-1}. Within five minutes, a solid scum (sublate) formed on the surface of the foam. Analysis indicated that this solid was a stoichiometric salt (surfactant—metal ratio, 2:1) of the surfactant and metal chloro complex anion.

The metal chloro complexes were recovered after separation by the following procedure. After the maximum flotation was achieved, the nitrogen flow was stopped and 25 ml of *n*-butyl acetate was slowly added to the top of the flotation sample solution. As the organic solvent was added, the foam collapsed and most of the sublimate was dissolved in *n*-butyl acetate. However, some of the sublimate was redispersed into the aqueous solution. Thus nitrogen was again passed through the solution for 10 min at 10 cm^3 min^{-1} in order to float all the redispersed sublate into the organic layer.

The organic and aqueous layers were then separated and analyzed to determine the extent of separation. The sublimate was recovered by rotary evaporation of the *n*-butyl acetate. The metal chloro complex was readily recovered from the sublimate by wet ashing with 30% hydrogen peroxide (or sulfuric or nitric acid) and fuming to dryness with a few drops of 1 M KCl and concentrated hydrochloric acid. The unfloated metal was recovered from the aqueous solution by evaporating to dryness on a hot plate. Duplicate flotations and recoveries were found to vary by no more than 1% (r.s.d.).

Measurement techniques

The progress of flotation experiments was monitored by removing 1—5-ml aliquots from the sample solutions at intervals and counting in the well crystal detector. The detector was incapable of discriminating the photon energies of the ^{109}Pd and ^{197}Pt decay. Therefore it was necessary to conduct duplicate flotations for mixtures with each run containing only one radioisotope. The concentration of metal in solution is directly proportional to the specific activity (counts per minute per unit volume) of the solution. Changes in concentration of the metal ion in solution during the flotation period were followed by dividing the specific activity at any time, S_t, by the original specific activity, S_o. Thus, $(1 - S_t/S_o) \times 100$ is the percentage of the metal floated at any time.

Spectrophotometric measurements were also used to supplement the tracer studies. Both platinum and palladium were quantified by the tin(II) chloride method of Sandell [5].

RESULTS AND DISCUSSION

Separation of tetrachloropalladate(II) and hexachloroplatinate(IV)

The flotation curves for the chloro complexes of Pd(II) and Pt(IV) in solutions of various hydrochloric acid concentrations are presented in Fig. 1. The surfactant HTPAB was chosen for the separation studies because each of the metal chloro complexes was floated quantitatively from 0.01 M HCl solutions by this surfactant. The initial concentration of each metal chloro complex in the flotation cell was set at 5×10^{-5} M and the surfactant at 2×10^{-4} M. These values were chosen so that the surfactant was in a stoichiometric amount with the metals and below its critical micelle concentration. The hydrochloric acid concentration was varied from 0.01 to 3.0 M. After flotation for 1 h, the bulk aqueous solutions were analyzed and the mole ratios of the metals in the foam, ϕ_f, and residual liquid, ϕ_l, were calculated. Plots of ϕ_f and ϕ_l vs. acid molarity are presented in Fig. 2. Clearly, the bulk liquid is enriched with respect to palladium and in 1 M HCl the concentration of palladium is 10 times the concentration of platinum. The foam is enriched with respect to platinum and contains only platinum when the hydrochloric acid concentration exceeds 2.0 M. Thus platinum(IV) can be recovered palladium-free, but the recovery is not quantitative. Additional data for the recovery of the two metals from various hydrochloric acid solutions with HTPAB and other surfactants are given in Table 1.

Separation of tetramminepalladium(II) and hexachloroplatinate(IV)

Several investigators [6—9] have made use of the charge selectivity of surfactants to achieve separations by adjusting the initial solution conditions so that the complex ions of interest had charges opposite to each other. It was noted that the cationic ammine complex of palladium can be formed in the presence of $PtCl_6^{2-}$. Thus it was thought that a single quantitative flotation separation could result if the cationic quaternary ammonium surfactants were used to float the $PtCl_6^{2-}$ from solutions containing sufficient ammonia to convert $PdCl_4^{2-}$ completely to $Pd(NH_3)_4^{2+}$.

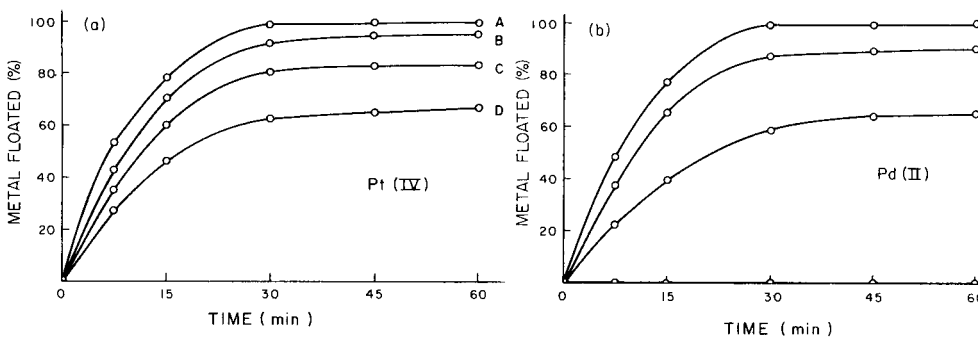

Fig. 1. Flotation of (a) platinum(IV) or (b) palladium(II) with HTPAB from solutions of various hydrochloric acid concentrations. Initial conditions: [Pt(IV)] = 5×10^{-5} M or [Pd(II)] = 5×10^{-5} M; [HTPAB] = 2×10^{-4} M, N_2 flow rate = 10 cm^3 min^{-1}. (A) 0.01 M HCl; (B) 0.5 M HCl; (C) 1.0 M HCl; (D) 3.0 M HCl.

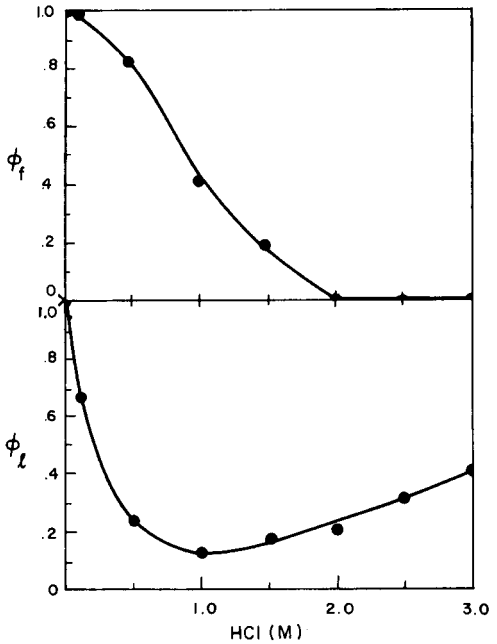

Fig. 2. Mole ratios of Pd to Pt in the foam and Pt to Pd in the residual bulk liquid as a function of hydrochloric acid concentration. Initial conditions: [Pt(IV)] = [Pd(II)] = 5×10^{-5} M, [HTPAB] = 2×10^{-5} M, N_2 flow rate = 10 cm^3 min^{-1}, flotation time 60 min. ϕ_f = [Pd]/[Pt] in foam; ϕ_l = [Pt]/[Pd] in liquid.

The reaction for the complete conversion of $PdCl_4^{2-}$ to $Pd(NH_3)_4^{2+}$ proceeds without heating and can be observed by the disappearance of the brownish-red color of the chloro complex as the colorless ammine complex forms. The ammine is very stable having an overall formation constant of 10^{30} [10]. However, the insoluble Vauquelin salt, $[Pd(NH_3)_4][PdCl_4]$, will form if insufficient ammonia is present to completely convert all the palladium(II) to the ammine complex.

Platinum(IV) does not readily form a complex ammine. In ammonium solutions, platinum(IV) will form the insoluble salt, $(NH_4)_2PtCl_6$ ($K_{sp} \approx 8 \times 10^{-6}$). However, the data of Linke [11] indicate that the salt exhibits significant solubility even in concentrated ammonium solutions. Thus, for the low concentrations of $PtCl_6^{2-}$ and NH_4^+ present in these studies, there was no reduction in the efficiency of platinum flotation caused by the precipitation of the ammonium chloroplatinate(IV).

The flotation sample solutions were prepared as for the previous studies except that hydrochloric acid was not added. Enough aqueous 2 M ammonia was added to give concentrations of 0.01—1 M. A compensation was made for small amounts which reacted with the hydrochloric acid that was added with the aliquots of the metal stock solutions. The sequence of mixing metal chloro complexes, surfactant or ammonia had no significance in the results of the flotation.

TABLE 1

Recovery data for the partial separation of Pd(II) and Pt(IV)
(Initial conditions: [Pd(II)] = [Pt(IV)] = 5×10^{-5} M, [surfactant] = 5×10^{-5} M, N_2 = 10 cm^3 min^{-1}, flotation time 60 min)

Surfactant	HCl (M)	Recoveries			
		Not floated		*Floated*	
		Pd[a] (mg)	Pd (%)	Pt[b] (mg)	Pt (%)
HTMAB	0.01	0.017	3	0.762	78
	0.10	0.042	8	0.752	77
	0.50	0.081	15	0.733	75
	1.00	0.378	71	0.644	66
	2.00	0.527	99	0.585	60
	3.00	0.538	101	0.510	52
HTEAB	0.01	0.011	2	0.819	84
HTPAB	0.01	0.012	2	0.965	98
	0.10	0.032	6	0.057	97
	0.50	0.053	10	0.934	96
	1.00	0.318	60	0.812	83
	2.00	0.505	95	0.761	78
	3.00	0.533	100	0.664	68
HTBAB	0.01	0.009	2	0.960	98
	0.10	0.027	5	0.955	98
	1.00	0.333	62	0.926	95
	2.00	0.521	98	0.897	92
	3.00	0.531	100	0.828	85

[a]Pd added, 0.532 mg. [b]Pt added, 0.975 mg.

Data for the separations of palladium(II) and platinum(IV) with HTMAB, HTEAB, HTPAB, and HTBAB and solutions of various ammonia concentration are given in Table 2. The ammonia concentration of 0.01 M was sufficient for the complete reaction of palladium(II). A simple, quantitative separation of palladium(II) and platinum(IV) was obtained from 0.01 M ammonia solutions by flotation of the platinum(IV) with HTPAB. There is a reduction in the flotation of platinum(IV) for solutions of greater ammonia concentration which leads to platinum(IV) contamination of the unfloated palladium(II). Thus, care must be taken in calculating the required volume of added ammonia in order to achieve the optimum separation of palladium and platinum.

Determination of separated metals by x-ray fluorescence

Upon completion of the flotation procedure, samples of both the collected froth and bulk solution were analyzed for the presence of platinum and pal-

TABLE 2

Recovery data for the separation of Pt(IV) and Pd(II)
(Initial conditions: [Pd(II)] = [Pt(IV)] = 5×10^{-5} M, [surfactant] = 2×10^{-4} M, N_2 = 10 cm^3 min^{-1}, flotation time 60 min)

Surfactant	NH_3 (M)	Recoveries			
		Not floated		*Floated*	
		Pd[a] (mg)	Pd (%)	Pt[b] (mg)	Pt (%)
HTMAB	0.01	0.520	98	0.751	77
	0.10	0.531	100	0.720	74
	1.00	0.522	98	0.672	69
HTEAB	0.01	0.533	100	0.809	83
	0.10	0.516	97	0.740	76
	1.00	0.521	98	0.721	74
HTPAB	0.01	0.532	100	0.974	100
	0.10	0.532	100	0.946	97
	1.00	0.518	97	0.889	91
HTBAB	0.01	0.519	97	0.984	101
	0.10	0.532	100	0.907	93
	1.00	0.528	99	0.878	90

[a]Pb added, 0.532 mg. [b]Pt added, 0.975 mg.

ladium by x-ray fluorescence to verify the efficiency of the separation. The metals were recovered from the floated samples and prepared as described earlier. Then, a small amount of each was placed on an aluminium disc for quantitation by x-ray fluorescence in a KEVEX Stereoscan 180 scanning electron microscope.

Platinum was separated from palladium by the procedure described earlier using HTPAB from an initially 3.0 M HCl solution. The collected foam samples showed clearly the x-ray lines for platinum but the lines for palladium were not discernible above the noise level after collecting data for 10 min. These data indicate that the platinum was separated and recovered (but not quantitatively) free of palladium by the procedure.

X-ray fluorescence analyses of the bulk solution for palladium and platinum after the flotation of platinum with HTPAB from 0.01 M ammonia showed traces of platinum in the palladium. These data were difficult to interpret quantitatively, but apparently the platinum contamination amounted to less than 0.5% of the original added platinum based on the recovery data and the relative line intensities. Therefore the separation of Pd(II) and Pt(V) by ion flotation in 0.01 M ammonia solution was essentially quantitative.

REFERENCES

1 E. W. Berg and D. M. Downey, Anal. Chim. Acta, 120 (1980) 237.
2 E. W. Berg and D. M. Downey, Anal. Chim. Acta, 121 (1980) 239.
3 E. W. Berg and D. M. Downey, Anal. Chim. Acta, 123 (1981) 1.
4 A. J. Rubin and J. D. Johnson, Anal. Chem., 39 (1967) 298.
5 E. B. Sandell, Colorimetric Determination of Traces of Metals (3rd edn.), Interscience, New York, 1959.
6 W. Walkowiak, D. Bhattachoryya and R. B. Grives, Anal. Chem., 48 (1976) 974.
7 C. Jacobelli-Turi, S. Terenzi and M. Palmera, Ind. Eng. Chem. Process Des. Dev., 6 (1967) 161.
8 B. L. Karger and M. M. Miller, Anal. Chem. Acta, 48 (1969) 273.
9 J. A. Lusher and F. Sebba, J. Appl. Chem., 15 (1965) 577.
10 A. V. Fasman, G. G. Kutyukov and D. V. Sotol'skii, Zh. Neorg. Khim., 10 (1965) 1338.
11 W. F. Linke, Solubilities of Inorganic and Metal-Organic Compounds (4th edn.), Vol. II, American Chemical Society, Washington, DC, 1965, p. 671.

Analytica Chimica Acta, 134 (1982) 321—326
Elsevier Scientific Publishing Company, Amsterdam — Printed in The Netherlands

UNLOADED POLYURETHANE FOAMS AS SOLID EXTRACTANTS FOR SOME METAL THIOCYANATE COMPLEXES FROM AQUEOUS SOLUTION

T. BRAUN* and M. N. ABBAS

Institute of Inorganic and Analytical Chemistry, L. Eötvös University, P.O. Box 123, 1443 Budapest (Hungary)

(Received 15th December 1980)

SUMMARY

Zinc, mercury, and indium are quantitatively extracted with unloaded polyurethane foams from aqueous thiocyanate solution. The unloaded polyester type foam will extract the thiocyanate complexes of the three metals as well as the polyether type. The extraction is strongly dependent on the thiocyanate concentration and is quantitative over a wide pH range.

The liquid—liquid extraction of metals from thiocyanate media has long been a subject of considerable interest in applied and analytical chemistry; several contributions have been made recently [1—5]. Open-cell polyurethane foams have attracted some attention as sorbents for preconcentrating inorganic and organic species from aqueous media [6, 7]. The quasi-spherical membrane structure of these foams has been shown to offer real advantages, providing an unusual geometrical form of the solid phase in analytical solid—liquid contact. Unloaded and reagent-loaded [8, 9, 10, 11] foams have been used successfully for extracting some metals from thiocyanate solutions. The use of unloaded polyurethane foams in a column arrangement offers special advantages over other techniques in trace analysis of water samples, for which a preconcentration step is usually needed. A column filled with unloaded foam is extremely cheap and simple to prepare. High flow rates can usually be attained by percolating aqueous solutions through such columns.

As an extension of earlier investigations in this laboratory [8, 9, 11], unloaded polyether and polyester types of foam were examined for the extraction of some metals from aqueous thiocyanate solution; the results were compared with those obtained with foams loaded with 1-(2-pyridylazo)-2-naphthol (PAN). Special attention was given to the extraction properties of foam of the polyester type because it contains less trace metal impurities than the ether type [12] (e.g., the tin content of the polyester type foam was shown to be about two orders of magnitude lower than that of the polyether type). This is of special importance when trace metals are determined non-destructively by activation analysis after the foam preconcentration step.

The extraction properties of foams of the polyester and polyether types were found to be nearly identical.

EXPERIMENTAL

Reagents, materials and equipment

All chemicals used were of analytical grade, and twice-distilled water was used.

Zinc stock solution (100 μg Zn ml^{-1}) was prepared by dissolving $Zn(NO_3)_2 \cdot 4H_2O$ in 1% nitric acid. Mercury stock solution (100 μg Hg ml^{-1}) was prepared by dissolving mercury(II) oxide in concentrated nitric acid and then diluting to yield a solution 1% in nitric acid. For the indium stock solution (100 μg In ml^{-1}), indium metal (99.99%) was dissolved in nitric acid and the solution was diluted to be 1% in nitric acid. Iron(III), cadmium(II), cobalt(II) and copper(II) solutions were prepared from their nitrate or sulphate salts in the same way. For the PAN solution, 0.1 g of 1-(2-pyridylazo)-2-naphthol was dissolved in 100 ml of chloroform.

Foams. The polyurethane foams used were of the polyether open-cell type (Greiner K. G. Schumstoffwerk, Kremsmünster, Austria) and the open-cell polyester type (Eurofoam, 9200 Wetteren, Belgium). The foam was used either in the form of small cubes (0.5 mm edge) or as cylinders of 25-mm diameter and 10-cm length. The PAN foam was prepared by soaking the foam in the appropriate amount of reagent solution to yield a PAN concentration of 1% (w/w) on the foam.

Tracers. The isotopes ^{65}Zn, ^{203}Hg, and ^{114m}In were obtained by irradiation of zinc metal, mercury(II) oxide, and indium metal for suitable times in the reactor of the Institute of Atomic Energy, Budapest, Hungary.

Equipment. Activities were measured with a NaI(Tl) well-crystal and an energy-selective counting device [(NC, 308) Gamma, Budapest].

Procedures

Batchwise experiments. The partition experiments were done batchwise at room temperature: 3 series of 20-ml flasks, each containing 0.10 g of foam cubes and 10 ml of solutions of different thiocyanate concentration in 1% nitric acid were spiked with ^{65}Zn, ^{203}Hg or ^{114m}In tracers. The flasks were shaken for 1 h and then the activity of 5 ml of the aqueous phase was counted. The initial concentrations of Zn, Hg and In in the aqueous phase were 0.5, 0.06 and 1.3 μg ml^{-1}, respectively. The distribution ratio D was calculated from the formula D = [metal in foam (μg g^{-1})]/[metal in solution (μg ml^{-1})].

The effect of pH of the aqueous phase on the extraction efficiency was studied as follows. Into 3 series of 20-ml flasks each containing 0.10 g of foam were added 10 ml of 0.20 M thiocyanate solution containing 10, 0.3, or 1.3 μg ml^{-1} of the spiked Zn, Hg or In solutions, respectively. The acidity was adjusted by addition of the calculated amount of nitric acid or sodium

hydroxide. After the flasks had been shaken for 1 h, 5 ml of the aqueous phase was counted and the percentage extraction was calculated.

To study the rate of uptake, portions (10 ml) of zinc or indium solutions in 1% nitric acid—0.2 M potassium thiocyanate, spiked with the corresponding isotope, were equilibrated with 0.1 g of foam cubes of the polyether type for 1, 3, 5, 10 and 30 min. The zinc or indium concentration in the initial aqueous solution was 1.0 or 1.3 $\mu g\ ml^{-1}$, respectively.

The effect of metal ion concentration on the percentage extraction was examined by shaking 10-ml portions of 0.2 M KSCN—1% nitric acid solution containing various concentrations of the metal under investigation spiked with the corresponding isotope, with 0.10 g of unloaded polyether foam cubes in 20-ml flasks for 1 h.

The effects of some cations were examined for a zinc concentration of 1 $\mu g\ ml^{-1}$ with five-fold amounts of the cation in question.

Dynamic experiments. The foam columns were prepared by placing the foam cylinders in glass columns, and applying gentle pressure with a glass rod. The columns were then filled with water under vacuum. Aliquots (100 ml) of zinc, mercury or indium thiocyanate solution spiked with the corresponding isotope, were allowed to percolate through the foam column at different flow rates. From activity measurements, the percentage extraction was calculated for the different flow rates examined.

RESULTS AND DISCUSSION

Extraction of zinc, mercury and indium

Extraction with PAN-loaded foams. The distribution ratio (D) for zinc, mercury and indium were found to be strongly dependent on the thiocyanate concentration. For example, when PAN-loaded foam was used to extract zinc from aqueous solution at pH 6, the distribution ratio was found to be 32 in the absence of thiocyanate, but 22600 in the presence of 0.2 M thiocyanate. In the extraction of mercury with PAN-loaded foam from neutral solution, the distribution ratio increased with increasing thiocyanate concentrations and reached a constant value of about 2000 at thiocyanate concentrations above 0.05 M (Table 1). The distribution ratio for indium in extractions from acidic solution (pH 2—3) increased from 4 in the absence of thiocyanate to 6270 at a 0.2 M thiocyanate concentration.

Extraction with unloaded foams. Both the polyether and polyester types of unloaded foams were found to extract the thiocyanate complexes of zinc,

TABLE 1

Effect of thiocyanate concentration on the distribution ratio of mercury on PAN-loaded foam (1% w/w PAN on foam; 0.06 $\mu g\ Hg^{2+}\ ml^{-1}$; pH 6.8)

KSCN (M)	—	0.02	0.05	0.2
D	193	1221	2069	2046

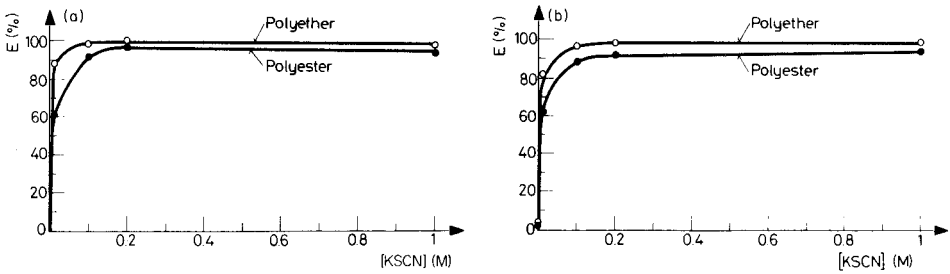

Fig. 1. Effect of thiocyanate concentration on percentage extraction with unloaded polyether (○) and polyester (●) type foams for (a) 10.5 μg Zn^{2+} ml^{-1} at pH 2.5; (b) 1.3 μg In^{3+} ml^{-1} at pH 2.

mercury and indium from aqueous solution. Figure 1 shows the effect of thiocyanate concentration on the extraction. The distribution ratios for zinc and indium on the unloaded polyether and polyester foams at different thiocyanate concentrations are given in Table 2. The mercury thiocyanate complex was also extracted by both types of unloaded foam; the distribution ratio on the ether-type foam increased from 277 in the absence of thiocyanate to 15050 at a 0.2 M thiocyanate concentration at pH 2.7.

Effect of pH on the extraction efficiency

The extraction of zinc from 0.2 M thiocyanate solution was almost quantitative over the pH range 0—6, but the distribution ratios improved as the pH increased. Thus at pH 6, the distribution ratios were 22630 and 24900 whereas at pH 2 the values were 4466 and 10320 for PAN-loaded and unloaded polyether foam, respectively.

Figure 2 shows the effect of pH on the extraction of mercury. With PAN-loaded foam from thiocyanate medium, the extraction was almost quantitative over the pH range 2.5—7.5. With the unloaded polyether foam, the extraction was essentially quantitative up to pH 6, but the polyester foam was less efficient. For indium, the extraction was quantitative in the pH range 2—5 with PAN-loaded foam and in the pH range 2—8 with unloaded

TABLE 2

Effect of thiocyanate concentration on the distribution ratios for zinc and indium on unloaded polyurethane foams of the ether and ester types (10.5 μg Zn^{2+} ml^{-1}; 1.3 μg In^{3+} ml^{-1}; pH 2—3)

KSCN (M)	Polyether type		Polyester type	
	D (Zn)	*D* (In)	*D* (Zn)	*D* (In)
—	2	62	2	120
0.02	744	450	155	166
0.1	—	3720	—	743
0.2	10320	8450	2260	1230
1.0	6000	17500	1490	2090

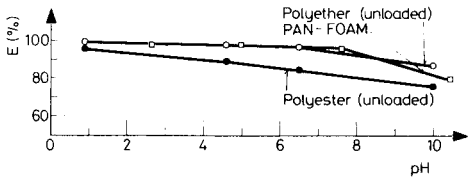

Fig. 2. Effect of pH on the extraction efficiency for mercury (0.363 μg Hg^{2+} ml^{-1}) in 0.2 M thiocyanate solution with different types of foam: (○) unloaded polyether; (□) loaded (1% w/w) with PAN; (●) unloaded polyester.

ether foam, the distribution ratios being higher at the lower pH values in the range. The extractions were rapid, with 98.8% and 95.3% of zinc (1 μg ml^{-1}) and indium (1.3 μg ml^{-1}), respectively, being extracted into the unloaded polyether foam after a 1-min contact time at pH 2. Longer contact times up to 30 min did not improve the percentage extractions.

Zinc and mercury at various concentrations in thiocyanate solution were quantitatively extracted on the unloaded polyether-type foam (Table 3). In the presence of 50-μg amounts of Hg(II), Fe(III), Cd(II) or Cu(II), 10.0 μg of zinc was still quantitatively extracted (99.3—99.6%) by the unloaded polyether foam.

Column experiments

When the column technique was used, the extraction of zinc with unloaded polyurethane foam was quantitative at flow rates up to 100 ml min^{-1}, and that of indium was quantitative at flow rates up to 87 ml min^{-1}, whereas the extraction of mercury was quantitative only when the flow rate did not exceed 25 ml min^{-1} (Table 4).

Recovery of zinc, mercury and indium from the foam. Zinc (50 μg) was first collected from 1 l of aqueous solution; about 98.5% of the zinc was recovered from the column by passing 150 ml of 1 M HNO_3 at a flow rate of 2 ml min^{-1}. A 1 M KSCN solution in 80% acetone was used to recover mercury from the foam; essentially quantitative recovery (98.95 ± 0.5%, n = 3) was obtained with 200 ml of this solution at flow rates of 15 ml min^{-1}.

TABLE 3

Effect of metal ion concentration on the extraction efficiencies for zinc and mercury on unloaded polyether-type foam from 0.2 M thiocyanate solution at pH 2—3

Zinc (μg ml^{-1})	% E	St. dev.[a] s	Confidence limit[b]	Mercury (μg ml^{-1})	% E	St. dev.[a] s	Confidence limit[b]
0.50	99.2	0.35	0.6	0.01	99.2	0.2	0.3
10.00	98.8	0.3	0.4	0.10	99.9	0.1	0.2
50.00	96.3	0.5	0.8	1.00	99.3	0.2	0.3

[a] n = 5. [b] $(ts/n)^{1/2}$ for t = 95.

TABLE 4

Effect of flow rate on the extraction efficiency for zinc (1 μg ml^{-1}), mercury (0.11 μg ml^{-1}), and indium (1.3 μg ml^{-1}) from 0.2 M thiocyanate solution at pH 2—3

Zinc		Mercury		Indium	
Flow rate (ml min^{-1})	E (%) and confidence limit[a]	Flow rate (ml min^{-1})	E (%) and confidence limit[a]	Flow rate (ml min^{-1})	E (%) and confidence limit[a]
25	99.85 ± 0.2	10	99.8 ± 0.3	20	99.4 ± 0.2
50	99.8 ± 0.2	25	98.3 ± 2.3	50	99.0 ± 0.0
100	99.4 ± 0.1	45	94.6 ± 5.7	87	97.3 ± 0.5

[a]For n = 5 at each level; t = 95.

Acetone alone can recover the mercury complex from the foam when the flow rate does not exceed 1 ml min^{-1}; 200 ml of acetone would be enough to recover mercury quantitatively. Indium was also recovered with the thiocyanate—acetone solution.

REFERENCES

1 J. P. Brunette, M. L. Arauso-Barreira, M. Taheri and M. J. F. Leroy, J. Inorg. Nucl. Chem., 41 (1979) 73.
2 M. Iqbal, M. A. Qureshi and M. Ejaz, Talanta, 25 (1978) 371.
3 S. Ahmed, W. Dil, S. A. Chaudhry and M. Ejaz, Talanta, 25 (1978) 563.
4 D. Singh and S. N. Tandon, Talanta, 26 (1979) 163.
5 D. Singh, O. V. Singh and S. N. Tandon, Anal. Chim. Acta, 115 (1980) 369.
6 T. Braun and A. B. Farag, Anal. Chim. Acta, 99 (1978) 1.
7 G. I. Moody and J. D. R. Thomas, Analyst, 104 (1979) 1.
8 T. Braun, A. B. Farag and M. P. Maloney, Anal. Chim. Acta, 93 (1977) 191.
9 T. Braun and M. N. Abbas, Anal. Chim. Acta, 119 (1980) 113.
10 H. J. M. Bowen, J. Chem. Soc. A, (1970) 1082.
11 T. Braun and A. B. Farag, Anal. Chim. Acta, 98 (1978) 133.
12 T. Braun, M. N. Abbas, A. Elek and L. Bakos, J. Radioanal. Chem., in press.

Analytica Chimica Acta, 134 (1982) 327—331
Elsevier Scientific Publishing Company, Amsterdam — Printed in The Netherlands

SOLVENT EXTRACTION OF ALKALINE EARTH METALS, AND LITHIUM WITH 1-PHENYL-3-METHYL-4-ACYLPYRAZOL-5-ONES AND TRIOCTYLPHOSPHINE OXIDE

SHIGEO UMETANI, KAZUE SASAYAMA and MASAKAZU MATSUI*
The Institute for Chemical Research, Kyoto University, Uji, Kyoto 611 (Japan)
(Received 7th August 1981)

SUMMARY

The synergic extraction of magnesium, calcium, strongium, barium and lithium into cyclohexane or benzene containing 1-phenyl-3-methyl-4-acyl-pyrazol-5-one (HA) and tri-*n*-octylphosphine oxide (TOPO) was investigated as a function of pH, HA and TOPO concentration. The extracted species when the 4-benzoyl compound was used, were $MA_2(TOPO)_2$ (M = Mg, Ca, Sr), $BaA_2(TOPO)_3$ and $LiA(TOPO)_2$. When the 4-trifluoroacetyl derivatives was used, the extracted species were the same except for $SrA_2(TOPO)_3$. Extraction constants for the synergic extractions were calculated.

4-Acylpyrazol-5-ones have proved to be very promising reagents for extracting metal chelates from acidic media [1—16], because they extract many metal ions at a lower pH than fluorinated β-diketones. In previous work in this laboratory, twenty 4-aroyl and 4-halogenated acyl derivatives of 1-phenyl-3-methylpyrazol-5-one were synthesized, and the extraction of europium and barium was investigated [15, 16]. Ghose et al. [17] developed a method for the extraction of radium and barium, using a mixture of 1-phenyl-3-methyl-4-benzoyl-pyrazol-5-one and tri-*n*-octylphosphine oxide (TOPO). However, no report seems to have appeared on a systematic study of the extraction of the alkaline earth metals. In the present paper, 1-phenyl-3-methyl-4-benzoyl-pyrazol-5-one (HPMBP) and 1-phenyl-3-methyl-4-trifluoroacetylpyrazol-5-one (HPMTFP) were chosen for a study of the synergic extraction of their chelates with alkaline earth metals and lithium, in the hope that a better understanding of the extraction system will lead to a wider use of these reagents in the extraction and separation of alkaline earth metals.

EXPERIMENTAL

Apparatus and reagents

Radioactivity measurements were carried out with a Metro Electronics NaI(Tl) well-type scintillation counter (44.5-mm diameter, 50.5-mm depth),

0003-2670/82/0000-0000/$02.75

Model PbW-6, equipped with a Metro automatic scaler, Model SS-1061H. Atomic absorption measurements were made with a Japan Jarrell-Ash Model AA-781 spectrometer.

HPMBP and HPMTFP were prepared by the method of Jensen [18]; analytical data for these reagents are shown in previous papers [15, 16]. Tri-*n*-octylphosphine oxide (TOPO) was purchased from Dojindo Co. Ltd. The $^{133}BaCl_2$ was supplied by New England Nuclear, Boston, MA. Stock solutions of alkaline earth metals and lithium were prepared by dissolving the carbonates in hydrochloric acid. All other chemicals were chemically pure or reagent-grade materials.

Extraction procedure

The procedure was essentially the same as that described previously [15]. A 10-ml portion of an aqueous solution containing the required amounts of metal ions, sodium perchlorate (0.1 M) and acetate (0.01 M) was placed in a 30-ml glass-stoppered centrifuge tube. After the pH of the solution had been adjusted to the desired value, 10 ml of the organic phase containing the pyrazolone (0.05 M) and various amounts of TOPO in benzene or cyclohexane were added. The two phases were shaken for 1 h at 25 ± 1°C. After centrifugation, the distribution of barium was determined radiometrically. The aqueous concentrations of magnesium, calcium, strontium and lithium were determined by atomic absorption spectrometry, and the metal concentrations in the organic phase were similarly measured in the aqueous solution after back-extraction with dilute hydrochloric acid. The pH of the aqueous phase was checked after the extraction process.

Data processing

In the synergic extraction of alkaline earth metals and lithium with a mixture of 4-acylpyrazolone (HA) and TOPO, the extraction equilibrium and the extraction constant, K_{ex}, can be expressed by

$$M^{n+} + nHA_o + sTOPO_o \rightleftharpoons MA_n(TOPO)_{s,o} + nH^+$$

$$K_{ex} = [MA_n(TOPO)_s]_o[H^+]^n_w/[M^{n+}]_w[HA]^n_o[TOPO]^s_o$$

where subscripts w and o, denote the concentrations of species in the aqueous and organic phases, respectively. If the concentrations of intermediate complexes such as MA^{n-1}, MA_n, $MA_n(TOPO)$ and $MA_n(TOPO)_2$ are negligible, the distribution ratio is given by $D = [MA_n(TOPO)_s]_o/[M^{n+}]$. Therefore, the extraction constant can be expressed as

$$K_{ex} = D[H^+]^n_w/[HA]^n_o[TOPO]^s_o$$

$$\text{or } \log K_{ex} = \log D - n\text{pH} - n\log[HA]_o - s\log[TOPO]_o \quad (1)$$

The number of TOPO molecules in the mixed complex can be determined from the slope of the graph $\log D$ vs. $\log[TOPO]_o$, at constant pH and $[HA]_o$.

RESULTS AND DISCUSSION

Figure 1 shows the log D vs. pH plots for the extraction of the HPMTFP chelates of the alkaline earth metals in the presence of TOPO, into benzene solution; results with cyclohexane were similar. In the absence of any adduct-forming organic bases, the extraction was very slight. As shown in Fig. 1, quantitative extraction (log $D > 2$) was achieved at pH $\geqslant$3.3 for magnesium, pH $\geqslant$3.6 for calcium, pH $\geqslant$4.7 for strontium and pH $\geqslant$5.7 for barium when benzene was used. The corresponding values for cyclohexane were $\geqslant$2.5, 2.6, 3.3 and 4.2, respectively. The slopes of the linear plots in both solvents for all the metal ions were close to 2, indicating that two hydrogen ions are released in the formation of each chelate.

The extraction curves for the HPMBP chelates of the same metals into benzene and cyclohexane in the presence of TOPO, are shown in Fig. 2. The slopes of all the plots are about 2, the theoretical value. As shown in Fig. 3, the log D vs. log$[\mathrm{HPMBP}]_o$ dependence at constant pH and TOPO concentration also indicates that two moles of the pyrazolone react with one mole of calcium ion to form the $MA_2(TOPO)_s$ type of chelate.

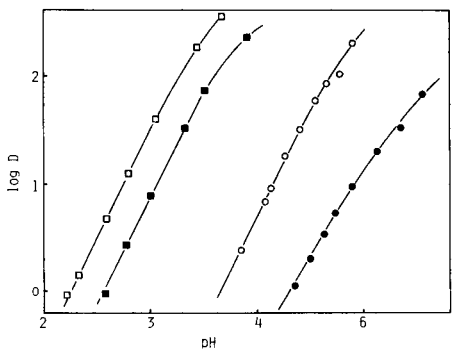

Fig. 1. Logarithm of the distribution ratio D as a function of pH. Benzene phase: 5×10^{-3} M HPMTFP, 1×10^{-2} M TOPO. (□) Mg; (■) Ca; (○) Sr; (●) Ba.

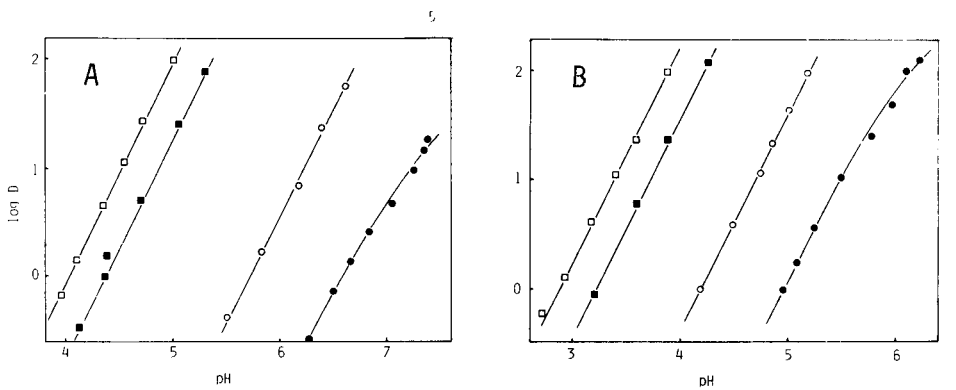

Fig. 2. Logarithm of the distribution ratio D as a function of pH. Organic phase: 5×10^{-2} M HPMBP and 1×10^{-2} M TOPO in (A) benzene, (B) cyclohexane. (□) Mg; (■) Ca; (○) Sr; (●) Ba.

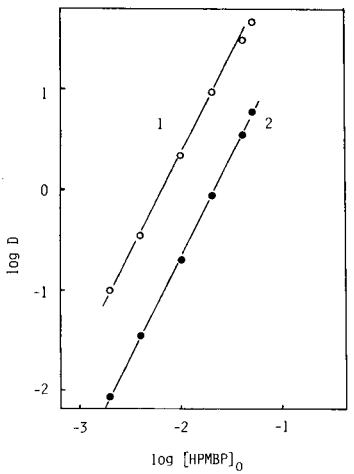

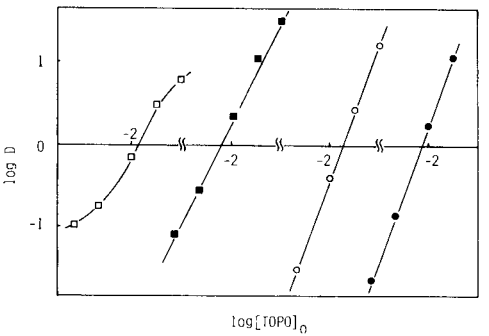

Fig. 3. Influence of HPMBP concentration (2×10^{-3}—5×10^{-2} M) on the extraction of calcium in the presence of 1×10^{-2} M TOPO: (1) cyclohexane, pH 4.0; (2) benzene, pH 4.7.

Fig. 4. Influence of TOPO concentration (2×10^{-3}—4×10^{-2} M) on the extraction into cyclohexane with 5×10^{-2} M HPMTFP. (□) Mg, pH 1.5; (■) Ca, pH 1.9; (○) Sr, pH 2.2; (●) Ba, pH 3.3. Log $[TOPO]_0$ scale as log D scale.

Figure 4 shows the increase in D with increasing TOPO concentration for HPMTFP in cyclohexane; similar results were achieved for HPMBP. The slopes are 2.0 for magnesium and calcium and 3.0 for strontium and barium in the HPMTFP extraction system; the same slopes were obtained with HPMBP except that the strontium slope was 2.0. When benzene was used, almost the same results were obtained. These differences in adduct formation are significant for the extractive separation of alkaline earth metals. Careful attention to the control of parameters such as the concentrations of chelating agent, organic solvent and especially TOPO, may result in considerably better separation between $MA_2(TOPO)_2$ and $MA_2(TOPO)_3$ adducts than is suggested by the simple chelate extraction system. The extraction constants calculated from the D values by means of Eqn. (1) are listed in Table 1.

TABLE 1

Extraction constants for $MA_n[TOPO]_s$

Ligand (HA)	Solvent	Mg $MgA_2(TOPO)_2$	Ca $CaA_2(TOPO)_2$	Sr $SrA_2(TOPO)_2$	Ba $BaA_2(TOPO)_3$	Li $LiA(TOPO)_2$
HPMBP	C_6H_6	−1.44	−2.27	−5.02	−4.56	−2.48
	C_6H_{12}	0.84	0.00	−2.02	−1.35	−1.10
		$MgA_2(TOPO)_2$	$CaA_2(TOPO)_2$	$SrA_2(TOPO)_3$	$BaA_2(TOPO)_3$	$LiA(TOPO)_2$
HPMTFP	C_6H_6	1.86	1.48	1.30	−0.04	−0.16
	C_6H_{12}	3.56	3.10	3.78	2.28	0.60

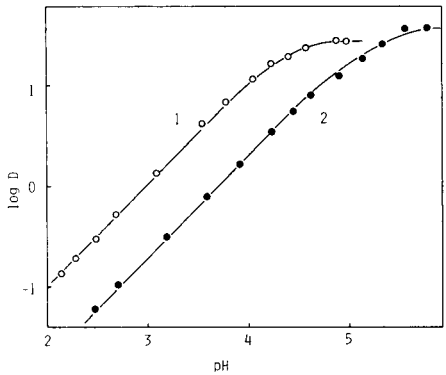

Fig. 5. Logarithm of the distribution ratio D for lithium as a function of pH with 5×10^{-2} M HPMTFP and 1×10^{-1} M TOPO in (1) cyclohexane, (2) benzene.

The extraction of lithium as a TOPO adduct of the pyrazolone chelates was also examined in the same way. Figure 5 shows that almost quantitative extraction was achieved at pH 4.5 in a 0.05 M HPMTFP—0.1 M TOPO—cyclohexane system. Plots of log D vs. log[TOPO] were linear and indicated that $LiA(TOPO)_2$ was extracted into cyclohexane. The extraction constants of the lithium chelates are also listed in Table 1.

REFERENCES

1 Yu. A. Zolotov and V. G. Lambrev, Zh. Anal. Khim., 20 (1965) 659.
2 Yu. A. Zolotov, M. K. Chmutova and P. N. Palei, Zh. Anal. Khim., 21 (1966) 1217.
3 M. K. Chmutova, P. N. Palei and Yu. A. Zolotov, Zh. Anal. Khim., 23 (1968) 1476.
4 M. K. Chmutova and N. E. Kochetkova, Zh. Anal. Khim., 24 (1969) 216.
5 B. F. Myasoedov and N. P. Molochnikova, Zh. Anal. Khim., 24 (1969) 702.
6 M. K. Chmutova, N. E. Kochetkova and Yu. A. Zolotov, Zh. Anal. Khim., 24 (1969) 711.
7 Yu. A. Zolotov, N. T. Sizonenko, N. T. Zolotovitskaya and E. I. Yakovenko, Zh. Anal. Khim., 24 (1969) 20.
8 Yu. A. Zolotov and L. G. Gavrilova, J. Inorg. Nucl. Chem., 31 (1969) 3613.
9 Yu. A. Zolotov, O. M. Petrukhin and L. G. Gavrilova, J. Inorg. Nucl. Chem., 32 (1970) 1679.
10 Y. Akama, T. Nakai and F. Kawamura, Jpn. Analyst, 25 (1976) 496.
11 Y. Akama, H. Naka, T. Nakai and F. Kawamura, Jpn. Analyst, 27 (1978) 680.
12 G. N. Rao and H. C. Arora, J. Inorg. Nucl. Chem., 19 (1977) 2057.
13 A. Roy and K. Nag, J. Inorg. Nucl. Chem., 40 (1978) 331.
14 B. Jensen, Acta Chem. Scand., 13 (1959) 1890.
15 S. Umetani, M. Matsui, J. Tôei and T. Shigematsu, Anal. Chim. Acta, 113 (1980) 315.
16 M. Matsui, J. Tôei, S. Umetani and T. Shigematsu, Bull. Inst. Chem. Res. Kyoto Univ., 57 (1979) 337.
17 A. K. Ghose, F. Sebesta and J. Starý, J. Radioanal. Chem., 24 (1975) 345.
18 B. Jensen, Acta Chem. Scand., 13 (1959) 1668.

Analytica Chimica Acta, 134 (1982) 333—339
Elsevier Scientific Publishing Company, Amsterdam — Printed in The Netherlands

KINETICS AND MECHANISM OF SOLVENT EXTRACTION OF COPPER WITH KELEX 100 IN PRESENCE OF NITRILOTRIACETIC ACID

SASWATI P. BAG[a] and HENRY FREISER*
Department of Chemistry, University of Arizona, Tucson, AZ 85721 (U.S.A.)
(Received 1st May 1981)

SUMMARY

A detailed study of the extraction kinetic behavior of copper(II) in aqueous media containing nitrilotriacetic acid (H_3Y) into chloroform solutions of Kelex 100, a high-molecular-weight alkylated 8-quinolinol, is described. The rate expression for the extraction of copper by Kelex 100, described by the expression $-d[Cu^{2+}]/dt = k'[Cu^{2+}][HL]_o/[HY^{2-}]^{0.5}$, supports a mechanism in which the rate-determining steps are the concurrent reactions of Cu^{2+} and CuY^- with a neutral Kelex 100 molecule in the aqueous phase.

Solvent extraction processes involving chelating extractants continue to be a separation technique of high significance for metal ion separations and trace organic determinations as well as for commercial process scale separations [1—5]. A great deal of research has been done to gain insight into existing processes, to understand fundamental equilibrium and kinetic aspects, and to exploit the technique for various analytical applications for the optimization of processing and design. For the last two decades, a series of systematic kinetic studies of chelating extraction systems has been conducted in this laboratory, and it has been demonstrated that the rate of extraction is attributable to the homogeneous chemical reactions in the aqueous phase [6—12].

During the last decade, kinetic studies of the extraction of metal ions by high-molecular-weight chelating extractants used in hydrometallurgy have been interpreted on the basis of rates of reactions taking place in interfaces [13—17]. Because several methods used to conduct rate studies involving Lewis cells [18], falling drops [19], and even automated centrifugal extraction apparatus [16, 20], have inadequate stirring efficiencies, kinetic results obtained may include contributions from diffusion processes.

This study addresses the question of whether by increasing the molecular weight of extractants to enhance the hydrophobicity of the ligand, the reaction site is relocated from the bulk aqueous phase to the interface as suggested by some workers [21]. The kinetics of the reaction for copper(II) with Kelex 100 is used as a model system for the study. Inasmuch as the rate

[a]On study leave from: Chemistry Department, Jadavpur University, Calcutta 70032, India.

0003-2670/82/0000-0000/$02.75

of extraction of hydrated copper ion is still too rapid for study in this system, nitrilotriacetic acid (H_3Y; NTA) is employed suitably to retard the reaction [22].

EXPERIMENTAL

Apparatus and reagents

The extraction kinetic apparatus has been described previously [23]. Copper was determined with a Varian AA-6 atomic absorption spectrometer equipped with a Westinghouse copper hollow-cathode lamp. Absorbances were measured at 324.7 nm with an air—acetylene flame and a spectral bandpass of 0.20 nm. Molecular absorptions were measured with a Gilford 2400 spectrophotometer using 10-mm quartz cells. All pH measurements were taken on an Orion 701 pH meter calibrated daily at pH 4.00 and 7.00 using buffer solutions (Micro Essential Laboratory, Inc.). A box-type Eberbach shaker with a shaking speed of 280 oscillations/min was used to equilibrate small volumes of aqueous and organic phases in 50-ml glass vials fitted with polyethylene stoppers and plastic screw caps.

An alkylated 8-quinolinol derivative, 7-(1-vinyl-3,3′,5,5′-tetramethylhexyl)-8-quinolinol (DDQ; commercially available as Kelex 100) was kindly supplied

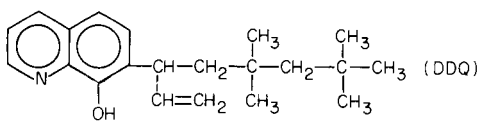

(DDQ)

in undiluted form by Sherex Chemical Company. The reagent was further purified for kinetic experiments by shaking a toluene solution of Kelex 100 with 1 M hydrochloric acid [24]. All other chemicals were reagent grade. Chloroform was washed and distilled twice, stored in the dark, and kept no longer than one week. A 0.01 M copper stock solution was prepared by dissolving pure copper wire (>99.9%) in a minimum volume of nitric acid, heating almost to dryness, a diluting to volume with water. The copper content of the stock solution was also determined by complexiметric titration with EDTA using murexide as indicator. All aqueous metal solutions were prepared daily from stock copper solution. The initial concentration of copper in the aqueous phase in kinetic experiments was 2×10^{-5} M, and the ionic strength was 0.1. Sodium sulfate was used throughout for this purpose and pH adjustments were made with sulfuric acid and sodium hydroxide solutions for equilibrium and kinetic studies.

Extraction kinetics procedure

Each phase was prepared in a 100-ml volumetric flask and immersed in a water bath thermostated at 25°C. After thermal equilibration (ca. 30 min), the aqueous solution was transferred to the reaction flask and thermostated in the same water bath. Next, the heavier chloroform solution was carefully

poured into the flask through a long-stem glass funnel to reduce the phase mixing so that metal extraction was negligible prior to starting the stirrer.

The reaction was begun by starting the stirring motor and a timer was started simultaneously. At predetermined intervals, samples (ca. 10 ml) were removed by purging the vessel with nitrogen gas to force an aliquot of the dispersion into a test tube without disturbing the course of the reaction in the flask. Samples were then centrifuged, and copper was determined in the aqueous phase by atomic absorption spectrometry. Since, at the low copper concentrations used, the response of the absorption spectrometer was linear with copper concentration, absorbance readings, A, were used in all calculations. The reaction rate constants, observed, k_{obs} were determined from

$$\ln [(A_o - A_e)/(A_t - A_e)] = k_{obs}t \quad (1)$$

where t is the sampling time, A_e and A_t are the aqueous phase absorbance at equilibrium and time t respectively. The equilibrium absorbance was obtained by collecting ca. 20 ml of the reaction mixture in a 50-ml glass vial at the end of the kinetic experiment and equilibrating the content on a shaker for 3 h.

The nature of the dependencies of the observed rate constant, k_{obs}, or the distribution coefficient of copper, D, on ligand as well as masking agent concentrations and pH was obtained from log—log plots of k_{obs} or D against the appropriate parameters.

RESULTS AND DISCUSSION

Inasmuch as the rate of extraction of copper by DDQ alone was found to be too fast to measure reliably by the usual method, the same stratagem was

TABLE 1

Summary of extraction kinetics of copper by Kelex 100 in presence of NTA ($[Cu^{2+}]_t = 2.00 \times 10^{-5}$ M; $I = 0.1$)

$[\text{Kelex 100}]_o(10^{-3}\text{ M})$	$[\text{NTA}](10^{-4}\text{ M})$	pH	$k_{obs}(10^{-4}s^{-1})$
0.50	1.00	4.00	2.51×10^{-4}
1.00	1.00	4.00	3.16×10^{-4}
1.50	1.00	4.00	4.47×10^{-4}
2.50	1.00	4.00	7.59×10^{-4}
3.50	1.00	4.00	10.0×10^{-3}
4.00	1.00	4.00	13.2×10^{-3}
5.00	1.00	4.00	15.1×10^{-3}
7.50	1.00	4.00	21.9×10^{-3}
10.0	1.00	4.00	30.9×10^{-3}
5.00	5.00	3.05	23.7×10^{-3}
5.00	5.00	3.55	9.48×10^{-4}
5.00	5.00	3.80	10.8×10^{-3}
5.00	5.00	4.05	26.1×10^{-3}
5.00	1.00	4.10	13.8×10^{-3}
5.00	1.00	4.22	12.0×10^{-3}
5.00	1.00	4.32	10.2×10^{-3}

TABLE 2

Summary of kinetic parameters

Dependent variable	Observed orders
$[HL]_o$	1.001 ± 0.027
$[H^+]$	−0.26 ± 0.28
[NTA]	−0.48 ± 0.04

used as was employed earlier [22], i.e., the addition of a complexing agent such as NTA to form a water-soluble copper complex which, by lowering the free copper concentration, slowed the overall extraction rate. Reaction orders in Table 2 were evaluated from data in Table 1 and were used to obtain the experimental rate expression

$$-d[Cu^{2+}]/dt = k'\,[Cu^{2+}][HL]_o/[H^+]^{0.26}[H_3Y]^{0.48} \quad (2)$$

Although the extraction is first order in both metal ion and DDQ, indicating that the formation of the 1:1 copper chelate is rate-determining, the fractional orders in both H^+ and H_3Y are, at first glance, somewhat puzzling. The expectation in the use of H_3Y was that the CuY^- would react very slowly or not at all with the extractant, leaving only the greatly decreased concentration of Cu^{2+} to react. This would lead to an inverse first-order dependence on H_3Y and zero order in H^+. The decrease in extraction rate with H_3Y addition does indeed signify that CuY^- reacts more slowly than Cu^{2+}, but taking the high concentration ratio of CuY^- to Cu^{2+} into account, it is not unreasonable to expect that both species reacting concurrently with DDQ might explain the fractional orders observed.

A reasonable explanation of the fractional dependences of $[HY^{2-}]$ and $[H^+]$ are their respective direct combination with DDQ as one of the possible pathways, i.e.

$$CuY^- + H^+ \overset{(K_{a3}\beta_{CuY})^{-1}}{\rightleftharpoons} Cu^{2+} + HY^{2-} \quad \text{(rapid pre-equilibrium)} \quad (3)$$

$$Cu^{2+} + HL \overset{k_1}{\rightleftharpoons} CuL^+ + H^+ \quad \text{(slow)} \quad (4)$$

$$-d[Cu^{2+}]/dt = k_1[Cu^{2+}][HL] = \{k_1/K_{a3}\beta_{CuY}K_{DR}\}$$

$$\{[CuY^-][HL]_o[H^+]/[HY^{2-}]\} \quad (5)$$

$$CuY^- + HL \overset{k_2}{\rightleftharpoons} CuL^+ + HY^{2-} \quad \text{(slow)} \quad (6)$$

$$-d[Cu^{2+}]/dt = k_2[CuY^-][HL] = \{k_2/K_{DR}\}\,[CuY^-][HL]_o \quad (7)$$

In these expressions, K_{DR} is the distribution coefficient of DDQ, β_{CuY} the formation constant of the Cu-NTA complex and K_{a3} the third acid dissociation constant of NTA.

If reactions (4) and (6) were both kinetically important in the determination of the rate of extraction of copper, then similar fractional orders of both $[H^+]$ and $[HY^{2-}]$ would be expected.

Also consistent with the observed order in $[H^+]$, is the following alternative pathway

$$Cu^{2+} + OH^- \overset{\beta_{CuOH}}{\rightleftharpoons} CuOH^+ \quad \text{(rapid pre-equilibrium)} \tag{8}$$

$$CuOH^+ + HL \overset{k_1'}{\rightleftharpoons} CuL^+ \quad \text{(slow)} \tag{9}$$

$$-d[Cu^{2+}]/dt = k_1'[CuOH^+][HL] = \{k_1'\beta_{CuOH}K_w/K_{a3}\beta_{CuY}K_{DR}\}$$

$$\{[CuY^-][HL]_o/(HY^{2-})\} \tag{10}$$

The overall rate expression combining reactions (4) and (6) would be

$$-d[Cu^{2+}]/dt = k_1[Cu^{2+}][HL] + k_2[CuY^-][HL] \tag{11}$$

$$= \left\{\frac{k_1[H^+]}{\beta_{CuY}K_{a3}K_{DR}}\frac{[HL]_o}{[HY^{2-}]} + \frac{k_2[HL]_o}{K_{DR}}\right\}[CuY^-] \tag{12}$$

which after integration becomes

$$\ln C_o/C_t = \left\{\frac{k_1[H^+][HL]_o}{\beta_{CuY}K_{a3}K_{DR}[HY^{2-}]} + \frac{k_2[HL]_o}{K_{DR}}\right\} t = k_{obs}t \tag{13}$$

where C_o and C_t represent the initial and time-dependent concentrations of total copper.

From Eqn. (13), a plot of k_{obs} vs. $[HY^{2-}]^{-1}$ should be linear with a slope proportional to k_1 and an intercept proportional to k_2 as follows

$$k_1 = (\text{slope})K_{DR}\cdot\beta_{CuY}K_{a3}/[H^+][HL]_o \tag{14}$$

$$k_2 = (\text{intercept})K_{DR}/[HL]_o \tag{15}$$

As shown in Table 3, the expected linearity was observed, giving a slope of $8.51 \pm 0.07 \times 10^{-8}$ and an intercept of $5.97 \pm 0.05 \times 10^{-4}$. Using values of $\log K_{DR} = 5.52 \pm 0.10$ [24], $\log \beta_{CuY} = 12.94$ [25], and $\log K_{a3} = 9.65$ [25], values for $k_1 = 1.10 \pm 0.15 \times 10^8$ M^{-1} s^{-1} and for $k_2 = 3.98 \pm 0.28 \times 10^4$ M^{-1} s^{-1} are obtained.

Alternatively, considering reactions (6) and (9), the overall rate expression would be

$$-d[Cu^{2+}]/dt = k_1'[CuOH^+][HL] + k_2[CuY^-][HL] \tag{16}$$

$$= \left\{\frac{k_1'\beta_{CuOH}K_w\,[HL]_o}{\beta_{CuY}K_{a_3}K_{DR}\,[HY^{2-}]} + \frac{k_2[HL]_o}{K_{DR}}\right\}[CuY^-] \tag{17}$$

which on integration yields

TABLE 3

The effect of $[HY^{2-}]^{-1}$ on the k_{obs} in presence of NTA

pH	$[HY^{2-}]^{-1}(10^3\ M^{-1})$	$k_{obs}(10^{-3}\ s^{-1})$	Slope	Intercept
3.96	1.02	0.76	8.51 (± 0.07) × 10^{-8}	5.97 (± 0.05) × 10^{-4}
3.96	5.56	1.11		
4.05	12.5	1.36		
4.07	2.08	0.75		
4.10	1.47	0.64		

$$\ln C_o/C_t = \left\{ \frac{k_1'\beta_{CuOH}K_w\,[HL]_o}{\beta_{CuY}K_{a3}K_{DR}\,[HY^{2-}]} + \frac{k_2\,[HL]_o}{K_{DR}} \right\} t = k_{obs}t \qquad (18)$$

A plot of k_{obs} vs. $[HY^{2-}]^{-1}$ should be linear with a slope proportional to k'

$$k_1' = (\text{slope})K_{DR}\beta_{CuY}K_{a3}/\beta_{CuOH}K_w\,[HL]_o \qquad (19)$$

and an intercept proportional to k_2 as indicated by Eqn. (15). From this, the value $k_1' = 5.5 \pm 0.33 \times 10^{11}\ M^{-1}s^{-1}$ is obtained. Inasmuch as the extraction kinetics was studied at pH 4.0, the likelihood of this alternative pathway is not as strong as that involving reactions (4) and (6).

An attempt to evaluate the rate constant assuming that CuY^-, Cu^{2+} and/or $CuOH^+$ react with $[L^-]$ instead of [HL], resulted in unrealistically high values for k_1, i.e., $10^{13.5}$ and $10^{13.75}$, respectively. Apparently, then, it is the unionized DDQ that participates in reaction with copper under the stated conditions. The value of k_1 of $1.10 \times 10^8\ M^{-1}s^{-1}$ is in accord with typical substitution reactions of Cu^{2+} [26].

This agreement with generally observed rate constants for copper substitution reaction in aqueous media represents strong evidence for the mechanism of Cu–DDQ extraction developed here rather than for any mechanism which suggests interfacial reaction. The results may be considered a helpful guide to the design of new metal extractants, more highly hydrophobic in character for both analytical and hydrometallurgical applications.

This work was supported by the National Science Foundation.

REFERENCES

1 G. H. Morrison and H. Freiser, Solvent Extraction in Analytical Chemistry, J. Wiley, New York, 1957.
2 E. B. Sandell, Colorimetric Determination of Traces of Metals, 3rd edn., Interscience, New York, 1959.
3 A. Leo, C. Hansch and D. Elkins, Chem. Rev., 71 (1971) 525.
4 G. Schill, in J. A. Marinsky and Y. Marcus (Eds.), Ion Exchange and Solvent Extraction, Vol. 6, M. Dekker, New York, 1974, pp. 1—57.
5 A. W. Ashbrook, Coord. Chem. Rev., 16 (1975) 285.
6 C. B. Honaker and H. Freiser, J. Phys. Chem., 66 (1962) 127.

7 B. E. McClellan and H. Freiser, Anal. Chem., 36 (1964) 2262.
8 J. S. Oh and H. Freiser, Anal. Chem., 39 (1967) 295.
9 P. R. Subbaraman, M. Cordes and H. Freiser, Anal. Chem., 41 (1969) 1878.
10 S. P. Carter and H. Freiser, Anal. Chem., 52 (1980) 511.
11 K. Ohashi and H. Freiser, Anal. Chem., 52 (1980) 767, 2214.
12 H. Freiser, Proc. Int. Solvent Extr. Conf., 1980, Vol. 1, 80-II.
13 D. R. Spink and D. N. Okuhara, Int. Symp. Hydrometall., AIME, New York, 1972, pp. 497.
14 D. R. Spink and D. N. Okuhara, Proc. Int. Solvent Extr. Conf., 1974, pp. 2527.
15 V. I. Lakshmanan, G. J. Lawson and P. S. Nyholm, Proc. Int. Solvent Extr. Conf., 1974, pp. 699.
16 D. S. Flett, J. A. Hartlage, D. R. Spink and D. N. Okuhara, J. Inorg. Nucl. Chem., 37 (1975) 1967.
17 D. S. Flett and D. R. Spink, Proc. Int. Solvent Extr. Conf., 1977, pp. 496.
18 C. A. Fleming, The Kinetics and Mechanism of the Solvent Extraction of Copper by LIX 64N and Kelex 100, N.I.M. Rep. No. 1793, 1976, Johannesburg, S. Africa.
19 C. Hanson, R. J. Whewell and M. A. Hughes, J. Inorg. Nucl. Chem., 37 (1975) 2303.
20 D. S. Flett, D. N. Okuhara and D. R. Spink, J. Inorg. Nucl. Chem., 35 (1973) 2471.
21 C. A. Fleming and M. J. Nicol, J. Inorg. Nucl. Chem., 42 (1980) 1327; 42 (1980) 1335.
22 V. V. Bagreev and H. Freiser, Sep. Sci., in press.
23 S. P. Carter and H. Freiser, Anal. Chem., 51 (1979) 1100.
24 S. P. Bag and H. Freiser, Anal. Chim. Acta, in press.
25 L. G. Sillén and A. E. Martell, Stability Constants of Metal Ion Complexes, Special Publ. No. 17, The Chemical Society, London, 1964.
26 R. G. Wilkins, The Study of Kinetics and Mechanism of Reactions of Transition Metal Complexes; Allyn and Bacon, New York, 1974.

Analytica Chimica Acta, 134 (1982) 341—348
Elsevier Scientific Publishing Company, Amsterdam — Printed in The Netherlands

CONSTANTES D'ACIDITE DE L'ACIDE PYROPHOSPHORIQUE ET CONSTANTES DE STABILITE DES COMPLEXES AVEC LE POTASSIUM ET LE SODIUM

ALBERT DELANNOY et JACQUES NICOLE

Laboratoire de Chimie Analytique, E.N.S.C. Lille, B.P. 40, 59650 Villeneuve d'Ascq (France)

JEAN HENNION*

Groupe d'Etudes Appliquées, U.E.R. Chimie, Université des Sciences et Techniques de Lille 59665 Villeneuve d'Ascq (France)

(Reçu le 13 Juillet 1981)

SUMMARY

(The acidity constants of pyrophosphoric acid and the stability constants of complexes with potassium and sodium ions)

The effect of potassium and sodium ions on the acidity constants of pyrophosphoric acid is studied by potentiometry at 25°C and at an ionic strength of 0.5 mol l^{-1}. Comparison of the results obtained in potassium chloride or sodium chloride medium with those found in tetramethylammonium chloride medium provides evidence of the formation of potassium and sodium complexes of the type $MHP_2O_7^{2-}$ and $MP_2O_7^{3-}$. Stability constants of these complexes are calculated and distribution diagrams of the species as a function of pH are given for the three different media utilized.

RESUME

L'influence des ions K^+ et Na^+ sur les constantes d'acidité de l'acide pyrophosphorique est étudiée à 25°C et à force ionique 0,5 mol l^{-1} par potentiométrie. La comparaison des résultats obtenus en présence de chlorure de potassium ou de sodium avec ceux obtenus en milieu chlorure de tétraméthylammonium permet de mettre en évidence la formation de complexes potassiques et sodiques du type $MHP_2O_7^{2-}$ et $MP_2O_7^{3-}$. Les constantes de stabilité de ces complexes sont déterminées et les diagrammes de répartition des espèces en fonction du pH sont établis dans les trois milieux considérés.

L'étude de la complexation de cations métalliques par un acide nécessite la connaissance de ses constantes d'acidité. Celles-ci sont souvent affectées par la présence d'ions alcalins dans le milieu expérimental, comme dans le cas de l'acide pyrophosphorique. Quoique de nombreuses publications aient été consacrées à son étude [1, 2], peu d'auteurs ont montré l'influence des ions alcalins. Les premiers travaux ont été réalisés par Monk [3] qui a mis en évidence par conductimétrie la présence du complexe $NaP_2O_7^{3-}$ dont il a déterminé la constante. D'autres travaux ont été réalisés par potentio-

0003-2670/82/0000-0000/$02.75

métrie [4—7] ou calorimétrie [8], Näsänen [9] n'a fait qu'évoquer la formation probable de complexes alcalins de l'acide pyrophosphorique.

Etudiant la complexation par les ions pyrophosphate de cations métalliques divalents en milieu chlorure de potassium et de sodium à 25°C et à force ionique 0,5 mol l^{-1}, nous avons en premier lieu déterminé les constantes d'acidité du complexant dans les mêmes conditions. Les résultats obtenus par potentiométrie sont exposés dans cet article.

PARTIE EXPERIMENTALE

Réactifs

Le pyrophosphate de tétraméthylammonium est préparé par échange d'ion. Une colonne de résine Dowex 50W-X2 (H^+) de 40 cm de hauteur et de diamètre 3 cm, est chargée avec une solution de chlorure de tétraméthylammonium (Fluka), puis un rinçage à l'eau est effectué pour éliminer l'excés de chlorure. L'élution est réalisée avec une solution de pyrophosphate de potassium (Carlo Erba, R.P.E.), dont la concentration est environ le double de la concentration finale en pyrophosphate de tétraméthylammonium désirée. Au cours de l'échange $(CH_3)_4N^+$—K^+, la résine passe du jaune pâle au rouge orangé, et cette variation de teinte peut servir de test de fin d'élution. Après avoir été rincée à l'eau, la résine est remise sous sa forme primitive avec une solution d'acide chlorhydrique. Toutes ces opérations se font sous atmosphère d'azote.

Les solutions d'acide chlorhydrique, de chlorure de sodium et de potassium sont obtenues à partir de produits pour analyse (Merck). Les solutions d'hydroxydes sont préparées exemptes de carbonate et stockées sous atmosphère inerte, les produits initiaux étant des produits pour analyse (Merck ou Sigma).

Toutes les solutions sont préparées avec de l'eau distillée, déionisée et bouillie avant emploi.

Techniques expérimentales

Les variations de pH d'une solution de pyrophosphate de tétraméthylammonium au cours de l'addition d'une solution d'acide chlorhydrique, les deux solutions étant à force ionique 0,5 mol l^{-1} en $(CH_3)_4NCl$, KCl ou NaCl, sont suivies par potentiométrie. Le volume initial est de 100 ml, et le vase de titrage est maintenu à 25 ± 0,1°C par circulation d'eau thermostatée. Les mesures de pH sont effectuées avec un potentiomètre Radiometer PHM 64 utilisé avec une électrode indicatrice de verre et une électrode de référence calomel—KCl saturé. La chaîne potentiométrique est standardisée avec les tampons hydrogénophthalate de potassium et tétraborate de sodium.

RESULTATS ET DISCUSSION

L'acide pyrophosphorique étant symbolisé par H_4A, les constantes d'acidité se notent sous la forme générale

$$K_j = [H^+]\,[H_{4-j}A^{j-}]/[H_{5-j}A^{(j-1)-}]$$

Le calcul de ces constantes requiert la détermination de la concentration en ions H^+ de la solution qui peut être reliée à la valeur expérimentale du pH. Dans ce but, nous avons étalonné la chaîne de mesure dans les différents milieux [$(CH_3)_4NCl$, KCl et NaCl] avec l'acide chlorhydrique pour les pH compris entre 2,5 et 6,5 et avec l'hydroxyde de sodium (milieu NaCl), l'hydroxyde de potassium (milieu KCl) et l'hydroxyde de tétraméthylammonium (milieu $(CH_3)_4NCl$) pour la zone de pH 7,5—10,5. Nous avons obtenu de cette manière des abaques donnant dans chaque milieu la valeur de $-\log_{10}[H^+]$ en fonction du pH.

La détermination des constantes d'acidité d'un acide suppose que les ions présents dans la solution ne réagissent pas avec une des formes de cet acide. Il faut donc opérer en présence de cations qui ne soient pas complexés par les espèces pyrophosphate. Il est admis que les ions tétralkylammonium répondent à cette exigence, et nous avons donc pris le chlorure de tétraméthylammonium comme milieu pour étudier les acidités de l'acide pyrophosphorique.

La courbe d'acidification d'une solution de pyrophosphate de tétraméthylammonium par une solution d'acide chlorhydrique présente deux sauts de pH pour les rapports [HCl]/[pyrophosphate] égaux à 1 et 2, respectivement dans les zones de pH 8—6,5 et 5,5—3,5; la décroissance du pH étant continue pour les rapports supérieurs à 2 (Fig. 1a). La forme de la

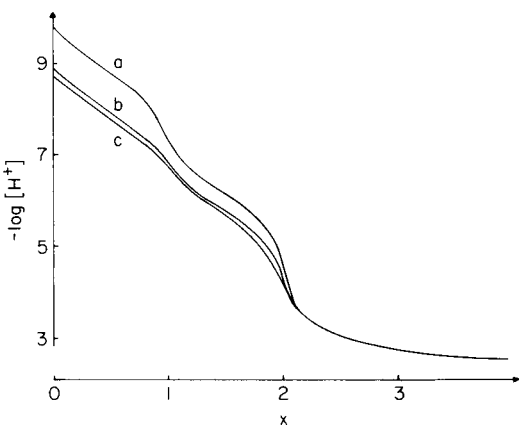

Fig. 1. Courbes d'acidification du pyrophosphate de tétraméthylammonium ($2{,}5 \times 10^{-3}$ mol l^{-1}) par l'acide chlorhydrique ($9{,}75 \times 10^{-2}$ mol l^{-1}) à 25°C et à force ionique 0,5 mol l^{-1}: (a) milieu $(CH_3)_4NCl$; (b) milieu KCl; (c) milieu NaCl.

courbe et les valeurs mises en évidence indiquent que l'acide pyrophosphorique possède deux acidités séparées et faibles et deux acidités fortes très voisines.

De ce fait, les constantes K_3 et K_4 peuvent être calculées séparément à partir de l'équation

$$pH = pK_j + \log [H_{4-j}A^{j-}]/[H_{5-j}A^{(j-1)-}] \quad (1)$$

A partir des bilans en concentration et de la neutralité électrique, nous pouvons déterminer les relations donnant $[H_{4-j}A^{j-}]$ et $[H_{5-j}A^{(j-1)-}]$.

En prenant la concentration initiale en pyrophosphate égale à C_o pour un volume initial V_o et la concentration initiale en acide ajouté égale à C, le volume versé étant V, nous avons pour le calcul de pK_4

$$[A^{4-}] = \{(C_oV_o - CV)/(V_o + V)\} + \{[H^+] - [OH^-]\}$$

$$\text{et } [HA^{3-}] = \{CV/(V_o + V)\} - \{[H^+] - [OH^-]\}$$

et pour le calcul de pK_3

$$[HA^{3-}] = \{(2\,C_oV_o - CV)/(V_o + V)\} + \{[H^+] - [OH^-]\}$$

$$\text{et } [H_2A^{2-}] = \{(CV - C_oV_o)/(V_o + V)\} - \{[H^+] - [OH^-]\}$$

Les valeurs de $[H^+]$ sont obtenues à partir des abaques et celles de $[OH^-]$ à partir de la relation $[H^+]\,[OH^-] = K_e$, avec pK_e égal à 13,75 en milieu $(CH_3)_4NCl$; 13,76 en milieu KCl et 13,71 en milieu NaCl. Ces trois valeurs ont été déterminées à force ionique 0,5 mol l^{-1} lors des étalonnages de la chaîne potentiométrique.

En portant sur un graphe les valeurs du pH en fonction de celles de $\log [H_{4-j}A^{j-}]/[H_{5-j}A^{(j-1)-}]$, nous obtenons une droite de pente égale à 1 et dont l'ordonnée à l'origine est égale à pK_j.

Les valeurs de K_1 et K_2 sont déterminées simultanément à partir de la relation

$$\{\bar{n}K_3K_4 + (\bar{n} - 1)\,K_3\,[H^+] + (\bar{n} - 2)\,[H^+]^2\}/(3 - \bar{n})\,[H^+]^3 = \{(4 - \bar{n})\,[H^+]/$$
$$K_1K_2\,(3 - \bar{n})\} + K_2^{-1} \quad (2)$$

dans laquelle $\bar{n}$ représente la fonction de Bjerrum. Avec les mêmes conditions que précédemment, nous avons

$$\bar{n} = \{CV - (H^+ - OH^-)(V_o + V)\}/C_oV_o$$

L'équation (2) est de la forme $y = ax + b$ avec $a = (K_1K_2)^{-1}$ et $b = K_2^{-1}$, ces deux grandeurs sont déterminées graphiquement.

Les valeurs de K_1, K_2, K_3 et K_4 trouvées en milieu chlorure de tétraméthylammonium sont regroupées dans le Tableau 1.

Lorsque le milieu contient des ions K^+ et Na^+ les courbes d'acidification du pyrophosphate de tétraméthylammonium par l'acide chlorhydrique sont semblables à celles obtenues en leur absence. Pour les rapports [HCl] /[pyro-

TABLEAU 1

Constantes d'acidité de l'acide pyrophosphorique à 25°C et à force ionique 0,5 mol l^{-1}

Valeur des constantes (mol l^{-1})	Milieu $(CH_3)_4NCl$	Milieu KCl	Milieu NaCl
K_1 (10^{-2})	4,2 ± 0,5	4,2 ± 0,5	4,2 ± 0,5
K_2 (10^{-2})	1,3 ± 0,2	1,3 ± 0,2	1,3 ± 0,2
K_3 (10^{-6})	1,07 ± 0,03	2,56 ± 0,05	2,90 ± 0,06
K_4 (10^{-8})	0,35 ± 0,01	2,37 ± 0,03	3,50 ± 0,07

phosphate] de 0 à 2, il y a un décalage entre les courbes obtenues dans les différents milieux: en présence de K^+ et Na^+ les courbes sont déplacées vers les pH plus acides. Ce décalage croît avec la concentration en ions alcalins. Il est plus grand en présence de Na^+ qu'en présence de K^+ et il est plus important pour les rapports molaires compris entre 0 et 1 que pour ceux compris entre 1 et 2. Pour les rapports supérieurs à 2, les trois courbes sont confondues (Fig. 1b et c).

De l'allure de ces courbes, nous pouvons déduire qu'il existe deux complexes entre les ions Na^+ et K^+ et les ions pyrophosphate du type MA^{3-} et MHA^{2-} (M^+ symbolisant l'ion alcalin) qui renforcent la troisième et surtout la quatrième acidité de l'acide pyrophosphorique.

A partir de l'équation (1) et en utilisant le même raisonnement que précédemment, nous pouvons déterminer en milieu chlorure de potassium et chlorure de sodium à force ionique 0,5 mol l^{-1} les valeurs des constantes des troisième et quatrième acidités; les deux premières constantes étant identiques. Le Tableau 1 regroupe les différentes valeurs obtenues. Ces résultats sont compatibles avec ceux de la littérature, en tenant compte de la grande divergence observée pour les valeurs de la première constante dans les travaux antérieurs, quelque soit la force ionique [1].

Les complexes alcalins dont les réactions de formation sont du type

$$M^+ + HA^{3-} \rightleftharpoons MA^{3-} + H^+ \text{ et } M^+ + H_2A^{2-} \rightleftharpoons MHA^{2-} + H^+$$

sont caractérisés par leur constante de stabilité

$$\beta_{MA} = [MA^{3-}]/[M^+][A^{4-}] \text{ et } \beta_{MHA} = [MHA^{2-}]/[M^+][HA^{3-}]$$

En milieu MCl, les constantes d'acidité apparentes de l'acide pyrophosphorique peuvent s'écrire

$$K_3' = [H^+]([HA^{3-}] + [MHA^{2-}])/[H_2A^{2-}] \text{ et } K_4' = [H^+]([A^+] + [MA^{3-}])/[HA^{3-}]$$

en faisant intervenir les constantes de stabilité des complexes, nous avons

$$K_3' = K_3 (1 + \beta_{MHA} [M^+]) \qquad (3)$$

et $K'_4 = K_4 (1 + \beta_{MA} [M^+])/(1 + \beta_{MHA} [M^+])$ (4)

Par approximations successives et en prenant pour première valeur $[M^+] = M_o - A_o$ (M_o et A_o étant respectivement les concentrations initiales en métal alcalin et en acide pyrophosphorique), nous pouvons calculer β_{MHA} à partir de l'équation (3) et β_{MA} à partir de l'équation (4). Les valeurs trouvées sont rassemblées dans le Tableau 2.

La filiation entre les différentes espèces en solution peut se résumer par le schéma

$$P_2O_7^{4-} \underset{K_4}{\overset{H^+}{\rightleftharpoons}} HP_2O_7^{3-} \underset{K_3}{\overset{H^+}{\rightleftharpoons}} H_2P_2O_7^{2-}$$

$$\beta_{MA} \Downarrow M^+ \qquad \beta_{MHA} \Downarrow M^+ \qquad H^+, M^+ \underset{K^{MHA}_{H_2A}}{\rightleftharpoons}$$

$$MP_2O_7^{3-} \underset{K^{MA}_{MHA}}{\overset{H^+}{\rightleftharpoons}} MHP_2O_7^{2-}$$

Pour déterminer $K^{MHA}_{H_2A}$ et K^{MA}_{MHA} nous utilisons les relations

$K^{MHA}_{H_2A} = [MHA^{2-}][H^+]/[H_2A^{2-}][M^+] = \beta_{MHA} K_3$

et $K^{MA}_{MHA} = [MA^{3-}][H^+]/[MHA^{2-}] = \beta_{MA} K_4/\beta_{MHA}$

Le Tableau 2 regroupe les valeurs obtenues pour les différentes constantes définies dans le schéma.

Dans les travaux antérieurs, seuls Botts et al. [7] ont mis en évidence la présence du complexe $KHP_2O_7^{2-}$, et compte tenu des diverses forces ioniques utilisées, nos résultats sont en accord avec ceux de la littérature.

Afin de mettre en évidence l'influence des ions alcalins présents en solution, nous avons établi le diagramme de répartition des espèces dans les trois milieux expérimentaux, en portant sur un graphe le rapport α_n (concentration d'une espèce/concentration initiale en acide pyrophosphorique) en fonction du pH (Fig. 2). Le rapport α_n est calculé à partir des constantes d'acidité et de stabilité et de la concentration en protons correspondant au pH.

TABLEAU 2

Constantes de stabilité des complexes potassiques et sodiques de l'acide pyrophosphorique à 25°C et à force ionique 0,5 mol l^{-1}

Constantes	$M^+ = K^+$	$M^+ = Na^+$
β_{MHA} (l mol^{-1})	2,9 ± 0,3	4,8 ± 0,3
β_{MA} (l mol^{-1})	32 ± 4	87 ± 8
$K^{MHA}_{H_2A}$	3,1 ± 0,7 × 10^{-6}	5,0 ± 0,4 × 10^{-6}
K^{MA}_{MHA} (mol l^{-1})	4,0 ± 0,9 × 10^{-8}	6,7 ± 0,6 × 10^{-8}

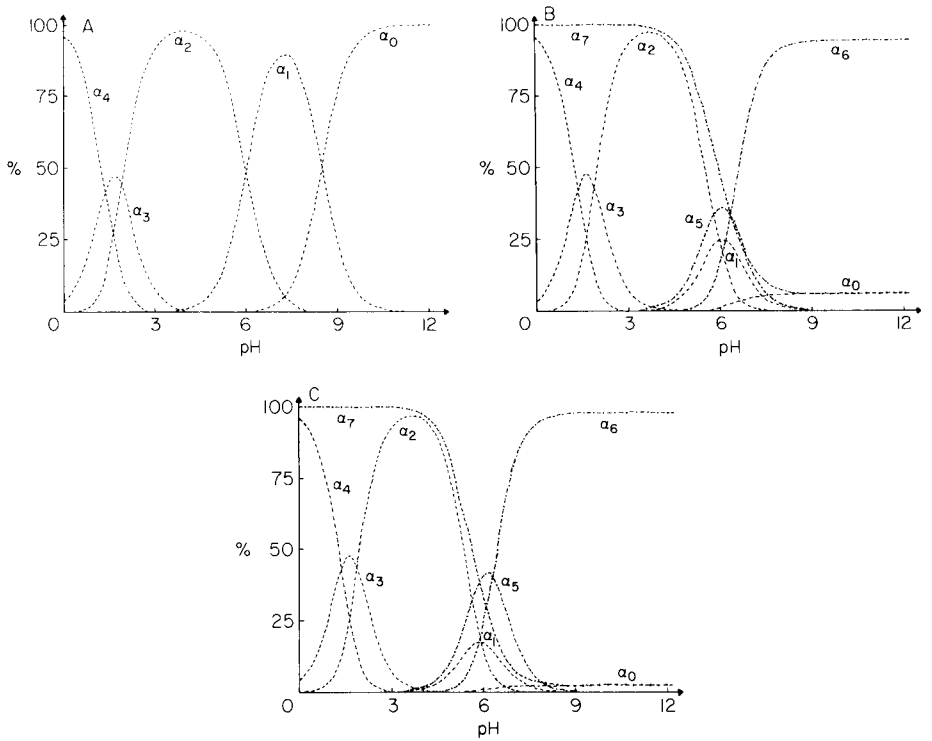

Fig. 2. Diagrammes de répartition des espèces dans les trois milieux expérimentaux à 25°C et à force ionique 0,5 mol l^{-1}: (A) $(CH_3)_4NCl$; (B) KCl; (C) NaCl. $\alpha_0 = [P_2O_7^{4-}]/C_0$, $\alpha_1 = [HP_2O_7^{3-}]/C_0$, $\alpha_2 = [H_2P_2O_7^{2-}]/C_0$, $\alpha_3 = [H_3P_2O_7^{-}]/C_0$, $\alpha_4 = [H_4P_2O_7]/C_0$, $\alpha_5 = [MHP_2O_7^{2-}]/C_0$, $\alpha_6 = [MP_2O_7^{3-}]/C_0$ et $\alpha_7 = [M^+]/M_0$.

La comparaison des trois diagrammes montre que seule la répartition des espèces $HP_2O_7^{3-}$ et $P_2O_7^{4-}$ est affectée par la présence d'ions alcalins. Le maximum de concentration en ions $HP_2O_7^{3-}$ libres passe de 90% à 25% de la concentration totale en pyrophosphate et celui des ions $P_2O_7^{4-}$ libres à pH 10 passe de 97% à 2%.

Il apparaît donc que, si ces deux espèces interviennent dans la complexation de cations métalliques, les ions alcalins présents dans la solution auront une action non négligeable sur les phénomènes et qu'il faudra en tenir compte dans la détermination des constantes de stabilité des complexes métalliques.

BIBLIOGRAPHIE

1 L. G. Sillén et A. E. Martell, Stability Constants of Metal—Ion Complexes, The Chemical Society, London, 1964, p. 190; Supplement No. 1, The Chemical Society, London, 1971, p. 112.
2 R. M. Smith et A. E. Martell, Critical Stability Constants, Vol. 4, Plenum Press, New York, 1976, p. 59.
3 C. B. Monk, J. Chem. Soc., (1949) 423.

4 J. A. Davis, Thèse, Indiana University, 1955.
5 S. M. Lambert, Thèse, Ohio University, 1957.
6 J. A. Wolhoff et J. T. G. Overbeek, Rec. Trav. Chim., 78 (1959) 759.
7 J. Botts, A. Chashin et H. L. Young, Biochemistry, 4(9) (1965) 1788.
8 V. P. Vasilev et S. A. Aleksandrova, Russ. J. Inorg. Chem., 18 (1973) 1089.
9 R. Näsänen, Suom. Kemistil. B, 33 (1960) 47.

Analytical Chimica Acta, 134 (1982) 349—352
Elsevier Scientific Publishing Company, Amsterdam — Printed in The Netherlands

Short Communication

GASEOUS CATALYSTS FOR END-POINT INDICATION IN TITRIMETRIC ANALYSIS IN THE MICROGRAM RANGE WITH IODIDE AND BROMIDE AS CATALYSTS

HERBERT WEISZ* and JOACHIM SCHLIPF

Institut für Analytische Chemie, Chemisches Laboratorium der Universität, Freiburg i. Br. (W. Germany)

(Received 20th July 1981)

Summary. A new technique for end-point detection in titrations with bromate is described. The first drop in excess causes evolution of bromine which is swept by nitrogen into an indicator vessel. There, the bromine reacts with iodide to form iodine which catalyzes the cerium(IV)—arsenic(III) reaction or with sulfite to form bromide which catalyzes the permanganate—iodine reaction. Microgram amounts of antimony(III) or arsenic(III) can be determined.

The application of catalytic reactions for end-point indication in titrimetric analysis has led to the development of numerous methods in recent years [1, 2]. In contrast to other kinetic catalytic methods, quantitative interpretation of the catalyzed reaction is not necessary; the catalyst only has to be present in an amount just sufficient to cause an observable acceleration of the indicator reaction. In the application of these methods, the catalyst itself serves as the titrant. Substances can be titrated which are able to decrease significantly the activity of the catalyst by precipitation, complex formation or oxidation [3, 4]. When all the inhibitor has been consumed (end-point of the titration), the first drop of the titrant (catalyst) in excess immediately accelerates the indicator reaction. This means that a very small excess will catalyze rather large amounts of the indicator reaction mixture. Such catalytic end-points are therefore remarkably sensitive.

Recently, a new method has been described in which a gas is evolved at the end-point and acts as a catalyst for the indicator reaction; this reaction takes place in a separate indicator vessel [4]. Two more possibilities for the application of gaseous catalysts are discussed in the present communication. Bromate can be used as titrant for the determination of various ions by oxidation reactions. At the end-point, the bromine formed is swept by nitrogen to a separate vessel where it reacts with iodide to form iodine; this in turn is swept into an indicator vessel containing cerium(IV)—arsenic(III) solution. The Ce(IV)—As(III) reaction is catalyzed by iodide and iodine [5]. The other possibility for titrations with bromate is to transfer the bromine formed at the end-point into several vessels each containing sulfite solution, where the

0003-2670/82/0000-0000/$02.75

bromine is reduced to bromide, which catalyzes the permanganate—iodine reaction [6].

Determination of antimony(III) and arsenic(III) by means of the cerium(IV)—arsenic(III) indicator reaction

Apparatus. Figure 1 shows a schematic representation of the necessary arrangement. A 15-ml test tube (1) serves as the titration vessel. Through the stopper lead three capillary tubes: one for the titrant, one for nitrogen and one to connect the titration vessel with the indicator reaction system (2). Tube A containing solid potassium iodide on glass wool is heated at about 185°C (3), and tube B contains the cerium(IV)—arsenic(III)—ferroin solution. The titrant solution is delivered at constant speed from an automatic syringe burette (4). The flow of nitrogen is regulated by a flow meter (Rota, Wehr, tube L 0, 063/4, 4).

General procedure. The following indicator reagent mixture is placed in the indicator reaction vessel (B) whilst nitrogen is flowing: 0.5 ml of 0.057 M cerium(IV) solution in 1 M H_2SO_4, 0.3 ml of 0.071 M arsenic(III) solution at pH 7.8, and 0.05 ml of 0.025 M ferroin solution diluted with water to about 2.5 ml.

A 0.00167 M bromate standard solution is delivered at a constant speed of 0.112 ml min^{-1} into the titration vessel. The temperature of the heater is maintained at 185 ± 5°C, and the flow of nitrogen is 50 ml min^{-1}. The glass wool impregnated with potassium iodide (2—5 mg; potassium iodide and glass wool 1:1) serves for 10—20 titrations. In all determinations, the time for the delivery of the bromate titrant is measured exactly with a stopwatch between the start of the titration and the end-point (colour change from green to red).

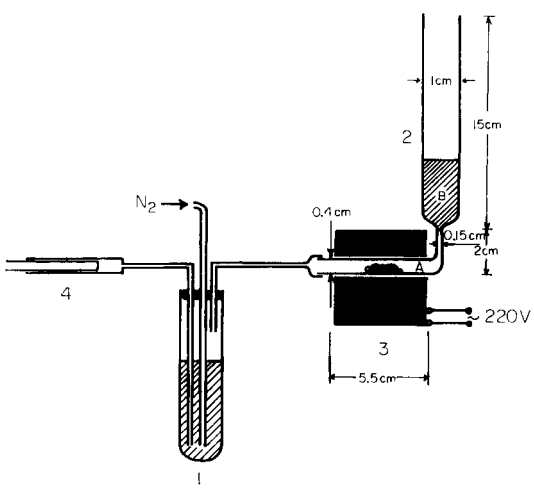

Fig. 1. Schematic representation of the titration arrangement: (1) titration vessel; (2) indicator system; (3) heater; (4) automatic syringe burette.

A non-catalytic method of indication is also applicable: instead of the indicator vessel, a cotton pad (about 30 mg) impregnated with iodide/starch (200 μl of 0.1 M KI and 200 μl of 0.5% starch solution) is placed directly into the nitrogen stream leaving the titration vessel. The time between the start of titrant addition and the first blue coloration is measured.

In both cases a standard graph is required (which is linear in all the examples described here) because blanks arise from the time difference between the liberation of the bromine in the titration vessel and the completion of the indicator reaction.

Determination of antimony(III). An aliquot (1 ml) of antimony(III) solution (sample or standard) containing 30—300 μg Sb(III) in 2 M HCl is mixed with 1 ml of 0.05 M KBr and 8 ml of water, and titrated with 0.00167 M bromate standard solution. Table 1 gives some results of single determinations evaluated by graphic extrapolation.

Determination of arsenic(III). An aliquot (1 ml) of arsenic(III) solution (sample or standard) containing 20—200 μg As(III) is mixed with 1 ml of 0.05 M KBr and 8 ml of 2 M HCl, and titrated with 0.00167 M bromate standard solution. In this case, only the cerium(IV)—arsenic(III)—ferroin system was used. Table 2 gives some results of single determinations.

Determination of arsenic(III) by means of the bromide-catalyzed permanganate—iodine reaction

Apparatus. Here only the titration vessel (1) and the burette (4) shown in Fig. 1 are used. The nitrogen tube leaving the titration vessel is placed successively into indicator test tubes (2.5 ml) containing sulfite solution.

Procedure. An aliquot (1 ml) of arsenic(III) solution (sample and standard) containing 20—200 μg As(III) is mixed with 1 ml of 0.05 M KBr and 8 ml of 2 M HCl, and titrated with 0.00167 M bromate standard solution. As before, the titrant is delivered at 0.112 ml min^{-1} and the flow of nitrogen is 50 ml

TABLE 1

Titration of antimony (μg/10 ml) with bromate by means of the cerium(IV)—arsenic(III) or iodide starch indicator reaction

Given	30	49	61	72	80	116	132	200	225	254
Found Ce/As	29	44	69	65	87	114	128	193	233	245
Iodide/starch	30	40	66	62	88	107	124	203	228	255

TABLE 2

Titration of arsenic (μg/10 ml) with bromate by means of the cerium(IV)—arsenic(III) indicator reaction

Given	21	22	28	41	58	66	131	138	140	187
Found	20	27	30	42	64	68	136	139	137	182

min^{-1}. Portions (0.5 ml) of 0.01 M sodium sulphite solution are added to ten indicator test tubes. In an initial titration, the indicator tube is changed every 30 s to determine the end-point approximately. After all ten tubes have been used 0.2 ml of 0.025 M hydrogen peroxide in 5 M H_2SO_4 is added to each to destroy the unconsumed sulphite. Then 0.2 ml of 0.008 M $KMnO_4$ is added followed by 0.1 ml of iodide solution (1 mg ml^{-1}). The bromine carried over at and after the end-point is reduced to bromide in all indicator tubes. In the tubes containing bromide the permanganate solution is decolorized within a few seconds; in the tubes without bromide, decolorization takes several minutes.

The end-point is determined as follows. For example, suppose that the first five indicator tubes (I—V) show no reaction, while tube VI shows a partial reaction and tubes VII—X show the completed decolorization reaction. The first tube in which a catalytic effect is recognizable (tube VI in this case) corresponds to the end-point. If in this particular tube decolorization is complete, as in tube VII, then the time necessary for the titration is given by multiplying the tube number by the change interval of the indicator tubes (in this case 30 s). If bleaching is not complete (as in tube VI), the arithmetic average between the tube before and after is used. In the example given, this would be 165 s for tube VI.

In two more titrations, the end-point is determined exactly. For this purpose, the nitrogen stream is led into the sulfite solutions only shortly before and after the approximate end-point and the tubes are changed every 15 s. In the third titration, the times are chosen so that they overlap with the times of the second titration. For example, in the second titration, the tubes can be changed over at intervals 120, 135, 150, 165, 180 and 195 s after the start of the titration; then in the third titration, the indicator tubes are changed over every 15 s at intervals 127, 142, 157, 172, and 187 s after the start of the titration. The titration times found in the second and third titration are averaged and so give the final titration times.

The concentration of the arsenic is evaluated by graphic extrapolation from a standard graph prepared in the same way. Table 3 gives some results.

TABLE 3

Titration of arsenic (μg/10 ml) with bromate by means of the permanganate indicator reaction

Given	22	36	42	42	70	90	110	154	156	192
Found	22	38	41	43	68	84	110	149	153	188

REFERENCES

1 H. Weisz and U. Muschelknautz, Fresenius Z. Anal. Chem., 215 (1966) 17.
2 T. P. Hadjiioannou, Rev. Anal. Chem. Isr., 3 (1976) 82.
3 S. Pantel and H. Weisz, Anal. Chim. Acta, 116 (1980) 421.
4 H. Weisz and J. Schlipf, Anal. Chim. Acta, 121 (1980) 257.
5 E. B. Sandell and I. M. Kolthoff, J. Am. Chem. Soc., 56 (1934) 1426.
6 M. Shiota, S. Usumi and J. Iwasaki, Nippon Kagaku Zasshi, 80 (1959) 753.

Analytica Chimica Acta, 134 (1982) 353—358
Elsevier Scientific Publishing Company, Amsterdam — Printed in The Netherlands

Short Communication

DETERMINATION OF SULFATE IN RIVER WATER BY FLOW INJECTION ANALYSIS

OSAMU KONDO, HARUO MIYATA and KYOJI TÔEI*

Department of Chemistry, Faculty of Science, Okayama University, Tsushima-naka 3-1-1, Okayama-shi 700 (Japan)

(Received 23rd August 1981)

Summary. Sulfate ion in river water is determined by flow injection analysis at a rate of 30 samples per hour; the sulfate contents are typically less than 30 ppm. The reagent solution contains dimethylsulfonazo-III, barium chloride, potassium nitrate and chloroacetate buffer in 70% (v/v) ethanol, and is saturated with barium sulfate. The aqueous carrier stream is also saturated with barium sulfate. The sample is filtered and treated with Amberlite IR120-B cation-exchanger before injection into the carrier stream, and the decoloration of the barium—dimethylsulfonazo-III complex by sulfate is measured at 662 nm. The calibration graph is linear over the range 0—30 $\mu g\ ml^{-1}$ for sulfate in water.

The content of sulfate ion in river waters in Japan is much less than that in Europe and the United States. The average content in Japan is 10.6 ppm, and in the Chugoku District the content is as low as 4.4 ppm [1]. Sulfate in river water has been determined successfully by flow injection analysis (f.i.a.) which was invented by Růžička and Hansen [2]; Krug et al. [3] used a turbidimetric method to determine 20—100 ppm sulfate in river water, but this method is not sensitive enough for Japanese river waters. Further, the JIS (Japanese Industrial Standard) K0102 (1974) procedure does not provide accurate results for low ppm sulfate contents. A sensitive spectrophotometric method has been developed, but its range is narrow and samples often require dilution before the determination [4—6]. Methods based on flow titrimetry [7], flow photometry [8] and flow-injection photometry [9] have been described by Reijnders et al., but the apparatus is very complicated.

The determination of sulfate ion by f.i.a. using the barium chelate of sulfonazo-III or dimethylsulfonazo-III is reported here. This method can be used directly for 1—30 ppm sulfate ion in river water, which range covers almost all river waters in Japan [1]. Thirty samples can be determined per hour within 1% relative error.

Experimental

Reagents. For the sulfonazo-III solution, transfer 5 ml of 10^{-2} M sulfonazo-III solution, 5 ml of 1 M KNO_3, 3.5 ml of 10^{-2} M $BaCl_2$, 20 ml of 1 M chloroacetic acid—sodium chloroacetate buffer (pH 2.8) and 700 ml of

ethanol into a 1-l volumetric flask and dilute to the mark with distilled water. Saturate the solution with barium sulfate in an ultrasonic bath and filter it through a Millipore filter (pore size 0.45 μm).

Prepare the dimethylsulfonazo-III (DMSA-III) solution similarly, but use 5.6 ml of 10^{-2} M DMSA-III and 3.9 ml of 10^{-2} M barium chloride solution.

For the barium sulfate solution, agitate distilled water with barium sulfate in an ultrasonic bath and filter through a Millipore filter (pore size 0.45 μm).

Other reagents used were of analytical-reagent grade.

Apparatus. The absorbance was measured with a Shimadzu double-beam spectrophotometer UV-140-02 with 1-cm micro flow cell (8 μl) and recorded by a Toa Dempa FBR-251A recorder. A double-plunger micro pump (Kyowa Seimitsu KHU-W-104) was used for the reagent and barium sulfate solutions. Sample solution (80 μl) was injected by a 6-way injection valve (Kyowa Seimitsu KMH-6V) into the carrier stream.

The flow lines were made from teflon tubing (1 mm and 0.5 mm i.d.). The reaction coil (1 mm i.d.) was optimally 5.5 m long and was wound around a glass rod (1.2 cm o.d.) to achieve complete mixing. The damping coils (0.5 mm i.d.) were 20 m long, to cancel the pulse from the reciprocal pump. The back-pressure tubing (0.5 mm i.d.) was 10 m long, to prevent formation of air bubbles.

A diagram of the flow system is shown in Fig. 1.

Recommended procedure. The flow rates of the reagent solution and barium sulfate solutions are optimally 2 ml min^{-1} each. Sample solutions are filtered through a Millipore filter (pore size 0.45 μm) and passed through an Amberlite IR120-B (H-form) column (1 cm i.d., 15 cm long) before being injected. From the sample loop, 80 μl of treated sample solution is injected into the carrier stream. Peak heights are measured at 645 nm for the sulfonazo-III method and at 662 nm for the DMSA-III method. The concentration of sulfate ion is measured from a calibration graph prepared with potassium sulfate standards.

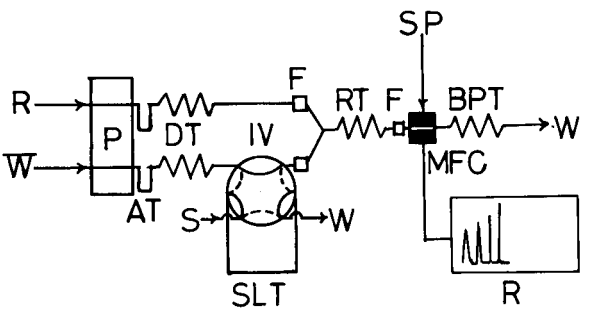

Fig. 1. Schematic flow diagram. R, Reagent solution; $\overline{W}$, water saturated with $BaSO_4$, P, double-plunger micro pump (2.0 ml min^{-1}); AT, air trap; DT, damping coil (0.5 mm × 20 m); IV, injection valve; SLT, sample injector (1.0 mm tubing 80 μl); F, line filter; RT, reaction coil (1 mm × 5.5 m); MFC, micro flow cell (1 mm × 10 mm); BPT, back-pressure coil (0.5 mm × 10 m); W, waste; SP, spectrophotometer; R, recorder.

Results and discussion

Sulfonazo-III method. The absorption spectra of sulfonazo-III and its barium chelate (Fig. 2, left) show maxima at 575 nm and 643 nm, respectively. The absorbance is measured at 645 nm for greatest sensitivity. Both sulfonazo-III and its barium chelate are soluble in water, but the molar absorptivity of the chelate increases when ethanol is added and reaches 5.4×10^4 l mol^{-1} cm^{-1} in 40% (v/v) ethanol [10]. Accordingly, the reagent solution is prepared in 70% (v/v) ethanol so that in the flow system the mixed solutions contain 35% ethanol. It must be recalled that ethanol reduces the solubility of barium sulfate seriously [11].

Barium ion reacts with sulfonazo-III at a mole ratio of 1:1 [10]; the molar ratio of barium to sulfonazo-III in the flow system was therefore fixed at 0.7:1. The flow injection system was tested at various pH values. Between pH 3.5 and 4.5, peak heights are constant; an equimolar solution of chloroacetic acid and sodium chloroacetate was therefore used to maintain pH 4.2 in 35% ethanolic solution. Further tests were made with different concentrations of the barium—sulfonazo-III solution to establish the difference in peak heights for 0 ppm and 10 ppm sulfate solutions. As the reagent concentration increases, the difference in peak heights increases but reaches a maximum at 5×10^{-5} M; this concentration of reagent is therefore recommended. As the sulfate ion in the sample solution should be converted to barium sulfate completely, it is best to saturate the reagent and carrier solutions with barium sulfate. This treatment improved the reproducibility remarkably. Addition of potassium nitrate to the reagent solution maintains constant ionic strength; without it, the base line fluctuates. The selected concentration of 5×10^{-3} M maximizes the absorbance difference between the blank and sample.

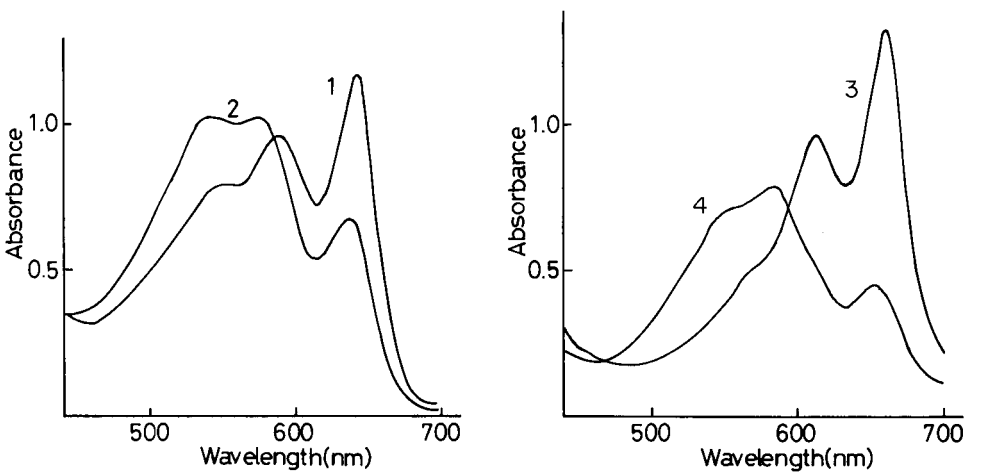

Fig. 2. Absorption spectra measured in 50% (v/v) ethanolic solution against a water reference. (1) 3.6×10^{-5} M barium—sulfonazo-III; (2) 3.6×10^{-5} M sulfonazo-III; (3) 2.5×10^{-5} M barium—dimethylsulfonazo-III; (4) 2.5×10^{-5} M dimethylsulfonazo-III.

When samples were injected with a micro syringe, the reproducibility of the peak height was not good and the signals were attenuated compared to those obtained when the 6-way injection valve was used.

Dimethylsulfonazo-III method. The absorption spectra of DMSA-III and its barium chelate are shown in Fig. 2 (right). The absorption maxima are 586 nm and 660 nm for DMSA-III and its chelate, respectively. Measurement at 662 nm provides the largest difference for the sulfate determination.

The reagent solution is prepared in 70% (v/v) ethanolic solution, and the molar ratio of DMSA-III to barium is 1:0.7. Other aspects of the reagent solution were likewise selected by considering the sulfonazo-III procedure. Maximum constant absorbance is achieved between pH 3.5 and 5.5, so that the monochloroacetate buffer is again appropriate.

A calibration run obtained with 0—16 ppm sulfate standards with the DMSA-III system is shown in Fig. 3. The reproducibility is good; linear calibration graphs can be obtained up to 30 ppm sulfate, with a correlation coefficient of 0.999. Calibration graphs for the sulfonazo-III system are similar, but the DMSA-III system is preferred because the pH range is wider. The sulfate content in almost all river waters in Japan can be determined directly without dilution or concentration.

The effects of co-existing ions are listed in Table 1. Calcium ion in ordinary

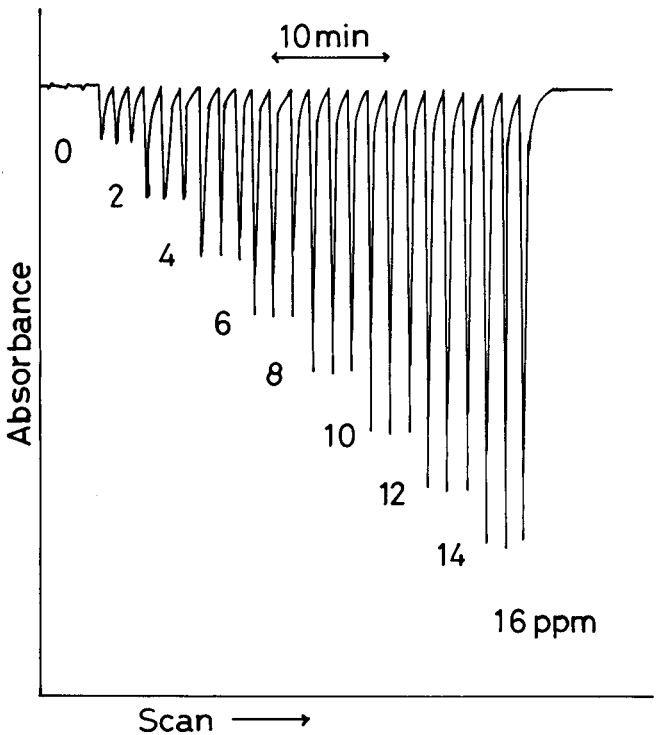

Fig. 3. A typical calibration run with the proposed flow injection system.

TABLE 1

Effect of co-existing ions

Ion	Added as	Conc. (M)	Found SO_4^{2-} (ppm)	Ion	Added as	Conc. (M)	Found SO_4^{2-} (ppm)
None	—	—	5.0	K^+	KCl	5×10^{-4}	5.1
Cl^-	KCl	5×10^{-4}	5.1	Na^+	NaCl	1×10^{-3}	5.0
HCO_3^-	$KHCO_3$	1×10^{-4}	5.0	NH_4^+	NH_4Cl	5×10^{-4}	5.0
NO_3^-	KNO_3	1×10^{-4}	5.0	Mg^{2+}	$MgCl_2 \cdot 6H_2O$	1×10^{-4}	5.0
$H_2PO_4^-$	KH_2PO_4	1×10^{-4}	5.1	Ca^{2+}	$CaCl_2 \cdot 2H_2O$	1×10^{-5}	4.9
SiO_3^{2-}	Na_2SiO_3	5×10^{-4}	5.0	Fe^{3+}	$FeCl_3 \cdot 6H_2O$	5×10^{-5}	5.0

TABLE 2

Determination of sulfate in river waters[a]

Sample	A1	A2	A3	A4	A5	A6	A7	A8	A9	A10
SO_4^{2-} (ppm)	2.8[b]	2.7	3.5	2.7	3.0	2.9	3.1	3.4	3.5	3.6[b]
Sample	Y1	Y2	Y3	Y4	Y5	Y6	Y7	Y8	Y9	
SO_4^{2-} (ppm)	3.6[b]	3.8	4.5	11.9	9.8	9.9	11.0	8.7	10.8[b]	
Sample	T1	T2	T3	T4	T5	T6	T7	T8	T9	T10
SO_4^{2-} (ppm)	4.7[b]	4.8	10.4	4.7	4.7	5.2	6.2	4.9	8.9	6.0[b]

[a]Samples A, Y and T were taken on 3rd, 3rd and 4th February 1981, respectively. The values given are the mean of three determinations. [b]These 6 samples were used in recovery tests. Sulfate (10 μg) was added to 1 ml of sample before injection. The recoveries were 98, 100, 100, 102, 101 and 102%, respectively.

river water interferes with the determination. To prevent this, samples are first passed through a column of cation-exchange resin; the first 20 ml of effluent is discarded and the next portion is used.

Application to river waters. The recommended procedure was applied to the determination of sulfate in waters from the Asahi, the Yoshii and the Takahashi Rivers in Okayama Prefecture. Sample waters were numbered from the upper to the lower reaches of the rivers. The results are shown in Table 2. Recovery tests indicated that this method is not affected by the various matters dissolved in these river waters.

The authors express their thanks to Nissan Science Foundation for financial support.

REFERENCES

1 J. Kobayashi, Nôgaku Kenkyu, 48 (1960) 63.
2 J. Růžička and E. H. Hansen, Anal. Chim. Acta, 78 (1975) 17.
3 F. J. Krug, H. Bergamin F°, E. A. G. Zagatto and S. Storgaad Jorgensen, Analyst, 102 (1977) 503.
4 S. Utsumi, Y. Oinuma and A. Isozaki, Bunseki Kagaku, 27 (1978) 278.
5 Y. Nasu, Bunseki Kagaku, 18 (1969) 1183.
6 T. Koita, H. Miyata and K. Tôei, Bunseki Kagaku, 29 (1980) 176.

7 H. E. R. Reijnders, J. J. van Standen and B. Griepink, Fresenius Z. Anal. Chem., 293 (1978) 413.
8 H. E. R. Reijnders, J. J. van Standen and B. Griepink, Fresenius Z. Anal. Chem., 295 (1979) 122.
9 H. E. R. Reijnders, J. J. van Standen and B. Griepink, Fresenius Z. Anal. Chem., 295 (1979) 410.
10 M. Zenki, Anal. Chim. Acta, 83 (1976) 267.
11 E. Suito, K. Takiyama, Bull. Chem. Soc. Jpn., 28 (1955) 305.

Analytica Chimica Acta, 134 (1982) 359—364
Elsevier Scientific Publishing Company, Amsterdam — Printed in The Netherlands

Short Communication

ENZYME SEQUENCE AND COMPETITION ELECTRODES BASED ON IMMOBILIZED GLUCOSE OXIDASE, PEROXIDASE AND CATALASE

R. RENNEBERG*, D. PFEIFFER and F. SCHELLER

Zentralinstitut für Molekularbiologie der Akademie der Wissenschaften der DDR, Berlin-Buch (E. Germany)

M. JÄNCHEN

Forschungsinstitut für Medizinische Diagnostik, Dresden (E. Germany)

(Received 14th April 1981)

Summary. The toxicologically important peroxidase substrates bilirubin and aminopyrine can be determined by combination of immobilized glucose oxidase, horseradish peroxidase and catalase, forming so-called enzyme sequence and enzyme competition electrodes. Bilirubin and aminopyrine are determined in the concentration range 5—50 μM.

The development of enzyme electrodes has led to highly efficient methods for the determination of various substances in biological fluids such as blood, serum, urine [1, 2]. In enzyme electrodes, the high selectivity of enzymes is combined with the high sensitivity of electrochemical measurements, which is a main reason for the increasing importance of enzyme electrodes, especially for medical purposes. To provide a wider range of substrates, enzymes can be coupled in so-called bi-enzyme electrodes [3, 4]. The term bi-enzyme electrode does not, however, reflect correctly the mode of cooperative reactions used by the enzymes for substrate conversion. That is why the term enzyme sequence electrode has been proposed [5] for a bi-enzyme electrode where two enzymes metabolize a substrate in a two-step sequence to form a product which can easily be detected. Some bi-enzyme electrodes developed by our research group, however, use the competition of two enzymes for the same substrate, so that the term enzyme competition electrode seems appropriate. This paper describes the coupling of immobilized glucose oxidase, with horseradish peroxidase and the coupling of horseradish peroxidase with catalase for enzyme sequence and enzyme competition electrodes, respectively. Toxicologically important peroxidase substrates like bilirubin and aminopyrine can be determined.

Free bilirubin is a highly toxic substance, especially for newborn infants. Bilirubin is usually determined in hemoglobin-free serum by spectrophotometric measurements either directly or after a diazo reaction [6]; more recently, the determination of bilirubin by an enzymatic peroxidase test has been suggested [7, 8]. Determination of the antipyretic drug aminopyrine

usually involves extraction procedures and spectrophotometric measurements after complex formation [9].

Experimental

Enzymes and cofactors used were commercial products. The materials used were bilirubin (FERAK), glucose oxidase (*P. notatum*; 46 U mg^{-1}), horseradish peroxidase (32 U mg^{-1}; RZ = 0.7), NADPH (all from VEB Arzneimittelwerk, Dresden) and catalase (beef liver; REANAL, Budapest).

All enzymes were immobilized or co-immobilized by entrapment in gelatin [10]. Liver microsomal cytochrome P-450 was obtained from rabbit liver as described by Imai and Sato [11].

For the determination of bilirubin, two dialysis membranes were sandwiched around a piece (3 × 3 mm) of the enzyme layer containing co-immobilized horseradish peroxidase (32 U cm^{-2}) and glucose oxidase (40 U cm^{-2}) in front of a normal platinum electrode (0.5-mm diameter). The first membrane separated the enzyme layer from the bulk solution (Fig. 1). The hydrogen peroxide produced was measured with the platinum indicator electrode polarized to +0.6 V against the Ag/AgCl reference electrode. The 20-ml test solutions were 0.1 M in phosphate buffer (pH 7.4) at 25° C.

The cytochrome P-450 batch reactor contained 10 μM microsomal cytochrome P-450 from rabbit liver, 2.5 mM NADPH and 1 mM aminopyrine in a 0.1 M sodium phosphate buffer (pH 6.5). Formaldehyde was determined as described by Nash [12].

For the determination of aminopyrine, a piece of immobilized enzyme layer was fixed with a dialysis membrane on a polyethylene membrane covering an oxygen electrode (Fig. 2). The enzyme layer contained horseradish peroxidase (32 U cm^{-2}) and/or catalase (1.000 U cm^{-2}). The enzyme electrode was dipped in 2 ml of a stirred 0.1 M phosphate-buffered solution (pH 6, 25° C).

Results and Discussion

Enzyme sequence electrode for determination of bilirubin. The principle of this enzyme sequence electrode is shown in Fig. 1. The reaction scheme is as follows:

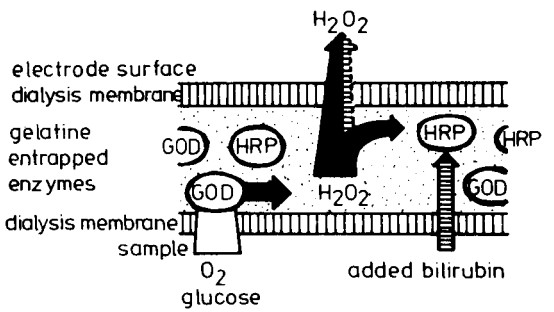

Fig. 1. Principle of the enzyme sequence electrode for determination of bilirubin with co-immobilized horseradish peroxidase (HRP) and glucose oxidase (GOD).

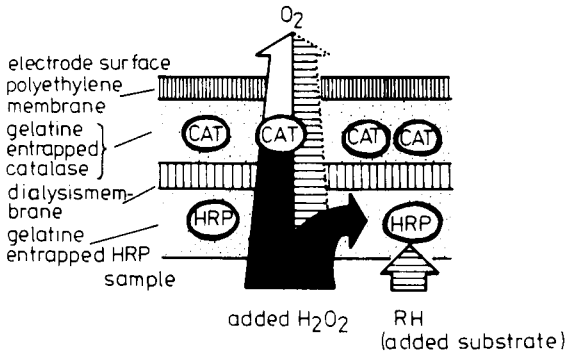

Fig. 2. Principle of the enzyme competition electrode for determination of aminopyrine and other peroxidase substrates with co-immobilized catalase and horseradish peroxidase.

$$\text{Glucose} + O_2 \xrightarrow{\text{GOD}} \text{gluconic acid} + H_2O_2$$

$$2H_2O_2 + \text{bilirubin} \xrightarrow{\text{HRP}} 2H_2O + \text{product}$$

The addition of glucose to the solution causes conversion of the oxygen dissolved in the enzyme membrane to hydrogen peroxide. Because of the high level of glucose added (1.0 mM), the anodic current is not increased by further addition of a sample containing moderate amounts of glucose, e.g., serum (see Fig. 3). When the anodic current reaches a constant level, 50 µl of bilirubin solution is added to the measuring cell. Part of the hydrogen peroxide formed in the glucose oxidase reaction inside the membrane is consumed by horseradish peroxidase for the conversion of bilirubin, and the anodic current is decreased in dependence on the bilirubin concentration.

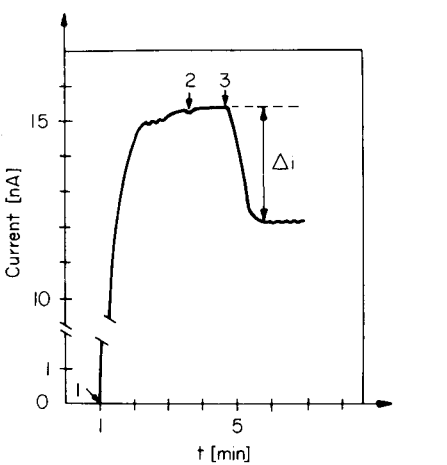

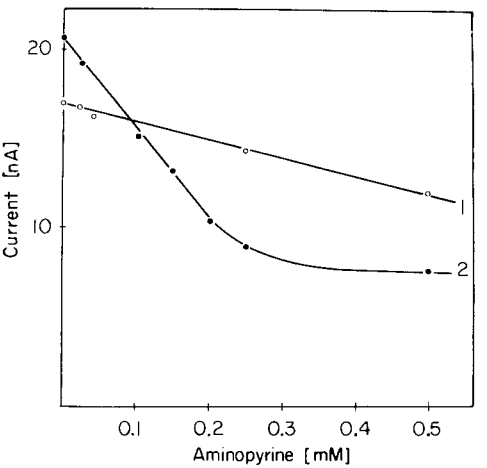

Fig. 3. Bilirubin assay with the enzyme sequence electrode: effect of addition of 50 µl of 0.4 M glucose (1), 50 µl of buffer solution (2), and 50 µl of 2 mM bilirubin solution (3).

Fig. 4. Calibration curves for aminopyrine assay with the enzyme competition electrode: (1) co-immobilized enzymes; (2) separated enzyme layer.

The calibration curve shows a linear range up to 0.05 mM bilirubin in the solution measured (i.e., 2 mM in the undiluted sample), the Δi values being 0.5 nA for 0.005 mM up to 4.25 nA for 0.05 mM bilirubin. At least 0.1 mM bilirubin in the sample can be detected with the enzyme electrode with reasonable precision. If the electrode surface were increased or a more sophisticated polarographic system were available, the sensitivity of the method should be further increased. However, in such cases, other peroxidase substrates or electrochemically active substances present in biological samples could cause disturbing effects.

Enzyme competition electrode for determination of aminopyrine. The reaction scheme for this determination is as follows

$$H_2O_2 \xrightarrow{\text{catalase}} H_2O + \tfrac{1}{2}O_2;\ 2RH + H_2O_2 \xrightarrow{\text{HRP}} 2R\cdot + 2H_2O$$

The oxygen reduction current is measured in order to prevent any interference with the oxidation of hydrogen peroxide by the electrode reactions of peroxidase substrates. The polyethylene membrane used to cover the electrode surface is permeable only to oxygen, not to peroxidase substrates.

Two variants were used: (1) horseradish peroxidase co-immobilized with catalase in a gelatin layer, and (2) horseradish peroxidase immobilized in gelatin separated by a dialysis membrane from the gelatin-immobilized catalase. In the test procedure, a defined amount of hydrogen peroxide is added to the air-saturated buffer solution. This peroxide is destroyed by the immobilized catalase, inducing an increase in the oxygen reduction current proportional to the concentration of peroxide [13]. If a peroxidase substrate is added, the horseradish peroxidase competes additionally with catalase for hydrogen peroxide. Thus the oxygen reduction current is decreased, depending on the substrate concentration. For calibration, increasing amounts of aminopyrine (0.025—1 mM final concentration) were added to the buffer solution followed by addition of constant amounts of hydrogen peroxide.

For the co-immobilized enzymes, the concentration dependence is linear up to 1 mM aminopyrine (Fig. 4, curve 1). However, this variant is much less sensitive than the enzyme electrode with separated enzyme layers (Fig. 4, curve 2); for the latter, the concentration dependence is linear up to 0.2 mM aminopyrine.

For application in connection with a cytochrome P-450 batch reactor, high sensitivity is required because the conversion of aminopyrine by cytochrome P-450 is catalyzed only very slowly. This is why the variant with separated enzyme layers is to be preferred despite the wider range of linearity of the reactions of the co-immobilized enzymes. The microsomal cytochrome P-450 system from rabbit liver catalyzes the demethylation of aminopyrine in a NADPH-supported reaction

$$\text{Aminopyrine} + \text{NADPH} + H^+ + O_2 \xrightarrow{\text{P-450}} \begin{matrix}\text{demethylation}\\ \text{products}\end{matrix} + \text{HCHO} + \text{NADP}^+ + H_2O$$

The time dependence of this reaction was monitored by simultaneously determining the unreacted substrate aminopyrine with the enzyme electrode and the amount of formaldehyde formed by the method of Nash [12]. A special calibration curve was required because of contamination of the cytochrome P-450 preparation by catalase. Inhibition of this catalase by sodium azide was not possible because azide would also inhibit the immobilized catalase. For the calibration curve and the measurements, the sensitivity of the system was increased by differentiation of the current—time curve of the oxygen reduction current and recording of the di/dt maximum value (Fig. 5). Figure 6 shows the correlation between aminopyrine consumption determined with the enzyme electrode and the amount of formaldehyde formed.

Conclusions

The viability of constructing enzyme electrodes based on two-step conversion of one substrate by two enzymes (enzyme sequence electrode) and on the competition of two enzymes catalyzing different reactions for one substrate (enzyme competition electrode) (Fig. 7) is demonstrated by the above results. Using these principles makes it possible to determine substrates which are not directly converted to polarographically detectable species.

The glucose oxidase—peroxidase enzyme sequence involves measurement of the difference between substrate concentrations and therefore depends on the precision of the concentration measurement. The systems were readily applied for measurements of ATPase activity [3] and of the cytochrome P-450 conversion of aminopyrine.

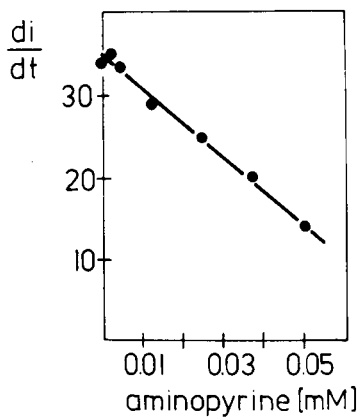

Fig. 5. Calibration curve for measurement of aminopyrine in a cytochrome P-450—buffer mixture.

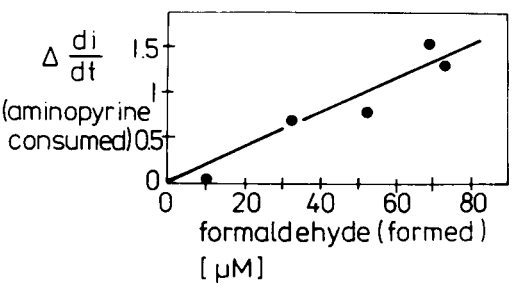

Fig. 6. Correlation between aminopyrine consumed in cytochrome P-450 reaction determined with the enzyme electrode and formed formaldehyde, respectively, determined by the method of Nash [12].

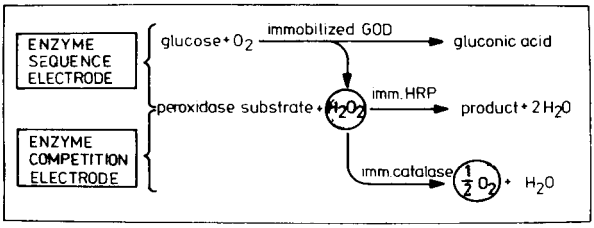

Fig. 7. General scheme of enzyme sequence and competition electrodes for determination of peroxidase substrates.

The enzyme sequence electrode undoubtedly reflects biological chain processes. That is why tissue slices and whole micro-organisms can replace the purified enzymes [14—17]. In the same way, the competition situation for substrates within tissues and micro-organisms could be used in bioprobes.

The authors thank M. Siepe, B. Bernard, and R. Gründer for technical assistance.

REFERENCES

1 G. G. Guilbault, Handbook of Enzymatic Methods of Analysis, M. Dekker, New York, 1976, 385 pp.
2 F. Scheller, M. Jänchen, D. Pfeiffer, I. Seyer and K. Müller, Z. Med. Labortech., 18 (1977) 312.
3 F. Scheller and D. Pfeiffer, Anal. Chim. Acta, 117 (1980) 383.
4 D. Pfeiffer, F. Scheller, M. Jänchen, K. Bertermann and H. Weise, Anal. Lett., 13 (1980) 1179.
5 M. A. Jensen and G. A. Rechnitz, J. Membr. Biol., 5 (1979) 117.
6 J. D. Bauer, P. G. Ackermann and G. Toro, Clinical Laboratory Methods, Mosby Company, Saint Louis, 1974.
7 J. Nakamura, J. Lee Y., Clin. Chim. Acta, 79 (1977) 411.
8 R. Brodersen, W. J. Cashore, R. P. Wennberg, C. E. Ahlfors, L. F. Rasmussen and D. Shusterman, Scand. J. Clin. Lab. Invest., 39 (1979) 143.
9 A. Neugebauer, F. Splinter, D. Häfke, R. Kober, H. Schirlitz and W. Klinger, Biochem. Pharmacol., 18 (1969) 1559.
10 F. Scheller, D. Pfeiffer, M. Jänchen, I. Seyer, M. Siepe and R. Pittelkow, GDR-Patent GO1 N/127 843, 19th December 1979.
11 Y. Imai and R. Sato, J. Biochem. (Tokyo), 75 (1974) 689.
12 T. Nash, J. Biochem. (Tokyo), 55 (1953) 416.
13 A. Aizawa, I. Karube and S. Suzuki, Anal. Chim. Acta, 69 (1974) 431.
14 G. A. Rechnitz, M. A. Arnold and M. E. Meyerhoff, Nature, 278 (1979) 466.
15 J. Kulys and K. Kadzianskiene, Biotechnol. Bioeng., 22 (1980) 221.
16 M. A. Arnold and G. A. Rechnitz, Anal. Chem., 52 (1980) 1170.
17 U. Wollenberger, F. Scheller and P. Atrat, Anal. Lett., 13 (1980) 825.

Analytica Chimica Acta, 134 (1982) 365—368
Elsevier Scientific Publishing Company, Amsterdam — Printed in The Netherlands

Short Communication

ON-LINE DETERMINATION OF POTASSIUM IN A LIQUID PROCESS STREAM BY γ-RAY SPECTROMETRY

M. A. LANGHORST*, J. W. THOMPSON[a] and A. J. KAMP[b]

Analytical Laboratories, The Dow Chemical Company, Midland, MI 48640 (U.S.A.)

(Received 20th January 1981)

Summary. The 1.46 MeV γ-ray associated with the decay of naturally radioactive ^{40}K is detected by using a NaI(Tl) scintillation detector, thus minimizing interferences from members of the uranium or thorium series. To overcome the problems of low count rates (<100 cps), an Intel 80/20 microcomputer is used to collect and correlate the data and provide an appropriate output for display. The response of the analyzer as a function of potassium concentration is linear over the range 0—2% KCl; based on counting statistics, the precision is about 1% at the 95% confidence level. By comparison to atomic absorption spectrometry, the accuracy is about 3% relative at the 1—2% KCl level.

The natural radioactivity of potassium has already been proposed as the basis of an analytical determination [1]. The naturally radioactive potassium isotope is ^{40}K ($t_{1/2}$ = 1.32 × 10^9 years [2]; relative abundance 0.012%). About 89% of its decay is by β-emission and the rest is by electron capture accompanied by emission of a 1.46-MeV γ-ray. This γ-ray, associated with the decay of ^{40}K, can be detected by a geiger tube or scintillation detector to yield a quantitative potassium determination. Possible interferences include members of the uranium or thorium series of fission products from modern sources, but these can be minimized by selecting a NaI(Tl) scintillation detector. This natural γ-ray counting has been successfully applied to the determination of potassium in fertilizers [3], and other solid samples [4]. The present communication is concerned with the use of the ^{40}K decay to determine the potassium concentration continuously and on-line in an aqueous process stream. An Intel 80/20 microcomputer is used to collect the data, correlate the radioactivity as a function of potassium concentration, and provide an appropriate output to display the results [5].

Experimental

The detector was a 12.7 cm × 12.7 cm sodium iodide, thallium-impregnated scintillation detector with integral photomultiplier (Bicron, Inc.). This detector and an Ortec tube base pre-amplifier were placed into a nickel well (3.4 mm wall thickness, 21.3 cm o.d. × 91.4 cm deep) located in the center of a tank (Fig. 1). The wall thickness was chosen as a compromise between

[a]Present address: Dow Chemical Company, Dowell Division, Tulsa, OK, U.S.A.
[b]Present address: Dow Chemical Company, Western Division, Walnut Creek, CA, U.S.A.

0003-2670/82/0000-0000/$02.75

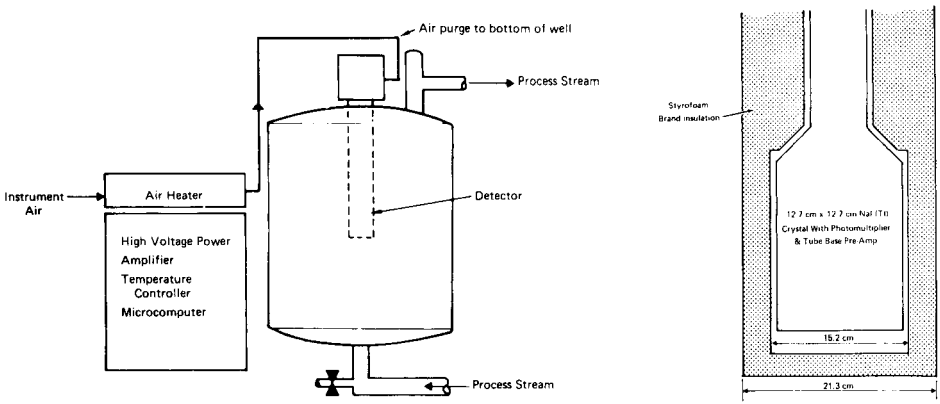

Fig. 1. Continuous analyzer for potassium in a process stream with detail of the detector in the well assembly (right hand side). Dimensions in cm.

losing counts by γ-ray absorption in the well material and maintaining a safe environment for the detector and electronics. The detector and pre-amplifier were surrounded by Styrofoam Brand polystyrene foam insulation (Dow Chemical Company) inside the well (Fig. 1) in order to minimize any thermal shock on the detector. The detector temperature was maintained at 32.5°C using a purge of clean, dry air which was thermostatted prior to entering the instrument. The point for controlling the purge air temperature was a thermocouple mounted on the detector. Additional electronic components, including a Canberra Model 3002 high-voltage power supply, an Ortec Model 485 amplifier, a Tracor Northern Model HEI-01 256-channel analog-to-digital converter, and an Intel SBC 80/20 microcomputer were housed in a weather-tight enclosure located adjacent to the tank.

An Elexon TLV-65 power supply provided operating voltages to the computer. Operating voltages for the amplifier and the A/D converter were provided by a Berkeley Nucleonics Model AP-1 portanim. The digital signal from the microcomputer was converted to an analog voltage signal by a Burr-Brown Model DAC 80-CBI-V 12-bit D/A converter. This voltage was converted to a current loop by an Acromag transmitter (10—50 mA output). A Foxboro strip-chart recorder was used to display the output continuously.

In order to monitor the 1.46-MeV γ-ray while minimizing the interferences from other γ-radiation sources, the energy spectrum from the NaI(Tl) detector was digitized by the A/D converter and input into the microcomputer memory. The computer was programmed to locate the center of the ^{40}K peak, which was stored in memory and the peak area integrated. This integration was completed every 200 s. The computer buffer contained the area for the last six ^{40}K integrations. Each time a new determination was completed, the oldest integration was dropped and the newest was placed into the buffer. The instrument was calibrated by using the sum of the six

integrations. The time constant of the system is then 13.3 min, which satisfies both precision and time requirements.

Results and discussion

With conventional pulse-counting instrumentation, energy discrimination is accomplished by setting energy "windows" and only counting the γ-rays which fall within the energy region of interest. An alternative means of data collection, reported here, utilizes an analog-to-digital (A/D) converter and a microcomputer for data collection. The A/D sorts the amplifier voltage pulses according to their height (i.e., energy) into one of 256 energy windows. This information is transmitted to the microcomputer which counts the number of pulses occurring in any given channel for a pre-determined time. This data collection approach has several unusual features. Two 64-word buffers, which are employed to input the data into the microcomputer, smooth out the random nature of the pulse-counting experiment and also remove the computer as a source of dead time, as long as the average rate of 27000 pulses per second is not exceeded. The buffers can accept a data burst from the A/D, while allowing the microcomputer to strobe data out of the buffers at its own rate. Another unusual aspect of this method of data collection is that stabilization of the system gain is not required. At the low count rates encountered here (<100 cps), it is virtually impossible for conventional counting equipment to track the movement of the system gain. To alleviate this problem, the entire energy spectrum is stored in the microcomputer memory. The region of interest can then be made to follow the ^{40}K peak instead of forcing the ^{40}K peak to remain in a region of interest.

Calculations indicate that ^{40}K decay events which originate farther than about 0.6 m from the detector do not significantly contribute to the observed count rate. A vessel larger than that required was chosen for the measurement, however, because the extra brine, while not contributing directly to the measurement, provided shielding for the detector against background radiation. In the present application, the activity detected with an empty tank was equivalent to several hundred ppm of potassium. But when the tank was filled with brine which did not contain potassium, the background count was essentially zero. In fact, the background subtraction feature of the software was not necessary because of this shielding.

The response of the scintillation detector, which is located in the center of a large tank filled with a brine containing 45% calcium chloride, as a function of potassium chloride concentration, is illustrated in Fig. 2. Potassium concentration was determined by atomic absorption spectrometry. The calibration function was programmed into the microprocessor so that the output was a voltage proportional to the % KCl in the brine from 0 to 2%. The pen variance was about 0.03% KCl at the 1.8% KCl level, or 1.6% relative. Based on counting statistics, the precision of this determination was approximately 1% at the 95% confidence level. The accuracy of the analyzer is estimated by comparison to atomic absorption spectrometry

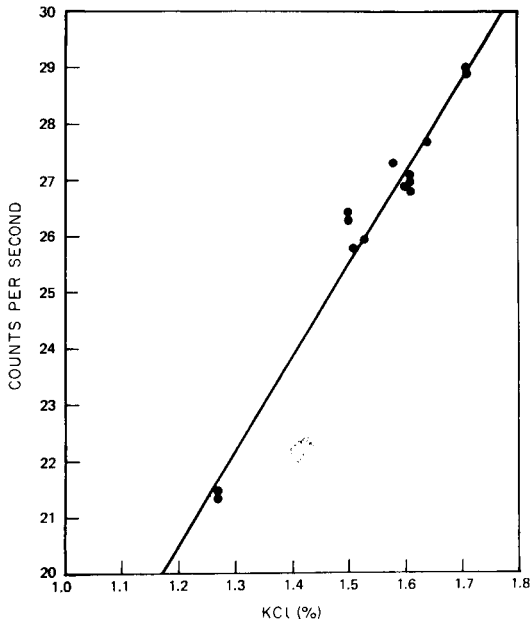

Fig. 2. Calibration of potassium analyzer in a brine containing 45% calcium chloride, showing counts per second in the 1.46-MeV region against % KCl determined by atomic absorption spectrometry. The linear regression equation is [KCl] = 0.06041 + 0.0413 with a standard deviation of 0.026 (% KCl).

TABLE 1

Performance of potassium analyzer

% KCl (Analyzer)	1.25	1.51	1.58	1.54	1.52	1.57	1.60	1.70	1.70
% KCl (a.a.s.)[a]	1.27	1.51	1.61	1.50	1.53	1.61	1.58	1.71	1.71
% Deviation	−1.6	0	−1.9	2.6	0.7	2.5	1.3	0.6	0.6

[a]Determined by a.a.s. for potassium with a double-beam instrument; standards were prepared fresh daily.

(a.a.s.) to be approximately 3% relative at the 1.8% KCl level in a brine containing 45% $CaCl_2$. Analyses of brine samples were correlated with the output of the calibrated analyzer to provide a check for the initial calibration. An example of such data are tabulated in Table 1; the average percentage deviation between the sets of results is 1.3%.

REFERENCES

1 R. B. Barnes and D. J. Salley, Ind. Eng. Chem. Anal. Ed., 15 (1943) 4.
2 W. R. Smyth and A. Henmendinger, Phys. Rev., 51 (1937) 178.
3 H. N. Wilson, P. S. Peco and W. Broomfield, Analyst, 76 (1951) 355.
4 A. M. Gaudin and J. H. Pannell, Anal. Chem., 20 (1948) 1154.
5 U.S. Patent Application pending.

Analytica Chimica Acta, 134 (1982) 369—373
Elsevier Scientific Publishing Company, Amsterdam — Printed in The Netherlands

Short Communication

COMPARISON OF ATOMIC ABSORPTION SPECTROMETRIC, SPECTROPHOTOMETRIC, AND FLUORIMETRIC METHODS FOR DETERMINATION OF ALUMINUM IN WATER

R. PLAYLE*, J. GLEED, R. JONASSON and J. R. KRAMER

Department of Geology, McMaster University, 1280 Main St. West, Hamilton, Ont. (Canada)

(Received 12th May 1981)

Summary. Three methods for quantifying aluminum in water samples are compared. An electrothermal atomic absorption method is assumed to be free of interferences and has an applicable range of 10 to above 1000 μg Al l^{-1}. The colorimetric ferron method has multiple interferences and is useful in the 50—1500 μg Al l^{-1} range. The fluorimetric method based on lumogallion has few important interferences and is useful to below 1 μg Al l^{-1}.

The aluminum content of water increases at low pH [1] and may be toxic [1—3]. There has been no study comparing the many current techniques used to quantify aluminum [4, 5]; perhaps no one method is suitable for all applications. In aquatic toxicology, for example, atomic absorption spectrometry (a.a.s.) [1, 3, 6], the colorimetric ferron method [7], and the aluminon and catechol violet techniques [8] have been used. The lumogallion fluorimetric method has been applied in fresh and sea-water studies [9—12]. In addition, inductively-coupled plasma emission spectrometry has been employed [13].

In this communication, the ferron colorimetric method, the lumogallion fluorimetric method, and the electrothermal a.a.s. method are compared and interferences are described. The ferron method has been suggested in government manuals [14, 15]; the fluorimetric lumogallion method has a low detection limit (0.05 μg l^{-1}); and a.a.s. is the most selective for aluminum.

Experimental

General methods. Water samples were collected in 1-l polypropylene or polyethylene acid-washed bottles that were also washed with the sample solution in the field. One sample was collected without pre-treatment, and an acidified sample was collected with a 1-ml aliquot of 6 M HNO_3 which lowered the pH of the sample to about 2.0. A third sample was filtered directly with a hand pump into a bottle already containing the 1-ml aliquot of acid. Samples were stored at room temperature. The filter units were

acid-soaked and washed in the laboratory and transported in sealed plastic bags, also acid-washed. Filter papers (Millipore 0.45 μm) were acid-washed with 50—100 ml of 10% HNO_3 followed by 300 ml of distilled—deionized water.

Lumogallion method. The lumogallion method used is similar to that of Hydes and Liss [9]. Stock aluminum solution was prepared from $AlK(SO_4)_2 \cdot 12H_2O$. The sodium acetate—acetic acid buffer was prepared by adjusting the pH of a 4 M sodium acetate solution from 9.6 to 8.0 with acetic acid, filtered through an acid-washed 0.45-μm membrane filter, and then adjusted to pH 5.0. The polyethylene and polypropylene bottles used for sample preparation were kept filled with 10% nitric acid between runs, being rinsed three times with distilled water and a further three times with distilled—deionized water before use. Lumogallion solution (1 ml of 0.02% w/v) and 0.5 ml of 4 M acetate—acetic acid buffer were added to the sample to reach a final volume of 100 ml. These 100-ml solutions were heated in a water bath for 1 h at 80°C. A Turner Model 111 fluorimeter was used for readings.

Atomic absorption spectrometry. A Perkin-Elmer 603 atomic absorption spectrometer was used with an HGA 2100 graphite furnace. Samples and standards were prepared as for the lumogallion method described above. Otherwise, standard a.a.s. procedures were followed. The furnace program was as follows: dry for 40 s at 140°C, char for 10 s at 800°C with a ramp time of 12 s, and volatize for 8 s at 2600°C. A 50-μl pipette was used to introduce the sample. The furnace was cleaned by brief heating at high temperature after each sample, and blanks were run between triplicate runs of each sample. A calibration curve was constructed using appropriate standards. When blanks gave consistently high readings, their values were subtracted from other peaks as a correction factor.

Ferron method. The procedure used was that outlined earlier [14], which is similar to that used by Driscoll [16]. After addition of ferron solution to three aliquots of each water sample to which known amounts of stock aluminum solution have been added, absorbance is read at 370 nm and the aluminum concentration is computed by linear regression. Interference by iron was avoided by reducing iron(III) with hydroxylammonium chloride, adding 1,10-phenanthroline along with the ferron, reading the absorbance at 520 nm, and substituting the absorbance into the correction equation [14].

Interference experiments. Potential interferences were studied by adding incremental concentrations of various substances to solutions. The sodium salt of humic acid (Aldrich Chemical Co.) was dissolved in distilled—deionized water and filtered through acid-washed 0.45-μm membrane filters. Metal ions were added as $FeSO_4(NH_2)_2SO_4 \cdot 6H_2O$, $MnSO_4 \cdot H_2O$, $ZnCl_2$, TiO_2 and $Zr(NO_3)_4 \cdot 5H_2O$. Organic substances studied were glycine, oxalate, boric acid, tartrate, glutamate, aspartate, L-alanine, nitriloacetic acid (NTA), 8-quinolinol and EDTA. Fluoride, sulfate, phosphate and silicate were used as their sodium or potassium salts.

Results and discussion

Contamination. Blanks of deionized water typically contain up to 1 μg Al l^{-1} of which about 0.5 μg l^{-1} can be due to the added lumogallion and buffer. Acid-washed filters should be used for samples, and, if possible, some sample should be passed through the filter and discarded as a further rinse. A 250-ml filtered sample preceded by a 250-ml sample rinse picks up about 0.5 μg Al l^{-1} from a washed 0.45-μm membrane filter and accumulates about 1 μg l^{-1} from an unwashed filter.

Comparison of the three methods. It was found that standard additions generally gave more reliable results than calibrations against a standard curve. The ferron method gave unreliable results below about 50 μg Al l^{-1}. The lumogallion and a.a.s. methods yielded similar results and when a large difference between the two methods occurred, it may have been because a.a.s. measures total aluminum while the lumogallion method does not measure unreactive aluminum.

To test the assumption that electrothermal a.a.s. quantified total aluminum in an aqueous sample, natural kaolinite was selected as a representative refractory material. Two kaolinite suspensions expected to contain 67 ± 1 and 72 ± 1 μg Al l^{-1} based on x-ray fluorescence and a chemical method, yielded values of 62 ± 2 and 58 ± 3 μg l^{-1} by the a.a.s. method. Although these data exhibit significant discrepancies, the a.a.s. method was used as a reference for comparison of the molecular absorption and fluorescence methods.

Interferences. Many interferences on the lumogallion method [9, 11, 12] occur only at high concentrations not often found naturally. Sulfate, phosphate, and silicate do not interfere at molar concentrations of up to 100 times that of the aluminum. Glycine, boric acid, and tartrate gave no interference when added in 2.0×10^{-4} M quantities to a 50 μg Al l^{-1} solution but oxalate interfered strongly and EDTA displaced lumogallion (5.8 μM) almost quantitatively. The addition of up to 40 μM glutamine, aspartate, and L-alanine to an 80 μg Al l^{-1} solution did not create interference but NTA addition did.

No interference with the lumogallion method was found from up to 2.7 mg Zr^{4+} l^{-1} added to a solution of 80 μg Al l^{-1}. Titanium(IV) at greater than 0.48 mg l^{-1}, gave apparent concentrations 5% higher than aluminum standards. Humic acid contributes about 0.5% Al by dry weight to a sample through contamination but does not interfere through fluorescence on its own or with lumogallion as previously reported [9]. Fluoride concentrations of 0.1, 1.0, and 3.8 mg l^{-1} added to 50 μg Al l^{-1} standards resulted in apparent aluminum concentrations of 48, 28, and 9 μg l^{-1}, respectively. Iron concentrations above 170 μg l^{-1} interfered above 50 μg Al l^{-1}. This interference can be overcome by diluting a sample so that the aluminum concentration is less than 50 μg l^{-1}. Manganese and zinc at concentrations up to 220 and 70 μg l^{-1}, respectively, increased the apparent aluminum concentrations by a maximum of only 1 μg l^{-1} in the range 10—50 μg Al l^{-1}.

Iron interference with the ferron method is corrected by the addition of 1,10-phenanthroline after reduction of iron(III). Manganese and fluoride and other ions [14] create small interferences. Glutamine and NTA reduced absorbance substantially for a 200 μg Al l^{-1} solution while L-alanine, glycine and aspartic acid did not consistently affect the results. The absorbance was increased markedly by 8-quinolinol which caused no interference with either the lumogallion or a.a.s. methods.

Detection limits and ranges of applicability. Detection limits between 0.05 and 0.1 μg Al l^{-1} have been reported for the lumogallion method [9, 10, 12, 17]. For routine work, a 1.0 μg l^{-1} standard was readily detected; the signal was linear up to about 120 μg Al l^{-1}. Lumogallion was used to obtain a constant matrix, and the detection limit for a.a.s. was then reduced to about 10 μg l^{-1}. Calibration curves were linear between 10 and 100 μg l^{-1} but had nonzero intercepts. The lower limit of usefulness of the ferron method was about 50 μg Al l^{-1}, although lower detection limits have been reported [14, 16] and the linear range was 50—1500 μg l^{-1}.

Conclusions

Although Hem and Roberson [18] suggested that mononuclear forms of aluminum are estimated in the ferron method, this must be considered speculative. The glutamic acid and NTA interferences are in accordance with the large stability constants (log K = 15.04 [19] and 11.4 [20] respectively) of the aluminum complexes. The interference of 8-quinolinol in the ferron method is not surprising. Because of the digestion step, the lumogallion method approximates total soluble aluminum.

REFERENCES

1 C. S. Cronan and C. L. Schofield, Science, 204 (1979) 304.
2 C. Decker and R. Menendez, Proc. W. Va. Acad. Sci., 46 (1974) 159.
3 C. S. Cronan, W. A. Reiners, R. C. Reynolds, Jr. and G. E. Lang, Science, 200 (1978) 309.
4 W. D. Burrows, Crit. Rev. Environ. Control, 7 (1977) 167.
5 J. R. J. Sorenson, J. R. Campbell, L. B. Tepper and R. D. Lingg, Environ. Health Perspect., 8 (1974) 3.
6 R. A. Freeman and W. H. Everhart, Trans. Am. Fish. Soc., 100 (1971) 644.
7 C. T. Driscoll, Jr., J. P. Baker, J. J. Bisogni, Jr. and C. L. Schofield, Nature, 284 (1980) 161.
8 J. B. Hunter, S. L. Ross and J. Tannahill, Water Pollut. Control, 79 (1980) 413.
9 D. J. Hydes and P. S. Liss, Analyst, 101 (1976) 922.
10 S. Cashetto and R. Wollast, Geochim. Cosmochim. Acta, 43 (1979) 425.
11 Y. Nishikawa, K. Hiraki, K. Morishige and T. Shigematsu, Jpn. Analyst, 16 (1967) 692.
12 T. Shigematsu, Y. Nishikawa, K. Hiraki and N. Nagama, Jpn. Analyst, 19 (1970) 551.
13 P. Allain and Y. Mauras, Anal. Chem., 51 (1979) 2089.
14 Inland Waters Directorate, Analytical Methods Manual, Environment Canada, Place Vincent Massey, Ottawa, 1979.
15 Techniques of Water-Resources Investigations of the United States Geological Survey, Methods for Collection and Analysis of Water Samples for Dissolved Minerals and Gases, 1970.

16 C. T. Driscoll, Cornell University, Thesis, 1980.
17 N. Ishibashi and K. Kina, Anal. Lett., 5 (1972) 637.
18 J. D. Hem and C. E. Roberson, Geological Survey Water Supply, Paper 1827-A.
19 M. K. Singh and M. N. Srivastava, J. Inorg. Nucl. Chem., 34 (1972) 567.
20 R. H. Smith and A. E. Martell, Critical Stability Constants, 1—4 (1974—1976).

Analytica Chimica Acta, 134 (1982) 375—378
Elsevier Scientific Publishing Company, Amsterdam — Printed in The Netherlands

Short Communication

DETERMINATION OF TRACES OF ZIRCONIUM IN SILICATE ROCKS BY INDUCTIVELY-COUPLED PLASMA EMISSION SPECTROMETRY

HIROSHI UCHIDA*, KIYOSHI IWASAKI and KATSU TANAKA

Industrial Research Institute of Kanagawa Prefecture 3173, Showa-machi, Kanazawa-ku, Yokohama 236 (Japan)

CHUZO IIDA

Laboratory of Analytical Chemistry, Nagoya Institute of Technology, Gokiso-cho, Showa-ku, Nagoya 466 (Japan)

(Received 5th August 1981)

Summary. The sample is fused with a mixture of sodium and potassium carbonates. Zirconium is separated from the large amounts of sodium and potassium by precipitation of hydrated oxides before nebulization. The detection limit is 0.32 μg Zr g^{-1}. Results for seven standard rocks are in accord with recommended values.

Traces of zirconium in silicate rocks have been determined by d.c. emission spectrography [1], x-ray fluorescence spectrometry [2] and neutron activation analysis [3], without any chemical treatment. These methods are simple and useful, but the results reported for zirconium are erratic, probably because of matrix effects. Spectrophotometric methods are also used but generally require complicated separation procedures. For example, zirconium must be isolated by ion-exchange separation prior to colour development with arsenazo-III [4] or xylenol orange [5].

Inductively-coupled plasma (i.c.p.) is the best excitation source for emission spectrochemical analysis because of its high sensitivity, wide dynamic range and comparative freedom from interferences. In previous work [6], minor and trace elements in various silicate rocks were determined by i.c.p. emission spectrometry after decomposition of the sample with a mixture of hydrofluoric acid and aqua regia in a sealed teflon vessel. This method generally proved effective, but for the determination of chromium and zirconium in some standard rocks, the results were significantly low probably because of incomplete sample decomposition.

The present communication deals with the determination of zirconium in silicate rocks by i.c.p. emission spectrometry; five methods for the decomposition of the sample were investigated. Fusion with alkali metal carbonates is recommended for complete decomposition of a variety of silicate rocks, although zirconium must be separated from the large amounts of alkali metals prior to the i.c.p. measurement.

Experimental

Instrumentation and operating parameters. An i.c.p. source (Model ICAP-1, Nippon Jarrell-Ash Co.) was used at 1.4 kW r.f. power, with argon flows of 14, 1.0 and 0.85 l min^{-1} as the coolant, plasma and carrier gases, respectively. The monochromator (Model JE-50, Nippon Jarrell-Ash Co.) was an Ebert-type (focal length 0.5 m) with a grating (1200 grooves mm^{-1}). The entrance and exit slit-widths were both 10 μm. The analytical line was Zr II 343.823 nm, and the observation height was 15.0 mm above the induction coil.

Sample preparation. In a platinum crucible, 0.5 g of silicate sample is fused with 2 g each of sodium carbonate and potassium carbonate for 30 min. After cooling, the melt is leached with 15 ml of 6 M hydrochloric acid, and diluted to 150 ml with water. Sodium hydroxide is added (with phenolphthalein as indicator) to precipitate zirconium as its hydrated oxide together with iron, magnesium, etc. The precipitates are filtered off, washed with water, transferred to a platinum vessel and dissolved in 10 ml of 47% hydrofluoric acid and 4 ml of 60% perchloric acid. The solution is heated gently under an i.r. lamp till acid fumes cease. The residue is dissolved in 10 ml of 6 M hydrochloric acid and diluted to 50 ml with water.

Stock solutions of zirconium and matrix elements were prepared as described previously [6, 7]. The standard solutions of zirconium used were 0—10 μg ml^{-1} in 1 M HCl. All contained aluminum (600 μg ml^{-1}), iron (600 μg ml^{-1}), calcium (500 μg ml^{-1}), magnesium (400 μg ml^{-1}), sodium (200 μg ml^{-1}) and potassium (200 μg ml^{-1}) as matrix elements.

Results and discussion

Zirconium shows great sensitivity in i.c.p. emission spectrometry [8]; three analytical lines, Zr II 339.198 nm [9], Zr II 343.823 nm [10] and Zr II 349.621 nm [6], have been generally used. For the determination of zirconium in silicate rocks, the 343.823-nm line is recommended because the other lines overlap with Th II 339.304 nm and Y II 349.608 nm, respectively, and thorium and yttrium are often present in silicate rocks at similar levels to zirconium. The effect of the viscosity of the sample solution could be decreased by preparing standard solutions of suitable matrix composition. The detection limit for zirconium (the concentration which gives an intensity equivalent to twice the standard deviation of the background from a blank matrix solution) was 0.32 μg g^{-1} in silicate rocks.

Five procedures for rock decomposition were first investigated for the standard silicate rock JG-1 (granodiorite; Geological Survey of Japan). The results for zirconium in each case are summarized in Table 1, together with an outline of the procedure. Decomposition with an acid mixture (method I) gave only about 30% recovery, though it was effective for most minor and trace elements [6]. The separation and fusion of the insoluble residue in method I with potassium hydrogensulfate (method II) was not successful. Most of the residue was dissolved after fusion with a mixture of sodium and potassium carbonates (method III) but some remained. Complete

TABLE 1

Decomposition procedures and results for zirconium in JG-1[a]

Method[b]	Reagents	Zr found ($\mu g\ g^{-1}$)	R.s.d.[c] (%)
(I) Decomposition with acids in sealed teflon vessel[d]	4 ml HF/3 ml HNO_3	36	9
(II) Fusion of insoluble matter in (I)[e]	0.5 g $KHSO_4$	34	—
(III) Fusion of insoluble matter in (I)[e]	0.25 g Na_2CO_3/0.25 g K_2CO_3	91	—
(IV) Initial fusion[f]	2 g Na_2CO_3/2 g K_2CO_3	123	3
(V) Fusion of the final residue in (IV)[g]	5 g $KHSO_4$	128	—

[a]Recommended value and r.s.d. are 111 $\mu g\ g^{-1}$ and 23.9%, respectively [11]. [b]0.5-g sample was decomposed and diluted finally to 50 ml with 1 M HCl. [c]Five determinations. [d]The method reported earlier [6] was modified by using nitric acid instead of aqua regia, and evaporating under an i.r. lamp. [e]Insoluble matter was filtered off and fused. The melt was dissolved in a few ml of 6 M HCl and combined with the primary filtrate. [f]As in experimental. [g]The melt was dissolved with 1 M HCl, and zirconium was separated with cupferron from the large amounts of potassium.

decomposition occurred on fusion of the original sample with this flux for 30 min (method IV). However, it has been stated that after fusion with alkali metal carbonates, any remaining insoluble matter must be fused with potassium hydrogensulfate (method V) [12]. However, there was no significant difference between the results of methods IV and V in the present experiments. On the basis of the above results, method IV is recommended. Zirconium could easily be separated from the large amounts of sodium and potassium by precipitation as its hydrated oxide, so that nebulization into the plasma became reproducible. The remaining small amounts of sodium and potassium did not cause ionization interferences.

TABLE 2

Results for zirconium in silicate rocks ($\mu g\ g^{-1}$)

Sample	Found[a]			Average reported ($\mu g\ g^{-1}$)	R.s.d. (%)	Recommended value [16]
	I	IV	V			
JB-1 (Basalt)	147	152	—	173 [11]	38.2	153[b]
MRG-1 (Gabbro)	99	113	—	112 [14]	26.6	105[c]
AGV-1 (Andesite)	229	237	—	227 [13]	13.9	225
BCR-1 (Basalt)	194	197	—	185 [13]	19.2	190
G-2 (Granite)	57	334	320	316 [13]	14.1	300
W-1 (Diabase)	78	115	109	108 [15]	22.6	105
GSP-1 (Granodiorite)	30	603	604	544 [13]	19.8	500

[a]By methods I, IV and V. [b]Ref. [11]. [c]Ref. [14].

Zirconium in other typical standard silicate rocks was determined by methods I and IV; method V was also used for samples that gave different results by methods I and IV. The results are listed in Table 2, and are compared with other reported values. Method I was simplest; it could be successfully applied to basalt, gabbro and andesite, but not to granite, diabase and granodiorite. The results of method IV compare reasonably well with the recommended values for all of the standard silicate rocks, though the procedure was more complicated. The secondary fusion with potassium hydrogensulfate (method V) seems to be unnecessary.

The authors express their gratitude to Dr. Tetsuo Uchida for his useful suggestions in this study.

REFERENCES

1 W. H. Champ and G. P. Bender, private communication, Geological Survey of Canada, Ottawa, 1973.
2 E. Murad, Anal. Chim. Acta, 67 (1973) 37.
3 K. Randle, Chem. Geol., 13 (1974) 237.
4 T. Kiriyama and R. Kuroda, Anal. Chim. Acta, 71 (1974) 375.
5 A. Mazzucotelli, R. Frache, A. Dadone and F. Baffi, Talanta, 24 (1977) 690.
6 H. Uchida, T. Uchida and C. Iida, Anal. Chim. Acta, 116 (1980) 433.
7 H. Uchida, T. Uchida and C. Iida, Anal. Chim. Acta, 108 (1979) 87.
8 P. W. J. M. Boumans and R. M. Barnes. ICP Inf. Newsl., 3 (1978) 445.
9 A. F. Ward and L. F. Marciello, Anal. Chem., 51 (1979) 2264.
10 H. Uchida and H. Matsui, Bunko Kenkyu, 27 (1978) 110.
11 A. Ando, H. Kurasawa, T. Ohmori and E. Takeda, Geochem. J., 8 (1974) 175.
12 K. Tada, Shin-Jikken Kagaku Koza, No. 9, Chemical Society of Japan, Maruzen, Tokyo, 1971, p. 269.
13 F. J. Flanagan, Geochim. Cosmochim. Acta, 33 (1969) 81.
14 S. Abbey, CANMET Rep. 79-35, Canada Centre for Mineral and Energy Technology, Energy, Mines and Resources, Canada, Ottawa, 1979, p. 49, 53.
15 M. Fleischer, Geochim. Cosmochim. Acta, 33 (1969) 65.
16 F. J. Flanagan, Geochim. Cosmochim. Acta, 37 (1973) 1189.

Analytica Chimica Acta, 134 (1982) 379—382
Elsevier Scientific Publishing Company, Amsterdam — Printed in The Netherlands

Short Communication

THE USE OF ALKALINE PERMANGANATE IN THE PREPARATION OF BIOLOGICAL MATERIALS FOR THE DETERMINATION OF MERCURY BY ATOMIC ABSORPTION SPECTROMETRY

J. F. CHAPMAN* and L. S. DALE

Chemical Technology Division, Australian Atomic Energy Commission, Research Establishment, Private Mail Bag, Sutherland 2232, N.S.W. (Australia)

(Received 7th July 1981)

Summary. Biological materials when treated with 1.5 M potassium hydroxide, rapidly disintegrate, and become dispersed in the aqueous phase. Addition of potassium permanganate causes rapid and almost complete sample oxidation. Dissolution is completed by addition of sulphuric acid, and excess of oxidant is reduced with oxalic acid. The homogenization step allows representative subsampling. The procedure is applicable to human hair, fingernails, urine, fish products, plant material, rat fur, blood and liver.

The determination of mercury by cold-vapour atomic absorption spectrometry requires the element to be in an ionic state to facilitate its reduction. For solid or liquid samples of organic origin, the determination is complicated by the need to destroy the organics and release the mercury without loss. The method of Omang [1] (sulphuric acid—potassium permanganate), has been used successfully to destroy small quantities of organic material. Disadvantages of this procedure are the time required to prepare the samples and the quantity of organic material that can be processed. By using homogenization with potassium hydroxide, larger samples may be processed with a significant reduction in preparation time.

Similar procedures have been used as an aid in dissolving organic matter. Giovanoli-Jakubczak et al. [2] used 11.2 M sodium hydroxide to dissolve hair. Skare [3] used 4% sodium hydroxide solution to homogenize fish samples and showed that, in general, alkaline homogenates showed no loss of mercury even after boiling in open containers. He also showed that methyl mercury was stable in alkaline media over extended periods and that protein was more effectively hydrolyzed by alkali than by acid. Alkaline potassium permanganate is very effective in decomposing many organic materials and acidified potassium permanganate is widely known for its oxidizing properties [4, 6].

In view of this it was considered that a three-stage chemical treatment of biological materials using sequential additions of potassium hydroxide, potassium permanganate and sulphuric acid should be capable of processing larger quantities of samples more rapidly than acidified permanganate alone, thereby allowing lower concentrations of mercury to be determined. This

aspect was investigated by analyzing various environmental materials including NBS orchard leaves and IAEA fish homogenate for mercury. The samples were analyzed by the standard addition technique using processed spiked samples.

Experimental

Reagents and equipment. All reagents were specially selected for their low mercury content: 1.5 M potassium hydroxide, 0.3 M potassium permanganate, 1.1 M oxalic acid and 9 M sulphuric acid (analytical grade).

All measurements were made on a Varian-Techtron model AA5 atomic absorption spectrometer operated at the recommended settings. The absorption cell and associated apparatus have been described elsewhere [7]. Erlenmeyer 100-ml flasks fitted with B14 cones and stoppers were used to store and process the samples.

Sample preparation. Details of preparation of individual samples are summarized in Table 1. In general, weighed samples were gently warmed with potassium hydroxide solution until dissolution or homogenization was evident. Blanks, samples and spikes were prepared simultaneously. After this initial treatment, potassium permanganate was added and the samples were allowed to stand for up to 30 min, or until the oxidant had obviously been consumed. More oxidant was added until the permanganate colour persisted. Samples were then acidified and allowed to stand for several hours. If the permanganate was depleted, more was added. This process was repeated until the permanganate colour persisted for about 4 h. A 1-ml aliquot of oxalic acid was added to the blank. After mixing and standing, a further 1 ml was added and the process was repeated until a clear solution was obtained. The same quantity of reagent was added slowly to the other samples. As reduction with oxalic acid proceeded, carbon dioxide was produced. It was therefore

TABLE 1

Typical quantities of reagents used to process the various samples

Sample	Weight[a] (g)	1.5 M KOH (ml)	0.3 M $KMnO_4$ (ml)	9 M H_2SO_4 (ml)
Human hair	0.01	1	1	2
Fingernail	0.01	1	1	2
Rat fur	0.01	1	1	2
Rat liver	0.1	1	2.5	2
Rat blood	0.5[b]	5	7	2.5
Urine	10[b]	4	14	3.5
Tinned fish	0.5	5	20	3
Dried fish	0.1	1	5	2
Vegetation	0.1	10	13	3.5

[a]Weight per determination. For most samples a larger quantity was homogenized with KOH and then subsampled into the reaction flasks. [b]Volume taken (ml).

necessary to ensure that the reaction flasks were kept only loosely stoppered to prevent them becoming pressurized. The mercury determination was completed by atomic absorption spectrometry as previously reported [7].

Results and discussion

The results for the analyses of the various materials for mercury are summarized in Table 2.

All sample types tested were readily homogenized in potassium hydroxide. Hair and fingernails dissolved completely in the alkaline solution. Most other materials left some residue but were readily homogenized. It has been shown that mercury partitions almost completely into the liquid phase in alkaline homogenates [3]. This was verified using a sample of IAEA fish homogenate in which small amounts of undissolved organic material remained after the chemical treatment. The result for mercury (Table 2) was within the range of the "most probable" value.

A urine sample was analyzed by the acid permanganate procedure [1] and with potassium hydroxide pretreatment. The same mercury result of 1.1 $\mu g\ l^{-1}$ was obtained with each procedure. However, the alkali treatment more than halved the processing time required by the acid permanganate procedure. Attempts to process a sample of orchard leaves large enough to provide a measurable mercury signal by using cold sulphuric acid—potassium permanganate [1] proved unsuccessful. When a similar sample was subjected to a preliminary alkali homogenization it was dispersed into the liquid phase and the decomposition proceeded rapidly. The mercury value obtained confirmed the accuracy of this procedure (Table 2).

TABLE 2

Results for mercury in various materials by the alkaline permanganate procedure

Sample	Hg found (mg kg^{-1})	Comments
Human hair	0.8—3.2	5 samples
Fingernail	3.1	
Rat fur	<0.05	Control
	0.14	After injection of 500 μg Hg
Rat liver	0.01	Control
	0.12	After injection of 500 μg Hg
Rat blood	0.045 ± 0.005 [a]	After injection of 10 μg Hg
Urine	1.1 ± 0.2[a]	
	3.4 ± 0.3[a]	
Tinned fish	0.08- 0.17	5 samples
Dried fish	10.1, 12.2	Shark (2 samples)
	1.4	Gem fish (*Rexea solandri*)
Fish homogenate	0.49 ± 0.03	Most probable value 0.48 ± 0.02
Orchard leaves NBS SRM 1592	0.16 ± 0.02	Reference value 0.155 ± 0.015

[a] $mg\ l^{-1}$.

The procedure was also suitable for use in the analysis of blood. Although the sample taken contained a higher than natural level of mercury (Table 2), the result indicated that the procedure would be suitable for lower levels. Skare [3] reported that mercury in blood could not be determined by using 4% sodium hydroxide homogenization followed by acid permanganate digestion; at no stage was an alkaline permanganate treatment tested.

Although all calibrations were linear in the range of observation (i.e., up to 150 ng Hg), some sample matrices adversely affected the sensitivity. For this reason the standard addition technique is recommended to cope with the wide range of materials for which this procedure is suitable.

Hydroxylammonium chloride, which had previously been used as a reducing agent to remove the excess oxidants remaining after the decomposition, was found to be unsatisfactory. This was because the large unconsumed quantity of permanganate in the blank required considerably more reductant than the samples. This excess resulted in erroneous blank absorbance readings owing to the "hold-back" effect mentioned by Stuart [8], who showed that even a small excess of hydroxylamine significantly diminished the mercury absorbance. The occurrence of this "hold-back" effect could be due to the formation of a stable mercury amide complex which is not completely reduced to mercury metal by tin(II) [9]. When oxalic acid is used as reductant, a stable mercury(I) oxalate complex [10] is formed. This complex, however, is reduced by tin(II). Thermodynamic data [11] support this. Experiments showed that with oxalic acid no loss of mercury occurred when carbon dioxide was evolved during the reduction of the excess of permanganate and manganese-(IV) oxide.

Conclusions

The procedure described above is applicable to a wide range of environmental samples and homogenization of a bulk sample facilitates representative subsampling. Although the accuracy has been verified by the results obtained on NBS orchard leaves and IAEA fish homogenate, the use of the standard addition technique is recommended for all sample types.

REFERENCES

1 S. H. Omang Anal. Chim. Acta, 53 (1971) 415.
2 T. Giovanoli-Jakubczak, M. R. Greenwood, J. C. Smith and T. W. Clarkson, Clin. Chem., 20 (1970) 222.
3 I. Skare, Analyst, 97 (1972) 148.
4 A. Y. Drummond and W. A. Waters, J. Chem. Soc., (1953) 435.
5 J. S. F. Pode and W. A. Waters, J. Chem. Soc., (1956) 717.
6 R. Stewart, Oxidation in Organic Chemistry, Academic Press, New York, 1965, Part A, Ch. 1.
7 J. F. Chapman and L. S. Dale, Anal. Chim. Acta, 101 (1978) 203.
8 D. C. Stuart, Anal. Chim. Acta, 106 (1979) 411.
9 H. Remy, Treatise on Inorganic Chemistry, Elsevier, Amsterdam, 1956, Vol. 2, p. 474.
10 T. Moeller, Inorganic Chemistry, An Advanced Textbook, J. Wiley, New York, 1952, p. 850.
11 W. M. Latimer, The Oxidation States of the Elements and their Potentials in Aqueous Solutions, Prentice-Hall, New York, 1952, p. 175.

Analytica Chimica Acta, 134 (1982) 383—388
Elsevier Scientific Publishing Company, Amsterdam — Printed in The Netherlands

Short Communication

A NUMERICAL AID FOR EVALUATION OF ATOMIC ABSORPTION SPECTROMETRIC RESULTS

J. A. S. ANDREWS

I.C.I. Central Research Laboratories, Newsom Street, Ascot Vale, Vic. 3032 (Australia)

A. JOWETT*

Division of Mineral Engineering, C.S.I.R.O., Bayview Ave., Clayton, Vic. 3168 (Australia)

(Received 1st July 1981)

Summary. A simple numerical method is described for evaluation of data from atomic absorption spectrometry; the method assumes an exponential relationship between absorption reading and concentration. It requires only that the concentrations of the calibrating solutions form an arithmetic progression. Evaluation of data indicates that the assumed exponential relationship holds to within the limits of experimental error normally regarded as adequate for routine work.

Atomic absorption spectrometry is extensively used in the mineral industry in the analysis of feed and products on mineral processing plants. Typical calibration plots for the instruments are not linear (e.g., Fig. 1) and the subjectivity and possible bias involved in drawing a smooth curve through the calibration points is known to lead at times to significant errors in estimation of the metal content of test solutions. An additional factor which can arise, and which is not easily detected on a calibration curve, is a calibrating solution which is slightly in error.

An alternative to the usual procedure of drawing a smooth curve through the calibrating points is to calculate a least-squares fit by computer to either a polynomial or a simple standard function (e.g. power law, exponential, etc.). However, such procedures are not entirely satisfactory on account of the non-linear equations used, and they are certainly unable to detect small calibrating errors. (In a routine analytical laboratory at a remote mineral production site, handling hundreds of samples daily, recalibration may not be carried out as frequently as desirable, mainly through a combination of shortage of experienced staff and pressure of work.) A better procedure is one which linearizes the data, and this is the basis of the numerical method described.

Linearization of data from atomic absorption spectrometry

The calibration curve has a simple form and should be describable by a mathematical expression incorporating very few curve-fitting parameters. Such an expression, with a shape and boundary conditions appropriate to the curve, is the exponential

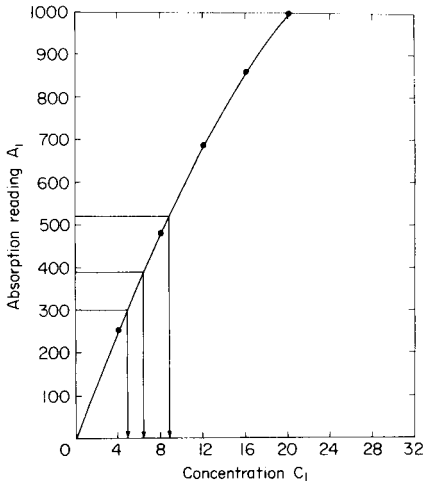

Fig. 1. Calibration chart for atomic absorption spectrometry of zinc.

$$A = A^* \left[1 - \exp(-BC)\right] \tag{1}$$

where A is the absorption reading of a solution with metal concentration C, A^* is a parameter having the dimensions of A, and B is a parameter having the inverse dimensions of C. This is an expression which in special circumstances can be linearized for fitting to a set of data to find (1) estimators of the parameters in the equation, and (2) criteria for the goodness of fit between the equation and the data.

In general, a simple method for finding estimates of A^* and B in terms of C_i and A_i $(i = 1 \ldots l)$, the concentrations and corresponding absorption readings of the set of standard solutions, is not possible because Eqn. (1) cannot be converted to a linear equation with respect to some transformation of these parameters.

However, for the special case where the concentrations of the set of calibrating solutions follow the arithmetic progression $C_i = ci$ $(i = 1 \ldots l)$, the corresponding absorption readings satisfy the linear difference equation

$$A_i = a + bA_{i-1} \quad (i = 1 \ldots l) \tag{2}$$

where c and a are parameters having the dimensions of C and A, respectively, and b is a dimensionless parameter. Also $A_0 = 0$, $A^* = a/(1 - b)$ and $B = -\ln b/c$.

The use of difference equations to aid interpretation of non-linear data is well known, and has been used for evaluation of particle size analysis results [1, 2] and of mineral flotation data [3]. Additionally, as Eqn. (2) is linear with respect to the parameters a and b, estimates of these parameters can be found in terms of $A_i (i = 1 \ldots l)$. The least-squares estimators of a and b are

$$\hat{a} = \left(\sum_{i=1}^{l} A_i - \hat{b} \sum_{i=1}^{l} A_{i-1} \right) \Big/ l \tag{3}$$

$$\hat{b} = \left[\sum_{i=1}^{l} A_{i-1}A_i - \left(\sum_{i=1}^{l} A_{i-1} \sum_{i=1}^{l} A_i\right)\Big/l\right]\Big/\left[\sum_{i=1}^{l} A_{i-1}^2 - \left(\sum_{i=1}^{l} A_{i-1}\right)^2\Big/l\right] \quad (4)$$

A measure of the goodness of fit between Eqn. (2) and the data is given by

$$R^2 = \frac{\left[\sum_{i=1}^{l} A_{i-1}A_i - \left(\sum_{i=1}^{l} A_{i-1} \sum_{i=1}^{l} A_i\right)\Big/l\right]^2}{\left[\sum_{i=1}^{l} A_{i-1}^2 - \left(\sum_{i=1}^{l} A_{i-1}\right)^2\Big/l\right]\left[\sum_{i=1}^{l} A_i^2 - \left(\sum_{i=1}^{l} A_i\right)^2\Big/l\right]} \quad (5)$$

where R is the correlation coefficient.

The calculated values of A_i ($i = 1 \ldots l$) are given by

$$\hat{A}_i = \hat{a} + \hat{b}\hat{A}_{i-1} \quad (i = 1 \ldots l) \quad (6)$$

where $\hat{A}_0 = 0$. If $A_j (j = 1, J)$ are the absorption readings of the set of solutions of unknown concentrations, the appropriate estimates of the concentrations are calculated from

$$\hat{C}_j = c \ln [1 - (1 - \hat{b})A_j/\hat{a}] / \ln \hat{b} \quad (7)$$

Data examination

A program was written for a HP67 pocket calculator to calculate Eqns. (3—7); a listing is available from the Division of Mineral Engineering, CSIRO.

The program was used to assess two blocks of data. The first block (I) was used to test the curve-fitting calculation and to arrive at some criteria representing an adequate fit to the calibration curve. A typical set of results is given in Table 1, which shows absorption readings for a set of calibrating solutions and the curve-fitting parameters. The R^2 value of 0.9994 indicates a very good fit to the curve, and in consequence the evaluated curve-fitting parameters were used to assess the zinc content of samples used in the preparation of unknown solutions. The calculated values are compared with graphical estimates made separately by two technicians; in this instance the differences between graphical and calculated values are not large, but bigger ones have been observed.

TABLE 1

Data relating to zinc content of ore samples (Zn range, 4—20%)

Calibrating solution (% Zn equivalent in sample)	Absorption readings	Mean (A_i)	Calculated value ($\hat{A}_i$)	Absorption reading for unknown solution	Graphical estimate		Calculated value ($\hat{C}_j$)
					Worker A	Worker B	
4.0	253,252	252.5	258.4	301	4.7	4.9	4.7
8.0	481,479	480.0	483.7	389	6.2	6.3	6.3
12.0	684,690	687.0	680.3	521	8.6	8.8	8.7
16.0	861,859	860.0	851.7				
20.0	999,1002	1000.5	1001.2				

Curve-fitting parameters: $a = 258.4$; $b = 0.8721$; $R^2 = 0.9994$.

TABLE 2

Summary of curve-fitting results for data block I

Set	Range	$\hat{a}$	$\hat{b}$	R^2
1	Zn (4—20%)	258.4	0.8721	0.9994
	Pb (4—20%)	270.8	0.8492	0.9998
	Cu (4—30%)	171.6	0.9168	0.9996
2	Zn (4—20%)	226.3	0.9381	0.9993
	Pb (4—20%)	270.5	0.8485	0.9999
	Cu (4—30%)	170.2	0.9199	0.9992

Table 2 summarizes curve-fitting results for six sets of data constituting block I. The minimum value of R^2 obtained was 0.9992, and the maximum deviation between observed (A_i) and calculated ($\hat{A}_i$) values of absorption readings was 8.6, which is about 1% deviation. In all cases, the curve-fitting was good enough to permit calculation of metal concentrations. These results were used to specify arbitrary standards for adequacy of the accuracy of curve-fitting. The standards were set initially at $R^2 > 0.9990$ and $|A_i - \hat{A}_i|_{max} < 10.0$, with the intention of adjusting to more appropriate values if necessary by reference to required standards of analytical accuracy as further data were examined.

If for any set of calibration data these criteria do not hold, further calculation should not proceed. The calibration must be checked by first ensuring that the standard solutions are in arithmetic progression, and then, if necessary, by checking the absorption readings of the standard solutions; if these also are correct, the calibrating solutions should be checked by an independent method. If all these are found satisfactory, Eqn. (1) does not fit the data, and the graphical method must be used.

To test the numerical method more thoroughly and to determine if the curve fitting criteria were adequate, more data were evaluated (block II). Table 3 gives R^2 and $|A_i - \hat{A}_i|_{max}$ values for sets of calibration data. With the exception of sets 2 and 4, the curve-fitting was good, and Table 4 gives a typical example of the comparison between numerical and graphical estimates of the metal content of unknown solutions in such circumstances. It is clear

TABLE 3

Summary of curve-fitting results for data block II

Set	Range	$\lvert A_i - \hat{A}_i \rvert_{max}$	R^2	Set	Range	$\lvert A_i - \hat{A}_i \rvert_{max}$	R^2
1	Pb (4—20%)	7.5	0.9991	5	Cu (4—20%)	5.5	0.9996
2	Zn (4—20%)	19.0	0.9970	6	Pb (4—20%)	2.0	0.9999
3	Pb (4—20%)	8.5	0.9993	7	Zn (4—20%)	6.5	0.9994
4	Zn (4—20%)	16.5	0.9984	8	Cu (4—20%)	6.0	0.9997

TABLE 4

Estimation of copper content of samples (data block II, Set 5)

Calibrating solutions (% Cu equivalent in sample)				Unknown solutions[a]				
C_i	A_i	$\hat{A}_i$	$A_i - \hat{A}_i$	Sample	A_j	$\hat{C}_j$	Graphical value	Difference
4	237.0	238.5	−1.5	1	256	4.3	4.4	−0.1
8	450.0	455.5	−5.5	6	681	12.6	12.3	+0.3
12	658.0	654.0	+4.0	7	262	4.4	4.5	−0.1
16	840.0	835.0	+5.0	8	544	9.7	9.6	+0.1
20	1000.0	1000.0	0.0	12	536	9.6	9.5	+0.1
		$R^2 = 0.9996$		14	678	12.5	12.2	+0.3
				18	307	5.2	5.3	−0.1
				23	286	4.8	4.9	−0.1

[a]Of the 23 unknown solutions evaluated, 15 showed zero difference between $\hat{C}_j$ and the graphical value and are not listed. The relevant A_j values were spread fairly evenly between 249 and 499.

that, when the calibration data accurately fit a smooth exponential curve, the discrepancies between numerical results and graphical estimates are mostly negligible; i.e., the numerical method is mainly useful in eliminating possible graphical errors and in giving a positive indication via the curve-fitting criteria of the reliability of the calibration curve and hence estimates of metal content.

The cases showing a relatively poor curve-fit are more interesting (Sets 2 and 4, both of which concern zinc assays using the same set of calibrating solutions). Table 5 shows the results for Sets 4 and 2, and several significant discrepancies are evident. In the case of Set 4 (which chronologically preceded Set 2), the calibrating solution for 16% zinc deviated markedly from the value corresponding to a fit to a smooth exponential curve; it is possible that the standard solution was incorrect. This view was confirmed by the results for Set 2, for which the correlation had worsened in the intervening period; the deviations from the curve-fitting criteria were larger, and also the calibrating solution for 12% zinc had changed; it was inferred that two calibrating solutions were then in error. Even so, the differences between numerical and graphical estimates of zinc content are quite small though significant. The numerical estimate is probably the more accurate, and it is clear that the curve-fitting procedure via the difference equation is a very sensitive method of detecting small calibrating errors.

Conclusions

The numerical method of estimating metal contents from atomic absorption readings, based on the assumption of an exponential form of calibration curve, can consistently give results at least as reliable as those obtained by graphical interpolation.

TABLE 5

Estimation of zinc content of samples (Data block II, Sets 4 and 2)

Calibrating solutions for Set 4 (% Zn equivalent in sample)				Unknown solutions in Set 4				
C_i	A_i	$\hat{A}_i$	$A_i - \hat{A}_i$	Sample	A_j	$\hat{C}_j$	Graphical value	Diff.
4	248.5	257.5	−9.0	1	745	13.5	13.2	+0.3
8	480.5	483.0	−2.5	2	810	15.0	14.7	+0.3
12	682.0	679.5	+2.5	3	750	13.6	13.3	+0.3
16	867.5	851.0	+16.5	4	338	5.4	5.5	−0.1
20	1000.0	1001.0	−1.0	5	498	8.3	8.3	0.0
	R^2 = 0.9984			6	728	13.1	12.8	+0.3
				7	575	9.8	9.7	+0.1
				8	566	9.6	9.5	+0.1
				9	292	4.6	4.7	−0.1
				10	281	4.4	4.6	−0.2
				11	406	6.6	6.6	0.0
				12	355	5.7	5.8	−0.1
				13	652	11.4	11.2	+0.2
				14	635	11.1	10.9	+0.2
				15	545	9.2	9.1	−0.1
				16	433	7.1	7.1	0.0

Calibration solutions for Set 2 (% Zn equivalent in sample)				Unknown solutions in Set 2				
C_i	A_i	$\hat{A}_i$	$A_i - \hat{A}_i$	Sample	A_j	$\hat{C}_j$	Graphical value	Diff.
4	246.5	260.0	−13.5	1	360	5.7	5.9	−0.2
8	477.0	486.0	−9.0	2	367	5.8	6.0	−0.2
12	701.5	682.5	+19.0	3	894	17.0	16.8	+0.2
16	866.5	853.0	+13.5	4	888	16.9	16.6	+0.3
20	1000.0	1001.5	−1.5	5	629	10.9	10.7	+0.2
	R^2 = 0.9970			6	268	4.1	4.4	−0.3
				7	274	4.2	4.5	−0.3
				8	508	8.4	8.4	0.0

The goodness-of-fit criteria specified for the curve-fitting appear to be satisfactory in providing analytical results of adequate accuracy. Also the method is robust to significant errors in one or even two calibrating solutions, but the method has special value in alerting technical staff to the possibility of deterioration of calibrating solutions.

The authors are pleased to acknowledge the collaboration of Mount Isa Mines Ltd. and Mr. Neil Richardson, Senior Analyst, particularly, in supplying analytical data.

REFERENCES

1 C. C. Harris and A. Jowett, Nature, 197 (1963) 1192.
2 C. C. Harris and A. Jowett, Nature, 208 (1965) 175.
3 A. Jowett, Trans. Inst. Min. Metall., 83C (1974) 263.

Analytica Chimica Acta, 134 (1982) 389—391
Elsevier Scientific Publishing Company, Amsterdam — Printed in The Netherlands

Short Communication

THE EFFECT OF pH ON THE CHELATION OF LEAD WITH AMMONIUM PYRROLIDINEDITHIOCARBAMATE FOR ATOMIC ABSORPTION SPECTROMETRY

D. M. JONAS and L. R. PARKER, Jr.*

Department of Chemistry, Vassar College, Poughkeepsie, NY 12601 (U.S.A.)

(Received 25th June 1981)

Summary. A standard method involving chelation of lead with ammonium pyrrolidinedithiocarbamate and extraction into methyl isobutyl ketone was investigated as to the effect of the pH of chelation on the absorbance and stability of the extracted lead. The maximum sensitivity to lead occurs at low pH values, but rapid degradation of the absorption also occurs at low pH values. Higher pH values give lower sensitivity, but provide better stability with time.

The standard method for quantifying lead by atomic absorption spectrometry specifies chelation by ammonium pyrrolidinedithiocarbamate (APDC) and extraction of the Pb—APDC complex into methyl isobutyl ketone (MIBK), followed by aspiration into an atomic absorption spectrometer [1]. Previous reports [2—4] have shown the absorption to be affected by the pH used during the chelation step, even though all the lead is chelated and extracted in the pH range 1—7 [2]; other workers have noted the change in absorption over time at a single pH [5]. This work investigated the two factors (pH and time) using a multivariate design, which is necessary to detect any interaction between the two factors.

Experimental

Apparatus. A Jarrell-Ash Dial-Atom III atomic absorption spectrometer was used with a 0.15-nm slit width and a Jarrell-Ash 45468 lead hollow-cathode lamp. Measurements were made at the 217-nm lead line, and a 10-mm burner height was maintained. Absorbance readings were taken every second from the digital display of the spectrometer, and were averaged over a 10-s period. Air (10 l min^{-1}) and acetylene (1 l min^{-1}) were used for the flame. An Orion 601A digital pH meter was used in the pH adjustment.

Chemicals. A stock solution (1.0 μg Pb ml^{-1}) was prepared from lead nitrate (Baker Analyzed Reagent) and was stabilized by the addition of 1 ml of concentrated nitric acid per liter. A 1.0% (w/v) solution of APDC (Baker Analyzed Reagent) was prepared fresh every week. Spectroscopic-grade MIBK (J. T. Baker Ultrex) was used. The pH was adjusted with 0.5 M hydrochloric acid or 0.5 M ammonia.

0003-2670/82/0000-0000/$02.75

Procedure. A 100.0-ml aliquot of the lead solution was added to a beaker and the pH was adjusted to the specified value. The solution was then placed into a Nalgene separatory funnel (to minimize carry-over) and 5.00 ml of the APDC solution was added. The solution was shaken for 1 min, and then 10.00 ml of MIBK was added. The mixture was shaken for 2 min, and then allowed to stand for the layers to separate. The organic layer was drawn off and stored in stoppered 25-ml Erlenmeyer flasks for the specified time interval.

Results and discussion

Method of storage. A preliminary study was undertaken to investigate whether refrigeration of the samples between the time of extraction and aspiration gave significantly different results than when the samples were allowed to stand at room temperature. The standard method was followed, including the pH of 3.0 for chelation. Samples were prepared on the same day as the absorbance measurement, as well as one, two, and three days prior to measurement (labelled day 1, 2, 3, and 4, respectively). The results of this study are shown in Table 1. An *F*-test on the variance between refrigerated and unrefrigerated samples compared to the variance among the replicates showed a low level of significance (29%). Therefore, it was decided to leave the samples unrefrigerated between extraction and measurement of the absorbance for the rest of the study.

pH vs. time study. Because previous work [6] had shown the aqueous APDC solution to be stable for up to a month, the stability of the extracted Pb—APDC complex at several different pH values was examined. The two ranges of pH studied were below (pH 1.0—2.5) and above (pH 4.0—6.0) the standard value. Modified factorial-type designs were used in each pH range.

The data from each experiment were used to fit a full second-order polynomial relating absorbance to pH and time

$$y = b_0 + b_1x_1 + b_{11}x_1^2 + b_2x_2 + b_{22}x_2^2 + b_{12}x_1x_2$$

where y is the absorbance, x_1 is the pH, and x_2 is the time in days for a particular sample. The resulting quadratic equations were then used to construct the pseudo-three-dimensional response surfaces shown in Fig. 1.

As the response surfaces show, the absorbance obtained when a low pH is used for chelation is larger than that obtained when a higher pH is used (compare the back surfaces of Fig. 1A and B). The response surfaces also show that the lower the pH, the more rapid the degradation of response.

TABLE 1

Absorbances for refrigerated and unrefrigerated samples at pH 3.0

Day	4	3	2	1	1
Refrigerated	0.427	0.465	0.471	0.436	0.445
Room temp.	0.431	0.438	0.464	0.447	0.445

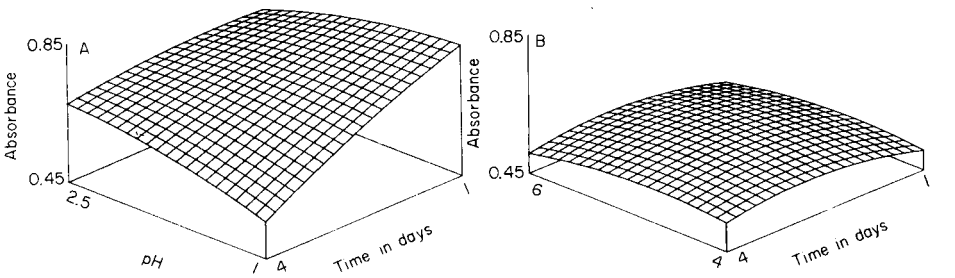

Fig. 1. Response surfaces for absorbance vs. pH and time (A) in the pH range 1.0—2.5 and (B) in the pH range 4.0—6.0.

At pH 1.0, the response decreases by 29% over the four-day period; at pH 2.5, the response decrease is only 12% over the same four-day period. At pH 4.0—6.0, there is no trend in absorbance with time; generally, there is no appreciable change in absorbance from the first day to the fourth day. As Fig. 1B shows, the response surface in this pH region is relatively flat.

The explanation for this behavior is not apparent. Since Everson and Parker [2] showed that all the lead is extracted throughout the pH range 1—7, the higher absorbance at low pH (with measurement on the same day as extraction) must be due to the nature of the complexed and extracted lead. In a flame atomic absorption spectrometer, it is difficult to separate an effect on transport (or nebulization) from an effect on free atom formation (dissociation and atomization). The change in absorbance at different levels of pH could be due to either effect, or a combination of the two. Future work, involving electrothermal atomic absorption (where the transport effect is absent), should distinguish between the two effects. Further, additional studies utilizing proton and carbon-13 nuclear magnetic resonance spectroscopy should help determine the mechanism of the pH and time effects.

Although there are insufficient data to draw firm conclusions, the results are important from an analytical point of view. For maximum sensitivity, the method should involve chelation at low pH, but the absorbance of all samples and standards must be measured at the same time interval after extraction, and within one day of extraction. For maximum insensitivity with respect to time and pH, chelation in the range pH 4—6 is advisable, if the lower sensitivity is not a problem. A pH in this range would allow for large tolerances on pH (e.g., pH 5.0 ± 1.0) and on the time elapsed between chelation/extraction and quantitation (up to four days) without significant change in the absorbance.

REFERENCES

1 American Public Health Association, Standard Methods for the Examination of Water and Wastewater, 14th edn., New York, 1976, pp. 144—162.
2 R. J. Everson and H. E. Parker, Anal. Chem., 46 (1974) 1968.
3 S. R. Koirtyohann and J. W. Wen, Anal. Chem., 45 (1973) 1986.
4 J. D. Kinrade and J. C. van Loon, Anal. Chem., 46 (1974) 1894.
5 H. A. Dabeka, Anal. Chem., 51 (1979) 902.
6 K. S. Subramanian and J. C. Meranger, Anal. Chim. Acta, 124 (1981) 131.

Analytica Chimica Acta, 134 (1982) 393—396
Elsevier Scientific Publishing Company, Amsterdam — Printed in The Netherlands

Short Communication

DETERMINATION OF THALLIUM IN GEOLOGICAL MATERIALS BY EXTRACTION AND ELECTROTHERMAL ATOMIC ABSORPTION SPECTROMETRY

C. M. ELSON*
Department of Chemistry, Saint Mary's University, Halifax, N.S. B3H 3C3 (Canada)
C. A. R. ALBUQUERQUE
Department of Geology, Saint Mary's University, Halifax, N.S. B3H 3C3 (Canada)

(Received 14th April 1981)

Summary. Thallium is determined in geological reference materials by acid digestion, extraction of thallium(III) from 0.5 M HBr solution into methyl isobutyl ketone and direct electrothermal atomic absorption spectrometry. The method yields results that agree with published values, has a detection limit of 0.04 μg Tl g^{-1}, and is relatively free of interferences.

Interest in the geochemistry of trace elements has been increasing in recent years with the hope that the level and distribution of these elements will further the understanding of geological processes. Thallium, which shows crystallochemical affinities with the geochemically important elements, potassium and rubidium, is one element of interest. The limited amount of information up to 1971 related to the geochemistry of thallium has been reviewed by Albuquerque and Shaw [1]. More recently, the thallium content of meteorites as well as lunar and terrestrial samples has been measured by neutron activation analysis [2—4]. Thallium was measured following a 5—7 day irradiation and radiochemical separation. Such methods have low detection limits (<1 ng Tl could be determined) but are also prolonged and require specialized facilities.

Thallium has also been determined in geological materials by a combination of solvent extraction and atomic absorption spectrometry (a.a.s.). Thallium(III) is readily extracted into organic solvents as a hydrated and solvated ion pair, $[H(H_2O)_nS_m^+\ TlX_4^-]$ where S is a molecule of solvent, X is a halide ion, and n and m are integers dependent upon the hydrohalic acid concentration and solvent [5, 6]. Previous work has involved extracting thallium with isopropyl ether and then evaporating the ether prior to a.a.s. with a tantalum boat [7] or redissolving the ether residue in dilute sulfuric acid [8]. Simplification is proposed here. Because methyl isobutyl ketone (MIBK) is a well-behaved solvent in the graphite furnace, a series of geological reference materials has been processed with a simple MIBK extraction of thallium from dilute hydrobromic acid solution followed by electrothermal a.a.s.

Experimental

Reagents and samples. All chemicals were reagent grade and water was distilled from an all glass apparatus. Glassware and teflon-ware were cleaned with warm (1 + 1) nitric acid. Methyl isobutyl ketone was presaturated daily with 0.5 M HBr.

The standard reference materials were obtained from the United States Geological Survey (USGS), Washington, DC, the Centre de Recherches Petrographiques et Geochimiques (CRPG), and the Association Nationale de la Recherche Technique (ANRT), Vandseuvre-les-Nancy, France.

Standard solutions of thallium(I) (200 ppm) were prepared from weighed amounts of thallium(I) sulfate in dilute hydrobromic acid. Solutions containing 200 ppb Tl(III) in 0.5 M HBr, used to spike samples, were prepared weekly by gently heating 10 ml of a 2 ppm Tl(I) solution with 4 ml of hydrobromic acid and 2—3 drops of bromine until all colour had disappeared and then diluting to 100 ml.

Equipment. The atomic absorption spectrometer (Model 403, Perkin-Elmer) was equipped with an electrothermal atomizer (Perkin-Elmer, HGA 2100), a deuterium arc background corrector, a thallium lamp (λ = 276.8 nm) and a time-base recorder (Hitachi—Perkin-Elmer). The temperature program was to dry for 25 s at 150°C, char for 30 s at 600°C, and atomize for 5 s at 2200°C. The internal nitrogen flow was interrupted during atomization.

Extractions were done with 125-ml separatory funnels fitted with teflon stopcocks on a wrist-action shaker (Burrell Corp.) for a period of 5 min.

Procedure. Weigh 0.5 g of sample into a 100-ml teflon beaker. Dampen the sample and then add 2 ml of concentrated nitric acid, 3 ml of 70% perchloric acid, and 8 ml of 49% hydrofluoric acid. (If the sample contains less than 0.5 μg Tl g^{-1}, use 1 g of sample and one and a half times the amount of acids.) Cover the beaker and heat in a sandbath for 2 h. Remove the cover and evaporate to dryness overnight. Add 2 ml of hydrobromic acid and 10—20 ml of water and warm to achieve dissolution. Transfer the solution to a 50-ml flask.

Pipette an aliquot of digested sample, usually 10 or 20 ml, into a separatory funnel; add 5 ml of MIBK and extract. Allow the phases to separate and transfer 10 μl of the MIBK layer into the graphite furnace. Spike the solution in the extraction flask with an aliquot of 200 ppb Tl(III) standard and repeat the extraction and atomic absorption measurement.

Results and discussion

The accuracy of the present method was evaluated by comparing the results (Table 1) with literature values [8—11]. The error limits represented one standard deviation based on at least three determination (USGS standards were analyzed at least six times). With the exception of the value for ANRT-DR-N, the agreement was quite good; however, the French standards have not been analyzed extensively for thallium. Because of the success in analyzing the fairly wide range of minerals and rock types, the method should be

TABLE 1

Thallium content of geological reference materials

Sample	Concentration ($\mu g\ g^{-1}$)					
	USGS-GSP-1	USGS-BCR-1	USGS-G-2			
This work	1.41 ± 0.10	0.27 ± 0.03	0.90 ± 0.09			
Other values	1.535 [8]	0.29 [8]	1.065 [8]			
	1.20 [9]	0.267 [9]	1.05 [9]			
	1.3 [10]	0.30 [10]	1.0 [10]			
Sample	CRPG-GA	CRPG-GH	CRPG-BR	CRPG-Mica-Fe	CRPG-Mica-Mg	
This work	0.92 ± 0.09	2.13 ± 0.17	0.01 ± 0.01	14.7 ± 1.15	5.94 ± 0.17	
Other values	1.10 [8]	2.60 [8]	0.110 [8]	12.4 [8]		
	1.90 [11]	5.00 [11]	1.00 [11]	15.5 [11]		
		2.20 [11]		19.0 [11]		
Sample	ANRT-FK-N	ANRT-GS-N	ANRT-UB-N	ANRT-DR-N	ANRT-BX-N	ANRT-VS-N
This work	2.7[a]	1.15 ± 0.09	0.06 ± 0.01	0.68 ± 0.07	0.07 ± 0.01	0.04 ± 0.01
Other values			0.045 [8]	1.02 [8]	0.15 [8]	0.05 [8]

[a]Result of a single determination.

applicable to other matrices. The result found for N.B.S. River Sediment (1645) was 1.24 ± 0.16 μg Tl g^{-1} which represented a 12% difference from the certified value of 1.44 ± 0.07 $\mu g\ g^{-1}$. The river sediment, however, contained 1.7% grease and oil which was carried through the procedure and into the MIBK extract. During a study of the trace metal content of fish oils [12], it was found that oil suppressed the metal signals significantly; this may account for part of the error in the case of the river sediment. Ten months after the original investigation had been completed and the method set aside, CRPG-GH was analyzed a further twelve times to check the reproducibility of the results. A value of 2.0 ± 0.15 μg Tl g^{-1} was obtained which was within 5% of the value listed in Table 1 and carried a relative standard deviation of approximately 8%.

The detection limit of the method (based on a signal equal to twice the background noise, a 10-μl injection into the graphite furnace, extraction of 40 ml of digested sample and a sample weight of 1 g) was 0.04 μg Tl g^{-1}. This value was ten times higher than that obtained by the tantalum boat—a.a.s. method [7] but similar to the detection limits of the back-extraction—a.a.s. method [8] and to the lengthy anion exchange-spectrographic method of Albuquerque and Muysson [9]. Reagent blanks gave no signals above the baseline noise.

Three main simplifications have been incorporated into the present method, the most important of which was the direct measurement of the organic extract. Furthermore, because digested samples that had been treated with bromine [7] or repeatedly evaporated to dryness with hydrobromic acid [8] yielded the same results as untreated samples, these steps could be omitted. This meant that thallium in the samples was oxidized to thallium-(III) during digestion.

Bromine was found to interfere because of its reaction with MIBK. Presumably, bromine added across the double bond of the enol form of the ketone and the brominated product, suppressed the thallium signal. Hence, care was taken to use fresh hydrobromic acid. The agreement between the present results and the published values of the well studied USGS standards was taken as evidence that the method was otherwise relatively free of interference.

Both authors gratefully acknowledge the financial support of the Natural Sciences and Engineering Research Council of Canada.

REFERENCES

1 C. A. R. Albuquerque and D. M. Shaw, in K. W. Wedepohl (Ed.), Handbook of Geochemistry, II-3, Springer, Berlin, 1971.
2 P. C. Fung and D. H. Shaw, Geochim. Cosmochim. Acta, 42 (1978) 703.
3 S. Biswas, H. T. Ngo and M. E. Lipschutz, Z. Naturforsch., 35A (1980) 191.
4 R. Wolf, A. Woodrow and E. Anders, Lunar Planet Sci., 10 (1979) 1361.
5 J. Korkisch, Modern Methods for the Separation of Rarer Metal Ions, Pergamon, New York, 1969, p. 310.
6 K. Henning and H. Specker, Z. Anal. Chem., 241 (1968) 81.
7 M. Fratta, Can. J. Spectrosc., 19 (1974) 33.
8 G. P. Sighinolfi, At. Abs. Newsl., 12 (1973) 136.
9 C. A. R. Albuquerque and J. R. Muysson, Chem. Geol., 9 (1972) 167 and references therein.
10 F. J. Flanagan, Geochim. Cosmochim. Acta, 37 (1973) 1189.
11 H. de la Roche and K. Govindaraju, Methods Phys. Anal., 7 (1971) 314.
12 C. M. Elson, E. M. Bem and R. G. Ackman, J. Am. Oil Chem. Soc., 1981, in press.

Analytica Chimica Acta, 134 (1982) 397—400
Elsevier Scientific Publishing Company, Amsterdam — Printed in The Netherlands

Short Communication

THE SPECTROPHOTOMETRIC AND FLUORIMETRIC DETERMINATION OF COBALT BY EXTRACTION AS 2,4-DICHLOROBENZYLTRIPHENYLPHOSPHONIUM TETRATHIOCYANATOCOBALTATE(II)

D. THORBURN BURNS*, P. HANPRASOPWATTANA and B. P. MURPHY

Department of Analytical Chemistry, The Queen's University of Belfast, Belfast, BT9 5AG, Northern Ireland (Gt. Britain)

(Received 3rd August 1981)

Summary. Cobalt (0—100 μg) can be determined by spectrophotometric or fluorimetric measurements after its extraction as 2,4-dichlorobenzyltriphenylphosphonium tetrathiocyanatocobaltate(II) into 1:9 acetone—dichloroethane. Cobalt quenches the fluorescence of the reagent. The effects of pH and diverse ions are reported. The system is applied to the determination of cobalt in mild steels without prior separation of the iron.

The reactions of onium ions are frequently very similar although some degree of selectivity may be achieved or enhanced by the use of reagents to form an appropriate anion or by variation in extracting solvent [1]. Many such systems have been used for the spectrophotometric determination of cobalt. In contrast, very few fluorimetric determinations, either direct or indirect by displacement reaction or by quenching of fluorescence, have been described for cobalt [2, 3]. Earlier, a method for the spectrophotometric and indirect fluorimetric determination of cobalt based on the extraction of protriptylinium tetrathiocyanatocobaltate(II) was reported [3]. The present communication reports on the 2,4-dichlorobenzyltriphenylphosphonium ion as an alternative fluorescent cation for the same determination. This species had advantages over protriptyline (*N*-methyl-5*H*-dibenzo-(α*d*)-cycloheptene-5-propylamine) as it is more sensitive, readily available and cheap, and is not a drug substance.

Experimental

Apparatus. A Unicam SP8000 recording spectrophotometer and a Baird Atomic SFR100 spectrofluorimeter were used. The wavelengths employed were 328 and 625 nm for absorption and 323 and 380 nm for fluorescence excitation and emission, respectively. Quartz 1-cm cells were used except for absorption measurements at 625 nm when 4-cm cells were used. The fluorimeter response was standardized with a 1 ppm phenanthrene solution in ethanol.

Reagents. 2,4-Dichlorobenzyltriphenylphosphonium chloride (Parish Chemical Co.) was used as supplied. Elemental analysis gave the results: theor. for $C_{25}H_{20}PCl_3$; 65.58% C, 4.40% H; found 65.85% C, 4.44% H. A

0003-2670/82/0000-0000/$02.75

0.005 M stock solution was made by dissolving 0.5722 g of reagent in 250 ml of 1:9 acetone—1,2-dichloroethane.

A stock 100 ppm cobalt(II) solution was prepared by dissolving 0.2630 g of anhydrous cobalt(II) sulphate (analytical-reagent grade dried to constant weight at 400°C) in 1 l of distilled water. More dilute standard solutions were prepared as required.

1,2-Dichloroethane was distilled twice (b.p. 83.5°C). All other reagents were of analytical grade and twice-distilled water was used throughout.

Choice of solvent. A variety of solvents including alcohols, ketones, esters, ethers and chlorinated and aromatic hydrocarbons were examined for extraction efficiency as before [3]. Ethyl acetate, nitrobenzene, isobutyl methyl ketone, 1,2-dichloroethane and chlorobenzene were the most efficient extractants. Extracts with chlorobenzene, ethyl acetate and 1,2-dichloroethane showed the highest fluorescence. The calibration graph using chlorobenzene was non-linear, but acetone—1,2-dichloroethane (1:9) gave a high response and a linear calibration graph, and was used for the rest of the study.

Optimum amounts of reagents. The effect of variation of thiocyanate concentration was similar to that noted earlier [3, 4], and a 1 M concentration was adopted for routine use and for experiments where the amount of 2,4-dichlorobenzyltriphenylphosphonium chloride was varied. Above a reagent: cobalt ratio of 3:1, the absorbance was constant. The effect of pH was not significant over the pH range 1—8.

It was found that some excess of reagent, as its thiocyanate, was extracted along with the cobalt complex. The reagent absorbance, mainly at 328 nm, could be compensated for by using a reagent blank, measurements at 328 nm being six times as sensitive for cobalt as at 625 nm ($\epsilon_{328} = 1.1 \times 10^4$ l mol^{-1} cm^{-1}, $\epsilon_{625} = 1.8 \times 10^3$ l mol^{-1} cm^{-1}). The fluorescence of the extracted reagent was increasingly quenched by increasing amounts of the cobalt complex although the shapes of the emission spectra were the same. This effect was used as the basis of a fluorimetric procedure.

Composition of the complex. This was established spectrophotometrically by Job's method of continuous variations [5] to be $(C_{25}H_{20}PCl_2)_2\ Co(SCN)_4$ at 625 nm but the complex is partly dissociated.

Analysis of steel samples. For steel samples containing 0.05—0.2% or 0.005—0.02% cobalt, dissolve 0.5 or 2.5-g samples, respectively, in 500-ml conical flasks containing 12 or 60 ml of distilled water, 6 or 30 ml of concentrated hydrochloric acid and 6 or 30 ml of 100-vol. hydrogen peroxide. When the initial reaction has subsided, add a further 6 or 30 ml of the hydrogen peroxide. Evaporate to 10 ml and dilute to 40 ml with distilled water. Adjust the pH to 0.1 by careful addition of 6 M ammonia solution. Transfer to a volumetric flask and dilute to 100 ml. To a 10- or 20-ml aliquot of this steel solution, add 5 ml of 1 M potassium thiocyanate solution and 2 or 10 ml of 40% (w/v) ammonium fluoride solution, and extract with exactly 25 ml of 0.005 M, 2,4-dichlorobenzyltriphenylphosphonium chloride solution, shaking for 1 min. Allow the phases to separate. Filter the lower phase

through a Whatman No. 1 filter paper, and determine the absorbance at 328 nm and at 625 nm, or the fluorescence at 380 nm with excitation at 323 nm.

Prepare calibration graphs over the range 0—100 μg of cobalt, adding 5 or 10 ml of iron solution containing 0.05 or 0.5 g of iron (depending on the size of sample taken), prepared from pure iron sponge dissolved as for the samples.

Results and discussion

Linear calibration graphs were obtained over the range 0—100 μg Co in the final 25-ml extract for absorbance measurements at 328 and 625 nm. The calibration graph for the indirect fluorimetric method was linear over the same range but with negative slope. At 50 μg of cobalt, the coefficients of variations estimated from 7 replicates were 0.63 and 0.77% for absorbance measurements at 328 nm and 625 nm, respectively, and 1.74% for the indirect fluorescence measurements.

The possible interferences of various cations, chosen on the basis of previous studies of onium extraction of tetrathiocyanatocobaltate(II) for the analysis of mild steels [3, 6], were checked spectrophotometrically for 60 μg of cobalt. The results are summarized in Table 1. The only ion that interfered significantly at the ratios likely to occur in mild steels was iron(III); this could be masked by the addition of 10 ml of 40% (w/v) ammonium fluoride for 0.5 g of iron. At high levels of iron, enhanced extraction was noted (+3% for 0.05 g and +9% for 0.5 g of Fe); these interfering effects in the determination of cobalt in steel and that of the blank were

TABLE 1

Effect of diverse ions on the determination of cobalt(II)

Ion[a]	Ratio to Co(II) (w/w)	Change in absorbance (%)	
		328 nm	625 nm
Zn^{2+}	50	−167	−15
	10	−2.7	0[b]
Mn^{2+}	500	+14	+19
	250	+7	+5
	50	0[b]	0[b]
Cu^{2+}	100	+25	+600
	100[c]	0[b]	−6
Pb^{2+}	20	−2	−3
	10	0[b]	0[b]
Fe^{2+}	50	460	5
Fe^{3+}	500	+2300	+1440
	500[d]	6	7
	5000[d]	41	43

[a]Added as chloride or sulphate. [b]Ions causing a change in absorbance less than twice the standard deviation for pure solutions are regarded as non-interfering. [c]In the presence of sodium thiosulphate (50 mg). [d]In the presence of ammonium fluoride.

TABLE 2

Determination of cobalt in mild steels

B.C.S. No.	Certified value (%)	Fluorimetry (%)	Spectrophotometry (%)	
			625 nm	328 nm
456	0.043—0.050	0.049 ± 0.0066[a]	0.049 ± 0.0009[a]	0.048 ± 0.0007[a]
459	0.073—0.080	0.080 ± 0.0060	0.080 ± 0.0008	0.080 ± 0.0006
458	0.16	0.158 ± 0.0067	0.157 ± 0.0009	0.160 ± 0.0007
460	0.008—0.009	0.0085 ± 0.00054	0.0090 ± 0.0009	0.0089 ± 0.0010
457	0.017—0.019	0.0186 ± 0.0063	0.0189 ± 0.0009	0.0179 ± 0.0011

[a]95% confidence limit, $n = 4$.

compensated for by the addition of an equivalent amount of iron to the standards. Linear calibration graphs were still obtained.

The results for the determination of cobalt in five British Chemical Standards steel samples (Table 2) are in good agreement with the certified values.

In common with other onium extractions of tetrathiocyanatocobaltate(II) [3, 6, 7], the procedure does not require prior separation of iron such as is required in other fluorimetric methods [8—10]. The mechanism of the quenching would appear to involve the photo-excited state, because there was no discernible change in the maximum or in the shape of the partially quenched fluorescent spectra [11, 12].

REFERENCES

1 A. G. Fogg, C. Burgess and D. Thorburn Burns, Talanta, 16 (1969) 719.
2 F. D. Snell, Photometric and Fluorimetric Methods of Analysis: Metals Part I, J. Wiley, New York, 1978.
3 D. T. Burns and P. Hanprasopwattana, Anal. Chim. Acta, 115 (1980) 389, and references therein.
4 M. Lehne, Bull. Soc. Chim. Fr., 18 (1951) 76.
5 P. Job, Ann. Chim. (Paris), 9 (1928) 113.
6 A. G. Fogg, C. T. Higgens and D. Thorburn Burns, Mikrochim. Acta, (1969) 546.
7 H. E. Affsprung, N. A. Barnes and H. A. Portraz, Anal. Chem., 23 (1951) 1680.
8 D. N. Lisitsyna and D. F. Shchebov, Zh. Anal. Khim., 28 (1973) 1203.
9 P. R. Haddad, P. W. Alexander and L. E. Smythe, Talanta, 23 (1976) 275.
10 S. B. Zamochnick and G. A. Rechnitz, Fresenius Z. Anal. Chem., 189 (1964) 424.
11 A. W. Varnes, R. B. Dodson and E. L. Wehry, J. Am. Chem. Soc., 94 (1972) 946.
12 G. G. Guilbault, Practical Fluorescence, Dekker, New York, 1973.

Analytica Chimica Acta, 134 (1982) 401—405
Elsevier Scientific Publishing Company, Amsterdam — Printed in The Netherlands

Short Communication

DIFFERENTIAL SPECTROPHOTOMETRIC DETERMINATION OF SILICA IN ROCKS AS α-MOLYBDOSILICIC ACID IN PRESENCE OF PHOSPHATE AND OTHER INTERFERENCES

R. C. SARKAR and M. SANKAR DAS*

Analytical Chemistry Division, Bhabha Atomic Research Centre, Trombay, Bombay 400 085 (India)

(Received 29th June 1981)

Summary. High concentrations of silica in rocks are determined by means of the stable α-12-molybdosilicic acid formed at around pH 4.2 in acetate buffer. Phosphate interference is avoided by acidification with sulphuric acid. Silica is quantified by differential spectrophotometry at 400 nm against standard rock solutions. Considerable amounts of phosphorus, arsenic and titanium and small amounts of germanium and vanadium do not interfere. The standard deviation is about 0.3%. The method is rapid and suitable for routine analysis of silicate and phosphate rocks.

It is well known that there are two forms of molybdosilicic acid; the α-form is stable and results from slow, spontaneous and irreversible transformation of the unstable β-form [1]. Most of the methods reported for the rapid determination of silica in rocks are based on formation of β-molybdosilicic acid followed by photometric measurement of the yellow complex [2—4] or of the blue complex after reduction [5]. The instability of the β-form with time calls for rigorous adherence to the recommended procedures and the use of potassium chromate solution as a permanent reference standard for high-precision differential spectrophotometry [3, 4].

Anderson [6] and Ringbom et al. [7] converted the β-acid to the stable α-form by heating the test solution. Truesdale and Smith [8], and Kato [9] determined silica in waters by methods based on the formation of α-molybdosilicic acid at pH 4.0 and pH 4.2, respectively, in the presence of acetate buffer without heating.

No particular procedure for eliminating interference from phosphate was suggested in these studies. Citric, tartaric and oxalic acids are not satisfactorily employed in most of the molybdosilicate methods for rock analysis, except in the methods based on formation of the molybdenum blue complex [5]. Morrison and Wilson [10], and Ringbom et al. [7] observed that these organic acids not only failed to mask the colour arising from phosphate but also caused fading of the molybdosilicate colour. The interference from phosphate is therefore normally corrected for, rather than removed by auxiliary complexing agents, in rock analysis by molybdosilicate methods

[3, 7]. As the determination of phosphorus present in the sample is then imperative, the rapidity of silica determinations suffers.

The molybdophosphoric acid can be destroyed, after full colour development, by acidification without harmful effects on the β-molybdosilicic acid [4, 11]. The present work takes advantage of the higher stability of the α-form of molybdosilicic acid even in the strongly acidic medium required for bleaching the coloured molybdophosphoric acid, to develop a differential spectrophotometric method for the determination of high silica contents in geological materials. The effects of other interfering elements are reported.

Experimental

Reagents. All reagents were of analytical grade. All solutions were prepared with distilled water and stored in polythene containers. Sulphuric acid (d. 1.84) was diluted for use.

For the buffer solution, dissolve sodium acetate trihydrate (25 g) in about 150 ml of water in a polythene beaker, add anhydrous acetic acid (18 ml), dilute to 250 ml, filter, and store.

Preparation of sample and standard solutions. Weigh accurately, by difference, 100—130 mg of ground dried rock sample (with not more than 70 mg of SiO_2 in the aliquot). Fuse for 10 min with the residue obtained on drying (hot plate) 5.0 ml of 30% (w/v) sodium hydroxide in a 50-ml nickel crucible. Cool, half-fill the crucible with water and heat on a steam bath for 15—20 min. Transfer the contents of the crucible to a polythene beaker containing about 350 ml of water and 15 ml of (1 + 5) sulphuric acid. Transfer the solution to a 500-ml volumetric flask and dilute to volume with water. If the solution is turbid, filter and take a clear aliquot for colour development.

Prepare the standard silica solution by taking a standard silicate rock through the above procedure. Soda feldspar (No. 99, U.S. National Bureau of Standards) was used here. Prepare a process blank solution in the same manner as the sample.

Colour development and differential measurement. Transfer a suitable aliquot (25 ml) of the sample solution (2.5—4 mg SiO_2) and different aliquots of the standard silica solution to 100-ml volumetric flasks. Equalize the volumes of these aliquots by adding the required volumes of the process blank solution, to remove any effect of the blank. Add a few drops of ca. 4×10^{-3} M permanganate solution to each solution until it becomes slightly purple. Add 10 ml of 0.06 M EDTA (disodium salt) and mix. Dilute to about 50 ml. Add 10 ml of buffer solution and 10 ml of filtered 6% (w/v) ammonium paramolybdate tetrahydrate solution, mixing after each addition. After 30 min, add 20 ml of (1 + 2.5) sulphuric acid, mix and let stand at room temperature for 10 min. Dilute to volume with water and mix. Measure the absorbance of the sample solution at 400 nm against a reference silica standard having a slightly lower absorbance than that of the sample, using a pair of matched cells (10 mm).

Measure the absorbances of as many silica standards of different concentrations as are needed to bracket all the sample solutions. Measure the absorbances of the sample solutions, with all the reagents except molybdate, against the blank solution treated similarly, to determine any corrections needed because of residual absorbance of the sample solutions. The magnitude of such corrections did not exceed 0.006 absorbance in this work.

Compute the silica content of the sample from the expression $\%SiO_2 = [c_L + (c_H - c_L)(A_X - A_L)/(A_H - A_L)]\,100/W$, where c_L and c_H are the weights of SiO_2 in the aliquots of the low and high standards, respectively, closely straddling the sample, W is the weight of sample in the aliquot taken for colour development, and A_L, A_H and A_X are the respective corrected absorbances. Since the actual concentration of the reference silica standard is not involved in the above expression, a permanent chromate standard can be used as reference [3, 4].

Results and discussion

The pH of the test solution is maintained at about 4.2 for the colour development described above because only the α-acid is formed at pH ⩾ 4.1 [9]. At this pH, full intensity of the colour of the solution develops in 20 min and is stable for at least 72 h; in contrast, the rate of bleaching is 2% in 30 min when the β-form is used [3, 4]. On subsequent acidification to 1 M in sulphuric acid the intensity of the colour increases by about 1% of the initial value and remains stable for at least 3 h. Later, the intensity decreases by about 2% after 24 h. Compared to molybdosilicic acid, the intensity of molybdophosphoric acid is highly sensitive to pH, particularly at pH below 2. Figure 1 shows that molybdophosphoric acid has no absorbance in sulphuric acid medium beyond 0.8 M.

The effects of possible interferences on the determination of silica are listed in Table 1. Considerable amounts of phosphorus, arsenic and titanium and low amounts of niobium, vanadium and germanium can be tolerated. Because of their low contents in silicate rocks, the effects of the last three

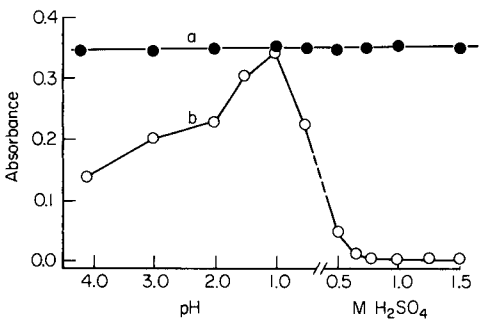

Fig. 1. (a) Molybdosilicic acid, 17.0 μg SiO_2 ml^{-1}, 0.04 M molybdate; (b) molybdophosphoric acid, 22.5 μg P_2O_5 ml^{-1}, 0.04 M molybdate. All absorbances were measured against the corresponding blanks at 400 nm.

TABLE 1

The effects of interfering species in the determination of silica (Concentration of SiO_2, 10 $\mu g\ ml^{-1}$; 1 M H_2SO_4)

Species	Conc.[a] ($\mu g\ ml^{-1}$)	Equivalent conc. in sample[b] (%)	Species	Conc.[a] ($\mu g\ ml^{-1}$)	Equivalent conc. in sample[b] (%)
P_2O_5	25.0	38.5	Nb_2O_5	2.0	3.1
As_2O_5	7.0	10.8	GeO_2	0.3	0.5
TiO_2	6.0	9.2	V_2O_5	0.25	0.4

[a]The observed deviation of the absorbance is less than 0.002 at the specified concentrations of the analyte and the interfering constituent. [b]Computed for a sample size of 130 mg in a volume of 500 ml with a 25-ml aliquot taken for colour development.

elements are insignificant. Molybdovanadic acid, like those of phosphorus and arsenic, is destroyed in strong acid; unlike the others, however, vanadium, leads to enhancement of the colour intensity of silicon, probably because of formation of a triple heteropoly complex. Hydrochloric acid was not used in these studies, to avoid the possible formation of coloured chloro complexes, e.g., with iron.

TABLE 2

Analytical results for silica in standard rocks by the proposed method

Standard rock	Type of rock	SiO_2 (%)	
		Recommended value	Present method
SY-3[a]	Syenite	59.68[12]	59.53
T-1[a]	Tonalite	62.70[12]	62.59
MRG-1[a]	Gabbro	39.32[12]	39.38
GSP-1[b]	Granodiorite	67.32[12] 67.38[13]	67.40
AGV-1[b]	Andesite	59.61[12] 59.00[13]	59.20
99[c]	Soda feldspar	68.66[f]	68.63
GS-N[d]	Granite	65.98[12] 65.80[14]	65.58
FK-N[d]	Pot. feldspar	65.11[12] 65.02[14]	65.26
DR-N[d]	Diorite	52.88[12]	52.74
UB-N[d]	Serpentine	39.93[12]	39.85
DT-N[d]	Kaynite	36.52[12]	36.62
B-1[e]	Basalt	50.60[4]	50.40
TKT[e]	Trachyte	67.57[3]	67.45

[a]Geological Survey of Canada. [b]U.S. Geological Survey. [c]U.S. National Bureau of Standards, Washington. [d]Association Nationale de la Recherche Technique (France). [e]Analytical Chemistry Division, BARC, Bombay. [f]Certified value.

Several international standard rocks containing a wide range of diverse elements, were analyzed by the proposed method with the results given in Table 2. The relative standard deviation of the determination of silica in a sample containing 67% SiO_2 was found to be 0.3%.

REFERENCES

1 J. D. H. Strickland, J. Am. Chem. Soc., 74 (1952) 862, 868, 872.
2 S. Abbey, N. J. Lee and J. L. Bouvier, Geol. Surv. Can. Pap., 74-19, 1974.
3 R. C. Sarkar and M. Sankar Das, J. Indian Chem. Soc., 57 (1980) 787.
4 R. C. Sarkar, J. Indian Chem. Soc., 58 (1981) 362.
5 L. Shapiro and W. W. Brannock, US Geol. Surv. Bull., 1144-A, 1962, A24.
6 L. H. Anderson, Acta Chem. Scand., 12 (1958) 495.
7 A. Ringbom, P. E. Ahlers and S. Siitonen, Anal. Chim. Acta, 20 (1959) 78.
8 V. W. Truesdale and C. J. Smith, Analyst, 100 (1975) 203, 797.
9 K. Kato, Anal. Chim. Acta, 82 (1976) 401.
10 I. R. Morrison and A. L. Wilson, Analyst, 88 (1963) 88.
11 O. A. Ohlweiler and J. O. Meditsch, Talanta, 24 (1977) 652.
12 S. Abbey, Geol. Surv. Can. Pap., 80-14, 1980.
13 F. J. Flanagan, Geochim. Cosmochim. Acta, 37 (1973) 1189.
14 H. de la Roche and K. Govindaraju, Analusis, 4 (1976) 347.

Analytica Chimica Acta, 134 (1982) 407—409
Elsevier Scientific Publishing Company, Amsterdam — Printed in The Netherlands

Short Communication

EXTRACTION—SPECTROPHOTOMETRIC DETERMINATION OF PALLADIUM WITH *n*-BUTYLXANTHATE

YOSHIAKI SASAKI

Department of Chemistry, Faculty of Science, Yamaguchi University, Yoshida, Yamaguchi-shi, Yamaguchi 753 (Japan)

(Received 22nd June 1981)

Summary. Palladium (6—180 nmol) is extracted quantitatively with potassium *n*-butylxanthate into benzene from an aqueous phase containing EDTA, and determined spectrophotometrically at 290 nm. The molar absorptivity of the complex is 7.5×10^4 dm^3 mol^{-1} cm^{-1}.

Alkylxanthates (O-alkyldithiocarbonates) react with various metal ions giving chelates which are sparingly soluble in water and soluble in organic solvents such as chloroform, and have been used for the extraction of metal ions [1]. Palladium(II) forms very stable 1:2 metal:ligand complexes with xanthates [2]. Methods for the chloroform extraction—spectrophotometric determination of milligram amounts of palladium with xanthates have been reported by Paria and Majumdar [3], who extracted at pH 2 and measured the absorbance of the extract at 460 nm. However, the molar absorptivity of the palladium complex at 460 nm was only 200 dm^3 mol^{-1} cm^{-1}, so that the method had poor sensitivity.

It is shown below that traces of palladium can also be extracted into benzene with a slight excess of *n*-butylxanthate from an alkaline medium containing a very large amount of EDTA. After such an extraction, the absorbance can be measured at 290 nm, because the reagent blank shows no absorption at this wavelength, and the molar absorptivity of the complex is 7.5×10^4 dm^3 mol^{-1} cm^{-1}. The use of EDTA eliminated the interferences from various metal ions.

Experimental

Reagents. Potassium *n*-butylxanthate was synthesized and purified as described previously [4], and the solution was freshly prepared daily. The standard palladium solution (1.2×10^{-2} mol dm^{-3}) was prepared by dissolving 1.0638 g of palladium(II) chloride in 400 cm^3 of (1 + 80) hydrochloric acid, and diluting to 500 cm^3 with water. The 2 mol dm^{-3} Tris buffer solution (pH 8.1) was prepared by dissolving 1 mol of tris(hydroxymethyl)aminomethane in water, adding hydrochloric acid until the pH reached 8.1, and diluting to 500 cm^3 with water.

Apparatus. Absorption spectra and absorbances were measured on a Shimadzu UV-200 spectrophotometer using 10-mm path-length quartz cells. The pH was measured on a Toa HM-5A pH meter with a glass electrode.

Procedure. In a 50-cm^3 separating funnel, mix the palladium solution (6—180 nmol Pd), 10 cm^3 of 0.25 mol dm^{-3} EDTA solution, 5 cm^3 of 2 mol dm^{-3} Tris buffer solution, and 1 cm^3 of 1×10^{-3} mol dm^{-3} potassium *n*-butylxanthate solution. Dilute to 20 cm^3 with water. Extract with 15 cm^3 of benzene for 5 min. Measure the absorbance of the organic phase at 290 nm against benzene.

Results and discussion

The extracted palladium complex was yellow, and exhibited three absorption maxima, at 290 nm ($\epsilon = 7.5 \times 10^4$), 385 ($\epsilon = 8.0 \times 10^3$), and 460 nm ($\epsilon = 2.0 \times 10^2$ dm^3 mol^{-1} cm^{-1}). It is well known that any free xanthate extracted also absorbs in the ultraviolet region. However, no free xanthate was detected in the extract when the extraction was done from neutral or alkaline medium with a small excess of xanthate.

The effect of the pH of the aqueous phase, adjusted with potassium hydroxide or hydrochloric acid, on the extraction of palladium was investigated at a level of 5×10^{-5} mol dm^{-3} *n*-butylxanthate. Below pH 7, the absorbance of the reagent blank increased with decreasing pH (Fig. 1). The optimum pH range for determination of palladium was 7—11. The pH of the aqueous phase was ultimately adjusted to 8.1 with Tris buffer, which did not affect the extraction of palladium.

The effect of *n*-butylxanthate concentration on the extraction of 6×10^{-6} mol dm^{-3} palladium at pH 8.1 was investigated. The results obtained are shown in Fig. 2. Palladium was extracted quantitatively if more than the equivalent amount of xanthate was present. The addition of 0.12 mol dm^{-3}

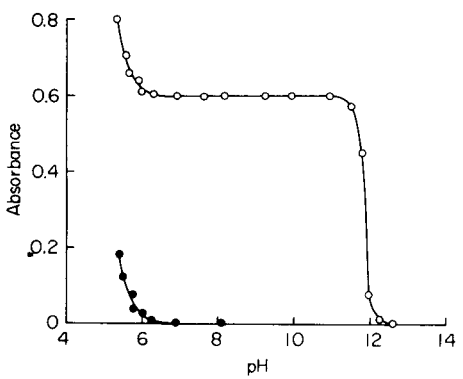

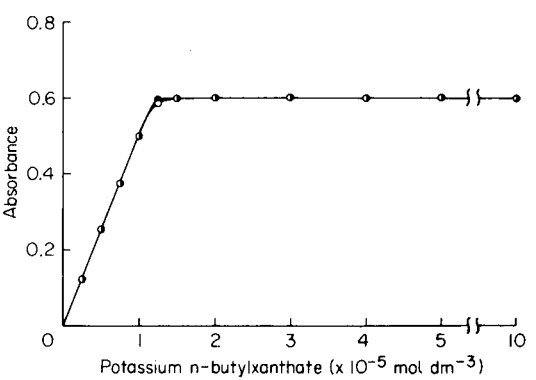

Fig. 1. Effect of pH on the benzene extraction of 6×10^{-6} mol dm^{-3} palladium with 5×10^{-5} mol dm^{-3} potassium *n*-butylxanthate: (○) sample; (●) reagent blank.

Fig. 2. Effect of *n*-butylxanthate concentration on the extraction of 6×10^{-6} mol dm^{-3} palladium at pH 8.1: (○) in the presence of 0.12 mol dm^{-3} EDTA; (●) in the absence of EDTA.

TABLE 1

Tolerable amounts of other ions in the determination of 120 nmol of palladium

Tolerable amount	Ion
5 mmol	Ammonium, alkali metals, alkaline earth metals, halides, NO_3^-, CO_3^{2-}, SO_4^{2-}, PO_4^{3-}, SCN^-, tartrate.
500 μmol	SO_3^{2-}, NO_2^-, oxalate.
200 μmol	Ni(II), Co(II), Fe(III), Cd(II), Pb(II), Zn(II), Al(III), Cr(VI), Mo(VI), Cu(II), Se(IV), Ce(III).

TABLE 2

Determination of palladium in synthetic samples

Other ions present	Palladium (nmol)	
	Taken	Found
Cr(VI), Cu^{2+}, Fe^{3+} (50 μmol of each)	120	118, 121, 120
	12	11, 13, 13
Ni^{2+}, Co^{2+}, Fe^{3+}, Cd^{2+}, Pb^{2+}, Zn^{2+} (10 μmol of each)	120	118, 121, 121
	12	13, 13, 13

EDTA did not affect the extraction of palladium if the xanthate concentration exceeded 1.5×10^{-5} mol dm^{-3}.

The calibration graph was linear over the range 6—180 nmol of palladium. The coefficient of variation was 1.2% (10 runs) for 120 nmol of palladium. Most ions did not interfere; Tl(I), Ag(I), Hg(II), Pt(II), Au(III), Ru(III), Os(VIII), thiosulfate and cyanide interfered seriously. The tolerable amounts of other ions are shown in Table 1. Palladium in synthetic samples was determined and excellent results were obtained, as is shown in Table 2. Thus the method for the determination of palladium is simple, precise and accurate.

The author expresses his appreciation to Dr. K. Hayashi, Professor of Yamaguchi University, for his valuable advice.

REFERENCES

1 E. M. Donaldson, Talanta, 23 (1976) 417.
2 D. Coucouvanis, Progr. Inorg. Chem., 11 (1970) 233.
3 P. K. Paria and S. K. Majumdar, Fresenius Z. Anal. Chem., 274 (1975) 127; Anal. Chim. Acta, 74 (1975) 197; Indian J. Chem., 13 (1975) 743; J. Indian Chem. Soc., 53 (1976) 421.
4 Y. Sasaki, J. Inorg. Nucl. Chem., in press.

Analytica Chimica Acta, 134 (1982) 411—415
Elsevier Scientific Publishing Company, Amsterdam — Printed in The Netherlands

Short Communication

SPECTROPHOTOMETRIC DETERMINATION OF MICROGRAM AMOUNTS OF PENICILLINS BY SOLVENT EXTRACTION WITH AZURE B

ANANT N. NAYAK*

Department of Chemistry, Government College for Boys, Mandya 571 401, Karnataka State (India)

P. G. RAMAPPA, H. S. YATHIRAJAN and S. MANJAPPA

Department of Post-Graduate Studies and Research in Chemistry, University of Mysore, Manasagangotri, Mysore 570 006 (India)

(Received 14th April 1981)

Summary. Penicillins are determined by means of ion-pair formation with azure B and extraction into chloroform: the absorbance of the extract is stable for several days. The apparent molar absorptivities for sodium penicillin G and potassium penicillin V at 634 nm are 3.91×10^3 and 1.25×10^4 l mol^{-1} cm^{-1}, respectively. Calibration graphs are linear over the range 60—950 μg of sodium penicillin G and 40—600 μg of potassium penicillin V in 10 ml. The method is successfully applied to pharmaceutical preparations.

The continuing introduction of new penicillin drugs has resulted in an extensive literature on their determination. The assay of antibiotics has been reviewed by Fairbrother [1]. Most chemical assays for the penicillins are based on the titration of unconsumed iodine after incubation with hydrolyzed penicillin [2]. An adaptation of this method is based on the reaction of penicillins with an excess of *N*-bromosuccinimide [3]. Adams et al. [4] proposed a novel enzymatic penicillin assay based on a pH-stat instrument incorporating coulometric generation of the titrant. Ibrahim et al. [5] determined penicillins by oxidizing with iodine monochloride and titrating the residual iodine monochloride with standard potassium iodate. Grime and Tan [6] determined some selected penicillins by direct titration with potassium iodate.

Spectrophotometric methods for penicillins have been based on the determination of the hydroxamic acid formed by reaction with hydroxylamine [7], or the penicillenic acid mercury(II) mercaptides formed by reaction with imidazole in the presence of mercury(II) chloride [8]. A method based on the formation of a coloured compound (λ_{max} = 750 nm) by boiling penicillins with ammonium vanadate solution in sulphuric acid has been reported [9].

Azure B forms ion-pairs with various anions; such reactions have been

used for extraction—spectrophotometric determinations of rhenium [10], antimony [11], uranium [12], etc. In a comprehensive investigation of analytical methods for penicillins, azure B was found to give extractable ion-pairs with sodium penicillin G and potassium penicillin V. The extraction of these ion-pairs provides a very sensitive spectrophotometric procedure which is applicable over a wide pH range with good selectivity.

Experimental

Apparatus and reagents. A Beckman DB spectrophotometer with 10-mm silica cells and in Elico L1-10 pH meter were employed. All chemicals were of analytical grade and were used without further purification. An azure B stock solution (5×10^{-3} M) was prepared by dissolving 340.5 mg of azure B in redistilled water, and diluting to 250 ml.

Penicillins. Pharmaceutical-grade benzyl penicillin sodium (sod. pen. G) and phenoxymethyl penicillin potassium (pot. pen. V) were obtained in sealed vials. Elemental analysis revealed no significant impurities. Standard stock solutions of penicillins were prepared by dissolution of appropriate amounts of solid in 100 ml of 0.1 M phosphate buffer solution, pH 5.91.

Procedure. Pipette an aliquot of sample or standard solution containing 60—950 μg of sod. pen. G or 40—600 μg of pot. pen. V into a 50-ml separating funnel. Add 5 ml of buffer pH 5.0 (14.74 g of Na_2HPO_4 and 10.20 g of citric acid per litre) and dilute to 20 ml with redistilled water. Add 1 ml of 1×10^{-3} M azure B solution and 10 ml of chloroform. Shake the funnel for 2 min to extract the ion-pair formed between azure B and penicillin. After standing for a fixed time between 5 min and 2 h, transfer the organic phase to a 15-ml glass-stoppered tube containing some anhydrous sodium sulphate. Shake the mixture vigorously until transparent and measure the absorbance at 634 nm against a reagent blank. Construct a calibration graph from the standard measurements.

For the analysis of pharmaceutical preparations, dissolve an appropriate amount of sample in the phosphate buffer to obtain a ca. 200-ppm solution of penicillin and filter if necessary. Then apply the above procedure.

Results and discussion

Figure 1 shows the absorption spectra of the azure B-penicillin ion-pairs extracted into chloroform, and of the reagent blank. All these spectra have their absorption maxima at 634 nm and this wavelength was used in all subsequent measurements. The wavelength of maximum absorption did not shift with a change in buffer composition at a given pH, when acetate and McIlvaine buffers were tested.

To establish the optimum pH range, penicillin was allowed to react with azure B in aqueous solutions buffered to pH 0.7—8.0 and the complex formed was extracted into chloroform for measurement. Sulphuric acid was used for adjustment to below pH 2.2, and McIlvaine buffers [13] for pH values in the range 2.2—8.0. Constant absorbances were obtained over the pH

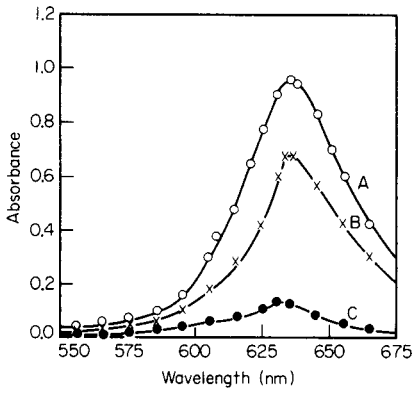

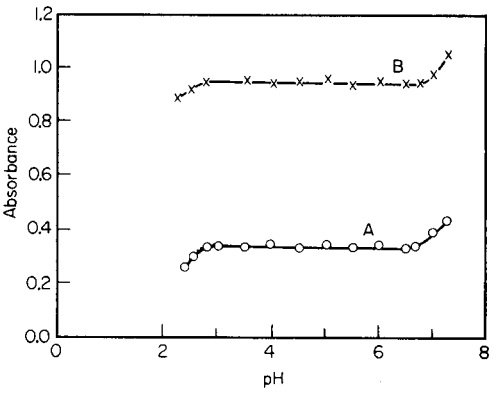

Fig. 1. Absorption spectra of azure B ion-pairs in chloroform: (A) 30 ppm potassium V (reagent blank subtracted); (B) 60 ppm sodium penicillin G (reagent blank subtracted); (C) reagent blank against chloroform.

Fig. 2. Effect of pH on the formation of the ion-pairs of azure B with (A) sodium penicillin G; (B) potassium penicillin V (reagent blank subtracted).

range 2.8—6.6 (Fig. 2). The decreased absorbance below pH 2.8 can be attributed to a decrease in the concentration of free penicillin ion caused by protonation. The increased absorbance above pH 6.6 is caused by the formation of an extractable azure B species. In all subsequent work, a pH of ca. 5.0 was used.

The extraction of the ion-pair was affected by the concentration of azure B. To establish the optimal amount, 1-ml aliquots of 10^{-4}—2×10^{-3} M azure B solutions were used in the conditions given above. Calibration graphs with 1 ml of 1×10^{-4} or 2.5×10^{-4} M azure B were not linear but the reagent blanks were low. The graphs with 5×10^{-4}—2×10^{-3} M azure B solutions were linear, but the more azure B used, the higher the reagent blank. In subsequent work 1 ml of 1×10^{-3} M azure B was employed. The method of continuous variations indicated that a single 1:1 ion-pair species was extracted.

To establish the optimal extraction conditions, solutions containing 400 μg of penicillin in redistilled water were treated with azure B as recommended and then extracted with successive 10-ml portions of chloroform, the absorbance of the organic phase after each extraction being measured against chloroform at 634 nm. The absorbance of the fifth extract was very similar to that of the fifth reagent blank, indicating that four 10-ml portions of chloroform suffice for complete extraction. However, the reproducibility with a single extraction was so good that, for simplicity, one 10-ml portion of chloroform was used in the recommended procedure. Tests made on sodium penicillin G (40 ppm) with the single extraction gave a mean result of 39.8 ppm with a standard deviation of 0.27 (n = 5). Other organic solvents were tested, but chloroform was found to be the most suitable.

Shaking times of 0.5—5 min produced constant absorbance, and so shaking for 2 min was used throughout. In contrast, increasing standing times (5 min—3 h) after shaking produced a slight increase in absorbance for both the reagent blank and the ion-pair. The reproducibility was good on standing for a fixed period; for example, measurements on 40-ppm solutions after 10-min standing times showed standard deviations of about 0.3 ppm (n = 10). The absorbances of the separated extracts were, however, stable for 5 days in a glass-stoppered tube at room temperature.

Calibration graphs showed a linear dependence of absorbance on concentration over the ranges 6—95 ppm of sodium penicillin G and 4—60 ppm of potassium penicillin V. For log I_0/I = 0.001, the Sandell sensitivities were 0.091 and 0.031 $\mu g\ cm^{-2}$, respectively, and the corresponding apparent molar absorptivities were 3.91×10^3 and $1.25 \times 10^4\ l\ mol^{-1}\ cm^{-1}$.

Effect of concomitant substances and applications to penicillin drugs. The effects of some compounds which often accompany penicillin in pharmaceutical products were studied. The compounds were added to 40-ppm penicillin solutions and studied by the recommended procedure. The tolerance limits are given in Table 1. The proposed method has the advantage of virtual freedom from interference and should be of value in the trace determination of penicillins in many samples.

The proposed method was successfully applied to the determination of penicillins in various pharmaceutical preparations. The results of the assays of tablets and vials (Table 2) compare favourably with the quoted values, and with those obtained by the official method of the British Pharmacopoeia [14].

The authors thank Hindustan Antibiotics Ltd., India, for the supply of pharmaceutical-grade penicillins.

TABLE 1

Effect of concomitant substances on the determination of penicillin (40 ppm)

Compound added	Tolerance limit[a] (ppm)		Compound added	Tolerance limit[a] (pp	
	Sod. pen. G	Pot. pen. V		Sod. pen. G	Pot. p
Ascorbic acid	120	130	Sucrose	6500	6300
Benzoic acid	250	275	Barbitone	2000	2200
Citric acid	4500	4300	Gelatin	5500	5800
4-Hydroxybenzoic acid	325	300	Gum acacia	10000	9500
Sorbic acid	500	550	Reserpine	300	300
Stearic acid	850	800	Sodium alginate	700	800
Tartaric acid	7800	8000	$NaHCO_3$	1400	1500
Dextrose	5500	5800	Starch	4000	4200
Lactose	4500	4500	Talc	4500	4600
Maltose	5000	5000			

[a]Amount causing an error of ±2.5%.

TABLE 2

Determination of penicillins in commercial pharmaceutical preparations

Preparations	Mean recovery[a] (%)	
	B.P. method	Proposed method
Pot. pen. V[b]		
(125 mg/tab)	102.3 ± 1.2	102.7 ± 1.4
(250 mg/tab)	98.8 ± 0.8	99.4 ± 0.7
Sod. pen. G[b]		
(500000 U/vial)	98.2 ± 1.1	98.6 ± 1.3
(1000000 U/vial)	101.6 ± 0.8	102.0 ± 0.6
Sod. pen. G[c]		
(200000 U/vial)	102.4 ± 0.6	102.1 ± 0.7
(500000 U/vial)	96.8 ± 1.5	96.4 ± 1.6
(1000000 U/vial)	101.2 ± 1.2	100.8 ± 0.8

[a]Average of five determinations with standard deviation. [b]Marketed by Hindustan Antibiotics Ltd. [c]Marketed by Squibb.

REFERENCES

1 J. E. Fairbrother, Pharm. J., 218 (1977) 509.
2 J. F. Alicino, Ind. Eng. Chem. Anal. Ed., 18 (1946) 619.
3 J. F. Alicino, J. Pharm. Sci., 65 (1976) 300.
4 R. E. Adams, S. R. Betso and P. W. Carr, Anal. Chem., 48 (1976) 1989.
5 E. A. Ibrahim, S. M. Rida, Y. A. Beltagy and M. M. Abd El-Khalek, J. Drug Res. (Egypt), 6 (1974) 13.
6 J. K. Grime and B. Tan, Anal. Chim. Acta, 105 (1979) 361.
7 G. E. Boxer and P. M. Everett, Anal. Chem., 21 (1949) 670.
8 H. Bundgaard and K. Ilver, J. Pharm. Pharmacol., 24 (1972) 790.
9 E. A. Ibrahim, Y. A. Beltagy and M. M. Abd El-Khalek, Talanta, 24 (1977) 328.
10 V. M. Tarayan and S. V. Vartanyan, Dokl. Akad. Nauk Arm. SSR, 47 (1968) 214.
11 V. M. Tarayan, E. N. Ovsepyan and M. G. Ekimyan, Uch. Zap. Erevan Univ. Estestv. Nauk, 1 (1972) 73.
12 V. M. Tarayan, E. N. Ovsepyan and A. A. Petrosyan, Zh. Anal. Khim., 26 (1971) 322.
13 H. T. S. Britton, Hydrogen Ions, Vol. 1, Chapman and Hall, London, 1955, p. 356.
14 British Pharmacopoeia, HMSO, London, 1973, pp. 52, 363.

Analytica Chimica Acta, 134 (1982) 417—419
Elsevier Scientific Publishing Company, Amsterdam — Printed in The Netherlands

Short Communication

IMPROVEMENTS TO THE SENSITIVITY, RESOLUTION AND BLANK VALUE IN THE SEMI-AUTOMATIC FLUORIMETRIC DETERMINATION OF SELENIUM

J. H. WATKINSON

Ministry of Agriculture and Fisheries, Ruakura Soil and Plant Research Station, Hamilton (New Zealand)

(Received 10th June 1981)

Summary. Purging of dissolved oxygen by nitrogen improves the sensitivity, resolution and blank values in the earlier procedure for selenium based on 4,5-benzopiazselenol fluorescence, by lessening fluorescence quenching as well as oxidative reactions of dissolved oxygen. The sensitivity and precision (at 0.1 ng Se ml^{-1}) can be more than doubled.

Although the semi-automatic fluorimetric method described earlier [1] is sensitive enough for selenium in most agricultural samples [2], some samples (e.g., natural waters [3]) are very low in selenium (<1 ng Se ml^{-1}) whereas others are of limited size.

The quenching factor for atmospheric oxygen on the fluorescence of 4,5-benzopiazselenol in cyclohexane reported by Parker and Harvey [4] is 3.1. Furthermore, oxygen is involved in the formation of the polymer from 2,3-diaminonaphthalene (DAN) which interferes in the fluorescence measurement of 4,5-benzopiazselenol [4]. In view of these observations, the possibility of improving the performance of the earlier method [1] by de-oxygenating the solutions with nitrogen was investigated.

Experimental

The earlier procedure [1] was followed except that: (1) dry, oxygen-free nitrogen was bubbled through the cyclohexane and DAN reagents in series to remove oxygen; and (2) the flow stream was segmented with bubbles of nitrogen instead of air by bleeding off gas from the nitrogen line to the two reagents. Air was still allowed as a bubble into the stream as the sample probe moved between sample and wash solutions, and no attempt was made to de-aerate either of these solutions.

Results and discussion

Sensitivity. The fluorescence quenching factor of 3.1 found by Parker and Harvey [4] was confirmed in a separate experiment where oxygen was totally purged from the cyclohexane extract passing through the flow cell of the fluorimeter. The full sensitivity increase of 3.1 could not be realized in the automatic system because of practical difficulties. However, an increase of

2.3 times, i.e., 75% of the potential increase, was readily and reproducibly achieved under the experimental conditions described above. It would be extremely difficult to de-oxygenate the sample and wash solutions reproducibly using the automatic sampler. Since the gain in sensitivity would be only 25%, with probably a loss of precision, no effort was made to gain this extra sensitivity. In the procedure, a small amount of atmospheric oxygen dissolved in the sample and wash solutions is unavoidably re-introduced into the cyclohexane, both directly and via the nitrogen-segmenting bubble equilibrated with oxygen from the aqueous phase during passage through the system.

Resolution. The air bubble between sample and wash solutions introduces oxygen into the cyclohexane in this region with a corresponding local drop in sensitivity at the trough from the additional oxygen quenching of fluorescence. The peak-to-peak resolution was improved by removal of oxygen at the peak but not at the trough. For a 1 ng Se ml^{-1} solution, the trough height to peak height, measured using a short time constant (0.2 s) with a digital voltmeter, was decreased from 33% to 25% when the reagent solutions were de-oxygenated.

Blank value. The DAN polymer was removed from the DAN reagent before use by shaking and extracting the polymer into the organic solvent or collecting it at the interface [1]. The fluorescence contribution from the reagent impurity was equivalent to <0.01 ng Se ml^{-1}, as was found by running all reagents with the reaction bath at ambient temperature (about 20° C). The DAN blank value therefore arises mainly from reactions occurring in the reaction coil at 50° C, most probably with dissolved oxygen in the aqueous solutions. Degassing the DAN reagent with nitrogen and segmenting the flow stream with nitrogen instead of air both decreased the dissolved oxygen level. The use of nitrogen as described decreased the blank value from the DAN from 0.06 ng Se ml^{-1} to 0.03 ng ml^{-1}. Segmenting with twice as many nitrogen bubbles decreased the blank to 0.02 ng Se ml^{-1}, but improved the sensitivity by only 5% because the cyclohexane was still exposed to about the same amount of oxygen, except that more was in the gas phase than in solution.

Precision. Better precision of measurement resulted from these improvements in resolution and blank value. For example, at 0.1 ng Se ml^{-1} the standard deviations ($n = 8$) were 0.014 and 0.0055 ng Se ml^{-1} by the original and modified methods, respectively, under comparable conditions.

In conclusion, the sensitivity and resolution were enhanced by the lowering of the fluorescence quenching by dissolved oxygen, and the blank value was lowered by the decreased concentration of oxygen involved in the formation of the interfering fluorescent polymer from DAN. This simple modification allows the sensitivity and precision of the method to be more than doubled.

The author thanks G. C. Milligan for competent technical assistance.

REFERENCES

1 J. H. Watkinson and M. W. Brown, Anal. Chim. Acta, 105 (1979) 451.
2 J. H. Watkinson, Anal. Chim. Acta, 105 (1979) 319.
3 J. H. Watkinson and F. C. C. Hupkens van der Elst, N. Z. J. Sci., 23 (1980) 383.
4 C. A. Parker and L. G. Harvey, Analyst, 87 (1962) 558.

ANALYTICA CHIMICA ACTA, Vol. 134 (1982)

AUTHOR INDEX

(continued from inside of cover)

ıtinued from cover)

rt Communications

*(continued on page **424**)*

CONTENTS

(continued on inside page of co